University of Venda

SCHOOL OF ENVIRONMENTAL SCIENCES

DEPARTMENT OF MINING AND ENVIRONMENTAL GEOLOGY

PALEOENVIRONMENTAL RECONSTRUCTION OF CRETACEOUS-TERTIARY KAOLIN DEPOSITS IN THE DOUALA SUB-BASIN IN CAMEROON

BY

BUKALO NTUMBA NENITA

STUDENT No: 14014934

A THESIS SUBMITTED TO THE DEPARTMENT OF MINING AND ENVIRONMENTAL GEOLOGY, SCHOOL OF ENVIRONMENTAL SCIENCES, UNIVERSITY OF VENDA, IN FULFILMENT OF THE REQUIREMENTS FOR THE PhD IN ENVIRONMENTAL SCIENCES (GEOLOGY)

PROMOTER: PROF G.E. EKOSSE

CO-PROMOTERS: PROF J.O. ODIYO
PROF J.S. OGOLA

SEPTEMBER 2017

DECLARATION

I, BUKALO Ntumba Nenita, Student Number 14014934, hereby declare that this thesis submitted to the Department of Mining and Environmental Geology, School of Environmental Sciences, University of Venda, for the PhD in Environmental Sciences (Geology) is my own work and has not been previously submitted, in whole or in part, to any university for any degree.

…….. ……..

Student's signature Date

Bukalo NN

We, the promoters, certify that this declaration is correct.

…….. ……

Promoter's signature Date

Professor Ekosse GE

…….. ……

Co-promoter's signature Date

Professor Odiyo JO

…….. ……

Co-promoter's signature Date

Professor Ogola JS

DEDICATION

This thesis is dedicated to my parents, Bukalo Bokassa Leade and Mbombo Kabunda Mimi, whose endless love and support are a continual blessing to my life.

ACKNOWLEDGEMENTS

"... the race is not to the swift, nor the battle to the strong, neither yet bread to the wise, nor yet riches to men of understanding, nor yet favour to men of skill; but time and chance happeneth to them all." Ecclesiastes 9:11 (KJV). I thank the Lord Almighty, whose grace and providence took me through this long journey.

I express my heartfelt gratitude to my promoter, Professor Georges-Ivo Ekosse, and co-promoters Professors John Odiyo and Jason Ogola for the mentorship and keenness towards this research. Through their fastidiousness and scrupulousness, I have learnt to always aim for excellence. I will always be grateful for that and for all the knowledge and skills imparted to me during these three years of working with them.

I thank Professor Jude Odhiambo, Head of Department of Soil Sciences in the School of Agriculture at the University of Venda for allowing me to use the Soil Science Laboratory. I also thank Mr Peter Tshidada for his assistance and guidance during the hydrometer test, colour, pH and electrical conductivity determination.

I thank Mr Tinyiko Nkuna for giving me access to the Hydrology and Water Resource Laboratory in the School of Environmental Sciences for particle size separation.

Dr Eduard Stam, Head of Department of Ecology and Resource Management, Professor Wilsom Gitari, Glynn Phindihama and Rabelani Mudzielwana, are hereby thanked for their permission, assistance and guidance in the Fourier transform infrared spectroscopic analyses of my samples.

I am grateful to Professor Antoine Mulaba, Head of the School of Mining, Metallurgy and Chemical Engineering; and Ms Nomsa Baloyi and Mr Edward Malenga from the Extraction and Engineering Metallurgy Department's Laboratory at the University of Johannesburg for carrying out X-ray diffractometry (XRD), X-ray fluorescence (XRF) spectroscopy and scanning electron microscopy-energy dispersive spectrometry (SEM-EDS). Thank you Edward for all the pieces of advice and tips I needed to understand XRF and XRD. I also thank Mrs Adeline Megne, of the same Department, who gave me shelter during my stay in Johannesburg. Still from the University of Johannesburg, I wish to thank Mr Thivhani Meshack, who assisted in differential thermal analysis (DTA), for his time and forever kindness.

I thank Dr Sabine Verryn from XRD Analytical and Consulting cc in Pretoria, who carried out the mineral phase identification and quantification from X-ray diffractometry scans.

My gratitude also goes to Professor Hlangani Tutu and Mr Chuene Mokgehle from Witwatersrand University who carried out the inductively coupled plasma mass spectrometry (ICP-MS).

I am grateful to Professor Chris Harris and his team at the Stable Isotopes Laboratory in the Department of Geological Sciences at the University of Cape Town for carrying out the stable isotopes analyses, sometimes during hard conditions. I am thankful for all the guidance and materials provided for the interpretation of the results.

The Central Analytical Facility of Stellenbosch University and its staff, who carried out U-Pb laser ablation-inductively coupled plasma mass spectrometry (LA-ICP-MS) dating of zircons are highly appreciated: Dr Jeanne Taylor, who greatly facilitated the analysis and who provided training for U-Pb dating and data processing, Ms Mareli Groobelar, who provided training for mineral separation and Mrs Riana Rossouw for supervising the analysis. Thank you Mareli for your guidance, patience and optimism during the mineral separation process. Dr Taylor, thank you for your availability, patience, guidance and materials provided for the interpretation of the results. In the same line, I thank Ms Elrika Harmzen-Pretorius and Mrs Madelaine Franzenburg for their assistance in acquiring cathodoluminescence and backscattered imaging of zircons.

My fieldwork went on smoothly thanks to Ms Avhatakali Raphalalani, Mr Ernest Ekosse and Mr Theophilus Neba. I thank Ms Raphalalani for going with me all the way to Cameroon for fieldwork. Her presence and assistance were much appreciated. I also thank Mr Ekosse for sacrificing his time to drive us to Ediki, Dibamba and Missole. Finally, Mr Neba is thanked for providing information on Yatchika kaolin and for driving us to Yatchika.

This PhD journey started with the help of Mr Ivo Arrey. I, therefore, wish to sincerely thank him for all the sacrifice he made during the pre-admission and admission processes, and for being a great friend. I also thank Mr William Ngou Njombe for his support during the preparations for my journey.

I thank the wonderful friends I met during my stay at Thohoyandou. Though from different backgrounds and cultures, we became a large family. I will start by thanking Mireille Bilonda, who showed me much kindness by giving me a warm welcome to her room without knowing me. She repeated the gesture at the end of my studies when I had no place to stay. Mireille, you have been a great sister and acting mother. I thank another sister, Mrs Oluebube Ibeh, with whom I shared a lot of tears and laughter. The moral support and love given to me by these two ladies are much appreciated. I pray that God blesses you abundantly. To continue in this vein, I thank Pie-Veilard Kalonji, Zongho Kom, Olatunde Durowoju and Oladipo

Ologundudu, whose friendships were uplifting, both spiritually and socially. I thank my other new brothers and sisters, Elizabeth Etta, Denis Kalobo, Joseph-Mathieu Mundadi, Andre Tiawoun, Babatunde Ojelade, Moses Oyebanjo, Lisa Tambe, and Malvin Loka, whose encouragements and company were most useful. To Johanna Molepo, who was my first companion during my research and with whom I spent a lot of time, discovered new places and shared a lot of emotions, I say *thank you*. I thank my younger ones, Unarine Mashao and Valery Phakoago, whose gleeful characters were always a source of delight every time we met. The presence of all these good people made the hardship of this research bearable.

I express my gratitude to Professor Christopher Agyingi, Dr Anatole Djieto-Lordon and Dr Andrew Ako from the University of Buea in Cameroon, who have always showed interest in all my academic endeavours. I also thank Dr Makia Diko, whose guidance and literature provided are appreciated. In the same line, I also thank my friends Odette Achu, Evelyn Manji, Giles Azia and Mathieu Bomia for their support and prayers.

Last but not least, I wish to thank my family; my parents, Leade Bukalo and Mimi Mbombo for their perennial love, care and support during my studies; my elder brother and his wife, Shiva and Alice Bukalo; my baby brother, Kevin Bukalo; and my cousin Gracia Madimba for their love and support.

The financial assistance of the National Research Foundation (NRF) towards this research is hereby acknowledged. Opinions expressed and conclusions arrived at, are those of the author and not necessarily to be attributed to the NRF. The NRF is also acknowledged for its Competitive Programme for Rated Researchers (CPRR) grant for the Cretaceous-Tertiary clay deposits and argillaceous sediments Project. The University of Venda, through its Research and Publications Committee (RPC) is also acknowledged for its financial support. I also thank the staff of the Directorate of Research and Innovation.

I thank the many whose names are not mentioned above, but whose help was most useful and much appreciated.

MAY GOD BLESS YOU ALL!

ABSTRACT

Cretaceous-Tertiary Periods marked the break-up of Gondwana, a large landmass composed of most of the present-day southern continents. In understanding the events of the supercontinental break-up, paleoenvironmental studies need to be carried out. In such studies, kaolinites could be used as paleoenvironmental proxies due to their small particle sizes and large surface area. It is in this context that this research sought to reconstruct the paleoenvironments in which selected Cretaceous-Tertiary kaolin deposits in the Douala Sub-Basin in Cameroon formed.

To achieve this objective, mineralogical and geochemical characterisations were carried out using x-ray diffractometry, scanning electron microscopy, Fourier transform infrared spectrometry, thermal analyses and x-ray fluorescence spectroscopy. Trace elements and stable isotopes were analysed using mass spectrometries. Ages of zircons in the kaolins were determined using laser ablation magnetic sector-field inductively coupled plasma mass spectrometry (LA-SF-ICP-MS) U-Pb geochronology. Diagnostic evaluation for industrial applications of the kaolins were carried out using particle size distribution, texture, moisture content, pH, and electric conductivity.

Six kaolin deposits from Cretaceous-tertiary Formations of the Douala Sub-Basin were studied; namely, Bomkoul (Tertiary), Dibamba (Tertiary), Ediki (Cretaceous), Logbaba (Cretaceous), Missole (Tertiary) and Yatchika (Cretaceous). The nature and occurrences of these kaolin deposits in Cameroon were determined through thorough mineralogical and geochemical characterisations of bulk (< 2 mm size fraction), silt (2-63 µm size fraction) and clay samples (< 2 µm size fraction). By quantifying the mineral phases present, the morphology and the functional groups in the kaolins are presented as the mineralogical characteristics of kaolins of each study site; whereas, the major oxides geochemistry and the micro-elemental composition constitute the geochemical characteristics of these kaolins. The minerals' geneses were also determined and the prevailing paleoenvironmental and paleoclimatic conditions in which they were formed were reconstructed using trace elements and stable isotopes of oxygen and hydrogen in kaolinite. The maximum age of the kaolins were determined using U-Pb LA-SFICP-MS dating of zircons in the kaolin deposits. Diagnostic evaluation of the kaolins was carried out, and involved the determination of physical characteristics (particle size, texture, colour and moisture content) and physico-chemical characteristics (pH and electrical conductivity).

Results showed that kaolinite and quartz (as major phases), smectite and/or illite (as minor phases), anatase and rutile (as minor or trace phases), goethite and hematite (as trace

phases) were the mineral phases present in bulk and silt samples. Whereas, in the < 2 µm fractions, the mineral phases are made up of kaolinite and smectite (as major phases), smectite and/or illite (as minor phases), anatase and rutile (as minor or trace phases), goethite and hematite (as trace phases). The kaolins are mostly made up of thin platy or pseudo-hexagonal particles or flakes, books or stacks of kaolinite. The Dibamba, Logbaba and Missole II kaolins have well-ordered structures. Exothermic peak temperatures were generally between 943-988^{o}C. The most abundant major oxides are silica and alumina, followed by iron oxide and titania; though Logbaba and Missole II had higher titania than iron oxide. 85% of the kaolins, portrayed extreme silicate weathering (chemical index of alteration > 80%) and are compositionally mature (index of compositional variability > 0.78). The geochemical composition of the kaolins showed that source rocks of these kaolins vary between rhyolite/granite and rhyolite/granite + basalt. The geochemistry also suggested that the kaolins formed in a marine environment (except Logbaba samples).

Trace elements results revealed that Cretaceous-Tertiary kaolins in the Douala Sub-Basin are mainly enriched in rare earth elements compared to the upper continental crust, and have negative Eu anomaly. Large ion lithophiles (mainly Rb and U) were highly enriched in samples, high field strength elements (Y and Nb) were enriched in studied samples of all fractions; and transition trace elements generally had concentrations quite similar to upper continental crust values. Stable isotopes showed that the kaolins were formed in a supergene environment; and temperatures of kaolinitisation (assuming equilibrium with the global meteoric water line) were 26.58^{o}C ± 9.65^{o}C for Cretaceous kaolins and 29.40^{o}C ± 7.22^{o}C for Tertiary kaolins. Assuming equilibrium with the local (Douala) meteoric water line, the temperatures of kaolinitisation were 24.64^{o}C ± 9.48^{o}C for Cretaceous and 27.42^{o}C ± 7.08^{o}C for Tertiary kaolins.

Four main zircon populations were identified from radiogenic dating: the 1st between 550 and 650 Ma, the 2nd between 950 and 1050 Ma, the 3rd around 1600 Ma and the 4th between 2800-3200 Ma. These four zircon populations belong to the Proterozoic (Neo-, Meso- and Paleoproterozoic) and the Archean. The maximum depositional ages of the kaolins, reflected by the youngest weighted averages of zircon populations varied between 588 ± 2 Ma and 612 ± 2 Ma, all belonging to the Ediacaran Period (Neoproterozoic).

The diagnostic evaluation of the kaolins revealed that the kaolins are very sandy, with 50% of the samples having a sandy loamy clay or sandy loam texture. The colour of the samples varied considerably from white to darker colours (dark grey); with 15% of the kaolins being light reddish brown. The moisture content was generally very low (< 2 wt %) in all size fractions, except in Yatchika samples (moisture content > 2 wt %). The kaolins are generally acidic, with

a $pH_{(KCl)}$ varying between 3.06 and 3.81, except in Missole I samples, which had a pH (KCl) < 2. The electrical conductivity (EC) generally varied between 20 to ~ 50 µS/cm, except Dibamba and MSL II 01 samples which had EC values in the interval 50 µS/cm < EC < 80 µS/cm; and Missole I samples having an EC > 7500 µS/cm.

In conclusion, no great distinction was found between Cretaceous and Tertiary kaolins of the Douala Sub-Basin based on their mineralogy and geochemistry. The best kaolins in terms of these characteristics, and in comparison with the Georgia Kaolins (known for their high kaolinite quality), were the Dibamba (Tertiary), Logbaba (Cretaceous) and Missole II (Tertiary) kaolins. Based on their compositional maturity and mineralogical characteristics, these three kaolins are considered to be second cycle sediments; unlike Bomkoul, Yatchika and Ediki kaolins, which are believed to be first cycle sediments. Based on the trace elements and stable isotopes composition, Cretaceous and Tertiary kaolins of the Douala Sub-Basin were derived from felsic rocks. However, Cretaceous kaolins were formed in a cooler anoxic reducing environment; whereas the Tertiary kaolins were formed in a warmer oxidising environment, with higher precipitation. Ages of zircons in Cretaceous-Tertiary kaolins suggested that the zircon formed during two main tectonic events: the Eburnean orogeny, during which older zircons crystallised and the Pan-African orogeny, during which younger zircons crystallised. The maximum depositional ages of the kaolins varied between 588 ± 2 Ma and 612 ± 2 Ma. The main identified sources of these zircons are the Archean Ntem Complex, the Paleoproterozoic Nyong Group and the Neoproterozoic Yaounde Group. The diagnostic evaluation indicated that the particle size greatly influences the mineralogy and geochemistry of the kaolins because the finer particles (< 2 µm) have higher amounts of kaolinite and Al_2O_3. The moisture content of the kaolins makes them suitable as paint fillers and in soap production. Paper coating, paper filler, ceramics, pharmaceutics and cosmetics are potential applications for the kaolins, though particle size reduction and beneficiation will give them a higher quality. However, because these kaolin deposits are not big and extensive, they cannot be recommended for large scale industrial applications; but they can be used for bricks, pottery and stoneware manufacturing.

Keywords: Cretaceous-Tertiary Periods, Douala Sub-Basin, kaolin, paleoenvironmental reconstruction, stable isotopes

TABLE OF CONTENTS

LIST OF FIGURES

LIST OF TABLES

LIST OF ABBREVIATIONS

Al : Aluminium

As : Arsenic

ATR : Attenuated total reflectance

BaO : Barium oxide

CIA : Chemical index of alteration

CIW : Chemical index of weathering

Co : Cobalt

Cr : Chromium

Cu : Copper

DTA : Differential thermal analysis

Eu : Europium

FTIR : Fourier transform infrared

GTS : Geologic time scale

H_2O : Water

HCl : Hydrogen chloride

HFSE : High field strength element

HNO_3 : Nitric acid

HREE : Heavy rare earth elements

ICP-MS : Inductively coupled plasma mass spectrometer

ICV : Index of compositional variability

La : Lanthanum

LA-SF-ICPMS : Laser ablation-sectorfield-inductively coupled plasma mass spectrometry

LREE : Light rare earth elements

Lu : Luthetium

Ma : Million years

MAS : Magic-angle-spinning

MAT	: Mean annual temperature
MC	: Moisture content
N	: Nitrate
Ni	: Nickel
NMR	: Nuclear magnetic resonance
Pb	: Lead
Pt	: Platinum
REE	: Rare earth elements
Se	: Selenium
SEM	: Scanning electron microscopy
Si	: Silicon
TMS	: Tetramethylsiane
UCC	: Upper continental crust
VSMOW	: Vienna Standard Mean Ocean Water
XRD	: X-ray diffraction
Zn	: Zinc

LIST OF APPENDICES

LIST OF UNITS AND SYMBOLS

%	: Percent
µl	: Microliter
µm	: Micromerter
Å	: Angstrom
g	: gram
kV	: Kilovolt
m	: meter
mHz	: Mega Hertz
ml	: Millilitre
^{o}C	: Degrees Celsius
Wt%	: Weight percent
δ	: Per mil deviation

CHAPTER 1

INTRODUCTION

1.1 Background

Kaolin is a soft, white plastic clay made up fundamentally of kaolinite, a hydrated aluminum silicate of formula: $Al_2 Si_2 O_5 (OH)_4$ (Murray, 2002). It is a dioctahedral 1:1 phyllosilicate formed by superposition of silicon tetrahedral and aluminum octahedral sheets (Frost *et al*., 2010). Depending on their modes of formation, kaolin deposits could be primary (hydrothermal, residual or mixed hydrothermal and residual deposits) or secondary (erosion and transportation of clay particles and their deposition in lacustrine, paludal, deltaic and lagoonal environments) (Bloodworth *et al*., 1993; Ekosse, 2005). Hydrothermal kaolins result from the hydrothermal alteration of alumina-silicate rocks (Bloodworth *et al*., 1993). These types of kaolins are closely related to the tectonic framework of a deposit and the alteration of parent rocks (Sayin, 2007). Residual kaolins usually form in a high rainfall, subtropical or tropical climate. This is because high temperatures and rainfall increase the rate of weathering of the primary minerals to clay minerals (Harvey and Murray, 1997 and Obaje *et al*., 2013). Secondary kaolins are those that have been transported, sorted and deposited in a sedimentary basin (Harvey and Murray, 1997). The type and composition of secondary kaolins usually reflect the degree of hydrolysis that prevailed within the basin (Fagel and Boës, 2007).

The formation of kaolins correlates with climatic factors, such as temperature and precipitation (Sheldon and Tabor, 2009). Kaolins also have small particle sizes and large surface area, which cause them to be affected by weathering, the relief, and climate (Moriarty, 1977; Heckroodt, 1991; Fürsich *et al*., 2005 and Fagel and Boës, 2007). In addition, weathering is controlled by climate change, which also affects soil formation and transport of terrigenous material into the sea (Das *et al*., 2013). Hence, the mineralogical, geochemical, and isotopic compositions of kaolins are potentially powerful proxies of paleoenvironmental conditions (Ortega *et al*., 1998 and Tabor *et al*., 2002).

Kaolin occurrences are reported on all continents of the world except Antarctica; with one of the best known and highly utilised deposits being the sedimentary kaolins from the Amazon region of Brazil, South America (Murray, 1999, Costa *et al*., 2009). This Brazilian Amazonian kaolin contains 10% of the world reserves of kaolins (Souza *et al*., 2007). Georgia (USA) also hosts high grade sedimentary kaolin deposits (Lang *et al*., 1965); whereas, the world-known primary kaolins are the Cornwall kaolins which occur in south-western England, Europe

(Murray, 1999). The Pugu kaolin deposit in Tanzania, Africa (Bloodworth *et al*., 1989), is globally recognised for providing the standard kaolinite (29-1488) in X-ray diffraction (Mineral Diffraction, 2001). In South Africa, Grahamstown hosts the largest kaolin deposit in the country, with reserves in excess of 50 million tons (Madi *et al*., 2013). The village Kauling, from which the word “kaolin” was derived, is a known kaolin locality in China (Chen *et al*., 1997).

In elucidating on kaolin genesis, an investigation of its environment of formation and age aids in interpreting environments of formation. Geochronology is the study of the ages of rocks and minerals (Kearey, 2001). It gives the absolute ages of rocks and minerals. In understanding the progression of continents, the evolution of continents through the geologic time is very significant. Therefore, determining the absolute ages of rocks and minerals that constitute these continental masses is fundamental in understanding their evolution.

The present research is part of the research project titled: “*Cretaceous-Tertiary clay deposits and argillaceous sediments*”, within the broader Clays and Clay Minerals in Africa programme. The research project covers the southern and south-western part of Africa (South Africa, Botswana, Namibia, Angola, Democratic Republic of Congo, Gabon, Cameroon and Nigeria) and eastern South America (Brazil and Argentina). This thesis, however, focuses on dating the Cretaceous-Tertiary kaolins of Cameroon, reconstructing the environments in which they were deposited, and promoting their exploitation, as paleoclimatic and paleoenvironmental reconstructions of kaolin deposits, and thus, provides useful guidelines for the kaolin exploration geologist (Harvey and Murray, 1997) to investigate Cretaceous and Tertiary argillaceous sediments. Outputs of this research also contribute to the body of knowledge.

1.2 Statement of the problem

The Cretaceous and Tertiary Periods were marked by a series of catastrophes and tectonic events, which affected both the geology and the climate of several countries in the world. These events included one of the five mass extinctions in the Earth’s history, which affected many groups of organisms; the Deccan Trap volcanism (Keller *et al*., 2009), the Chicxulub impact event (Sutherland, 1996 and Martinez-Ruiz *et al*., 2006) and the breakup of Gondwana. Gondwana was a large landmass composed of most of India, Australia, Africa, South America and Antarctica. The geology of each of the countries and correlation studies between different countries of the aforementioned continents have to be studied to better understand the events of the super continental break-up.

Several studies have been undertaken in Cameroon regarding the breakup of Gondwana, amongst which are studies by Congleton *et al*. (1992); Tchameni *et al*. (2000); Toteu *et al*. (2001; 2004); Penaye (2004); Lerouge *et al*. (2006); and Oliveira *et al*. (2006). However, studies involving the correlation between South America and Cameroon, using kaolin deposits in sedimentary basins have not been carried out, despite the occurrence of at least 27 kaolin deposits in Cameroon (Ekosse, 2010).

The Douala Sub-Basin is part of the West-Central Coastal Province delineated by Brownfield and Charpentier (2006). This province also includes the Kribi-Campo, Rio Muni, Gabon, Congo, Kwanza, Benguela, and Namib Basins, which together form the Aptian salt basins of equatorial west Africa (Brownfield and Charpentier, 2006). These basins formed during the breakup of Gondwana. Therefore, reconstructing the paleoenvironments in which Cretaceous-Tertiary kaolins of the Douala Sub-Basin in Cameroon have been deposited will greatly contribute to the research on the Gondwana continent.

Most kaolin deposits around the world have not been dated. Their ages are usually inferred from the ages of the formations in which they occur (Siddiqui and Ahmed, 2008; Baioumy, 2014). This is the case with kaolin deposits in Cameroon (Diko and Ekosse, 2013; Logmo *et al*., 2013; Ngon Ngon *et al*., 2014). Successful dating of kaolin deposits has been a challenge due to their origin and small particle sizes (Gilg and Frei, 1997; Gilg, 2003). Using a different method to date Cretaceous-Tertiary kaolins could yield useful results.

Cameroon is a low-middle income country with a population of 22.77 million people (World Bank, 2016a). It ranks 172 out of 189 on the *Doing Business 2016 Report* (World Bank, 2016b). Average poverty stands at about 40%; which is high compared to other countries in the region with similar economic characteristics (World Bank, 2015). Boosting Cameroon's economy will, therefore, require new investments; and kaolin exploration and exploitation could be one of these. Kaolin deposits in Cameroon are easily accessible, and can be processed and beneficiated for industrial uses (Ekosse, 2010). Therefore, determining the physical, chemical and mineralogical properties of Cameroon's kaolin, will provide baseline knowledge for their exploitation, thereby contributing to Cameroon's economic development.

1.3 Motivation

This research is part of a larger project (NRF CPRR UID 91559): "*Cretaceous-Tertiary clay deposits and argillaceous sediments*" that involves parts of South America (Brazil and Argentina) and parts of Southwestern Africa (South Africa, Botswana, Namibia, Angola,

Democratic Republic of Congo, Gabon, Cameroon and Nigeria). It will contribute to knowledge on clays and clay minerals in Africa. The fit of these two continents (South America and Africa) proposed by Bullard *et al*. (1965) has been widely recognised as one of the most precise continental reconstructions. Several studies and correlations have been made in these two parts of the world to confirm this fit. These studies were based on metamorphic and igneous rocks (Kusky and Polat, 1999; Carvalho *et al*., 2000; Pedrosa-Soares *et al*., 2001; Chaves and Neves, 2005; King, 2005; Rainaud *et al*., 2005; Lerouge *et al*., 2006; Oliveira *et al*., 2006; Babinski *et al*., 2012; Ernst *et al*., 2013), geodynamics and structural geology (Bullard *et al*., 1965; Owen, 1976; Martin *et al*., 1981; Murphy and Nance, 1991; Brito Neves *et al*., 1999; Matos, 2000; Neves, 2003; Tohver *et al*., 2006; Aslanian *et al*., 2009) and sedimentary rocks (Pletsch *et al*., 2001; Brito Neves, 2002; Dickson *et al*., 2005; Guadagnin *et al*., 2013). None of these studies focused on continental argillaceous sediments. However, Petschnick *et al*. (1996) studied clay minerals' distribution in surface sediments of the South Atlantic. They presented their sources, transport, and relation to oceanography, though their study was limited to marine argillaceous sediments.

Unlike most of these previous studies, this research project focuses on clay deposits and argillaceous sediments. The present research particularly focuses on Cameroon kaolins, as kaolins could be important paleoenvironmental indicators. Without information on the distribution, modes of formation and ages of kaolins in eastern South America and southern West Africa, many assumptions could remain debatable.

Environmental changes, such as climatic changes, occurring at present and predicted for the future, have increased interest on paleoclimatic and paleoenvironmental studies (Becker *et al*., 2006). Hence, records of paleoenvironments and paleoclimates (isotopic data and rare earth elements' ratios) may elucidate the causes of climate change (Stern *et al*., 1997). Therefore, a better understanding of the environment in which we live and predicting future environmental changes is a motivation behind this research.

Kaolin exploitation is a financially sustainable profit-making mining industry that continues to contribute positively to national economies of the world (Ekosse, 2010). The physical and chemical properties of kaolins are important in establishing their proper utilisation in various industrial applications; and help to identify impurities, such as Fe_2O_3, that gives the red colouration to kaolin and significantly decreases its industrial worth (Prasad *et al*., 1991; Murray and Kogel, 2005; Siddiqui and Ahmed, 2008). With increasing new industrial applications of kaolin, any promising deposit is worth exploiting, particularly in developing countries (Nyakairu *et al*., 2001 and Njoya *et al*., 2006). However, Ekosse (2010)

recommended that any exploration of kaolins in Africa should focus on Cretaceous-Tertiary kaolins.

This research equally focused on thorough characterisation of the kaolins using mineralogy, geochemistry, stable isotopes, geochronology and diagnostic evaluation of kaolins for industrial uses. It, therefore, added new knowledge in understanding Cretaceous-Tertiary periods' events. It also contributes to poverty alleviation by determining the industrial properties of kaolins in Cameroon, and beneficiating the kaolins for industrial uses.

1.4 Hypotheses

A. The studied Cretaceous-Tertiary kaolin deposits in Cameroon have similar mineralogical and geochemical characteristics.
B. The studied Cretaceous-Tertiary kaolin deposits formed in similar paleoenvironmental conditions.
C. Kaolinisation in Cretaceous-Tertiary Formations of the Douala Sub-Basin occurred during Cretaceous and Tertiary Periods.
D. The physico-chemical properties of these kaolins can assist in determining their potential industrial applications.

1.5 Research questions

A. What are the mineralogical and geochemical characteristics of Cretaceous-Tertiary kaolins in Cameroon?
B. In what paleoenvironmental conditions did they form?
C. When were the kaolins deposited?
D. What are potential industrial applications of the kaolins based on their physical and physico-chemical properties?

1.6 Objectives

1.6.1 Main objective

The main objective of the study was to reconstruct the environments and time span in which Cretaceous-Tertiary kaolins in the Douala Sub-Basin in Cameroon were formed, and characterise them for possible industrial applications.

1.6.2 Specific objectives

The specific objectives of the study were to:

A. Investigate the nature and occurrence of selected kaolins of Cretaceous-Tertiary ages in the Douala Sub-Basin, by carrying out a thorough mineralogical and geochemical characterisation of kaolins of selected kaolin deposits.
B. Determine the minerals' geneses and reconstruct the prevailing paleoenvironmental conditions in which they formed, using trace elements and stable isotope ratios of kaolinite in the kaolin samples.
C. Carry out radiogenic dating of zircons in the kaolins to constrain the time of kaolinisation.
D. Carry out diagnostic evaluation on selected kaolin samples, by evaluating their particle size distribution and inferring their possible industrial applications.

1.7 Study area

The different countries investigated in the mega research project on "Cretaceous-Tertiary clay deposits and argillaceous sediments" are shown in Figure 1.1. This component of the research took place in Cameroon, and considered six Cretaceous-Tertiary kaolin deposits, namely; Bomkoul, Dibamba, Ediki, Logbaba, Missole and Yatchika kaolins, as shown Figure 1.2.

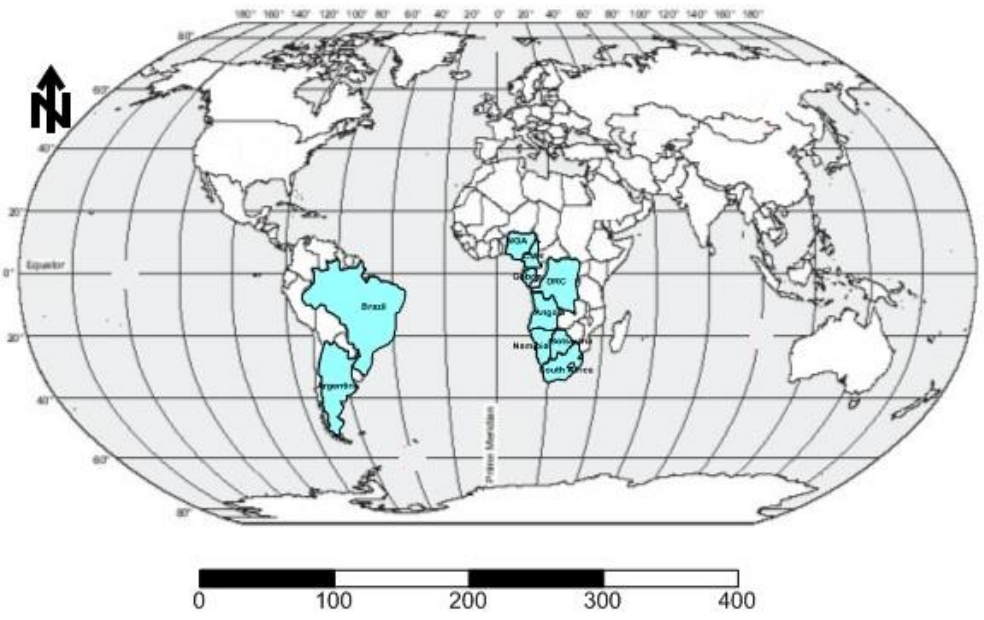

Figure 1.1: Study area of the mega research project (www.google.co.za)

Countries related to the study in which Cretaceous-Tertiary kaolins are located

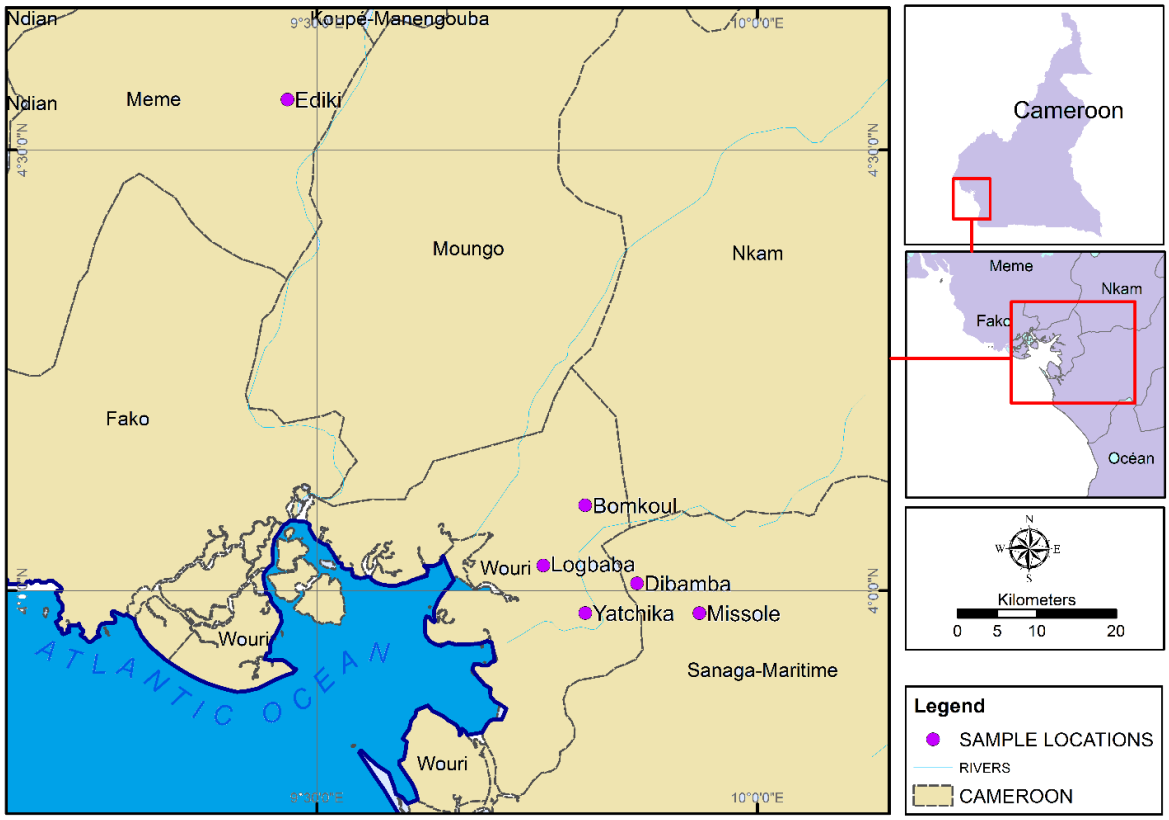

Figure 1.2: Location map of the studied Cretaceous-Tertiary deposits in Cameroon (SNH/UD, 2005)

1.7.1 Geology of the study area

The studied kaolin occurrences are found in the Douala Sub-Basin, which stretches on the South coast of Cameroon, covering a total surface area of 19, 000 km^2 (Mbesse *et al*., 2012). It is subdivided into seven Formations (Logmo *et al*., 2013). The studied kaolins belong to four Cretaceous-Tertiary Formations: the Early Cretaceous Mundeck Formation made up of sandstones; the Late Cretaceous Logbaba Formation, made up of sandstones and clays with intercalations of sands and rare occurrence of limestones; the Paleocene to Middle Eocene Nkapa Formation composed of marls, shales and calcareous sandstones; and the Upper Eocene to Oligocene Souellaba Formation, composed of sandstones and marls, shales, clayey sands, sands and gravels (Effoudou-Priso *et al*., 2014). Figure 1.3 shows the geology of the Douala Sub-Basin.

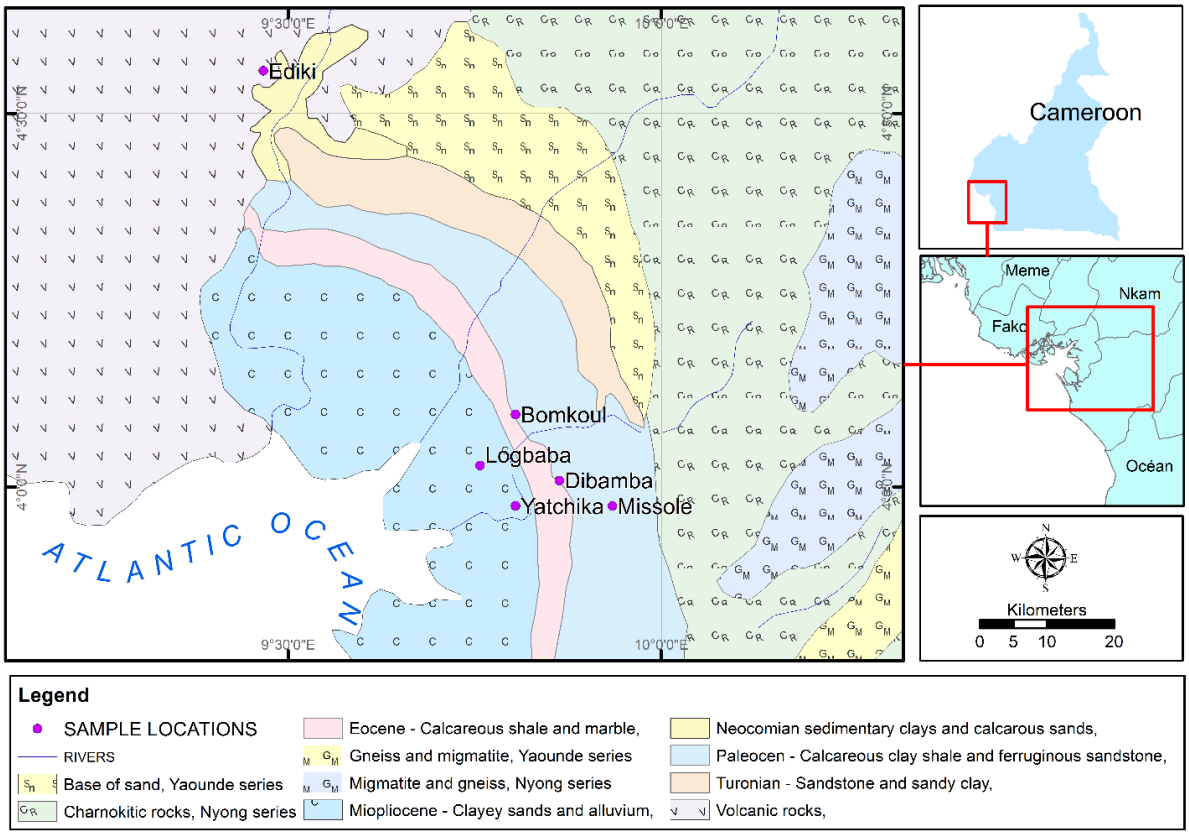

Figure 1.3: Geologic map of the Douala Sub-Basin (SNH/UD, 2005)

The geotectonic history of the Douala Sub-Basin described by Kenfack *et al*. (2012a, b) is as follows (Figure 1.4):

- Pre-rift phase: Jurassic continental sediments were deposited in an Afro-Brazilian depression that extended over this Sub-Basin;
- Rifting phase (Jurassic-Barremian): The stratigraphic sequence appeared to be controlled by listric faulting and associated roll over anticlines;
- Syn-rift phase: Characterised by an intensive erosion activity of the highlands and deposition in the previously formed graben;
- Rift-drift transition phase (Mid-Late Aptian): Marked by salt deposition and the transform direction resulting in a series of cross-faults which have segmented the rift structure; and
- Post-rift phase (Albian-Present): Sedimentation was dominated by marginal clastic sedimentation with sporadic build ups between the Albian and Paleocene.

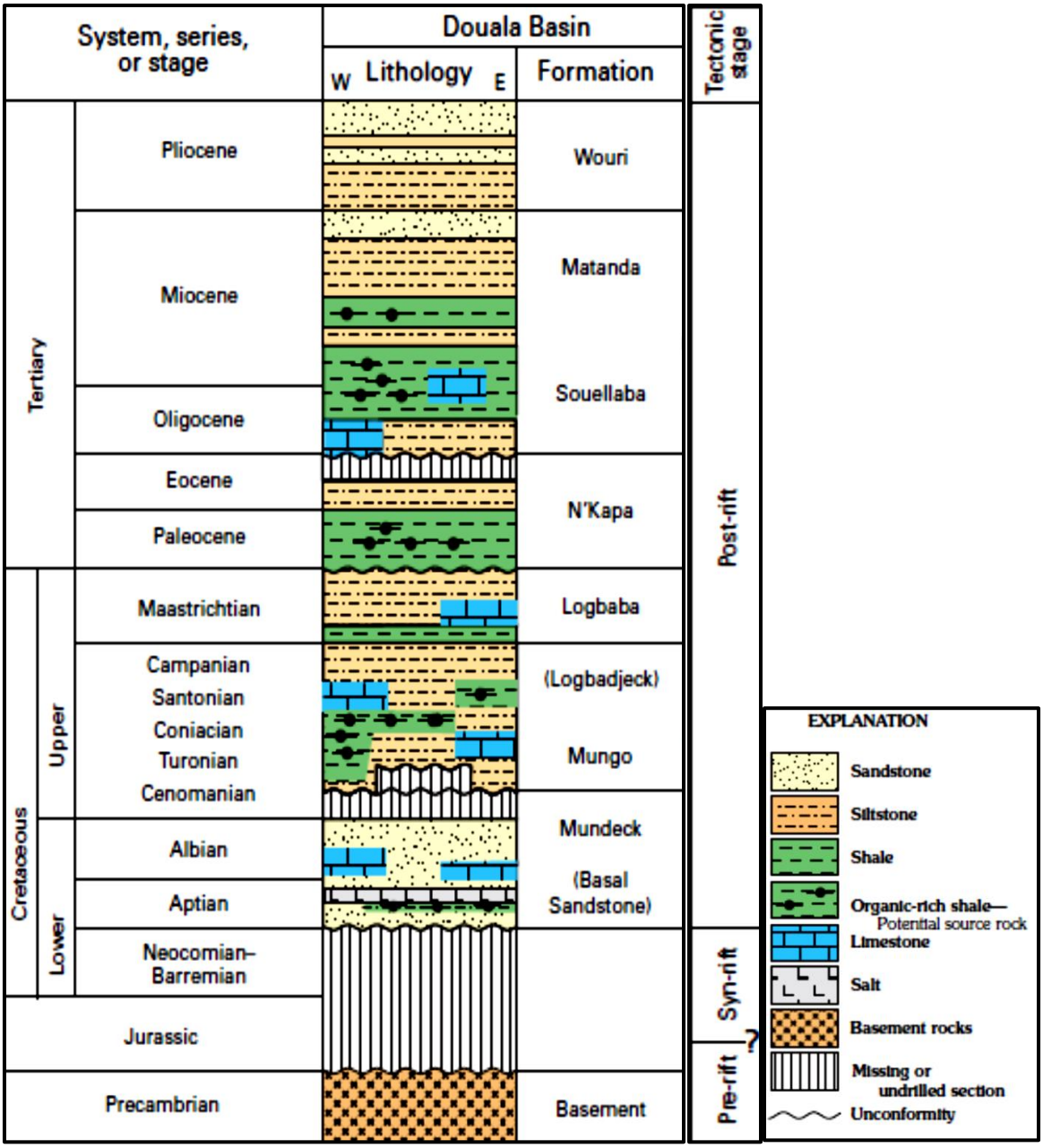

Figure 1.4: Generalised lithostratigraphy and geotectonic history of the Douala Sub-Basin (Brownfield and Charpentier, 2006)

1.7.2 Climate

The study areas have the Guinean type of the equatorial climate; resulting from the combined effect of convergence of the tropical oceanic low pressure zone and the inter-tropical front within the continent. There are two main seasons; namely a long rainy season which lasts from April to September, and a short dry season, which generally stretches from October to March. Between these two seasons are transitional seasons: the wet-dry season (September to November) and the dry-wet season (March to May). The climate is also characterised by Monsoon winds of the Guinea type, predominantly southwesterly (Folack and Gapche, 2000).

Annual rainfall locally reaches 5-10 m/year (CDC, 2010). Douala monthly temperatures and precipitation over the past years are shown in Figures 1.5 and 1.6, respectively.

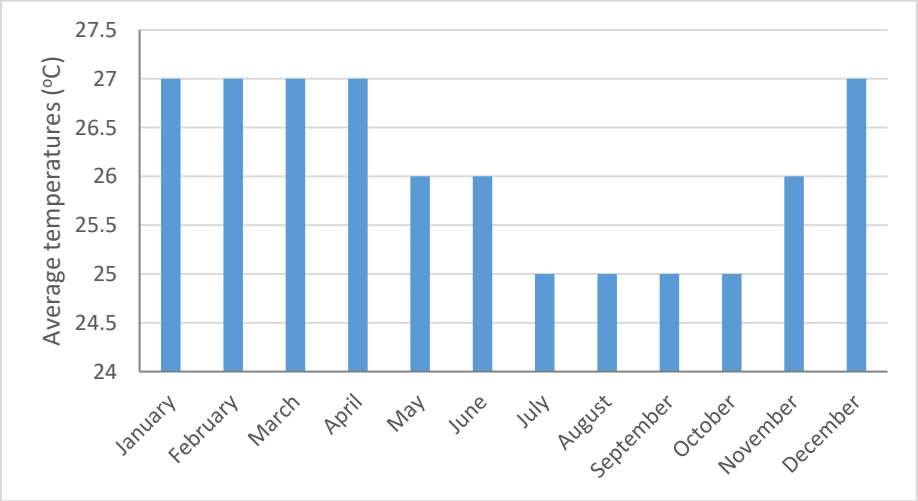

Figure 1.5: Average temperature in Douala over the past 16 years (1999-2015) (www.weatherbase.com)

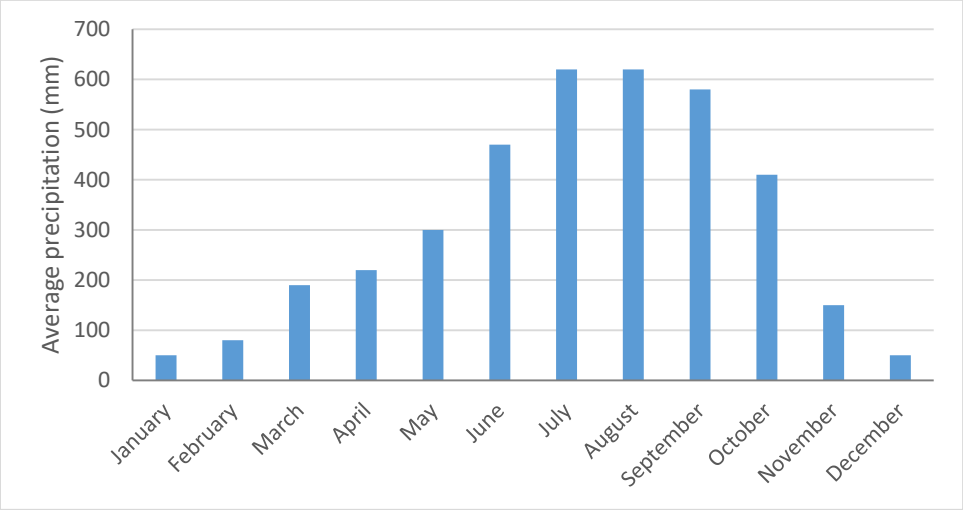

Figure 1.6: Average precipitation in Douala over the past 100 years (1915-2015) (www.weatherbase.com)

There are two broad climatic zones in Cameroon: the equatorial climatic zone and the tropical climatic zone. The two climatic zones of Cameroon have been described by Pamo (2008) and summarised in Figure 1.7.

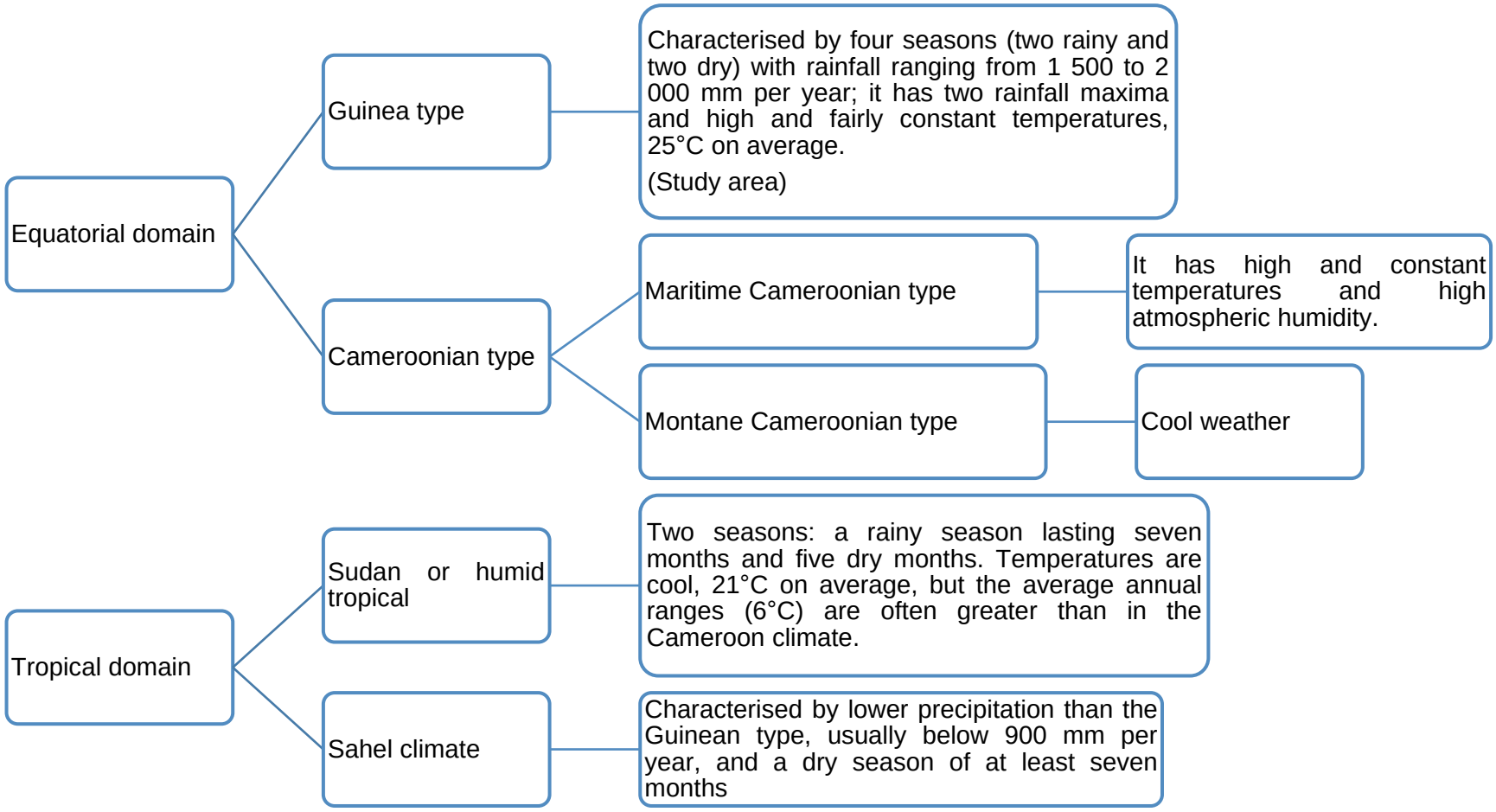

Figure 1.7: Climatic zones in Cameroon (Pamo, 2008)

CHAPTER 2

LITERATURE REVIEW

2.1 Preamble

This chapter presents a review of available literature related to this research. It highlights on the Periods of the Geologic Time Scale, the Precambrian to Tertiary geology of Cameroon, kaolin genesis, Cretaceous-Tertiary paleoclimates, geochronology, the use of kaolins as paleoenvironmental and paleoclimatic proxies, occurrences of kaolins in Cameroon, paleoenvironmental reconstruction in the Douala Sub-Basin, and kaolin applications and beneficiation methods.

2.2 Geologic Time Scale

The Geologic Time Scale (GTS) is an “absolute time scale made up of standard stratigraphic divisions based on rock sequences” (Kearey, 2001). The old and new versions of the GTS are shown in Figures 2.1 and 2.2.

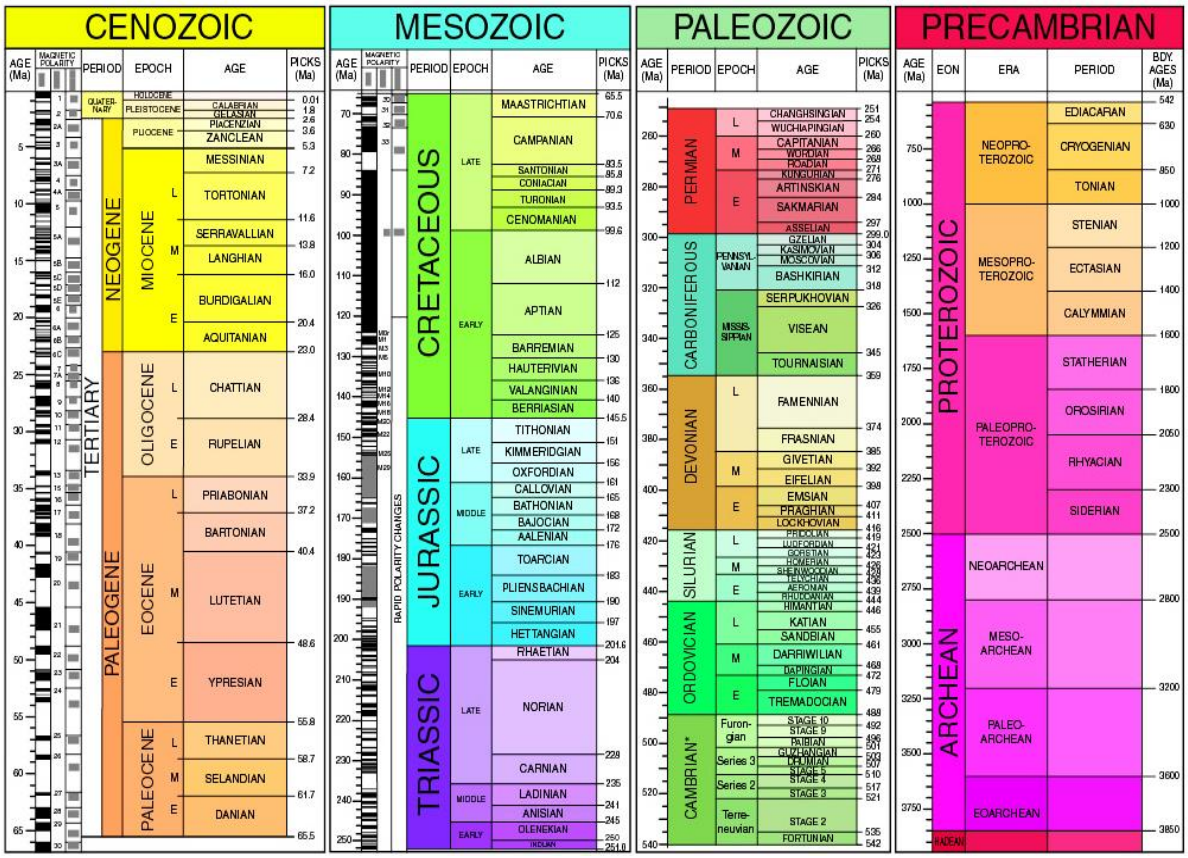

Figure 2.1: Geologic Time Scale (Walker *et al*., 2013)

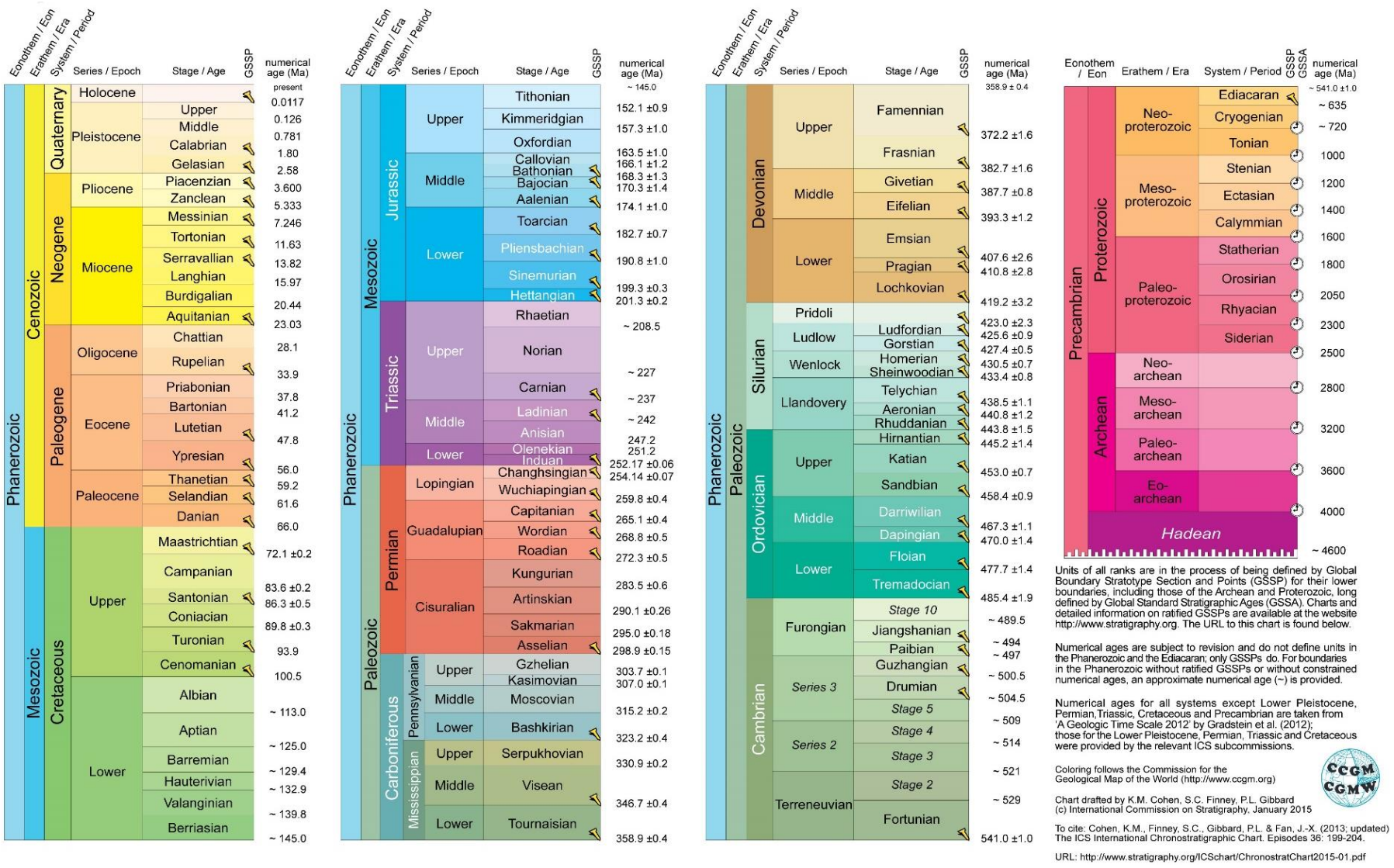

Figure 2.2: New International Chronostratigraphic Chart (Cohen *et al.*, 2013)

The GTS is subdivided into two Eons (the Precambrian and Phanerozoic Eons), and ten Eras (the Hadean, Archean, Paleoproterozoic, Mesoproterozoic, Neoproterozoic, Paleozoic, Mesozoic and Cenozoic eras). The Cretaceous (145-66 Ma) is a Period of the Mesozoic whereas the Tertiary (66-23.03 Ma) is a Period of the Cenozoic. Each Period is divided into Epochs and each Epoch is divided into Ages. In the new Geologic Time Scale, the Tertiary is not mentioned; the Paleogene is the Period that follows the Cretaceous (Figure 2.2).

2.3 Precambrian to Tertiary Geology of Cameroon

The geology of Cameroon is highly dominated by Precambrian basement rocks. This section provides a synopsis of the geologic history of Cameroon. A geologic map of Cameroon is shown in Figure 2.3.

2.3.1 The Precambrian Geology of Cameroon

The oldest geologic unit in Cameroon is the Ntem Complex. It constitutes the Archean cratonic basement of southern Cameroon and the north-western part of the Congo Craton in Central Africa (Tchameni *et al*., 2000). The Ntem complex comprises Palaeoarchaean to Mesoarchaean and Late Archaean charnockites, Mesoarchaean greenstone formations, Late Archaean tonalite–trondhjemite–granodiorite (TTG) basement, dolerite dykes and high-K granites (Shang *et al*., 2010). The Ntem Complex is mainly made up of dome and basin tectonics related to diapiric movements in the mid to lower crust (Tchameni *et al*., 2001). Two major episodes of deformation affected the Ntem complex (Shang *et al*., 2004): The first episode is characterised by vertical foliation, stretching and vertical lineation and isoclinal folds; and the second episode is marked by the development of sinistral shear planes trending north–south to N45^{o} E, and partial melting of charnockitic and tonalitic members of the TTG suite and the greenstone belt country rocks.

The Ntem Complex is bordered on the west by the Palaeoproterozoic Nyong series metamorphic complex which formed as a result of the Eburnean-Trans-Amazonian orogeny, during the collision of the Congo and São Francisco cratons (Toteu *et al*., 2001). The Nyong series is a high-grade gneiss unit which includes the Kama, the Akongo and the Ngovayang Groups (Owona *et al*., 2013). These groups are dominated by biotite–hornblende gneisses, which locally appear as grey gneisses of TTG composition, orthopyroxene– garnet gneisses (charnockites), garnet–amphibole–pyroxenites, and banded iron formations (BIF) (Lerouge *et al*., 2006). It is also made up of magmatic rocks which include augen metadiorites, granodiorites, and syenites (Lerouge *et al*., 2006).

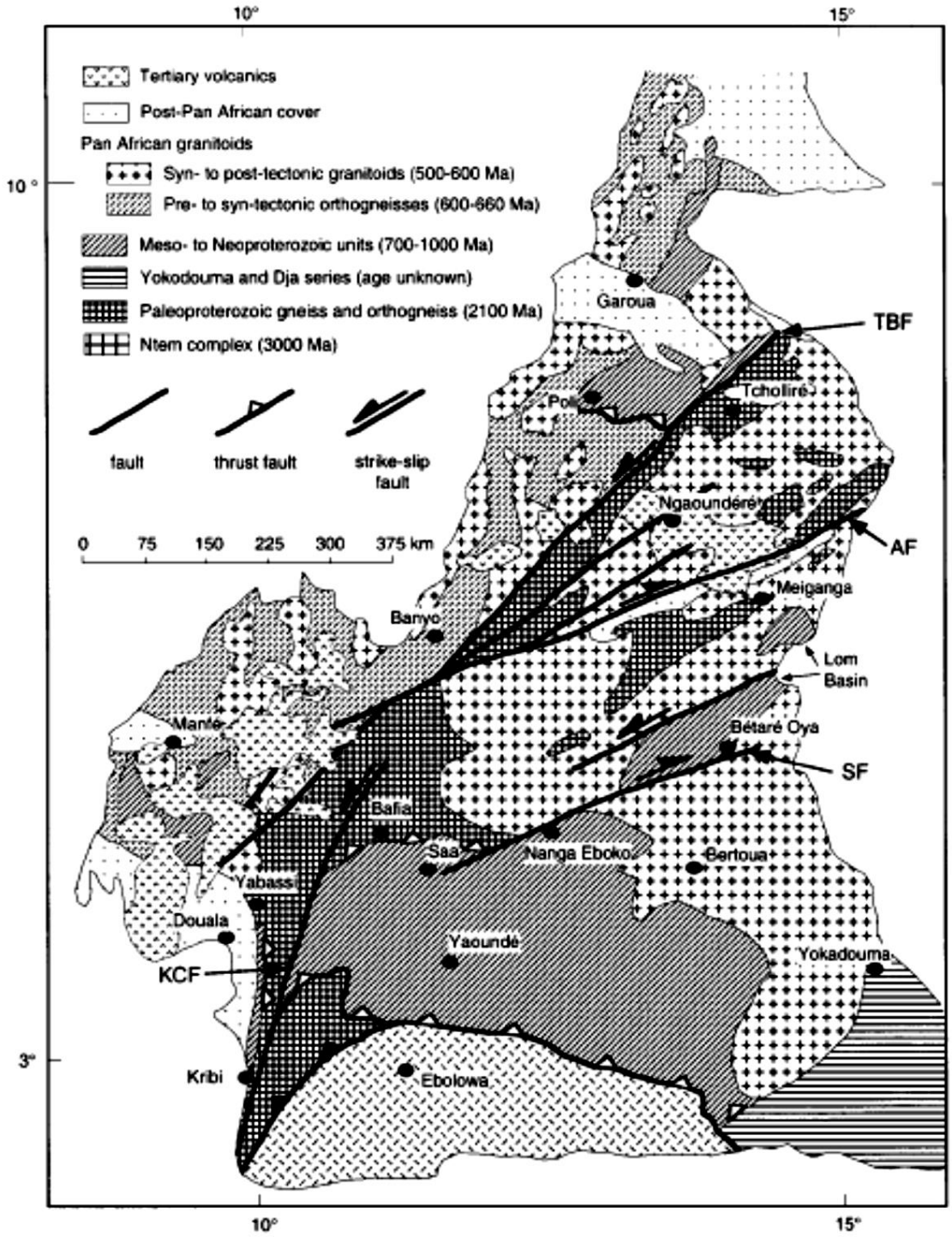

Figure 2.3: The geologic map of Cameroon. *AF: Adamaoua fault, KCF: Kribi-Campo fault, SF: Sanaga fault and TBF: Tcholliré-Banyo fault* (Toteu *et al*., 2001)

The Proterozoic is also represented in Cameroon by the Yaounde Group (Late Neoproterozoic), which forms the southern limit of the Central African Fold Belt. It comprises low- to high-grade garnet-bearing metapelites, and orthogneisses metamorphosed under a medium to high-pressure metamorphism reaching the granulite facies (Stendal *et al*., 2006). It is also part of the Yaounde Belt (the southern limit of the Central African Fold Belt) (Oliviera

et al., 2006). Rock types in the Yaoundé series include chlorite-rich schists, garnet- and/or kyanite-bearing micaschists and garnet- and kyanite-bearing high-grade gneisses (Shang *et al*., 2010).

Pan-African granitoids also occur in Cameroon. They are usually found along the Cameroon Orogenic Belt, and they intrude the older Paleoproterozoic basement gneisses, migmatites and granulites, and the Meso- to Neoproterozoic deformed and metamorphosed volcano-sedimentary sequences (Djouka-Fonkwé *et al*., 2008). The Tcholliré-Banyo fault, the central Cameroon shear zone, the southwestern Cameroon shear zone, and the Sanaga fault are the major shearing and late-tectonic that occur in the Cameroon orogenic belt (Djouka-Fonkwé *et al*., 2008).

2.3.2 The Paleozoic-Triassic Geology of Cameroon

The Paleozoic to the Triassic rocks are either non-existent in Cameroon or they have not been reported. This could probably be periods of non-deposition.

2.3.3 The Cretaceous-Tertiary Geology of Cameroon

Cretaceous and Tertiary Periods in Cameroon are mostly represented by sedimentary basins (the Mamfe and the Douala/Kribi-Campo Basins) and the Cameroon Volcanic Line (CVL). The Mamfe Basin is a rifting basin formed during the separation of the South American and African plates (Nguimbous-Kouoh *et al*., 2012). It is a NW-SE splay segment of the Benue trough in Cameroon (Eseme *et al*., 2006). The Mamfe Basin is made up of Cretaceous sedimentary rocks (the Cross River sandstone series, the clayey sandstone series, the upper conglomeratic sandstone series, the Manyu sandy clay series, the lower conglomeratic sandstone series), which are underlain by Precambriam rocks consisting of gneisses, granites and schist (Eseme *et al*., 2002).

The Douala/Kribi-Campo extends from the edge of the Niger Delta in Cameroon to the Walvis Ridge near the Angola–Namibia border (Ntamack-Nida *et al*., 2008). The stratigraphy of the Douala Sub-Basin is made up of the Mundeck, Logbadjeck, Logbaba, N'kapa, Souellaba, Matanda and Wouri Formations (Ngon Ngon *et al*., 2012a). The sediments of the Kribi-Campo Sub-Basin form a series of asymmetrical horst-and-graben basins; and they include continental conglomerates and arkosic sandstones interlayered with fluviatile-lacustrine black micaceous shales, and some intercalation of limestones and marls (Ntamack-Nida *et al*., 2008).

Smaller Neocomian-Early Aptian sedimentary basins (130-118 Ma) have also been reported in northern Cameroon (Loule and Pospisil, 2013). They contain interstratified alkali basalt flows associated with dolerite dykes and sills, as well as post-sedimentary intrusive igneous bodies which cut through the sedimentary sequence also occur (Loule and Pospisil, 2013).

The main Tertiary feature in Cameroon is the Cameroon Volcanic Line (CVL), which is an alignment (1600 km long) of Tertiary continental and oceanic volcanic massifs trending N30^{o} from Pagulu Island to Lake Chad (Kamgang *et al*., 2013). The oceanic horsts are represented by the four Islands of the Gulf of Guinea (Pagalu, Bioko, Sao Tome and Principe) and the continental ones are of high relief (Mounts Cameroon, Rumpi, Manenguba, Bamboutos, Mbam, and Oku) (Ngako and Njonfang, 2011). The CVL is made up of granites or syenites, to which subordinate intermediate, basic and ultrabasic rocks are sometimes associated (Ngako *et al*., 2006). Lavas from Mount Cameroon are generally mafic and they comprise basanites, alkali basalts, hawaiites and mugearites; whereas, the silicic lavas comprise benmoreites, trachytes, phonolites and/or rhyolites (Ngako *et al*., 2006).

2.4 Kaolin genesis

2.4.1 Kaolin mineralogy

Four minerals constitute the kaolin group, namely; kaolinite ($Al_2Si_2O_5$ $(OH)_4$), halloysite ($Al_4Si_4O_{10}(OH)_8.8H_2O$), nacrite ($Al_2Si_2O_5(OH)_4$) and dickite ($Al_2Si_2O_3(OH)_4$) (Kearey, 2001; Obaje *et al*., 2013). Halloysite is a fairly common mineral that develops in tropical and moderate-temperature soils and weathering crusts, particularly on basalts; and through a range of hydrothermal alterations that affect particularly volcaniclastic formations (Melka *et al*., 2000). Nacrite is usually formed through hydrothermal processes or found in high temperature environments (Chen *et al*., 2001). Dickite is quite rare, and it isusually associated with hydrothermal alteration zones and veins of ore minerals, whereas kaolinite can form over a wide range of temperatures, as a result of weathering, diagenesis, or hydrothermal deposition and alteration (Schroeder and Hayes, 1968).

2.4.2 Kaolinite chemistry

Kaolinite is a two-layer clay (phyllosilicate mineral) which has a sheet of silica tetrahedral combined through octagonal hydroxyls which are shared with an alumina octahedral sheet (Murray, 1999). The kaolinite structure is shown in Figure 2.4.

The alumina octahedral sheet and the silica tetrahedral sheet share a common plane of oxygen atoms and repeating layers of the mineral are hydrogen bonded together (Miranda-Trevino and Coles, 2003). The functional groups are principally made up of the outer and the inner hydroxyl groups (Frost, 1998). The theoretical formula of kaolin is 46.54% SiO_2, 39.50% Al_2O_3 and 13.96% H_2O (Deer *et al*., 1992).

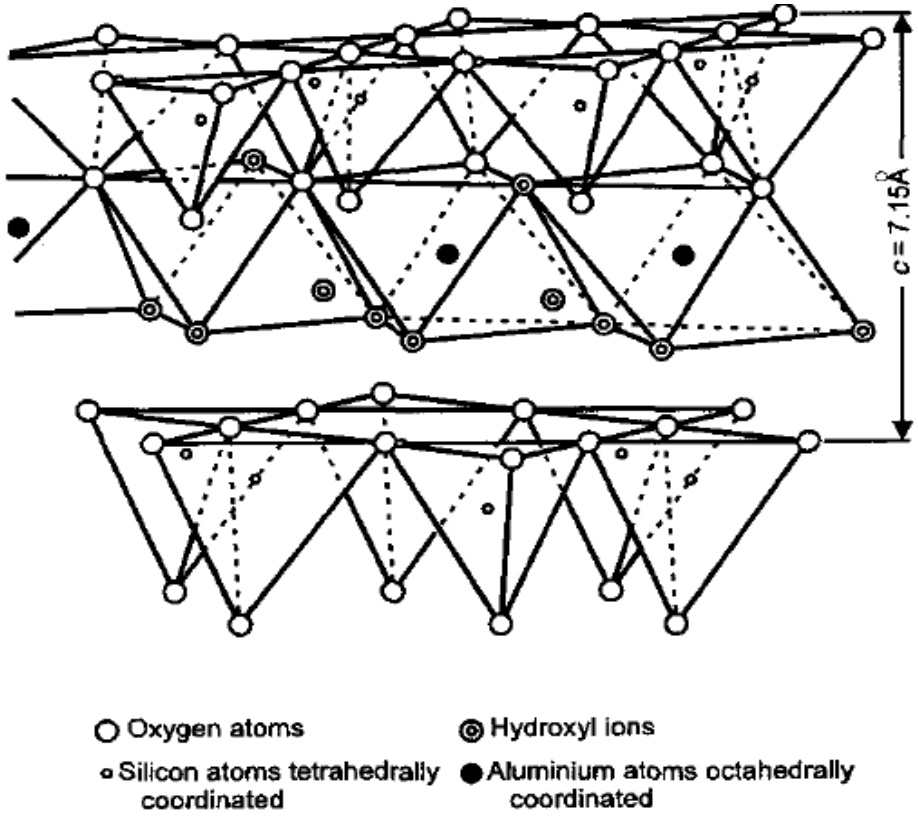

Figure 2.4: Kaolinite structure (Murray, 1999)

2.4.3 Environments of formation

Kaolin genesis could be either primary or secondary. Primary kaolins form *in situ* and they could either be hypogene or supergene. Hypogene kaolins form from the weathering of alumino-silicate rocks, whereas, hypogene kaolins result from hydrothermal activities (Gilg *et al*., 1999). Sometimes, primary kaolins could be formed as a combination of both supergene and hypogene processes (Gilg *et al*., 1999). Unlike primary kaolins, secondary (sedimentary) kaolins are those that have been formed elsewhere, then they were transported and deposited (Bloodworth *et al*., 1993). According to Dill *et al*. (1997), kaolin minerals are extensively developed in a wide range of lithologies and form in various depositional environments.

2.4.3.1 Primary kaolins

The formation of residual kaolins is influenced by climate, topography, permeability of the parent rock and temperature of alteration (Harvey and Murray, 1997). Kaolinite is the main mineral in soils of humid climates, where abundant vegetation makes the pH of soils to be acidic (Obaje *et al*., 2013). An example of residual kaolin is the Lastarria kaolin in south-central Chile. These kaolins formed on two subvolcanic quartz porphyry stocks which cut across the low-grade metamorphic basement of the Chilean Andes (Gilg *et al*., 1999).

For hypogene kaolins, there must be sufficient fractures in the host rock to allow the circulation of thermal groundwater, which will lead to hydrothermal alteration of the host rock (Bloodworth *et al*., 1993). For example, high-heat-flow granites may provide optimum thermal conditions required to drive groundwater convection cells (Bloodworth *et al*., 1993). Kaolinite may also form in humid soils formed from volcanic ash and pumice (Yuan *et al*., 2014). The Cornwall kaolins in southwestern England are an example of hydrothermal kaolins, where weathering occurred after a long hydrothermal alteration (Harvey and Murray, 1997).

2.4.3.2 Secondary kaolins

Secondary kaolins are those that are transported and deposited in a sedimentary basin (Murray, 1999). They often contain more than 60% of kaolinite (Bloodworth *et al*., 1993). According to Baouimy (2014a), the geochemistry of sedimentary kaolins is controlled by three main factors: (1) the detrital minerals (quartz, feldspars, zircon, rutile, and leucoxene) that reflect the source area composition; (2) the neo-minerals (kaolinite and non-clay minerals such as anatase) resulting from weathering; and (3) post-depositional alterations (diagenesis and weathering).

The Pugu kaolins (Tanzania) are secondary kaolins whose source rocks are believed to be the Precambrian metamorphic rocks of the Uluguru Mountains (Schwaighofer and Muller, 1987). These kaolins then resulted from a rapid erosion and transportation of sediments from the Pugu Hill Formation, which occurred during the Upper Cretaceous (Robertson *et al*., 1954).

2.5 Cretaceous-Tertiary paleoclimates

Extensive distribution of biota and sedimentary indicators only present in lower latitudes show that the Cretaceous climate was warm, non-varying and ice-free (Barron, 1983). According to

Valdes (2000) and Sijp *et al*. (2014), the Earth's surface was significantly hotter than today during the Cretaceous and the Tertiary, with the Cretaceous having one of the warmest climate extremes of the Phanerozoic (Barron, 1993). A summary of Cretaceous-Tertiary climates is given in Table 2.1.

Table 2.1: Summary of the Cretaceous-Tertiary climates (Zachos *et al*., 1993; Keller, 2008; Sijp *et al*., 2014)

PERIODS	EPOCHS	DESCRIPTION OF THE CLIMATE
TERTIARY	Pliocene	
	Miocene	
	Oligocene	Glacial maximum
	Eocene	No or only mild cooling of tropical waters but substantial cooling of high latitude waters (Sijp *et al*., 2014)
	PALEOCENE-EOCENE THERMAL MAXIMUM (PETM)	
	Paleocene	
K-T BOUNDARY		GRADUAL COOLING
CRETACEOUS	Maastrichtian	Gradual cooling through most of the Maastrichtian; followed by an abrupt greenhouse warming 200-400 Ky before the end of the Cretaceous
	Campanian	Rapid cooling of surface water
	Santonian	Warming and Fluctuating climate conditions
	Coniacian	Warm but reduced temperatures (28^{o}C)
	Turonian	
	Cenomanian	Warming reaching maximum marine surface temperatures (28^{o}C) in high southern latitudes
	Albian	Significant cooling
	Aptian	Increased warming and greenhouse conditions associated with the Ontong Java I volcanic province
	Barremian	Warming associated with the Parana-Etendeka volcanic province
	Hauterivian	Coolest temperatures
	Valanginian	Cooling
	Berriasian	

The breakup of Gondwana greatly influenced the climate of the southern hemisphere (Maley, 1996), moderating seasonal thermal variations (Fluteau *et al*., 2007). The eastern part of Africa, for instance, experienced the most displacement, and their paleoclimates were greatly affected as a result of the drift of the Africa and South America, since the Upper Cretaceous (Maley, 1996).

Norris *et al*. (2002) suggested that Uppermost Cenomanian tropical sea-surface temperatures may have been as much as 4–7^{o}C warmer than the highest modern mean annual temperatures. Geological evidence for these Cretaceous sea level fluctuations could be recognised in regional unconformities (Flögel *et al*., 2011). This is further supported by isotopic data which support a gradual decrease in deep water temperatures from 15°C to 2-3°C throughout the Tertiary (Barron, 1983). The greenhouse warming that occurred during the end of the Cretaceous was linked to catastrophs such as the Deccan volcanism (65–66 Ma) and the Chicxulub impact (Keller, 2008).

The Tertiary was characterised by a general cooling of global climates which ended with warm temperate in the mid-latitudes, and alternsting cool-temperate climates in the Late Neogene (Ehlers and Gibbard, 2007). However, the Early Paleogene is identified as a particularly warm period in Earth's history (Sewall and Sloan, 2001). Like the Early Aptian (Cretaceous), the Paleogene-Eocene boundary was characterised by a remarkable increase in temperature (Jenkyns, 2003).

Zachos *et al*. (1993) distinguished two thermal events during the Tertiary: the first was the Paleocene-Eocene thermal maximum, characterised by reduced oceanic turnover and decreases in global $\delta^{13}C$ and in marine productivity; the second was the Early Oligocene glacial maximum, which was accompanied by intensification of deep ocean circulation and elevated $\delta^{13}C$ and productivity.

The middle Eocene was marked by mild cooling of tropical waters; whereas there was insignificant cooling of high latitude waters (Sijp *et al*., 2014). In West Africa, the Eocene-Oligocene transition determined a non-reversible turnover observed through rapid environmental evolution (Seranne, 1999).

2.6 Geochronology

2.6.1 Review of kaolin dating

Several attempts have been made to date kaolin deposits. Gilg and Frei (1997) studied isotope dating of residual kaolin deposits in Europe, with the objective to explore the use of radiogenic

(K-Ar and Rb-Sr) and stable (H) isotopes in direct dating of kaolin formation in the Tirschenreuth (Germany) and St. Yrieix (France) residual kaolin deposits. They concluded that secondary kaolinites cannot be dated using the K-Ar or Rb-Sr methods because they preferentially incorporate Ar and Sr (daughter elements) from their precursor minerals.

The most successful attempts to date kaolins were made using stable isotopes of oxygen and hydrogen (Gilg, 2000; 2013); as they are an indirect method of dating. Gilg (2000) studied the stable isotope evidence of the timing of kaolinisation in Northeast Bavaria in Germany. He showed that under specific conditions, kaolins keep their original hydrogen isotope ratios and that they can yield valuable geochronological information. He further discussed the palaeoclimatic, palaeogeographic and palaeohydrological implications. Conclusions were obtained by comparing the hydrogen isotope ratios of the studied kaolins with those of sedimentary kaolins of known age. Therefore, stable isotope geochemistry can provide indirect evidence for the age of weathering products. The D/H ratios of the kaolins yielded Mid-Cretaceous ages for the deposit. Hence, stable isotope data of kaolins have a good potential in constraining the timing of weathering (Gilg, 2000).

Gilg (2003) reviewed isotopic tools for dating palaeoweathering in Europe. This review presented geochronological methods using radiogenic isotope systems (K-Ar, ^{40}Ar-^{39}Ar and Rb-Sr) and stable isotopes of oxygen and hydrogen; and their application in weathering ranging from Mesozoic to Cenozoic. The K-Ar method is suitable for dating K-rich minerals (Gilg, 2003). Several authors have used the K-Ar method to date potassium-rich clay minerals (Burley and Flisch, 1989; Środoń *et al*., 2002; Meunier *et al*., 2004; Zwingmann *et al*., 2004 and Clauer *et al*., 1995, 2012 and 2014). The ^{40}Ar-^{39}Ar method, however, is usually not suitable for dating very fine-grained clay minerals due to ^{39}Ar recoil during irradiation (Gilg, 2003). Due to the short half-times of ^{230}Th and ^{234}U, the uranium series are principally restricted to Quaternary samples.

Souza *et al*. (2007) successfully used single zircon direct evaporation geochronology with the Pb-Pb method to determine the provenance of soft and flint kaolin facies of the Capim River (Brazil) by correlating ages found in the region. The zircon crystals in these kaolins were grouped into four morphologic types: type I, characterised by long and euhedral crystals; type II, characterised by intermediate, subhedral to subrounded crystals; type III, characterized by short euhedral crystals; and type IV, characterised by ovoid to spherical crystals. Type II zircons predominated at 39%, followed by type III with 32%, type IV with 17%, and type I with 12%. Among the four age plateaus, 2.15 and 2.02 Ga were the best defined age intervals for the Capim kaolin zircons, because they corresponded to the intervals with the highest amount of zircons and four morphologic types. The results of this study identified two main sediment

sources: one located to the northeast of Capim River, in the Gurupi Region, and the other located in the southwestern and southern portion of the Amazon Craton.

2.6.2 Pb-Pb geochronology

The ability of zircon to fractionate radioactive uranium (U) and thorium (Th) from lead (Pb) during their crystallisation makes zircon an important mineral in provenance and geochronology studies (Kober, 1987). Pb-Pb geochronology uses the crystallisation ages of zircon to infer the ages of the samples being dated. The single zircon Pb-evaporation technique determines the $^{207}Pb/^{206}Pb$ age of a zircon grain through "step-by-step heating of the filament in a solid source thermal ionisation mass spectrometer" (Gaudette *et al*., 1998).

The technique consists of loading an untreated single zircon grain in an outgassed Re filament (Kober, 1986). The sample is then heated in steps from about 1400 to about 1650°C. The Pb driven off from the zircon is deposited on a second filament and subsequently analysed for its isotopic composition. However, only $^{207}Pb/^{206}Pb$ ages are obtained because the zircon grains are not spiked (Ansdell and Kyser, 1993).

2.7 Kaolins as paleoenvironmental and paleoclimatic proxies

2.7.1 Use of stable isotopes of H and O of kaolinite

2.7.1.1 Stable isotopes of H and O

The isotopic abundances of several light elements, including oxygen and hydrogen, usually differ in different phases, different chemical compounds, and sometimes in different atomic positions within the same compound. These differences are caused by physico-chemical processes and reflect slight differences in the physical and chemical properties of the isotopes (Savin and Hsieh, 1998). The commonly used stable isotopes of oxygen and hydrogen are ^{18}O and ^{2}H or deuterium (D). Their average relative abundances in natural systems are 0.204 ‰ and 0.015 ‰, respectively (Savin and Hsieh, 1998).

Stable isotopes geochemistry of water was one of the first to be developed for natural systems, and Craig (1961) came up with the equation of the meteoric water line (Equation 2.1). Sheppard *et al*. (1969) developed the Hypogene-Supergene line which is equivalent to kaolinite in equilibrium with meteoric waters at about 35°C (Parnell *et al*., 2000). Later, studies by Savin and Epstein (1970) led to the development of the kaolinite line (Equation 2.2), which represents the location of isotopic data for pure kaolinites formed in approximate equilibrium

with meteoric water at surface temperatures (Faure, 1998). The meteoric water, supergene-hypogene and kaolinite lines are illustrated in Figure 2.5.

$$\delta D = 8\delta^{18}O + 10 \quad \text{(Eqn. 2.1)}$$

$$\delta D = 7.5\delta^{18}O - 220 \quad \text{(Eqn. 2.2)}$$

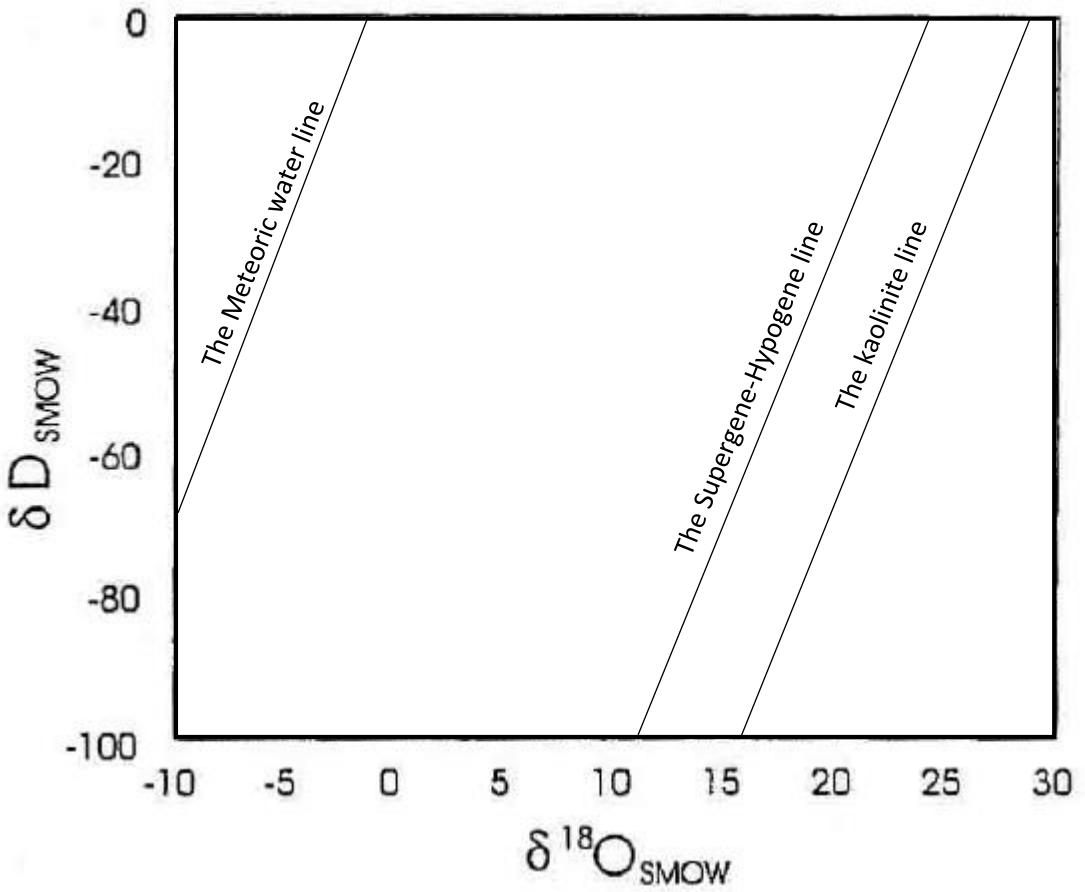

Figure 2.5: The meteoric water, supergene-hypogene and kaolinite lines (Modified from Gilg *et al*., 1999)

The δD and δO values of meteoric water vary with change in latitude and altitude. Therefore, the stable isotope composition of secondary kaolins is considered to reflect the environment of formation (Mizotta and Longstaffe, 1996). The stable isotope composition of kaolins can also provide paleoenvironmental information on the isotope composition of soil waters, paleotemperatures, isotope values of gases in the soil and the partial pressure of soil and tropospheric gases (Sheldon and Tabor, 2009). Several studies have applied stable isotope geochemistry of clay minerals to various disciplines, such as: geothermometry; clay minerals' genesis, diagenesis, and palaeoenvironments, amongst other disciplines (Sheppard and Gilg,

1996). This is because oxygen and hydrogen isotopic signatures of naturally occurring kaolin minerals contain information about the conditions under which these minerals formed (Gilg and Sheppard, 1996; Savin and Hsieh, 1998). Several authors applied stable isotopes of oxygen and hydrogen to reconstruct paleoenvironments of formation of kaolins (Elliot *et al*., 1997; Savin and Hsieh, 1998; Gilg *et al*., 1999; Tabor *et al*., 2002; Tabor and Montanez, 2005; Ekosse, 2007; Horbe, 2011; Das *et al*., 2013; Gilg *et al*., 2013; Roseneau and Tabor, 2013; Turc *et al*., 2013; Westermann *et al*., 2013 and Martinez-Ruiz *et al*., 2014).

In their study on stable isotopes of clay minerals, Sheppard and Gilg (1996) proposed equations for the approximation of the equilibrium H- and O-isotope fractionations, based on experimental, empirical and/or theoretical data for kaolinite (Equations 2.3 and 2.4). Variations in kaolinite chemistry are generally too minor, causing the fractionation factor not to vary much; with an error margin in Equation (2.3) being of ± 5 (Gilg and Sheppard, 1996).

Hydrogen: $1000 \ln \alpha_{kaolinite-water} = -2.2x10^6 x\, T^{-2} - 7.7$ (Eqn. 2.3)

Oxygen: $1000 \ln \alpha_{kaolinite-water} = -2.76x10^6 x\, T^{-2} - 6.75$ (Eqn. 2.4)

Where T is the temperature.

2.7.1.2 Previous investigations of stable isotopes of H and O of kaolinites as paleoenvironmental and paleoclimatic proxies

Elliot *et al*. (1997) interpreted palaeoclimates using pedogenic clay minerals from the Piedmont Province in Virginia, USA. The objective of the study was achieved by carrying out isotopic (stable oxygen isotope) and mineralogical studies of kaolinite. The relatively low ^{18}O (18.3-19.9 ‰) led them to conclude that the kaolinite formed in a climate cooler than that of 1997, probably during the Pleistocene.

Gilg *et al*. (1999) carried out a study on the supergene origin of the Lastarria kaolin deposit in South-Central Chile; then addressed the palaeoclimatic implications. The objective of the work was to prove the supergene origin of the Lastarria kaolin deposit and to discuss the various criteria proposed to distinguish between supergene and hypogene kaolins. They determined the mineralogical composition of the kaolin samples, carried out differential thermal analysis (DTA), studied the fluid inclusions in the quartz phenocrysts and determined the oxygen and hydrogen isotopic compositions of the samples analysed. The results showed that there was no significant hydrothermal alteration of the quartz porphyries. Stable isotopes data indicated that the kaolin formed in a supergene environment, with higher mean annual air temperatures

than the mean temperatures in 1999. These results converged to show that the deposit had a supergene origin.

Boulvais *et al*. (2000) determined the origin of kaolinisation of deposits overlying granites in Brittany (France), using the isotopic compositions of O and H. Kaolin deposits in Brittany occur abundantly in various types of rocks. Hence, the necessity to determine their origin. The results ($\delta^{18}O_{kaolinite}$ = 20.2 ± 1 ‰, $\delta D_{kaolinite}$ = - 55 ‰ to – 67 ‰) were coherent with a supergene origin. However, the association of kaolinite with quartz veins in deposits is probably as a result of an increase in permeability caused by a former hydrothermal alteration event.

Gilg *et al*. (2013) studied D/H and $^{18}O/^{16}O$ ratios of kaolins from sites on the Fennoscandian Shield (Southern Sweden) in order to estimate groundwater palaeotemperatures during weathering and infer ages of phases of deep kaolinisation. Weathering profiles containing high concentrations of kaolinite occur on Proterozoic Shield rocks beneath Pleistocene glacial deposits. The oxygen and hydrogen isotopic ratios indicated weathering by cool groundwater under mean annual temperatures of 13-15^{o}C, which are below Cretaceous mean annual temperatures (MATs), and slightly above Plio-Pleistocene MATs. The Cretaceous-Paleogene uplift might have caused a selective intense weathering of fractured shield rocks. Therefore, the assumption that kaolinisation only occurs in humid tropical environments is questionable (Gilg *et al*., 2013).

2.7.2 Use of trace elements in kaolins

2.7.2.1 Trace elements

Some elements are less mobile during sedimentary processes. This enables them to stay in the solid phase during erosion and sedimentation, thereby preserving the chemical signatures of their source rocks (López *et al*., 2005). These elements constitute the group of trace elements, and include rare earth elements (REEs), large ion lithophile elements (LILE), high field strength elements (HFSE) and transition trace elements (TTE).

The REEs are a group of elements belonging to the Lanthanides, with atomic numbers ranging from 57 (La) – 71 (Lu). Individual REE or group of REEs have similar but distinct geochemical behaviour in natural systems (Laveuf *et al*., 2008). The immobility of REEs during geological processes makes them useful indicators of provenance of sediments (Cavalcante *et al*., 2014). Like REEs, high field strength elements (HFSE) (Zr, Hf, Nb, U and Ta), Th, Sc, Ti, Y and Co are the most suitable ones for provenance determination (Nyakairu and Koeberl, 2001; Banner, 2004).

Large ion lithophile elements and TTEs include Cr, Se, Co, Pb, As, Ni and Cu, and U. Their mobility is depedent on the pH, sorbent nature, presence and concentration of organic and inorganic ligands, including humic and fulvic acids, root exudates and nutrients (Violante *et al*., 2010). Moreover, kaolinite is highly dependent on pH; this causes the adsorption of metals based on the pH of the environment (Bhattachryya and Gupta, 2008).

Dill *et al*. (1997) showed that some REEs are more concentrated in kaolin during hydrothermal processes (Au and Ag), whereas others are more concentrated during weathering. Hence, unlike major oxides, trace elements are useful in interpreting the genesis of kaolinisation (Cravero *et al*., 2001; Laveuf *et al*., 2008).

2.7.2.2 Previous investigations of trace elements as paleoenvironmental and paleoclimatic proxies

Dill *et al*. (1997) studied the mineralogical and geochemical variations in hypogene and supergene kaolin deposits in a mobile fold belt of the Central Andes in north-western Peru. The aim of the study was to differentiate between hypogene and supergene kaolinisation using their trace elements' chemistry and mineralogy. According to these authors, S, Ba, and Sr are more concentrated in kaolins during hypogene processes, unlike Cr, Nb, Ti and lanthanides which preferentially concentrate within a supergene environment. The P_2O_5 vs. SO_3, Zr vs. Ti, Cr + Nb vs. Ti + Fe, and Ce + Y + La vs. Ba + Sr diagrams were used to determine the origin of the kaolin deposits. During the Lower Cretaceous, kaolins were deposited in flood plain to delta plain environments. In the magmatic arc/back-arc basin, kaolinisation occurred during uplift and peneplanation; and during the Late Miocene, kaolinisation of volcanic rocks was similar (Dill *et al*., 1997).

Late Cretaceous sea-level changes in Tunisia were studied by Li *et al*. (2000) using a multidisciplinary approach. This approach included bulk rock and clay mineral compositions, carbon isotopes, total organic carbon (TOC), Sr/Ca ratios, and macro- and microfaunal associations. In this study, they used the kaolinite / (chlorite + mica) ratios to determine sea-level changes. The results of clay mineral analyses led to the interpretation of ckimatictrends in Tunisia. The high kaolinite and variable mica and chlorite abundances suggested that the Late Maastrichtian was increasingly humid. The kaolinite distribution and abundance indicated that the overall climate in Tunisia was generally more humid during the late Maastrichtian. Low kaolinite / (chlorite + mica) ratios corresponded to low sea-levels, and warm or humid climates.

Baioumy (2014) studied the geochemistry and origin of Cretaceous sedimentary kaolin deposits of the Red Sea in Egypt. The aim of the study was to determine the source of the aforementioned deposits using their mineralogy and geochemistry. Baioumy (2014) found that

the deposits were derived from a mixture of mafic, granitic and alkaline rocks. The REE pattern, the negative europium anomaly and the high Zr and Y contents suggested the contribution of granitic rocks; the relatively high TiO_2 and Ti contents suggested the contribution of mafic rocks; and the abnormally high Nb indicated a contribution of alkaline rocks to the source rocks. The conclusion was that the Cretaceous sedimentary kaolins of the Red Sea were deposited in a non-marine depositional environment, due to abundant organic matter, absence of marine fossils and presence of kaolinite as single mineral phase.

2.8 Occurrence of kaolins in Cameroon

Ekosse (2010) reported the existence of 27 kaolin deposits in Cameroon (Table 2.2), of both primary and secondary origins. A summary of characterised kaolins in Cameroon is shown in Table 2.2. Other kaolin deposits in Cameroon include the Misselele, Dizangue, Mbanga, Bomkoul, Nkolbisson, Mbankomo, Etoug-Ege Mbe, Mbe, Mora and Lembo (Ekosse, 2010), amongst others.

Table 2.2: Kaolin deposits in Cameroon (Ekosse, 2010)

Deposits	Genesis	Minerals	Applications
Mayouom	Hydrothermal alteration of gneiss mylonite and magmatic intrusive veins	Kaolinite, quarts, illite/muscovite, anatase	Ceramics
Bana	Primary, from alteration of Bana Tertiary ring complex	Quartz, illite, hematite, kaolinite	Ceramics
Balengou	Meteoric alteration of granites of the Bana ring complex		
Ntamuka (Bafut)	Primary, from alteration of trachyte	Halloysite	
Santa	Primary, from weathering of trachyte and phonolite from Mount Bamenda	Kaolinite, Quartz	Ceramics
Bali	Residual weathering of trachyte and phonolite from Mount Bamenda	Kaolinite, quartz and halloysite	Ceramics, pottery, bricks

Deposits	Genesis	Minerals	Applications
Bambili	Secondary, from weathering of feldspathic arenites within the Douala sedimentary basin	Kaolin	Ceramics
Sabga	Primary, from alteration of ferrugineous lateritic profiles	Kaolinite, quartz, goethite	Bricks
Banga	Primary, from alteration of granites	Kaolin	Bricks, pottery

Of these deposits, only four have been studied, namely; the Mayouom, Ediki, Missole and Bomkoul kaolins.

2.8.1 Mayouom kaolins

The Mayouom kaolin deposit is located in the Foumban shear zone (550-660 Ma) (Njoya *et al*., 2006). Njoya *et al*. (2006) studied the genesis of the Mayouom kaolin deposit. The sand-rich and the sand-poor kaolins were the two main facies distinguished in this deposit. In addition to the quantitative analyses, semi-quantitative analyses using X-ray diffraction spectroscopy (XRD), scanning electron microscopy (SEM) and Fourier Transform Infrared (FTIR) techniques were also carried out. Results obtained from this study showed that the Mayouom kaolin deposit is of hydrothermal origin, formed from the kaolinisation of veins and neighbouring mylonite.

Sequel to the study made by Njoya *et al*. (2006), Tassongwa *et al*. (2014) studied the geochemistr and mineralogy of the Mayouom kaolin deposit. The study focused on a particular outcrop in the deposit, suggesting a possible vertical variation of the Mayouom kaolin. Determination of the chemical index of alteration (CIA) was included in the study in order to determine the degree of alteration of the samples. The industrial suitability of the Mayouom kaolin deposit was evaluated by Nkoumbou *et al*. (2009). Mayouom kaolins were recommended for ceramic applications (porcelain, ceramic glass, sanitary ware and silico-alumina-based refractory ceramics).

2.8.2 Ediki kaolins

The Ediki kaolin deposit occurs within the Mungo River (Logbadjeck) Formation of Turonian-Cenomanian ages (93.9-72.1 Ma) of the Douala Sub-Basin (Diko and Ekosse, 2012). The Ediki kaolin is acidic, with quartz and kaolinite as the dominant mineral phases, and muscovite + microcline and illite + goethite as the minor and trace phases, respectively. Kaolinisation was favoured by a hot humid tropical climate, and low pH (Diko and Ekosse, 2012). Two kaolin facies can be distinguished from this deposit (Diko and Ekosse, 2013): the sand-rich and the sand-poor facies. The difference in mineralogy and geochemistry between the two facies were attributed to physical controls on weathering (Diko and Ekosse, 2013).

2.8.3 Missole II kaolins

The Missole II kaolin deposit is found in the Paleocene-Eocene N'Kapa Formation of the Douala Sub-Basin (Logmo *et al*., 2013). According to the study carried out by Logmo *et al*. (2013), the main minerals of this deposit are kaolinite, illite and quartz. A study conducted by Ngon Ngon *et al*. (2012a) showed that average elemental ratio values of Eu/Eu* (0.5), La/Sc (8.0), Th/Sc (0.99), La/Co (26.9), Th/Co (4.1), and Cr/Th (8.3); coupled with light rare earth elements (LREE) enrichment and flat heavy rare earth elements (HREE) of the kaolins favour a felsic rocks source for Missole II kaolins. This was later confirmed by Ngon Ngon *et al*. (2014). The Missole II kaolins are suitable for the manufacturing of bricks and tiles (Logmo *et al*., 2013).

2.8.4 Bomkoul kaolins

The Bomkoul kaolins are found in the Matanda-Wouri-Formation (Miocene-Pliocene age), on the eastern part of the Douala Sub-Basin (Ngon Ngon *et al*., 2012b). The kaolin deposit is mainly made up of kaolinite and smectite, and could be used for pottery and manufacturing of bricks and tiles. Ngon Ngon *et al*. (2014) investigated the Bomkoul kaolins deposit to identify its parent rocks. The high CIA depicted extreme weathering if the kaolins under humid tropical climate before and after its deposition in the coastal plain. The values of elemental ratios, together with the chrondrite-normalised rare earth elements (REE) patterns, and the negative Europium anomaly corroborated a silicic or felsic parent rock.

2.9 Paleoenvironmental reconstruction in the Douala Sub-Basin

The Douala- Kribi-Campo Basin has usually been studied for its hydrocarbon potential. However, in the past decade, paleoenvironmental research on the Douala Sub-Basin sediments focused on the use of palynostratigraphy and the study of the lithology of some outcrops in this Sub-Basin (Ngaha, 2005; Kenfack *et al*., 2012b, Mbesse *et al*., 2013; Chavom *et al*., 2014).

Kenfack *et al*. (2012b) proposed a paleoenvironmental reconstruction (geochronology and paleoecological interpretations) of the sediments in the Northern border of the Douala Sub-Basin using fossils dinoflagellates. All the collected dinoflagellates belonged to the Dinophyceae class. Correlating these results with those obtained in other studies gave a Maastrichtian-Paleocene age to sediments, which is in accordance with the hosting Formation's age. The results also proved that the sediments were deposited in a shallow marine coastal environment, with warm waters and normal salinity (Kenfack *et al*., 2012b).

Mbesse *et al*. (2012) suggested a paleoenvironmental reconstruction of the Paleocene-Eocene boundary of the Douala Sub-Basin, using palynostratigraphy (Dinocysts' ecology and the Dinoflagellates/Pollen-Spores' ratio in the studied sequences). An important marine transgression phase took place from the Lower to Mid Paleocene, while one of the study sites (Moulongo) showed a clear regression phase during the Lower Eocene (Mbesse *et al*., 2012). The two other sites showed a break in sedimentation, which was interpreted as the beginning of the tectonic activity, which caused a general regression in the Douala Sub-Basin.

Chavom *et al.* (2014) used the lithology, grain size and sedimentary structures of selected Tertiary outcrops of the Douala Sub-Basin to reconstruct the paleoenvironments of deposition of its sediments. They came up with five depositional environments, namely; the fluvial-braided channels, meandered channels, delta plain, continental shelf and the marginal-littoral.

2.10 Kaolin applications and beneficiation methods

2.10.1 Kaolin applications

Kaolin genesis has a direct link to its industrial applications (Ekosse, 2000). Mineralogical and chemical characteristics are important properties for a good quality control of kaolins, and physical properties are closely related to the mineralogy and chemistry (Cravero *et al*., 1997). Moreover, the wide applications of kaolins in industry strongly depend on their purities.

The excellent firing properties and relatively high melting point of kaolin (Aja and Randy, 2013) have made kaolin an intensively used industrial mineral (Choudhary *et al*., 2012). The wide range of applications of kaolins include construction, agricultural, textile, paper, pharmaceutical, ceramic, electrical, paint, nuclear energy, polymer and petroleum industries (Heckroodt, 1991; Ekosse, 2000; Matike *et al*., 2011; Obaje *et al*., 2013 and Tassongwa *et al*., 2014).

In the soap production industry, kaolin is used as a filler and it gives the structure and acts as a riser (Aja and Randy, 2013). Kaolin is also used as a filler and coater in the paper industry (Jepson, 1984). Kaolins could also be used for ceramics. Ceramic applications if kaolins include the production of sanitary ware, tableware, fine china, electrical porcelain, wall tiles and floor tiles, whereas, in the paint and polymer industry, kaolins are used as extenders due to their fineness, aspect ratio and whiteness (Jepson, 1984). Testing for the physico-chemical characteristics of kaolins is known as diagnostic evaluation, and the degree of response to beneficiation determines the specific industrial application of a kaolin deposit (Ekosse, 1994).

2.10.2 Diagnostic evaluation

Diagnostic evaluation consists of evaluating the physical properties of kaolins, such as the grain size distribution, viscosity, colour, pH, electrical conductivity, and plastic and liquid limits. The liquid limit is taken as the water content of the soil at which it will just begin to flow when jarred in a specific manner, while the plastic limit is the minimum water content at which the soil can just be rolled by hand into threads 3 mm thick without crumbling (Bain, 1971).

2.10.3 Beneficiation methods

Beneficiation enhances kaolin applications (Ajayi and Adefila, 2012). The two principal objectives of kaolin beneficiation are the removal of impurities and production of a desired particle size distribution (Kirabira *et al*., 2007).

Particle size reduction could be done by conventional sieving and/or by using a sedigraph (Ngon Ngon *et al*., 2012b).
Magnetic separation processes are simple and economic; they therefore, hold great promise for the clay manufacturer (Oder and Price, 1973). Cravero *et al*. (1997) determined the technological properties of three kaolin deposits in the Neuquén Basin (Argentina) and suggested their most suitable uses. The degree of plasticity of the kaolins positively correlated

with illite/smectite ratio content; whereas the kaolin's viscosity and pH correlated negatively. These results led to the conclusion that kaolins could be used as stoneware clays in ceramic. Bacterial leaching involves three main processes (Roy *et al*., 2010): isolation and cultivation of the bacteria; bioleaching of the kaolin; and the identification of the bacteria. Bacteria of Bacillus species are the most widely used because they break down the silicate structure during weathering and in the genesis of kaolins (Štyriaková and Štyriak, 2000). The most commonly used bacteria in bioleaching is the *Aspergillus niger*, which is used commercially in the production of organic acids, such as citric acid, oxalic acid, and gluconic acid (Ajayi and Adefila, 2012).

2.11 Concluding remarks

In this Chapter, a concise literature review on aspects discussed in this research is presented. It covered the Periods of the Geologic Time Scale, the Precambrian to Tertiary geology of Cameroon, kaolin genesis, Cretaceous-Tertiary paleoclimates, geochronology, the use of kaolins as paleoenvironmental and paleoclimatic proxies, occurrences of kaolins in Cameroon, paleoenvironmental reconstruction in the Douala Sub-Basin, and kaolin applications and beneficiation methods

CHAPTER 3

METHODS

3.1 Preamble

This chapter presents the methods used throughout this research. They cover methods used during fieldwork and sampling, sample preparation techniques, analytical methods, and methods used for data analysis and interpretation. Samples used for analyses were in three fractions: bulk (< 2 mm), silt (between 2 µm and 63 µm) and clay (< 2 µm).

3.2 Fieldwork and sampling

3.2.1 Fieldwork

Fieldwork was carried out in December 2015 at the different study sites in Cameroon. A Global Positioning System (Garmin Etrex H) was used to determine the location and elevation of kaolin deposits. The thickness of outcrops and the distance between sampling points were measured using a tape. At each study site, records of the lithologies and physical characteristics of kaolins outcrops were made in a field book, and photographs were taken.

3.2.2. Sampling

Sampling was done during fieldwork at the different study sites. The method of sampling was judgemental (Tan, 1996), based on the presence of kaolin deposits in known Cretaceous-Tertiary Formations of the Douala Sub-Basin. The number of samples and sampling intervals were a function of the availability of the outcrop, and the size and differences in lithological characteristics of the kaolin occurrences (Diko and Ekosse, 2012).

The collection of samples was done using a trowel (Figure 3.1). Prior to the collection of samples, the exposed surface of outcrops was cleared to enable the collection of fresh samples (Figure 3.1). Samples were either collected vertically or laterally, depending on the presence of profile. Approximately 500 g of fresh sample was collected and stored in labelled air tight sample bags. After field work, samples were air-dried and preserved for sample preparation (van Reeuwijk, 2002). The location of studied kaolin deposits is found in Table 3.1.

Figure 3.1: Collection of fresh kaolin sample with a trowel

Table 3.1: Location of studied kaolin deposits

Period	Deposits	Location	Coordinates
Cretaceous	Ediki kaolin	Ediki, Mbonge Sub-Division, Meme Division, South-West Region	N04°33'25.4" E09°27'59.9"
	Logbaba kaolin	Douala, Douala 3eme Sub-Division, Wouri Division, Littoral Region	N04°01'42.9" E09°45'25.7"
	Yatchika kaolin	Douala, Douala 3eme Sub-Division, Wouri Division, Littoral Region	N03°58'28.8" E09°48'16.8"
Tertiary	Bomkoul kaolin	Douala, Douala 5eme Sub-Division, Wouri Division, Littoral Region	N04°05'49.1" E09°48'16.7"
	Dibamba kaolin	Dibamba, Sanaga Maritime Division, Littoral Region	N04°00'30.4" E09°51'48.3"
	Missole kaolin	Missole, Mouanko Sub-Division, Sanaga Maritime Division, Littoral Region	N03°58'27.9" E09°56'03.7"

3.1.2 Sample coding

The collected samples were given codes for ease of handling and processing of results, according to their locations as in Table 3.2.

Table 3.2: Sample codes according to their locations

Location	Sample	Sample code
Bomkoul	Bomkoul 01	BKL 01
	Bomkoul 02	BKL 02
	Bomkoul 03	BKL 03
Dibamba	Dibamba	DBB
	Dibamba clay nodule 01	DBB CN 01
	Dibamba clay nodule 02	DBB CN 02
Ediki	Ediki 01	EDK 01
	Ediki 02	EDK 02
	Ediki 03	EDK 03
Logbaba	Logbaba 01	LBB 01
	Logbaba 02	LBB 02
	Logbaba 03	LBB 03
Missole	Missole I 01	MSL I 01
	Missole I 02	MSL I 02
	Missole II 01	MSL II 01
	Missole II 02	MSL II 02
Yatchika	Yatchika 01	YTK 01
	Yatchika 02A	YTK 02A
	Yatchika 02B	YTK 02B
	Yatchika 03	YTK 03

3.3 Sample preparation

Sample preparation involved sieving, removal of organic matter, dispersion, particle size separation and packaging. Sieving, removal of organic matter and dispersion were carried out in the Soil Science Laboratory in the School of Agriculture; whereas particle size separation was done in the Hydrology and Water Resources Laboratory in the School of Environmental Sciences. Both laboratories are in the University of Venda.

3.3.1 Sieving

Air-dried samples were gently crushed, to ensure that the internal structure of the particles were not destroyed, with a mortar and pestle in order to disaggregate clods. After being gently crushed, samples were placed in a nest of sieves comprising from top to bottom of 2 mm, 1 mm, 125 µm, 105 µm, 63 µm sieves and the collection plate. This nest of sieves was then placed on a Fritsch Spartan Analysette3-Pulverisette 0 electric sieve (Figure 3.2). The samples were sieved for 10 minutes.

Figure 3.2: Nest of sieves comprising 2 mm, 1 mm, 125 µm, 105 µm, 63 µm sieves and the collection plate

The collected < 63 µm samples were used afterwards to separate the clay fraction from silt fraction. Whereas, for bulk samples, the collected samples from the field were sieved using the 2 mm sieve, and samples < 2 mm were used as bulk samples (van Reeuwijk, 2002).

3.3.2 Removal of organic matter

The presence of organic matter in samples can affect analyses; for example by producing broad X-ray diffraction peaks, increasing the background, and inhibiting dispersal of other minerals. The method used to remove organic matter from samples was slightly modified from that described in van Reeuwijk (2002), which involves the use of hydrogen peroxide (H_2O_2). Fifty grams of samples were used instead of 20 g. The reason for this is because more than 10 g of < 2 µm fraction were needed for mineralogical, geochemical and isotopic analyses. An amount of 50 g instead of 20 g of sample would not affect the results (GTM-13, 2015).

Hence, 50 g of < 63 µm of each sample were transferred into 600 ml beakers. Twenty millilitres of (H_2O_2) were added to the samples. Distilled water was then added to a volume of 300 ml. The samples were placed in a sand bath (Figure 3.3) at a temperature of 200^{o}C for approximately 4 hours until the supernatant was clear, indicating that the decomposition of organic matter was completed. The samples were then removed from the sand bath and let to cool for about one hour. They were allowed to settle and the supernatant was then decanted.

Figure 3.3: Samples being heated in a sand bath for oxidation of organic matter

For analysed bulk samples, organic matter was removed from < 2 mm samples. The samples were then dried in an oven at 105°C, then packaged for subsequent mineralogical, geochemical and isotopic analyses.

3.3.3 Dispersion

While the samples were cooling, a dispersing agent (calgon) was prepared using 40 grams of sodium hexametaphosphate $(NaPO_3)_6$ and 10 grams of soda (Na_2CO_3) (van Reeuwijk, 2002). This solution was transferred in a 1 L volumetric flask and filled to volume with distilled water. Twenty ml of calgon was then added in each cooled beaker and distilled water was also added up to 300 ml volume. The solutions in the beakers were allowed to stand overnight. The following day, each solution was mixed for 15 minutes using an Eijkelkamp Mechanical Analysis Stirrer. Immediately after which each mixed solution was either transferred to one litre polyethylene bottles for particle size separation (Section 3.3.4) and eventual mineralogical, geochemical and isotopic analyses; or to a sedimentation cylinder, for particle size determination (Section 3.4.4.2).

3.3.4 Particle size separation

Particle size separation was carried out to obtain the silt and clay fractions. Particle size separation is based on the principle of Stoke's Law of sedimentation of spherical particles falling freely at a steady velocity under the influence of gravity, and with the fluid's viscosity being the only resistance (Gaspe *et al*., 1994). The principle is illustrated in Equation 3.1.

$$V = \frac{g(d_p - d_w)D^2}{18\eta} \qquad \text{Eqn. 3.1}$$

Where, V is the settling velocity in cm/sec,

D is the particle diameter in cm,

η is the viscosity in poises

g is the gravitational constant (980 cm/sec^2)

d_p is the density of the liquid in g.cm^{-3}

d_w is the density of water in g.cm^{-3}

3.3.4.1. Silt fraction (2-63 µm fraction)

Silt fraction was separated for six samples, one sample for kaolin deposit. For those six samples, the mixed solution transferred in polyethylene bottles (Section 3.3.3) were vigorously agitated and immediately poured into 250 ml beakers, at a height of 7 cm. The 7 cm depth solutions were allowed to stand undisturbed for 4 hours and 54 minutes. This is the appropriate time for particles > 2 µm, with a specific gravity of 2.65 to settle in a 7 cm suspension at a temperature of 25°C (Jackson *et al*., 1979; CRC Press, 2005) (Figure 3.4). After 4 hours and 54 minutes, the supernatant was poured in another beaker for clay size fraction separation. The silt fraction deposited in previous beakers was dried in an oven at 105°C for at least one hour.

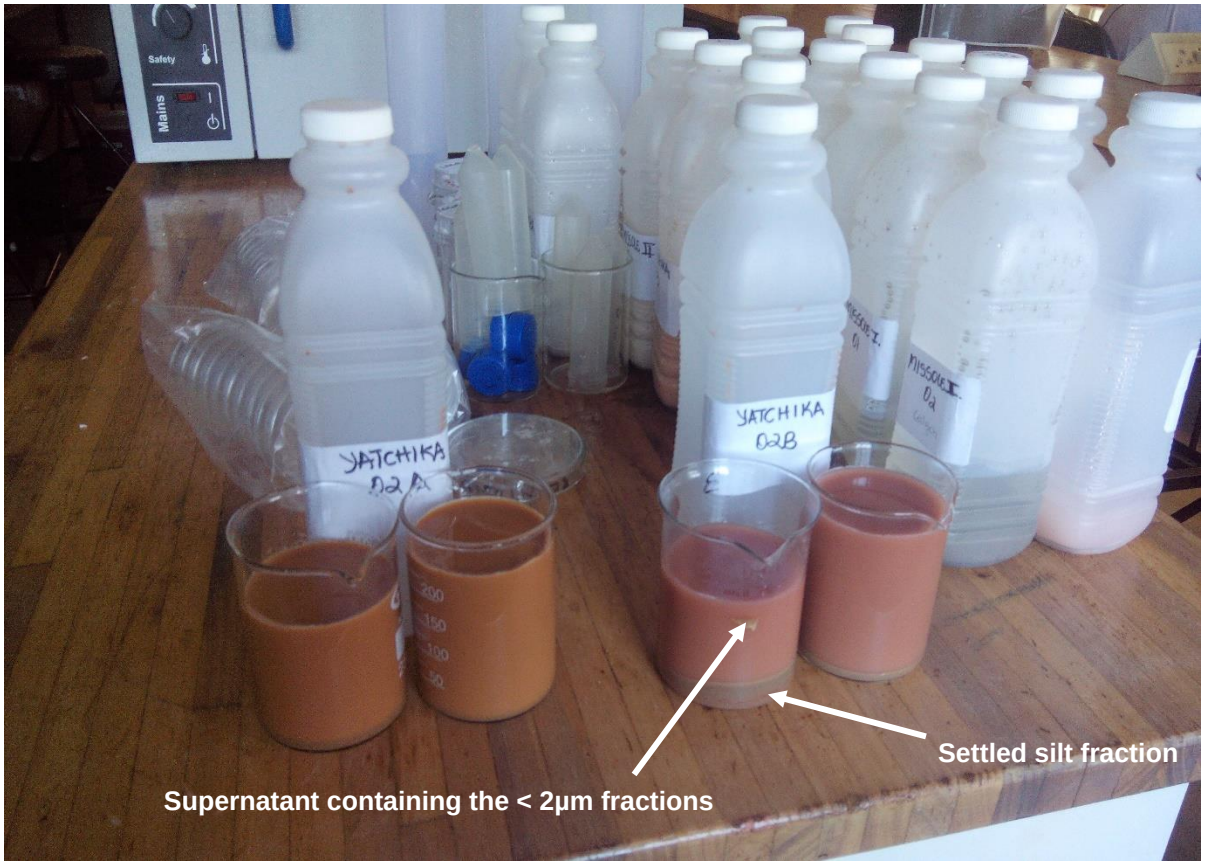

Figure 3.4: Settled silt fraction and supernatant containing the < 2µm fraction

3.3.4.2 Clay fraction (< 2µm)

As in Section 3.3.4.1, the mixed solution transferred in polyethylene bottles were vigorously agitated and immediately poured into 250 ml beakers, at a height of 7 cm. The 7 cm depth solutions were allowed to settle undisturbed for four hours and 54 minutes. This time is the approximate time needed for all particles with a specific gravity of 2.65 and a particle size ≥ 2

µm to settle in a 7 cm suspension at 25°C (Jackson *et al*., 1979; CRC Press, 2005). The supernatant was then transferred to centrifuge tubes (Figure 3.5); then centrifuged at least twice at a speed of 2400 rpm for about 50 minutes, using a Grant-bio LMC-3000 centrifuge, so as to also get the finest particles (0.2 µm) (Jackson *et al*., 1979). The collected < 2µm fraction from the centrifuge tubes (Figure 3.6) were oven-dried at 105°C for about 3 hours.

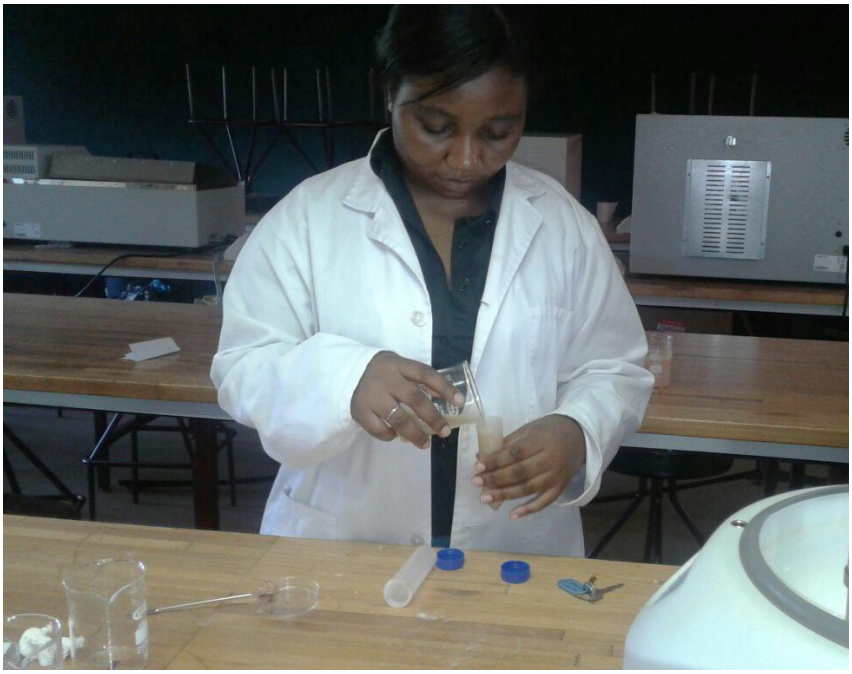

Figure 3.5: Collection of the settled < 2µm fraction from a centrifuge bottle by author

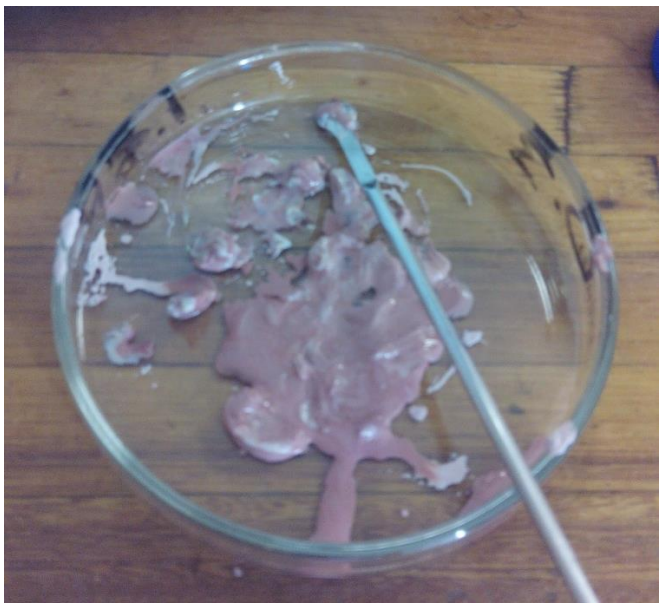

Figure 3.6: Collected < 2µm fraction from centrifuge bottles

3.3.5 Packaging

After drying the different fractions of samples (bulk, silt and < 2µm samples), samples were let to cool and they were later packaged in air-tight bags and labelled (Figure 3.7).

Figure 3.7: Labelled samples in polyethylene bags

3.4 Laboratory analyses

Laboratory analyses involved mineralogical analyses (X-ray diffraction, scanning electron microscopy, Fourier transform infrared spectroscopy and, thermogravimetric analysis and differential scanning calorimetry), geochemical analyses (X-ray fluorescence spectroscopy and energy-dispersive X-ray spectroscopy), trace elements analysis (Inductively coupled plasma mass spectroscopy) and stable isotopes analyses, radiogenic dating of zircons in kaolins (U/Pb) and analyses to determine physico-chemical characteristics of samples (diagnostic evaluation). A summary of analyses carried out, particle sizes that were analysed and number of samples analysed is shown in Table 3.3.

Table 3.3: Summary of analyses carried out, analysed particle sizes and number of samples analysed

Analyses	Particle sizes analysed	No. of samples
X-ray diffraction	Bulk samples Silt samples < 2 µm samples	20 06 20
Scanning electron microscopy	< 2 µm samples	20
Fourier transform infrared spectroscopy	< 2 µm samples	20
Thermogravimetric analysis and Differential scanning calorimetry	< 2 µm samples	20
X-ray fluorescence spectroscopy	Bulk samples Silt samples < 2 µm samples	20 06 20 + 1*
Energy-dispersive X-ray spectroscopy	< 2 µm samples	20
Inductively coupled plasma mass spectroscopy	Bulk samples Silt samples < 2 µm samples	20 06 20 + 1*
Stable isotopes analyses	< 2 µm samples	09
U/Pb dating of zircons	Bulk samples	06
Analyses to determine physico-chemical characteristics of samples (diagnostic evaluation)	Bulk samples	20

(*): One duplicate sample for quality assurance

Samples for stable isotopes analyses were chosen based on their high kaolinite content (> 85 wt%) and less amount of other minerals. Two samples per kaolin deposits were chosen, except Ediki kaolins which contained < 70 wt% in all samples. Therefore, the sample with the highest kaolinite content was chosen. Composite samples of each kaolin deposit were used for U/Pb dating of zircons, this gave a total of 6 samples (one sample per kaolin deposit).

3.4.1 Mineralogical and geochemical analyses

3.4.1.1 Mineralogical analyses

X-ray diffraction analysis (XRD)

X-ray diffraction (XRD) is a very useful and non-destructive analytical technique used in identifying mineral phases and their abundances in a sample. The method uses Bragg's Law, which relates the 2θ angle of the incident beam of X-rays and the spacing between ordered layers or sheets of atoms. Bragg's Law, shown in Equation 3.2 and illustrated in Figure 3.8.

$$n\lambda = 2d \, X \sin\theta \qquad \text{Eqn. 3.2}$$

Where:

n = order of the reflection. This number is an integer.

λ = wavelength of the incident beam of x-rays.

d = spacing of the layers or sheets of atoms in Angstroms (Å).

θ = angle between the incident beam and the atomic planes of the layers or sheets.

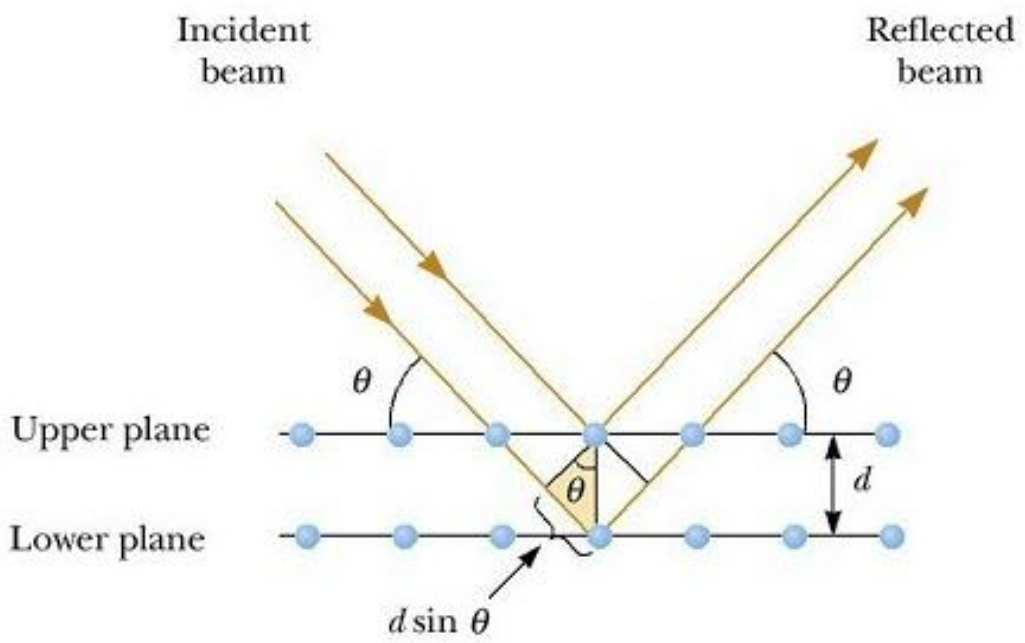

Figure 3.8: Illustration of Bragg's Law

X-ray diffraction analysis was done at the Extraction & Engineering Metallurgy Department's Laboratory at the University of Johannesburg using a Rigaku Ultima IV diffractometer (Figure 3.9), working with 40 kV and 30 mA, and using a cobalt source (λ = 1.789 Å) and an alpha filter (CoKα). Samples were scanned from 3° 2θ to 90° 2θ at a rate of 2° per minute, though results are reported up to 40° 2θ. Mineral phase identification and quantitative analysis of

these mineral phases were carried out at XRD Analytic and Consulting cc. The mineral phases were identified using X'Pert Highscore Plus Software. The relative phase amounts (weight %) were estimated using the Rietveld method.

Figure 3.9: Rigaku Ultima IV X-ray diffractometer used for XRD analysis of samples

Scanning Electron Microscopy with an energy dispersive X-ray spectrum (SEM-EDX)

Scanning Electron Microscopy (SEM) with an energy dispersive X-ray spectrum (EDX) was used to determine the micromorphological and microchemical characteristics of the kaolin samples. The method used was similar to that described in Ekosse (2000). Particle images were obtained with a secondary electron detector. Samples were mounted on Al stumps using a conductive glue. Very small amounts of the < 2 µm fraction of each sample was set on carbon tapes. They were then coated with carbon using a Quorum Q150T carbon coater

(Figure 3.10). Samples were viewed from a VEGA3 TESCAN analytical scanning electron microscope (Figure 3.11). The analysis was carried out at the Extraction & Engineering Metallurgy Laboratory at the University of Johannesburg.

Figure 3.10: Quorum Q150T carbon coater, which was used to coat the samples

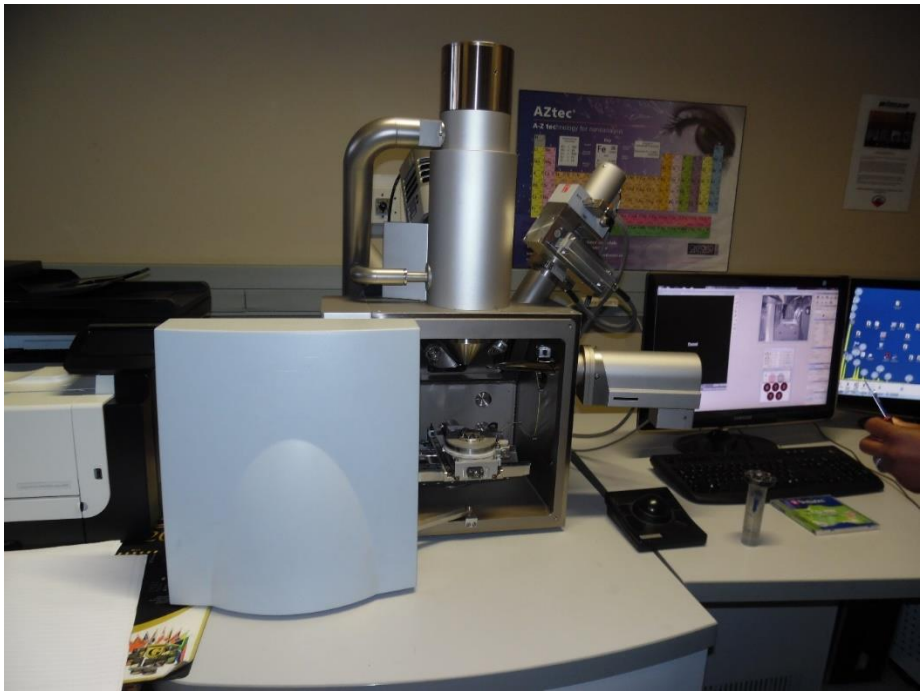

Figure 3.11: VEGA3 TESCAN equipment used for SEM-EDX analysis

Fourier transform infrared spectroscopy (FTIR)

The FTIR spectroscopy is used to characterise functional groups in clay minerals and to fingerprint specific minerals (Madejová and Komadel 2001; Ekosse 2005). It has proven to be a rapid and cost-effective technique in determining the degree of structural disorder of clay minerals (Madejová and Komadel 2001). In this research, FTIR was carried out using a reflectance technique attenuated total reflectance (ATR) at the Ecology and Resource Management Laboratory in the School of Environmental Sciences at the University of Venda.

The method used was that described by Madejová and Komadel (2001): Each sample was placed in contact with an ATR crystal (ZnSe), and the evanescent wave was attenuated in the regions of infrared (IR) spectrum, where the sample transmits (absorbs) energy. The IR spectra were recorded using a Brucker Alpha Platinum ATR FTIR spectrometer (Figure 3.12), in the mid-infrared regions (MIR) (4000-400 cm^{-1}) and with a resolution of 4 cm^{-1}.

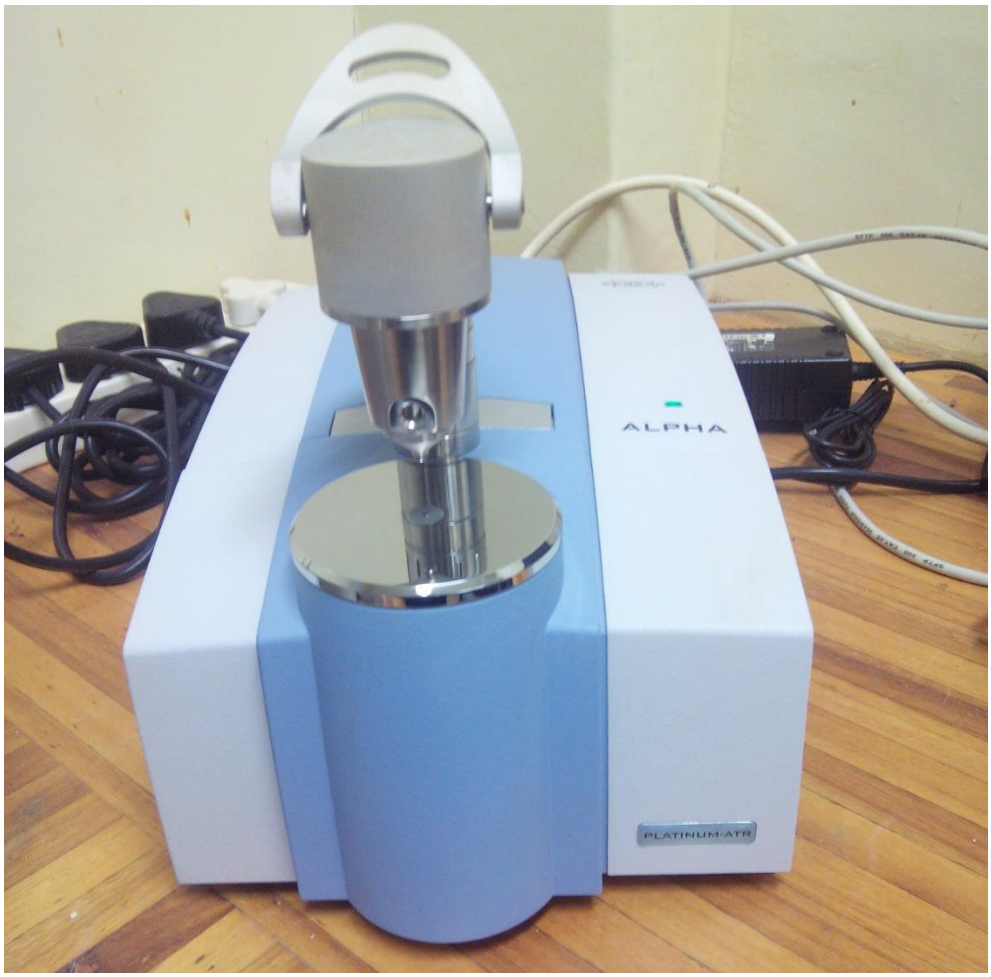

Figure 3.12: Brucker Alpha Platinum ATR FTIR spectrometer used to determine the functional groups in the samples

The peaks obtained were compared to those of the Georgia kaolins (KGa-1b and KGa-2), known for their high grade (high purity and crystallinity), which were also analysed using ATR (Madejová and Komadel, 2001). Peaks were reported based on % transmittance to given wavelengths. The samples were later described as ordered, partially ordered, poorly ordered and disordered based on the empirical classification of Vaculíková *et al*. (2011).

Thermogravimetric analysis and Differential scanning calorimetry (TGA-DSC)

Thermogravimetric analysis and differential scanning calorimetry are thermal analyses (TA) techniques which involve a recording of a change of a material (in this case, kaolin) as it is being heated. Changes in heat content of the analysed sample are indicated by deflections (called peaks) shown by curves representing the differential temperature, and peak temperature (T_m) values are obtained from the classic Equation 3.3 (Kissinger, 1956).The curves show the weight changes during heating (TGA) and the effect of energy changes (endothermic or exothermic reactions) in a sample (DSC) (Guggenheim and van Groos, 2001).Thermal analyses have also been successfully used as a method to determine the kaolinite disorder degree (Vaculíková *et al*., 2011; Diko *et al*., 2016).

$$\ln(\theta T_m^{-2}) = C - E(RT_m^{-2}) \qquad \text{Eqn. 3.3}$$

Where θ is the heat rate,

T_m is the peak temperature,

C is an integrating constant,

E is the activation energy and

R is the gas constant

The TGA-DSC analysis was carried out at the Department of Chemistry Laboratory at University of Johannesburg. The method used was similar to that in Diko *et al*. (2016). An average mass of 10 mg of sample was heated in nitrogen atmosphere at a rate of 10 °C/min, from 25 °C to 1000 °C using a TA instrument SDT Q600 (Figure 3.13). Thermal gravimetric analysis (TGA), derivative thermal gravimetric (DTG) analysis and heat flow were reported.

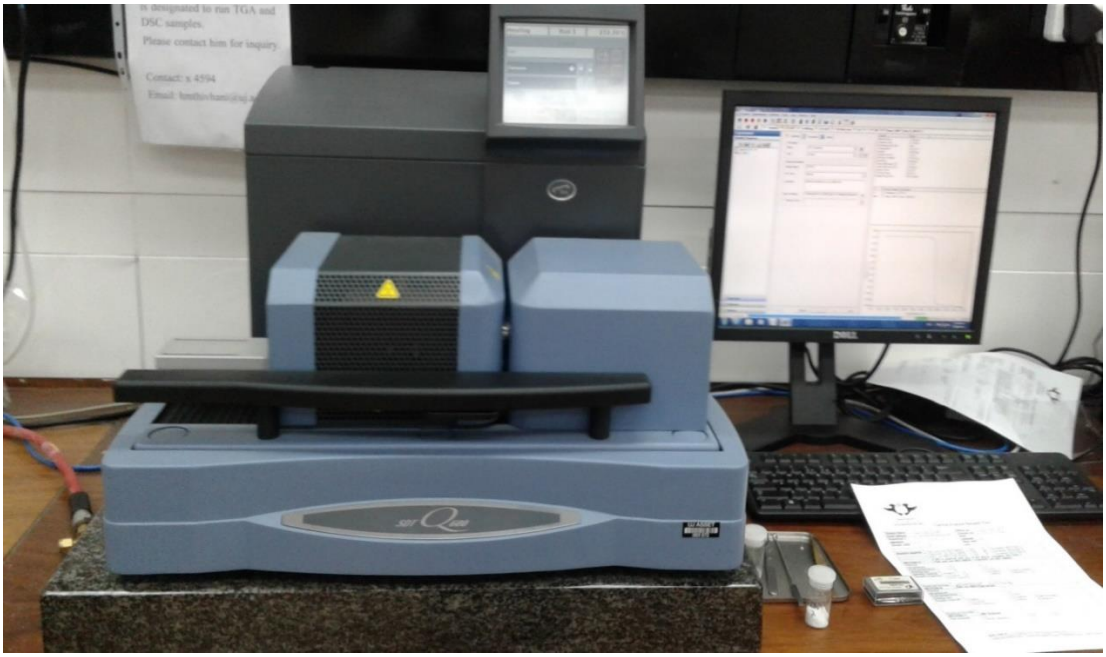

Figure 3.13: TA instrument SDT Q600 used for TGA-DSC analyses of samples

3.4.1.2 Geochemical analyses

X-ray fluorescence (XRF) spectrometry

X-ray fluorescence (XRF) spectrometry is an X-ray technique used for chemical analyses of rocks, minerals, sediments and fluids. It is based on wavelength-dispersive spectroscopic principles. Fluorescent rays are emitted as samples are being irradiated by an intense X-ray beam. The emitted fluorescent rays are detected by a wavelength-dispersive detector, which identifies and quantifies elements or oxides of elements present in samples, based on the intensity of the X-rays. It is one of the most widely used techniques for major elements (oxides) in rocks, minerals and sediments due to the simple and cost efficient samples preparation.

X-ray fluorescence spectrometry analysis was carried out at the Extraction & Engineering Metallurgy Laboratory at the University of Johannesburg. Prior to analysis, pellets (Figure 3.14) were produced using a hydraulic press and a die set (die body, base, plunger, and two polished metal disks), made up of tungsten alloy. Then the pressed pellets were placed in an oven at 105^{o}C for one hour. After removal from the oven, the pellets were allowed to cool; then XRF analysis was carried out using a Rigaku ZSX Primus II XRF spectrometer (Figure 3.15).

Figure 3.14: Pellets of samples produced with a hydraulic press

Figure 3.15: Rigaku ZSX Primus II XRF spectrometer used for XRF analysis of samples

Loss on ignition (LOI)

The LOI is an essential part of major oxides determination, which accounts for constituents such as H_2O and CO_2, which cannot be measured by XRF and are lost during glass formation, so requiring a correction to be made in the determination of the major elements (Ramsey *et al*., 1995). Loss on ignition was determined at the Extraction & Engineering Metallurgy Laboratory at the University of Johannesburg.

To determine the LOI, samples were initially heated for 24 hours at 105^{o}C. Then, they were weighed to determine their moisture content. Thereafter, the samples were placed in a muffle furnace and heated at 1000^{o}C for two hours. After two hours, the samples were removed from the furnace and were placed in desiccators. When cooled, samples were weighed, and LOI was calculated using Equation 3.4 (van Reeuwijk, 2002).

$$MC = \frac{m_A - m_B}{m_B - m_C} x100 \qquad \text{Eqn 3.4}$$

Where, MC is the moisture content

m_C is the mass of tin (g)

m_A is the mass of kaolin sample after heating for 24 hours at 105^{o}C + tin (g)

m_B is the mass of kaolin sample heating for two hours at 1000^{o}C + tin (g)

3.4.2 Trace elements and stable isotopes analyses

3.4.2.1 Inductively coupled plasma-mass spectrometry (ICP-MS)

Inductively coupled plasma-mass spectrometry (ICP-MS) is a powerful tool used to analyse trace elements in samples. It was used to determine trace elements, including rare earth elements. Inductively coupled plasma-mass spectrometry combines a high-temperature ICP source with an MS. The ICP source converts the atoms of the elements in the sample to ions, which are then separated and detected by the mass spectrometer. Before carrying out the analysis, the samples were digested using an Anton Paar Multiware GO Microwave Digestion System (Figure 3.16). The analysis was carried out at the Environmental Analytical Chemistry Laboratory at the Witwatersrand University using an Agilent 7700 series ICP-MS spectrometer (Figure 3.17).

Figure 3.16: Multiware GO Microwave Digestion System used to digest the samples

Figure 3.17: Agilent 7700 series ICP-MS spectrometer used for trace elements analysis

A quantity of 250 mg of each sample was weighed and placed in a Teflon tube. Nine millilitres of HCl, 3 ml HNO_3 and 1 ml HF were added to each sample. The samples were then placed in an Anton Paar Multiware GO Microwave Digestion System for about one hour. After digestion, 6 ml boric acid was added to the samples to remove excess fluoride. Samples were then diluted with distilled water and filled up to 50 ml. Trace elements were then measured using an Agilent 7700 series ICP-MS spectrometer. This ICP-MS spectrometer measures the concentrations of elements in triplicates and provides mean concentrations and standard deviations of each element.

3.4.2.2 Stable isotopes analyses

Stable isotopes analyses were carried out at the Stable Isotopes Laboratory in the Department of Geological Sciences at the University of Cape Town. The samples analysed were the < 2 µm fraction, enriched in kaolinite and with less amounts of other minerals based on the XRD results, in order to avoid oxygen contamination from other minerals. The method used for stable isotopes analyses was similar to the method described by Harris *et al*. (1999). Approximately 20 mg of each sample was placed in a glass container and attached to the vacuum line. The content was then frozen in liquid nitrogen. The air in the sample was then outgassed and the absorbed water was cryogenically distilled to a second vessel by heating the sample at 150^{o}C with an air gum. The mass of the original sample and the produced water were measured and used to determine the wt % of absorbed water. Figure 3.18 shows the set-up for sample preparation; whereas Figure 3.19 shows Finnegan DeltaXP mass spectrometer used to determine oxygen and hydrogen stable isotopes.

Figure 3.18: Set up for sample preparation for oxygen and hydrogen stable isotopes ratios

Figure 3.19: Finnegan DeltaXP mass spectrometer used for stable isotopes analyses

Oxygen isotopes

The samples were outgassed under high vacuum at 200°C for 2 hours, after being dried in an oven at 110°C. Then, the samples were reacted with an excess of ClF_3 at ~560°C for 12-16 hours. The evolved O_2 was quantitatively converted to CO_2 using a hot platinised carbon rod. The $\delta^{18}O$ of the CO_2 was then measured using the Finnegan DeltaXP mass spectrometer. Duplicate splits of the MQ quartz standard were analysed with each batch of eight samples. These values were used to normalise the raw $\delta^{18}O$ to the SMOW scale, using $\delta^{18}O$ = 10.1‰ for MQ.

Hydrogen isotopes

Prior to analysis, three replicate analyses of the kaolinite standard, Bulk Serina Kao (SB8) from Serina Mine near Cape Town, gave structural water contents 11.93, 12.24 and 12.56 wt%, and a mean δD value of -57 wt% (Appendix 3.1). The extracted absorbed water were converted to hydrogen gas using a variation of the closed tube Zn reduction (Harris *et al*., 1999). Hydrogen isotopic composition was then measured on the Finnegan DeltaXP mass spectrometer (Figure 3.19) calibrated using SMOW. Internal standards (CTMP2010 and RMW, exactly 2 mg) were used to calibrate the raw data to the SMOW scale. This was done by correcting the raw data versus the reference gas value, then adjusted so that CTMP2010 = -7.4, then “stretched” so that RMW = -131.4. The silicates were then adjusted so that kaolinite = -57 (i.e. the δD value of SB8, used as kaolinite standard).

3.4.3 Radiogenic dating of kaolins

Radiogenic dating of kaolins was carried out using laser ablation magnetic sector-field inductively coupled plasma mass spectrometry (LA-SF-ICP-MS) U-Pb geochronology on detrital zircons in kaolin samples. Six composite samples, representing each location, were analysed. The analysis was carried out at the Central Analytical Facilities (CAF) ICP-MS & XRF Laboratory at Stellenbosch University, and it involved heavy mineral separation, cathodo-luminescence (CL) imaging, LA-SF-ICP-MS U-Pb geochronology and data processing.

3.4.3.1 Heavy mineral separation

Heavy mineral separation was carried out in eight steps: crushing, sieving, panning, magnetic separation, picking, mounting and polishing.

Crushing

An amount of 3 Kg of each whole sample was crushed to about pea size using a Jaw crusher (Figure 3.20a). The size was tested by passing each sample through 1 cm sieve and bigger pieces were re-crushed. The crushed pea-size samples were fed in scoops through a Disc mill (Figure 3.20b).

a)  b) 

Figure 3.20: a) Jaw crusher; b) Disc mill used to crush samples

The first milling was done at 1 cm spacing, the second at 5 mm, the third at 2 mm and the fourth at 1 mm. The Disc mill gave sand size grains of individual minerals.

Sieving

The product of the Disc mill was sieved through a 350 µm sieve. All the material that passed through the sieve was placed in a bag and labelled < 350 µm; whereas the material that did not go through the sieve was placed in a bag and labelled > 350 µm.

Panning

Each < 350 µm milled sample was hand-washed by placing it in a large 5 L beaker. The beaker was filled to the top with water while stirring the sample. After waiting for 20 seconds for grains to settle, the water containing the clay fraction was poured out (Figure 3.21). This decanting process was repeated several times until there were no more suspended clay particles and water was clear.

Figure 3.21: Hand-washing of < 350 µm sample

After hand-washing samples to remove clay-size fractions, spoons of each sample were consecutively placed in a Super Panner (Figure 3.22). The Super Panner is a small scale water table which aids in the gravitational separation of samples less than 500 g. Two main

taps were opened (one for water flow and one for suction). The small spout on the narrow end of the pan was also opened to start water flow over the pan, which was slightly inclined towards the wide end of the pan. The motor (used for shaking mechanism) was switched on.

Figure 3.22: Super Panner used for separating heavy minerals from light minerals

A spoon full of each sample was placed at the narrow end of the pan. The water flow and the tilt were adjusted to create a continuous flow, where heavy minerals (on narrow end) remained more or less in one place, moving slowly towards the wider end, and the light minerals moved at a more rapid pace towards the wider end into the suction hose. Heavy minerals were identified by a change in colour from the light minerals (Figure 3.23).

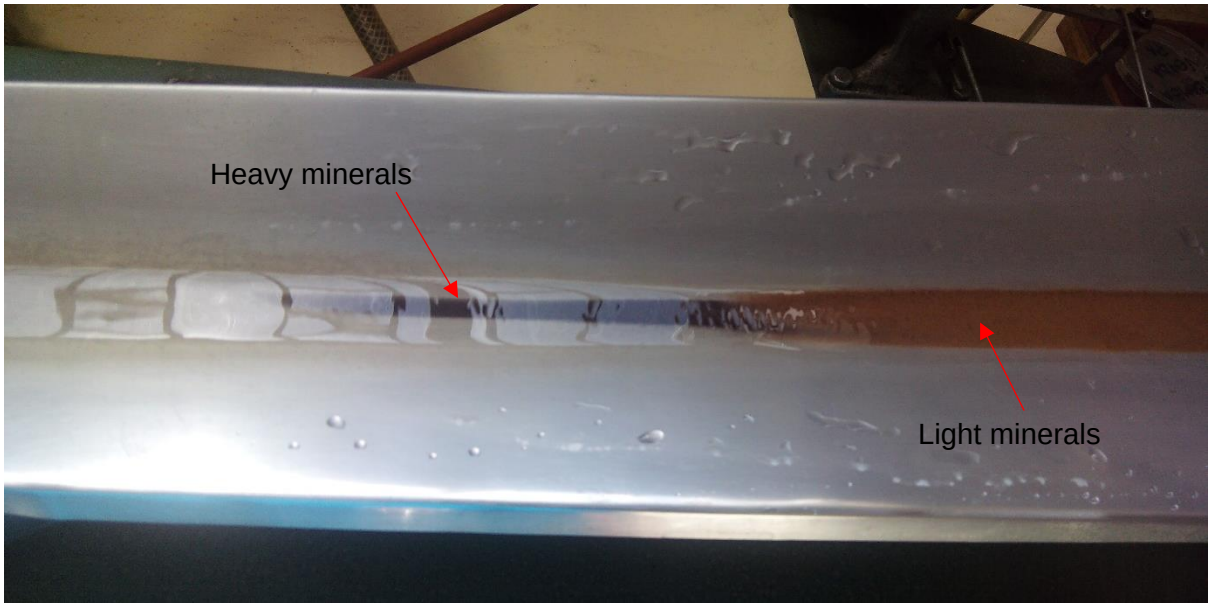

Figure 3.23: Separation of heavy minerals from light minerals

The heavy minerals were collected using a disposable pipette and they were placed in a petri-dish. The petri-dishes containing heavy minerals of each sample were placed in an oven to dry at 40^{o}C. The light minerals were placed in a beaker, covered with a paper towel and placed in an oven to dry.

Magnetic separation

Magnetic separation was carried out in three steps. The first step involved the use of a hand magnet to remove ferro-magnetic minerals such as magnetite and pyrrhotite, as follows: A small amount of sample was spread on a clean sheet of A4 paper and the hand magnet (wrapped in small wax paper) was passed through the sample. The hand magnet was then lifted from the sample and tapped to free loosely bound grains. Then the magnet was removed to another clean sheet of paper and the wax paper was unwrapped to free the magnetic grains. The process was repeated with each sample until no further magnetic material was picked up. The ferro- magnetic sample was stored in a tube and labelled “FM” (ferro-magnetic).

The second step was to remove paramagnetic minerals from the non-ferro-magnetic sample. This was done using the Franz magnetic separator (Figure 3.24 and 3.25). The magnetic separation of minerals was made according to the intensity of the current generated by the Franz magnetic separator (Table 3.4).

Figure 3.24: Franz magnetic separator used for separating paramagnetic minerals

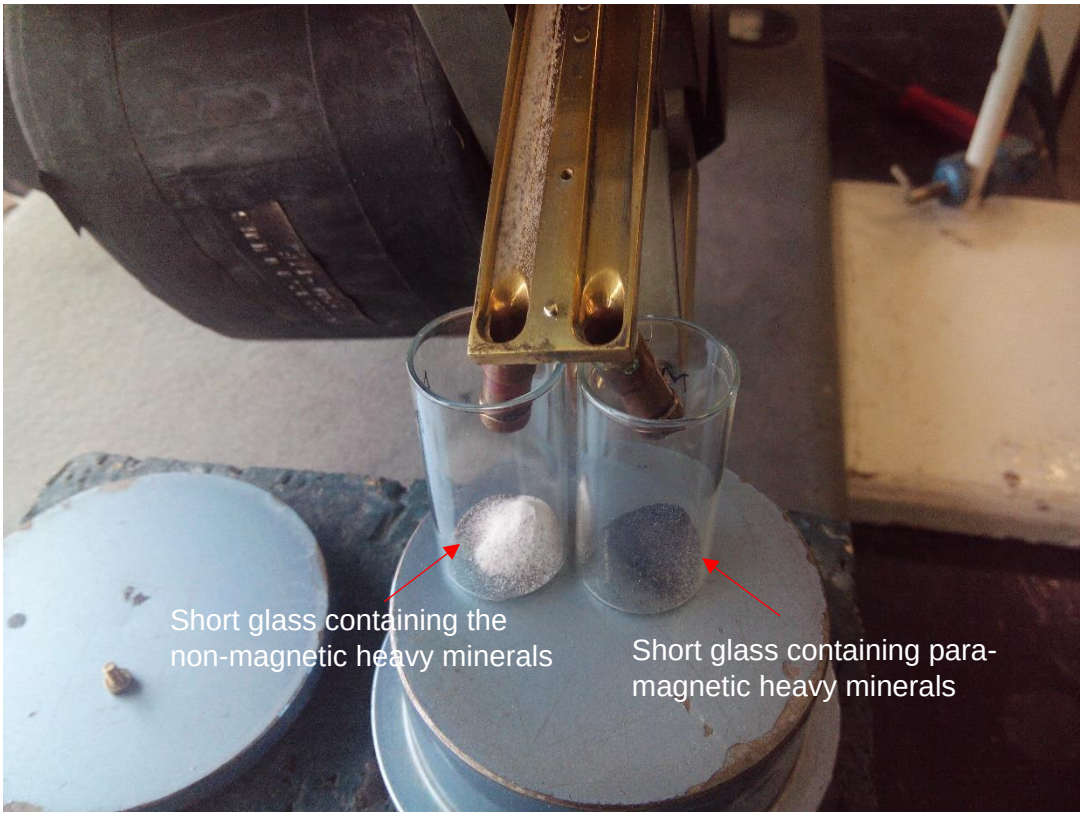

Figure 3.25: Short glasses containing non-magnetic heavy minerals (left) and paramagnetic minerals (right)

Table 3.4: Magnetic separation of minerals according to the intensity of the current of the Franz separator

Magnetic at 0.4 A	Magnetic at 0.8 A	Magnetic at 1.5 A	Non-Magnetic at 1.5 A
Garnet	Biotite	Muscovite	Zircon
Ilmenite	Hornblende	Spinel	Rutile
Chromite	Hypersthene	Enstatite	Sphene
Chloritoid	Augite	Tourmaline	Leucoxene
Olivine	Actinolite	Clinozoisite	Apatite
	Staurolite	Diopside	Corundum
	Epidote	Tremolite	Barite
	Chlorite		Fluorite
			Sillimanite
			Kyanite

Two clean short glass tubes (Figure 3.25), marked “M” (magnetic) and “NM” (non-magnetic), were placed on the split end. Using a side slope of 20° and a tilt of 25°, each sample was run slowly and steadily through the feed tube at 0.4 amperes. The non-magnetic fraction obtained after running the sample at 0.4 amperes was run through the feed tube for the second time, but at 0.8 amperes; and a third time at 1.5 amperes. The magnetic sample obtained from the Franz magnetic separator was placed in a tube and labelled “PM” (paramagnetic); whereas, the non-magnetic sample, obtained after separation at 1.5 amperes, was placed in a tube and labelled “NM” (non-magnetic).

The third step was to carry out heavy liquid separation on the non-magnetic sample obtained from the previous steps. Heavy liquid separation is used to further concentrate heavy minerals by removing other non-magnetic minerals found in the NM sample and which are not heavy minerals. Heavy liquid separation was done using Tetrabromoethane (TBE) of density 2.96. The principle was to set up a separatory funnel on the high stand and two conical funnels on low stands on either side of separatory funnel (Figure 3.26). A small glass beaker (marked Pure TBE) with conical funnel and filter paper (marked HM + sample code) was placed under the separatory funnel. A conical funnel marked “TBE” was placed on top of the separatory funnel. The separatory funnel valve was set in the “close” position. Then, TBE was carefully poured into the separatory funnel, filling to the infection point of the glass. The “TBE” funnel was then removed and set aside in a glass beaker marked “Waste”.

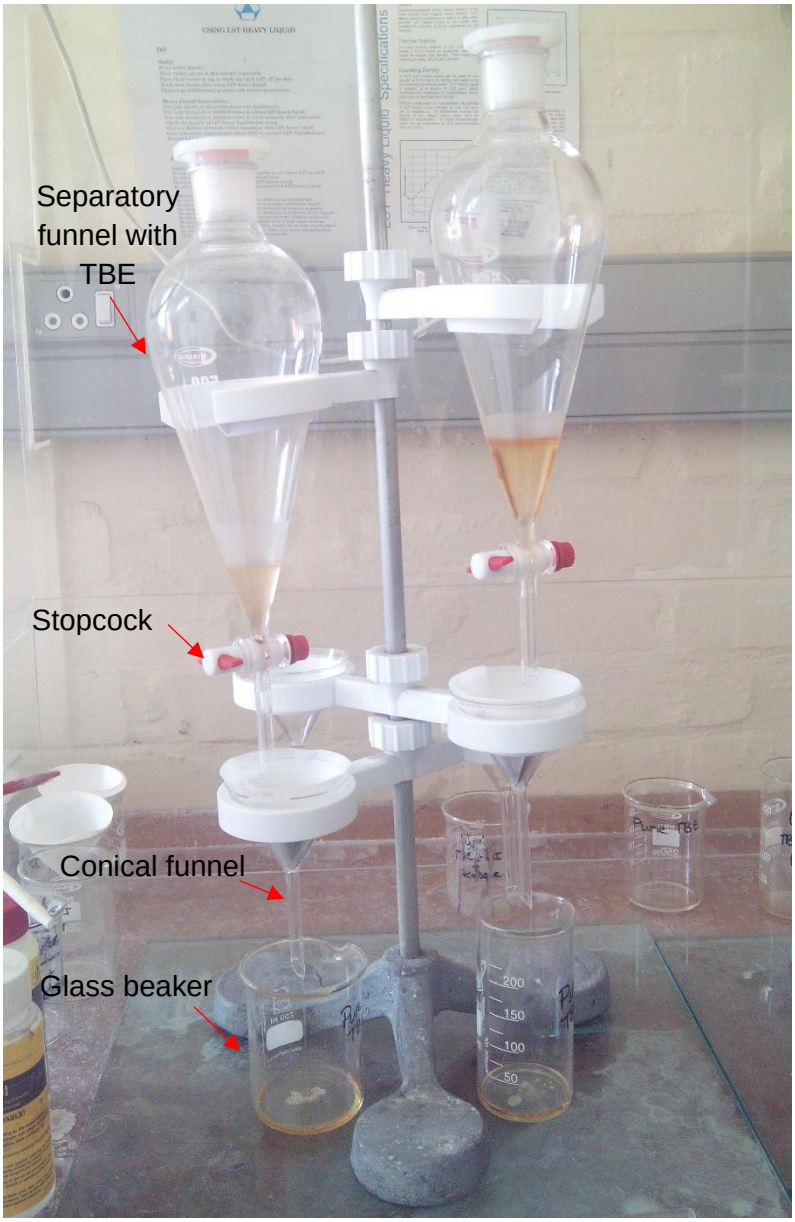

Figure 3.26: Set up for heavy liquid separation

The sample funnel marked “Sample Code” was placed on top of the separatory funnel. Then slowly and carefully, the sample (non-magnetic fraction) was poured into the separatory funnel. The glass tube and the plastic funnel were tapped a few times to ensure that all grains were removed. The plastic funnel was then removed. A glass rode was inserted to gently stir the mixture until the sample clouds the liquid; then it was slowly retracted to minimise grains sticking to it. The rod was lightly shaken to remove excess TBE and was placed in a beaker marked “waste”. After the 30 minutes (allowed for grains settlement and separation), the TBE was gently stirred with the glass rod by trying not to disrupt settled grains at the bottom. After another 30 minutes (or more), the grains completely separated. Once the complete separation of grains was achieved, the stopcock was quickly turned open and closed to release heavy

minerals onto the filter paper below. The stopcock was quickly turned open and closed in the opposite direction to ensure no grains were stuck between the valve and the glass. The TBE was then allowed to drain from the heavy minerals grains in the filter paper.

Another small glass beaker marked “pure TBE” with conical funnel and filter paper (marked “Light Mineral + Sample Code”) was placed under the separatory funnel. The stopcock was opened to drain all TBE and light minerals fraction (LM) onto the filter paper. The TBE was allowed to drain off the light minerals grains in the filter paper. The heavy and light minerals filter papers were each placed on separate glass beakers marked “Waste – TBE + DI (deionised water) + Acetone”. Both the HM and LM grains were washed first with acetone, then with DI (until the TBE smell disappeared), all draining into waste beakers. After the TBE was removed from the HM and LM, the filter papers were placed in separate glass beakers, marked “HM + Sample Code” and “LM + Sample code”. They were then placed in an oven to dry. The “Pure TBE” was poured back in the original TBE bottle using a TBE funnel.

Handpicking and mounting

The dried heavy mineral grains obtained from the heavy liquid separation were placed in a petri-dish. This petri-dish was placed under the microscope. A glass mounting plate with double sided tape was prepared. About 120 zircon grains were handpicked using a needle, from the petri dish to the double sided taped-mount. The zircon grains were placed in a row for each sample. In order to avoid confusion, a mount map was created to distinguish between samples on the mount (Figure 3.27).

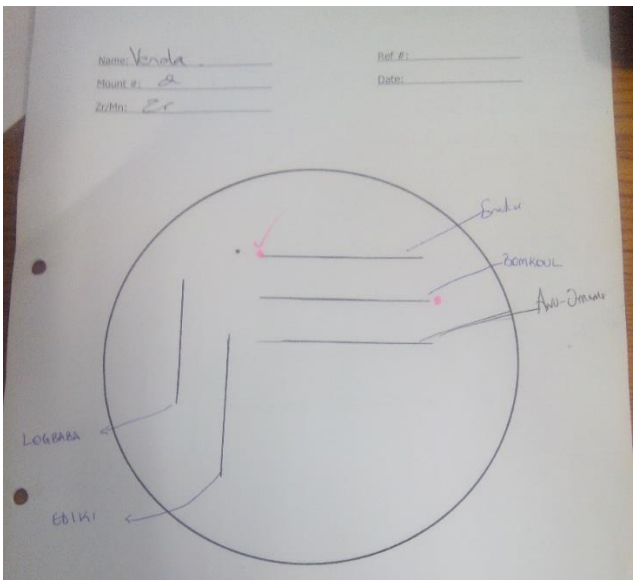

Figure 3.27: Mount map reflecting the location of samples on the mount

After all zircon grains were picked, a mould ring was placed over the mounted grains, and epoxy was poured into the mould. The mould was then placed in an oven to set. Epoxy was obtained by mixing SpeciFix Resin and SpeciFix-40 Curing Agent (2.5 parts of Resin into 1 part of Curing Agent by weight). The curing time was 3 hours and 30 minutes at 50^{o}C. Stirring was done thoroughly for about 5 minutes to avoid the formation of many bubbles.

Polishing

The following day, the mould ring was removed from the oven and the mount was removed from the mould. The sticky residue on the mount's surface, caused by the double sided tape, was removed. A coarse sand paper was made wet, then used to grind the bottom rim of the mount. The mount was then polished using a 3-micron polishing pad and a 3 micron diamond paste for 10 minutes; then using a 1-micron pad and a 1-micron diamond paste for 5 minutes (Table 3.5) using a Struers Rotopol-35 (Figure 3.28). Care was taken not to polish too long in order to avoid very small grains plucking out of the mount.

Figure 3.28: Struers Rotopol-35 used for mount polishing

Table 3.5: Polishing materials and their application

Polishing pad	Composition	Abrasive/grain size	Applicable Suspension	Polishing Time (min)	Application
MD-Dac	Satin woven acetate	Diamond/9-3 µm	DiaPro-Dac3 (3 µm)	3-5	Polishing of all materials
MD-Nap	Synthetic short nap	Diamond, oxide polishing/≤1µm	DiaPro-Nap B1 (1 µm)	3-5	Final polishing of all materials

3.4.3.2 Cathodo-luminescence imaging

After the mounts were polished, they were coated with gold using an S150A sputter coater (Figure 3.29). The gold-coated mounts were then inserted in a Zeiss MERLIN Field Emission Scanning Electron Microscope (FE-SEM) (Figure 3.30). The Zeiss MERLIN Field Emission Scanning Electron Microscope (FE-SEM) was used for the acquisition of cathodo-luminiscence (CL) and backscatter (BS) images of zircon grains. Cathodo-luminescence images distinguished between different zonings in the zircon grains (core and rims); whereas BS images were used to best view parts of the zircon grains that had cracks and holes.

Figure 3.29: S150A sputter coater used for gold coating of mounts

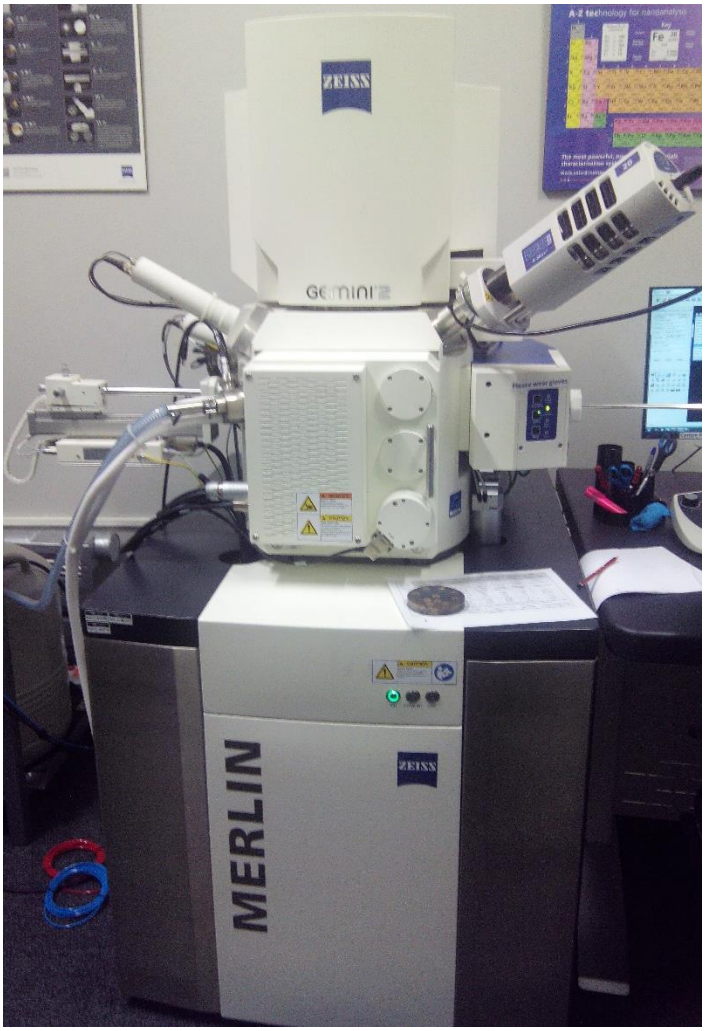

Figure 3.30: Zeiss MERLIN Field Emission Scanning Electron Microscope (FE-SEM) used for CL and BS imaging

3.4.3.3 U-Pb dating for determination of zircon ages

Determined zircon ages were U-Pb ages. These ages were acquired using a laser ablation – single collector – magnetic sector field – inductively coupled plasma – mass spectrometry (LA-SFICP-MS), employing a Thermo Finnigan Element *2* mass spectrometer coupled to a NewWave UP213 laser ablation system (Figure 3.31). The instrumentation and analysis are described in detail by Gerdes and Zeh (2006) and Frei and Gerdes (2009). Data were obtained by single spot analyses, with spots of 30 µm diameter and a crater depth of approximately 15-20 µm. Decision on the location of the spots on the zircon grain to be ablated was taken based on the CL and BS images, by avoiding cracks and holes (using BS images) and by choosing single cores and/or rims (using CL images) in each zircon grain. Each spot was referred to “unknown zircon”.

Figure 3.31: Laser ablation – single collector – magnetic sector field – inductively coupled plasma – mass spectrometer (LA-SFICP-MS) associated to a Thermo Finnigan Element *2* mass spectrometer coupled to a NewWave UP213 laser ablation system

During the analysis of “unknown zircons”, the primary zircon reference material, GJ1 (608 ± 1 Ma) , was also analysed and used for correction of uncertainties due to elemental fractionation and instrumental mass bias on measured isotopic ratios (Jackson *et al*., 2004). The Plešovice zircon (337 ± 1 Ma) (Slama *et al*., 2008) and M127 zircon (524 ± 1 Ma) (Nasdala *et al*., 2016) were equally analysed and used as secondary reference materials for quality control purposes. In order to analyse all six samples, a total of two sequences were analysed. The first sequence was made up of four samples (Bomkoul, Dibamba, Ediki and Logbaba) and the second sequence was made up of two samples (Missole and Yatchika). In the first sequence, 34 GJ1 zircons, 10 Plešovice zircons, seven M127 and 460 “unknown zircons” (zircons from Bomkoul, Dibamba, Ediki and Logbaba kaolins) were analysed; whereas in the second sequence, 18 GJ1 zircons, 15 Plešovice zircons, eight M127 zircons and 199 “unknown zircons’ (zircons from Missole and Yatchika kaolins) were analysed. Each sequence began with three analyses of GJ1 zircon and ended with two or three analyses of GJ1 zircon. The

remaining GJ1 zircons, as well as all Plešovice and M127 zircons were randomly analysed in between analyses of “unknown zircons”.

3.4.3.4 Data processing

The processing of U-Pb data was done using the LA-ICP-MS data reduction software package Iolite v.3.1 (Paton *et al*., 2011), combined with VizualAge (Petrus and Kamber, 2012). A detailed description of the data processing is found in Frei and Gerdes (2009). The calculation of zircon population ages and plotting of weighted average diagrams, were performed using Isoplot/Ex 3.0 (Ludwig, 2003). Zircon ages were reported as $^{206}Pb/^{238}U$ ages for ages < 1300 Ma, and as $^{207}Pb/^{206}Pb$ ages for ages > 1300 Ma. For both primary and secondary reference materials (GJ1, Plešovice and M127), concordant ages were calculated and presented in concordia diagrams. Whereas, for each kaolin sample, a concordia (showing both discordant and concordant ages), a probability density plot (showing different zircon populations) and weighted average plots of each zircon population were displayed. Concordance filters for each plot was as in Table 3.6.

Table 3.6: Plotted diagrams and corresponding discordance rejection and concordance filters

Diagrams	Discordance rejection	Concordance filter
Concordia diagrams for reference materials	> 3 %	97-103
Probability density plots for zircons in kaolin samples	> 10 %	90-110
Weighted average plots for zircons in kaolin samples	> 5 %	95-105
Concordia diagrams for zircons in kaolin samples	No rejection (discordant and concordant ages plotted)	No filter

3.4.4 Diagnostic evaluation

Diagnostic evaluation of samples involved the determination of physical (particle size, texture, colour and moisture content) and physico-chemical (pH and electrical conductivity) characteristics. These analyses were carried out at the Soil Science Laboratory in the School

of Agriculture at University of Venda; except moisture content which was determined at the Extraction & Engineering Metallurgy Laboratory at the University of Johannesburg.

3.4.4.1 Particle size distribution

The particle size distribution of samples was determined using a Microtrac S3500 equipment (Figure 3.32). The system uses a tri-laser system, which in turn uses precise angular measurement of scattered light through a full 180 degree angular range with three lasers and two detector arrays (www.batatekinc.com). A small amount of the sample was placed in the equipment, where a built-in ultrasonic probe is used to disperse the sample and data were generated.

Figure 3.32: Microtrac S3500 used to determine the particle size distribution

3.4.4.2 Texture

The first step to determining the texture of the samples was the determination of different particle size fractions (sand, silt and clay). The hydrometer method was used to achieve this, as described by van Reeuwijk (2002). After carrying out dispersion and mixing the solution for 15 minutes using a milkshake, the dispersed solution was transferred to 1 L sedimentation cylinders (Section 3.3.3) (Figure 3.33). A blank solution was prepared with 20 ml calgon, then poured in a sedimentation cylinder and filled to volume (1 L) with distilled water.

Figure 3.33: Solutions poured in sedimentation cylinders for particle size determination

Each sedimentation cylinder was vigorously shaken for about one minute, then let to settle. Immediately after letting the cylinder to settle, the temperature of the solution was measured in both the solutions containing the sample and the blank, using an alcohol and mercury thermometer. After 5 minutes of settling, the first hydrometer reading was taken in both the solution containing the sample (R_1) and the blank (R_{bl1}), and recorded. The second hydrometer reading was taken after two hours for both the solutions containing the sample (R_2) and the blank (R_{bl2}), and recorded. At each hydrometer reading, the temperature of both solutions were taken. Hydrometer readings were taken after dropping an ASTM 152H soil hydrometer in the solution and letting it rise and stabilise in the solution. The time between each reading was recorded using a stopwatch.

Hydrometer readings from the solution containing the sample (R_1 and R_2) were corrected using readings from the blank using the equation below (van Reeuwijk, 2002):

$$C_n = R_n - R_{bln} \qquad \text{Eqn 3.5}$$

Where, *n* is 1 or 2 (first or second reading)

The summation percentage of clay particles (P_{Clay}) was determined using Equation 3.6.

$$P_{Clay} = \frac{C_2}{50} \times 100$$ Eqn 3.6

The summation percentage of silt particles (P_{Silt}) was determined using Equation 3.7.

$$P_{Silt} = \frac{C_1}{50} \times 100$$ Eqn 3.7

The summation percentage of sand particles (P_{Sand}) was determined using Equation 3.8.

$$P_{Sand} = 100 - (P_{Clay} + P_{Silt})$$ Eqn 3.8

Where, 50 stands for the mass of the sample before removal of organic matter (Section 3.3.2),

C_2 is the corrected R_2 reading,

C_1 is the corrected R_1 reading.

The second step was to plot the different particle size percentages (P_{Sand}, P_{Silt} and P_{Clay}) in a texture triangle (Figure 3.34). The texture of each sample corresponds to the field in which the sample plotted.

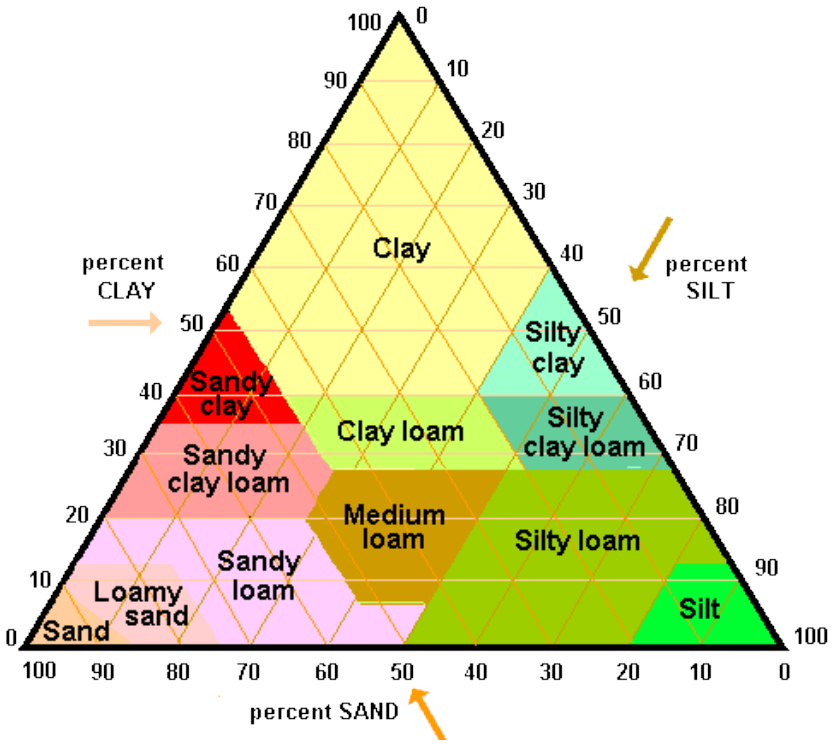

Figure 3.34: Texture triangle showing different textures based on particle sizes

3.4.4.3 Colour

The colour of samples was determined using the Munsell ® Soil Colour Charts (2000). These charts use the Munsell Colour System (Figure 3.35), which is based on three attributes, being hue, value and chroma (Torrent and Barrón, 1993). The hue is the angular displacement from an arbitrary position. It is also known as the specific colour of the sample; the valueis the vertical distance to the basal plane of the sample; and the chroma is the distance to the central black-white axis.

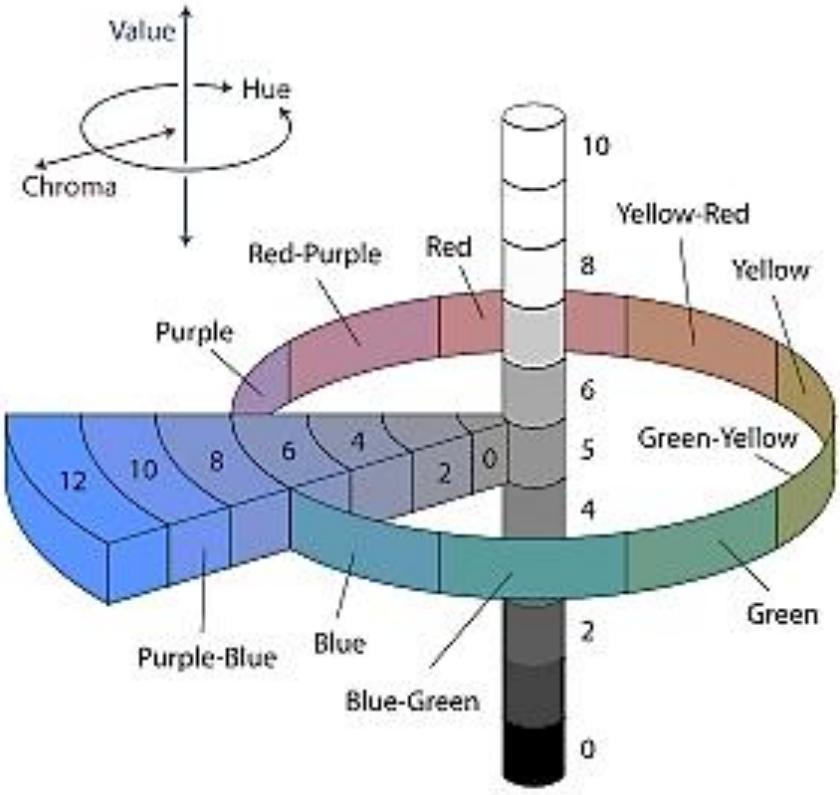

Figure 3.35: Munsell colour system

Each sample was placed on a white paper and was visually compared with soil colours in the Munsell Soil Colour Charts to obtain its hue, value and chroma characteristics (Matike *et al*., 2011). The colour of the sample was then deduced from its characteristics.

3.4.4.4 Moisture content

The method used to determine the moisture content was the method described by van Reeuwijk (2002). Five grams of each sample was weighed in a 2.11 g tin. The samples were

heated in an oven for 24 hours at 105°C. After removing the samples from the oven, they were placed in a desiccator in order to preserve the moisture (Figure 3.36). Each sample was weighed again to note the weight difference. The moisture content (MC) was calculated using Equation 3.9 (van Reeuwijk, 2002).

$$MC = \frac{m_2 - m_3}{m_3 - m_1} x100 \qquad \text{Eqn 3.9}$$

Where, MC is the moisture content

m_1 is the mass of tin (g)

m_2 is the mass of wet kaolin + tin (g)

m_3 is the mass of dry kaolin + tin (g)

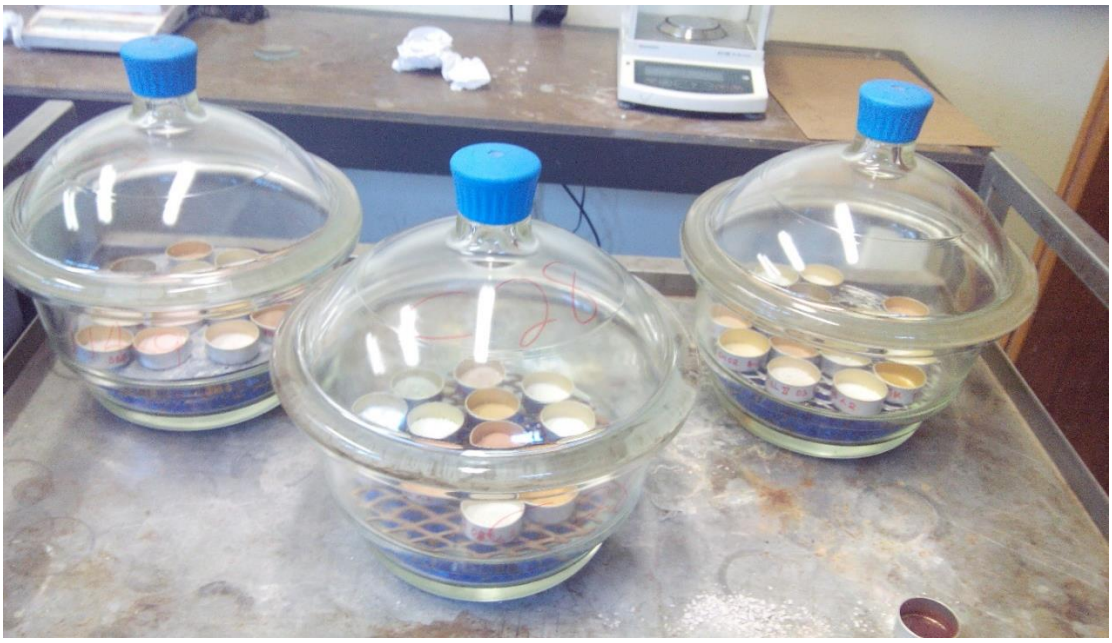

Figure 3.36: Samples placed in desiccators after heating for 24 hours

3.4.4.5 pH

The pH was determined using the method modified from that described in The Non-Affiliated Soil Analysis Working Committee (1990). Prior to measurements, a Crison BasiC 20 pH meter (Figure 3.37) was calibrated with buffers of pH = 7 and pH = 4.

Ten grams of dry sample (< 2 mm) was weighed and placed in a beaker. 50 ml of 1 M potassium chloride (KCl) solution (74.5 g KCl dissolved in 1 L of distilled water) was added in the beaker. The mixture was stirred rapidly for 5 seconds, using a glass rod then allowed to

stand. After 50 minutes, the mixture was stirred again, then allowed to stand for 10 minutes. Then the pH was measured with the calibrated pH meter, with the electrodes placed in the supernatant.

Figure 3.37: Crison BasiC 20 pH meter

3.4.4.6 Electrical conductivity

Prior to measurement, a Crison BasiC 30 Conductimeter was calibrated using a standard of EC = 1413 µS/cm at a temperature of 25^{o}C (Figure 3.38). The EC was determined by weighing 10 g of each sample and placing it in a beaker. Distilled water was then added to the sample and the mixture was vigorously stirred using a glass rod. The EC was then measured using the calibrated conductimeter, with the electrode placed in the supernatant.

Figure 3.38: The Crison BasiC 30 Conductimeter being calibrated

3.4.5 Quality assurance

The following measures were taken for quality assurance:

Precautions were taken during sampling to avoid contamination by other samples.
During sample preparation, all instruments (mortar, sieves, pestle, glass rods, beaker, milkshake mixer, etc.) were thoroughly cleaned with distilled water before using them for other samples, in order to avoid contamination.
For most analyses (those related to abundance quantification), a duplicate coded sample of MSL II 01 < 2 µm (MSL II 03) was analysed.

3.5 Data analysis

Data analyses were carried out using several programs such as Excel 2013 for basic plots, Origin Pro 8 for XRD Diffractograms, FTIR spectra and particle size distribution, Triplot version 2 for all ternary diagrams excluding texture and ProSim Ternary Diagram for texture analysis.

Several indices, ratios and geochemical discrimination plots were used for data interpretation. These are, but are not restricted to:

3.5.1 Weathering indices

From the oxides determined by ICP-MS, chemical weathering indices or alteration indices (chemical index of alteration (CIA), chemical index of weathering (CIW), index of compositional variability (ICV) and silica-titania index (STI)) were calculated (Equations 3.10-3.12). These indices are commonly used for characterising modern and ancient weathering profiles and as proxies to subtle geochemical changes such as hydrothermal alteration along a fault and/or alteration at the water table (Price and Velbel, 2003). For example, very strong chemical weathering implies specific paleoclimatic conditions (humid and warm) in the source area (López *et al*., 2005).

The CIA is interpreted as a measure of the extent of the conversion of feldspar to clays and it is a good measure of the degree of weathering (Shao *et al*., 2012). It is defined as:

$$CIA = \left[\frac{Al_2O_3}{Al_2O_3+CaO+Na_2O+K_2O}\right] x\ 100$$ (Nesbitt and Young, 1982) (Eqn. 3.10)

The CIW is defined as:

$$CIW = \left[\frac{Al_2O_3}{Al_2O_3+CaO+Na_2O}\right] x\ 100$$ (Fiantis *et al*., 2010) (Eqn. 3.11)

The ICV is used to measure the abundance of Al_2O_3 relative to the other major oxides in the kaolins. It is defined in Equation 3.12, in which SiO_2 is excluded to eliminate problems of quartz dilution (Cox *et al*., 1995).

$$\mathrm{ICV} = \frac{\mathrm{CaO+K_2O+Na_2O+Fe_2O_3(t)+MgO+MnO+Ti_2O}}{\mathrm{Al_2O_3}}$$ (Cox *et al*., 1995) (Eqn.3.12)

For calculation of these indices, all values are in molar contents, with CaO being the amount of CaO incorporated in the silicate fraction of the rock.

3.5.2 Elemental ratios

La/Sc, Th/Co, Th/Sc, Zr/Sc and Cr/Th ratios

The La/Sc, Th/Co, Th/Sc, Zr/Sc and Cr/Th ratios when compared with the Upper Continental Crust (UCC) values can be used to determine the source-area composition (Taylor and McLennan, 1985) of kaolins.

3.5.3 Geochemical discrimination diagrams

Binary and ternary scatter plots of selected element abundances were used as “geochemical discrimination diagrams” for inferring the character or tectonic setting of source rocks to a clastic sedimentary basin and the amount of weathering that the detrital sediments have undergone (Baioumy *et al*., 2014). These plots (Figures 3.39 to 3.41) include the TiO_2/Al_2O_3 binary plot (Ekosse, 2001), the La-Th-Sc ternary diagram and the Th/Co vs La/Sc binary plot (López *et al*., 2005).

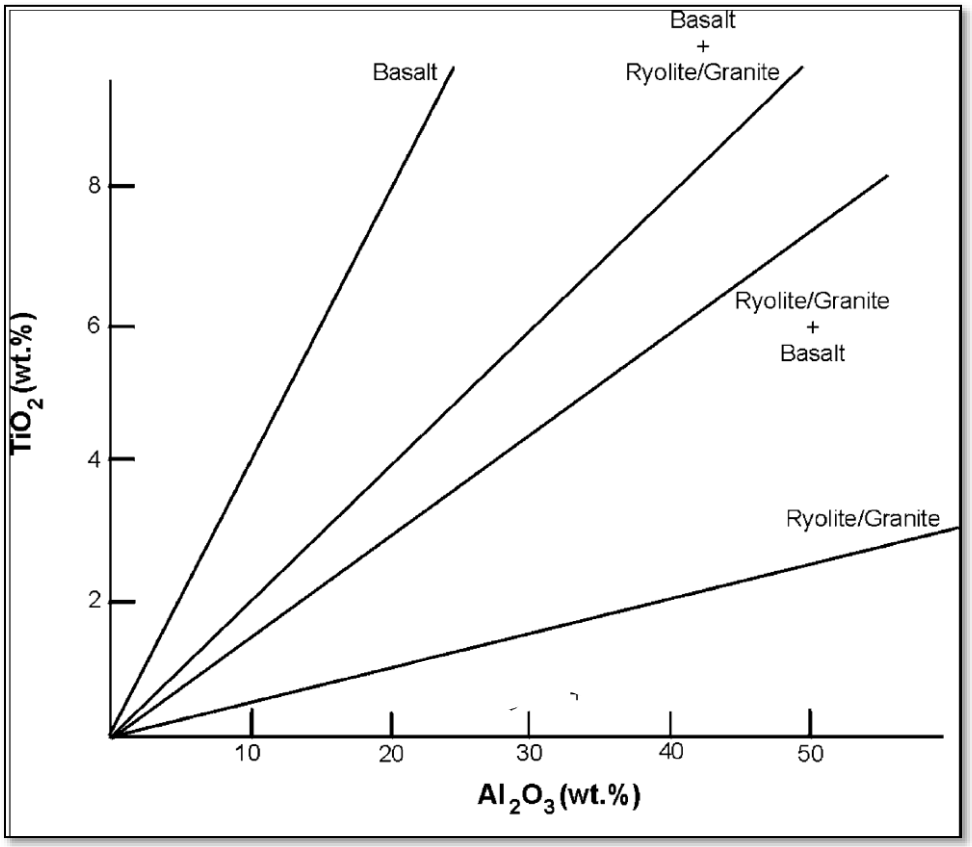

Figure 3.39: TiO_2/Al_2O_3 binary plot of kaolinitic samples (Modified from Ekosse, 2001)

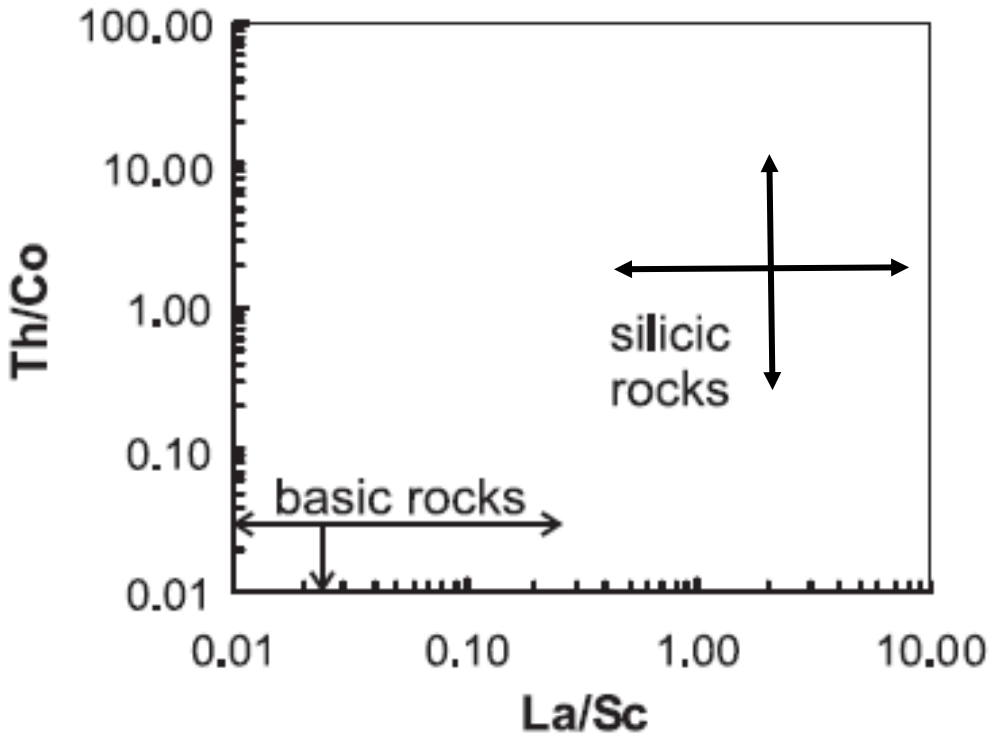

Figure 3.40: Th/Co vs La/Sc binary plot (Modified from López *et al*., 2005)

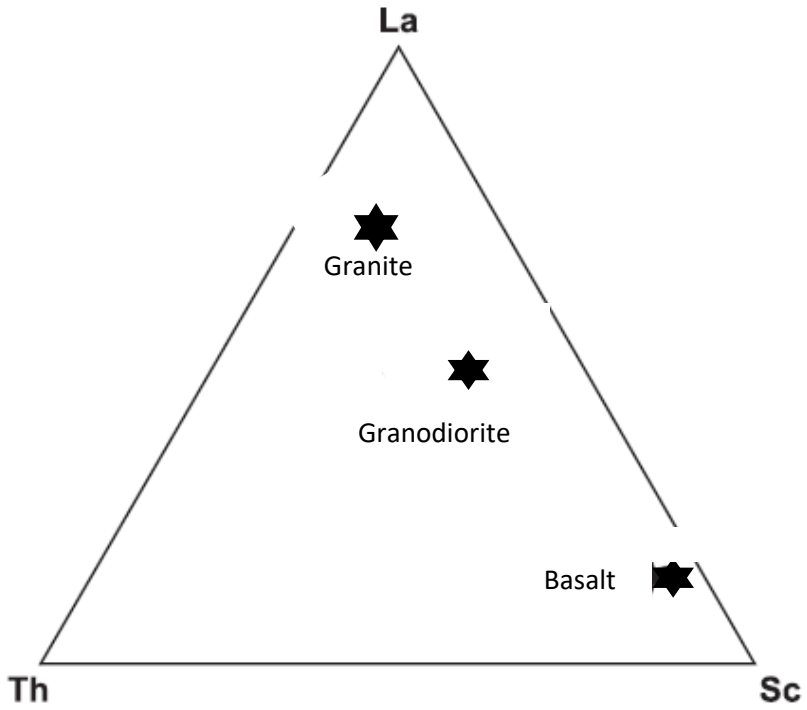

Figure 3.41: La-Th-Sc ternary diagram (Modified from López *et al*., 2005)

3.6 Concluding remarks

This chapter presented the different methods that were used from field work to data analysis through laboratory analyses. Several precautions, listed under quality assurance, were taken to ensure the reliability of the results.

CHAPTER 4

NATURE AND OCCURRENCES OF CRETACEOUS-TERTIARY KAOLINS: MINERALOGICAL AND GEOCHEMICAL CHARACTERISATION

4.1 Preamble

The objective of this chapter is to investigate the nature and occurrence of Cretaceous-Tertiary kaolins in the Douala Sub-Basin, by carrying out a thorough mineralogical and geochemical characterisation of kaolins of selected kaolin deposits (Specific Objective A). It presents a field description and reports on the mode of occurrence and characteristics of the mineralogy and geochemistry of bulk, silt and < 2 µm samples of studied Cretaceous-Tertiary kaolins in Douala Sub-Basin. The quantification of the mineral phases present, the morphology and the functional groups in the kaolins are presented as the mineralogical characteristics of kaolins of each study site; whereas, the major oxides geochemistry and the micro-elemental composition constitute the geochemical characteristics of these kaolins. This chapter is based on Hypothesis A.

HYPOTHESIS A: The studied Cretaceous-Tertiary kaolin deposits in Cameroon have similar mineralogical and geochemical characteristics.

4.2 Field description of studied kaolins

4.2.1 Bomkoul kaolin

The exposure of the studied Bomkoul kaolin occurrence varied between 80 cm to ~1.5 m thick, with no distinct horizons (Figure 4.1). Bomkoul kaolins are characterised by three facies (mottled, grey and dark grey clayey materials) with generally fine particles (Ngon Ngon *et al*., 2012b). The area is found in the Cameroon coastal plain, which is characterised by hills with flat and sharp summits and is deeply dissected by V- and U-shaped valleys (Ngon Ngon *et al*., 2012b).

Figure 4.1: Bomkoul kaolin occurrence showing the mottled texture of the kaolin

4.2.2 Dibamba kaolin

Dibamba kaolin is embedded in the Dibamba Sandstone deposit 1.5 to 3 m thick. The Dibamba Sandstone deposit occurs as layers 1mm to few centimetres thick of yellowish, pinkish, reddish and whitish sandstones. The embedded kaolins occur as whitish layers (5-10 cm thick) and nodules, and they have a soapy feel. The whitish layers are found between two reddish sandstone layers, whereas the nodules are surrounded by yellowish or pinkish layers (Figure 4.2). In some places of the outcrops, the different laminae and layers of sandstones are deposited in a cross-bedding structure (Figure 4.3).

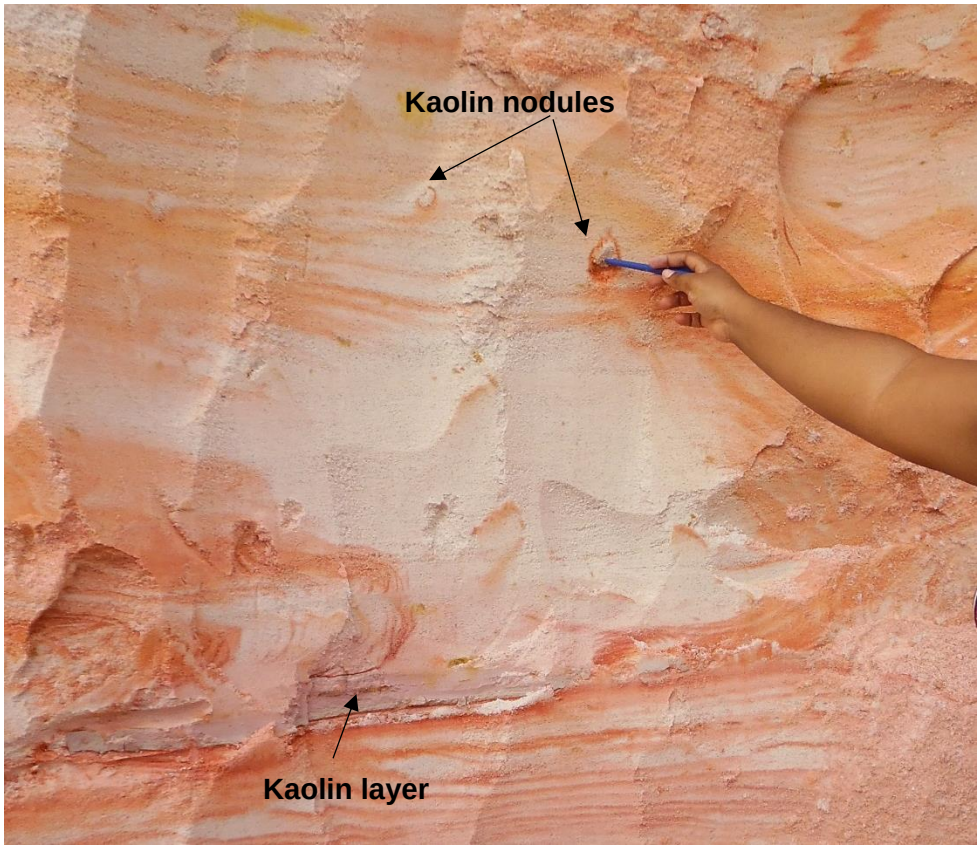

Figure 4.2: Kaolin layer and nodules occurring in Dibamba sandstones

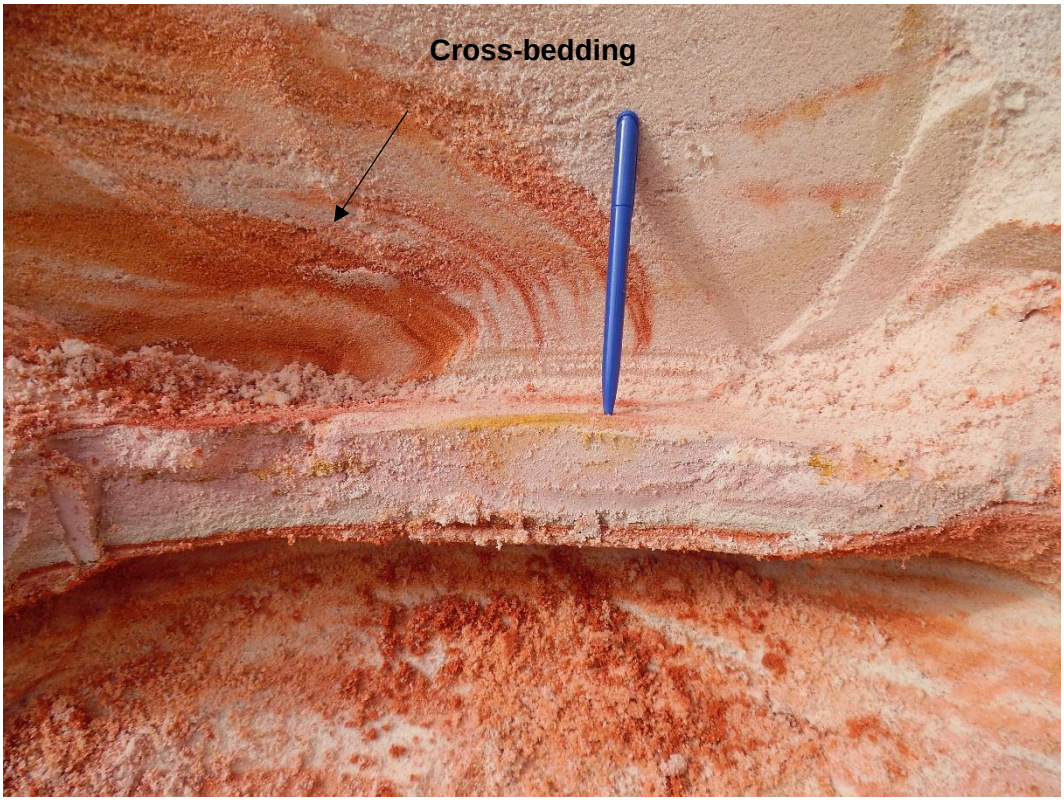

Figure 4.3: Cross-bedding occurring in Dibamba sandstones

4.2.3 Ediki kaolin

Ediki kaolin is embedded in the Ediki Sandstone deposit varying between 2 - 3 metres thick. The Ediki Sandstones are weathered grey to greenish sandstone unit with a gradient of 35 to 40° (Diko and Ekosse, 2013). The thickness of the studied kaolin occurrence varied between 30-60 cm. Though there are no clear profiles in these outcrops, the kaolins can be distinguished into two main facies, as described by Diko and Ekosse (2013); namely, a sand-rich facies and a sand-poor facies. The latter is pink, orange and grey (Figure 4.4). Whereas the former is greyish green (Figure 4.5).

Figure 4.4: Sandy kaolins at Ediki

Figure 4.5: Clayey kaolins at Ediki

4.2.4 Logbaba kaolin

Logbaba kaolin in found in Logbaba, which is a gas field. The gas condensate is found in Campanian and Santonian sandstones reservoirs of the Logbaba Formation (Blackwatch, 2016). These sandstones source rocks are capped by shales, which also make up the Logbaba Formation. Though few studies (reports) have been made on the Logbaba gas field, none reported on the kaolins in this Formation. The studied outcrop of the Logbaba kaolins is a whitish outcrop. The deposit, of about 5 metres high and 16 metres wide (Figure 4.6), is made up of clayey sand with no distinct profiles (Figure 4.7).

Figure 4.6: Logbaba kaolin outcrop

Figure 4.7: White clayey sands in Logbaba

4.2.5 Missole kaolins

Missole is found in the Cameroon coastal plain, having low altitudes (40-120 m). The geomorphology shows hills with flat and sharp summits and is deeply dissected by V and U shape valleys, with MBongo, Bongougou, Missolo and Bongo being the main rivers in the area (Ngon Ngon *et al*., 2012b). Two facies were distinguished in the area: a dark grey sand-rich kaolin at Missole I, and a white clay-rich kaolin at Missole II. The dark grey sand-rich kaolin is about 70 cm thick and outcrops on the road side. It is overlain by sandstones (Figure 4.8). Whereas, the white clay-rich kaolin is found close to a spring and it is about 50 cm thick (Figure 4.9).

Figure 4.8: Dark grey sand-rich kaolin occurring at Missole I

Figure 4.9: White clay-rich kaolin occurring at Missole II

4.2.6 Yatchika kaolin

Yatchika kaolin has an exposure of ~5 m high and 20 m wide with an overburden of about 10 cm thick. The deposit is mainly characterised by alternating layers of reddish white and brown kaolins and layers of white and pink kaolins (Figure 4.10). The former show weak kaolinisation. Where there is alternation, these layers are separated by a thin iron-rich layer (Figure 4.11).

Figure 4.10: Layer of kaolins with pink tints occurring at Yatchika

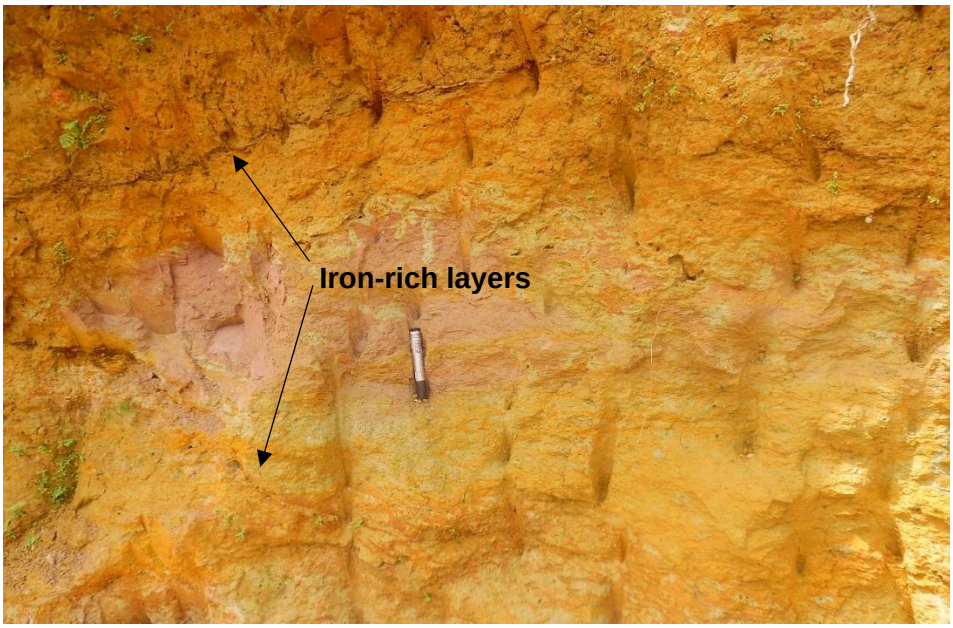

Figure 4.11: Iron-rich layer within the Yatchika kaolins

4.3 Mineralogical characterisation

4.3.1 Mineral phases present in the studied kaolins

4.3.1.1 Qualitative analysis

Diffractograms of samples are shown in Figures 4.12-4.25. The qualitative analysis of kaolin samples did not show great variations between mineral phases present in bulk, silt and < 2 µm samples. Mineral phases present were anatase, goethite, illite, kaolinite, quartz, rutile and smectite. In addition, Ediki samples were the only ones containing microcline and Yatchika samples were the only ones containing hematite (Table 4.1).

Table 4.1: Minerals identified by XRD in Cretaceous-Tertiary kaolins in the Douala Sub-Basin

Name of mineral	Compound name	Chemical formula	Main diagnostic peaks (dÅ)
Anatase	Titanium oxide	TiO_2	3.51
Goethite	Iron oxide hydroxide	$FeO(OH)$	4.15
Hematite	Iron oxide	Fe_2O_3	2.71
Illite	Potassium magnesium aluminum silicon oxide hydroxide hydrate	$K_{0.78}Mg_{0.34}Al_{2.34}Si_{3.35}O_{10}(H_2O)_{0.15}$	4.32, 9.94, 4.47
Kaolinite	Aluminum silicate hydroxide	$Al_2Si_2O_5(OH)_4$	7.13, 4.36, 4.16, 3.57
Microcline	Potassium aluminum silicate	$K(AlSi_3O_8)$	4.22, 3.24
Quartz	Silicon oxide	SiO_2	4.25, 3.34
Rutile	Titanium oxide	TiO_2	3.25
Smectite	Calcium aluminum magnesium silicate hydroxide hydrate	$Na_{0.3}(Al,Mg)Si_4O_{10}(OH)_{2\cdot x}H_2O$	12.52
	Sodium aluminum magnesium silicate hydroxide hydrate	$Ca_{0.2}(Al,Mg)_2Si_4O_{10}(OH)_{2\cdot 4}H_2O$	15, 5.01, 4.50

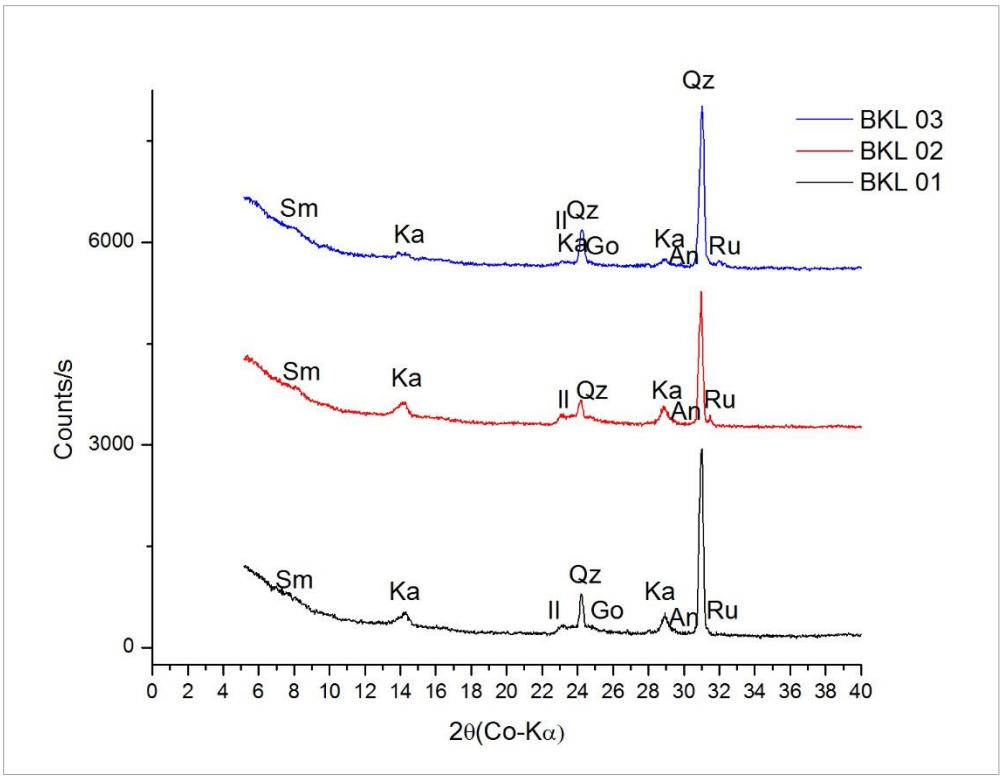

Figure 4.12: Diffractograms of Bomkoul bulk samples. An: Anatase, Go: Goethite, Il: Illite, Ka: Kaolinite, Qz: Quartz, Ru: Rutile, Sm: Smectite

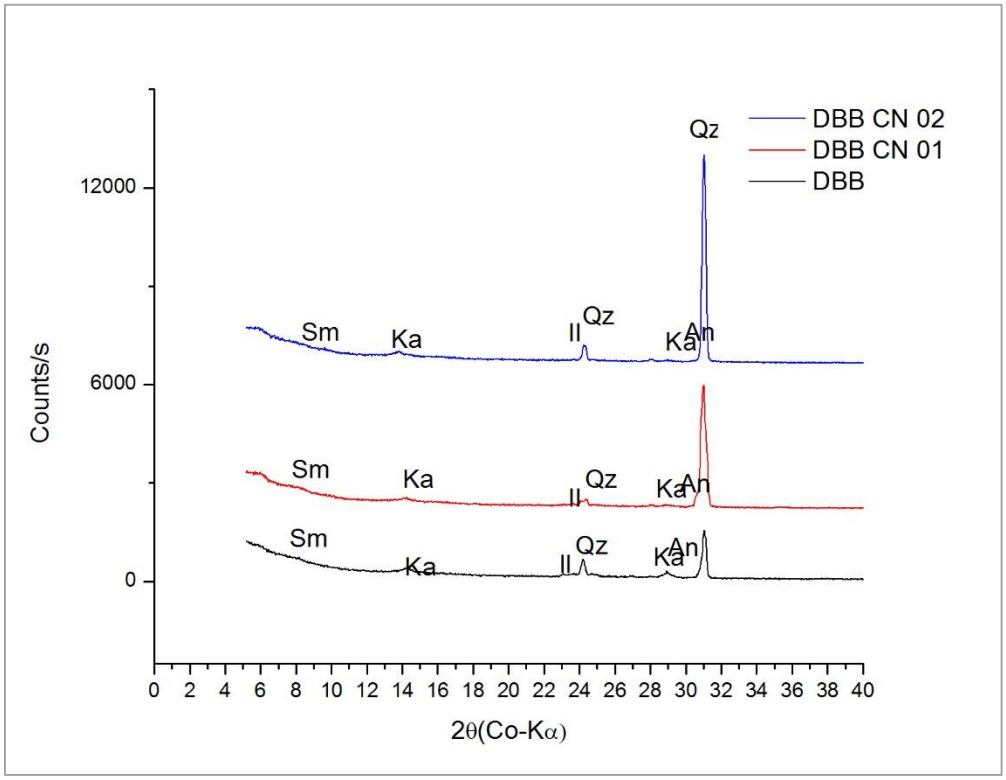

Figure 4.13: Diffractograms of Dibamba bulk samples. An: Anatase, Il: Illite, Ka: Kaolinite, Qz: Quartz, Sm: Smectite

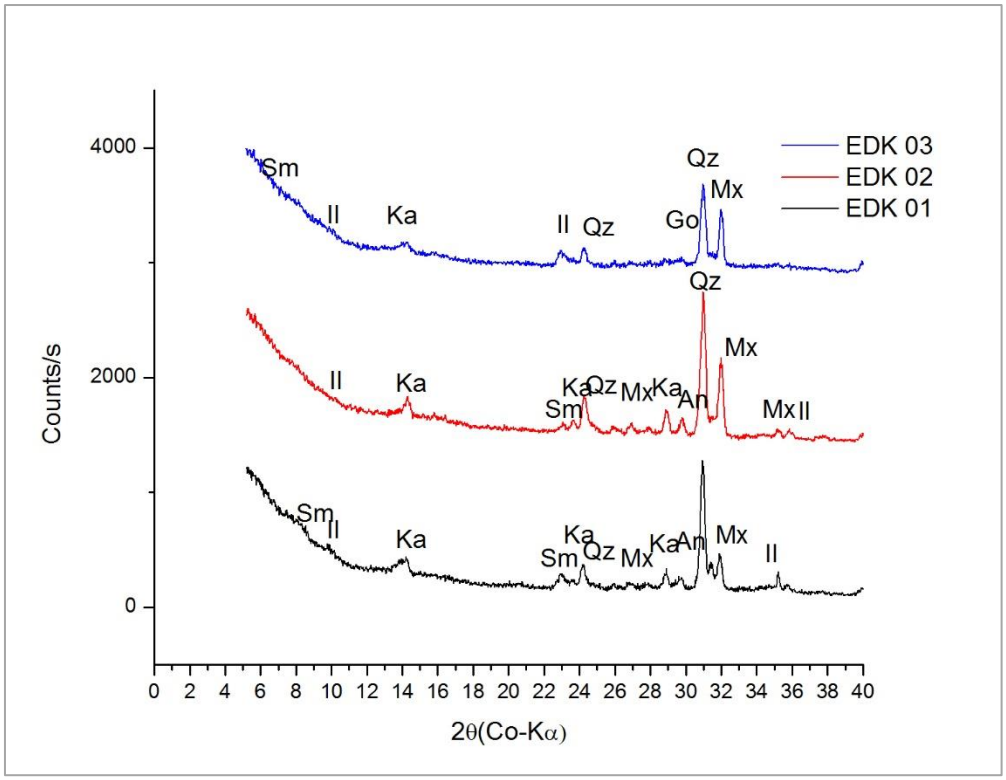

Figure 4.14: Diffractograms of Ediki bulk samples. An: Anatase, Go: Goethite, Il: Illite, Ka: Kaolinite, Mx : Microcline, Qz: Quartz, Ru: Rutile, Sm: Smectite

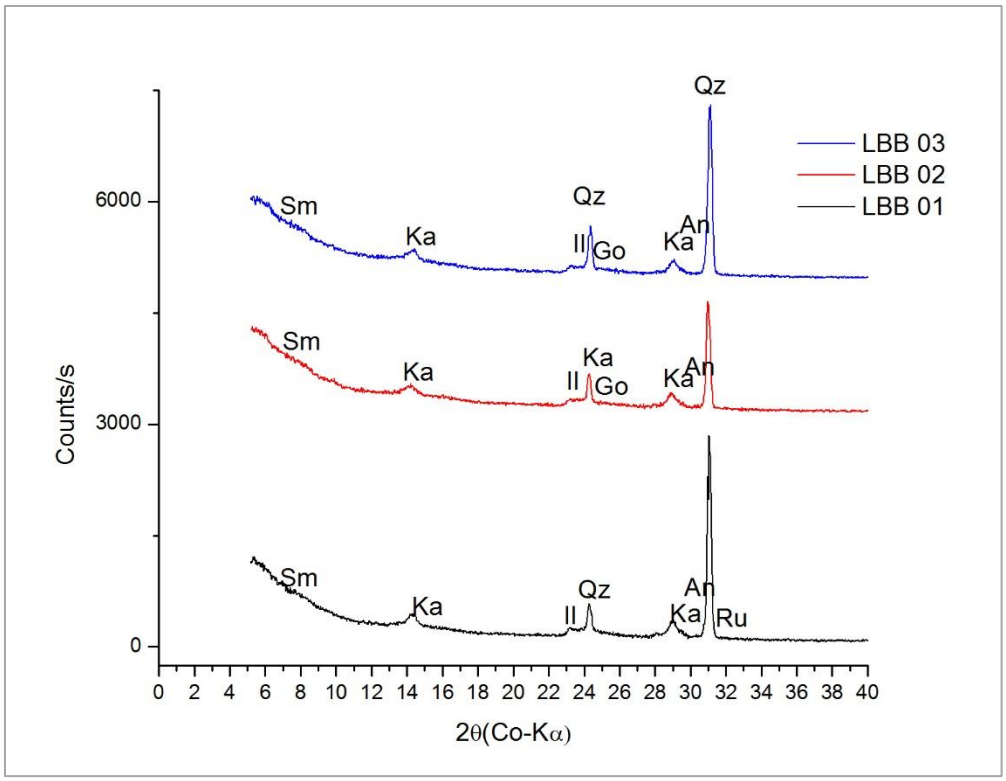

Figure 4.15: Diffractograms of Logbaba bulk samples. An: Anatase, Go: Goethite, Il: Illite, Ka: Kaolinite, Qz: Quartz, Ru: Rutile, Sm: Smectite

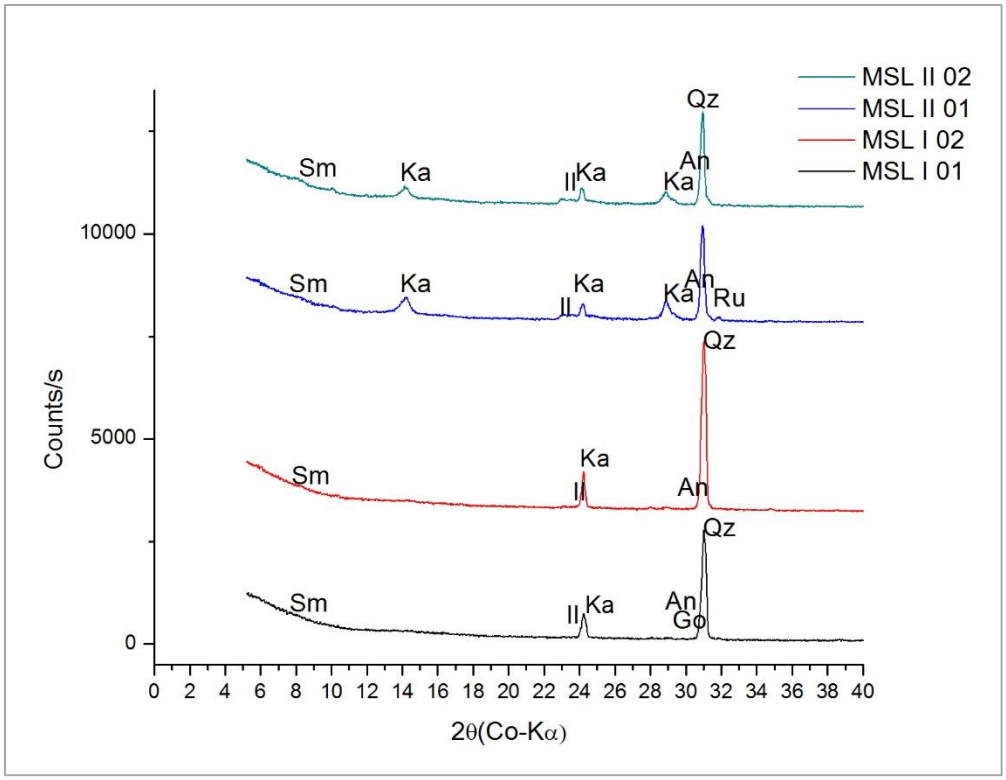

Figure 4.16: Diffractograms of Missole bulk samples. An: Anatase, Go: Goethite, Il: Illite, Ka: Kaolinite, Qz: Quartz, Ru: Rutile, Sm: Smectite

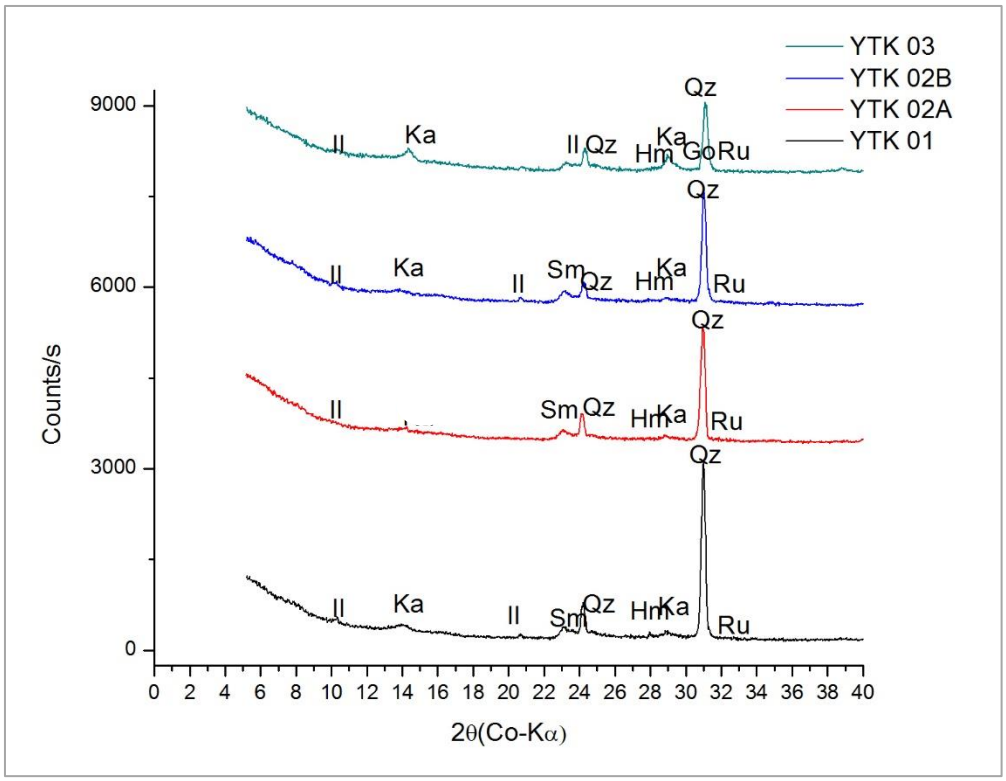

Figure 4.17: Diffractograms of Yatchika bulk samples. An: Anatase, Go: Goethite, Hm: Hematite, Il: Illite, Ka: Kaolinite, Qz: Quartz, Ru: Rutile, Sm: Smectite

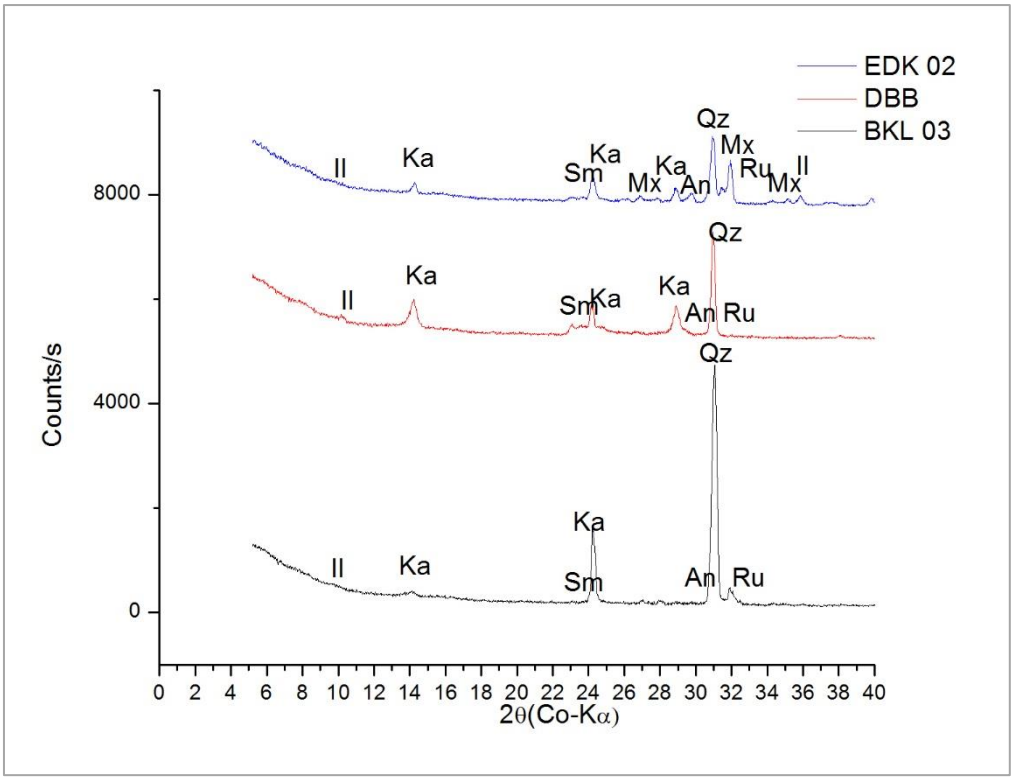

Figure 4.18: Diffractograms of BKL 03, DBB and EDK 02 silt samples. An: Anatase, Go: Goethite, Il: Illite, Ka: Kaolinite, Qz: Quartz, Ru: Rutile, Sm: Smectite

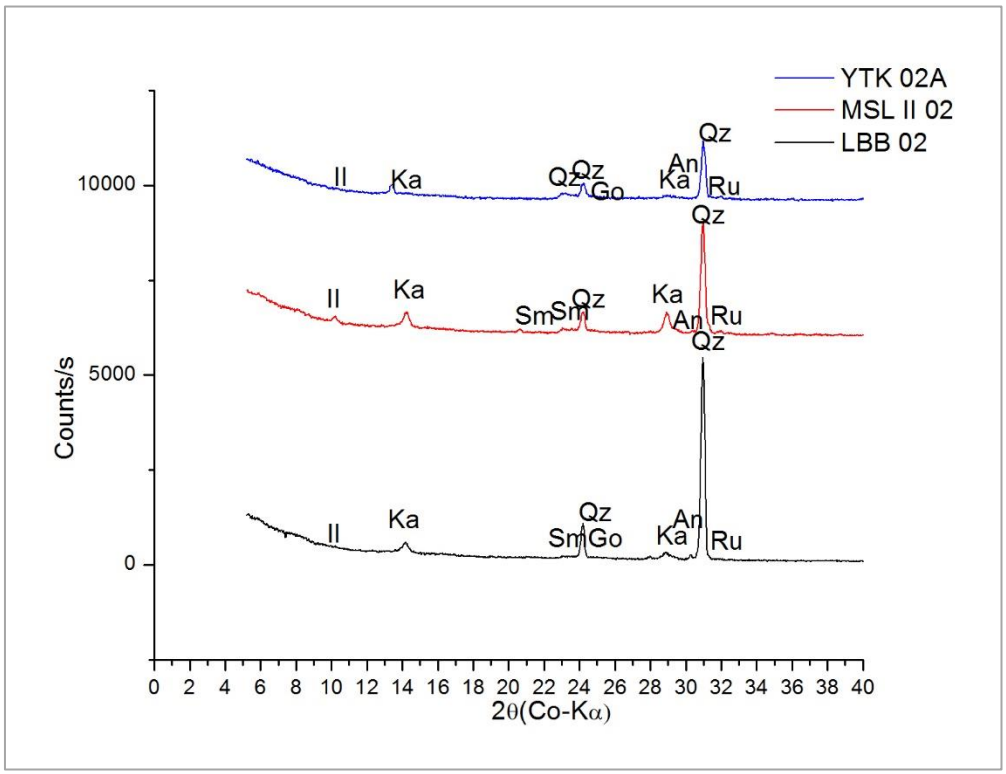

Figure 4.19: Diffractograms of LBB 02, MSL II 02 and YTK 02A silt samples. An: Anatase, Go: Goethite, Il: Illite, Ka: Kaolinite, Qz: Quartz, Ru: Rutile, Sm: Smectite

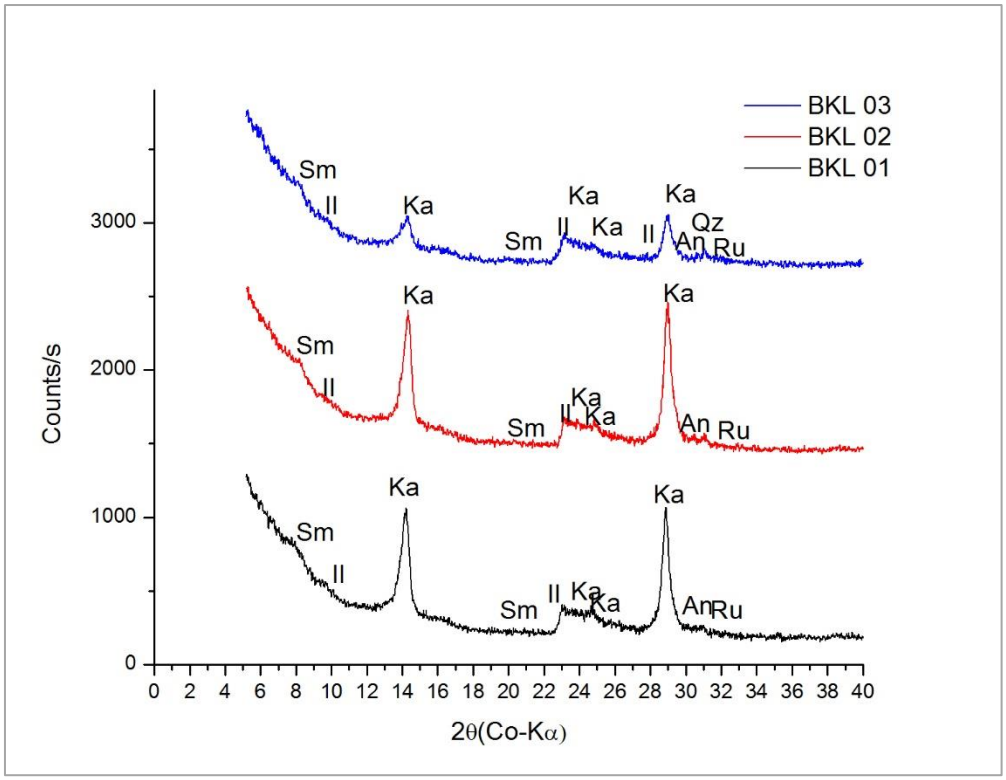

Figure 4.20: Diffractograms of Bomkoul < 2 µm fraction samples. An: Anatase, Go: Goethite, Il: Illite, Ka: Kaolinite, Qz: Quartz, Ru: Rutile, Sm: Smectite

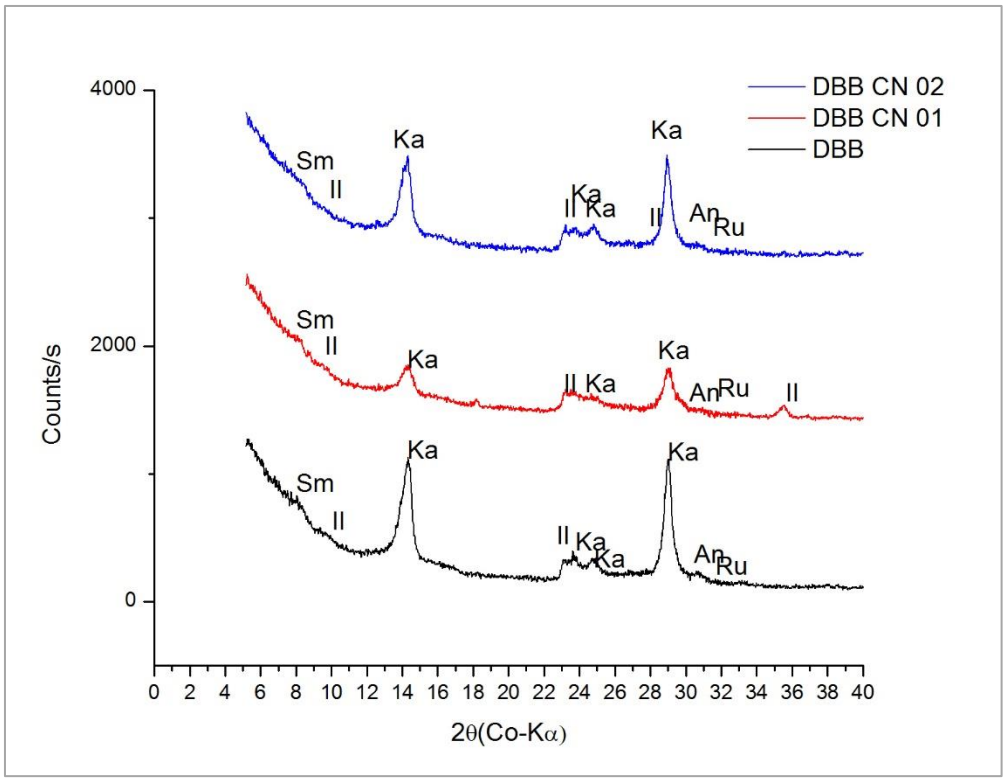

Figure 4.21: Diffractograms of Dibamba < 2 µm fraction samples. An: Anatase, Go: Goethite, Il: Illite, Ka: Kaolinite, Qz: Quartz, Ru: Rutile, Sm: Smectite

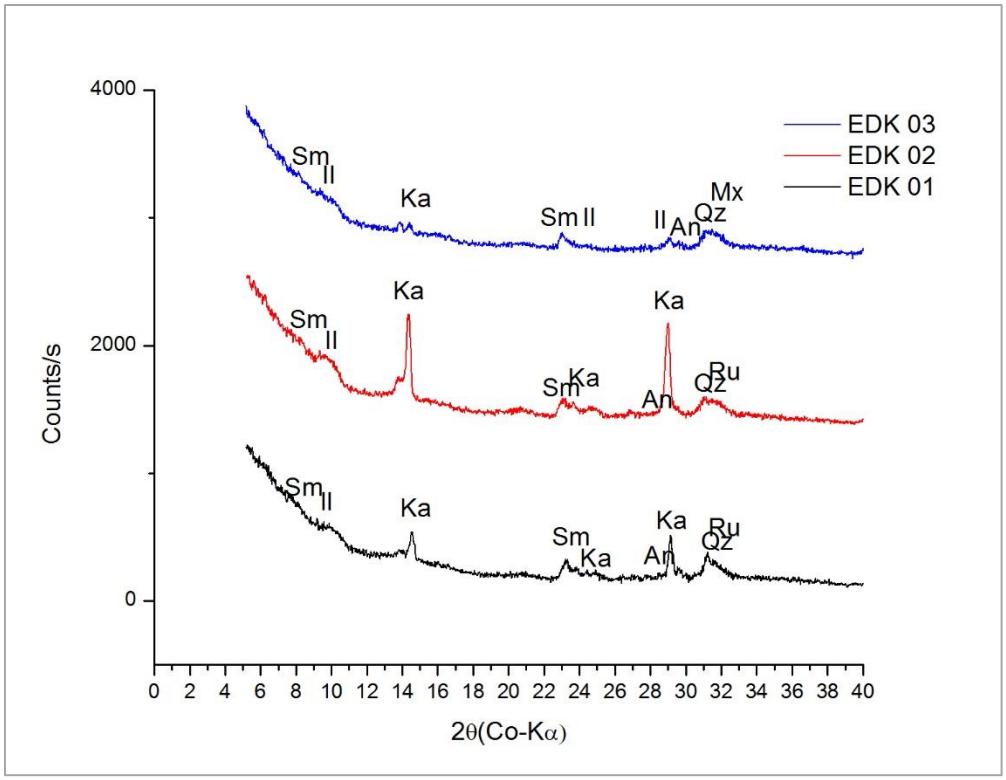

Figure 4.22: Diffractograms of Ediki < 2 µm samples. An: Anatase, Go: Goethite, Il: Illite, Ka: Kaolinite, Mx: Microline, Qz: Quartz, Ru: Rutile, Sm: Smectite

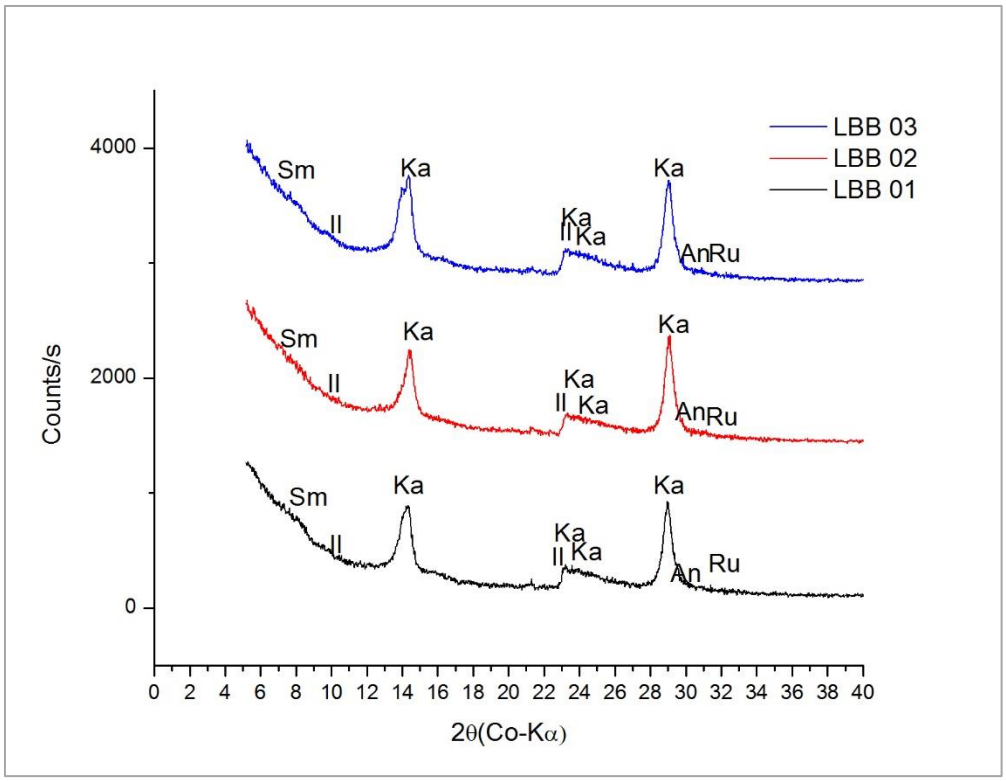

Figure 4.23: Diffractograms of Logbaba < 2 µm samples. An: Anatase, Go: Goethite, Il: Illite, Ka: Kaolinite, Qz: Quartz, Ru: Rutile, Sm: Smectite

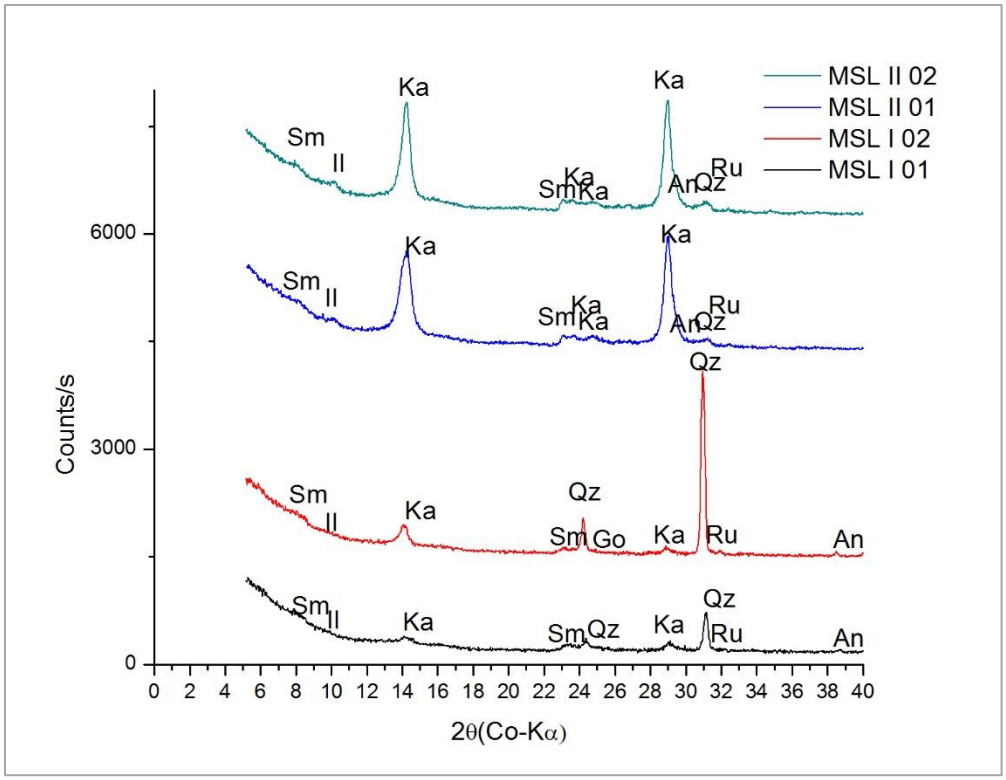

Figure 4.24: Diffractograms of Missole < 2 µm samples. An: Anatase, Go: Goethite, Il: Illite, Ka: Kaolinite, Qz: Quartz, Ru: Rutile, Sm: Smectite

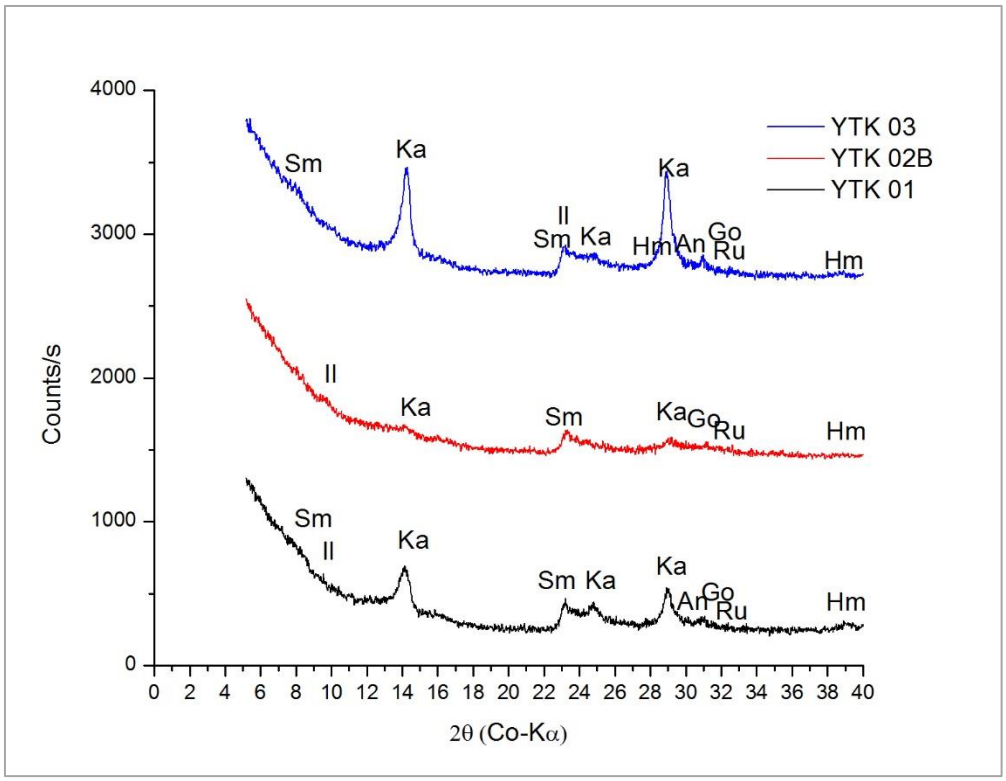

Figure 4.25: Diffractograms of Yatchika < 2 µm samples. An: Anatase, Go: Goethite, Hm: Hematite, Il: Illite, Ka: Kaolinite, Qz: Quartz, Ru: Rutile, Sm: Smectite

4.3.1.2 Semi-quantitative and quantitative analyses

Bulk kaolins (< 2 mm fraction)

Results of semi-quantitative and quantitative analyses of minerals identified in bulk Cretaceous-Tertiary kaolin samples in the Douala Sub-Basin are shown in Appendix 4.1 and Table 4.2.

Table 4.2: Results of semi-quantitative analysis of minerals identified in bulk samples

	Kaolinite	Illite	Smectite	Quartz	Microcline	Anatase	Rutile	Goethite	Hematite
BKL 01	+++	++	++	+++	-	++	+	+	-
BKL 02	+++	++	++	+++	-	++	+	-	-
BKL 03	+++	++	+++	+++	-	+	+	++	++
DBB	+++	++	++	+++	-	+	-	++	-
DBB CN 01	+++	++	++	+++	-	++	-	-	-
DBB CN 02	++	++	++	+++	-	+	-	-	-
EDK 01	+++	+++	+++	+++	-	++	++	-	-
EDK 02	+++	++	++	+++	+++	+	+	+	-
EDK 03	+++	++	++	+++	+++	++	++	-	-
LBB 01	+++	++	++	+++	-	++	+	-	-
LBB 02	+++	++	++	+++	-	++	-	++	-
LBB 03	+++	++	++	+++	-	++	-	+	-
MSL I 01	+++	+	++	+++	-	+	-	+	-
MSL I 02	++	++	++	+++	-	+	-	-	-
MSL II 01	+++	++	++	+++	-	++	-	-	-
MSL II 02	+++	++	++	+++	-	++	-	-	-
YTK 01	+++	+++	++	+++	-	+	+	++	+
YTK 02A	+++	++	+++	+++	-	++	+	++	+
YTK 02B	+++	+++	+++	+++	-	+	+	+	+
YTK 03	+++	++	++	+++	-	++	+	++	++

(+++) Major, (++) Minor, (+) Trace, (-) Not detected

Samples BKL 01, BKL 02, DBB, LBB 01, LBB 02, MSL II 01, MSL II 02, YTK 01, YTK 02B and YTK 03 had kaolinite and quartz as the most abundant mineral phase with abundances of

55.82, 57.64, 53.5, 50.23, 53.8, 52.43, 55.9, 41.50, 46.24 and 58.43 wt %, respectively; constituting 50 % of the samples (Figure 4.26). Smectite was the second most dominant clay mineral, with abundances of 35.53 and 38.07 wt % for EDK 01 and EDK 03, respectively (Figure 4.27), constituting 10% of the samples. Illite was most dominant in EDK 01 (12.24 wt %).

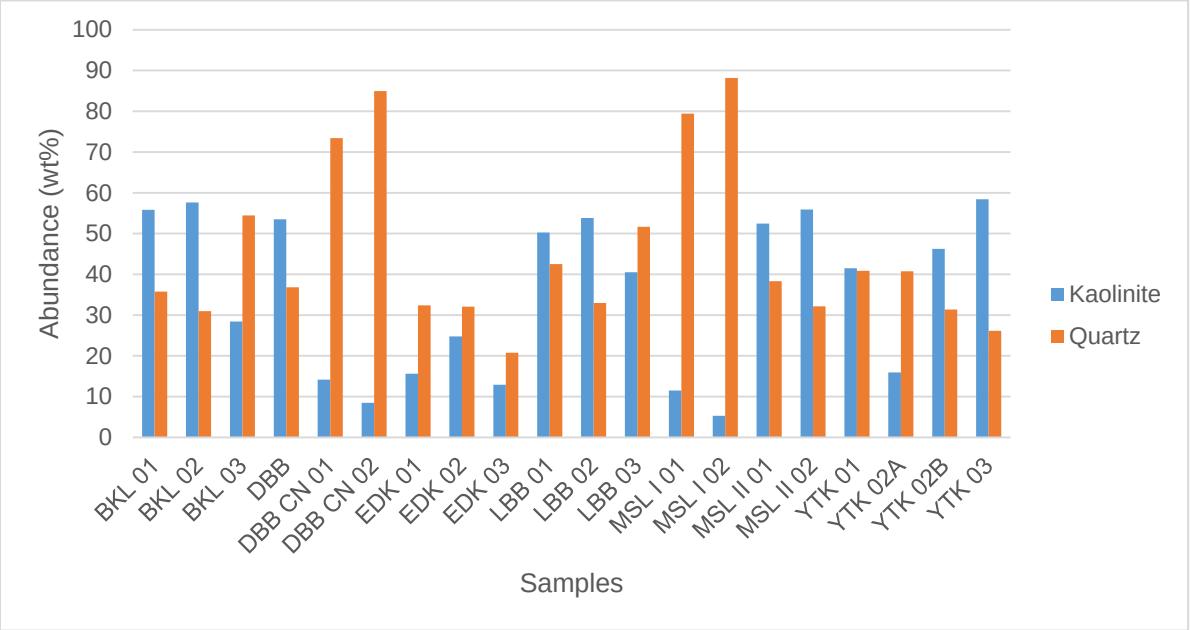

Figure 4.26: Abundance in wt% of kaolinite and quartz in bulk kaolin samples

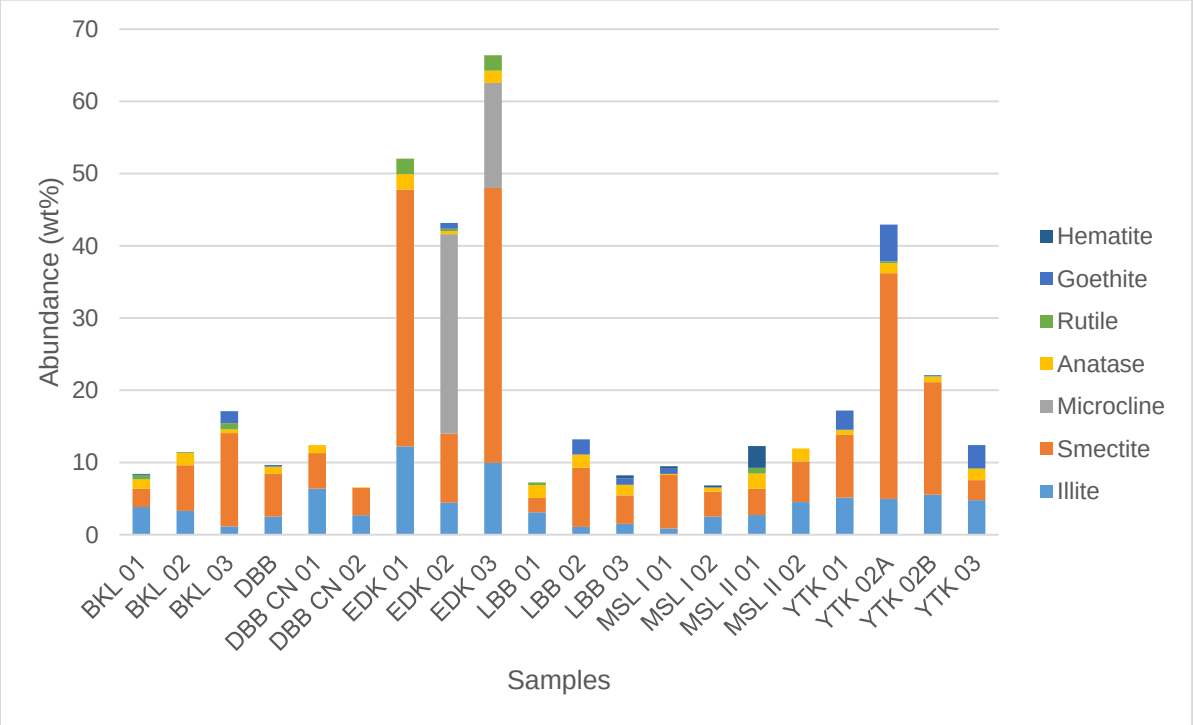

Figure 4.27: Abundance in wt% of other minerals in bulk kaolin samples

Quartz was the dominant mineral in 40% of the samples; namely, BKL 03, DBB CN 01, DBB CN 02, EDK 02, LBB 03, MSL I 01, MSL I 02 and YTK 02A, with abundances of 54.43, 73.40, 84.95, 32.08, 51.66, 79.40, 88.19 and 40.75 wt %, respectively (Figure 4.26). Microcline was only present in EDK 02 and EDK 03 in abundances of 27.61 and 14.53 wt%, respectively. Fe-bearing minerals were present in trace to minor amounts, as goethite and hematite. Goethite was more abundant than hematite, with abundances ranging from 0 (in 35% of the samples) to 5.09 wt % (YTK 02A). Hematite was only present in YTK samples, with a mean abundances of 0.27 wt %. Ti-bearing minerals, anatase and rutile, were mainly present in minor and trace amounts, having means of 1.20 and 0.37 wt % for anatase and rutile, respectively (Figure 4.27).

Silt samples (2-63 µm fraction)

Results of semi-quantitative and quantitative analyses of minerals identified in silt fractions of Cretaceous-Tertiary kaolin samples in the Douala Sub-Basin are shown in Appendix 4.2 and Table 4.3.

Table 4.3: Results of semi-quantitative analysis of minerals identified in silt samples

	Kaolinite	Illite	Smectite	Quartz	Microcline	Anatase	Rutile	Goethite	Hematite
BKL 03	++	++	++	+++	-	+	+	-	-
DBB	+++	++	++	+++	-	+	+	-	-
EDK 02	+++	++	++	+++	+++	+	+	-	-
LBB 02	+++	+	++	+++	-	+	+	+	-
MSL II 02	+++	++	++	+++	-	+	+	-	-
YTK 02A	+++	++	+++	+++	-	+	+	+	+

(+++) Major, (++) Minor, (+) Trace, (-) Not detected

Kaolinite was the most abundant clay mineral in DBB, EDK 02, LBB 02 and MSL II 02, with abundances of 67.6, 27.77, 19.44 and 36.74 wt %, respectively (Figure 4.28). Smectite was the second most abundant clay mineral, ranging from 2.66 wt % (DBB) and 40.55 wt % (YTK 02A). Whereas, illite concentrations ranged from 0.95 wt % (LBB 02) to 5.6 wt % (YTK 02A) (Figure 4.28).

Quartz was the most dominant mineral phase in BKL 03, LBB 02 and MSL II 02, with abundances of 87.49, 73.92 and 49.93 wt %, respectively (Figure 4.29). Microcline only occurred in the EDK 02 (32.02 wt %) and it was the most dominant mineral in this sample. Ti-bearing minerals were present in all samples, with anatase being more abundant than rutile, except in BKL 03. However, Fe-bearing minerals were not present in all samples. Goethite

was only present in traces in LBB 02 (0.57 wt %), and in minor amounts in YTK 02A (3.21 wt %); whereas traces of hematite were detected in YTK 02A (0.9 wt %) (Figure 4.29).

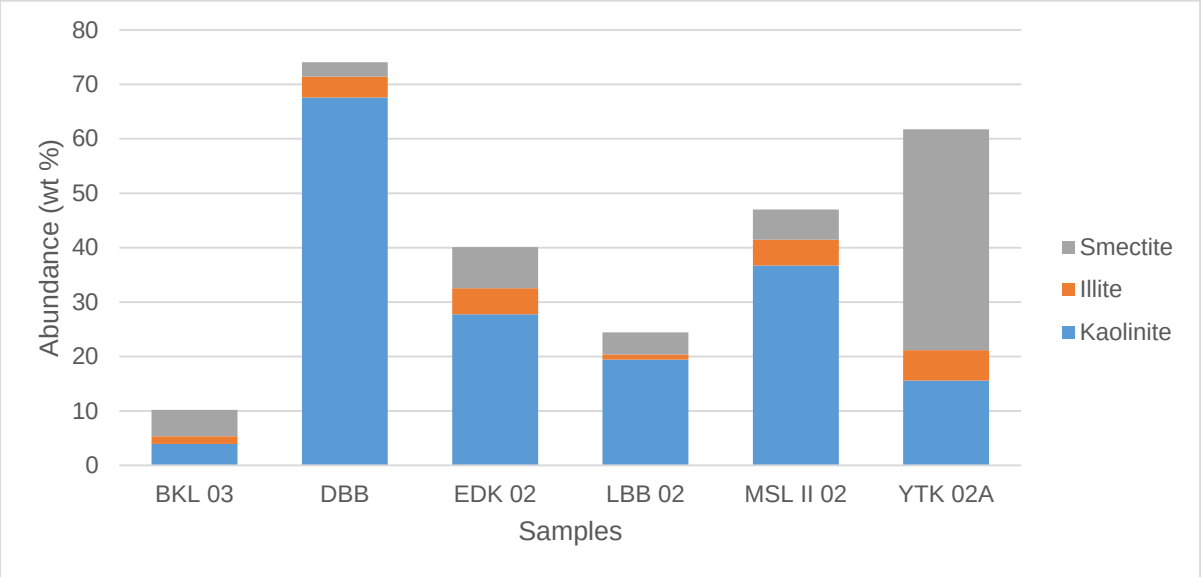

Figure 4.28: Abundance in wt% of clay minerals in silt samples

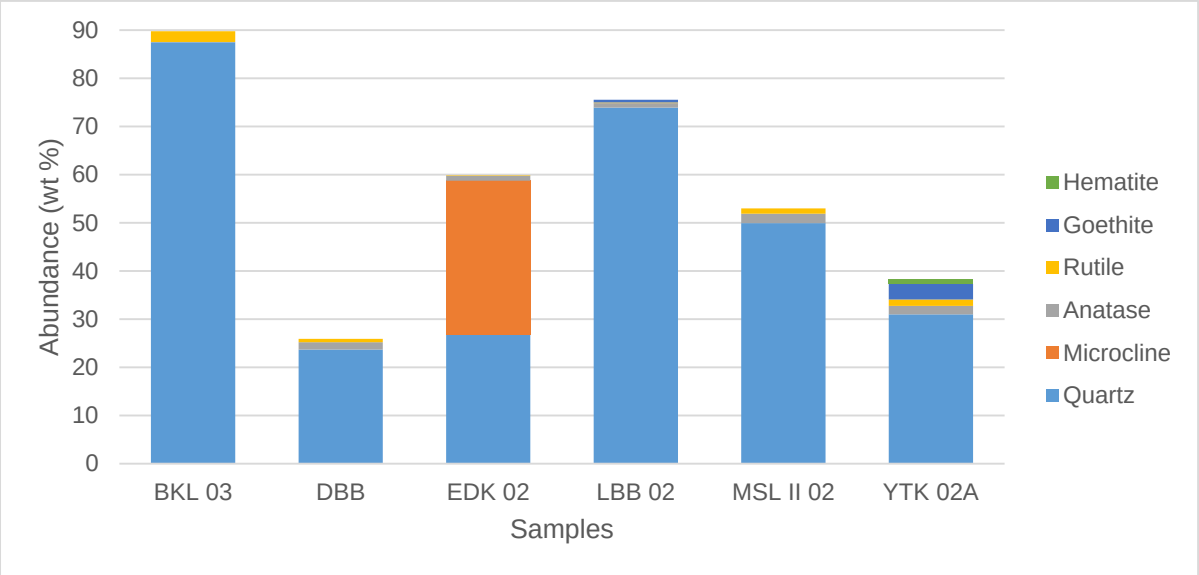

Figure 4.29: Abundance in wt% of other minerals in silt samples

Clay samples (< 2 µm fractions)

Results of semi-quantitative and quantitative analyses of minerals identified in < 2 µm samples of Cretaceous-Tertiary kaolin in the Douala Sub-Basin are shown in Appendix 4.3 and Table 4.4.

Table 4.4: Results of semi-quantitative analysis of minerals identified in < 2 µm samples

	Kaolinite	Illite	Smectite	Quartz	Microcline	Anatase	Goethite	Hematite	Rutile
BKL 01	+++	++	++	-	-	++	-	-	+
BKL 02	+++	++	++	-	-	++	-	-	+
BKL 03	+++	++	+++	-	-	++	-	-	+
DBB	+++	++	++	-	-	++	-	-	+
DBB CN 01	+++	++	++	-	-	++	-	-	+
DBB CN 02	+++	++	++	-	-	++	-	-	+
EDK 01	+++	+++	+++	++	-	++	-	-	++
EDK 02	+++	++	+++	++	-	+	-	-	++
EDK 03	++	+++	+++	++	+++	++	-	-	++
LBB 01	+++	++	++	-	-	++	-	-	+
LBB 02	+++	++	++	-	-	++	-	-	+
LBB 03	+++	++	++	-	-	++	-	-	+
MSL I 01	+++	++	+++	+++	-	++	-	-	+
MSL I 02	+++	+	++	+++	-	+	+	-	+
MSL II 01	+++	++	++	+	-	++	-	-	+
MSL II 02	+++	++	++	+	-	++	-	-	+
YTK 01	+++	-	++	+	-	++	++	+	+
YTK 02A	+++	-	+++	+++	-	+	+++	++	-
YTK 02B	+++	++	+++	-	-	+	-	++	+
YTK 03	+++	++	++	+	-	+	-	+	+

(+++) Major, (++) Minor, (+) Trace, (-) Not detected

Figure 4.30 shows the abundance of clay minerals in < 2 µm samples. Kaolinite was the most dominant clay mineral in 90% of the samples, with abundances ranging from 8.00 wt % (EDK 03) to 92.17 wt % (DBB CN 01). Except in Ediki samples (EDK 01, EDK 02 and EDK 03), MSL I 01, MSL I 02 and YTK 02A, kaolinite was the most dominant mineral phase (>80 wt % in most samples).Smectite was the most dominant clay mineral in EDK 03 (41.6 wt %) and YTK 02A (20.48 wt %). Illite was the least abundant clay mineral (mean of 4.69 wt %); however, it is the most abundant clay mineral in EDK 03 (21.9 wt %), after smectite (41.6 wt %).

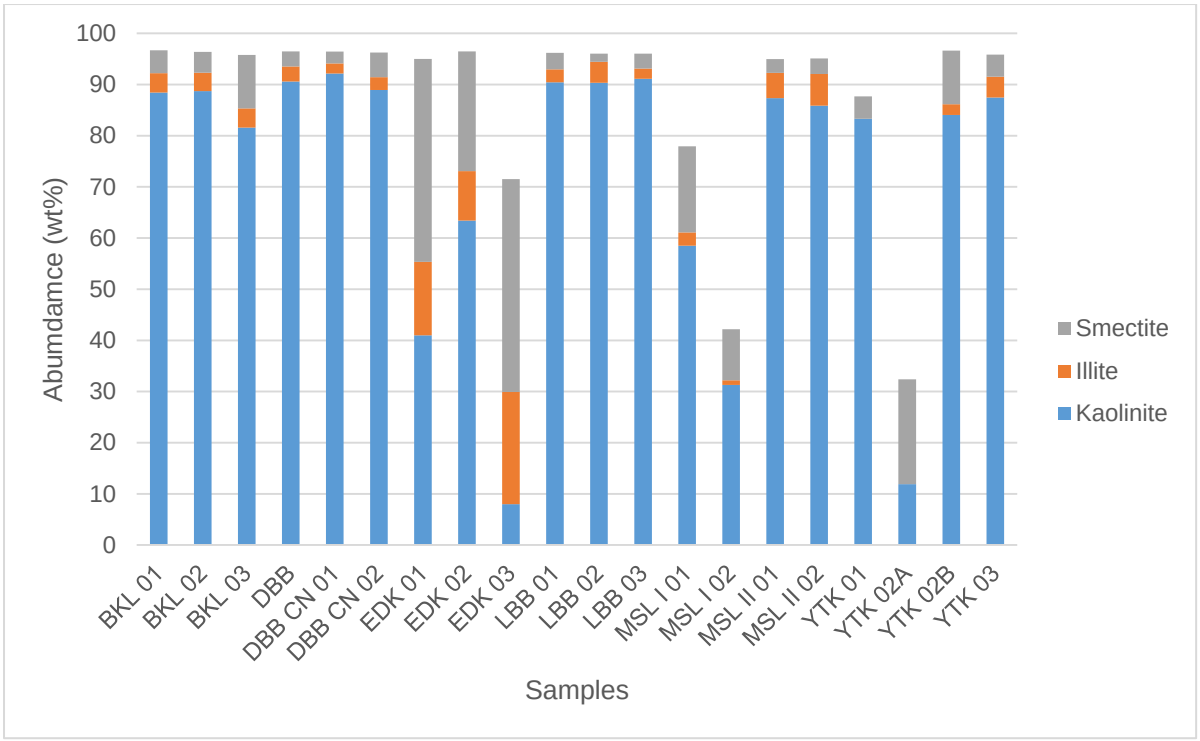

Figure 4.30: Abundance in wt% of clay minerals in < 2 µm samples

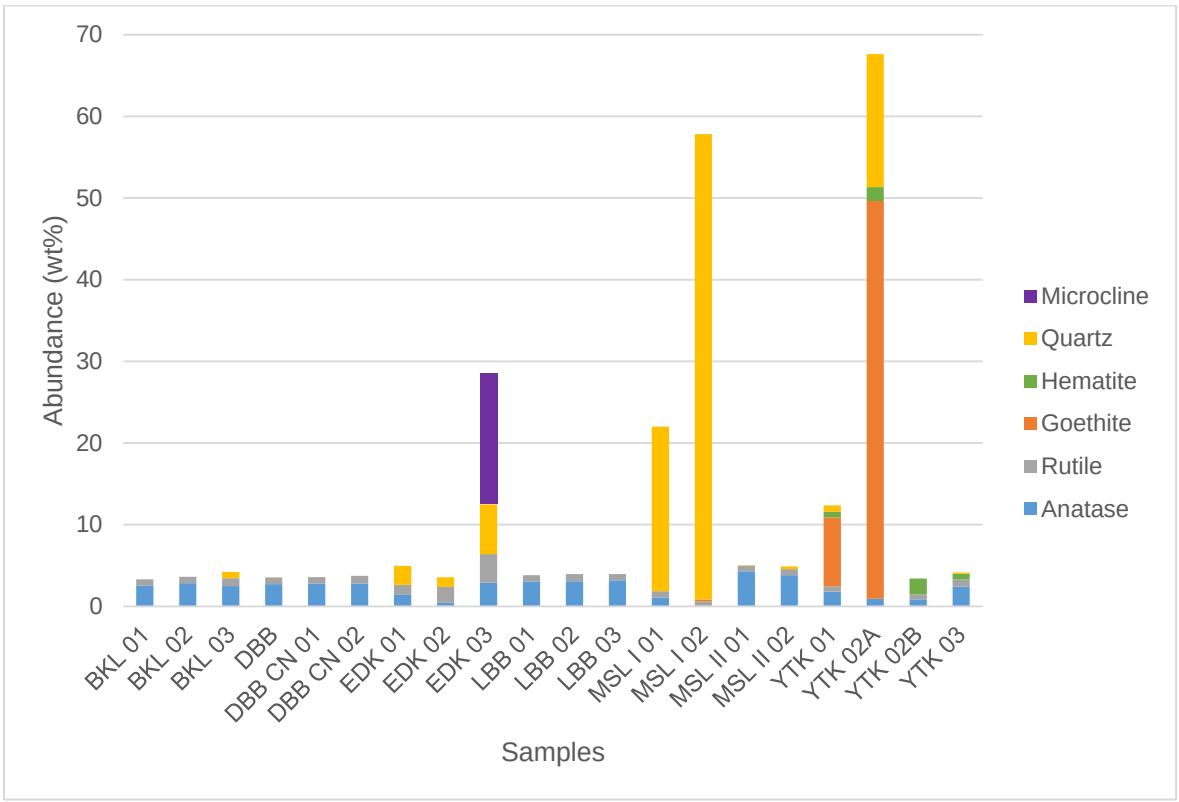

Figure 4.31: Abundance in wt% of other minerals in < 2 µm samples

Non-clay minerals (Figure 4.31) constituted < 10 wt % in 80% of the samples. MSL I 02 had quartz as the most dominant mineral phase. Samples MSL I 01 and YTK 02A had > 15 wt % of quartz. Microcline was only present in EDK 03 (16.03 wt %). Goethite was the most dominant mineral in YTK 02A (48.70 wt %). It was present as minor phase in YTK 01 (8.42 wt %), and as trace in MSL I 02 (0.23 wt %). As in bulk samples, hematite was present only in YTK samples, as minor phase in YTK 02A and YTK 02B (1.69 and 1.93 wt %, respectively), and as trace phase in YTK 01 and YTK 03 (0.69 and 0.70 wt %, respectively). Anatase was the most abundant Ti-bearing mineral phase, with concentrations >2.70 wt % in Dibamba, Logbaba and Missole II samples. Rutile was mostly present in traces in all samples, except in Ediki samples in which it was more abundant than anatase.

4.3.2 Morphology of studied kaolins

Scanning electron microscopy images showing the different morphologies of Cretaceous-Tertiary kaolins of the Douala Sub-Basin are depicted in Figures 4.32-4.51. Different morphologies present can be grouped into three categories:

- Pseudo-hexagonal particles or flakes and thin platy particles: Dibamba (DBB, DBB CN 01 and DBB CN 02), EDK 02, LBB 02, LBB 03, MSL I 01, MSL I 02, Bomkoul (BKL 01, BKL 02 and BKL 03), LBB 03, MSL I 01, YTK 01, YTK 02A, YTK 02B and YTK 03.

- Books or stacks of kaolinite: Made up of well-formed, unaltered pseudo-hexagonal plates, and observed in EDK 01, MSL II 01 and MSL II 02. This texture is reported to occur during transport of kaolinite flakes (Keller, 1978).

- Swirl texture: Characterised by a tight binding or agglutination of these plates into laminar ribbon-like structures, which could have been caused by movement during packing, settling, dewatering, or other soft-rock deformation (Keller, 1978). It was depicted in EDK 03 and LBB 01.

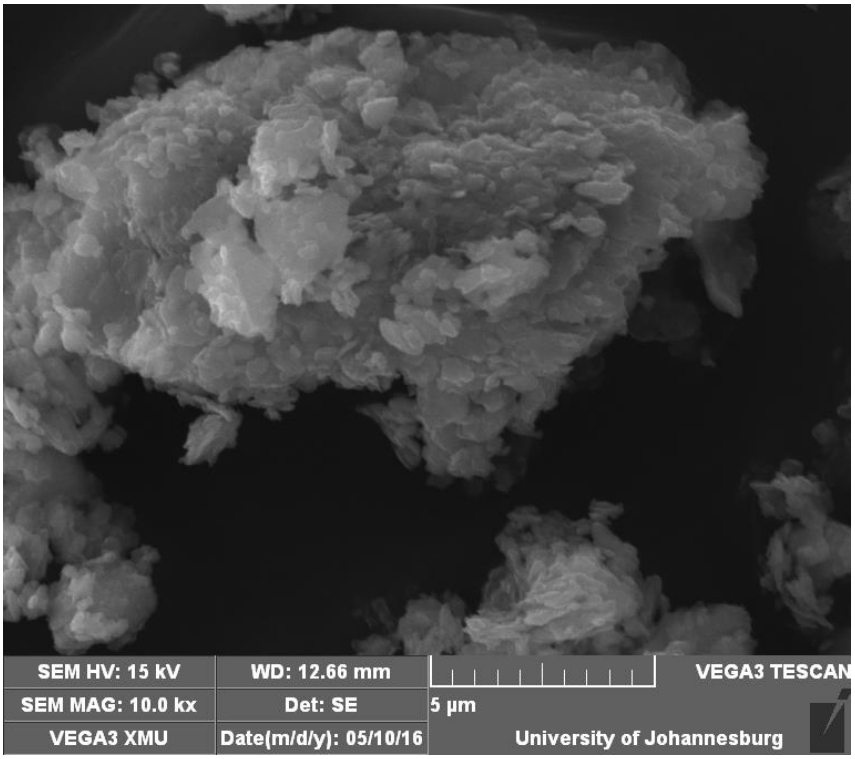

Figure 4.32: SEM image of BKL 01 showing thin platy kaolinite particles

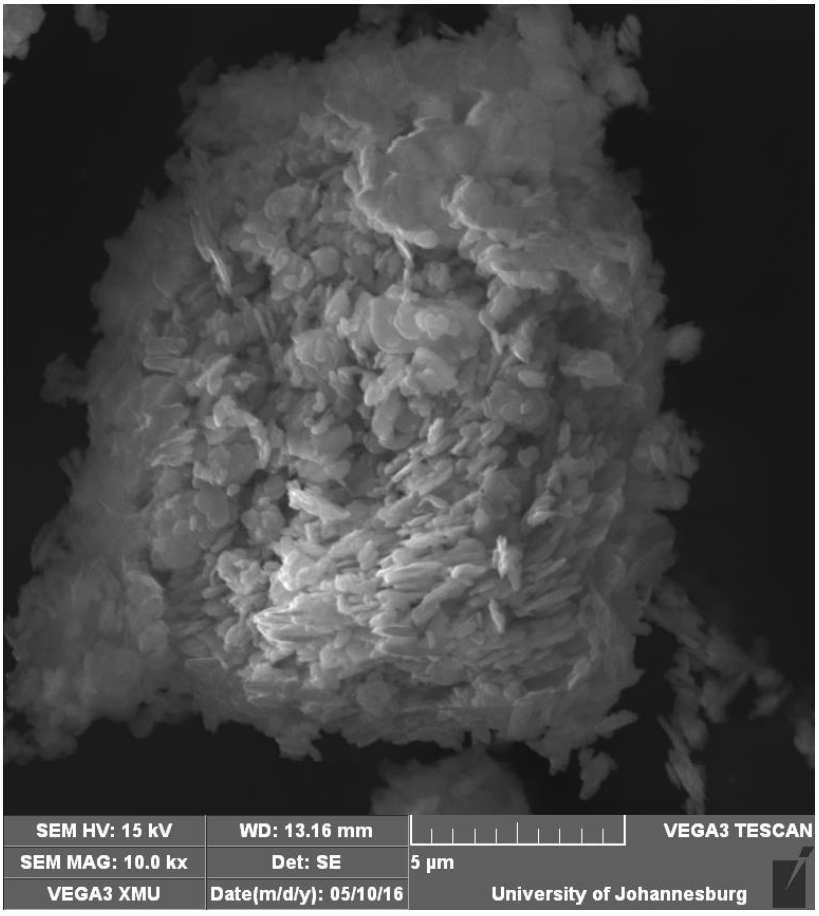

Figure 4.33: SEM image of BKL 02 showing thin platy kaolinite particles

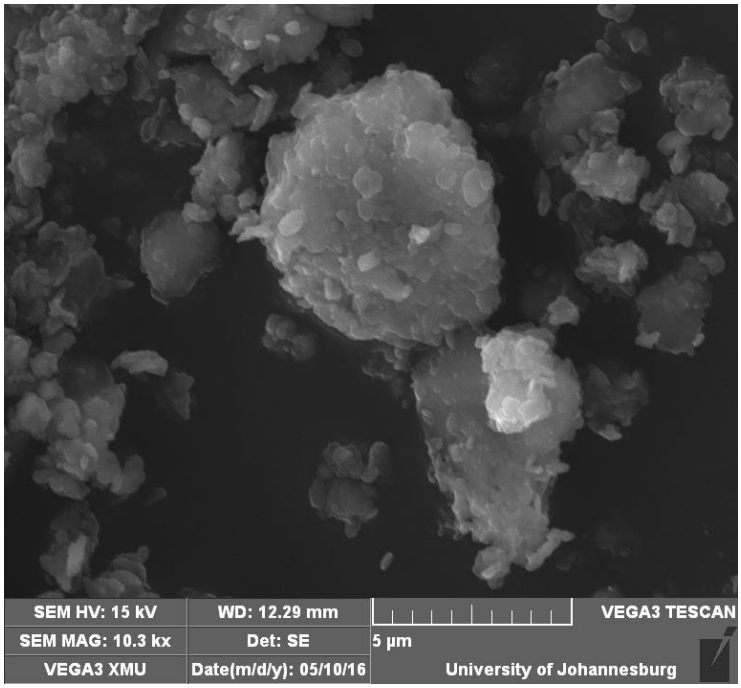

Figure 4.34: SEM image of BKL 03 showing thin platy kaolinite particles

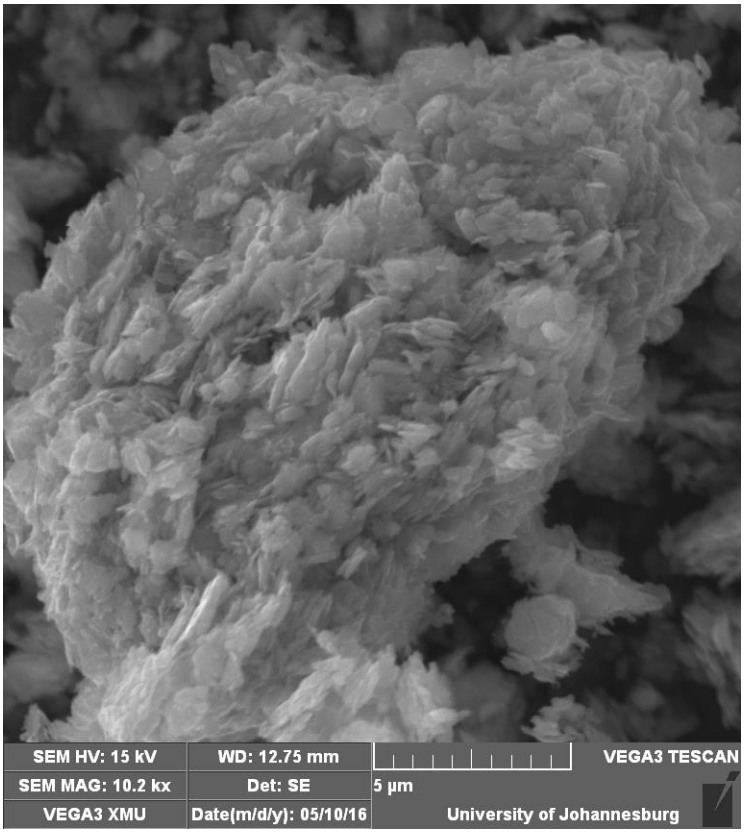

Figure 4.35: SEM image of DBB showing pseudo-hexagonal kaolinite particles

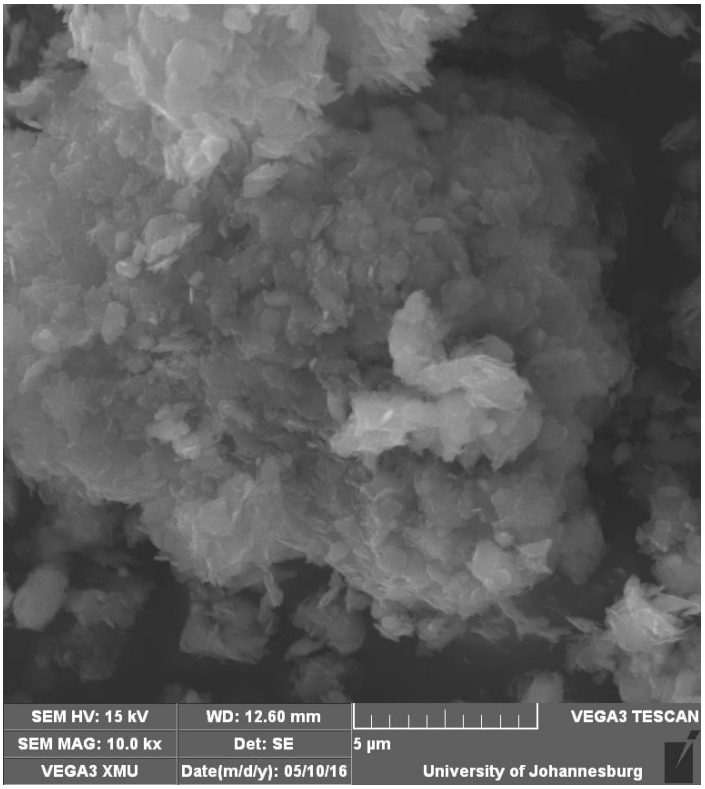

Figure 4.36: SEM image of DBB CN 01 showing pseudo-hexagonal kaolinite particles

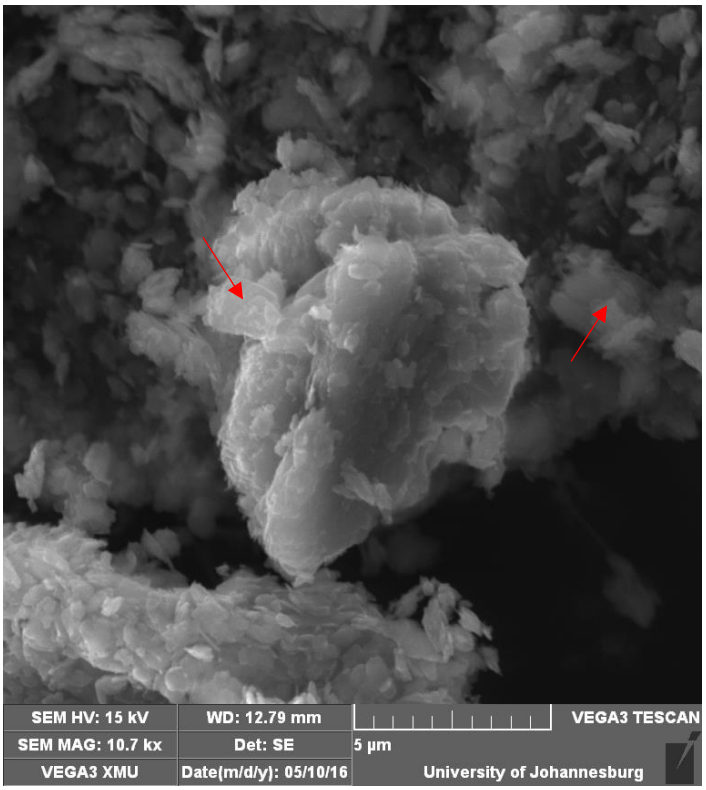

Figure 4.37: SEM image of DBB CN 02 showing thin platy particles and stacks of kaolinite

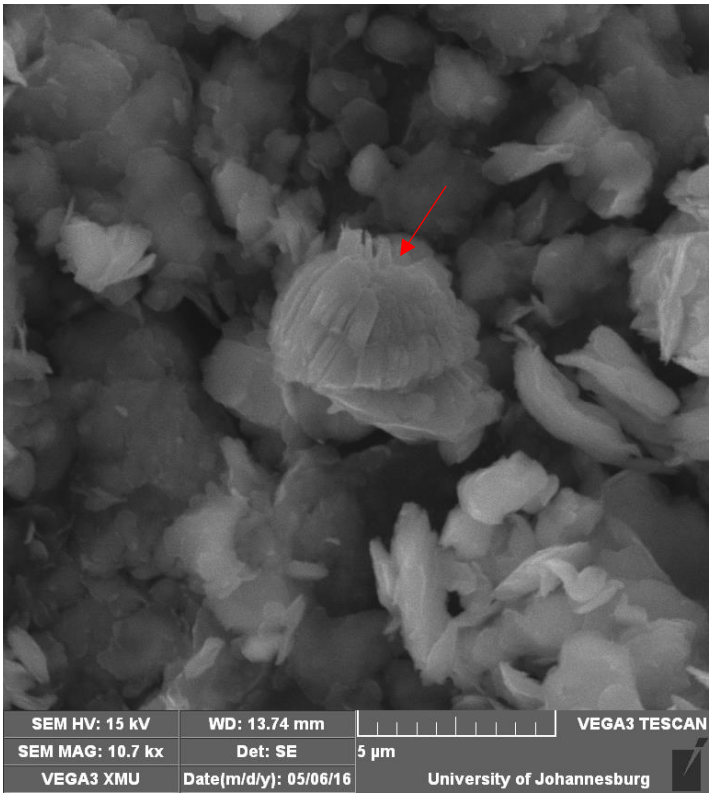

Figure 4.38: SEM image of EDK 01 showing a kaolinite book

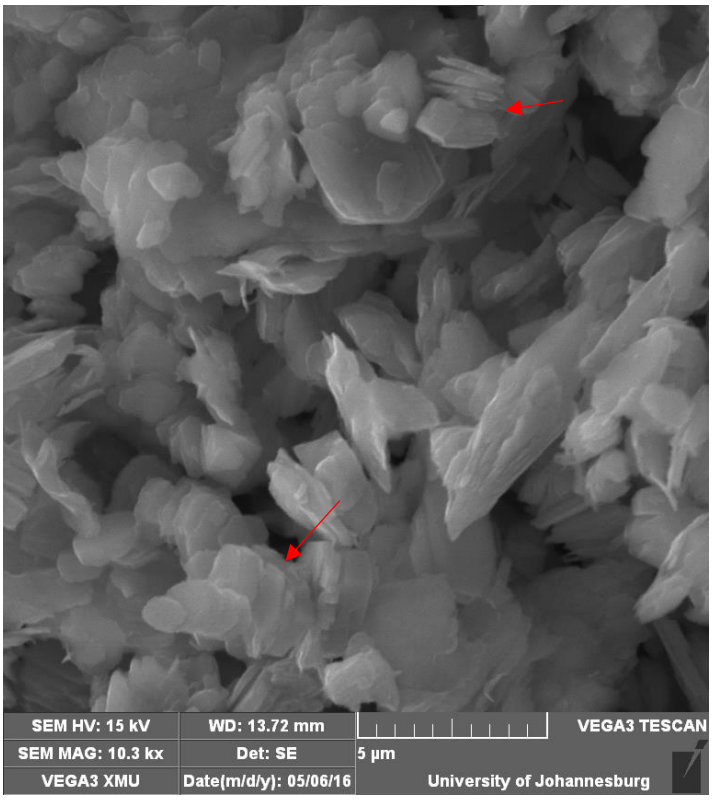

Figure 4.39: SEM image of EDK 02 showing stacks of pseudo-hexagonal kaolinite particles

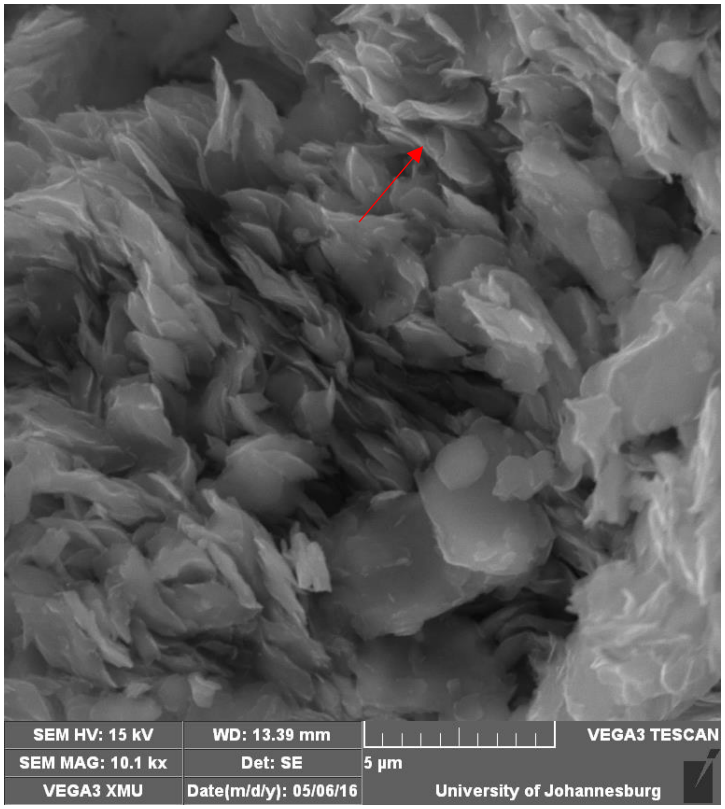

Figure 4.40: SEM image of EDK 03 showing swirl texture with face to face arrangement of kaolinite grains

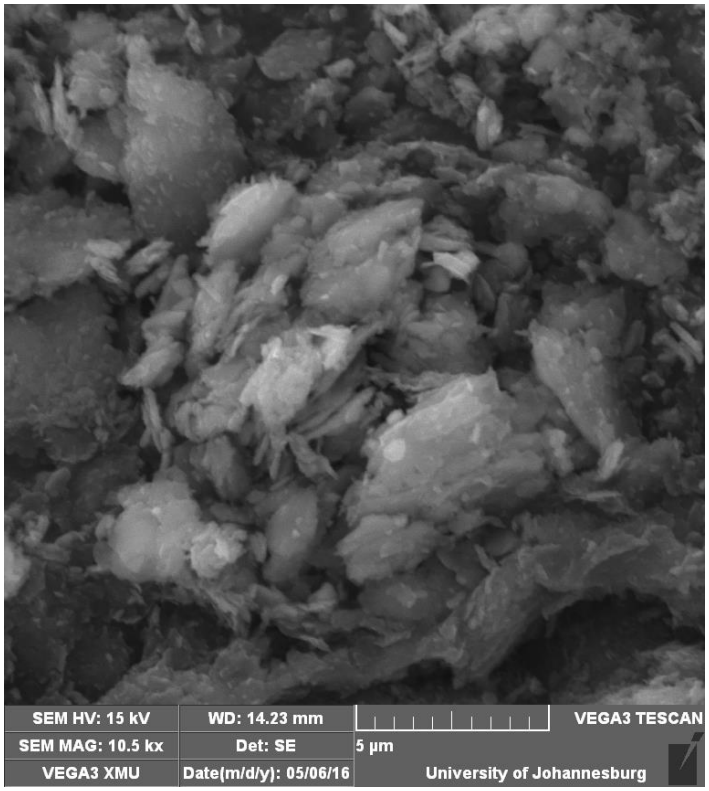

Figure 4.41: SEM image of LBB 01 showing a swirl texture of kaolinite particles

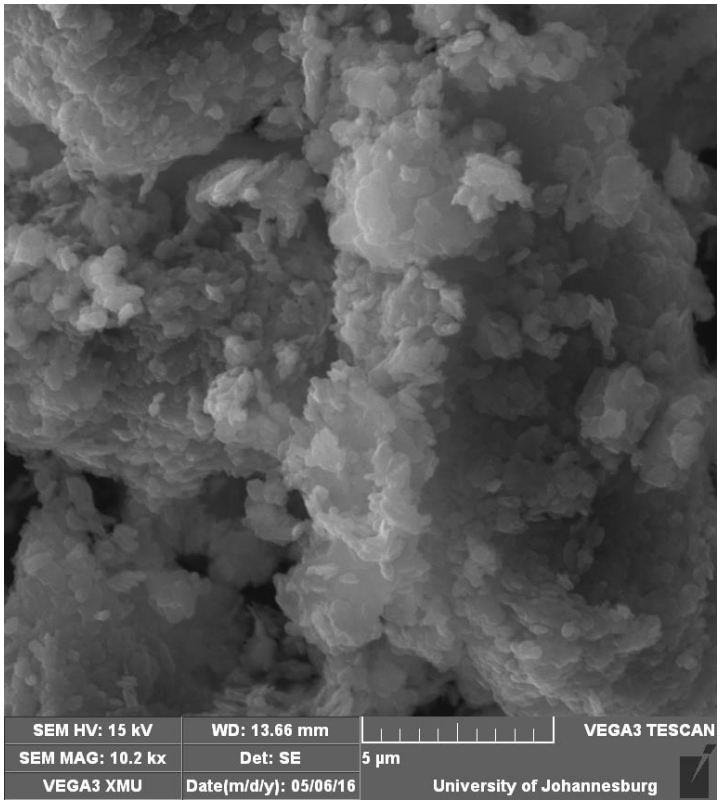

Figure 4.42: SEM image of LBB 02 showing pseudo-hexagonal kaolinite particles

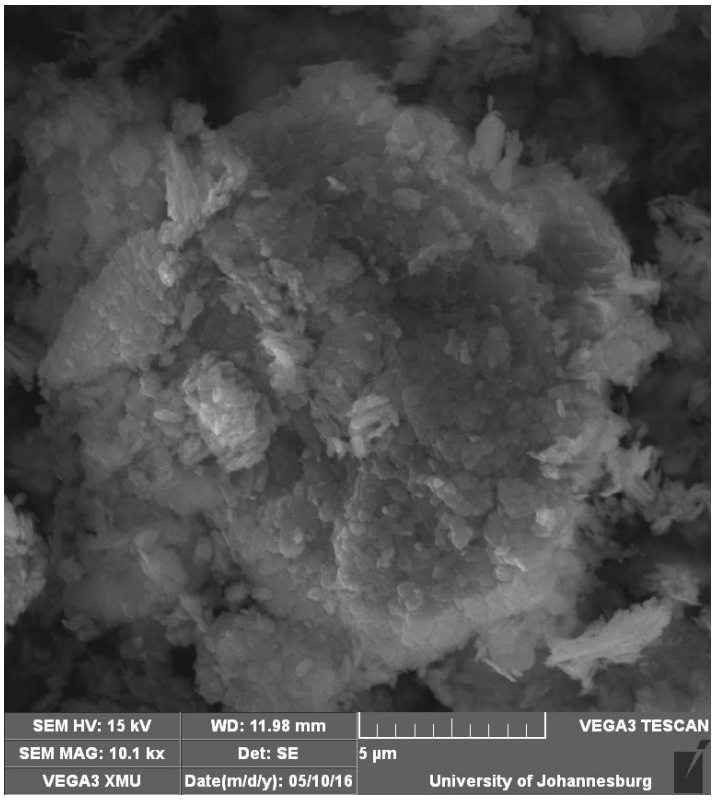

Figure 4.43: SEM image of LBB 03 showing thin platy kaolinite particles

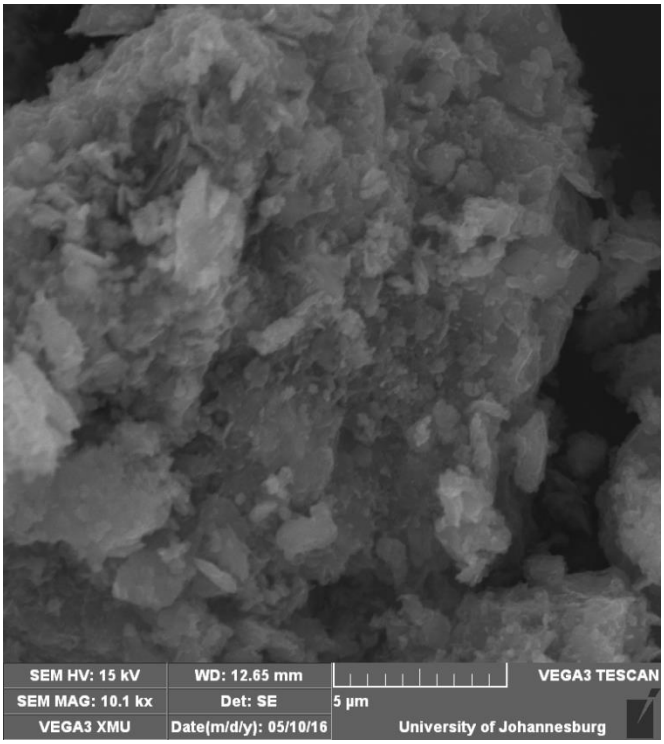

Figure 4.44: SEM image of MSL I 01 showing thin platy kaolinite particles

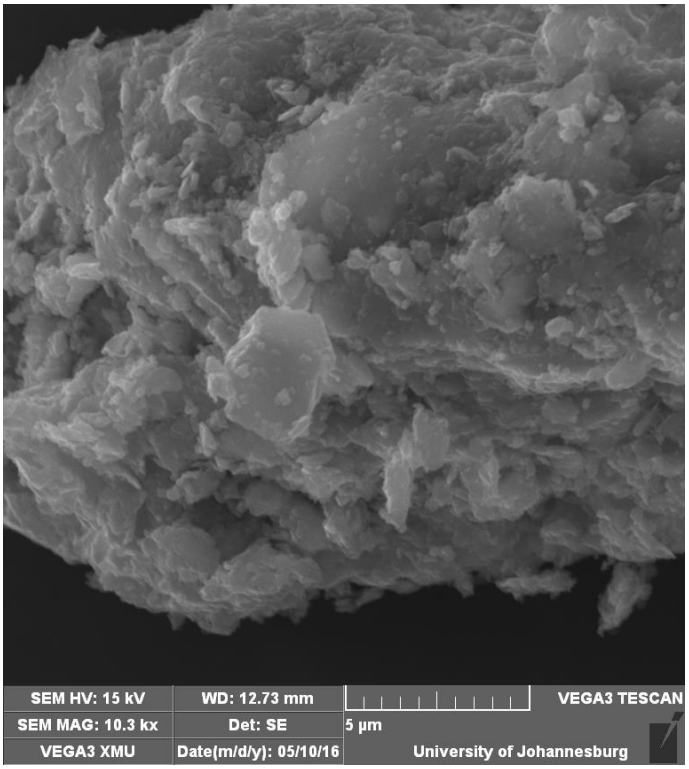

Figure 4.45: SEM image of MSL I 02 showing thin platy kaolinite particles

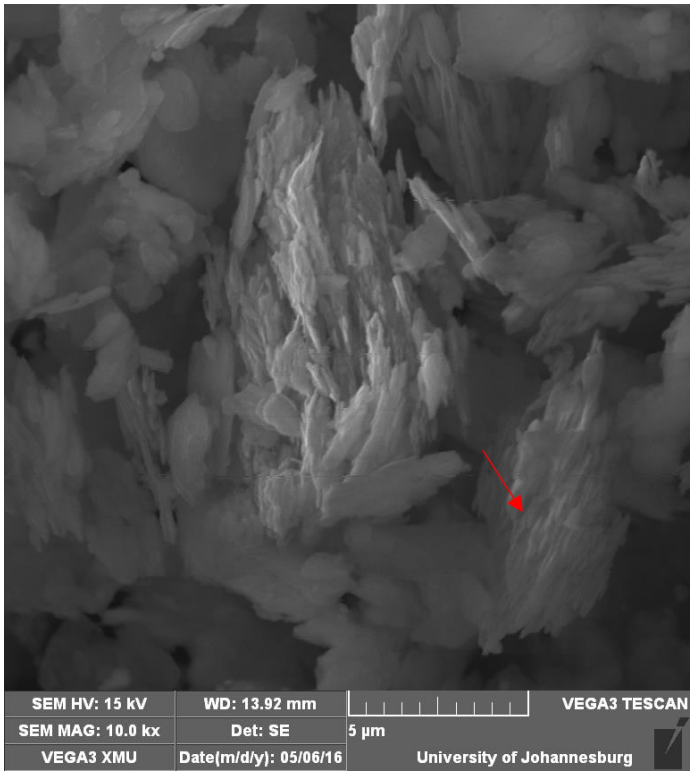

Figure 4.46: SEM image of MSL II 01 showing stacks of kaolinite particles

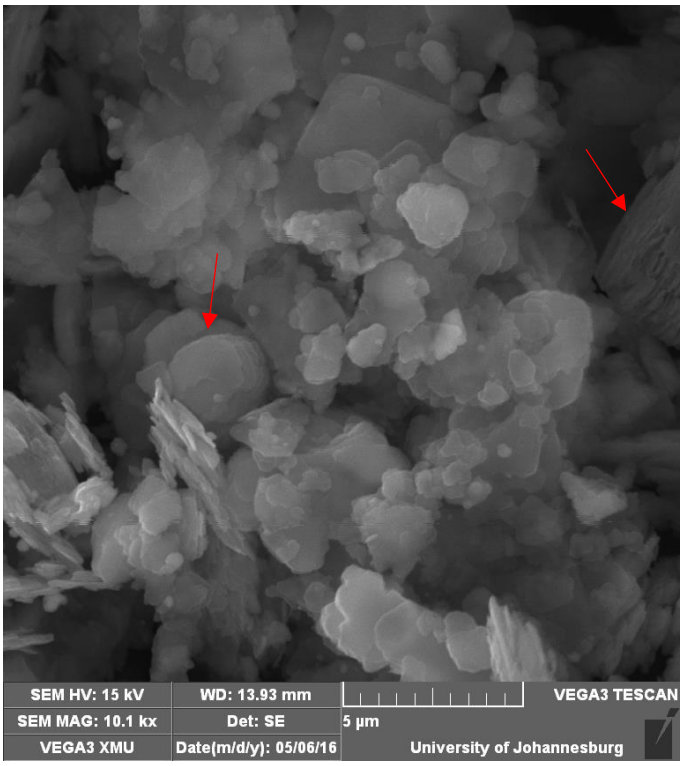

Figure 4.47: SEM image of MSL II 02 showing stacks of pseudo-hexagonal kaolinite particles

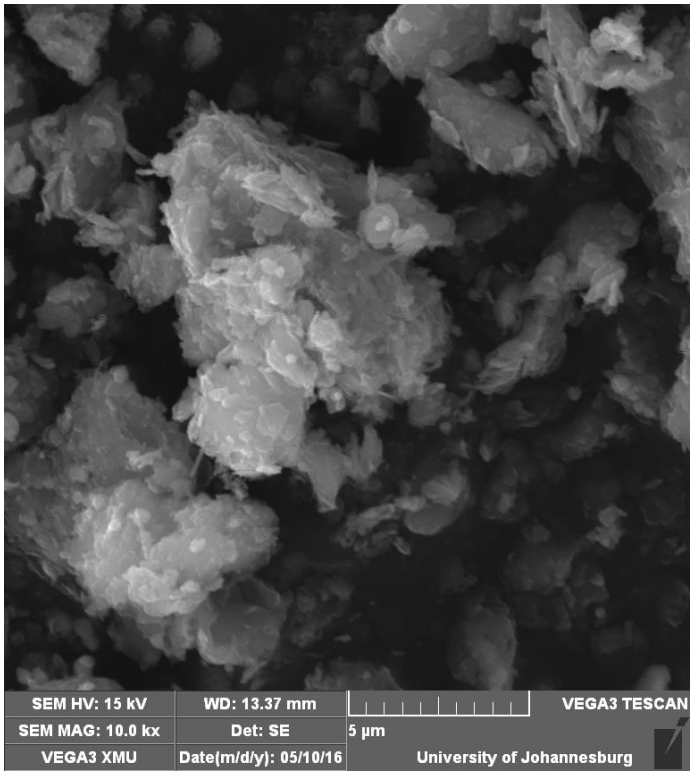

Figure 4.48: SEM image of YTK 01 showing thin platy kaolinite particles

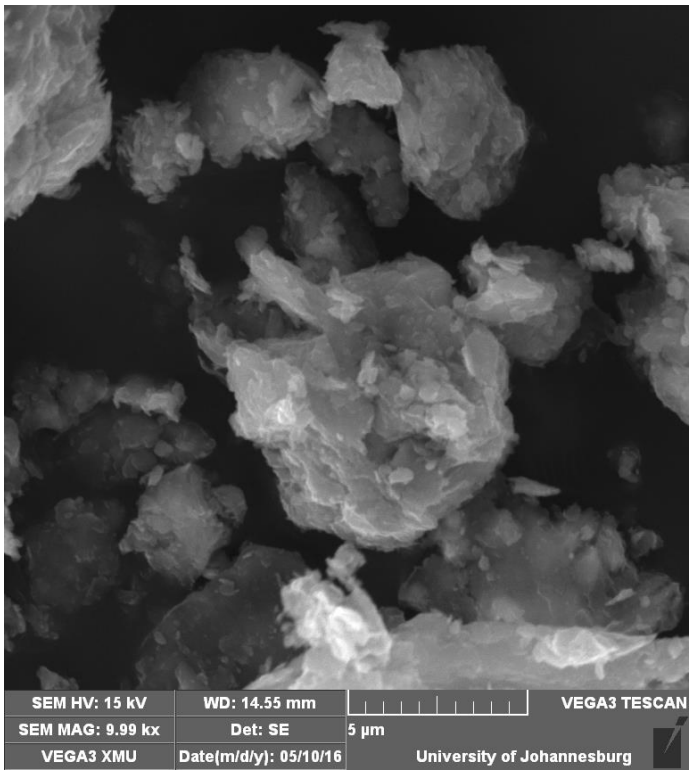

Figure 4.49: SEM image of YTK 02A showing thin platy kaolinite particles

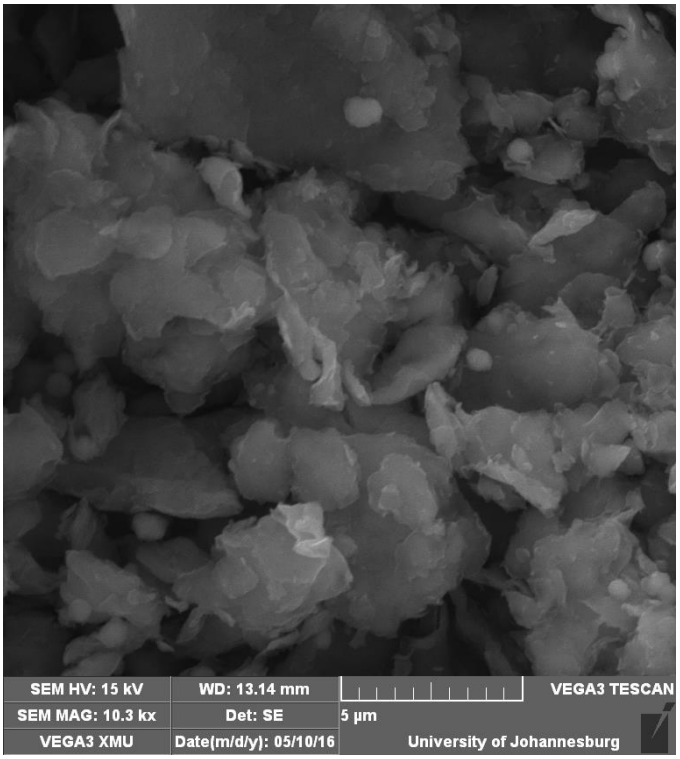

Figure 4.50: SEM image of YTK 02B showing thin platy kaolinite particles

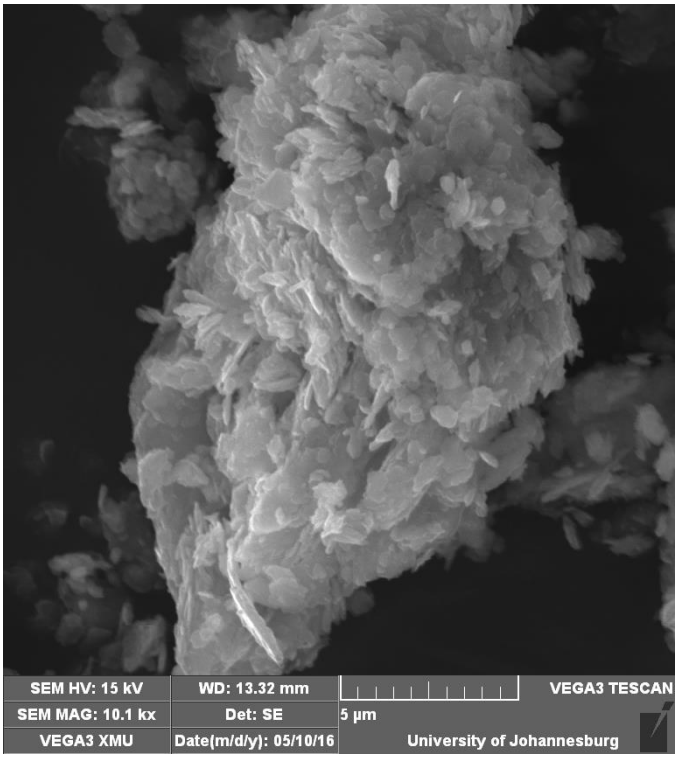

Figure 4.51: SEM image of YTK 03 showing thin platy kaolinite particles

4.3.3 Functional groups in the kaolins

Fourier transform infrared spectra of the OH stretching hydroxyl group, OH stretching of water, Si-O stretching bands, OH deformation of inner-surface hydroxyl groups and OH deformation of inner hydroxyl groups, and the Si-O band were analysed. Figures 4.52-4.54 show FTIR spectra of studied Cretaceous-Tertiary kaolin samples in the Douala Sub-Basin, and Appendices 4.4 – 4.6 summarise the assignment of the different bands.

OH stretching of hydroxyl group

The OH stretching of hydroxyl groups is an important band region because it provides information on the environment of formation of different minerals, such that mineral groups portray almost similar transmittance/absorption in this region (Farmer and Russel, 1967). It also determines the order/disorder in the kaolin mineral's structure. Kaolin minerals usually have four distinguishable bands in the hydroxyl stretching region (3695, 3670, 3650 and 3620 cm^{-1}), with bands around 3695 and 3620 cm^{-1} being specific to kaolin minerals (Vaculíková *et al*., 2011).

OH stretching of hydroxyl group is found between 3500 and 4000 cm^{-1}. Figures 4.52 A-F show FTIR spectra of studied Cretaceous-Tertiary kaolin samples in the Douala Sub-Basin, and Appendices 4.4 – 4.6 summarise the assignment of the different bands. Most of the samples had the four distinguishable bands, though the second transmittance band (3670 cm^{-1}) had low intensities. This band usually appears in well crystallised kaolinite (Fehli *et al*., 2008). This transmittance band was not present in BKL 03, EDK 03, MSL I 01, MSL I 02 and YTK 02A, which therefore were not well crystallised. The 3695 cm^{-1} band had a low intensity in all Ediki samples (EDK). EDK 03 specifically showed broadening of the four hydroxyl stretching bands. Transmittance bands 3670 and 3650 cm^{-1} were totally absent in YTK 02B; this is indicative of the disorder in the kaolinite's structure (Vaculíková *et al*., 2011).

OH stretching of water

OH stretching of water bands (3457 and 3442 cm^{-1} for KGa-1b and KGa-2, respectively) was not present in all the samples. It was mainly observed in all Logbaba samples at 3443 cm^{-1} for LBB 01 and LBB 03, and 3445 cm^{-1} for LBB 02 (Figure 4.53). Besides the band corresponding to the OH stretching of water, all three Logbaba samples had an additional band around 3530 cm^{-1} (3526, 3530 and 3527 cm^{-1} for LBB 01, LBB 02 and LBB 03, respectively). This is similar to the Cretaceous-Tertiary kaolins from Sidi El Bader in Tunisia (Fehli *et al*., 2008), it is attributed to H bonding between surface OH groups and adsorbed water (Ece *et al*., 2003).

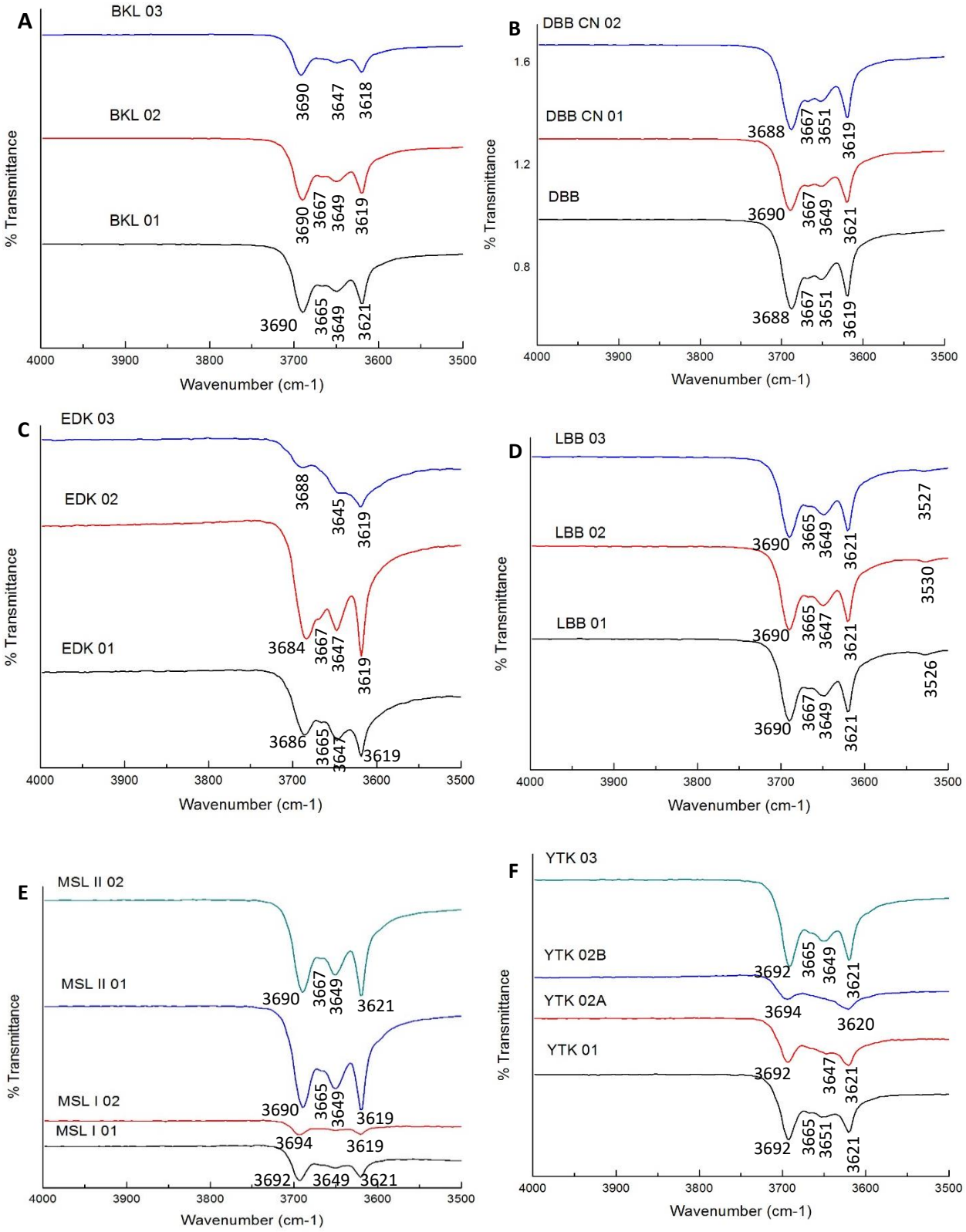

Figure 4.52: FTIR spectra of kaolin samples between 3500 and 4000 cm^{-1}

A- Bomkoul; B-Dibamba C-Ediki D-Logbaba E-Missole F-Yatchika

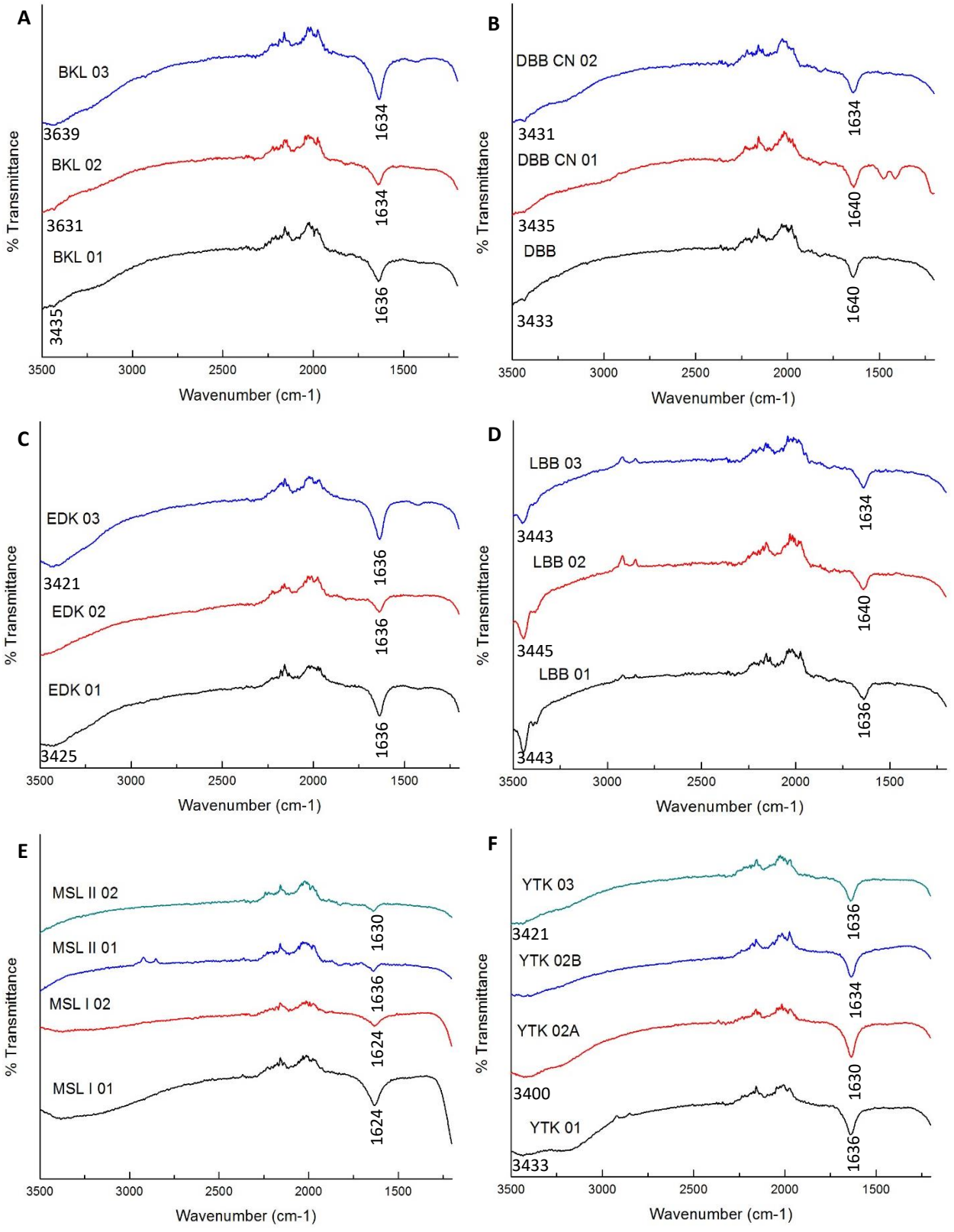

Figure 4.53: FTIR spectra of kaolin samples between 1200 and 3500 cm^{-1}

A- Bomkoul; B-Dibamba C-Ediki D-Logbaba E-Missole F-Yatchika

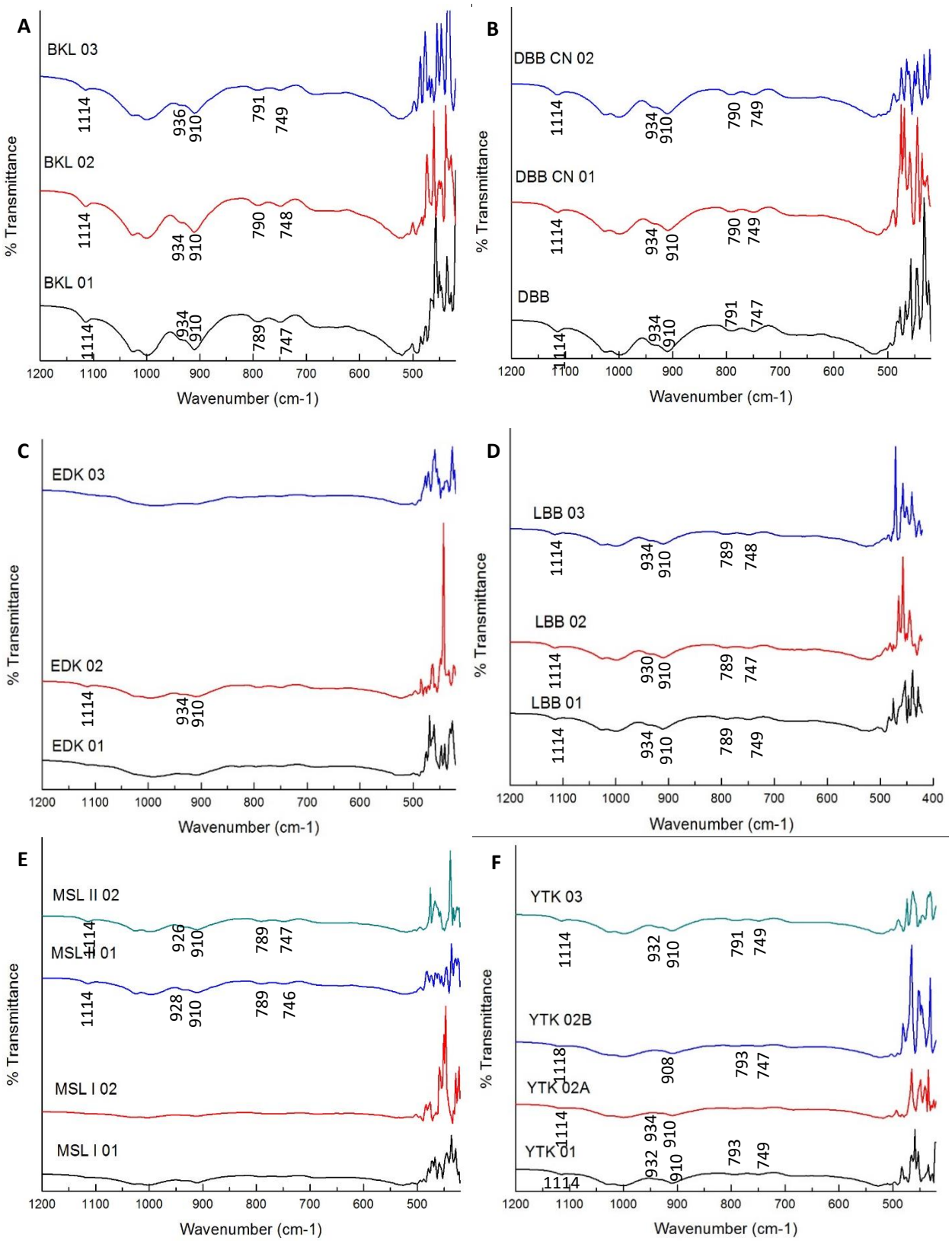

Figure 4.54: FTIR spectra of kaolin samples between 420 and 1200 cm^{-1}

A- Bomkoul; B-Dibamba C-Ediki D-Logbaba E-Missole F-Yatchika

The 3439 cm^{-1} band in BKL 03 could either be attributed to the OH stretching of water in this sample or to the presence of smectite (Ojima, 2003; Ekosse, 2005). EDK 01 (3425 cm^{-1}), EDK 03 (3421 cm^{-1}), YTK 01 (3433 cm^{-1}), YTK 02A (3400 cm^{-1}) and YTK 03 (3421 cm^{-1}) also had a band around 3426 cm^{-1}. Bomkoul kaolins are reported to also be smectitic (Ngon Ngon *et al*., 2012b; Ngon Ngon *et al*., 2014). This explains the presence of a band around 3426 cm^{-1}.

Si-O stretching bands

Longitudinal mode Si-O stretching bands were observed in all samples at 1114 cm^{-1}, except in EDK 03 (1111 cm^{-1}) and YTK 02B (1118 cm^{-1}); whereas the perpendicular mode Si-O stretching bands was only exhibited in MSL I 02. The first in-plane Si-O stretching was observed between 983-1002 cm^{-1} in all samples (Figure 4.54), and the second in-plane Si-O stretching bands were observed in all the samples between 1022 and 1028 cm^{-1}.

OH deformation of inner-surface hydroxyl groups and OH deformation of inner hydroxyl groups

OH deformation of inner-surface hydroxyl and inner hydroxyl groups were observed around 937 and 935 cm^{-1}, respectively for KGa kaolinites (Madejová and Komadel, 2001). In the studied kaolins, OH deformation of inner-surface hydroxyl groups were observed between 926 cm^{-1} (MSL II 02) and 936 cm^{-1} (BKL 03) (Figure 4.54), with most samples having this OH deformation at 934 cm^{-1}. OH deformation of inner hydroxyl groups occurred between 908 and 912 cm^{-1}. These two bands reflecting OH deformation of inner-surface hydroxyl and inner hydroxyl groups were very visible in the BKL, DBB, LBB and MSL II samples; slightly visible in all the YTK samples, EDK 01 and EDK 02; and not visible in MSL I 01, MSL I 02 and EDK 03.

Si-O band

Two weak bands of about equal intensities around 795 and 758 cm^{-1} were observed in BKL, DBB, LBB, EDK 02, MSL II 01, MSL II 02, and YTK 03 samples. These bands are not visible in the remaining samples (Figure 4.54).

Classification of the degree of structural order of kaolinite in the samples

Vaculíková *et al*. (2011) used an empirical method to classify the degree of structural order of kaolinite. Four attributes were taken into consideration: 1) Distinguishable four bands 3695, 3670, 3650 and 3620, 2) General broadening of all bands was not observed, 3) OH deformation bands around 938 and 916 were visible, 4) two weak bands of about equal intensities were found around 795 and 758. Table 4.5 shows a summary of the classification of studied Cretaceous-Tertiary kaolins of the Douala Sub-Basin. BKL 01, BKL 02, DBB, DBB

CN 01, DBB CN 02, LBB 01, LBB 02, LBB 03, MSL II 01 and MSL II 02 had ordered kaolinite structures. BKL 03, YTK 01 and YTK 03 had partially ordered kaolinite structures. EDK 01, EDK 02, YTK 02A and YTK 02B exhibited poorly ordered structures; whereas MSL I 01 and MSL I 02 had disordered structures. The poorly and partially ordered kaolins might contain some amounts of smectite and/or illite, causing some variance in their IR spectra (Vaculíková *et al*. 2011).

Table 4.5: Classification of the degree of structural order in the studied Cretaceous-Tertiary kaolins of the Douala Sub-Basin

	Attributes				**Class**
	1	**2**	**3**	**4**	
BKL 01	Y	Y	Y	Y	Ordered
BKL 02	Y	Y	Y	Y	
DBB	Y	Y	Y	Y	
DBB CN 01	Y	Y	Y	Y	
DBB CN 02	Y	Y	Y	Y	
LBB 01	Y	Y	Y	Y	
LBB 02	Y	Y	Y	Y	
LBB 03	Y	Y	Y	Y	
MSL II 01	Y	Y	Y	Y	
MSL II 02	Y	Y	Y	Y	
BKL 03	N	Y	Y	Y	Partially ordered
YTK 01	Y	Y	N	Y	
YTK 03	Y	Y	Y	N	
EDK 01	Y	N	Y	N	Poorly ordered
EDK 02	Y	N	Y	N	
YTK 02A	N	N	N	Y	
YTK 02B	N	N	N	Y	
EDK 03	N	N	N	N	Disordered
MSL I 01	N	N	N	N	
MSL I 02	N	N	N	N	

Attributes used by Vaculíková *et al*. (2011) as described in-text. Y = Yes, N = No

4.3.4 Thermogravimetric analyses and differential scanning calorimetry (TGA-DSC)

Four main reactions occur with increasing heating of kaolinite. The first is an endothermic reaction, which involves dehydroxylation of kaolinite to form metastable kaolinite between 450-700°C (dehydroxylation peak temperatures (T_d)) (Equation 4.1); the second is an exothermic reaction involving the formation of cubic spinel and amorphous silica (transformation into crystalline phases) between 925-1050°C (transformation peak temperatures (T_t)) (Equation 4.2); the third is an exothermic reaction involving the formation of mullite between 1050-1200°C (Equation 4.3); and the fourth reaction occurs above 1200°C and it involves the crystallisation of cristobalite from amorphous silica (Equation 4.4) (Ptáček *et al*., 2010; Fodvari, 2011; Diko *et al*., 2016).

$$Al_2O_3.2SiO_2.2H_2O \rightarrow Al_2O_3.2SiO_2 + 2H_2O \quad \text{Eqn. 4.1}$$

$$2(Al_2O_3.2SiO_2) \rightarrow 2Al_2O_3.3SiO_2 + SiO_{2\,(amorphous)} \quad \text{Eqn. 4.2}$$

$$3(2Al_2O_3.3SiO_2) \rightarrow 2(3Al_2O_3.2SiO_2) + 5SiO_2 \quad \text{Eqn. 4.3}$$

$$SiO_{2\,(amorphous)} \rightarrow SiO_{2\,(cristobalite)} \quad \text{Eqn. 4.4}$$

Moreover, release of adsorbed water in pores occurs at T ≤ 150°C (Ptáček *et al*., 2010) or at T ≤ 200°C (Ilić *et al*., 2010) and pre-dehydroxylation of kaolinite can occur between 200 and 450°C, causing a mass loss due to reorganisation in the octahedral layer (Ilić *et al*., 2010).

Results of TGA-DSC are shown in Tables 4.6-4.7 and Figures 4.55-4.74. Three endothermic peaks were noted. The low temperature endothermic peak in each sample was observed between 48-109°C. It was present in all the samples and it was linked to the dehydration of samples. The second low temperature peak was observed between 223-285°C. This temperature peak was only present in BKL 01, BKL 02, DBB CN01, LBB 01, LBB 02, LBB 03, MSL I 02, YTK 01 and YTK 02A. This peak was attributed to the pre-hydroxylation of the samples. The third endothermic peak was found between 469-531°C, and it was attributed to the dehydroxylation of the kaolins.

One exothermic peak, corresponding to the formation of mullite, was observed between 943-988°C. However, in YTK 02A, it was observed at 905°C; and in BKL 01, BKL 03, EDK 01, EDK 02, EDK 03, MSL I 01, YTK 01 and YTK 03, it was greater than 1000°C. Samples were heated up to 1000°C, therefore exothermic peak temperatures above 1000°C were not recorded.

Table 4.6: TGA-DSC endothermic and exothermic peak temperatures and main reactions of < 2 µm kaolin samples

	Endothermic Peak Temperatures			Exothermic Peak Temperatures[#]
Reactions	Dehydration* ($T \leq 200^oC$)	Pre-dehydroxylation* ($200 \leq T \leq 450^oC$)	Dehydroxylation[#] ($450 \leq T_d \leq 700^oC$)	Mullite formation from metakaolinite ($925 \leq T_t \leq 1050^oC$)
Samples				
BKL 01	56.54	266.89	483.81	nr
BKL 02	68	244.25	494.23	971.56
BKL 03	86.74	-	478.34	nr
DBB	50	-	494.34	985.4
DBB CN 01	57.49	238.15	496.5	987.39
DBB CN 02	47.76	-	492.25	974.47
EDK 01	68.36	-	524.56	nr
EDK 02	56.03	-	517.38	nr
EDK 03	84.91	-	530.77	nr
LBB 01	73.17	234.26	492.85	983.79
LBB 02	56.43	234.19	492.21	985.26
LBB 03	66.23	223.76	482.18	986
MSL I 01	108.84	-	505.17	nr
MSL I 02	65.02	266.82	491.8	981.68
MSL II 01	50.34	-	496.12	968.03
MSL II 02	54.75	-	498.65	970.11
YTK 01	60.83	284.01	478.82	nr
YTK 02A	64.92	266.54	491.5	905.86
YTK 02B	82.37	-	469.53	943.56
YTK 03	55.69	-	491.67	nr
Minimum	47.76	223.76	469.53	905.86
Maximum	108.84	284.01	530.77	987.39

*Dehydration and pre-dehydroxylation temperatures were derived from TGA-DTG curves
[#]Dehydroxylation and exothermic peak temperatures were derived from DSC curves
(-): No peak; (nr): Not recorded, $T_t > 1000^oC$

Weight loss at T ≤ 450°C varied between 0.6% (DBB CN 01) and 6% (MSL I 01); it was due to the release of adsorbed water in pores. Dehydroxylation of kaolinite caused higher weight loss, varying from 5.6% (EDK 03)-13.6% (DBB CN 01).

Table 4.7: Weight loss during heating of kaolin samples

Samples	Weight loss at T ≤ 450°C	Weight loss at 450°C ≤ Td ≤ 700°C	Total weight loss
BKL 01	2.0%	12.0%	14.0%
BKL 02	1.6%	12.3%	13.9%
BKL 03	0.8%	5.7%	6.5%
DBB	0.8%	13.5%	14.3%
DBB CN 01	0.6%	13.6%	14.2%
DBB CN 02	1.6%	12.6%	14.2%
EDK 01	1.0%	6.6%	7.6%
EDK 02	-	8.6%	8.6%
EDK 03	0.9%	5.6%	6.5%
LBB 01	1.4%	12.8%	14.2%
LBB 02	1.6%	12.8%	14.4%
LBB 03	1.6%	12.9%	14.5%
MSL I 01	6.0%	9.2%	15.2%
MSL I 02	1.6%	12.6%	14.2%
MSL II 01	0.8%	12.4%	13.2%
MSL II 02	-	12.2%	12.2%
YTK 01	4.0%	10.2%	14.2%
YTK 02A	4.0%	9.2%	13.2%
YTK 02B	2.8%	8.4%	11.2%
YTK 03	2.0%	11.0%	13.0%
Minimum	0.6%	5.6%	6.5%
Maximum	6%	13.6%	15.2%

(-): No weight loss

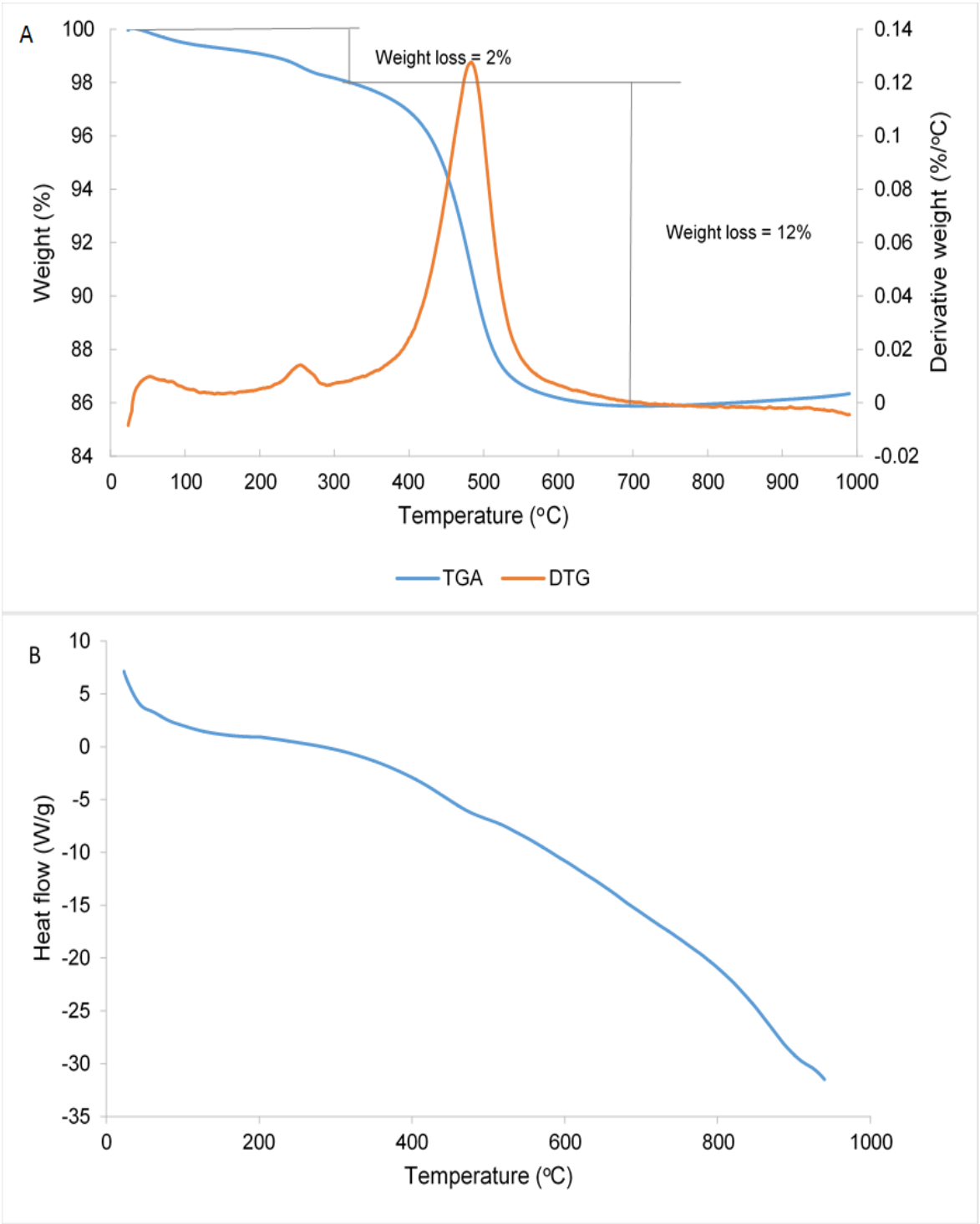

Figure 4.55: Thermal analysis of BKL 01: A) TGA-DTG curve; B) DSC curve

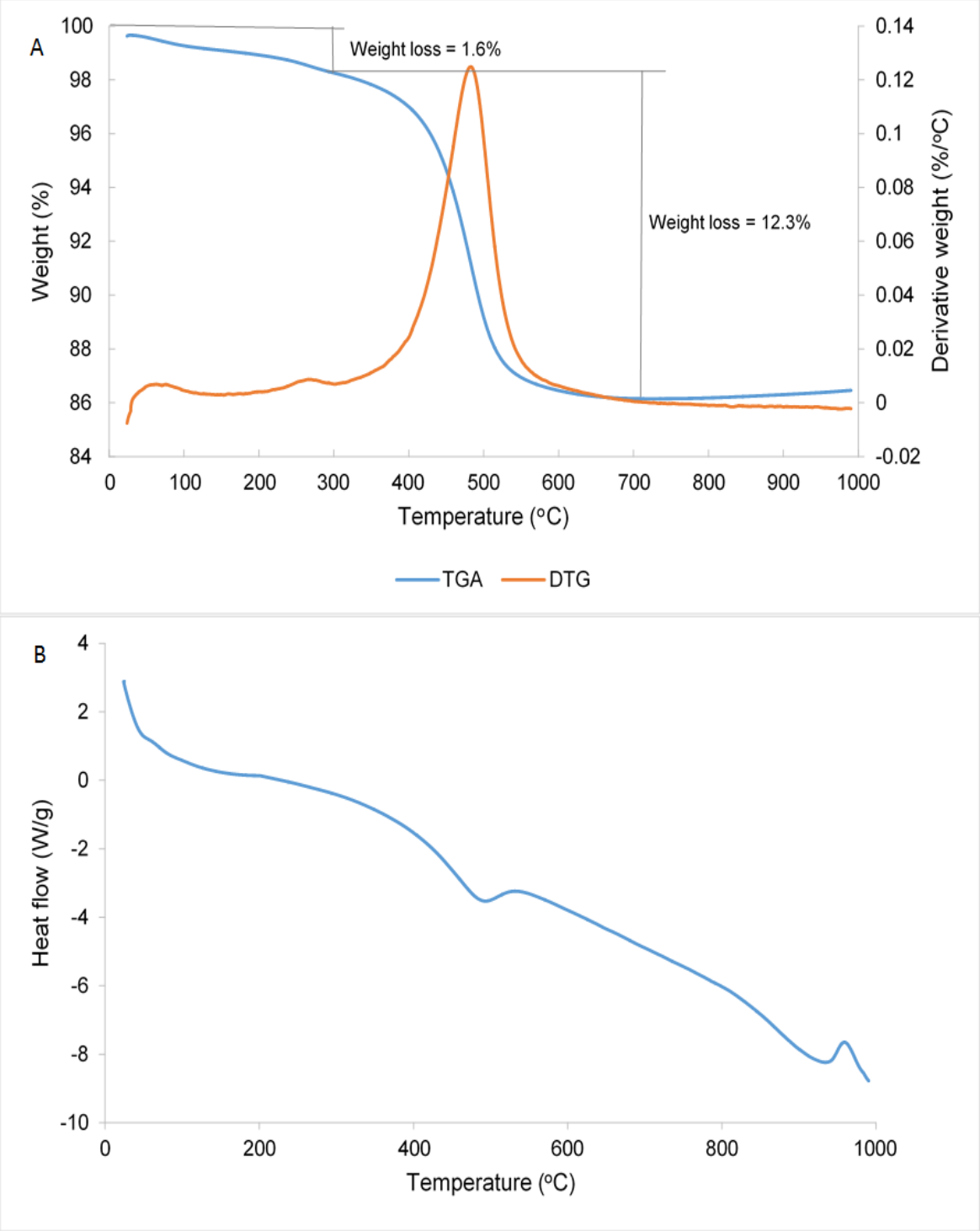

Figure 4.56. : Thermal analysis of BKL 02: A) TGA-DTG curve; B) DSC curve

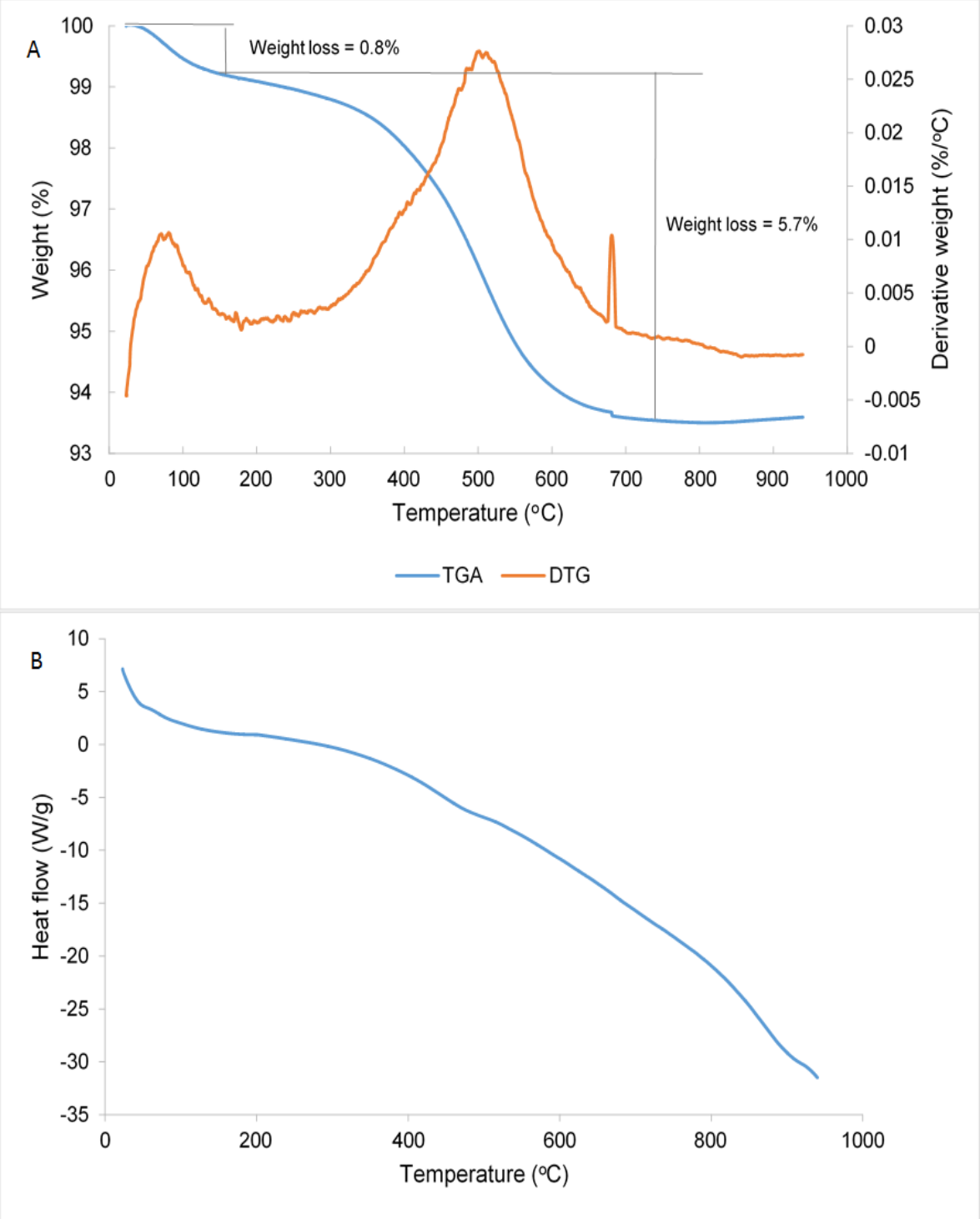

Figure 4.57: Thermal analysis of BKL 03: A) TGA-DTG curve; B) DSC curve

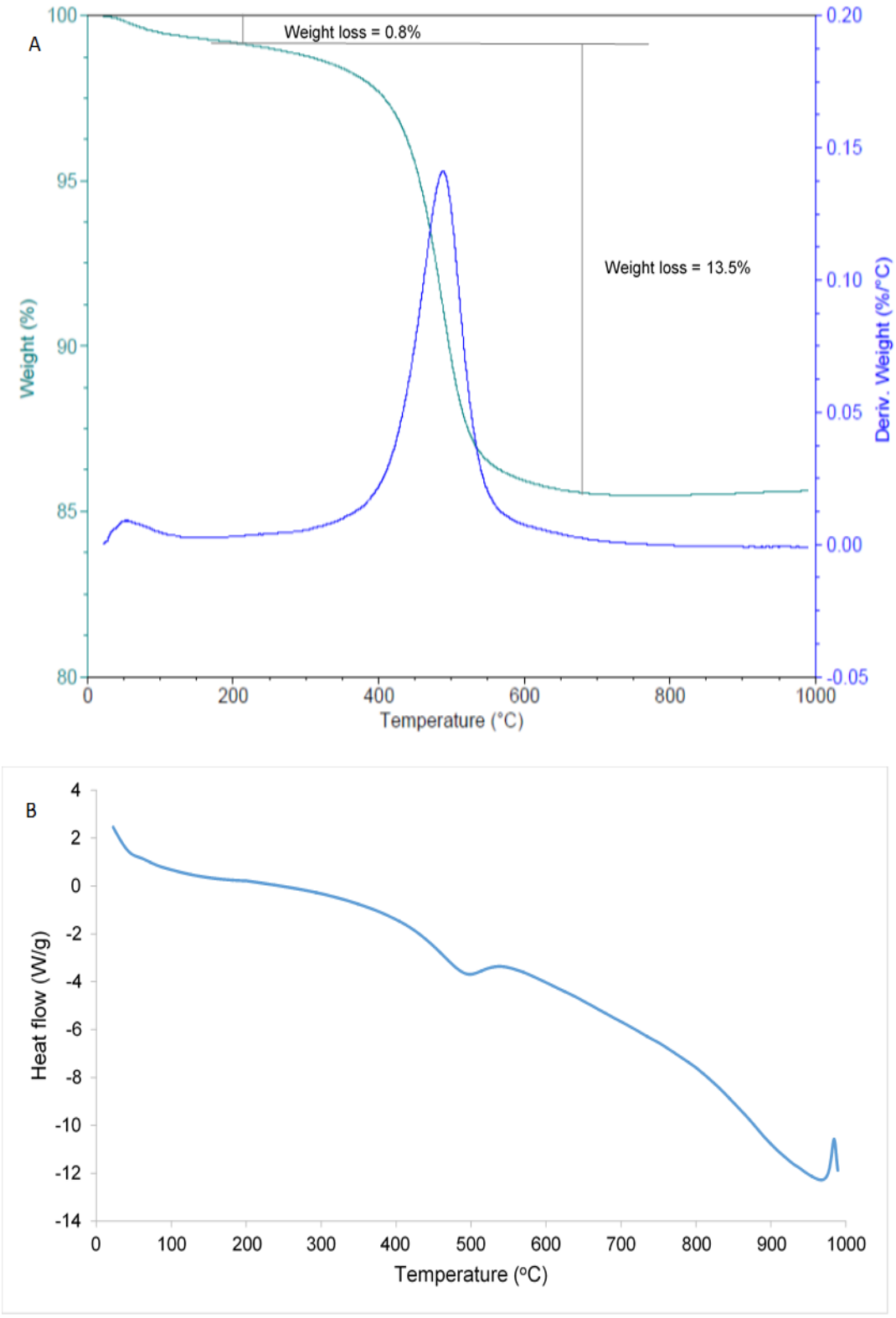

Figure 4.58: Thermal analysis of DBB: A) TGA-DTG curve; B) DSC curve

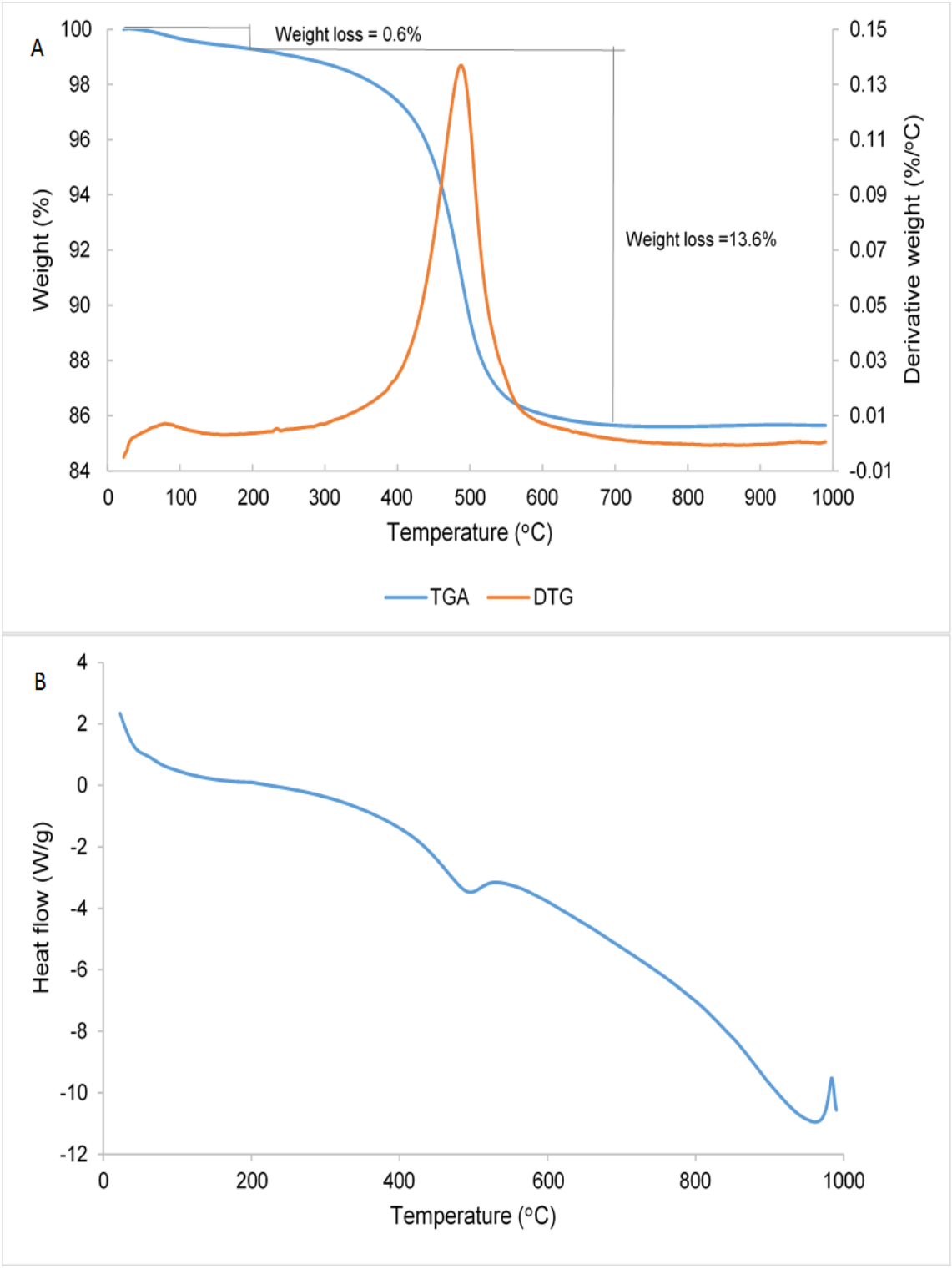

Figure 4.59: Thermal analysis of DBB CN 01: A) TGA-DTG curve; B) DSC curve

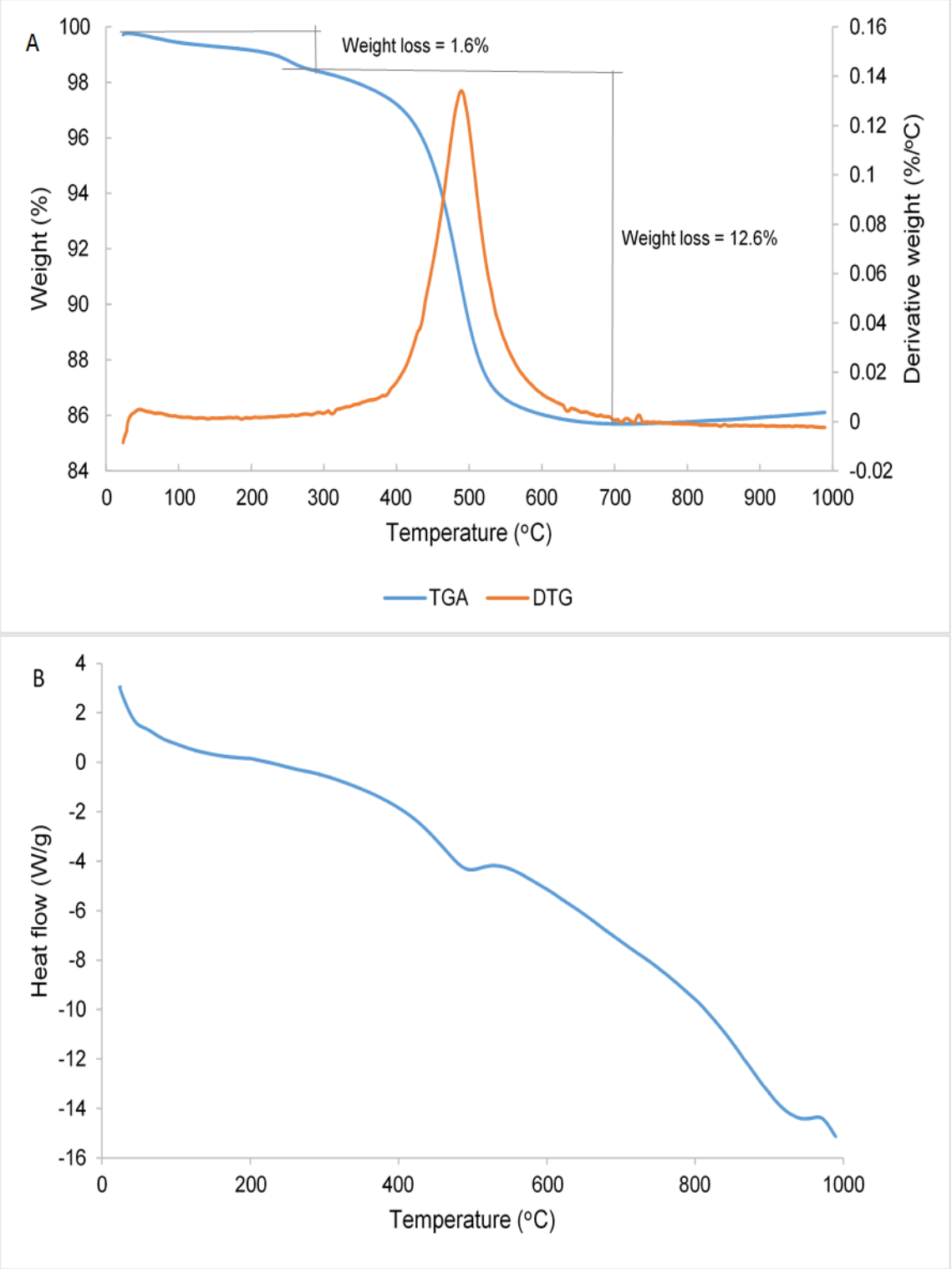

Figure 4.60: Thermal analysis of DBB CN 02: A) TGA-DTG curve; B) DSC curve

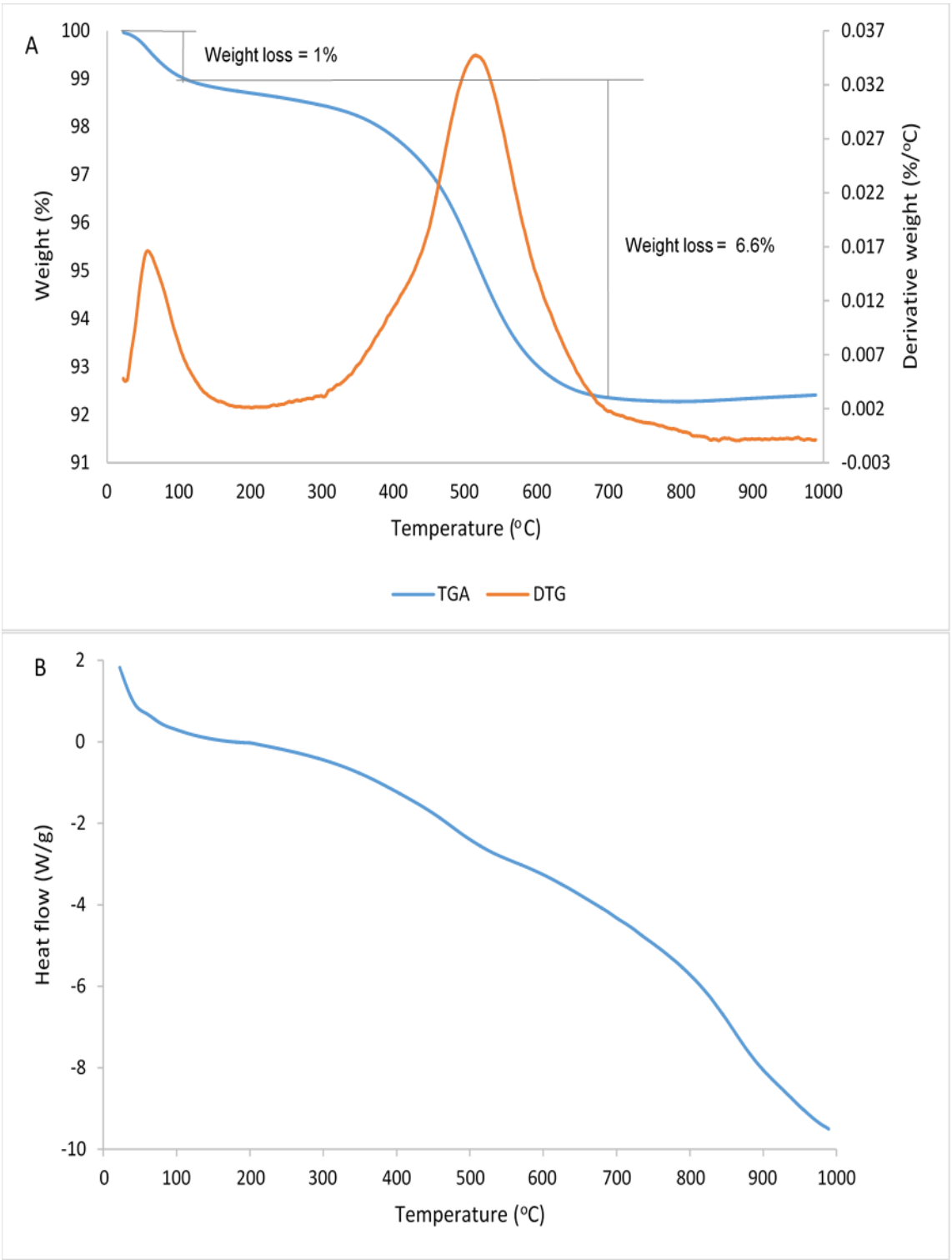

Figure 4.61: Thermal analysis of EDK 01: A) TGA-DTG curve; B) DSC curve

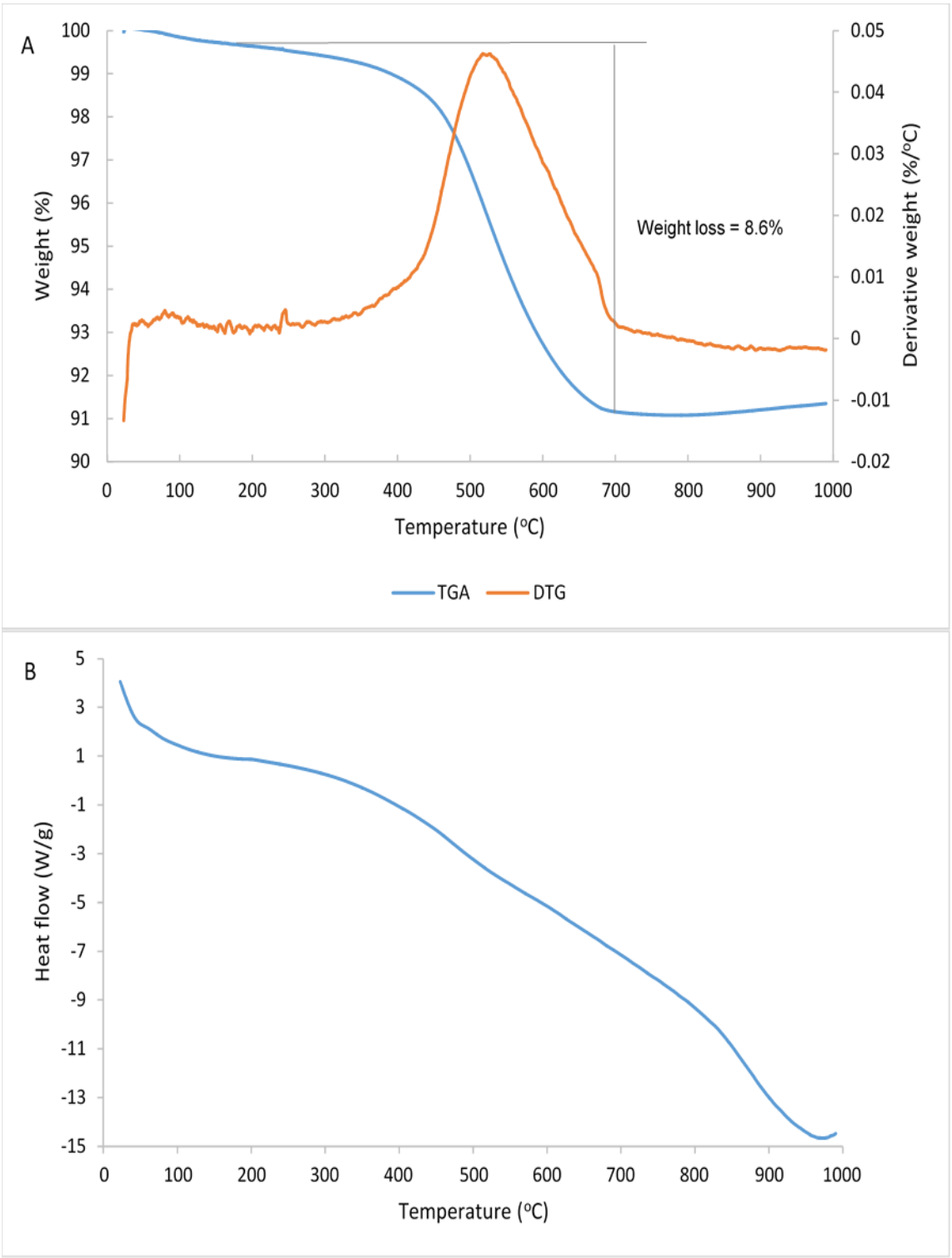

Figure 4.62: Thermal analysis of EDK 02: A) TGA-DTG curve; B) DSC curve

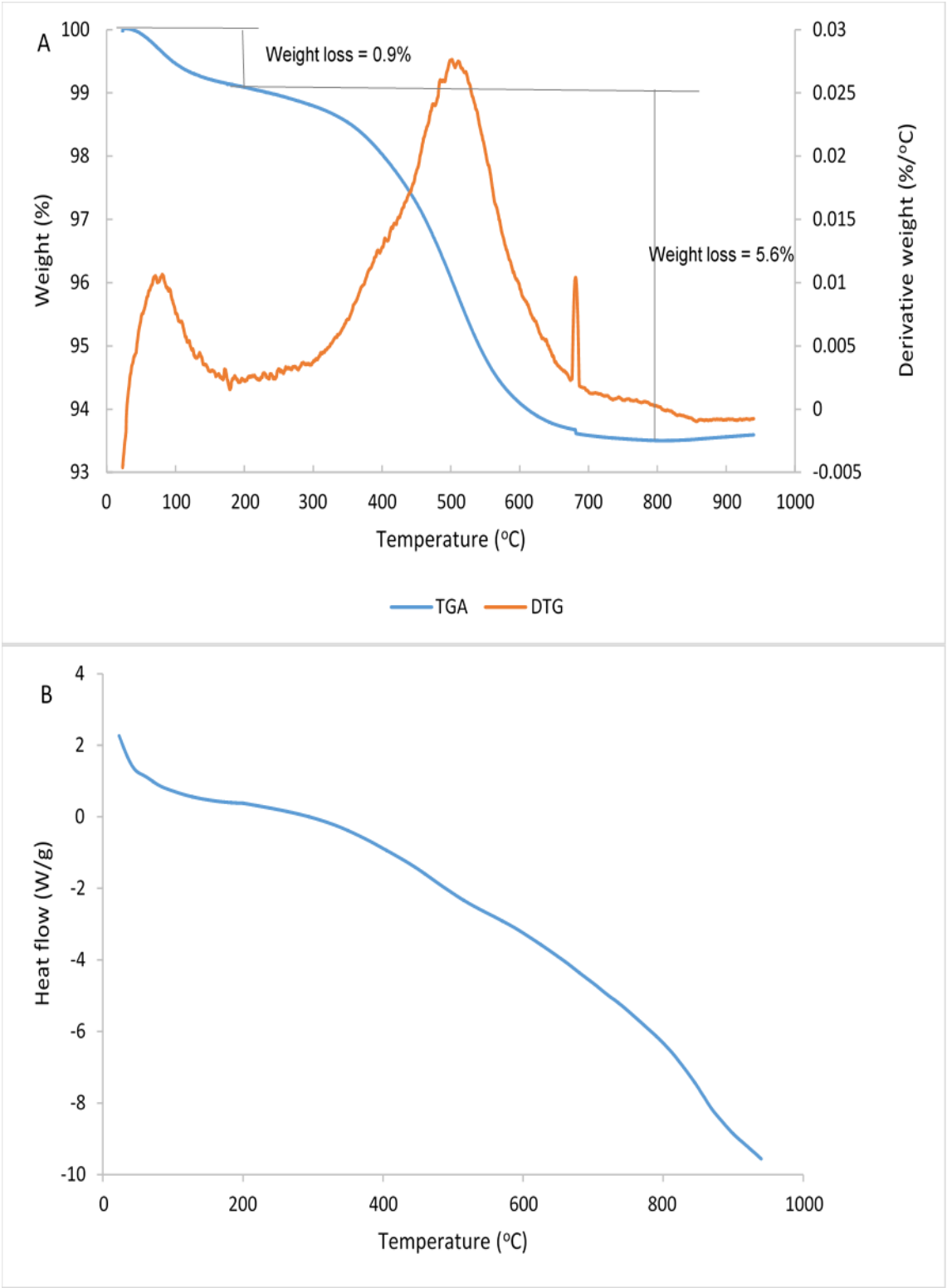

Figure 4.63: Thermal analysis of EDK 03: A) TGA-DTG curve; B) DSC curve

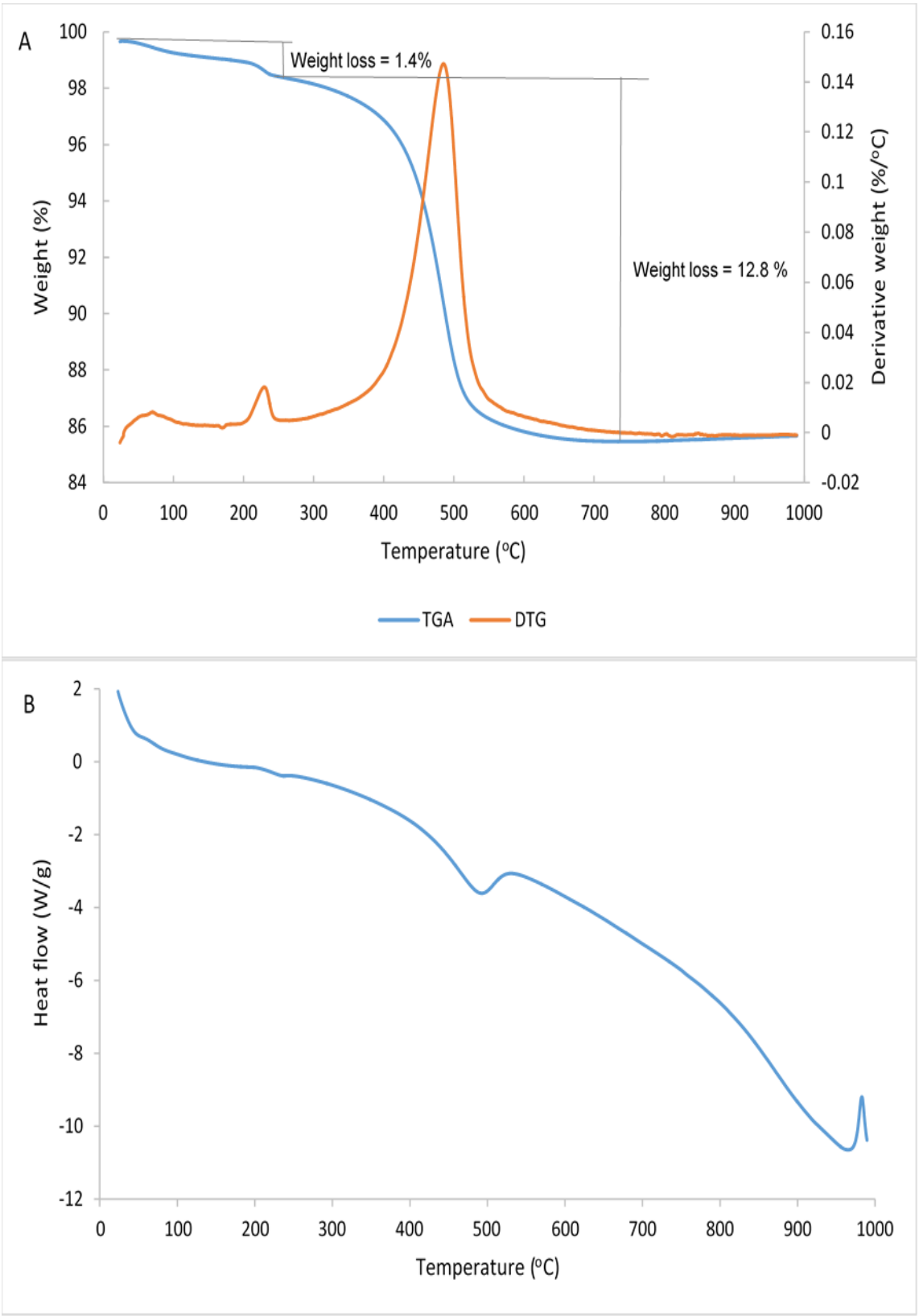

Figure 4.64: Thermal analysis of LBB 01: A) TGA-DTG curve; B) DSC curve

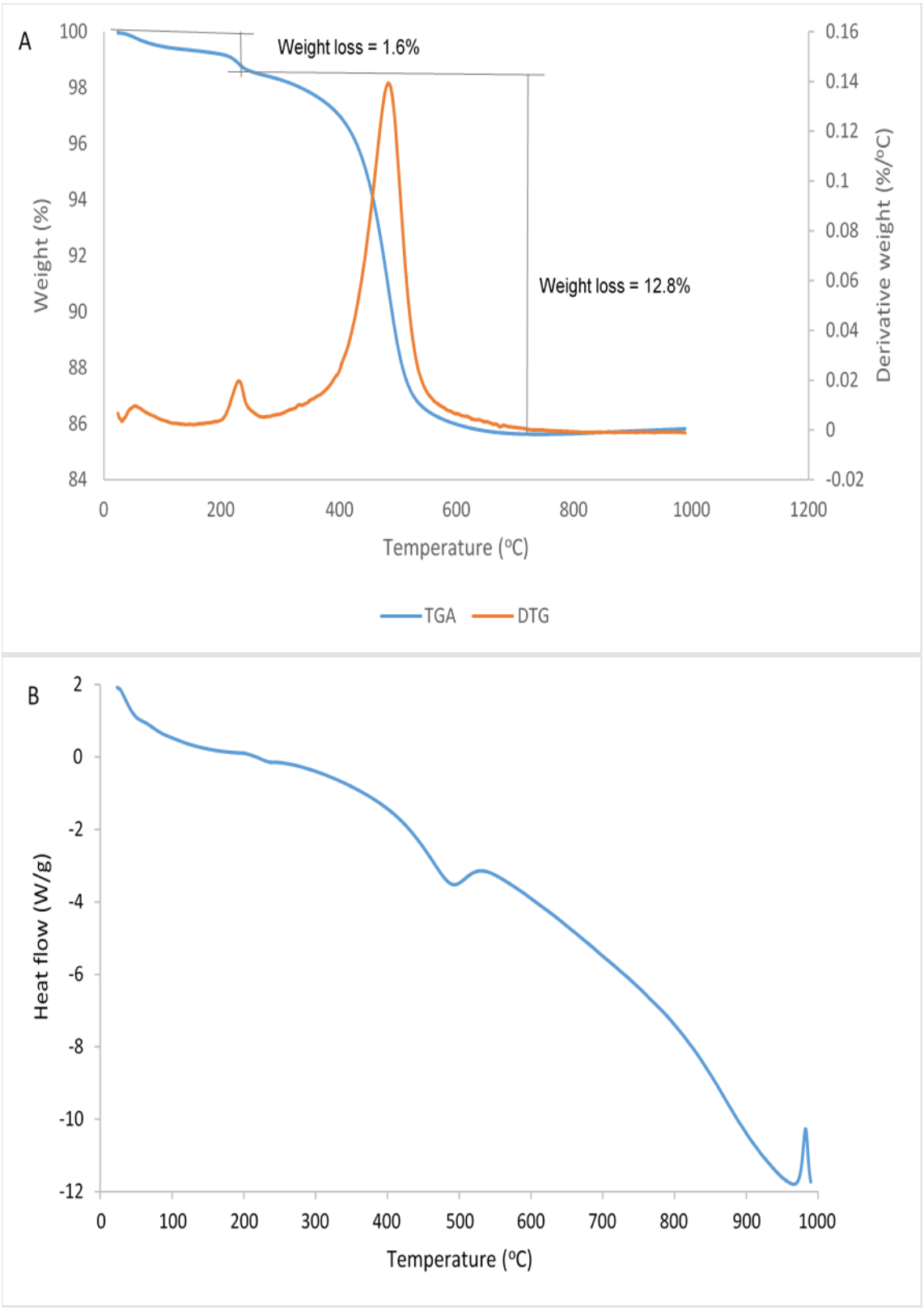

Figure 4.65: Thermal analysis of LBB 02: A) TGA-DTG curve; B) DSC curve

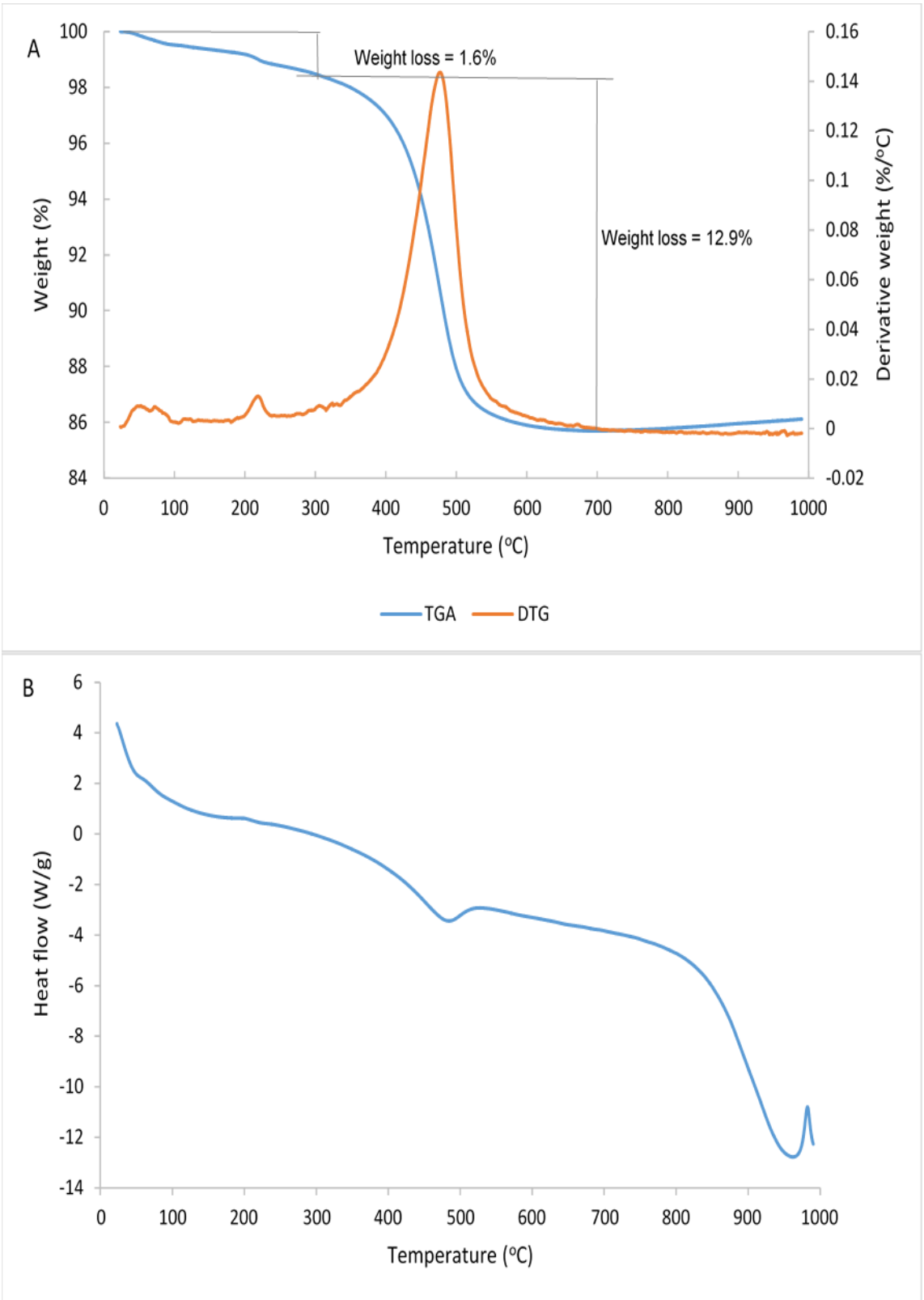

Figure 4.66: Thermal analysis of LBB 03: A) TGA-DTG curve; B) DSC curve

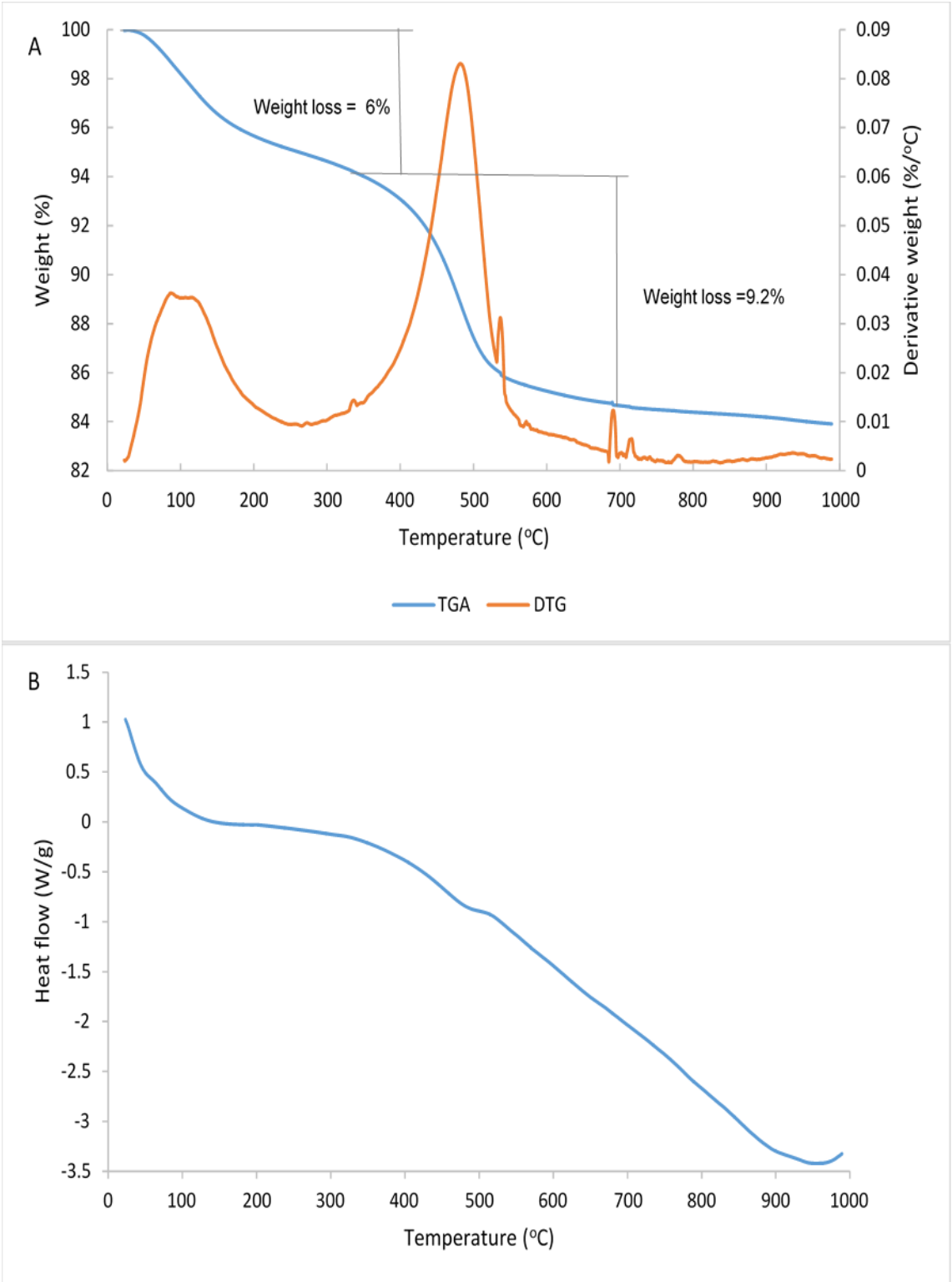

Figure 4.67: Thermal analysis of MSL I 01: A) TGA-DTG curve; B) DSC curve

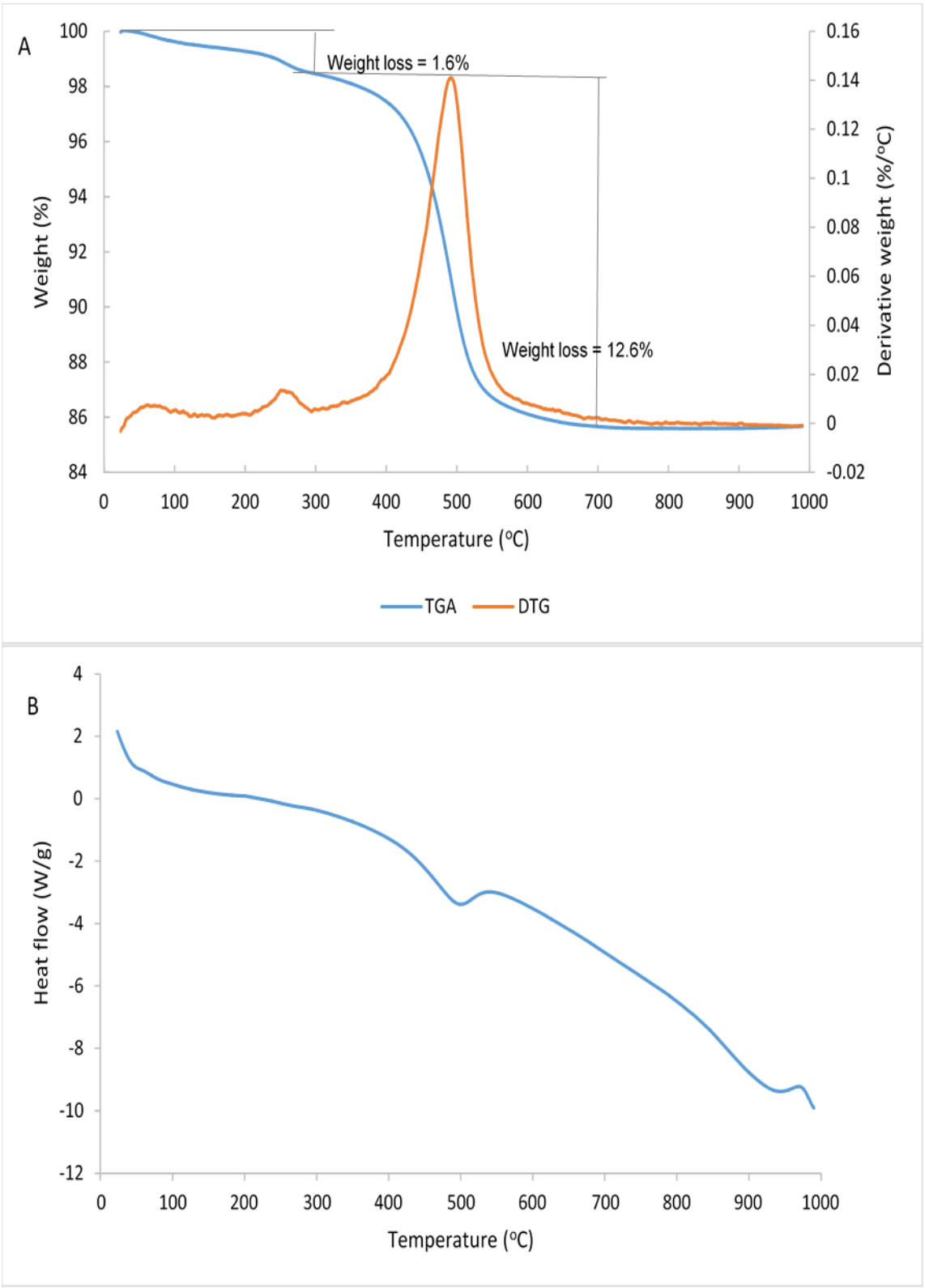

Figure 4.68: Thermal analysis of MSL I 02: A) TGA-DTG curve; B) DSC curve

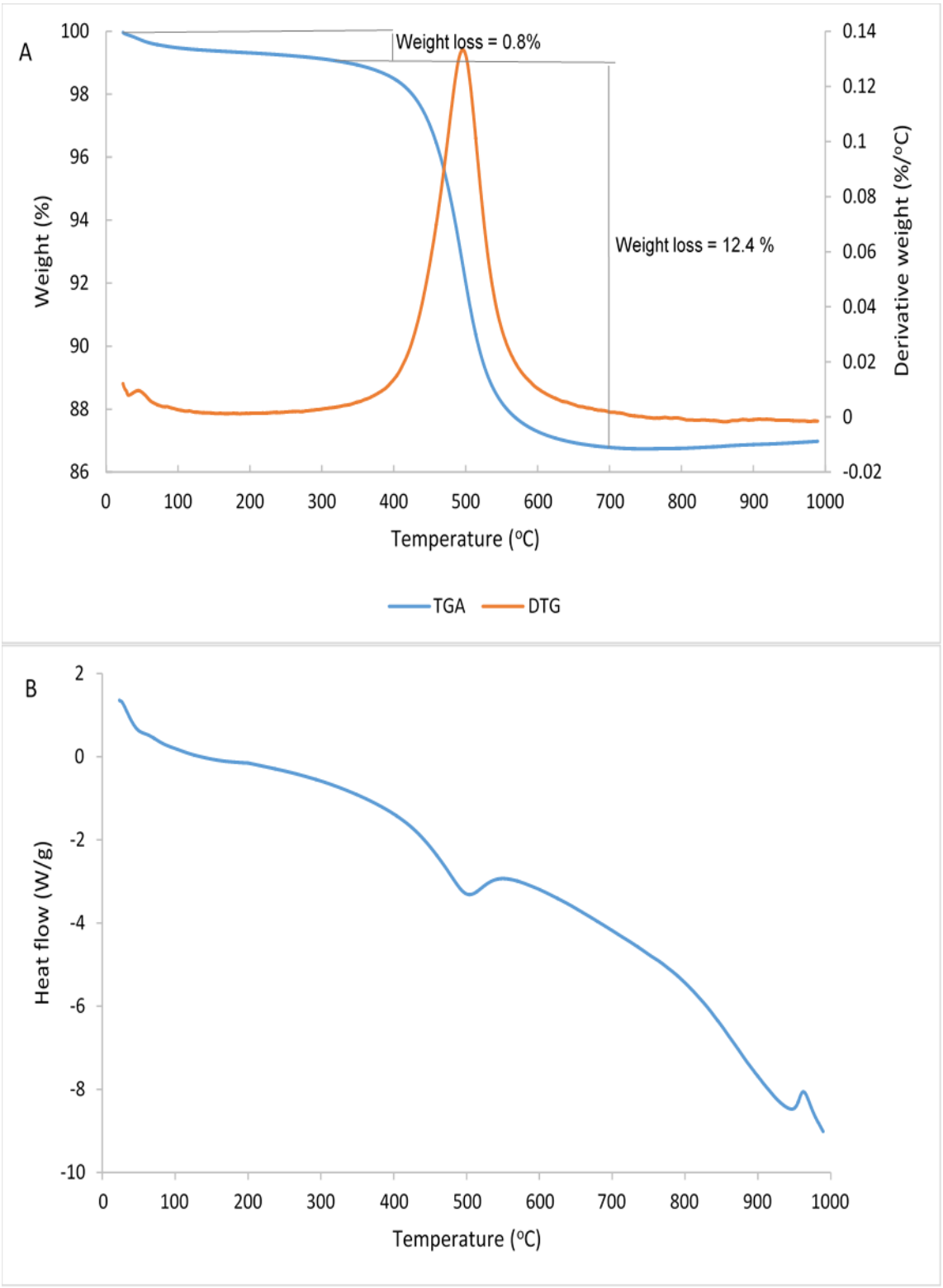

Figure 4.69: Thermal analysis of MSL II 01: A) TGA-DTG curve; B) DSC curve

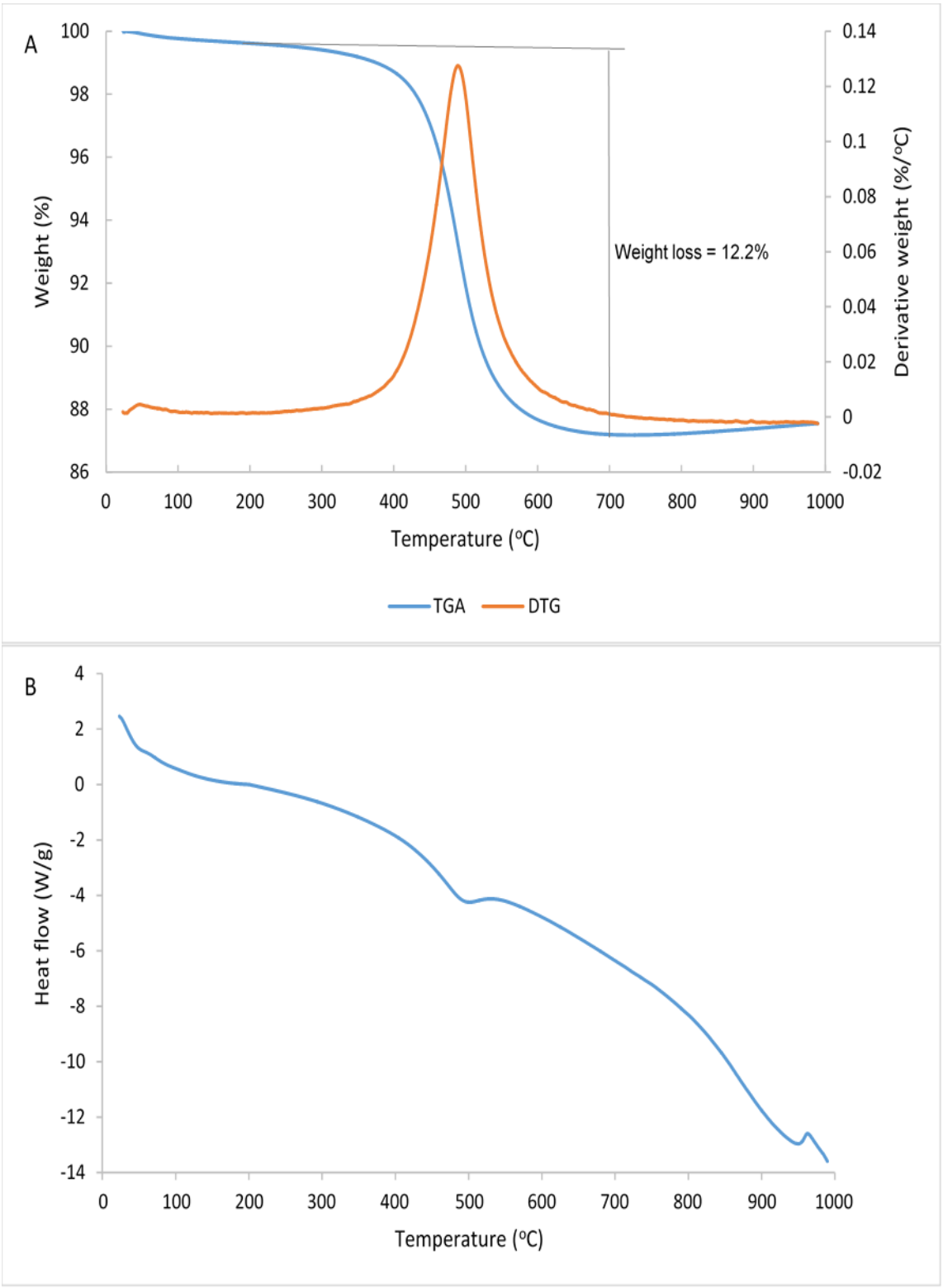

Figure 4.70: Thermal analysis of MSL II 02: A) TGA-DTG curve; B) DSC curve

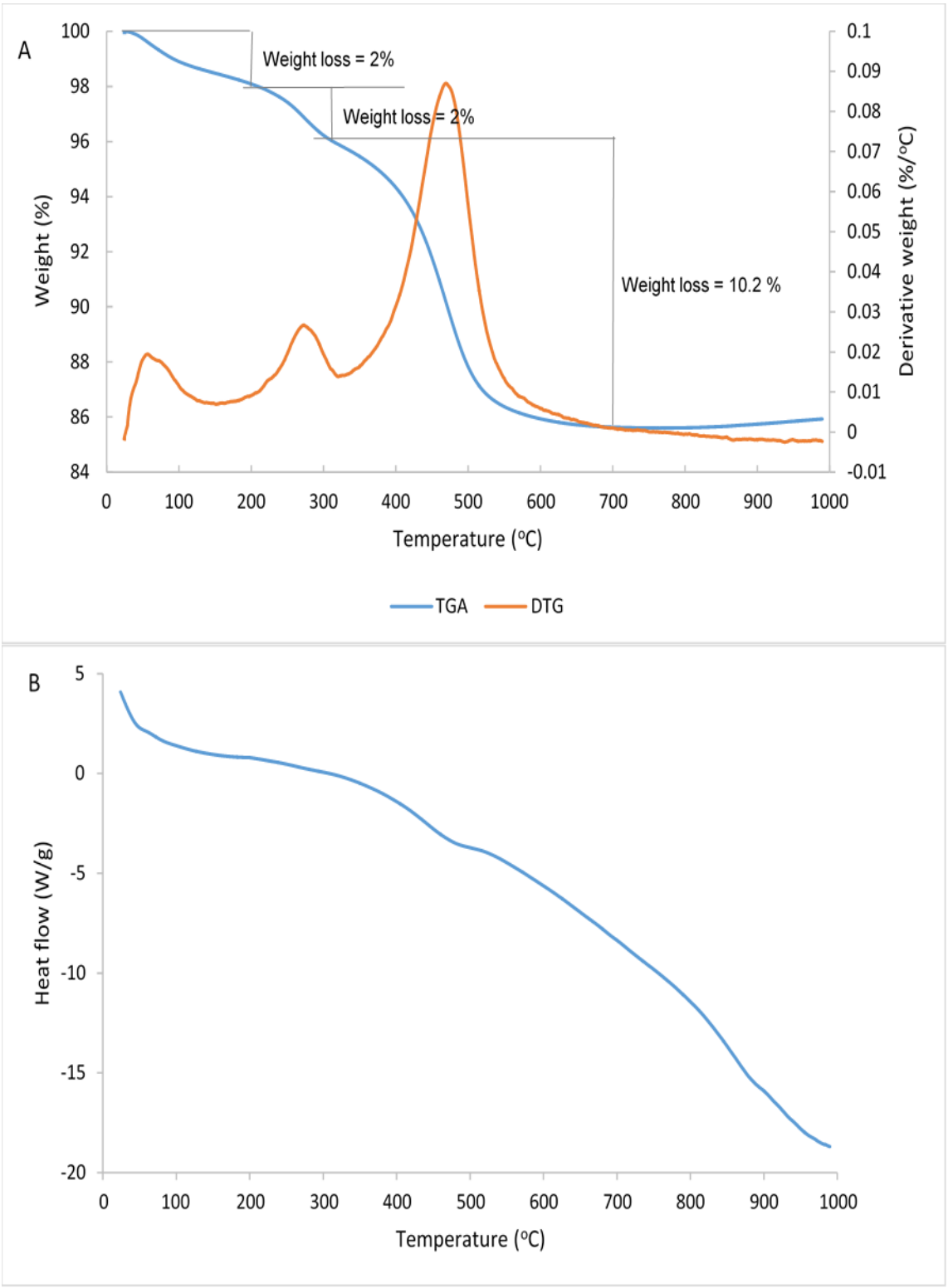

Figure 4.71: Thermal analysis of YTK 01: A) TGA-DTG curve; B) DSC curve

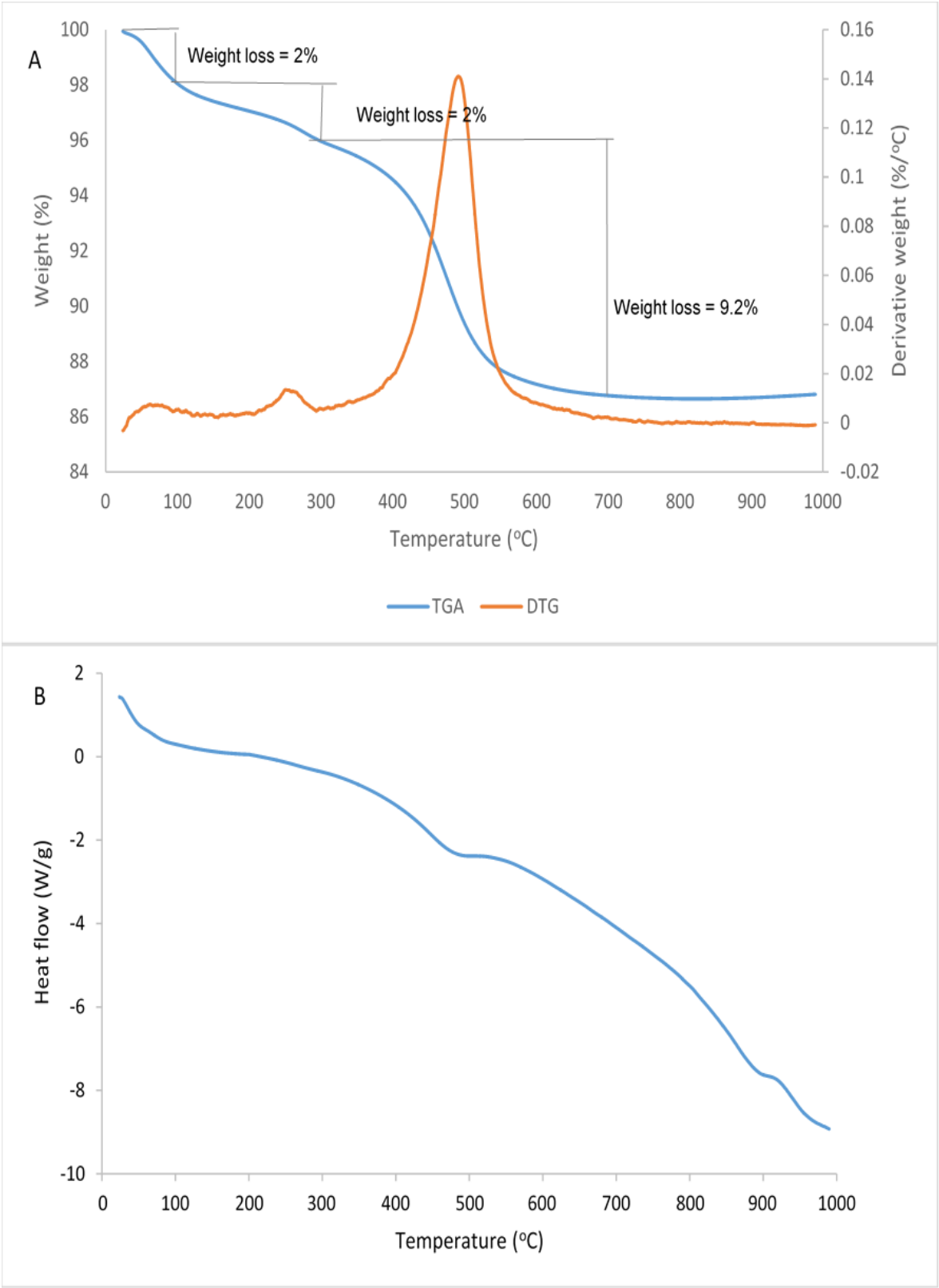

Figure 4.72: Thermal analysis of YTK 02A: A) TGA-DTG curve; B) DSC curve

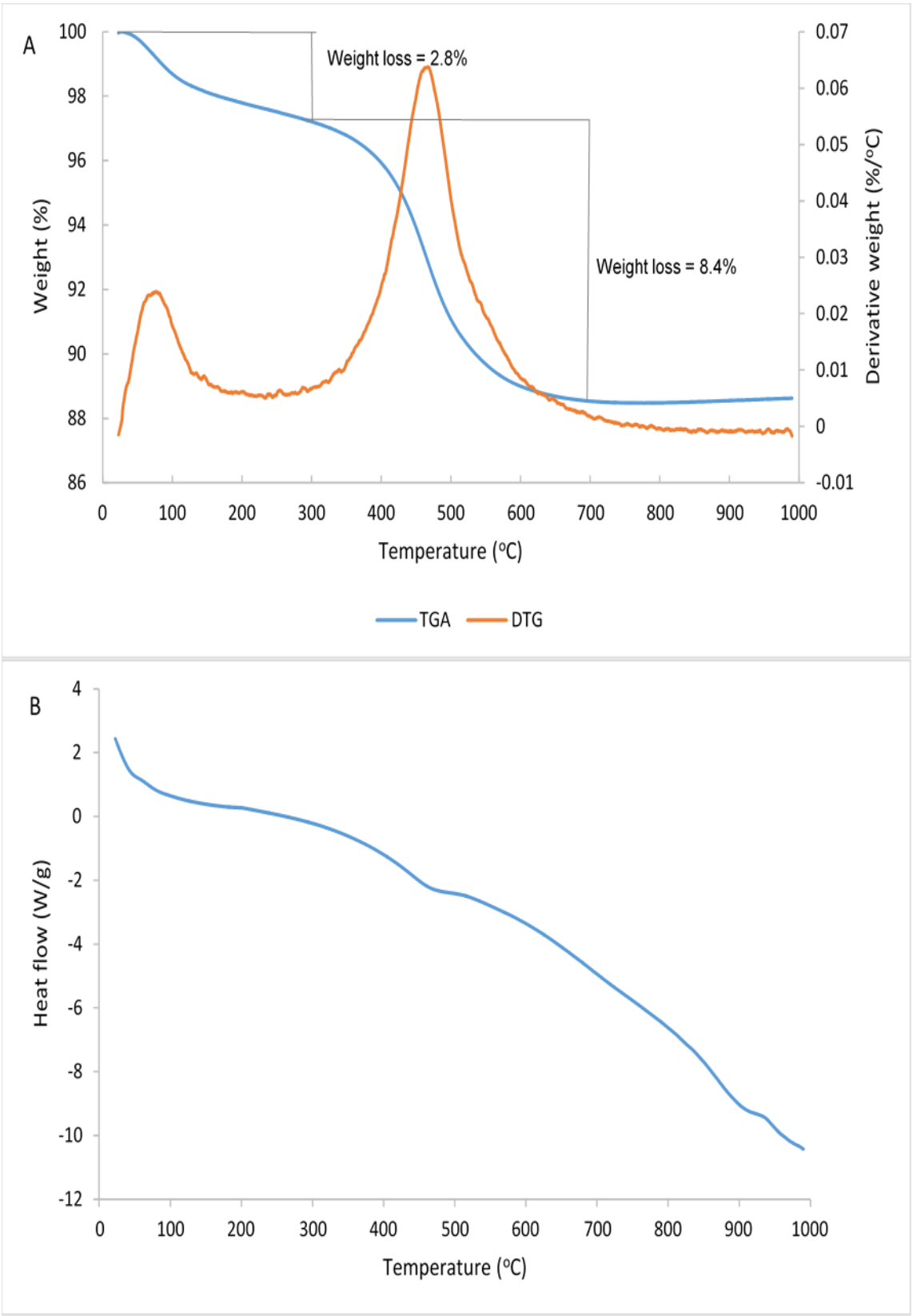

Figure 4.73: Thermal analysis of YTK 02B: A) TGA-DTG curve; B) DSC curve

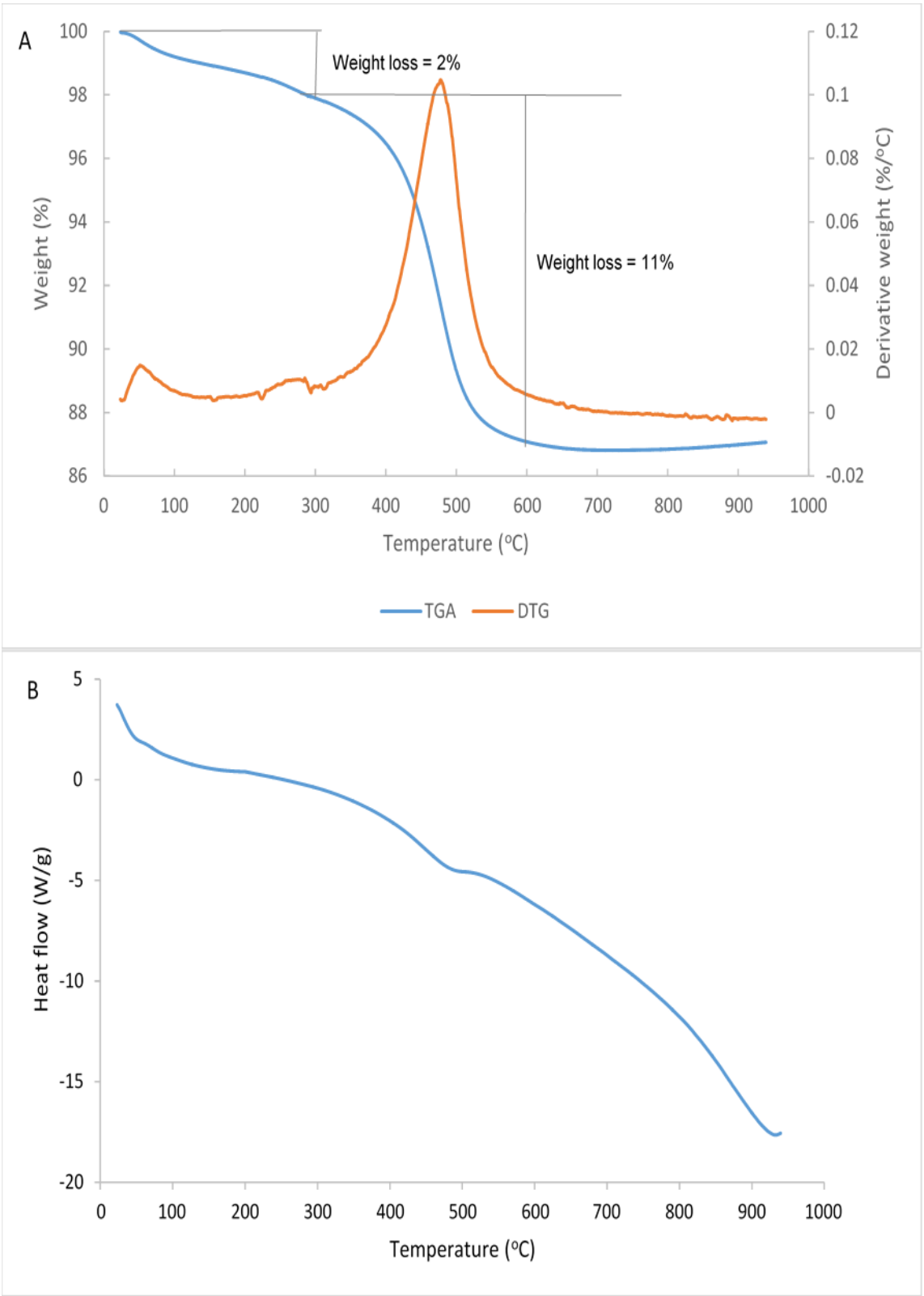

Figure 4.74: Thermal analysis of YTK 03: A) TGA-DTG curve; B) DSC curve

4.4 Geochemical characterisation

4.4.1 Major oxides geochemistry

Results of the chemical analysis of bulk samples, silt and < 2 µm fractions are summarised in Appendices 4.7 - 4.9.

4.4.1.1 Bulk kaolins (< 2 mm samples)

SiO_2 and Al_2O_3

DBB, DBB CN 01, DBB CN 02, LBB 03, MSLI 01, MSLI 02 bulk samples had SiO_2 concentrations greater than 60.5%. Other bulk samples had SiO_2 concentrations varying between 46.87-60.31 wt %. Al_2O_3 varied between 9.14 wt % (DBB CN 02) to 32.90 wt % (MSL II 01) (Figure 4.75). Bulk samples portrayed an inverse relationship between Al_2O_3 and SiO_2 concentrations, with r^2 =0.72 (Figure 4.76)

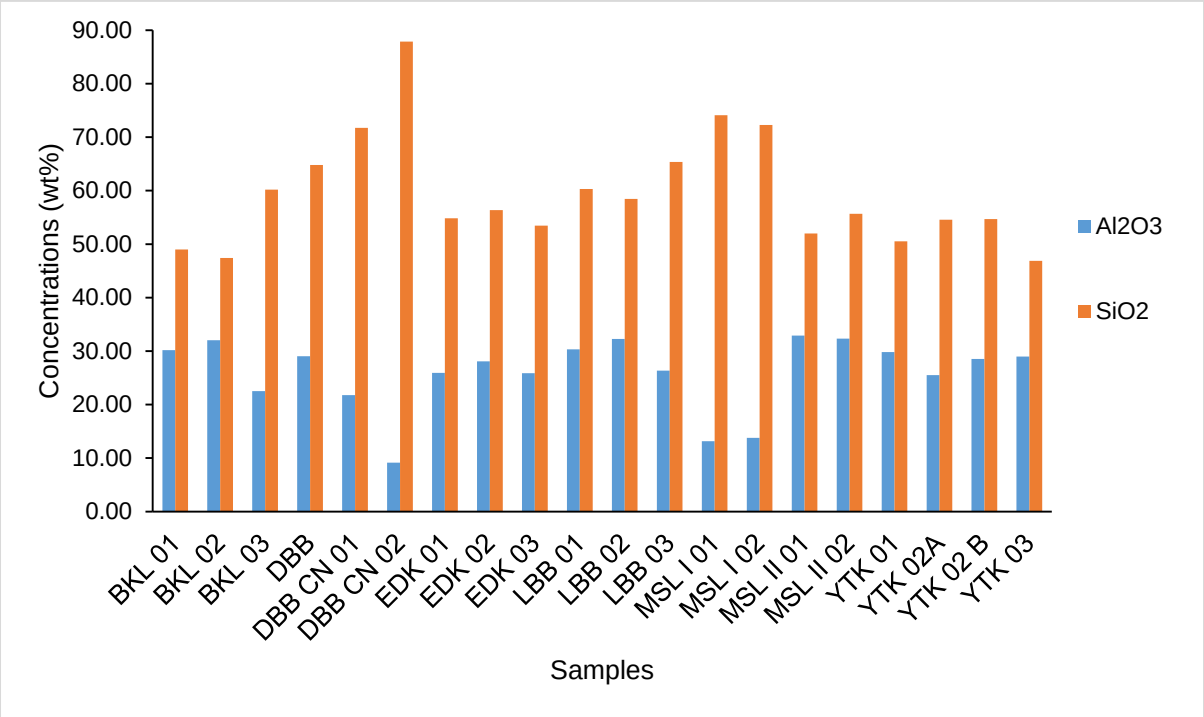

Figure 4.75: Al_2O_3 and SiO_2 concentrations of bulk samples

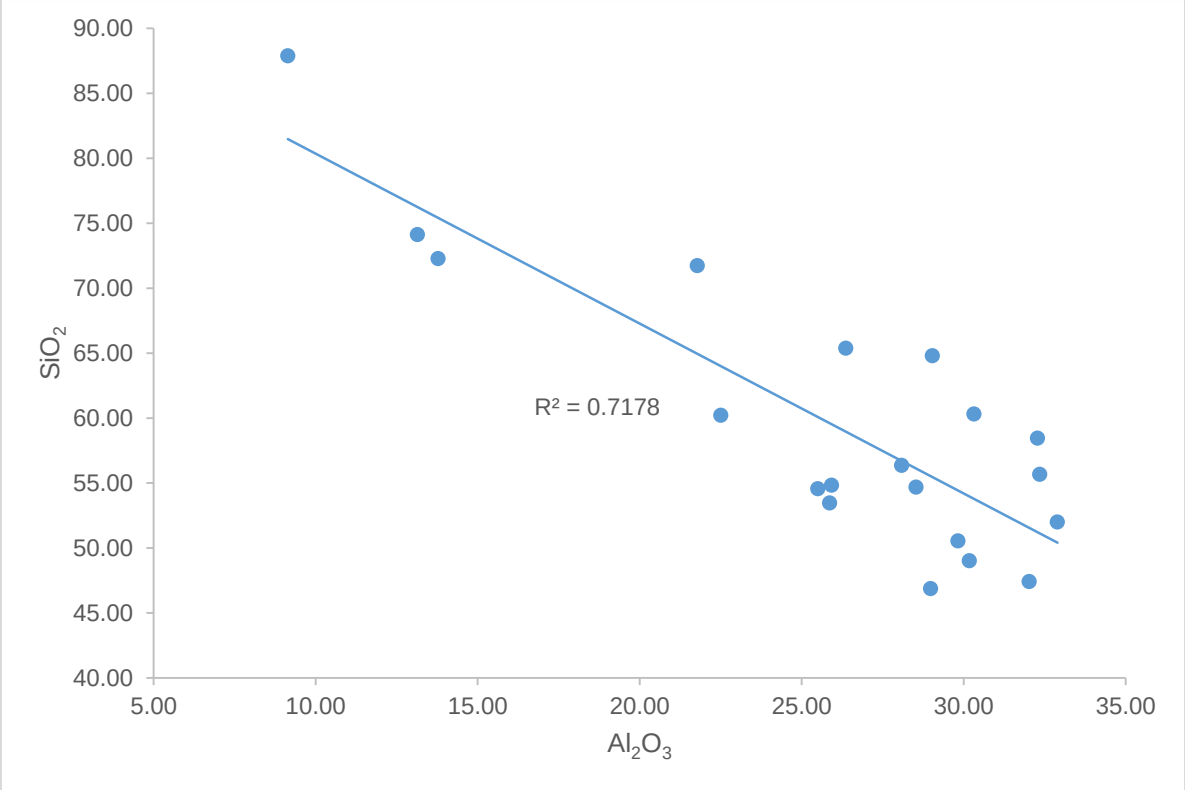

Figure 4.76: Scatter plot diagram of SiO_2 versus Al_2O_3 concentrations of bulk samples

CaO, Na_2O, K_2O and MgO

Concentrations of CaO, Na_2O, K_2O and MgO in bulk samples are plotted in Figure 4.77. CaO had very low concentrations in all samples. CaO was < 0.1 wt %. Na_2O had concentrations less than 0.1 wt %, except BKL03 (0.13 wt %) and EDK 02 (0.11 wt %). Na_2O was not detected in DBB CN 01, DBB CN 02 and LBB 03. Ediki samples had the highest K_2O concentrations (mean of 7.95 wt %). Other samples had K_2O concentrations < 2 wt %.

MgO concentrations were generally less than 1.00 wt% (Figure 4.77). However, EDK 01 and EDK 03 had MgO concentrations of 1.08 and 1.57 wt%, respectively. In YTK 02A and YTK 02B, MgO concentrations did not vary with particle size. Logbaba samples had the lowest MgO concentrations (< 0.1 wt %).

70% of bulk samples had the sum of CaO, Na_2O, K_2O and MgO (CNKM) less than 2 wt%. Ediki samples had the highest CNKM (>6 wt %). BKL 03, YTK 02A and YTK 02B had CNKM varying between 2.33 and 3.05 wt % (Figure 4.78).

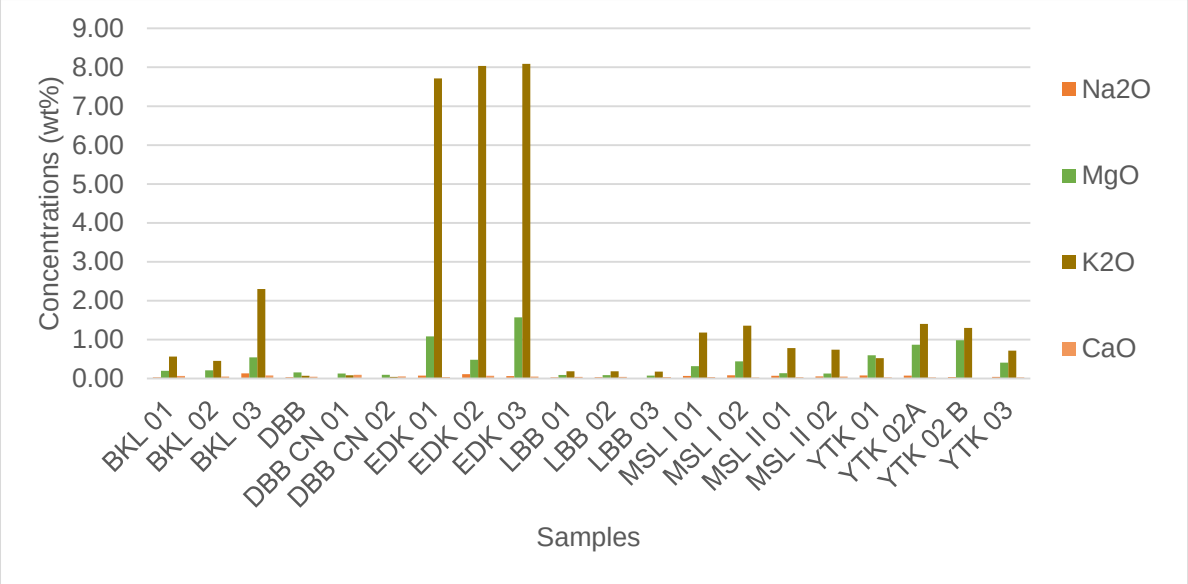

Figure 4.77: CaO, Na_2O, K_2O and MgO concentrations in bulk samples

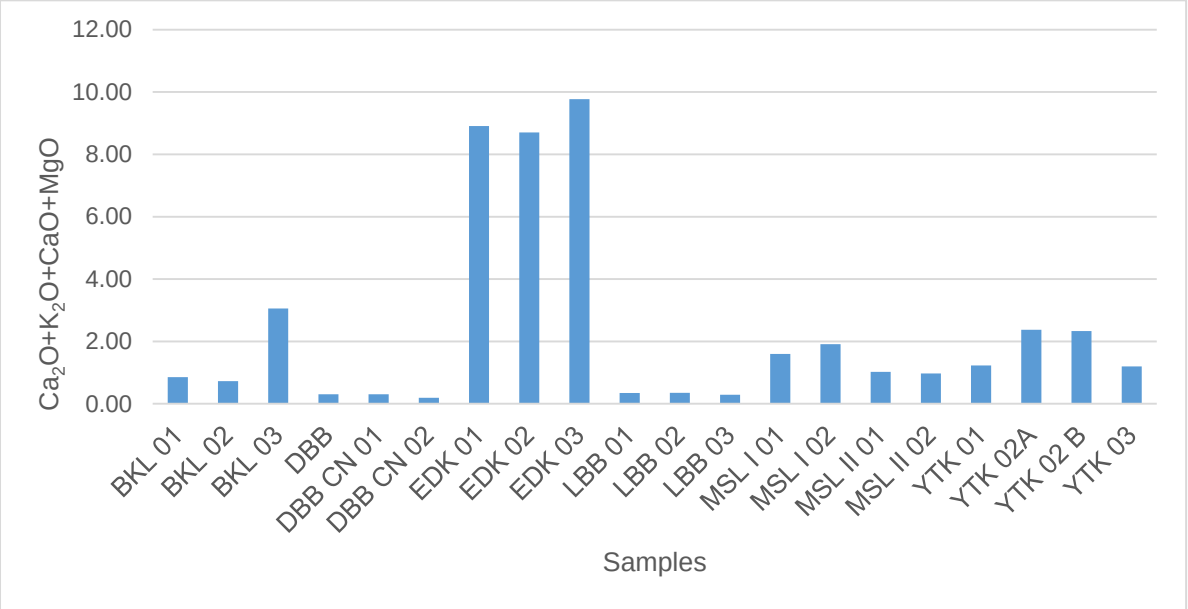

Figure 4.78: Sum of CaO, Na_2O, K_2O and MgO concentrations in bulk samples

TiO_2 and Fe_2O_3

TiO_2 and Fe_2O_3 are usually considered as impurities in kaolins. DBB CN 01 and DBB CN 02 had the lowest TiO_2 concentrations (< 0.40 wt %). High titania contents were observed in MSL II 01 and MSL II 02 (> 3.00 wt %). Fe_2O_3 was higher than TiO_2 in all samples, except in Logbaba samples, where Fe_2O_3 concentrations were less than 2 wt % (Figure 4.79). High

Fe_2O_3 concentrations (> 6.00 wt %) were found in Yatchika and Bomkoul samples, except in YTK 02B (4.56 wt %).

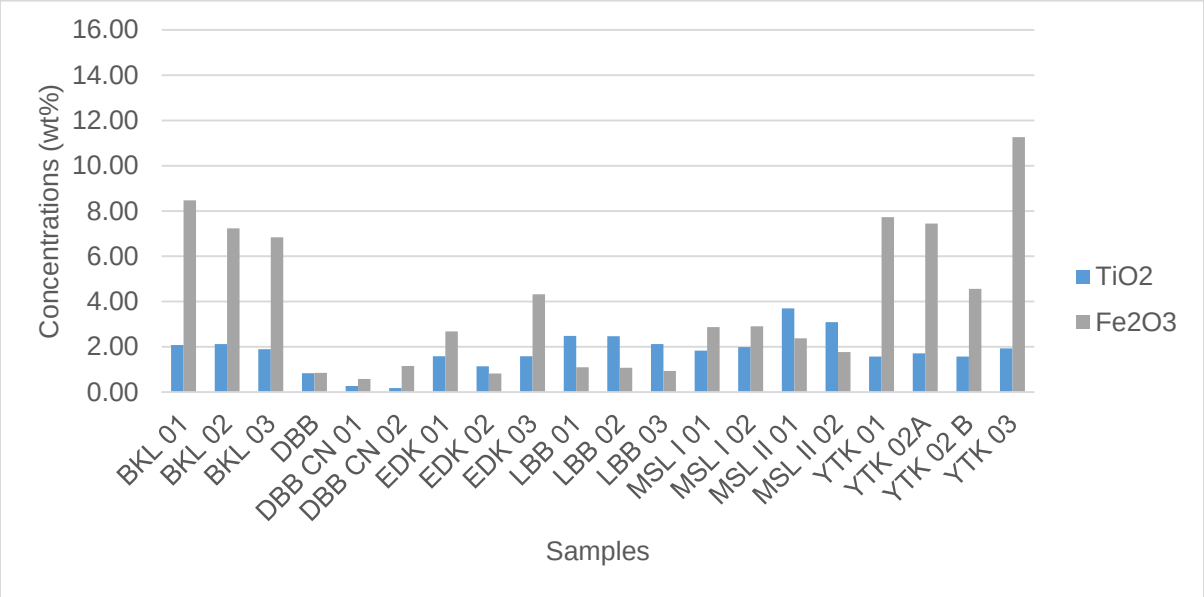

Figure 4.79: TiO_2 and Fe_2O_3 concentrations in bulk samples

P_2O_5 and SO_3

Bulk samples had P_2O_5 concentrations less than 0.40 wt %, except DBB CN 01, which had a P_2O_5 concentration of 0.93 wt%. SO_3 was less than 0.20 wt%; the only exception being in MSL I 01 and MSL I 02, in which SO_3 concentration was slightly above 3.00 wt% (Figure 4.80).

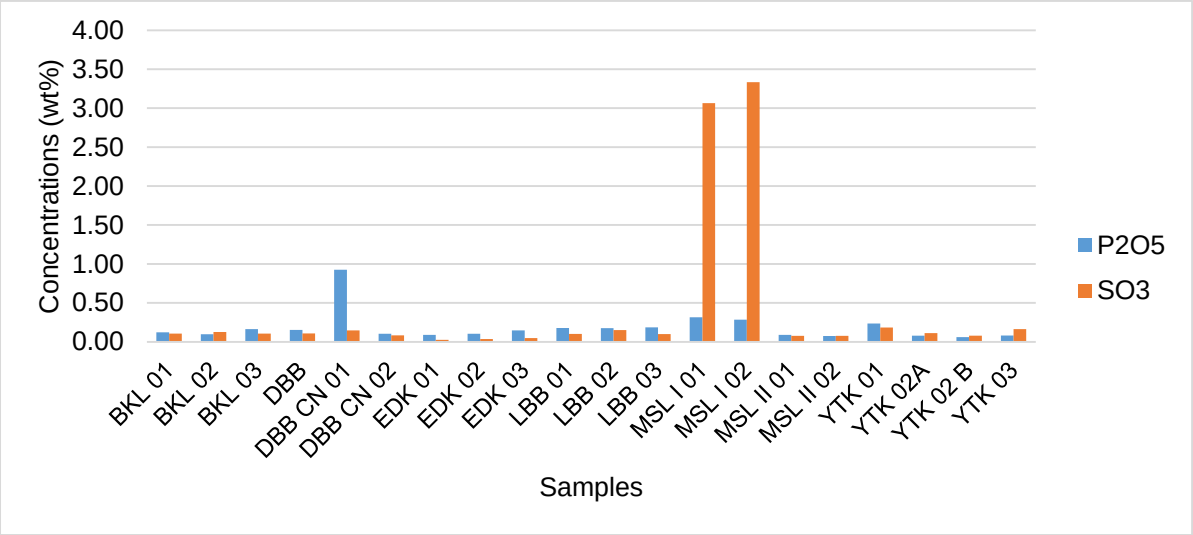

Figure 4.80: P_2O_5 and SO_3 concentrations in bulk samples

K_2O/Al_2O_3

The plot of K_2O/Al_2O_3 is shown in Figure 4.81. Logbaba and Dibamba samples had the lowest ratio (≤ 0.01), whereas Ediki samples had a K_2O/Al_2O_3 ratio greater than 0.250, with EDK 03 having a K_2O/Al_2O_3 ratio greater than 0.300.

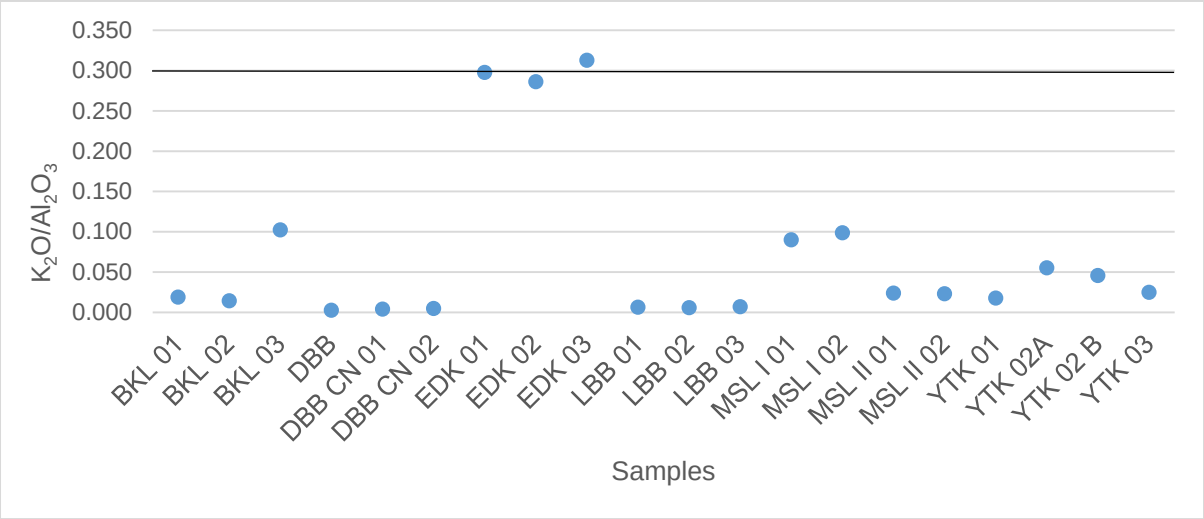

Figure 4.81: Plot of the K_2O/Al_2O_3 ratio of bulk samples showing most samples having a ratio < 0.3

4.4.1.2 Silt samples (2-63 µm fraction)

SiO_2 and Al_2O_3

Silica (SiO_2) was most abundant in BKL 03 (75.18 wt %) and least abundant in DBB (51.34 wt %). Whereas, Al_2O_3 varied between 9.86 wt % (BKL 03) and 32.29 wt % (DBB) (Figure 4.82). Therefore, there was an inverse relationship between SiO_2 and Al_2O_3, with $r^2 = 0.93$ (Figure 4.83).

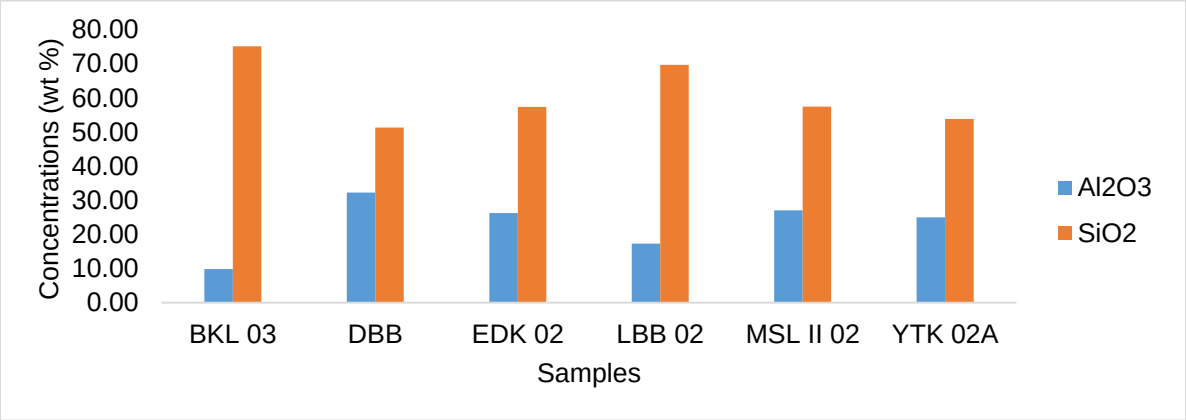

Figure 4.82. : Al_2O_3 and SiO_2 concentrations in silt samples

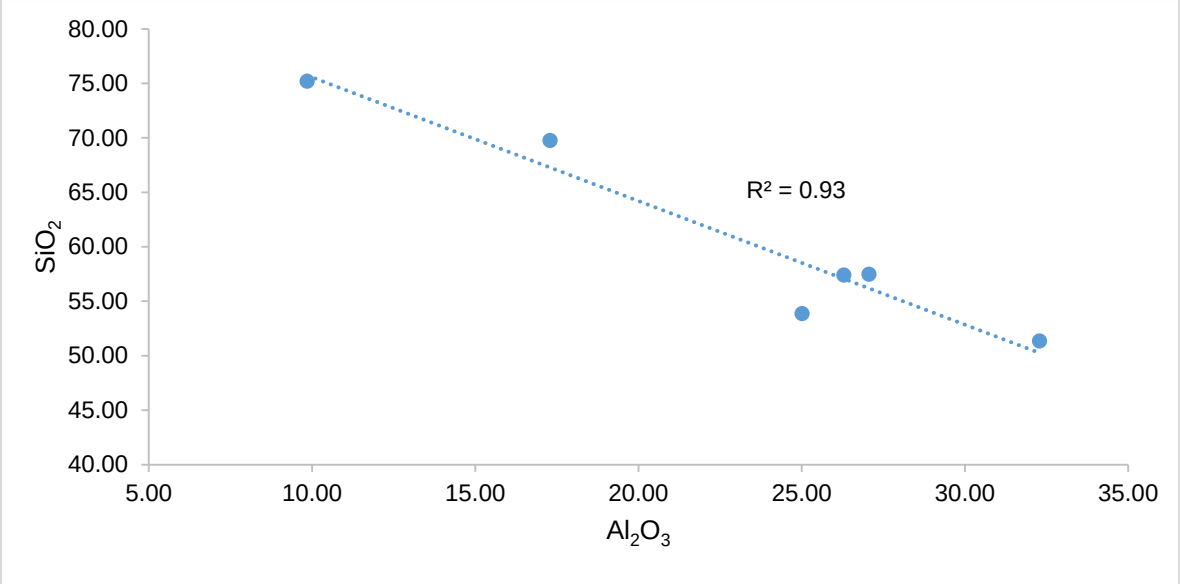

Figure 4.83: Scatter plot diagram of SiO_2 versus Al_2O_3 concentrations of silt samples

CaO, Na_2O, K_2O and MgO

The concentrations of CaO were the lowest of all major oxides, varying from 0.3 wt % (DBB) to 0.29 wt % (BKL 03). Na_2O had concentrations varying between 0.27 wt % (DBB, EDK 02 and MSL II 02) and 0.87 wt % (YTK 02A). Concentrations of K_2O varied between 0.21 wt % (DBB) and 8.27 wt % (EDK 02). MgO had concentrations < 0.30 wt % in all samples, except in YTK 02A (0.87 wt %) (Figure 4.84).

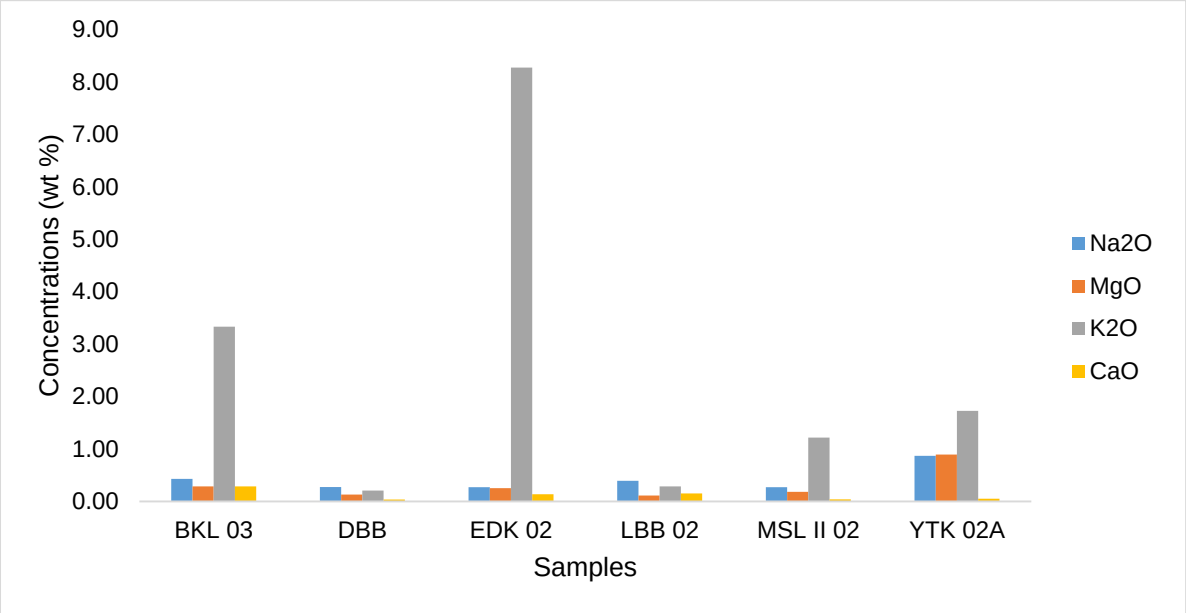

Figure 4.84: CaO, Na_2O, K_2O and MgO concentrations in silt samples

The sum of CaO, Na_2O, K_2O and MgO (CNKM) is < 1 wt % in DBB and LBB 02. In other samples, it varied between 1.71 wt % (MSL II 02) and 8.93 wt % (EDK 02) (Figure 4.85).

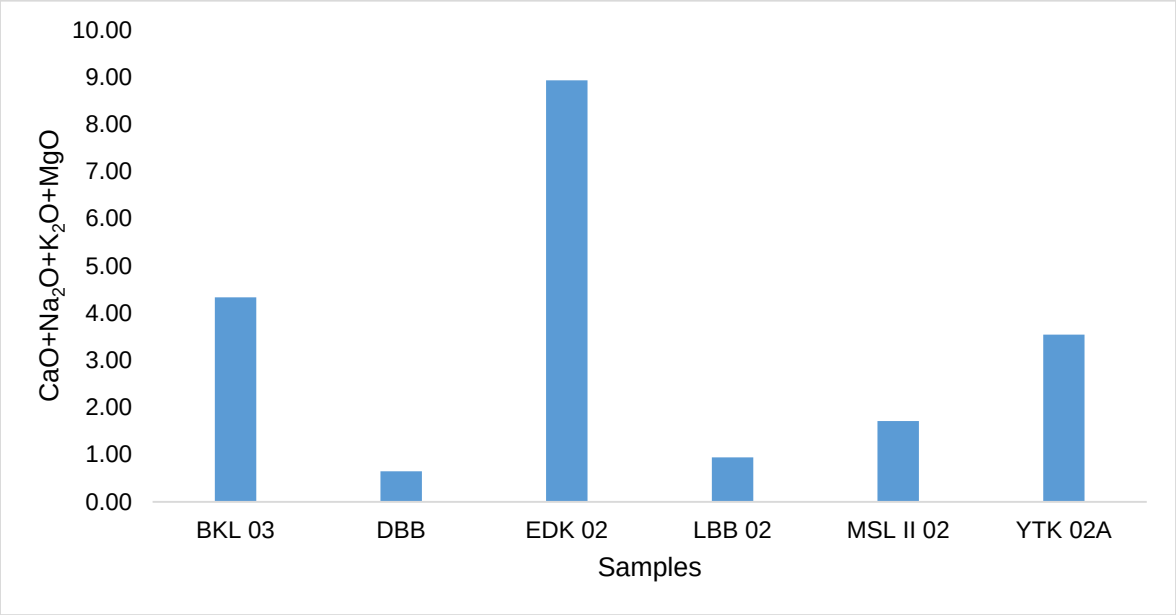

Figure 4.85: Sum of CaO, Na_2O, K_2O and MgO concentrations in silt samples

TiO_2 and Fe_2O_3

Concentrations of Fe_2O_3 were higher than those of TiO_2 in BKL 03 (5.65 wt %) and YTK 02A (7.20 wt %). In other samples, TiO_2 was more abundant, varying between 1.59 wt % (EDK 02) and 4. 34 wt % (LBB 02) (Figure 4.86).

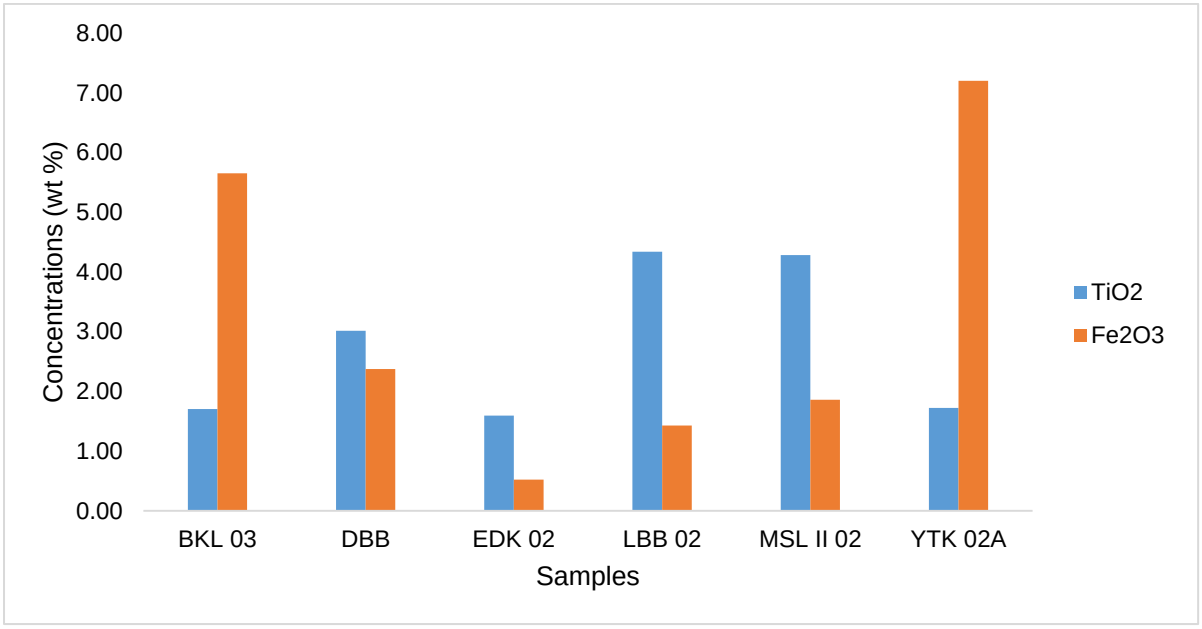

Figure 4.86: TiO_2 and Fe_2O_3 concentrations in silt samples

P_2O_5 and SO_3

SO_3 had concentrations less than 0.05 wt % in all samples. However, P_2O_5 had abnormally high concentrations, varying between 0.29 wt % (MSL II 02) and 0.98 wt % (LBB 02) (Figure 4.87).

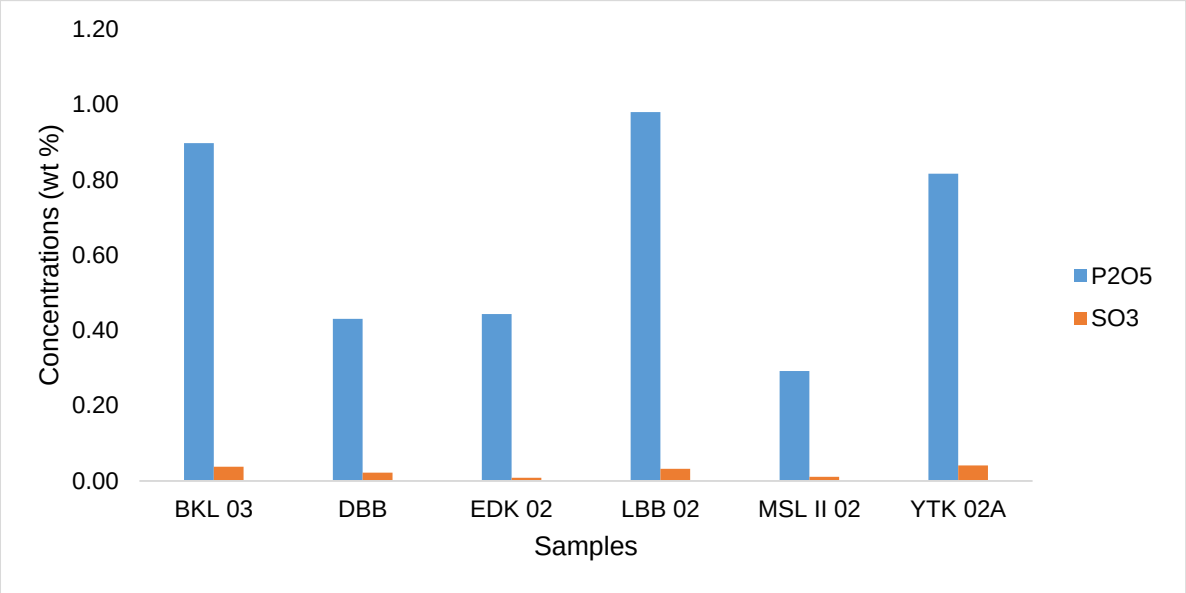

Figure 4.87: P_2O_5 and SO_3 concentrations in silt samples

K_2O/Al_2O_3

Values of K_2O/Al_2O_3 are less than 0.1, except in BKL 03 (0.34) and EDK 02 (0.31) (Figure 4.88).

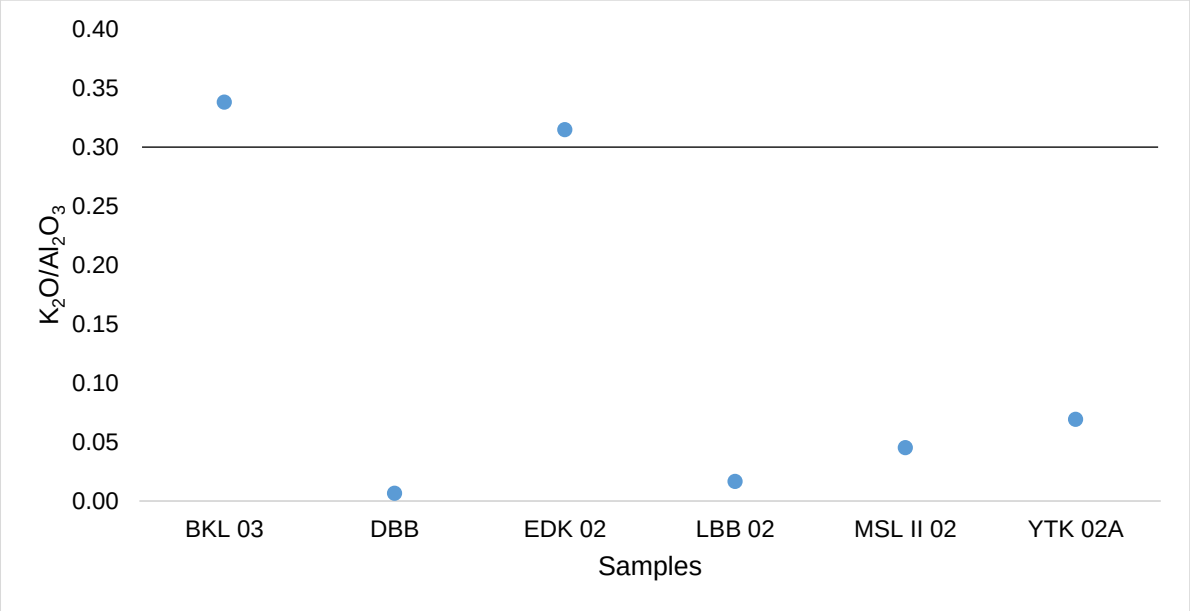

Figure 4.88: Plot of the K_2O/Al_2O_3 ratio of silt samples

4.4.1.3 Clay samples (< 2 µm fraction)

SiO_2 and Al_2O_3

In the < 2 µm samples, MSLI 02 had the highest SiO_2 concentration (54.70 wt %), whereas all other samples had SiO_2 concentrations < 50.00 wt % (Figure 4.89).

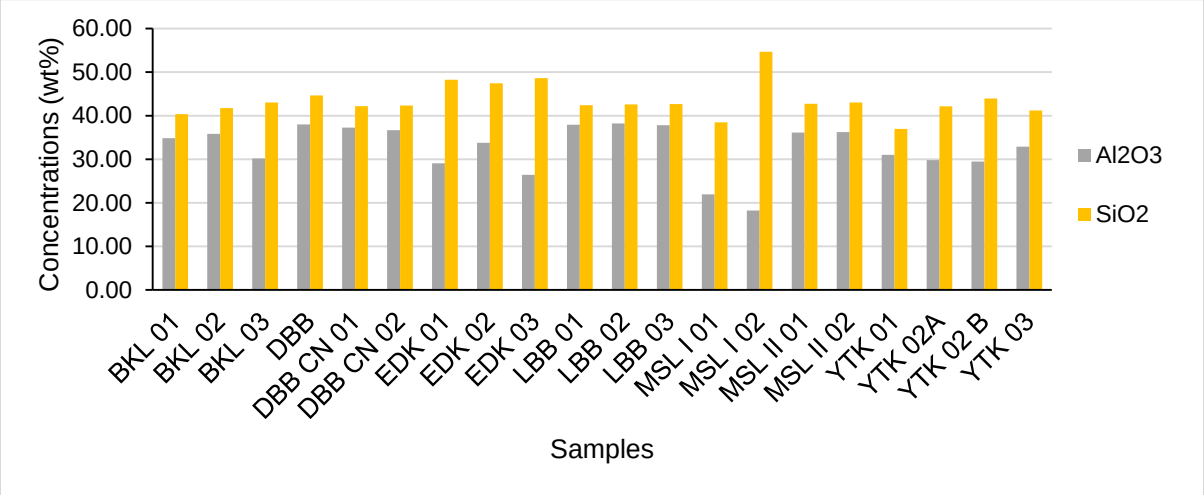

Figure 4.89: Al_2O_3 and SiO_2 concentrations in < 2 µm samples

YTK 01 had the lowest SiO_2 concentration (36.99 wt %). Logbaba samples had high Al_2O_3 concentrations (37.91, 38.21 and 37.82 wt % for LBB 01, LBB 02 and LBB 02, respectively). MSLI 01 and MSLI 02 had Al_2O_3 concentrations less than 26 wt % (Figure 4.89). The < 2 µm samples portrayed a slight inverse relationship between Al_2O_3 and SiO_2 concentrations, with r^2 =0.18 (Figure 4.90).

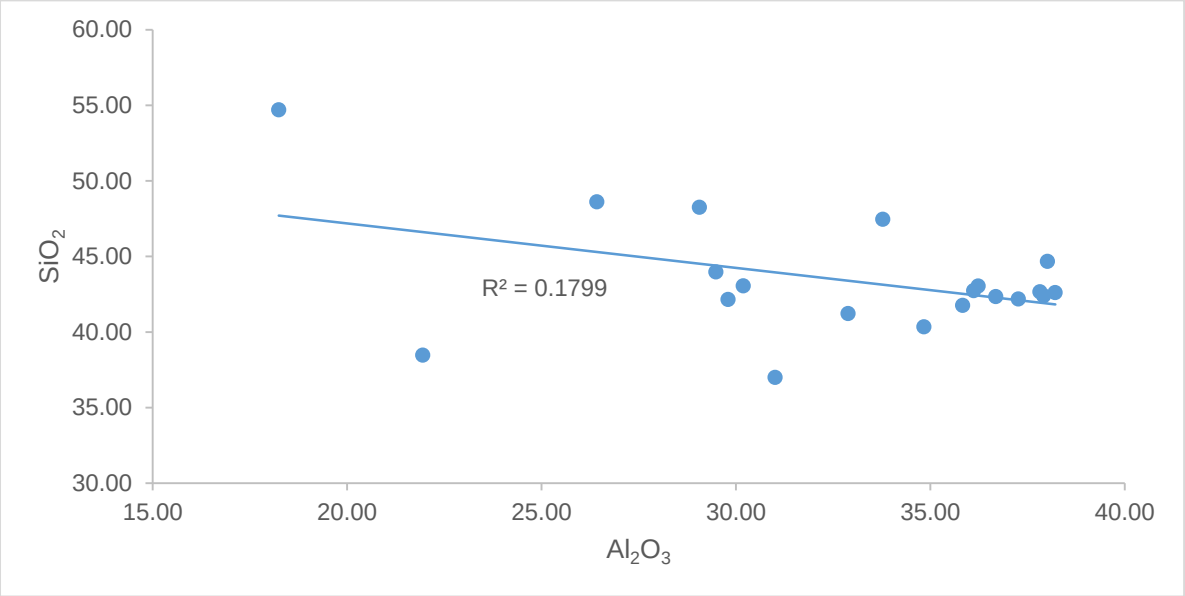

Figure 4.90: Scatter plot diagram of SiO_2 versus Al_2O_3 concentrations of < 2 µm samples

CaO, Na_2O, K_2O and MgO

Concentrations of CaO, Na_2O, K_2O and MgO of < 2 µm samples are plotted in Figure 4.91. CaO had very low concentrations in all samples. Most CaO concentrations were slightly lower in the < 2 µm samples than in bulk samples, except the < 2 µm sample of DBB CN 01, which had CaO concentration of 0.11 wt%.

NaO_2 had higher concentrations (> 0.25 wt %). Logbaba and Missole I samples had the lowest NaO_2 concentrations (≤ 0.35 wt %). Ediki and Yatchika samples had relatively higher NaO_2 content (between 0.48 and 1.61 wt %). Ediki samples had the highest K_2O concentrations (mean of 6.31 wt %). Other samples had K_2O concentrations < 2 wt%. All < 2 µm samples had K_2O concentrations lower than their corresponding bulk samples. MgO concentrations were generally less than 1.00 wt % and showed a similar trend as in bulk samples, with EDK 01 and EDK 03 having the highest MgO concentrations (1.33 and 1.83 wt %, respectively). Though < 2 µm samples had lower MgO concentrations than their corresponding bulk samples, exceptions were found in BKL 03 and all Ediki samples, whose < 2 µm samples had higher MgO concentrations than their corresponding bulk samples. In YTK 02A and YTK 02B, MgO concentrations did not vary with particle size. Logbaba samples had the lowest MgO concentrations (< 0.1 wt %).

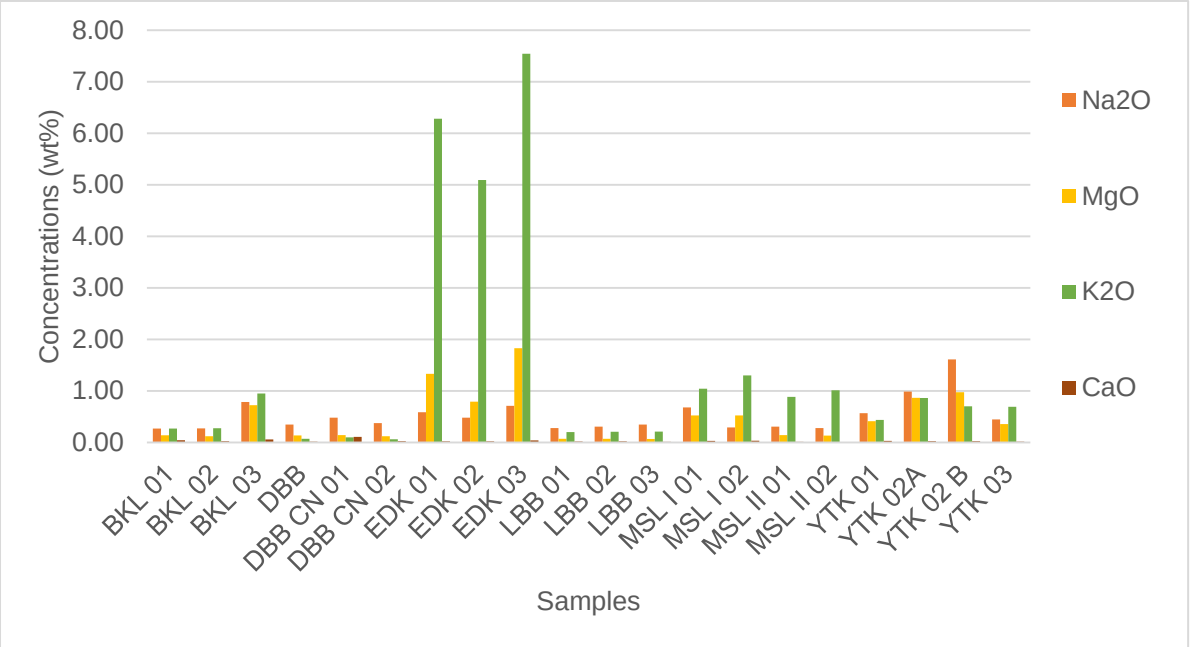

Figure 4.91: CaO, Na_2O, K_2O and MgO concentrations in < 2 µm samples

60% of clay fraction samples had the sum of CaO, Na_2O, K_2O and MgO (CNKM) less than 2 wt%. Ediki samples had the highest CNKM (> 6 wt %) in < 2 µm samples. BKL 03, YTK 02A and YTK 02B had CNKM varying between 2.52 and 3.31 wt % (Figure 4.92).

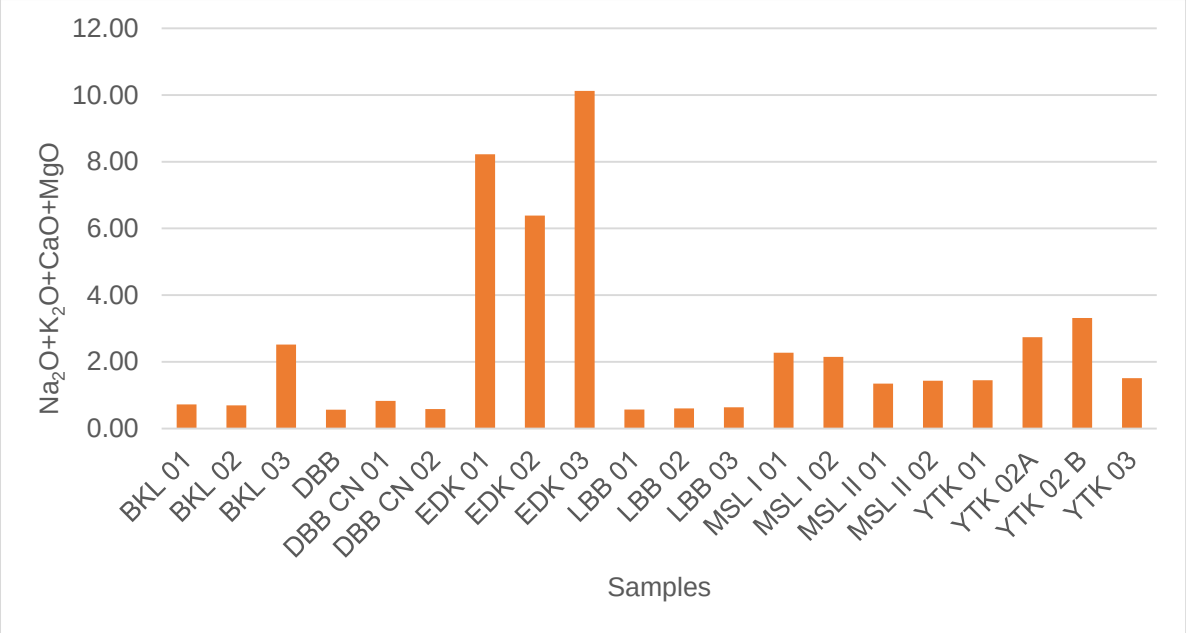

Figure 4.92: Sum of CaO, Na_2O, K_2O and MgO concentrations in < 2 µm samples

TiO_2 and Fe_2O_3

As in bulk samples, DBB CN 01 and DBB CN 02 also had the lowest TiO_2 concentrations in both bulk samples and clay fractions (< 0.40 wt %). High titania contents were observed in MSL II 01 and MSL II 02 (> 3.00 wt %). Fe_2O_3 was higher than TiO_2 in all samples, except in Logbaba and Missole II samples. As a general trend, Fe_2O_3 was higher in clay fractions than in bulk samples (Figure 4.93). High Fe_2O_3 concentrations (>6.00 wt %) were found in Bomkoul, MSL I 01 and Yatchika samples.

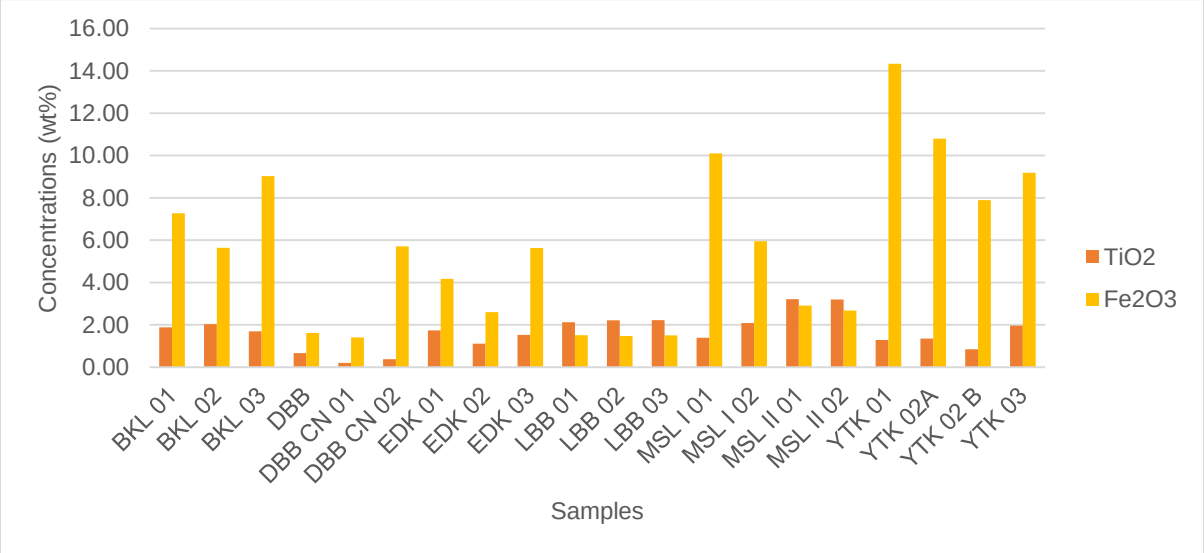

Figure 4.93: TiO_2 and Fe_2O_3 concentrations in < 2 µm samples

P_2O_5 and SO_3

< 2 µm samples had higher P_2O_5 concentrations than their corresponding bulk samples (up to 7.56 wt% in MSL I 01). SO_3 was less than 0.20 wt% in < 2 µm samples; the only exception being in MSL I 01 and MSL I 02, in which SO_3 concentration was up to 4.48 wt% (Figure 4.94).

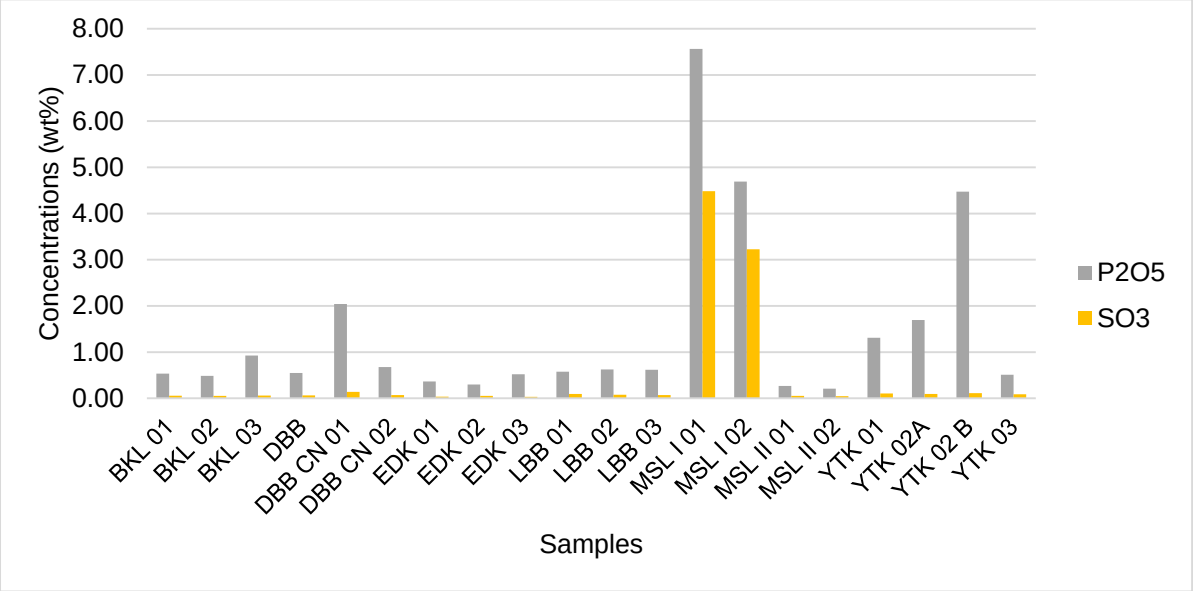

Figure 4.94: P_2O_5 and SO_3 concentrations in < 2 µm samples

K_2O/Al_2O_3

The plot of K_2O/Al_2O_3 of < 2 µm samples is shown in Figure 4.95. Logbaba and Dibamba samples had the lowest ratio (≤ 0.01), whereas Ediki samples had a K_2O/Al_2O_3 ratio between 0.15 and 3.00.

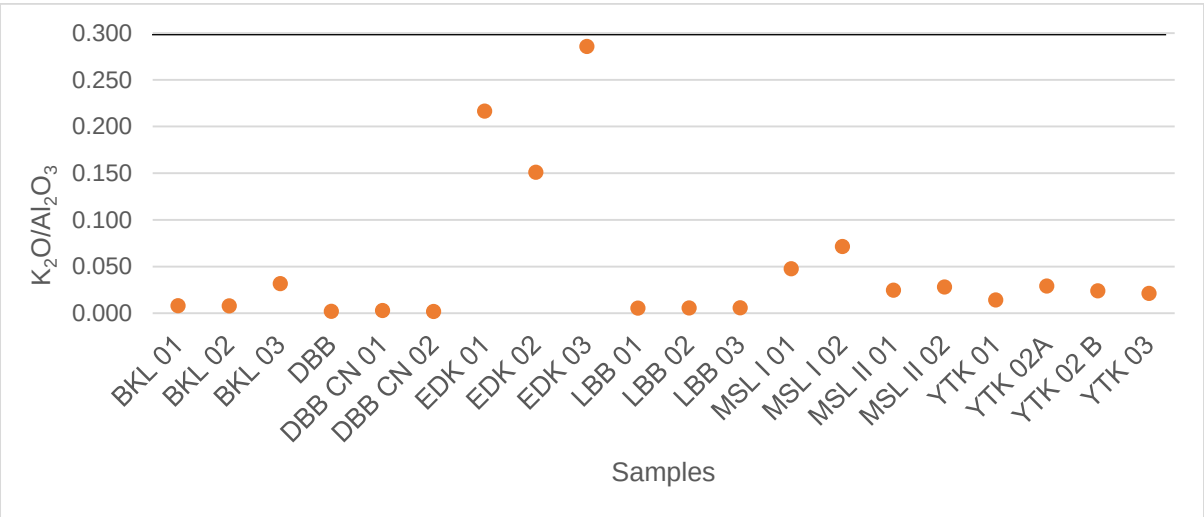

Figure 4.95: Plot of the K_2O/Al_2O_3 ratio of < 2 µm samples

4.4.2 Hacker diagrams

Hacker diagrams (Figure 4.96) show the relationship between alumina and various oxides, silica and titania, loss on ignition (LOI) and CaO and Al_2O_3. In general, these relationships were weak, either positive or negative. Positive correlations were noted between Al_2O_3 and Na_2O ($r^2 = 0.04$), Al_2O_3 and TiO_2 ($r^2 = 0.06$), Al_2O_3 and LOI ($r^2 = 0.54$) and SO_3 and P_2O_5 ($r^2 = 0.39$). Negative relationships were noted between Al_2O_3 and CaO, Al_2O_3 and K_2O, Al_2O_3 and P_2O_5, and CaO and LOI, with r^2 values of 0.07, 0.03, 0.03 and 0.14, respectively.

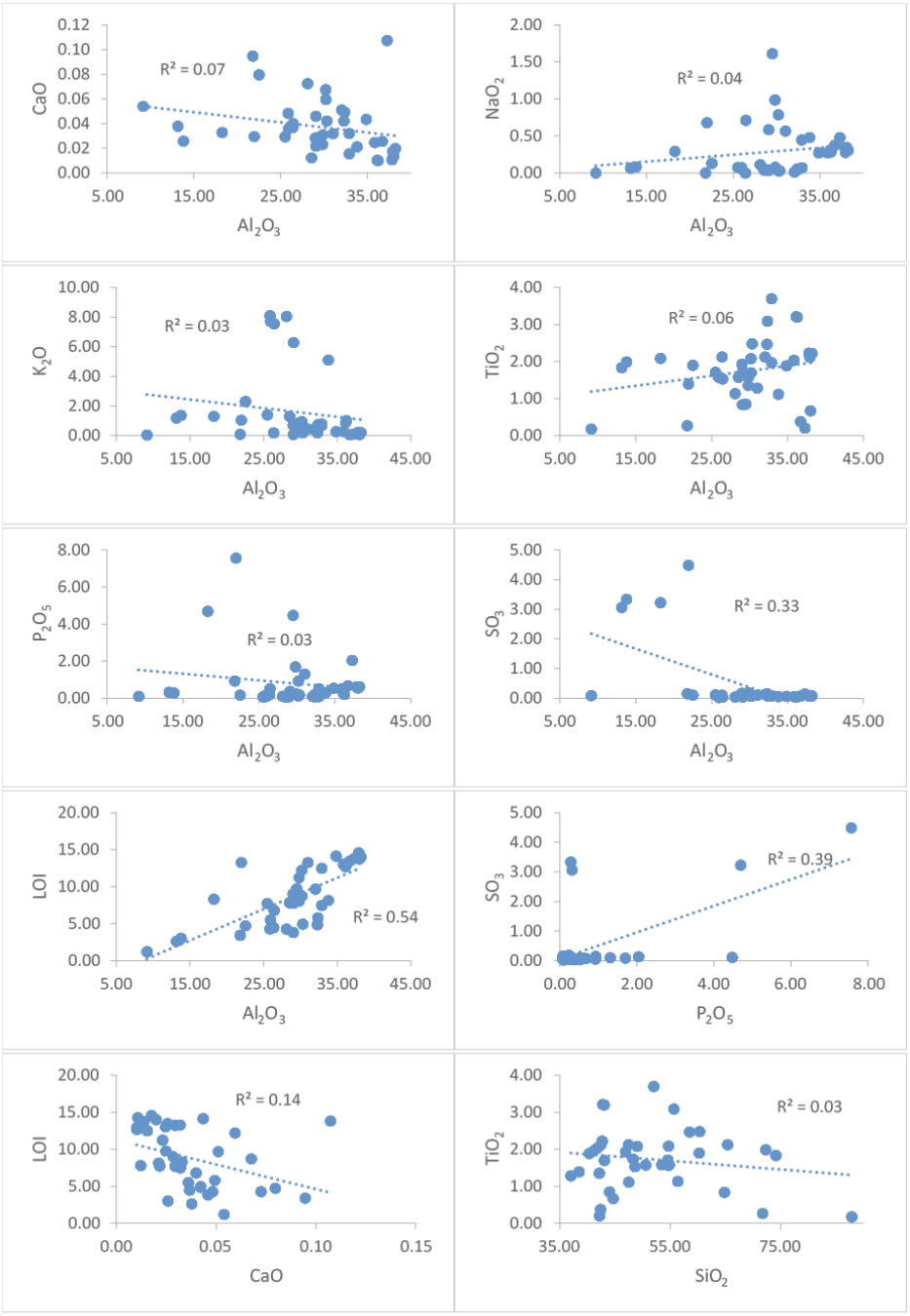

Figure 4.96: Hacker diagrams showing relationships between various oxides and alumina, silica and LOI

4.4.3 Microelemental composition of < 2 µm fraction of kaolin samples

The microelemental composition of kaolin samples was in agreement with the major oxides composition of these samples. In general, concentrations of elements in samples were in the following order of abundance: O > Si > Al > Fe > Ti > P > Na > K > Mg. In samples from Dibamba, Logbaba and Missole II, Mg was not detected; whereas in Bomkoul, Ediki, Missole I and Yatchika samples, Mg concentrations could be up to 0.87% (EDK 01). Potassium was generally less than 1%, except in Ediki samples in which it varied between 3.68 and 5.73%.

Missole II and Logbaba had Ti concentrations greater than Fe concentrations, as in their major oxides, where TiO_2 concentrations were greater than Fe_2O_3 concentrations. Fe concentration was high in Bomkoul, Ediki, Missole I and Yatchika samples, with its concentration being up to 9.3% in MSL I 01. High Fe concentrations corresponded to high Mg concentrations.

Some elements, like Cu and S were only detected in one or two samples. Copper was only detected in DBB CN 01 and EDK 01; whereas S was only detected in Missole I samples, with the highest concentration being 3.05%. The microelemental composition of kaolin samples is given in Table 4.8 and plotted in Figures 4.97-4.102.

Table 4.8: Percentage of different elements present in studied kaolins

	Na	Mg	Al	Si	P	S	K	Ti	Fe	Cu	O	Total
BKL 01	0.34	nd	20.32	24.13	0.48	nd	0	1.13	5.09	nd	48.51	100
BKL 02	0.41	nd	20.49	24.08	0.41	nd	0.24	1.31	4.53	nd	48.54	100.01
BKL 03	0.8	0.44	16.76	25.11	0.74	nd	0.82	1.14	6.41	nd	47.79	100.01
DBB	0.43	nd	21.59	25.91	0.42	nd	nd	0.44	1.16	nd	50.05	100
DBB CN 01	0.49	nd	21.49	25.07	1.46	nd	0.05	nd	0.95	0.36	50.12	99.99
DBB CN 02	0.36	nd	20.99	25.03	0.58	nd	nd	nd	3.87	nd	49.17	100
EDK 01	0.56	0.87	15.68	26.48	0.26	nd	4.77	1.02	2.4	0.32	47.64	100
EDK 02	0.42	0.43	18.49	25.93	0.24	nd	3.68	0.79	1.57	nd	48.45	100
EDK 03	0.61	1.1	14.13	26.26	0.43	nd	5.73	1.15	3.65	nd	46.95	100.01
LBB 01	0.39	nd	22.16	24.75	0.42	nd	nd	1.33	1.14	nd	49.8	99.99
LBB 02	0.37	nd	22.07	24.86	0.42	nd	nd	1.42	1	nd	49.86	100
LBB 03	0.46	nd	21.56	25.31	0.53	nd	0.14	1.19	0.9	nd	49.93	100.02
MSL I 01	1.32	0.34	11.79	20.4	4.39	3.05	0.81	0.68	9.3	nd	47.92	100
MSL I 02	0.3	0.3	8.26	30.22	2.24	1.54	0.94	1.12	5.33	nd	49.74	99.99
MSL II 01	0.42	nd	20.69	24.89	0.38	nd	0.73	1.89	1.7	nd	49.29	99.99
MSL II 02	0.36	nd	20.83	25.27	0	nd	0.94	1.81	1.5	nd	49.28	99.99
YTK 01	0.77	nd	18.2	23.01	0.81	nd	0.29	0.82	9.16	nd	46.95	100.01
YTK 02A	0.96	0.62	16.8	24.1	0.92	nd	0.77	0.81	7.77	nd	47.25	100
YTK 02B	1.92	0.62	15.63	23.14	3.74	nd	0.49	0.5	5.71	nd	48.24	99.99
YTK03	0.57	0.26	19.06	24.34	0.35	nd	0.52	1.08	5.82	nd	48	100

nd = not detected

A)

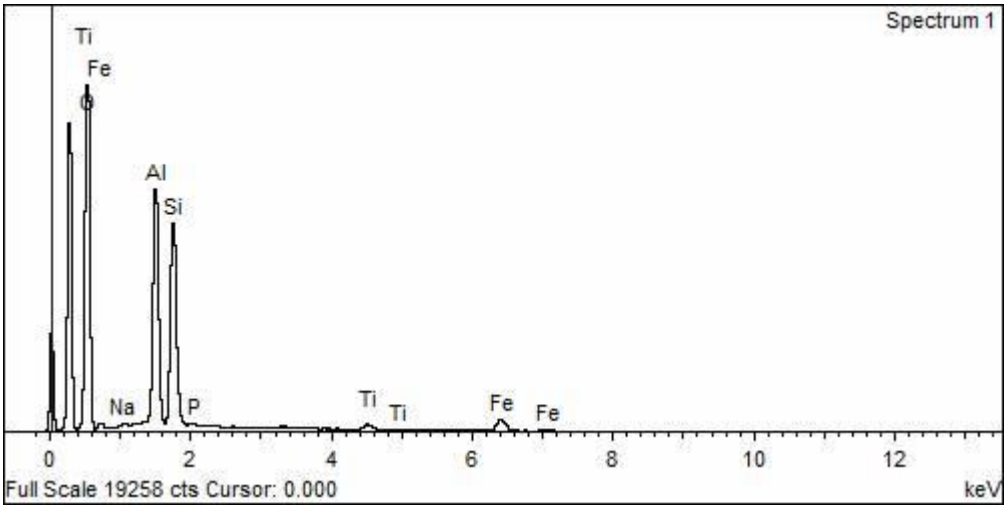

B)

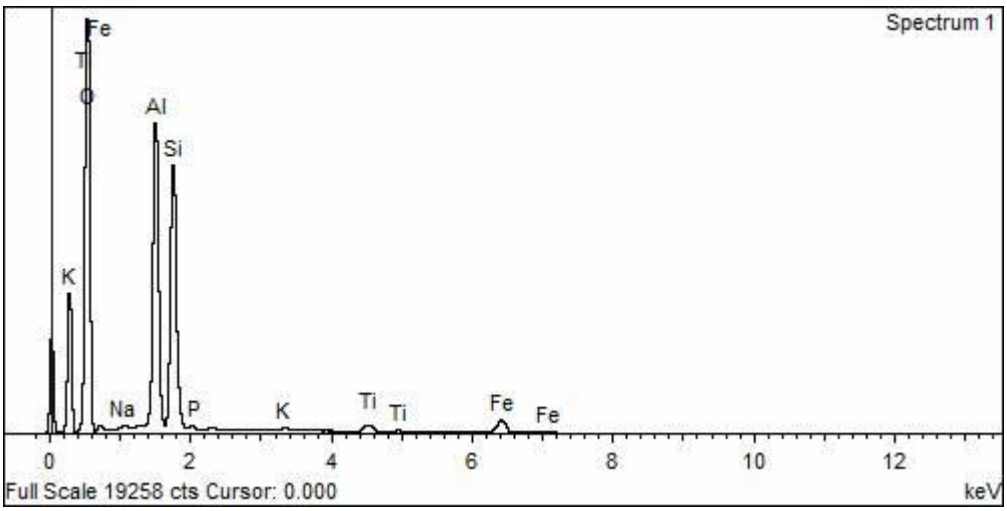

C)

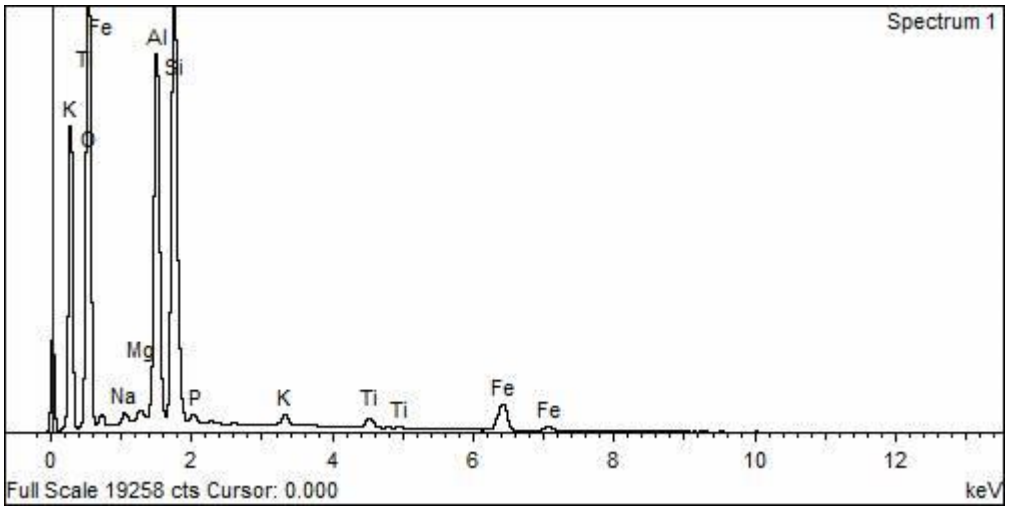

Figure 4.97: Microelemental composition of Bomkoul samples: A) BKL 01, B) BKL 02, C) BKL 03

A)

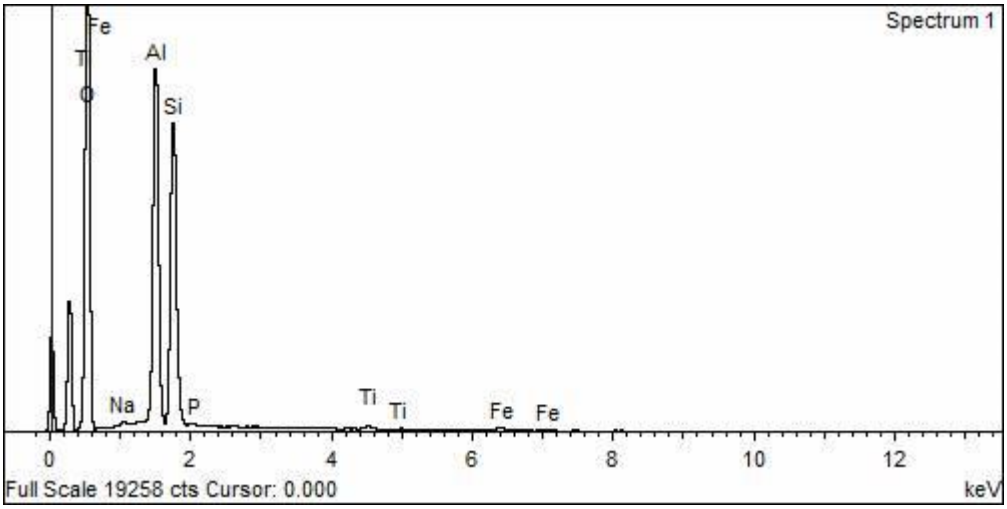

B)

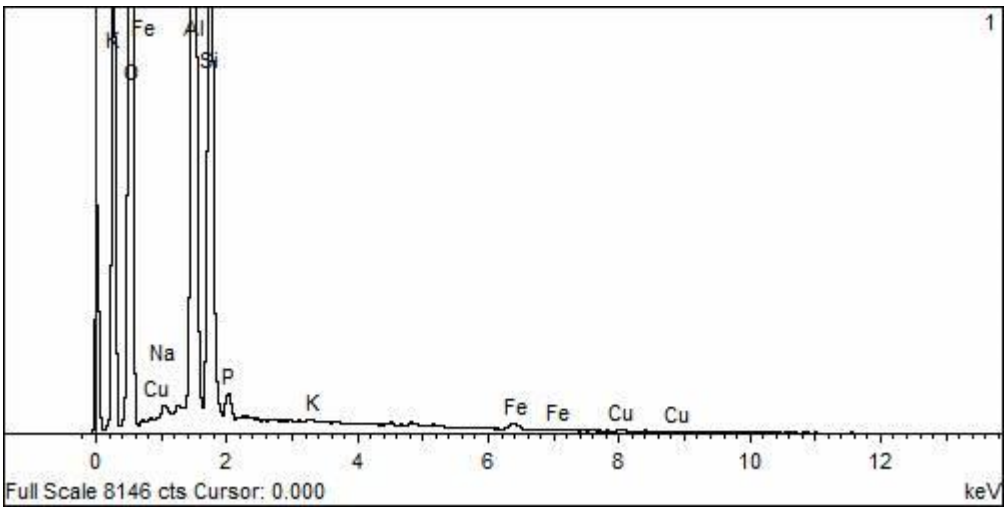

C)

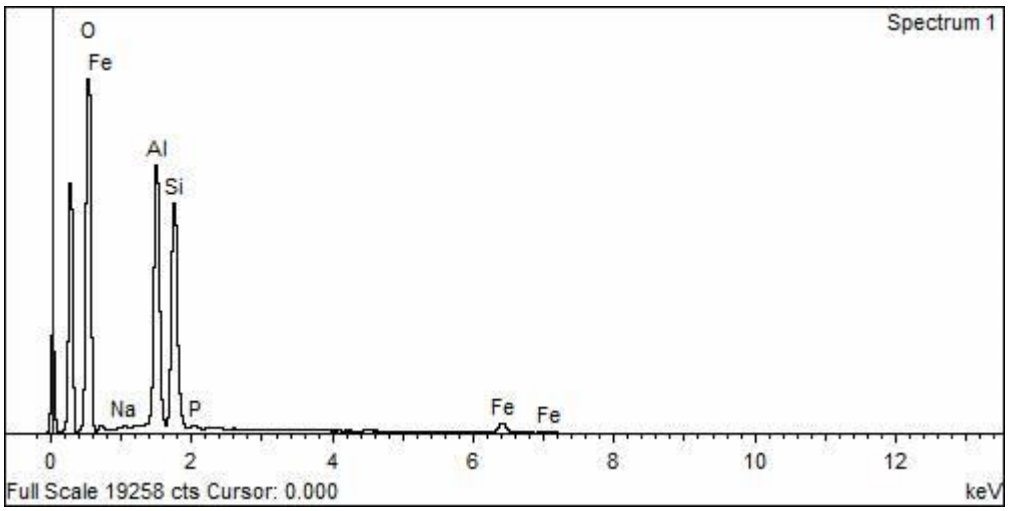

Figure 4.98: Microelemental composition of Dibamba samples; A) DBB, B) DBB CN 01, C) DBB CN 02

A)

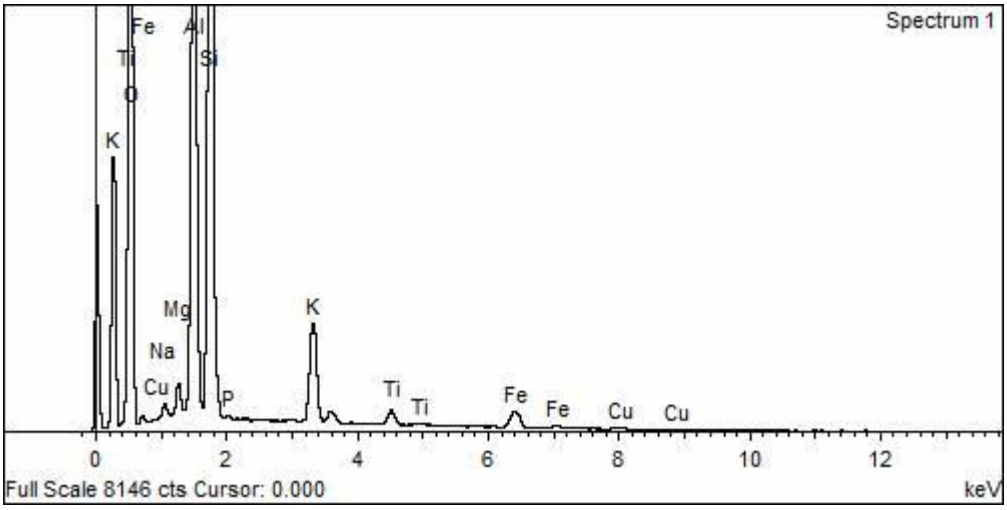

B)

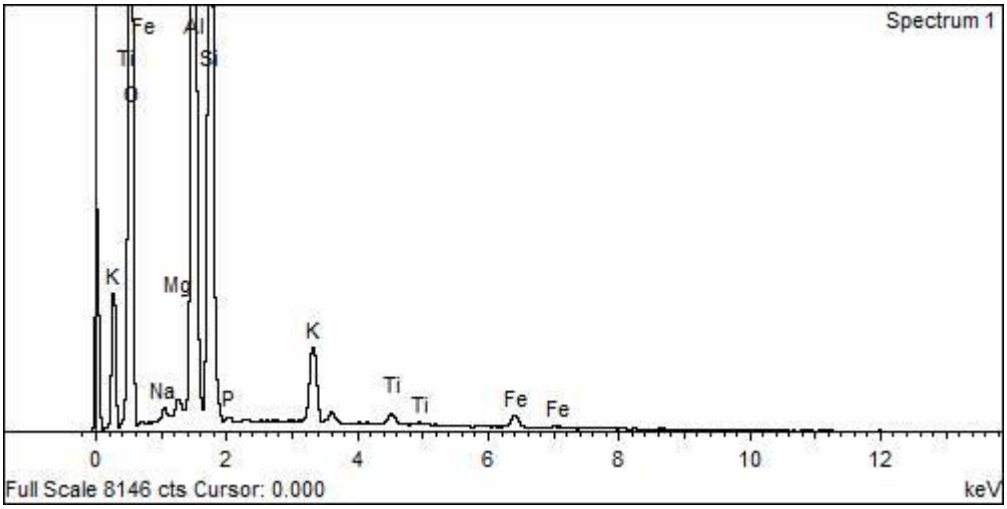

C)

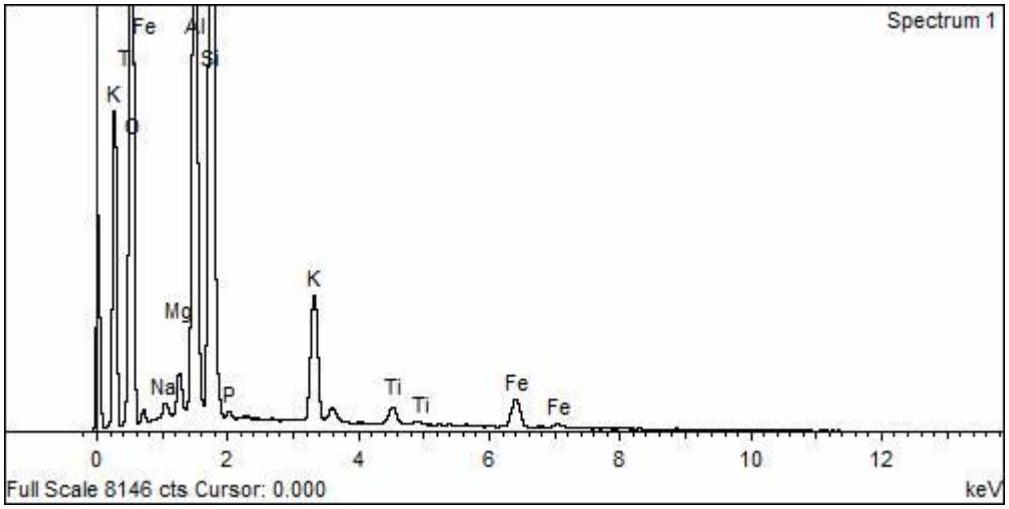

Figure 4.99: Microelemental composition of Ediki samples; A) EDK 01, B) EDK 02, C) EDK 03

A)

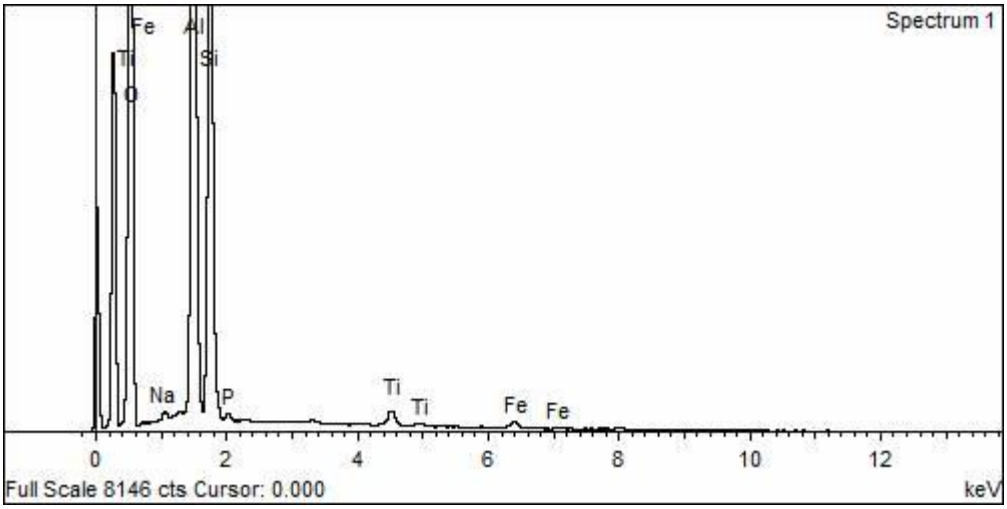

B)

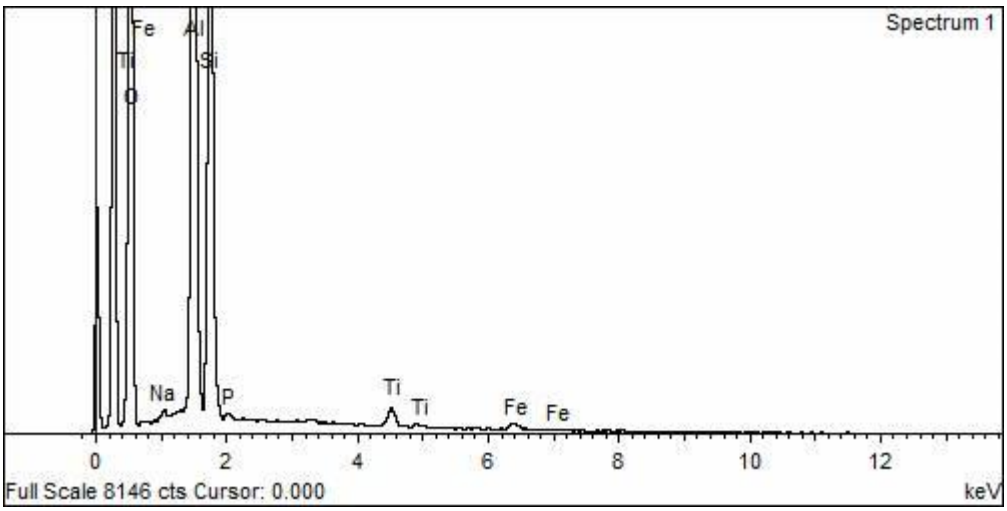

C)

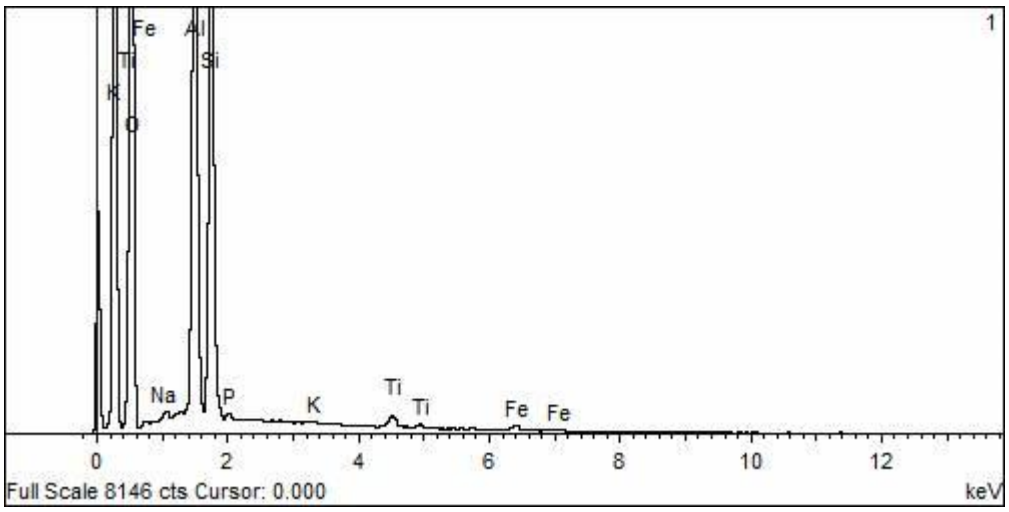

Figure 4.100: Microelemental composition of Logbaba samples; A) LBB 01, B) LBB 02, C) LBB 03

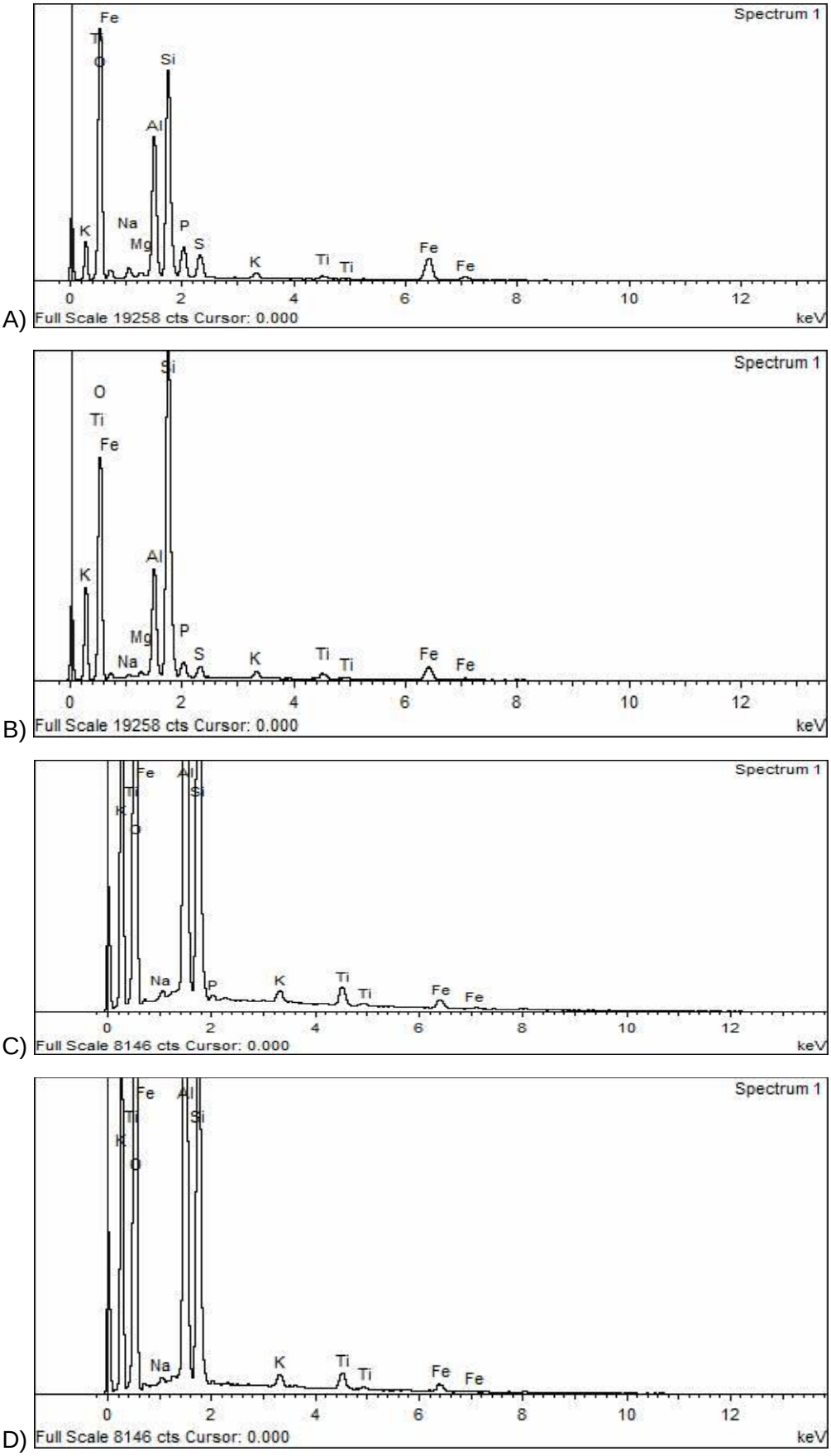

Figure 4.101: Microelemental composition of Missole samples; A) MSL I 01, B) MSL I 02, C) MSL II 01, D) MSL II 02

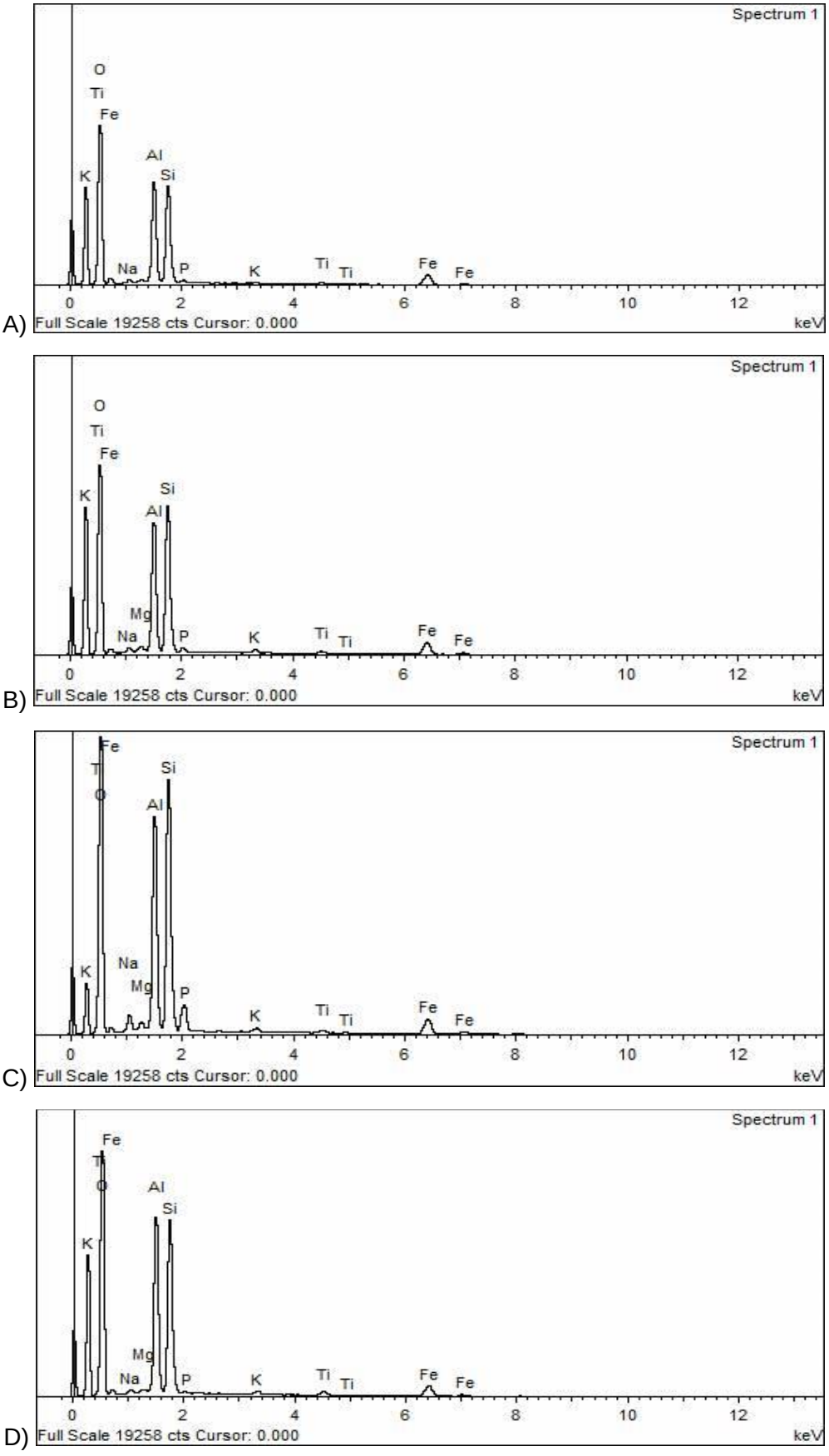

Figure 4.102: Microelemental composition of Yatchika samples; A) YTK 01, B) YTK 02A, C) YTK 02B, D) YTK 03

4.5 Discussion

4.5.1 Mineralogy and geochemistry of Cretaceous-Tertiary kaolins in the Douala Sub-Basin

Kaolins are secondary minerals, which result from the alteration of primary minerals from host rocks (Dhannoun *et al*., 2010). Hence, their mineralogy and geochemistry strongly depend on the mineralogy and geochemistry of their source rocks and minerals.

The main mineral phases present in studied Cretaceous-Tertiary kaolins of the Douala Sub-Basin are kaolinite > smectite > illite, with mean values of 33.01 wt % > 11.20 wt % > 4.41 wt %, 28.52 wt % > 10.87 wt % > 3.54 wt %, and 72.23 wt % > 10.69 wt % > 4.69 wt %, in bulk, silt and clay fractions of kaolins, respectively. The increase of kaolinite in clay fractions was associated with an increase in Al_2O_3 and a decrease in SiO_2 concentrations in the samples, hence the negative correlation between these two oxides (Figures 4.89 and 4.90).

The relatively higher CaO and Na_2O concentrations in clay fractions is associated with the presence of smectite and illite, which could also be linked to decrease in particle size. Higher CaO and Na_2O concentrations in clay fractions justify the relatively lower values of the chemical index of alteration (CIA) and chemical index of weathering (CIW) in some of the < 2 µm samples (Appendix 4.9), because CIA and CIW are inversely proportional to CaO and Na_2O concentrations (Nesbitt and Young, 1982; Fiantis *et al*., 2010).

The main impurities in these kaolins are TiO_2 and Fe_2O_3, which are also reflected in the mineralogy by the presence of rutile (TiO_2), anatase (TiO_2), goethite (αFeO.OH) and hematite (Fe_2O_3). Anatase was present in minor amounts, whereas rutile was mainly in trace. Baioumy (2014b) also reported anatase to be the principal Ti-bearing mineral phase in Cretaceous kaolins in Egypt, though other Ti-bearing minerals (rutile, ilmenite and leucoxene) were in trace amounts. High TiO_2 concentrations corresponded to high anatase content e.g. in Missole II and Logbaba samples. Schroeder *et al*. (2003) evaluated the difference between total TiO_2 and anatase-TiO_2 in selected kaolin deposits, including the Cretaceous-Tertiary kaolins from Georgia and Brazil. They all had an amount of anatase that was slightly equal to their TiO_2 content. Therefore, anatase accounted for most of the TiO_2 content.

Logbaba samples, which had lower Fe_2O_3 concentrations than TiO_2, also had very high CIA (> 98%) in both bulk and < 2 µm fraction (Appendices 4.7 and 4.9). This could suggest that anatase, in these samples, is derived from the oxidation of Fe-Ti-bearing precursors, as in Georgia kaolins (Schroeder *et al*., 2004). However, the absence of Fe-Ti-bearing mineral phases, such as ilmenite, and Fe-bearing mineral phases, such as goethite and hematite, in

these kaolins is explained by the extreme weathering undergone by the kaolins. Dibamba kaolins also displayed similar characteristics as Logbaba kaolins.

Unlike anatase and rutile, goethite and hematite were mostly present in minor or trace amounts, and in few of the samples. The possible substitution of Fe^{3+} into octahedral sites (made up of Al^{3+}) in these samples may be associated with interlayer oxides or hydroxides. This possible substitution may have affected the crystallinity of the kaolinite structure of these samples (Ekosse, 2000), giving them a partially to poorly ordered structure. Moreover, kaolins in tropical areas are usually associated with oxide and oxyoxide minerals, such as goethite and hematite (Sheldon and Tabor, 2009).The substitution of Al^{3+} by Fe^{3+} was more evident in YTK 02A, in which kaolinite, smectite and illite abundances considerably dropped from 15.93, 4.97 and 31.23 wt %, respectively in bulk samples to 11.91, 0 and 20.48 wt %, respectively in < 2 µm fraction; whereas, goethite abundance increased from 5.09 wt % in bulk sample to 48.07 wt % in the < 2 µm fraction. A particularity about Yatchika kaolin is that they were the only samples having hematite in both bulk and clay fractions. It is believed that the hematite might have been derived from the dehydroxylation of goethite, or vice versa depending on prevailing conditions, according to Equation 4.5.

$$2\alpha.FeOOH \rightleftharpoons \alpha.Fe_2O_3 + H_2O \qquad \text{Eqn. 4.5}$$

Goethite Hematite

The general trend of Ediki samples (EDK) confirmed the results obtained by Diko and Ekosse (2012; 2013); and Diko *et al*. (2016). The presence of microcline, illite and smectite in these samples are consistent with the relatively high K_2O and Na_2O concentrations in their geochemistry. As a consequence, the CIA of these samples were the lowest (< 86%), indicating moderate silicate weathering; the index of compositional variability values (ICV) were the highest (0.61 and 0.65 in bulk and clay fractions, respectively) (Appendices 4.7 and 4.9); and K_2O/Al_2O_3 ratios were the highest. These indicators showed the compositional immaturity of Ediki kaolin (Cox *et al*., 1995; Nagarajan *et al*., 2013). The high degree of structural disorder in the kaolinite structure of Ediki samples reported in Diko *et al*. (2016) was also observed.

Missole samples were in two categories, both reported in previous works by Logmo *et al*. (2013) and Ngon Ngon *et al*. (2014). The dark grey Missole I kaolins, hosted in shales of the Nkapa Formation, had more quartz and less kaolinite in the bulk samples, and the clay fractions were more kaolinitic and smectitic. The geochemistry of Missole I kaolins reflected their mineralogy; relatively higher SiO_2 and lower Al_2O_3 concentrations. In addition, Missole I kaolins had high SO_3, P_2O_5, MgO and Fe_2O_3 in both bulk samples and clay fraction. High SO_3 and P_2O_5 concentrations were also reported in Cretaceous-Tertiary hypogene kaolins in Peru

(Dill *et al*., 1997) and in Tertiary hypogene kaolins from the El-Gideda iron ore in Egypt (Baioumy and Hassan, 2004). The absence of high temperature minerals in Missole I samples, the relatively high SO_3 and P_2O_5 concentrations in these samples but negative correlations between SO_3 and Al_2O_3, and P_2O_5 and Al_2O_3 (Figure 4.96) showed that SO_3 and P_2O_5 contents may have been favoured by organic matter contained in shales (Yaalon, 1961). High MgO contents could be attributed to the presence of altered femic minerals (such as hornblende), which may not be detected by diffractometry (Ligas *et al*., 1997). However, high MgO concentrated in the clay fractions could also be attributed to presence of smectite (Manju *et al*., 2001). For example, the smectite mineral identified in YTK 02A is saponite $[Mg_2Al)(Si_3Al)O_{10}(OH)_2{\cdot}4H_2O]$, which is the Mg-rich member of smectites.

The whitish Missole II kaolin was predominantly made up of kaolinite in both bulk and < 2 µm fraction (up to 87.33 wt %), and contained illite in minor amounts, as reported by Logmo *et al*. (2013) and Ngon Ngon *et al*. (2014). The only impurities found in Missole II kaolins was anatase, which was more abundant in these samples than in other samples. No Fe-bearing mineral was detected, hence their whitish colour. These kaolins were well structured and fell under the class of well-ordered kaolins based on FTIR analysis.

Thermogravimetric analyses and differential scanning calorimetry (TGA-DSC) of the < 2 µm samples showed that dehydroxylation temperatures (T_d) were lower than that of the Cretaceous-Tertiary Georgia kaolin Standard (576 °C) (Vaculíková *et al*., 2011). In the latter, well-ordered kaolin samples had a T_d > 571 °C, ordered sample had T_d between 561-570 °C, poorly ordered kaolin samples had T_d between 546 and 560 °C, and disordered kaolin samples had values of T_d < 545 °C. All studied Cretaceous-Tertiary kaolins of the Douala Sub-Basin had T_d < 545 °C.

However, this classification by Vaculíková *et al*. (2011) based on dehydroxylation temperatures of kaolins could not be applied in this research because (i) this classification is applicable only if analyses were carried out under the same conditions (Vaculíková *et al*., 2011), (ii) the particle size of samples and the size of individual crystals affect all reactions involving water (Guggenheim and van Gross, 2001), (iii) differences in the purging technique will produce difference in T_d values (Guggenheim and van Gross, 2001; Ilić *et al*., 2010). The results obtained by Diko *et al*. (2016) also confirmed that this classification cannot be used in all circumstances. Moreover, the total weight loss recorded during heating of the kaolin samples are similar to the LOI, as shown in Figure 4.103.

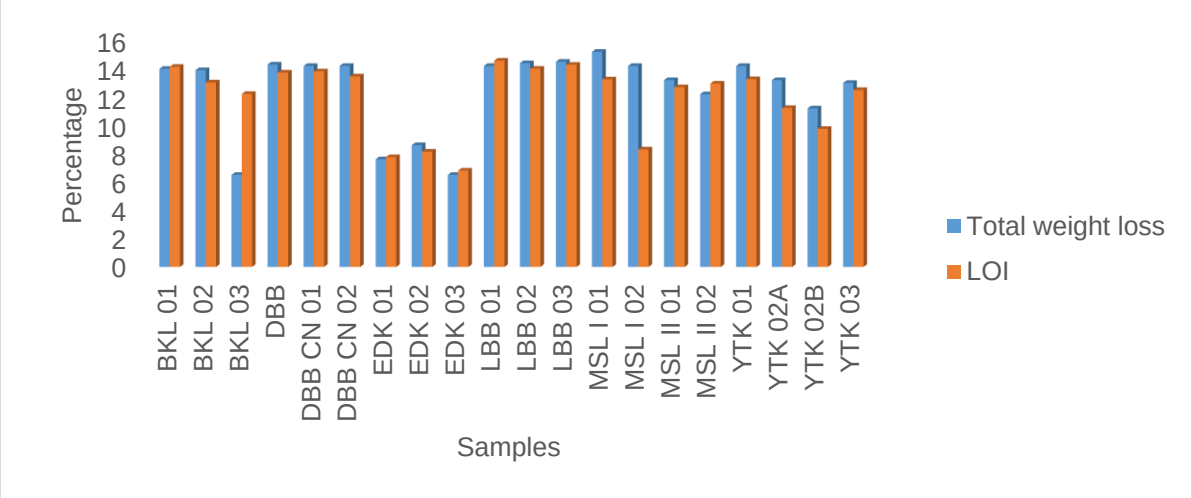

Figure 4.103: Comparison of the total weight loss during heating and the LOI of < 2 µm samples

4.5.2 Paleoenvironmental reconstruction using major oxides

4.5.2.1 Paleoweathering

CIA vs CIW

Ninety percent of bulk kaolins exhibited extreme silicate weathering (CIA > 80%) against 10% (Ediki kaolins) that exhibited moderate silicate weathering (Figure 4.104). Clay fractions had lower CIA and CIW values than bulk samples. Logbaba and Dibamba samples had higher CIA values (> 98%).

On the plot of CIA vs CIW of silt samples, EDK 02 and BKL 03 portrayed moderate silicate weathering (CIA < 80%); unlike DBB, LBB 02, MSL II 02 and YTK 02A, which portrayed extreme silicate weathering, with DBB and LBB 02 having the highest CIA (> 95%) (Figure 4.105).

In the clay fractions, 95% of samples exhibited extreme silicate weathering against 5% (EDK 03) that exhibited moderate silicate weathering (Figure 4.106). Clay fractions had lower CIA and CIW values than their corresponding bulk samples, this is due to higher amounts of Na_2O in < 2 µm fractions. Logbaba and Dibamba samples had higher CIA (> 98%) and CIW (> 99%) values.

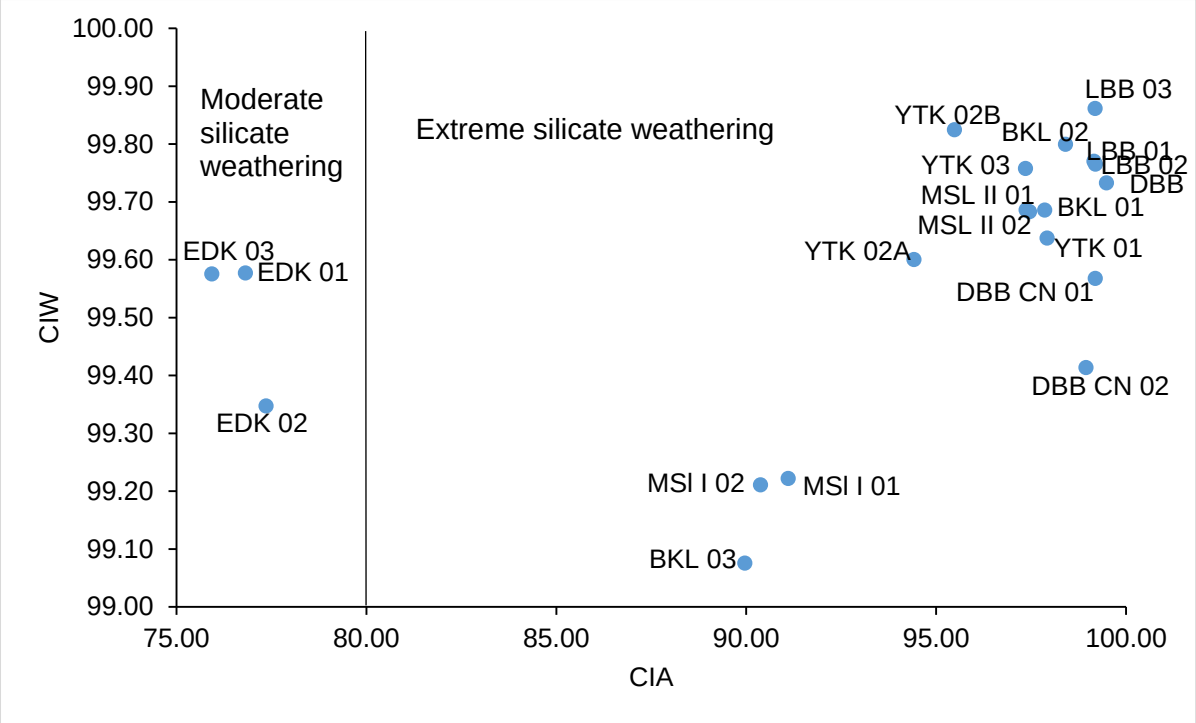

Figure 4.104: Chemical index of weathering (CIW) versus chemical index of alteration (CIA) of bulk samples

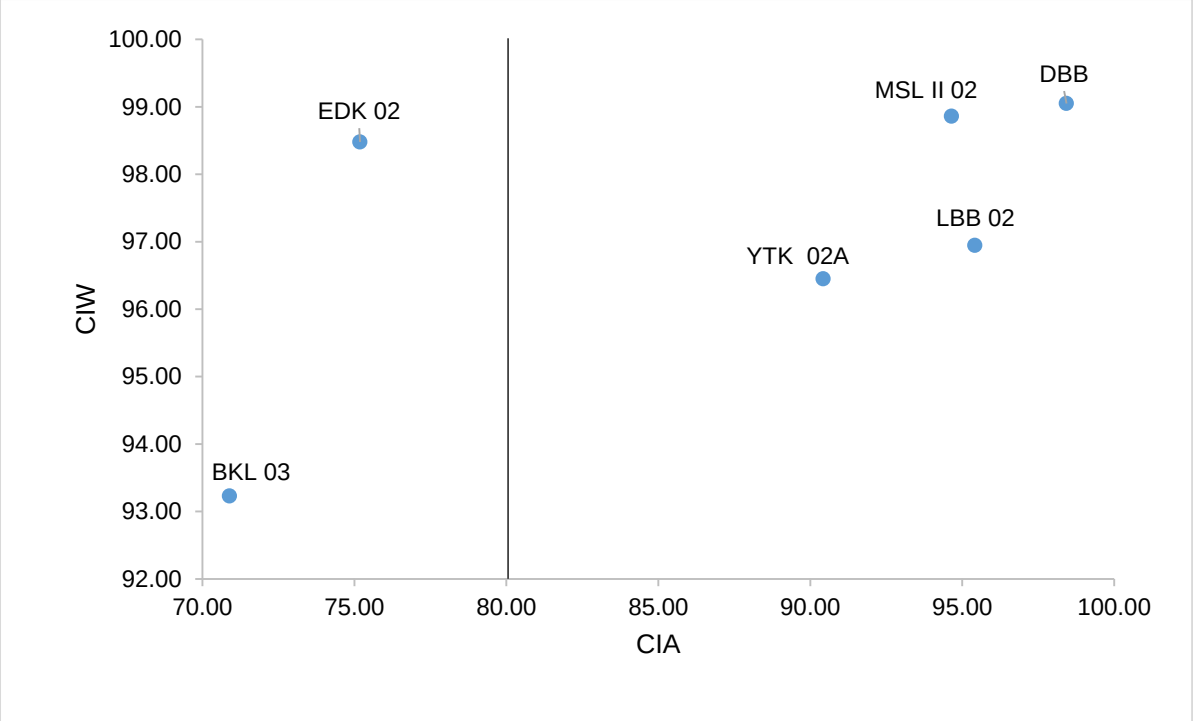

Figure 4.105: Chemical index of weathering (CIW) versus chemical index of alteration (CIA) of silt samples

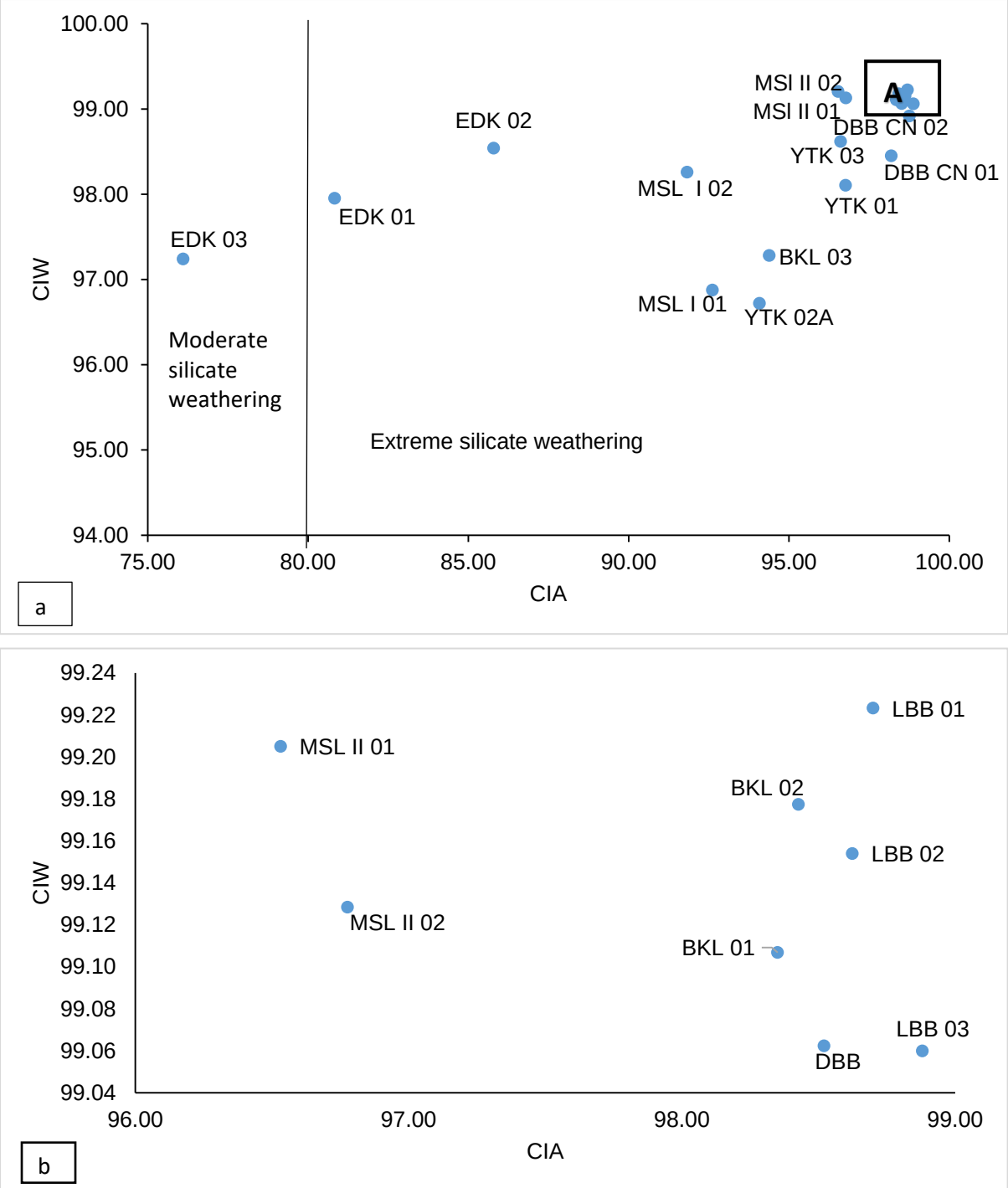

Figure 4.106: a) Chemical index of weathering (CIW) versus chemical index of alteration (CIA) of < 2 µm samples; b) CIW versus CIA of < 2 µm kaolins, expanded from Box A

Index of compositional variability (ICV)

The ICV values of bulk samples ranged from 0.05 (DBB CN 01) to 0.61 (EDK 03). Dibamba, Logbaba and Missole II samples had ICV values < 0.3; whereas, other samples had ICV values between 0.3 and 0.61 (Figure 4.107). The ICV values of silt samples ranged from 0.19 (DBB) to 1.19 (BKL 03). BKL 03 was the only sample with an ICV value greater than 0.60

(Figure 4.108). Of the six samples, BKL 03 was the sample with the highest ICV value in its corresponding bulk sample (0.52).

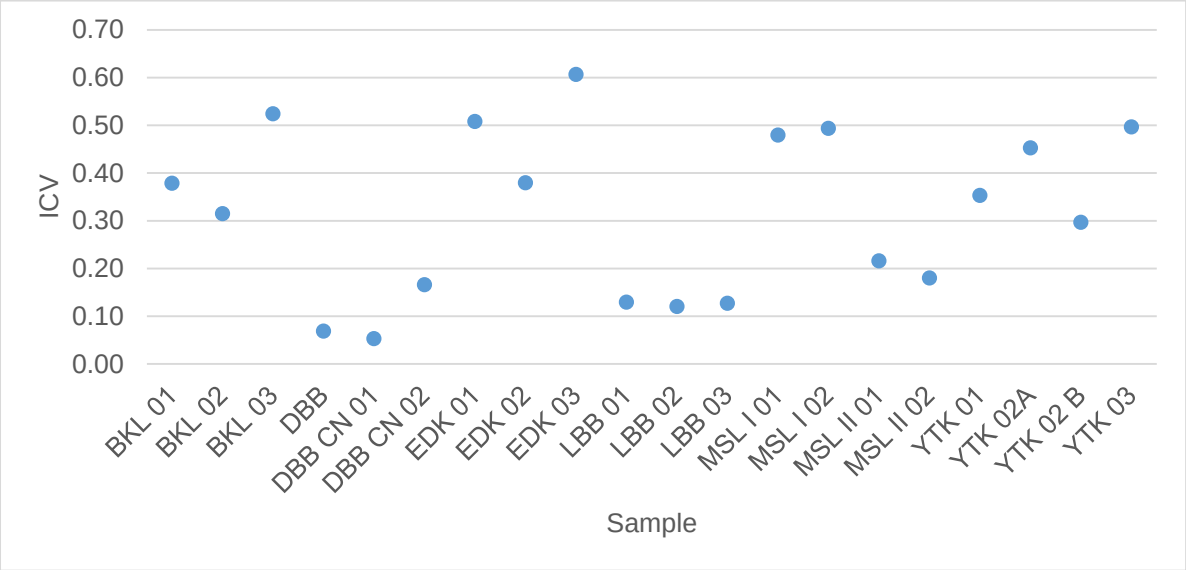

Figure 4.107: ICV of bulk samples

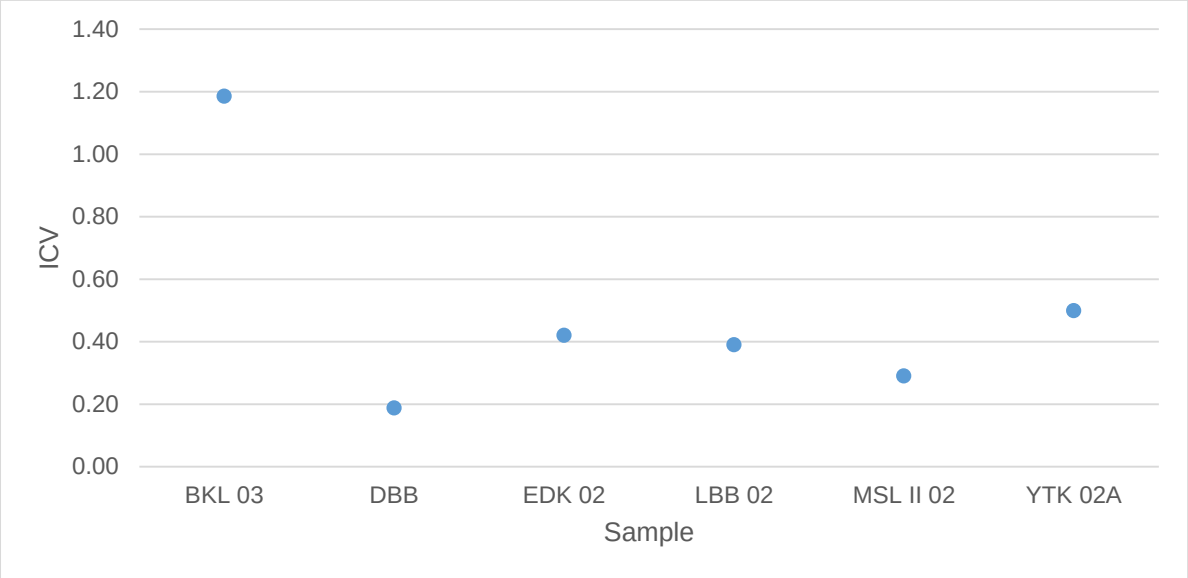

Figure 4.108: ICV of silt samples

The ICV values of < 2 µm samples ranged from 0.07 (DBB and DBB CN 01) to 0.65 (EDK 03). This is a similar trend as in bulk samples. Dibamba, Logbaba and Missole II had ICV values < 0.22 (Figure 4.109).

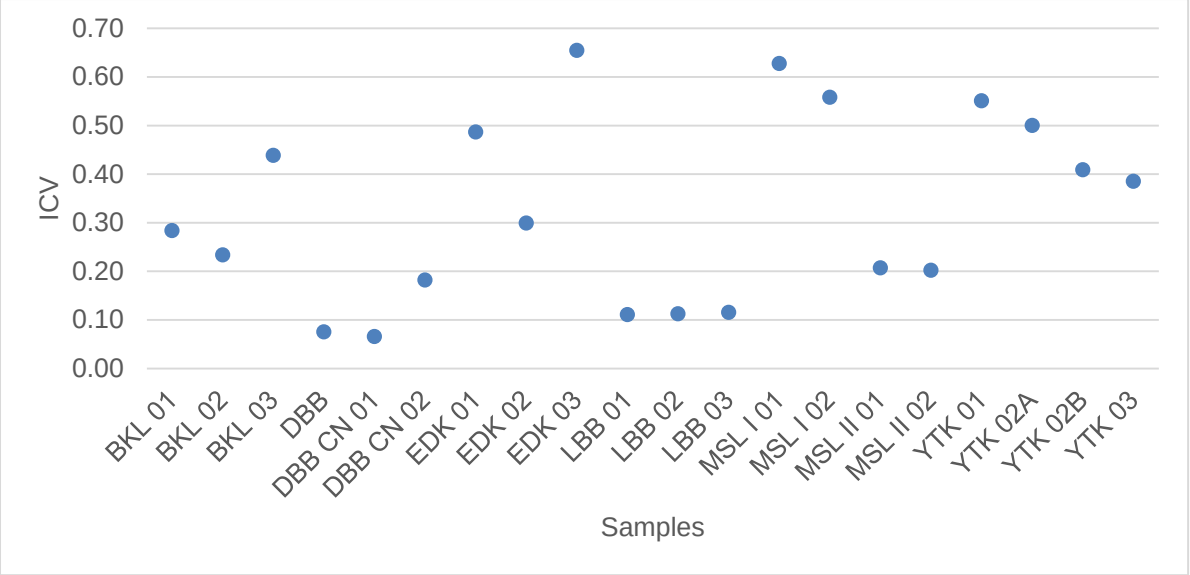

Figure 4.109: ICV of < 2 µm samples

4.5.2.2 Sedimentary provenance

Major oxides geochemistry of clay minerals could be a best indicator for their compositional variability, thereby giving insights on their provenance, as well as environmental conditions prevailing during diagenesis (Cox *et al*., 1995). Geochemical discrimination diagrams could be used to deduce the provenance of kaolins. An example, the relationship between climate and the degree of weathering shows that higher rainfall corresponds to increased weathering and higher CIA values in the resulting sediments (Ahmad *et al*., 2014). A similar positive relationship exist between the intensity of weathering and CIW due to the immobility of Al and higher mobility of Na, K, and Ca (Akinyemi *et al*., 2014). However, as weathering progresses, ICV decreases due to conversion of feldspars to Al-bearing clays, such as kaolins.

The lowest ICV values (< 0.22) were observed in Dibamba, Logbaba and Missole II samples. Low ICV values correspond to high degree of maturity of the samples. Therefore they might have been deposited in tectonical quiescent or cratonic environments, which is a characteristic of second cycle deposits; unlike immature sediments which tend to be found in tectonically active settings and are characteristic of first-cycle deposits (Cox *et al*., 1995). Though other samples did not have very low ICV values, their values however, fall in the range for clay minerals (0.03-0.78), which confirm the mineralogy varying from dominant clay minerals to minor feldspars (Nagarajan *et al*., 2013).

The TiO_2-Al_2O_3 binary plots of both bulk and < 2 µm samples (Figures 4.110 and 4.111) suggest that the source rocks of these kaolins vary between rhyolite/granite and

rhyolite/granite + basalt, with Missole I samples being the closest to the rhyolite/granite + basalt line.

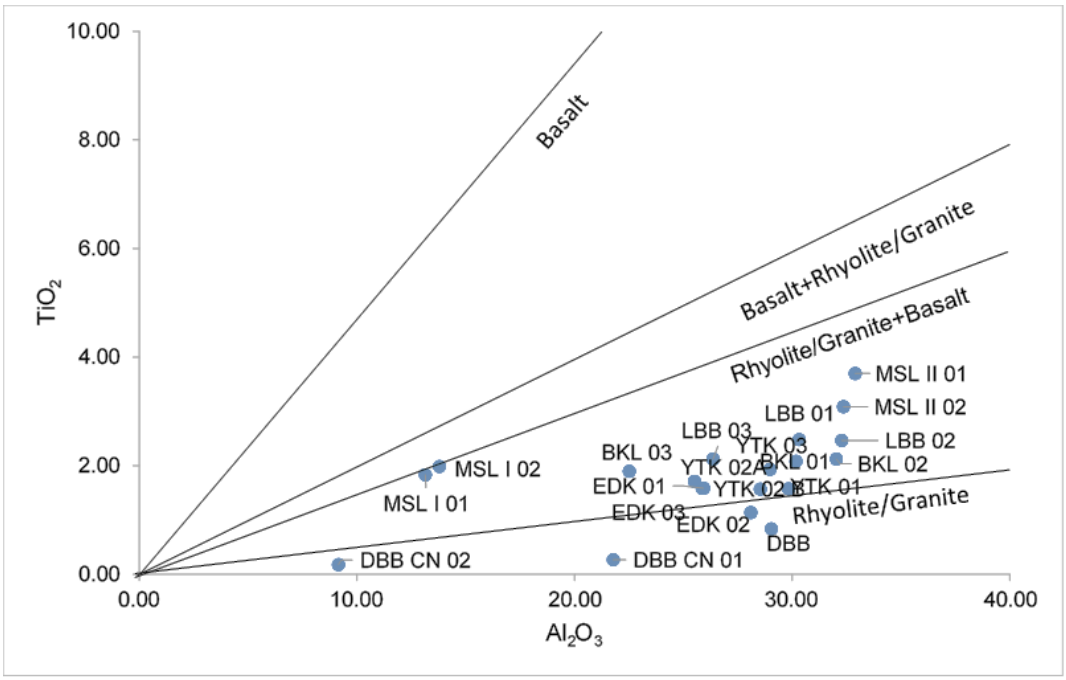

Figure 4.110: TiO_2-Al_2O_3 binary plot of bulk samples (Fields are from Ekosse, 2001)

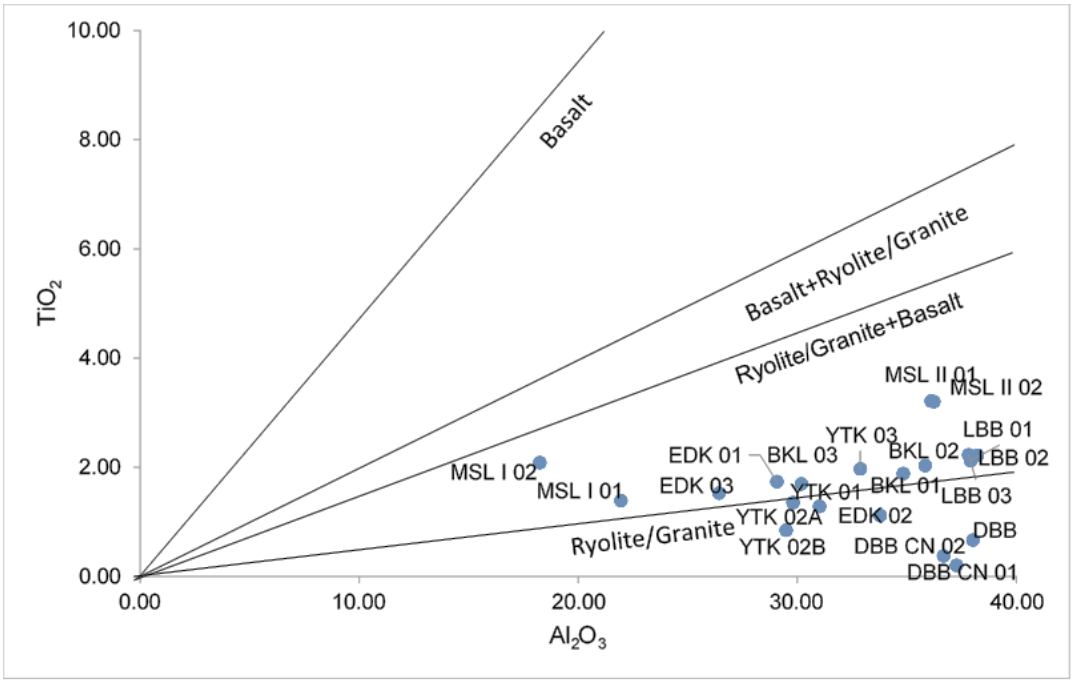

Figure 4.111: TiO_2-Al_2O_3 binary plot of < 2 µm samples (Fields are from Ekosse, 2001)

The A-CN-K ternary plots (Figures 4.112 and 4.113) were used to evaluate the geochemical alteration of studied kaolins and infer their possible provenance (Fedo *et al*., 1995; Bahlburg

and Dobrzinski, 2009). Most samples plotted close to the kaolinite point. Unlike the mineralogy, however, these plots show that the kaolins had more illite than smectite. Ediki kaolins plotted in the illite field, this is because Ediki kaolins contained microcline; therefore the excess K_2O in the samples was taken for illite.

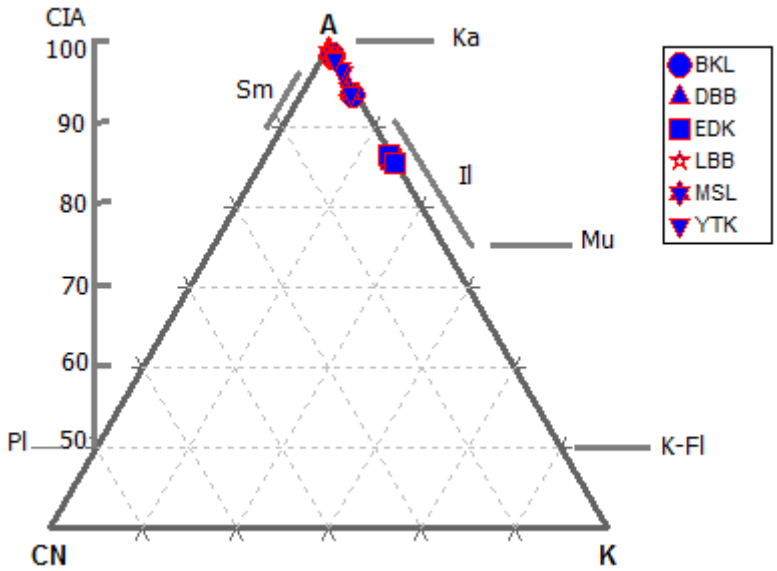

Figure 4.112: A-CN-K plot of bulk samples

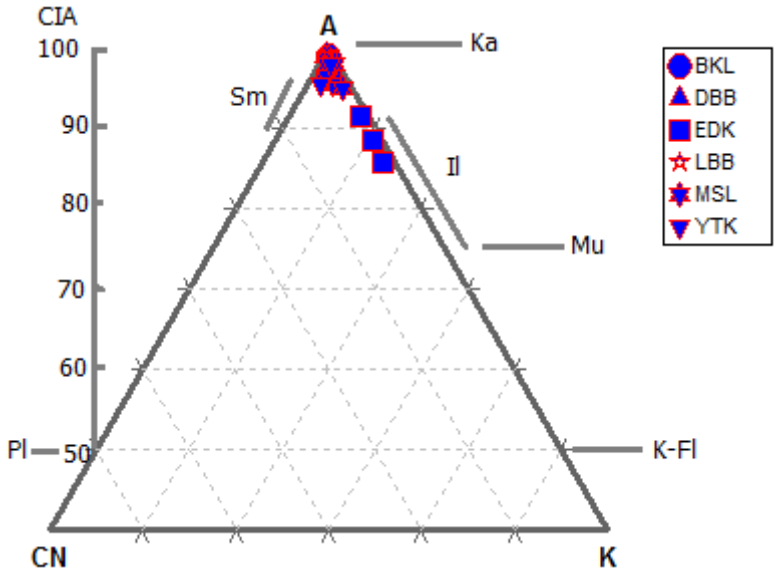

Figure 4.113: A-CN-K plot of < 2 µm samples

As in the A-CN-K plots, the A-CNK-FM plots (McLennan *et al*., 1993) of both bulk and < 2 µm kaolins (Figures 4.114 and 4.115) showed that kaolinite was the most dominant mineral, with few amounts of illite in Ediki kaolins. Dibamba, Logbaba and Missole II kaolins plotted very close to the kaolinite point.

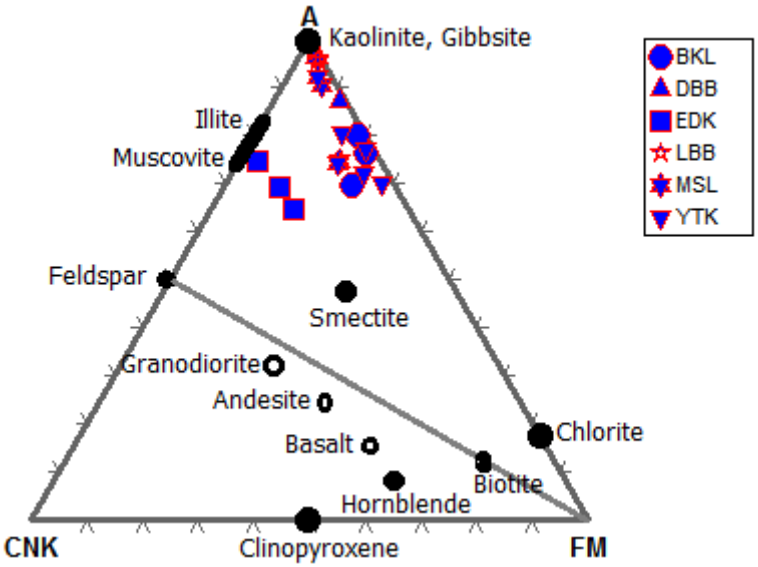

Figure 4.114: A-CNK-FM plot of bulk samples

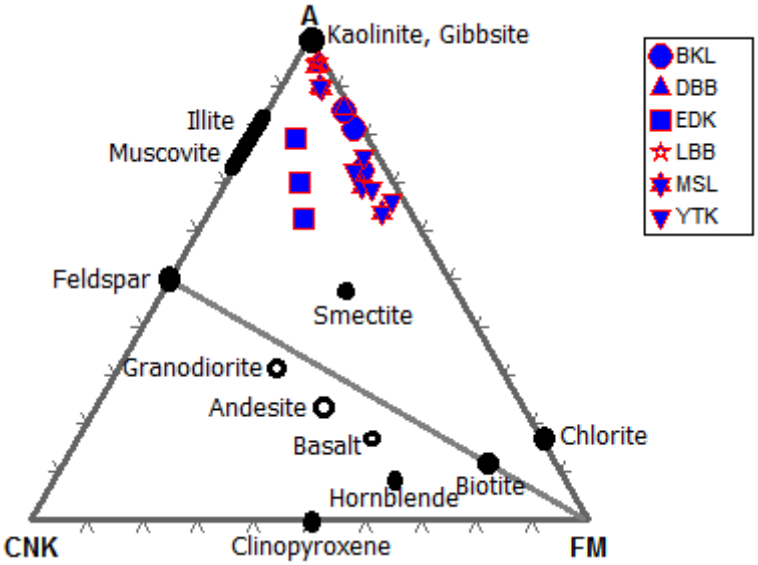

Figure 4.115: A-CNK-FM plot of < 2 µm samples

4.5.2.3 Environments of formation or deposition

The plot of log (K_2O/Al_2O_3)/log (MgO/Al_2O_3) has been used by Mousa *et al*. (2014) to discriminate between marine and non-marine environments or formation or deposition. For the studied kaolins, the plot of log (K_2O/Al_2O_3)/log (MgO/Al_2O_3) showed that the kaolins are dominantly of marine origin, except the Logbaba samples, which show a non-marine/deltaic environment (Figures 4.116 and 4.117). The Logababa samples are found in the Upper Cretaceous Logbaba Formation, which is believed to have sediments of lacustrine origin (Chavom *et al*., 2014).

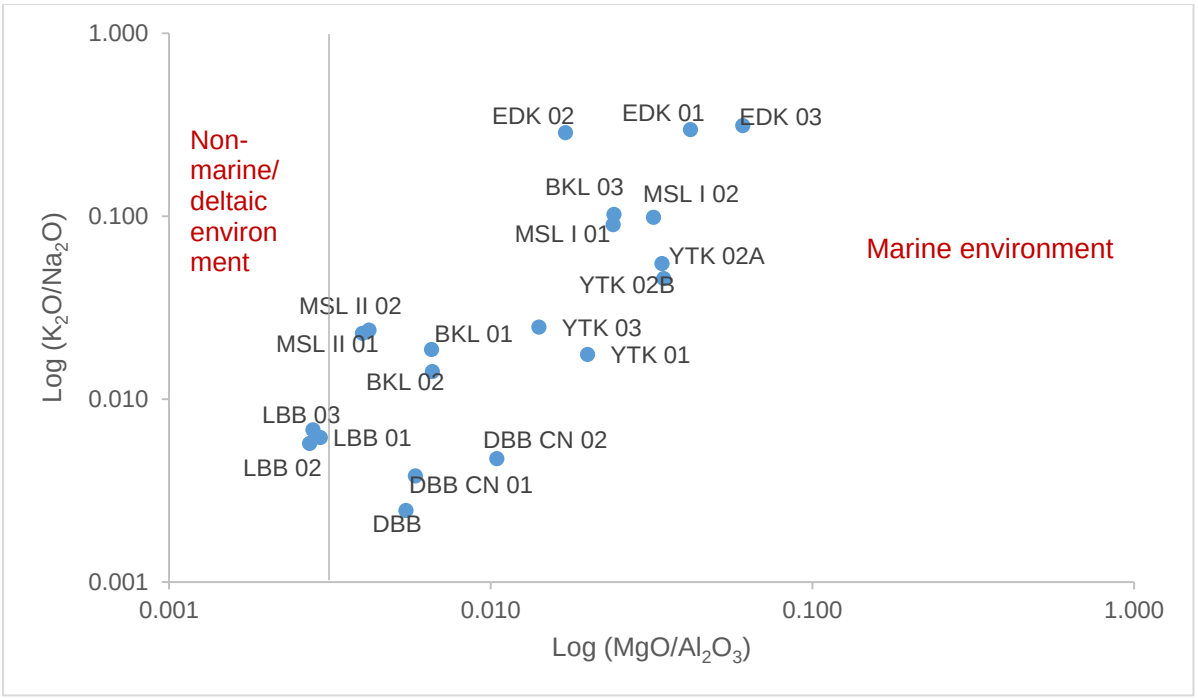

Figure 4.116: Plot of log (K_2O/Al_2O_3)/log (MgO/Al_2O_3) of bulk kaolins showing a marine environment of formation

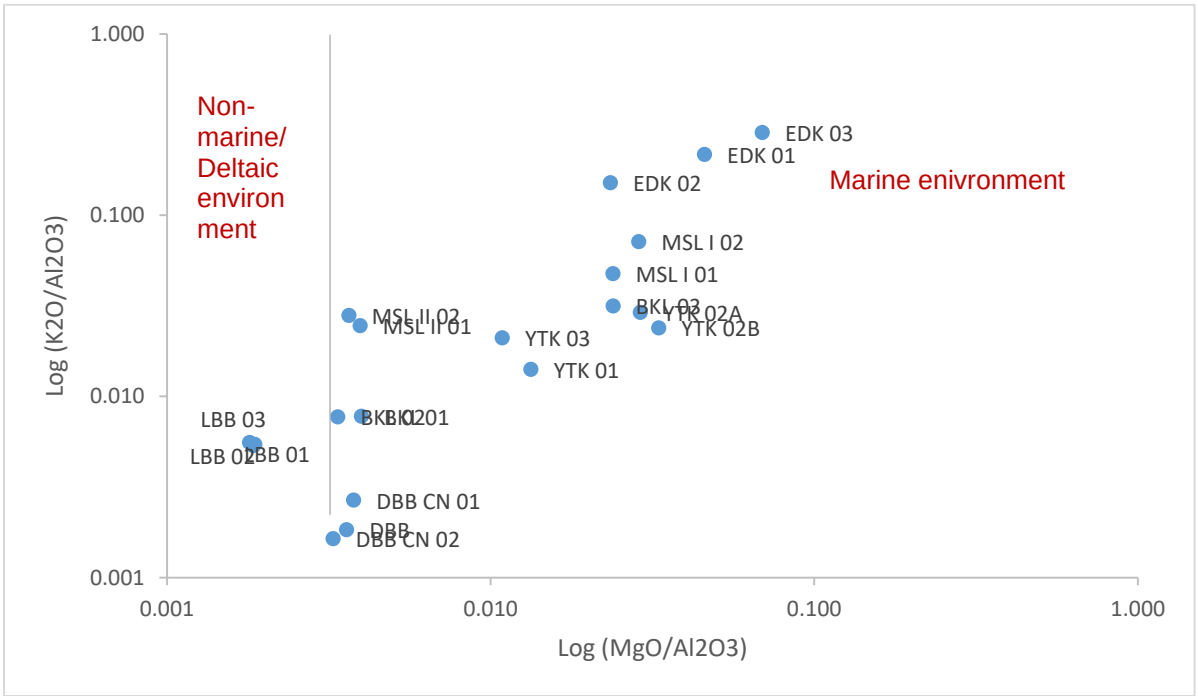

Figure 4.117: Plot of log (K_2O/Al_2O_3)/log (MgO/Al_2O_3) of < 2 µm kaolins showing a marine environment of formation

4.6 Synopsis

The objective of this chapter was to investigate the nature, occurrence, mineralogy and geochemistry of Cretaceous-Tertiary kaolins of the Douala Sub-Basin (Specific Objective A). The following results were obtained:

- Generally, Cretaceous-Tertiary kaolins of the Douala Sub-Basin are hosted by sandstone deposits. They occur as layers varying from 1 mm to 5 m thick. Texturally, the kaolins can be divided into two facies: sandy and clayey kaolins.
- The mineral phases present in bulk and silt samples are kaolinite and quartz (as major phases), smectite and/or illite (as minor phases), anatase and rutile (as minor or trace phases), goethite and hematite (as trace phases). In the clay fractions, the mineral phases are made up of kaolinite and smectite (as major phases), smectite and/or illite (as minor phases), anatase and rutile (as minor or trace phases), goethite and hematite (as trace phases); though goethite was a major phase in YTK 02A. Dibamba, Logbaba and Missole II kaolins contained the highest amount of kaolinite (> 85 wt %) in all samples; whereas, Ediki kaolins contained the least amount of kaolinite and were mostly smectitic. Anatase was the main impurity in most of the samples.
- The kaolins are mostly made up of thin platy or pseudo-hexagonal particles or flakes, books or stacks of kaolinite. A swirl texture was also noted in a sample (EDK 03). The Dibamba, Logbaba and Missole II kaolins have well-ordered structures, based on the FTIR classification of Vaculíková *et al*. (2011). Bomkoul and part of Yatchika kaolins have partially to well-ordered kaolinite structure; and Ediki and Missole I kaolins have poorly ordered or disordered kaolinite structures.
- The three main reactions occurring during kaolin heating were observed in all samples. In addition, pre-dehydroxylation reaction occurred in all Logbaba samples. Dehydroxylation temperatures were generally lower than those of the Cretaceous-Tertiary Georgia kaolins used as standards, but this difference was attributed to difference in parameters used in the analysis. Exothermic peak temperatures were between 943-988^{o}C; though all of Ediki samples and some of Bomkoul, Missole I and Yatchika samples had exothermic peak temperatures above 1000^{o}C. The total weight loss were close to respective LOI of samples.
- The most abundant major oxides are silica and alumina, followed by iron oxide and titania; though Logbaba and Missole II had higher titania than iron oxide. Potassium and magnesium oxides were relatively higher in some samples. All kaolins, portrayed extreme silicate weathering, except Ediki kaolins, which portrayed moderate silicate weathering. This was also supported by ICV values, which showed that Cretaceous-Tertiary kaolins

of the Douala Sub-Basin are compositionally mature, but Ediki kaolins are less mature. The geochemical composition of the kaolins showed that source rocks of these kaolins vary between rhyolite/granite and rhyolite/granite + basalt; and they are mostly enriched in kaolinite with some amounts of illite (Ediki kaolins). The geochemistry also suggested that the kaolins formed in a marine environment (except Logbaba samples).

Validation of hypothesis: Cretaceous-Tertiary kaolins of the Douala Sub-Basin have similar mineralogical and geochemical parameters, depending on their composition variability.

CHAPTER 5

PALEOENVIRONMENTAL RECONSTRUCTION OF CRETACEOUS-TERTIARY KAOLINS

5.1 Preamble

This chapter attempted to determine the genesis of studied Cretaceous-Tertiary kaolins in Douala Sub-Basin and reconstruct the prevailing paleoenvironmental conditions in which they formed (Specific Objective B). Trace elements geochemistry (trace elements' abundances, elemental ratios, binary and/or ternary plots) and stable isotopes geochemistry, from which the genesis and paleoenvironmental reconstruction are deduced, are presented. This chapter is based on Hypothesis B.

HYPOTHESIS B: The studied Cretaceous-Tertiary kaolin deposits formed in similar paleoenvironmental conditions.

5.2 Trace elements geochemistry

5.2.1 Rare earth elements (REEs)

Results of REEs are found in Appendices 5.1-5.3. Holmium (Ho) was not detected in all the samples. Other elements such as Ce, Nd, Eu, Tm and Lu were not detected in some samples. Therefore, the traditional spider diagrams were substituted to histograms to show the enrichment or depletion of REEs in Cretaceous-Tertiary kaolins relative to upper continental crust (UCC) values (Rudnick and Gao, 2003).

Bulk samples

The normalised concentrations of REEs to UCC values in bulk samples is shown in Figure 5.1. Bomkoul samples were enriched in most REEs relative to UCC, except La and Yb (BKL 01). Dibamba samples were mostly enriched in REEs; however, La and Pr were depleted in DBB CN 02 (0.40 and 0.44 for La and Pr, respectively) and DBB Cn 01 was depleted in Yb (0.20). Ediki samples (EDK 01 and EDK 02) and all Logbaba samples were also depleted in La and Yb. Logbaba samples were also depleted in Ce. Unlike other kaolins, Missole kaolinss were mostly enriched in La and Yb. All kaolins were mostly enriched in Er, with normalised

values ranging from 100.06 (DBB CN 01) to 3557.55 (BKL 03). Europium was enriched in BKL 03 (2.17), DBB CN 01 (3.39), EDK 02 (1.60), EDK 03 (2.34) and all Missole samples (1.56-14.67); and it was depleted in DBB (0.79), DBB CN 02 (0.40), EDK 01 (0.20) and all Logbaba samples (0.58-0.79). Europium was not detected in Yatchika samples. However, all samples in which it was detected had a negative Eu anomaly.

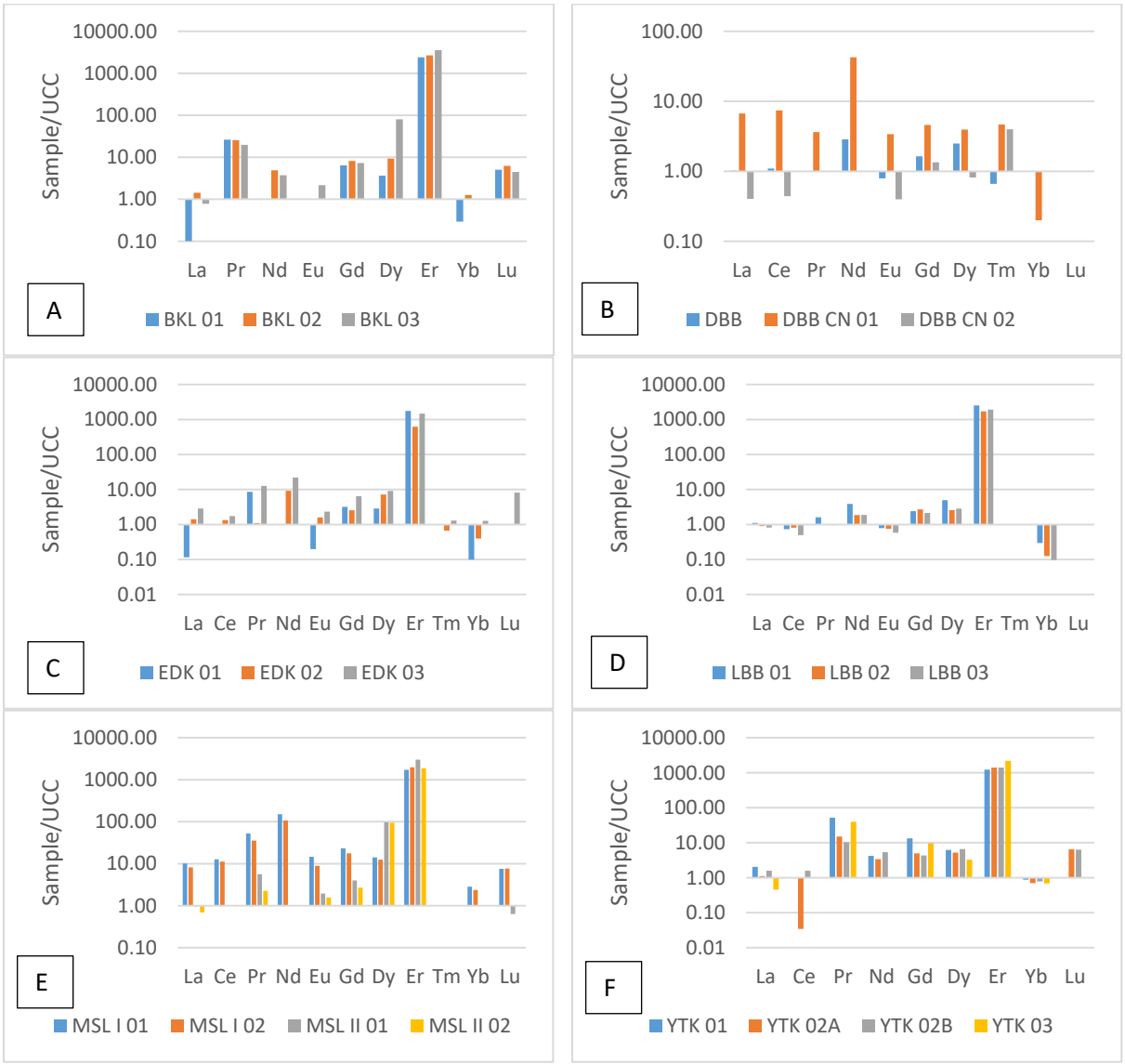

Figure 5.1: Normalised concentrations of REEs to UCC values in bulk samples from A) Bomkoul, B) Dibamba, C) Ediki, D) Logbaba, E) Missole, F) Yatchika

Silt samples

All silt samples were enriched in most REEs, with Er being the most abundant (1038.69-3731.22) (Figure 5.2). All samples were depleted in Yb (0.40-0.80). Samples BKL 03 and MSL

II 02 were also depleted in La (0.22 and 0.47, respectively). A negative Eu anomaly (0.40) was observed in MSL II 02 and in EDK 02 (1.78). Eu was not detected in BKL 03, DBB, LBB 02 and YTK 02A.

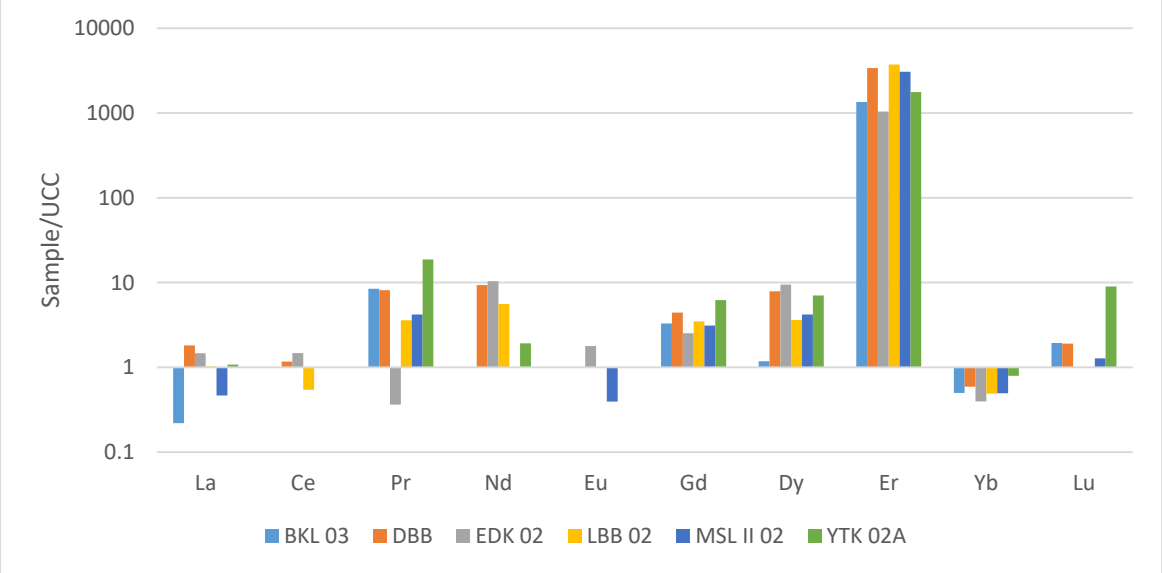

Figure 5.2: Normalised concentrations of REEs to UCC values in silt samples

< 2 µm fraction samples

Unlike in their corresponding bulk samples, the < 2 µm fraction samples were mostly enriched in La (Figure 5.3). However, they were also depleted in Yb. Er was the most abundant REE, with values ranging between 203.94 (DBB CN 01) to 3755.80 (MSL II 02). Europium was enriched in BKL 02 (1.40), DBB CN 01 (15.17) and all Logbaba samples (1.56 - 1.77); and it was depleted in DBB (0.58) and DBB CN 02 (0.40). Eu was not detected in Missole and Yatchika samples. In samples where Eu was detected, there was a negative Eu anomaly.

A negative anomaly was observed in BKL 02 (1.40), DBB (0.58) and DBB CN 02 (0.40); whereas a positive Eu anomaly was observed in DBB CN 01 (15.17) and all Logbaba samples (1.56 - 1.77). Eu was not detected in Missole and Yatchika samples.

Figure 5.3: Normalised concentrations of REEs to UCC values in < 2 µm fraction samples from A) Bomkoul, B) Dibamba, C) Ediki, D) Logbaba, E) Missole, F) Yatchika

5.2.2 Other trace elements

Results of trace elements other than REEs, i. e. the large ion lithophile elements (LILE), high field strength elements (HFSE) and transition trace elements (TTE) are found in Appendices 5.4-5.6. Tungsten (W) was not detected in all the samples. Other elements such as Co, Cu, Hf, Nd, Ta and Th were not detected in some samples. Therefore, as for REEs, the traditional spider diagrams were substituted with histograms to show the enrichment or depletion of Cretaceous-Tertiary kaolins relative to UCC values (Rudnick and Gao, 2003) in trace elements.

Bulk samples

For the LILE (Rb, Ba, Sr, Th and U), Sr and Ba were depleted in all samples relative to UCC, with normalised values varying between 0.10 and 1.00 in Bomkoul, Ediki and Missole samples; and up to < 0.1 in Dibamba, Logbaba and Yatchika samples (Figure 5.4). Rb, Th and U were enriched in all samples, though Th, where detected, was generally similar to UCC values. The normalised values of Rb and U were > 100 in all samples.

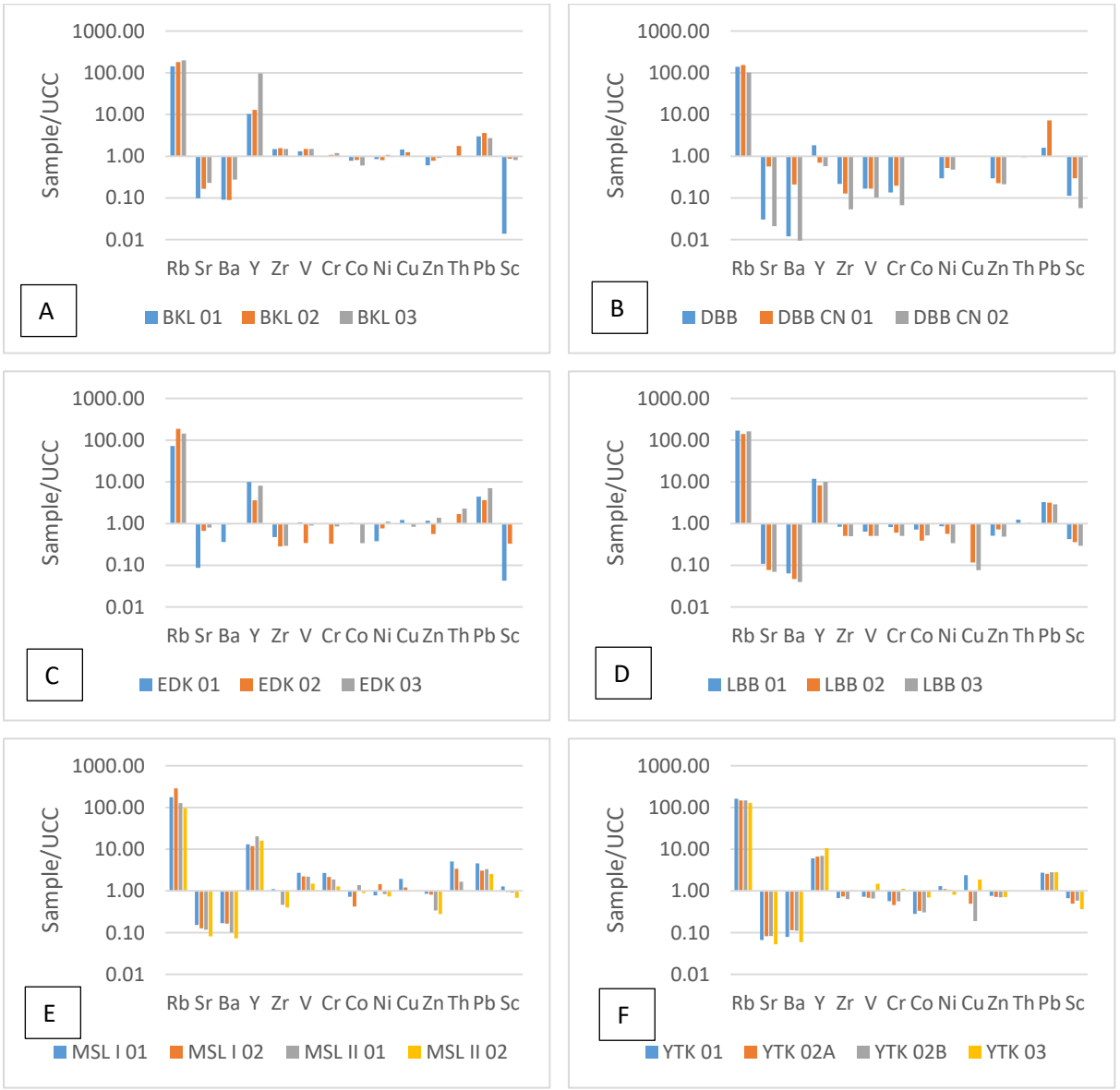

Figure 5.4: Normalised concentrations of trace elements to UCC values in bulk samples from A) Bomkoul, B) Dibamba, C) Ediki, D) Logbaba, E) Missole, F) Yatchika

High field strength elements (Y, Zr, Nb and Hf). Yttrium was enriched in all samples relative to UCC; whereas Zr concentrations were generally similar to UCC values in Bomkoul, Ediki,

Logbaba, Missole and Yatchika, though slightly depleted (Figure 5.4). Zirconium was more depleted in Dibamba, with normalised values being up to 0.1. Niobium (Nb) was enriched in all samples relative to UCC but was below detection limit in all Dibamba samples. Hf was only detected in Dibamba clay nodules (DBB CN 01 and DBB CN 02) and EDK 02 (Appendix 5.4) and with concentrations varying between 229.63 ppm (EDK 02) and 1666.67 ppm (DBB CN 01).

Transition trace elements (V, Co, Cu, Ni and Sc): Vanadium, Co, Cu and Ni concentrations are quite similar to UCC values, except in Dibamba samples in which normalised values could be below 0.10. Scandium was mainly depleted in all samples, but had similar values to UCC in Yatchika, Missole and some Bomkoul samples (Figure 5.4).

Silt samples

LILE (Rb, Ba, Sr, Th and U): Rubidium and U were more enriched in all samples relative to UCC, with normalised values being > 100 in all samples. Ba was depleted in all samples but was slightly enriched in EDK 02 relative to UCC. Strontium was depleted in all samples; and Th had slightly similar values as UCC (Figure 5.5).

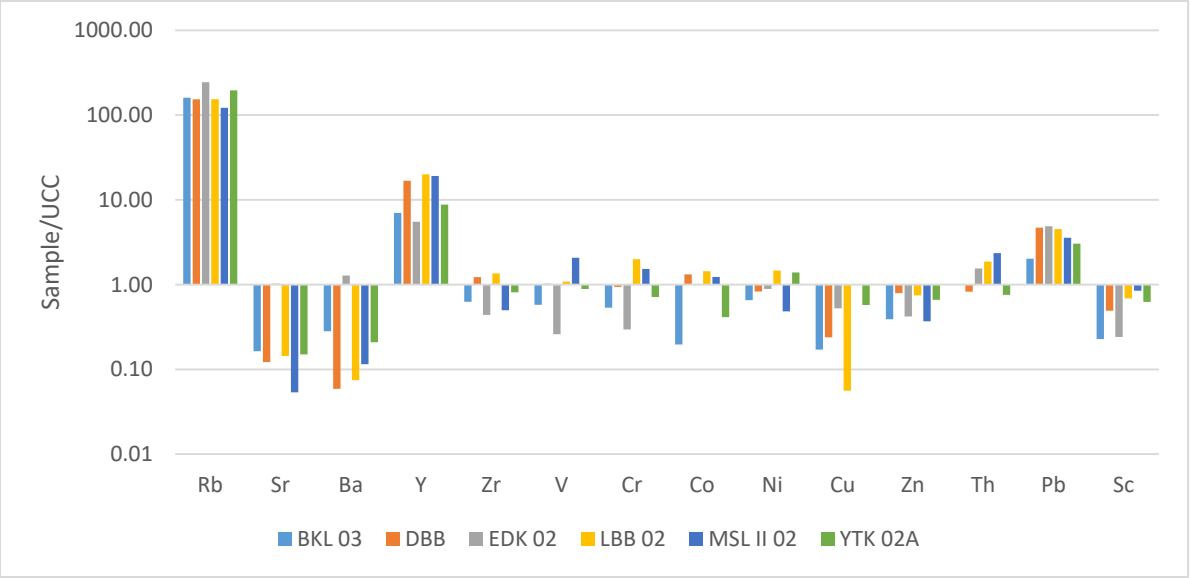

Figure 5.5: Normalised concentrations of trace elements to UCC values in silt samples

High field strength elements (Y, Zr, Nb and Hf): Yttrium and Nb were enriched in all samples relative to UCC (Figure 5.5). Zirconium values were slightly similar to UCC values. Zirconium enriched in DBB and LBB 02, but depleted in BKL 03, EDK 02, MSL II 02 and YTK 02A. Hf was only detected in EDK 02, with a concentration of 565.03 ppm.

Transition trace elements (V, Co, Cu, Ni and Sc): Copper and Sc were depleted in all samples, relative to UCC. Vanadium, Co and Ni had values similar to UCC, though V was mainly depleted in EDK 02 and Co was mainly depleted in MSL II 02.

< 2 µm fraction samples

The LILE (Rb, Ba, Sr, Th and U): As in other fractions, Rb and U were highly enriched in all samples relative to UCC (Figure 5.6). Barium and Sr were depleted in all samples relative to UCC. In Bomkoul, Ediki, Missole and Yatchika samples, Th concentrations were similar to UCC; but Th was more enriched in Logbaba samples.

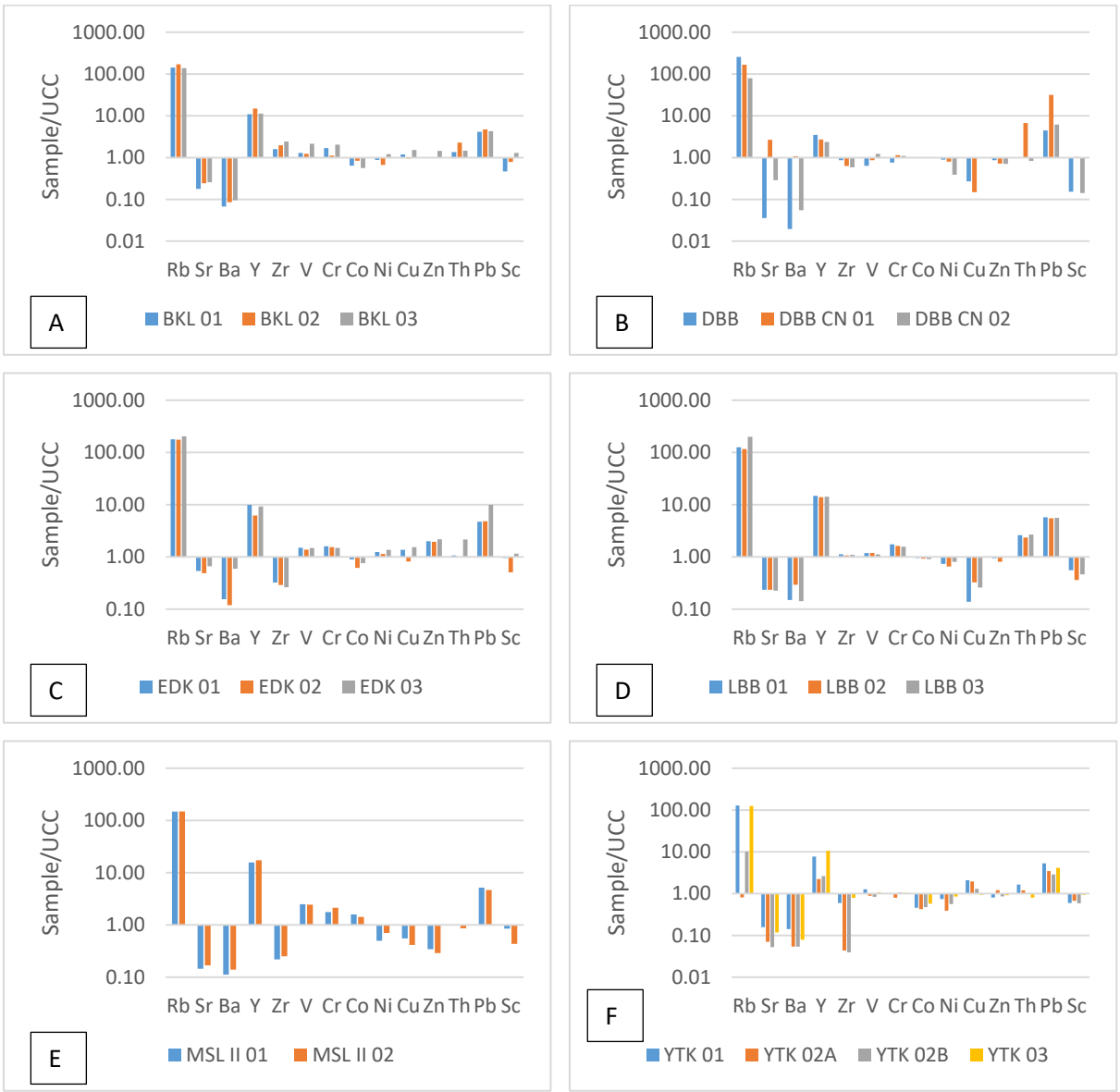

Figure 5.6: Normalised concentrations of trace elements to UCC values in < 2 µm fraction samples from A) Bomkoul, B) Dibamba, C) Ediki, D) Logbaba, E) Missole, F) Yatchika

High field strength elements (Y, Zr, Nb and Hf): Yttrium and Nb were enriched in all the samples, as in other fractions. Zr was mainly depleted in all samples relative to UCC, except in Bomkoul and Logbaba samples; though Logbaba samples had Zr concentrations very similar to UCC (Figure 5.6). Hafnium was only detected in DBB CN 01 (1666.67 ppm) and DBB CN 02 (243.12 ppm).

Transition trace elements (V, Co, Cu, Ni and Sc): Averagely, TTEs were very similar to UCC values in all samples (Figure 5.6).

5.3 Stable isotopes geochemistry

Eleven samples were analysed for ^{18}O and D stable isotopes. $\delta^{18}O$ and δD of the samples are shown in Table 5.1 and plotted in Figure 5.7. For reference, the local meteoric water line (LMWL) for Douala (Wirmvem *et al*., 2016), the global meteoric water line (GMWL) (Craig, 1961), the supergene-hypogene line (Sheppard *et al*., 1969) and the kaolinite line (Savin and Epstein, 1970) are also plotted in Figure 5.7, according to Equations 5.1-5.4.

Local meteoric water line for Douala: $\delta D = 7.92\delta^{18}O + 12.99$ (Eqn. 5.1)

Global meteoric water line: $\delta D = 8\delta^{18}O + 10$ (Eqn. 5.2)

Supergene-hypogene line: $\delta D = 7.5\delta^{18}O - 185$ (Eqn. 5.3)

Kaolinite line: $\delta D = 7.5\delta^{18}O - 220$ (Eqn. 5.4)

Table 5.1: $\delta^{18}O$ and δD values of analysed Cretaceous-Tertiary kaolins

	$\delta^{18}O$	δD
BKL01	15.3	-68
BKL02	18.2	-69
DBB	21.0	-57
DBB CN02	20.5	-60
EDK02	16.9	-48
LBB 03	20.3	-64
LBB01	20.1	-63
MSL(2)01	18.7	-53
MSL(2)01	18.7	-53
YTK01	18.6	-68
YTK03	20.2	-64
Mean	19.0	-60.5
Standard deviation	1.6	6.7

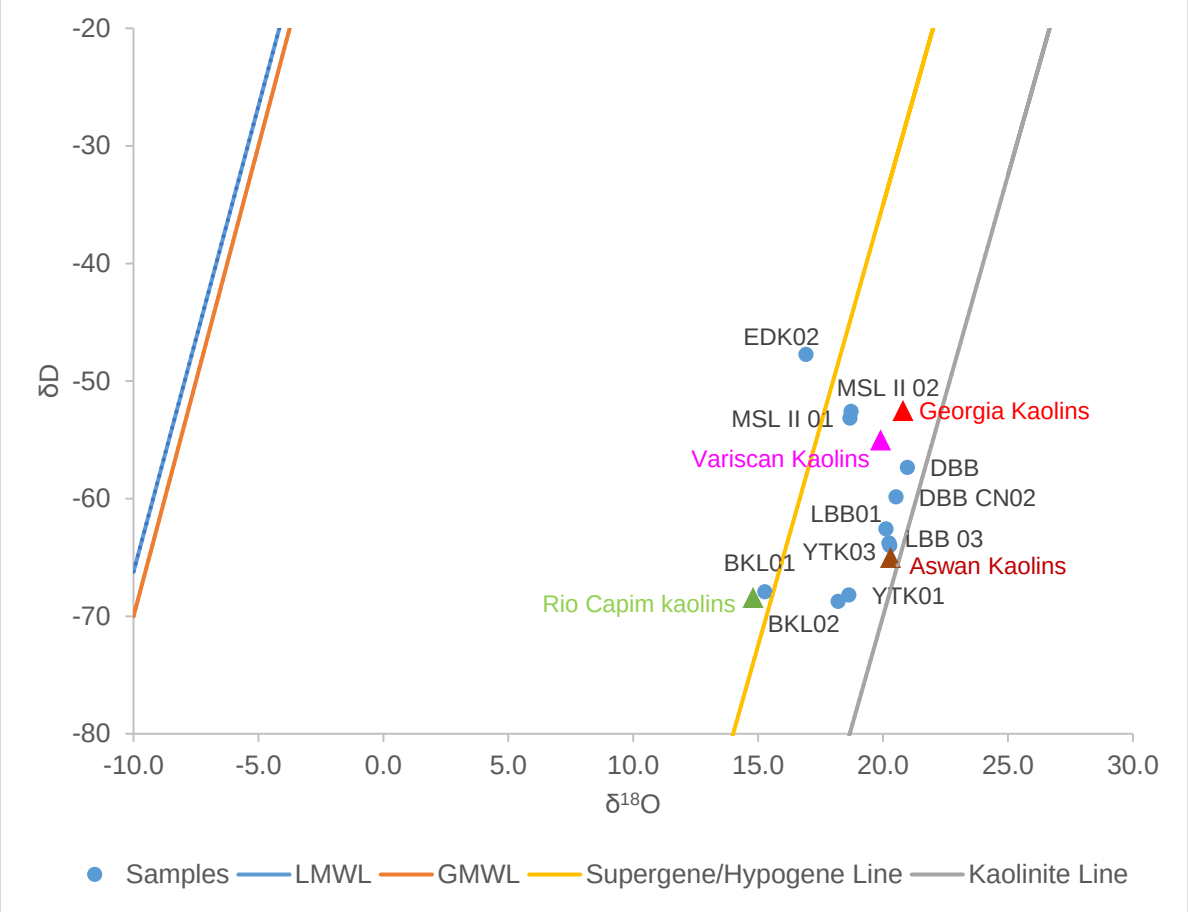

Figure 5.7: $\delta^{18}O$ versus δD plot of clay fractions of selected samples: *The LMWL, GMWL, S/H line and the kaolinite line were plotted for reference. Values of the Cretaceous-Tertiary Georgia kaolins in USA (Hassapinak and Elsinger, 1985), Cretaceous Rio Capim kaolins in Brazil (Santos et al., 2007), Cretaceous Aswan kaolins in Egypt (Baouimy, 2013) and Tertiary Variscan kaolins in Spain (Clauer et al., 2015) were also included for comparison.*

The $\delta^{18}O$ values varied between 15.3‰ (BKL 01) and 21.0‰ (DBB); whereas, δD values varied between -69‰ (BKL 02) and -53‰ (MSL II 01 and MSL II 02). The means of $\delta^{18}O$ and δD are 19.0 ± 1.6‰ and -60.5 ± 6.7‰, respectively, indicating that $\delta^{18}O$ have homogenous values. About 82% of the samples fall between the kaolinite line and supergene-hypogene line. Two samples (EDK 02 and BKL 01) fall on the left of the supergene-hypogene line, suggesting a possible hypogene genesis for these two samples. However, Clauer *et al*. (2015) suggested that supergene kaolins could plot in the hypogene field if they formed in isotopic equilibrium with their parental fluid without subsequent isotopic exchange or alteration.

Dibamba and Logbaba samples (DBB, DBB CN 02, LBB 01 and LBB 03) plot very close to the kaolinite line. These samples all have a kaolinite content > 90.0 wt %. Missole II kaolins (MSL II 01 and MSL II 02) plot on the right side of the supergene-hypogene line, but closer to this line than other samples. These kaolins have an illite content of 4.94 and 6.18 wt %, for

MSL II 01 and MSL II 02, respectively; and lower kaolinite content 87.33 and 85.87 wt %, for MSL II 01 and MSL II 02, respectively. EDK 02, which plots more to the left of the supergene-hypogene line, has the lowest kaolinite content (63.4 wt %) and the highest illite content (9.69 wt %) than all other samples. The isotopic composition of illite and kaolinite in equilibrium with meteoric waters at 20^{o}C are similar (Gilg *et al*., 1999). Therefore, the lower the amount of kaolinite, the farther the sample from the kaolinite line.

5.4 Discussion

5.4.1 Paleoenvironmental reconstruction based on trace elements and major oxides geochemistry

Trace elements, including REEs, high field strength elements (Zr, Hf, Y and Nb) and transition trace elements (TTE) e.g. Sc, Co, Cr and Ni are relatively immobile during sedimentary processes and thus they are used as geochemical proxies to determine paleoenvironments of formation (Madukwe *et al*., 2016). Paleoenvironmental reconstruction of Cretaceous-Tertiary kaolins of the Douala Sub-Basin using trace elements and some major oxides involved the determination of the following: sedimentary provenance, hydraulic sorting and sediment recycling, and paleo-redox conditions.

5.4.1.1 Sedimentary provenance

The concentration of some trace elements and/or their ratios varies in different source rocks composition (silicic or acidic and basic). Of these trace elements, Th, Sc, Cr, Ni and Co, which are among the least soluble, are the widely used for provenance studies, because they are transported almost exclusively in the terrigenous component of a sediment and, therefore, reflect the chemistry of their source rocks (Lopez *et al*., 2005). Felsic rocks are richer in Th, and La; whereas, mafic rocks are richer in Co, Sc, Ni and Cr (Armstrong-Altrin *et al*., 2013). Hence, these elements and their ratios (La/Sc, Th/Sc, Th/Co, and Cr/Th) could be used to infer the sedimentary provenance or source rock composition (Cullers, 1995; 2000). The Th/Co vs La/Sc and TiO_2 vs Ni plots and the Th/Sc, Th/Co, Cr/Th ratios (Figure 5.8-5.12) all showed that Cretaceous-Tertiary kaolins in the Douala Sub-Basin have a silicic or felsic source.

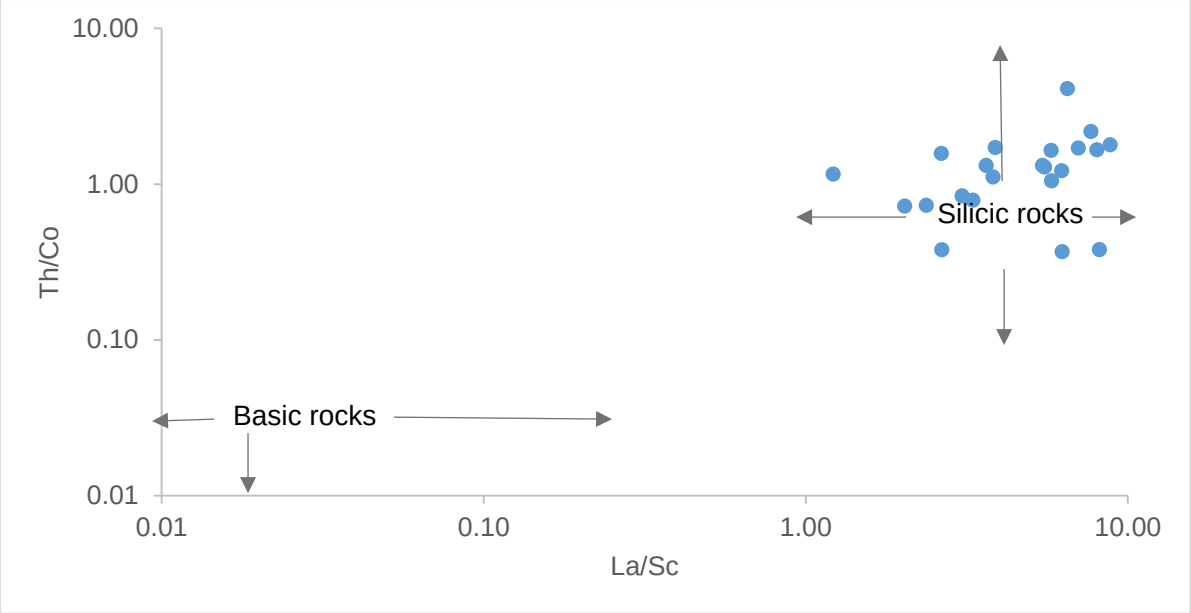

Figure 5.8: Th/Co vs La/Sc showing the source rocks of Cretaceous-Tertiary kaolins (bulk, silt and clay) samples

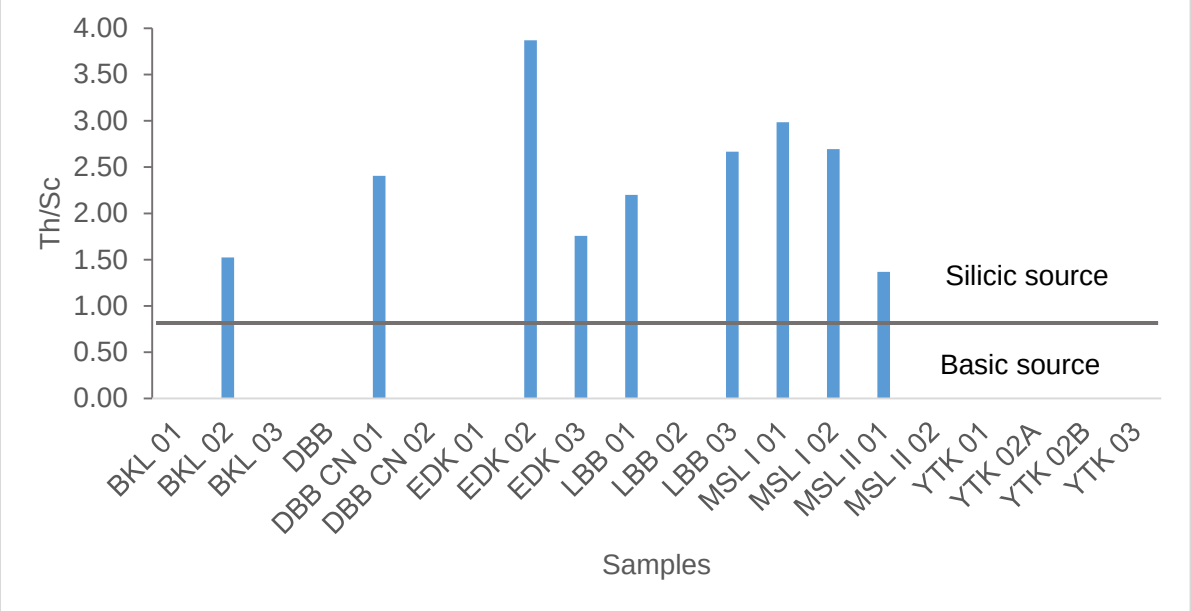

Figure 5.9: Plot of Th/Sc of bulk samples

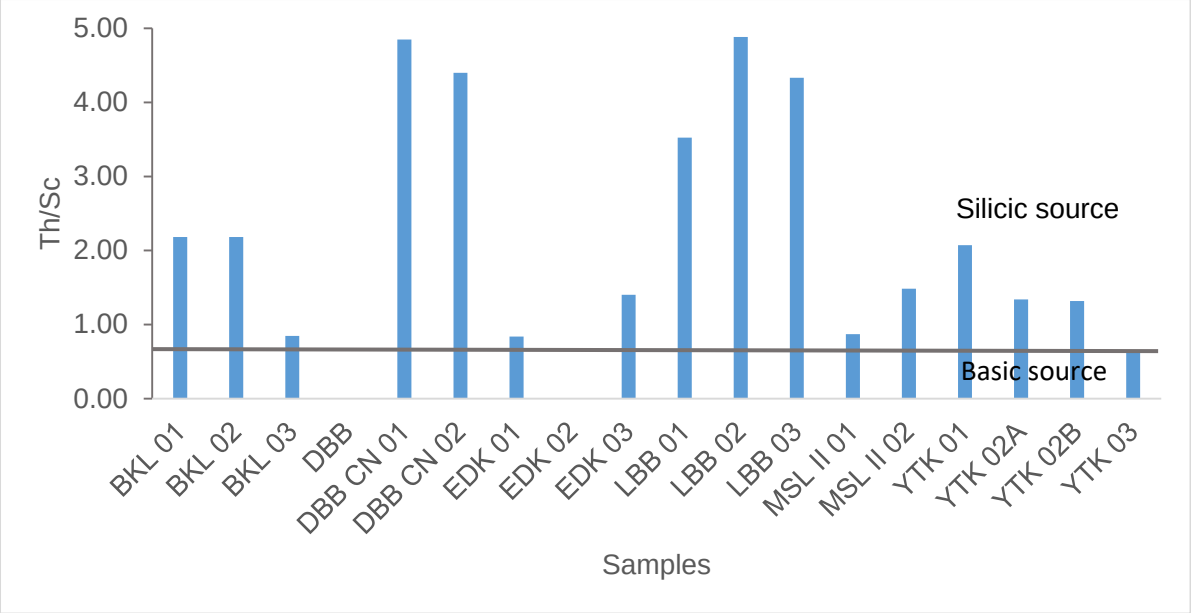

Figure 5.10: Plot of Th/Sc of < 2 µm fraction samples showing the silicic source of the kaolins

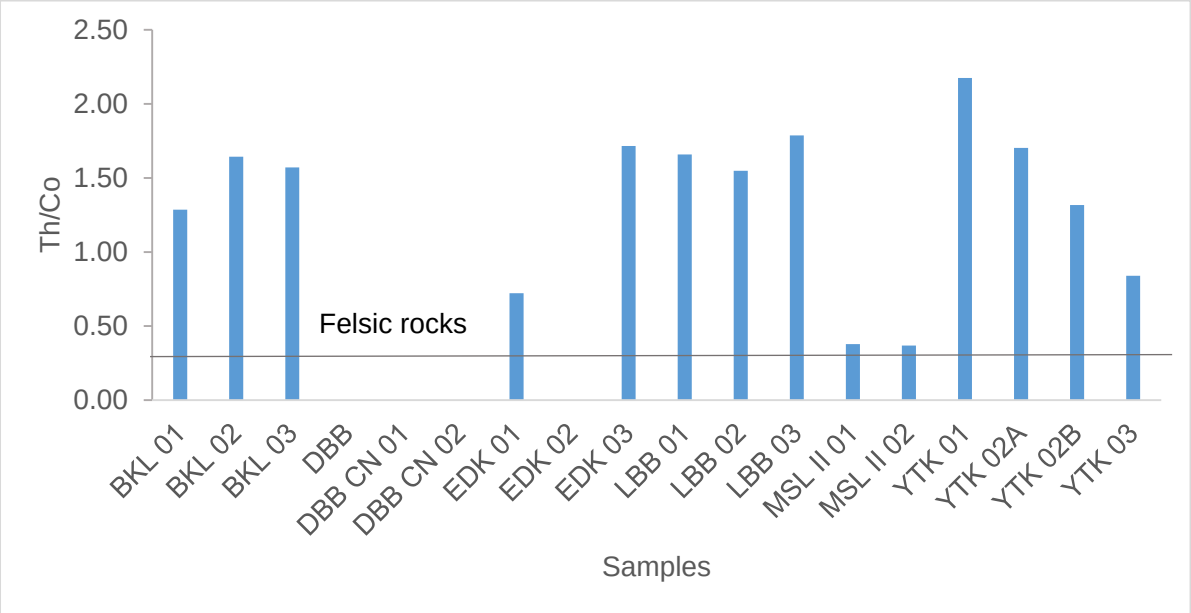

Figure 5.11: Plot of Th/Co of < 2 µm fraction samples showing the felsic source of the kaolins

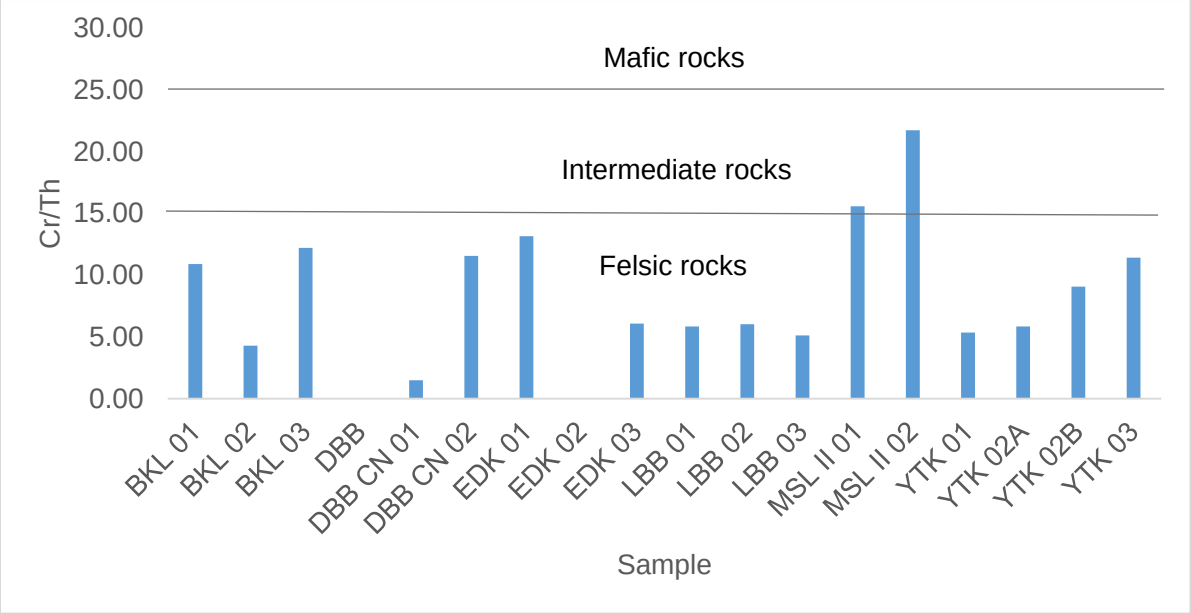

Figure 5.12: Plot of Cr/Th of < 2 µm fraction samples showing a felsic to intermediate source

Titanium and Ni are immobile elements that can be used to determine the composition of rocks and discriminate between a basic source and a felsic (acidic) source (Madukwe *et al*., 2016). Most samples plotted in the acidic field or close to the acidic field, suggesting that the kaolins have intermediate to acidic sources (Figures 5.13 and 5.14).

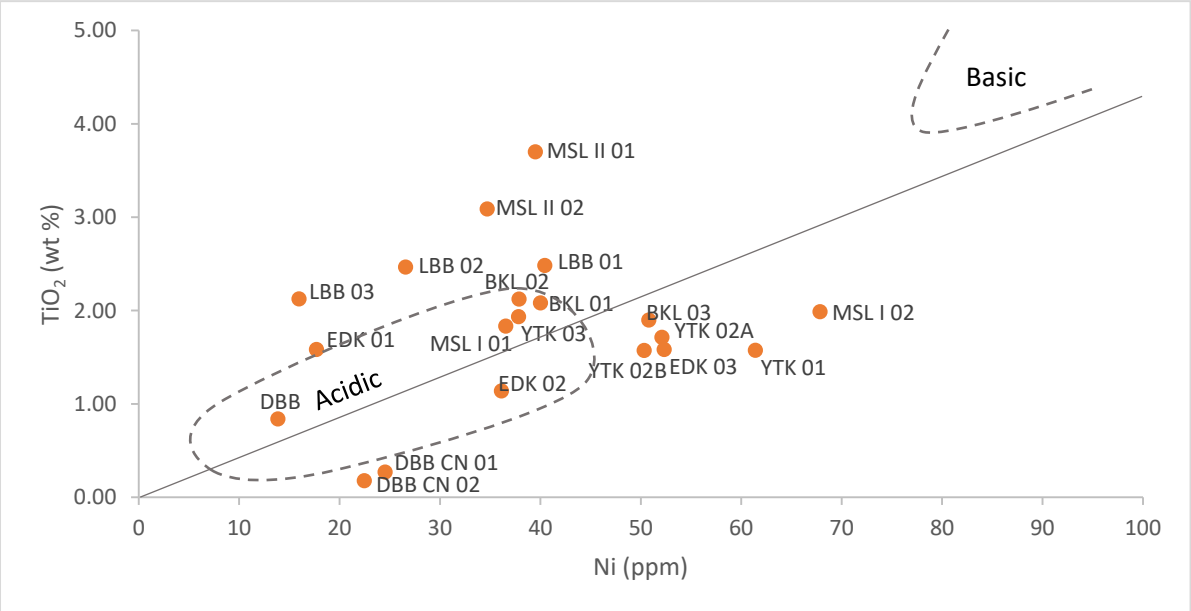

Figure 5.13: TiO_2 vs Ni plot showing intermediate to acidic source rocks of bulk samples

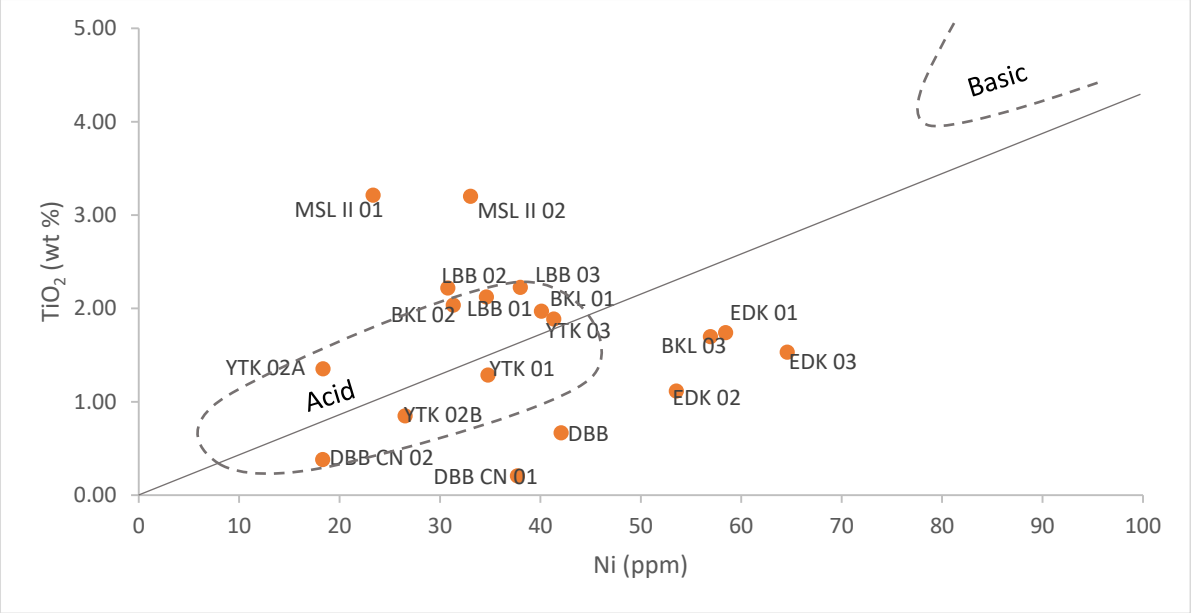

Figure 5.14: TiO_2 vs Ni plot showing intermediate to acidic source rocks in clay samples

High Cr (> 150 ppm) and Ni (> 100 ppm) concentrations, low Cr/Ni ratios (between 1.3 and 1.5) and a high correlation coefficient between Cr and Ni (> 0.90) are indicative of ultramafic rocks source; whereas a Cr/Ni ration > 2.0 indicates mafic-volcanic detritus (Garver *et al*., 1996). In this research, concentrations of Cr and Ni were very varied, even among samples in the same location. In general, samples had Ni concentrations < 100 ppm; Cr concentrations were > 150 ppm mainly in Missole. Moreover, there was a very weak positive correlation (r^2 = 0.09) between Cr and Ni. These show that the ultramafic or mafic source rock cannot be deduced from the Cr and Ni concentrations in this research; and, Cr and Ni input in Cretaceous-Tertiary kaolins in the Douala Sub-Basin might have been from different sources, other than ultramafic (mafic).

5.4.1.2 Hydraulic sorting and sediment recycling

The concentration of some trace elements, such as Zr and Th can be controlled by hydraulic sorting in sedimentary rocks (Nagarajan *et al*., 2015). McLennan *et al*. (1993) used the Th/Sc vs Zr/Sc bivariate plot to illustrate hydraulic sortng and sedimentary recycling. Thorium is incompatible but Sc is compatible in igneous systems (Lee, 2009). Hence, the Th/Sc ratio is a good proxy for igneous chemical differentiation processes. Unlike Zr which is strongly enriched in zircon, Sc is not enriched but generally preserves a signature of the provenance. The ratio Zr/Sc is a useful index of zircon enrichment (McLennan *et al*., 1993). Trend 1, in Figures 5.15 and 5.16, shows the normal igneous differentiation trend, which does not involve

zircon enrichment. An enrichment of zircon occurs during sedimentary sorting or recycling (Trend 2) (Nagarajan *et al*., 2015) (Figures 5.15 and 5.16).

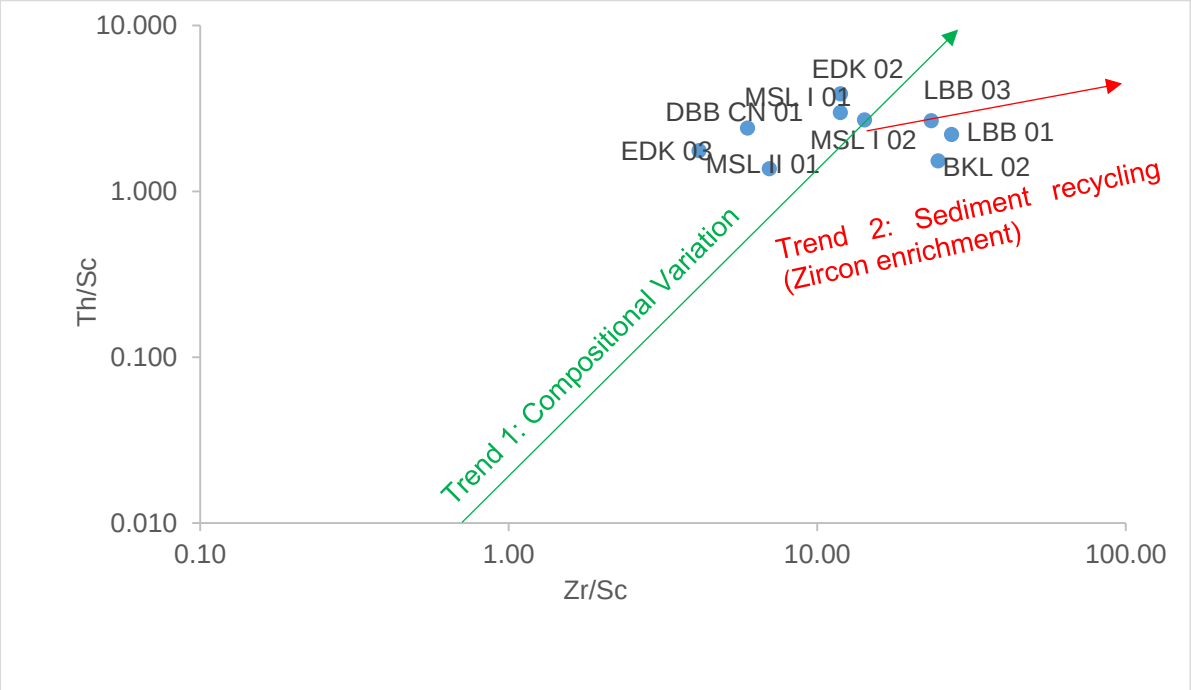

Figure 5.15: Th/Sc versus Zr/Sc plot showing sedimentary recycling in bulk samples

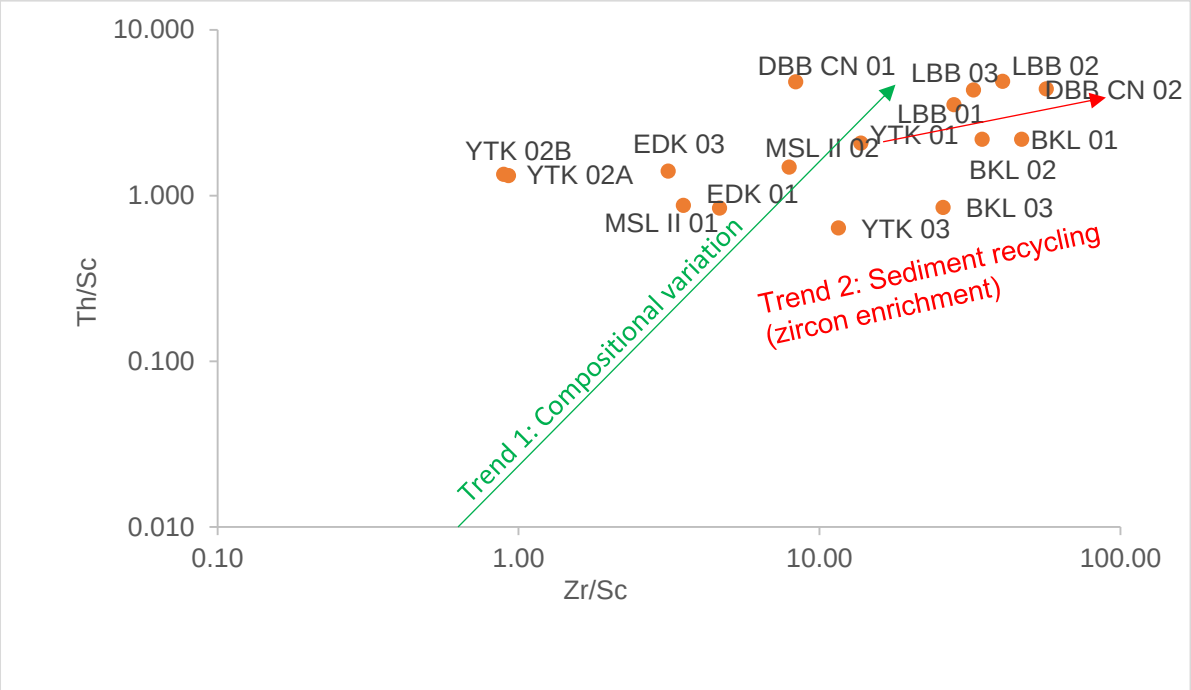

Figure 5.16: Th/Sc versus Zr/Sc plot showing sedimentary recycling in < 2 µm fraction samples

Thorium was below detection limit in most of the bulk samples. However, Logbaba kaolins aligned according to Trend 2, indicating sediment recycling and zircon enrichment. Other samples followed Trend 1. In < 2 µm fraction samples, Logbaba and Bomkoul kaolins portrayed sediment recycling. Two of Yatchika samples and one Dibamba sample also aligned according to Trend 2. Other samples showed compositional variations (Trend 1).

5.4.1.4 Paleo-redox conditions and environments of deposition

Some trace elements such as Ni, V, Cr and Co can be used to evaluate paleo-redox conditions during the time of formation of deposition of kaolins. Nickel and V are preferentially preserved under anoxic conditions; whereas, Cr and Co are believed to be related to the detrital fraction and they are not affected by redox conditions (Sari and Koca, 2012). Several studies used the Ni/Co, V/Cr and V/(V+Ni) to deduce the redox conditions during the deposition or formation of sediments (Rimmer, 2004; Sari and Koca, 2012; Kuscu *et al*., 2015; Tobia and Shangola, 2016). For example, the V/Cr ratio is suggested as a paleo-oxidation indicator, and high Ni/Co ratios are believed to be related to anoxic conditions (Rimmer, 2004).

Figures 5.17-5.20 show cross-plots of different paleo-redox indicators used in this research. The Ni/Co ratios in bulk samples showed that 75% of studied kaolins were formed (deposited) under oxic conditions, against 25% that were formed under suboxic to anoxic conditions (Figures 5.17-5.20). Whereas in the clay fractions, the Ni/Co ratios showed that all samples formed in oxic conditions, except BKL 03, which formed in dysoxic conditions. The V/Cr ratio in both bulk and clay samples showed that all the samples were formed under oxic conditions (Figures 5.17 and 5.18). The V/(V+Ni) ratios showed that most samples (bulk and clay) formed under anoxic conditions, and few (10% in bulk and 11.11% in clay samples) formed under euxenic conditions (Figure 5.19 and 5.20).

Samples that are suboxic or anoxic (Ni/Co proxy) or dysoxic to anoxic (V/(V+Ni) proxy) are mainly Cretaceous samples. This suggests that Cretaceous kaolins were deposited in an anoxic reducing environment; whereas Tertiary kaolins were deposited in an oxic or oxidising environment. This is in accordance with the low oxygen levels recorded in several Cretaceous stratigraphic units (Turgeon and Brumsack, 2006).

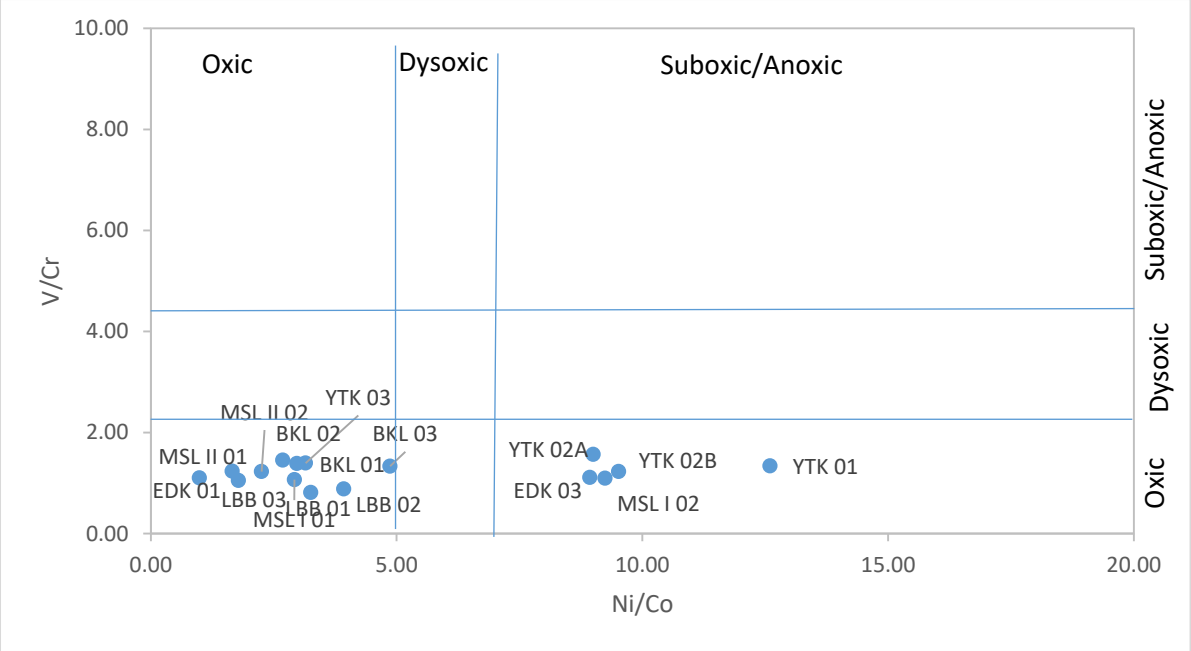

Figure 5.17: Cross-plot of V/Cr and Ni/Co used as paleo-redox indicators in bulk samples

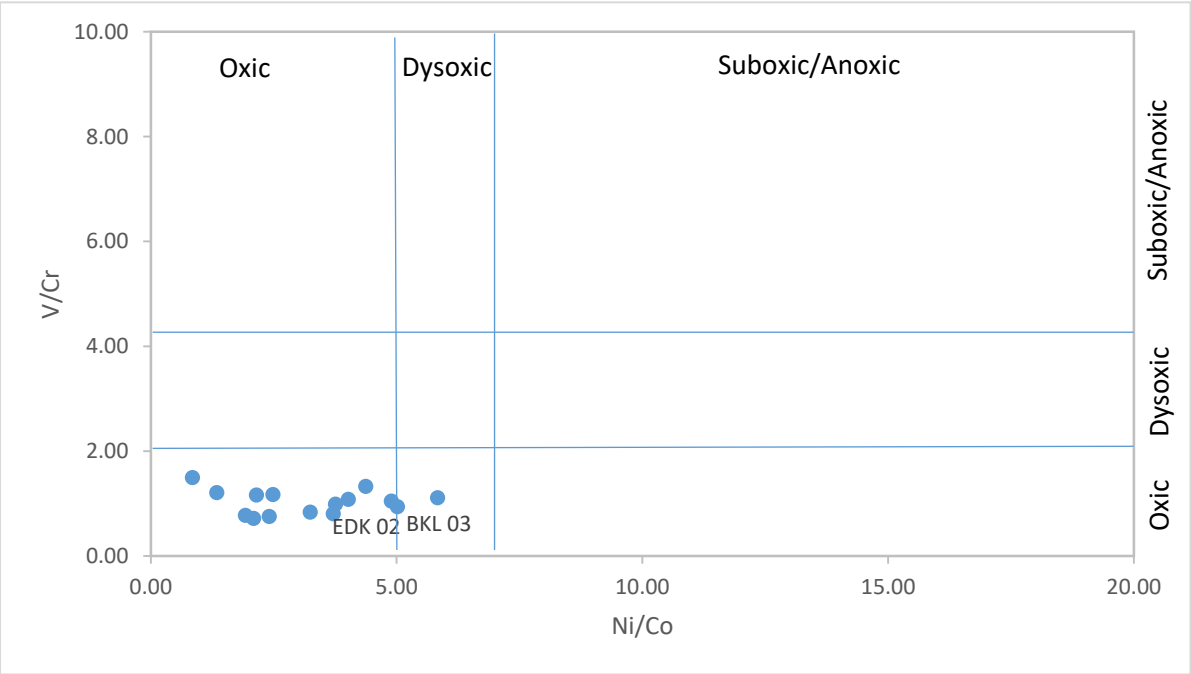

Figure 5.18: Cross-plot of V/Cr and Ni/Co used as paleo-redox indicators in < 2 µm fraction samples

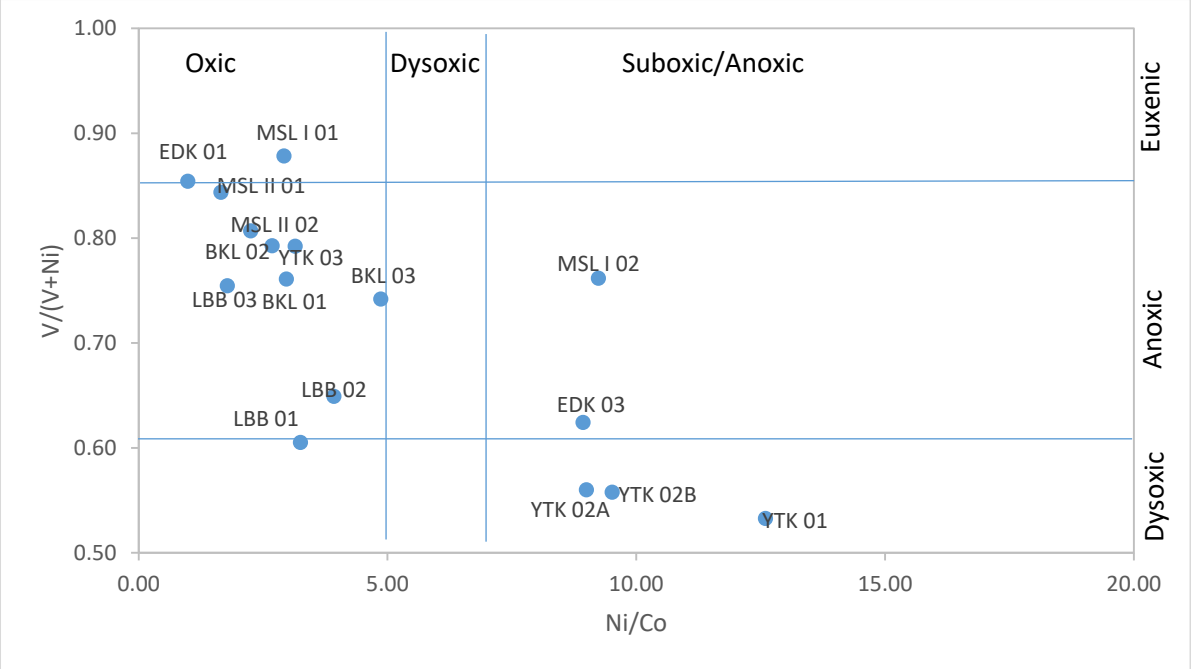

Figure 5.19: Cross-plot of V/(V+Ni) and Ni/Co used as paleo-redox proxies for bulk samples (Fields from Rimmer, 2004)

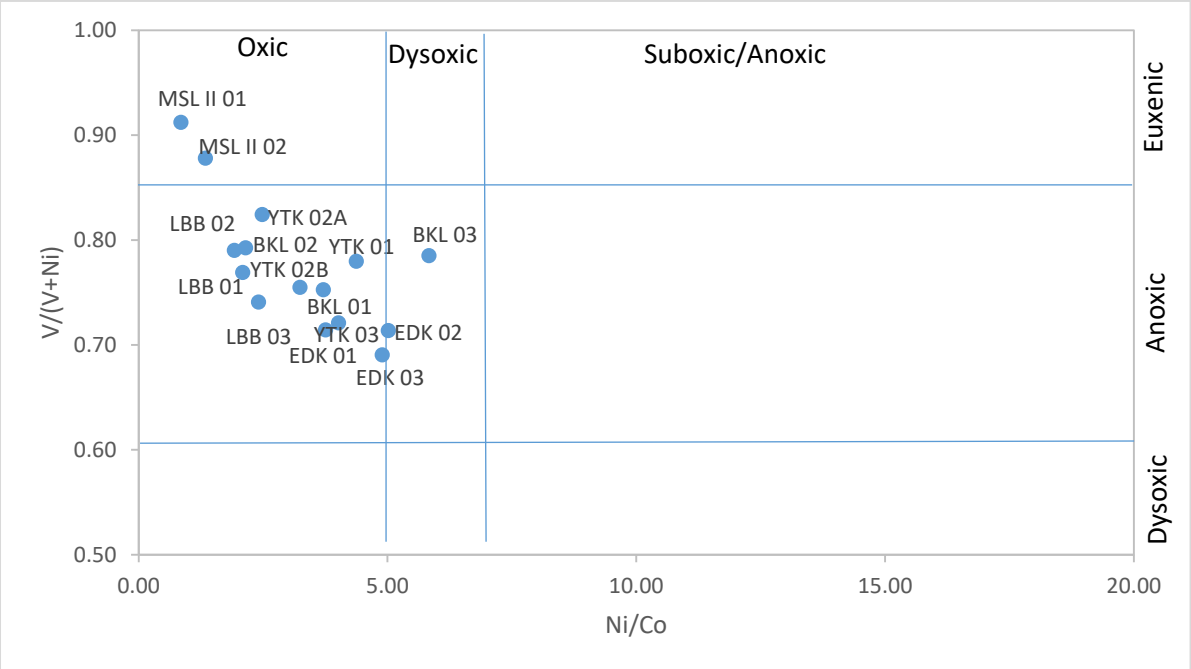

Figure 5.20: Cross-plot of V/(V+Ni) and Ni/Co used as paleo-redox proxies in clay samples (Fields from Rimmer, 2004)

5.4.2 Paleoenvironmental reconstruction based on stable isotope data

5.4.2.1 Assessing the influence of modern meteoric water

The studied kaolins are exposed occurrences, which might have been formed through interactions with modern local meteoric water. Knowing the present day mean isotopic composition of meteoric water in Douala, -3.09 and -10.22‰ for $\delta^{18}O_W$ and δD_W, respectively (Wirmvem *et al*., 2016) and present day mean annual temperature (26.95°C) (IAEA/WMO, 2017), it is possible to evaluate the influence of modern local meteoric water on the kaolinisation of Cretaceous-Tertiary sediments in the Douala Sub-Basin. This could be done by computing the isotopic composition of Cretaceous-Tertiary kaolins in the Douala Sub-Basin in two ways (dos Santos *et al*., 2007):

By determining the isotopic composition of kaolinite using the mean isotopic composition of modern meteoric water in Douala, and equilibrium fractionation factors between kaolinite and water as in Equations 5.5 and 5.6 by Savin and Epstein (1970):

$$\alpha_{K-W}^{O} = \frac{\delta^{18}O_K + 1000}{\delta^{18}O_W + 1000} \quad \text{(Eqn 5.5)}$$

$$\alpha_{K-W}^{D} = \frac{\delta D_K + 1000}{\delta D_W + 1000} \quad \text{(Eqn 5.6)}$$

Where, α_{K-W}^{O} and α_{K-W}^{D} are equilibrium fractionation factors between kaolinite and water (meteoric water) with respect to oxygen and hydrogen, respectively; and they have values of 1.027 and 0.97, respectively (Lawrence and Taylor, 1971).

Hence, kaolinites in equilibrium with modern meteoric water should have an isotopic composition of 23.83 and -39.91‰ for $\delta^{18}O_K$ and δD_K, respectively. However, these values are much heavier than those obtained for Cretaceous-Tertiary kaolins in the present research, and it implies that Cretaceous-Tertiary kaolins of the Douala Sub-Basin are not in equilibrium with modern meteoric water.

By determining the isotopic composition of kaolinite using the modern mean annual temperature (26.95°C in 2015) (IAEA/WMO, 2017), as in Equations 5.7 and 5.8 (Gilg and Sheppard, 1996; Sheppard and Gilg,1996):

Hydrogen: $1000 \ln \alpha_{kaolinite-water} = -2.2x10^6 x\, T^{-2} - 7.7$ (Eqn. 5.7)

Oxygen: $1000 \ln \alpha_{kaolinite-water} = 2.76x10^6 x\, T^{-2} - 6.75$ (Eqn. 5.8)

Where, T is the temperature (°K) and $\alpha_{kaolinite-water}$ is the equilibrium isotopic fractionation factors between kaolinite and water.

Hence, kaolinites that formed under modern mean annual temperature should have an isotopic composition of 20.84 and -39.91‰ for $\delta^{18}O_K$ and δD_K, respectively.

The δD_K value is the same using both methods; whereas, $\delta^{18}O_K$ values are close. Though DBB has a slightly heavier $\delta^{18}O_K$, Cretaceous-Tertiary kaolins have lighter $\delta^{18}O_K$ and δD_K than computed modern kaolins. Thus, it can be concluded that Cretaceous-Tertiary kaolins of the Douala Sub-Basin are not in equilibrium with modern meteoric water.

5.4.2.2 Temperature of kaolinisation

The stable isotope composition of kaolins, as well as other clay minerals, is a function of the isotopic composition of the water from which they formed. The equilibrium isotopic fractionation factors between kaolinite and water were developed by Gilg and Sheppard (1996) and Sheppard and Gilg (1996) (Equations 5.7 and 5.8). These fractionation factors are a function of the temperature of kaolinisation; therefore, the isotopic composition of kaolinite can provide information about its genesis (Fernandez-Caliani *et al*., 2010).

Delgado and Reyes (1996) developed an equation of the formation temperature of smectite, based on the assumption of plausible formation in an open system with high water (meteoric water) – rock (clay mineral) ratios and near-surface temperatures. This equation was extrapolated for a kaolinite-water system by Clauer *et al*. (2015), using Equations 5.2, 5.7 and 5.8. The derived equation of the temperature of water from which kaolinite formed is as follows:

$$3.04x10^6T^{-2} = \delta O_k - 0.125\delta D_k + 7.04 \qquad \text{(Eqn. 5.9)}$$

Temperatures of kaolinisation (T_G) of studied kaolins were computed and presented in Table 5.2. Kaolins found in Cretaceous Formations had a mean T_G of 21.83°C ± 2.19°C; whereas those found in Tertiary Formations had a mean T_G of 27.09°C ± 6.17°C. These temperatures suggest that kaolins hosted in Cretaceous Formations formed at temperatures about 5°C cooler than those found in Tertiary Formations; and both Cretaceous and Tertiary temperatures are humid temperatures, favouring the formation of kaolins.

The local meteoric water line of Douala was developed for the years 2013 and 2014 by Wirmvem *et al*. (2016) (Equation 5.1). Using the same method and based on the same assumptions as in Delgado and Reyes (1996) and Clauer *et al*. (2015), the temperature of kaolinisation in equilibrium with the local meteoric water line of Douala is derived as follows:

$$3.04x10^6T^{-2} = \delta O_k - 0.126\delta D_k + 7.42 \qquad \text{(Eqn. 5.10)}$$

Hence, the temperatures of kaolinisation (T_L) of studied kaolins in equilibrium with the local meteoric water line were computed and presented in Table 5.2. The T_L values were slightly lower than T_G values, with Cretaceous kaolins having a mean of 19.97°C ± 2.14°C; and Tertiary kaolins having a mean of 25.16°C ± 6.07°C. These values also show that kaolins hosted in Cretaceous Formations formed at temperatures about 5°C cooler than those found in Tertiary Formations. Moreover, in both cases (kaolinites in equilibrium with the global meteoric water line or with the local meteoric water line), kaolinisation temperatures in Tertiary kaolins (the warmest) are slightly higher than present day mean annual temperatures in Douala (26.95°C) (IAEA/WMO, 2017).

Table 5.2: Kaolinisation temperatures T_G and T_L of analysed samples

		$d^{18}O$	dD	T_G(°C)	T_L(°C)
Tertiary	BKL01	15.28	-67.93	40.98*	38.72
	BKL02	18.21	-68.75	26.56	24.59
	DBB	20.98	-57.35	20.77	18.96
	DBB CN02	20.53	-59.85	21.37	19.54
	MSL II 01	18.68	-53.16	33.32	31.28
	MSL II 02	18.73	-52.59	33.45	31.42
	Mean			27.09	25.16
	Standard Deviation			6.17	6.07
Cretaceous	EDK02	16.92	-47.74	45.57*	43.31
	LBB 03	20.28	-64.00	20.23	18.40
	LBB01	20.13	-62.58	21.61	19.77
	YTK01	18.64	-68.20	24.99	23.06
	YTK03	20.25	-63.78	20.48	18.65
	Mean			21.83	19.97
	Standard Deviation			2.19	2.14

Values with an * were not taken into consideration while calculating the means and standard deviations

5.4.2.3 Stable isotope composition of the meteoric water in equilibrium with Cretaceous-Tertiary kaolinites in the Douala Sub-Basin and equilibrium fractionation factors

The positioning of the Ediki sample (EDK 02) in the hypogene field could be interpreted as being formed in isotopic equilibrium with its parental fluid, without subsequent isotopic exchange with meteoric water (Clauer *et al*., 2015). However, Lawrence and Meaux (1993)

argued that the high salinity of formation fluids might not favour the formation of kaolinite. In the regional stratigraphy of Ediki, the sandstones and clays are overlain by Tertiary undifferentiated basalts from Mount Cameroon (Diko and Ekosse, 2012). But the studied kaolin occurrence is exposed to the surface. Therefore, it is believed that the Ediki kaolins might have been buried at some point in geologic time, during which they might have interacted with low temperature hydrothermal fluids; and later, they might have been exposed due to uplift in the area.

One of the Bomkoul samples (BKL 01) had the lowest $\delta^{18}O$. It is believed that at this location, the kaolin might have had isotopic exchange with surface water depleted in oxygen, causing the low $\delta^{18}O$ in this sample. Hence, the values of BKL 01 and EDK 02 were not taken into consideration in the calculation of the isotopic composition of ancient meteoric waters.

Mean temperatures of kaolinisation determined using the GMWL and LMWL were used to determine the mean stable isotope composition of the meteoric water in equilibrium with Tertiary kaolins (300.24^{o}K and 298.39^{o}K) and Cretaceous kaolins (294.98^{o}K and 293.12^{o}K), using Equations 5.5-5.8. The results are shown in Table 5.3. Using the GMWL equation, the mean isotopic composition of the meteoric water in equilibrium with Cretaceous kaolins is -5.15 and -31.67‰, for $\delta^{18}O_W$ and δD_W, respectively; whereas its mean isotopic composition when in equilibrium with Tertiary kaolins is -4.44 and -26.24‰, for $\delta^{18}O_W$ and δD_W, respectively (Table 5.3 and Figure 5.21). This shows that the meteoric water is becoming enriched (heavier) in $\delta^{18}O_W$ and δD_W when moving from Cretaceous to Recent, with present day mean values of -3.09 and -10.22‰ for $\delta^{18}O_W$ and δD_W, respectively (Wirmvem *et al*., 2016).

Table 5.3: Mean isotopic composition of meteoric water in equilibrium with Cretaceous and Tertiary kaolins and kaolinite-water fractionation factors

		$\delta^{18}O_K$	δD_K	T (^{o}K)	$\delta^{18}O_W$	δD_W	$\alpha_{K\text{-}W}$ ^{18}O	$\alpha_{K\text{-}W}$ D
Present day compositions		20.84	-39.91	300.10	-3.09	-10.22	1.024	0.97
GMWL	Tertiary	19.43	-58.34	300.24	-4.44	-26.24	1.024	0.97
	Cretaceous	19.82	-64.64	294.98	-5.15	-31.67	1.025	0.97
LMWL	Tertiary	19.43	-58.34	298.39	-4.82	-25.93	1.024	0.97
	Cretaceous	19.82	-64.64	293.12	-5.55	-31.33	1.026	0.97

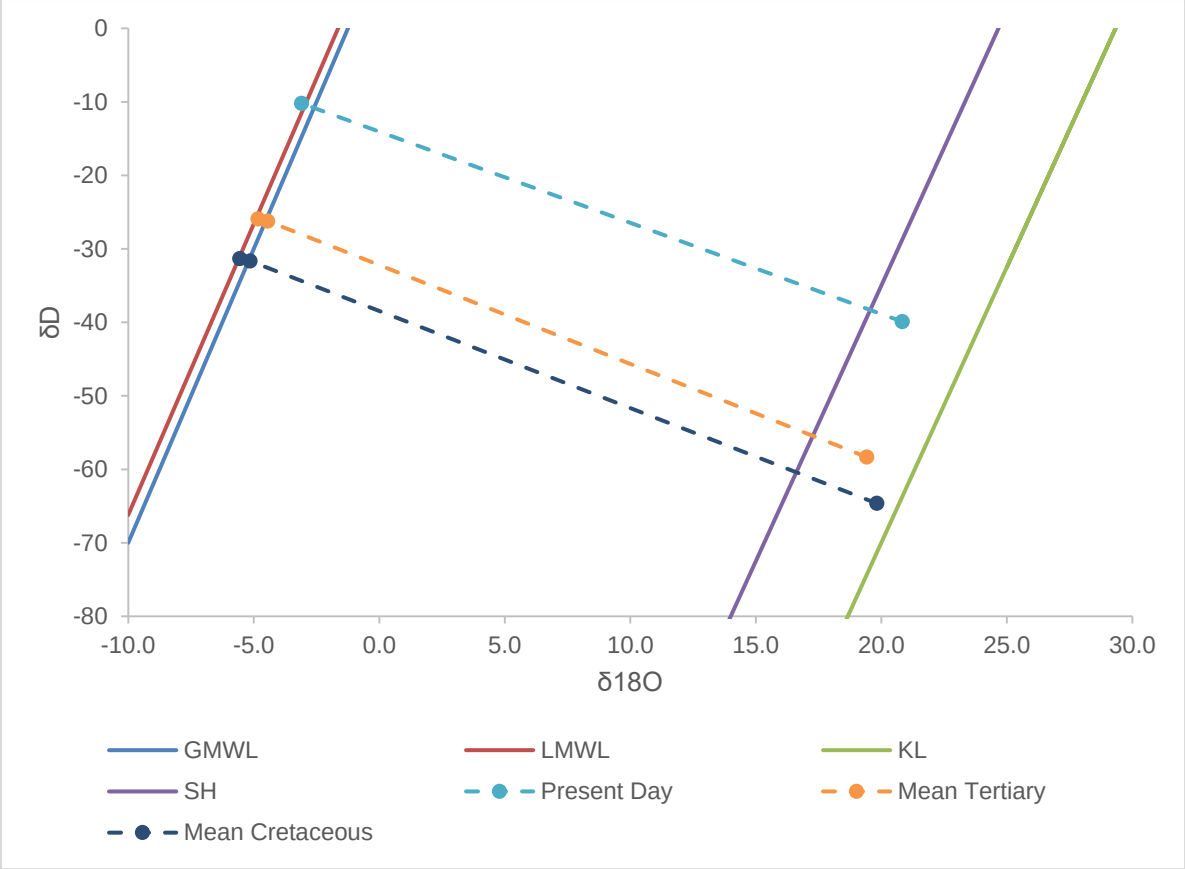

Figure 5.21: Plot showing the mean isotopic composition of meteoric water in equilibrium with Cretaceous and Tertiary kaolins

Using the LMWL equation, the mean isotopic composition of Tertiary meteoric waters (in equilibrium with Tertiary kaolins) is -4.82 and -25.93‰, for $\delta^{18}O_W$ and δD_W, respectively; whereas the mean isotopic composition of Cretaceous meteoric waters (in equilibrium with Cretaceous kaolins) is -5.55 and -31.33‰, for $\delta^{18}O_W$ and δD_W, respectively (Table 5.3 and Figure 5.21). These results, as well as the temperature of kaolinisation, are slightly lower than results obtained when using the GMWL equation.

However, the equilibrium fractionation factor of δD between kaolinite and water ($\alpha_{K\text{-}W}D$) using the GMWL or the LMWL has remained constant from Cretaceous to present ($\alpha_{K\text{-}W}D = 0.97$). Whereas, the equilibrium fractionation factor of ^{18}O between kaolinite and water ($\alpha_{K\text{-}W}\,^{18}O$) has decreased from 1.025 or 1.026, during the Cretaceous, to 1.024 since the Tertiary.

5.4.2.4 Paleoenvironmental reconstruction

The isotopic composition of Cretaceous-Tertiary kaolins in the Douala Sub-Basin indicates that they are of weathering origin; therefore, they were formed in a supergene environment. As indicated by Bird and Chivas (1988), kaolins in a supergene environment generally have $\delta^{18}O$ values between 17 and 23‰, and δD values between -80 and -40‰. This is sustained by the isotopic compositions of other kaolins formed by weathering, amongst which, the Cretaceous-Tertiary Georgia kaolins in the USA (Hassapinak and Elsinger, 1985), the Tertiary Lastarria kaolins (Gilg *et al*., 1999), the Cretaceous-Tertiary Rio Capim semi-flint kaolins in Brazil (Santos *et al*., 2007), the Permian Variscan kaolins in Spain (Fernandez-Caliani *et al*., 2010; Clauer *et al*., 2015), the Cambrian Burela kaolin deposit in Spain (Galan *et al*., 2016) and the Cretaceous-Tertiary Patagonia kaolins in Argentina (Dominguez *et al*., 2016).

Since kaolinite mostly preserves its original $\delta^{18}O$ compositions, isotopic exchange after deposition is unlikely (Boulvais, 2000). However, the little oxygen isotopic exchange between kaolinite and water reported by several authors was exhibited in the studied kaolins from Cretaceous (19.4‰) to present (20.8‰). An increase in $\delta^{18}O$ values with time was also observed in Australian kaolinites (Bird and Chivas, 1989). In the present research, this increase corresponds to an interaction of the kaolins with isotopically heavier meteoric waters with time, which is due to the upward migration of Cameroon towards the Equator since the Cretaceous (Figures 5.22-5.23).

Conversely, hydrogen isotopic exchange between kaolinite and water occurs more at more rapidly and is responsible for the displacement of samples from the kaolinite line (Bird and Chivas, 1989). Cretaceous-Tertiary kaolins in the Douala Sub-Basin become heavier from Meteoric water in the study area is shown to become heavier when moving from Cretaceous to present. Therefore, the samples have been undergoing continual low-temperature isotopic exchange with meteoric waters of successively heavier isotopic compositions since their formation. This is a contrary trend from to values of Bavaria kaolins obtained by Gilg (2000).

Subsequently, kaolinisation temperatures of Cretaceous-Tertiary kaolins in the Douala Sub-Basin (< 45^{o}C) reflect supergene environments, with Tertiary temperatures being higher than Cretaceous temperatures. This suggests a cooler climate during the Cretaceous than the Tertiary. An increase in precipitation usually corresponds to an increase in δD, either in kaolinite or its corresponding meteoric water (Sheppard and Gilg, 1996). Therefore, the increasing mean δD values of kaolins in the Douala Sub-Basin means there has been an increase in precipitation in the study area since the Cretaceous, favouring the formation of kaolins.

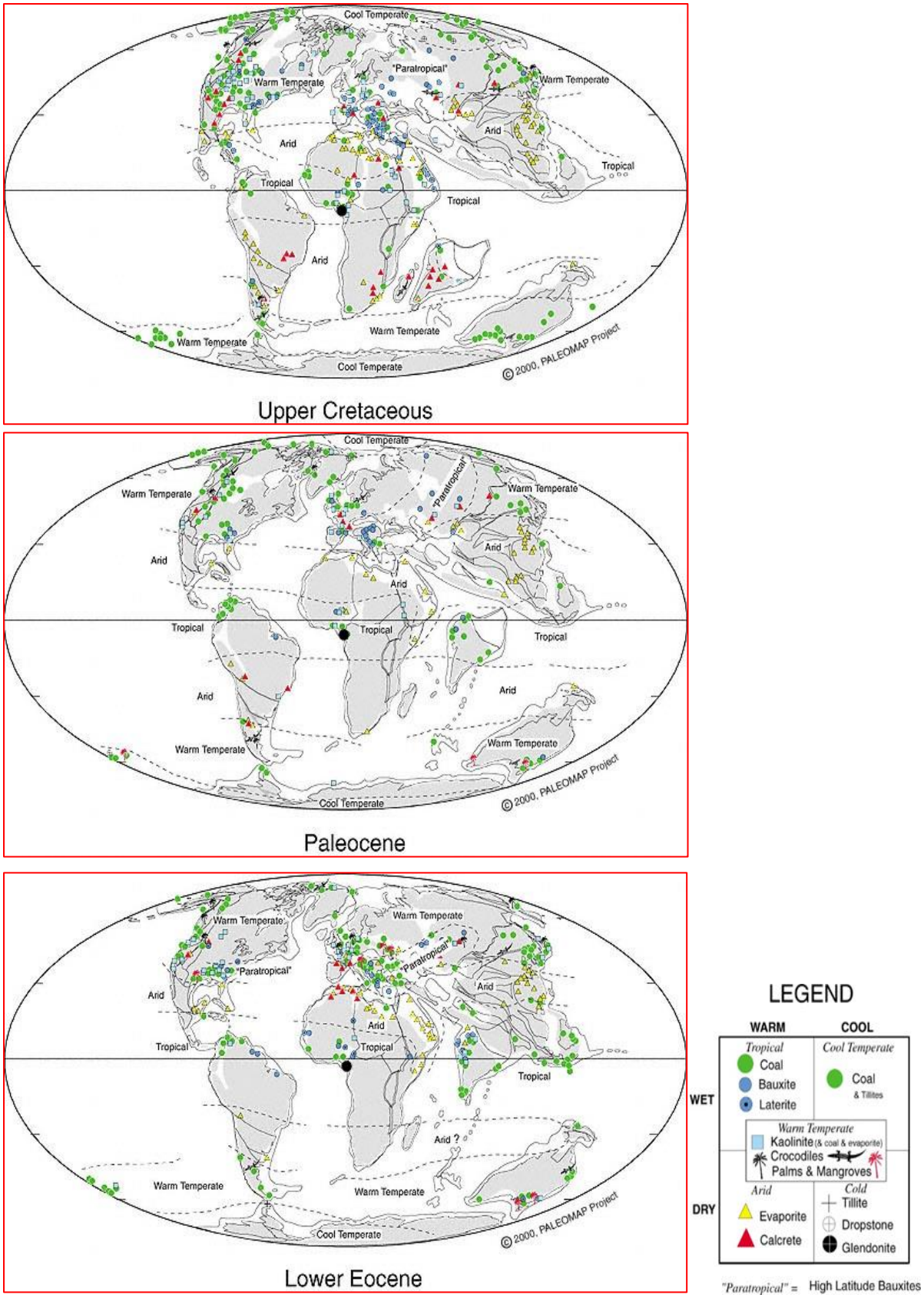

Figure 5.22: Paleoclimate maps from Upper Cretaceous to Lower Eocene (Scotese, 2001)

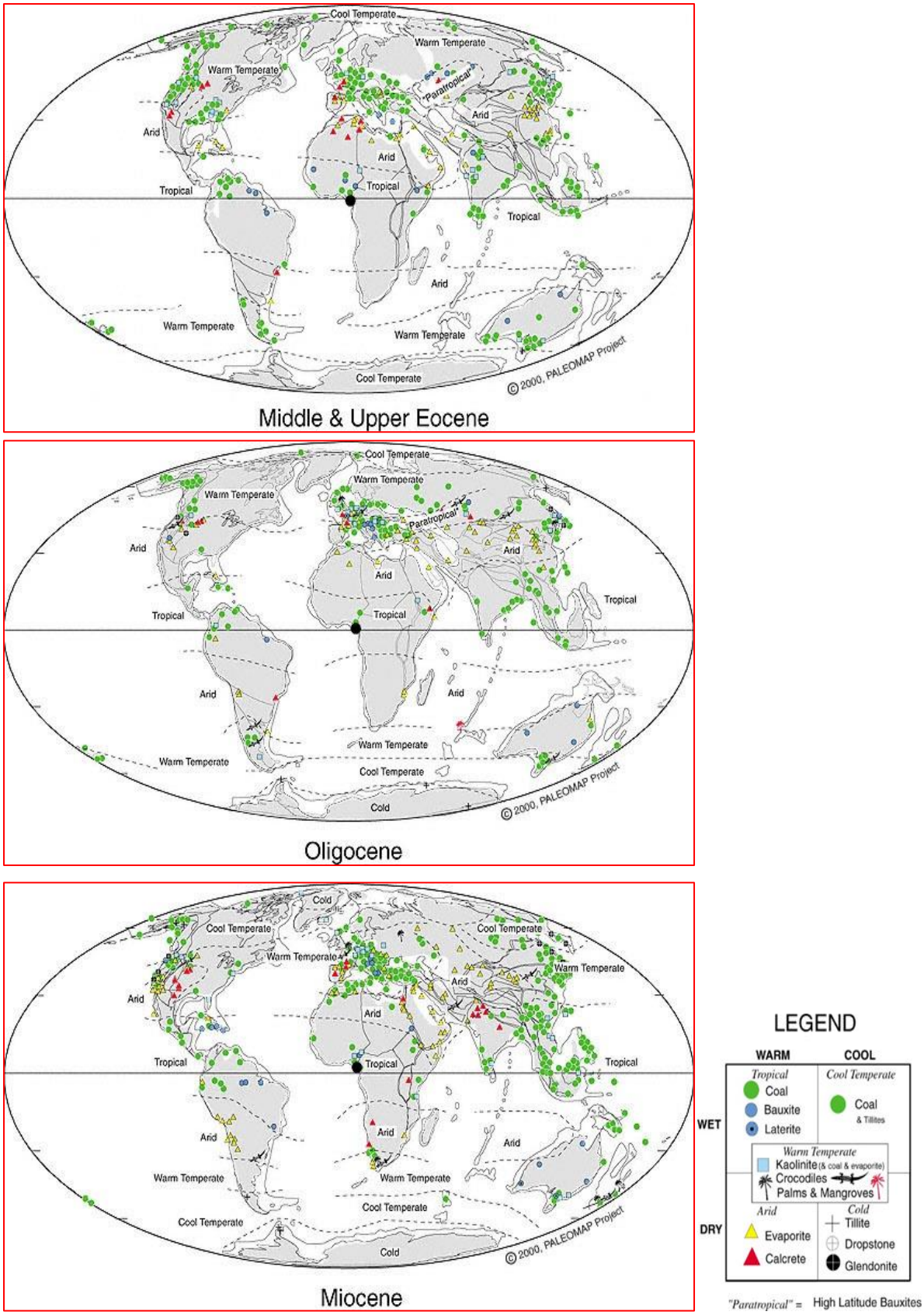

Figure 5.23: Paleoclimate maps from Middle and Upper Eocene to Miocene (Scotese, 2001)

The Douala Sub-Basin is found in the Equatorial domain, which has precipitations ranging between 1 500 to 2 000 mm, and mean temperatures around 25 °C (Pamo, 2008). In west and Central Africa, this Equatorial domain has a humid tropical climate, due to their low-altitudes (Tardy *et al*., 1991). Regarding temperatures, Tardy *et al*. (1991) argued that West and Central Africa have higher temperatures at the Equator (> 5-6^{o}C) and at the Tropics (> 20^{o}C) than the same latitudes in South America (Brazil) and East Africa. Hence, when moving northwards from the Equator to the Tropic of Cancer, temperatures increase; whereas when moving southwards from the Equator to the Tropic of Capricorn, temperatures decrease (Tardy *et al*., 1991).

Using the paleolatitude calculator for paleoclimatic studies developed by van Hinsbergen *et al*., (2015) and the reference frame for paleoclimate studies by Torsvik and Van der Voo (2002) on www.paleolatitude.org, the paleolatitude of the Douala Sub-Basin has been moving northwards, towards the Tropic of Cancer from Cretaceous to Present (Figure 5.24). According to the argument of Tardy *et al*. (1991), the climate in the Douala Sub-Basin has been becoming warmer from Cretaceous to present. Results obtained in this research converge towards this conclusion, showing that the Cretaceous had cooler temperatures than the Tertiary in the Douala Sub-Basin (19.97^{o}C ± 2.14^{o}C and 25.16^{o}C ± 6.07^{o}C, respectively); with mean annual temperatures between 2006 and 2015 being 27.08 ^{o}C ± 0.35.

Though warm temperatures are required for kaolin formation, precipitation and leaching are the main factors influencing the formation of kaolins (Bird and Chivas, 1988). According to the rainfall patterns during the Mesozoic to Cenozoic derived by Parrish *et al*. (1982), Douala and its environs fall in the high rainfall domain since the Cretaceous. However, the wettest months (June-October) also correspond to the coolest months. Therefore, the formation of Cretaceous-Tertiary kaolins in the Douala Sub-Basin was more influenced by high precipitation than high temperatures; and seasonal characteristics show that these kaolins were formed in a humid tropical climate. it implies that Douala had a humid climate during the Cretaceous, and the climate is gradually becoming hotter as concluded by Tardy *et al*. (1991), regarding the climate in West and Central Africa; but more humid.

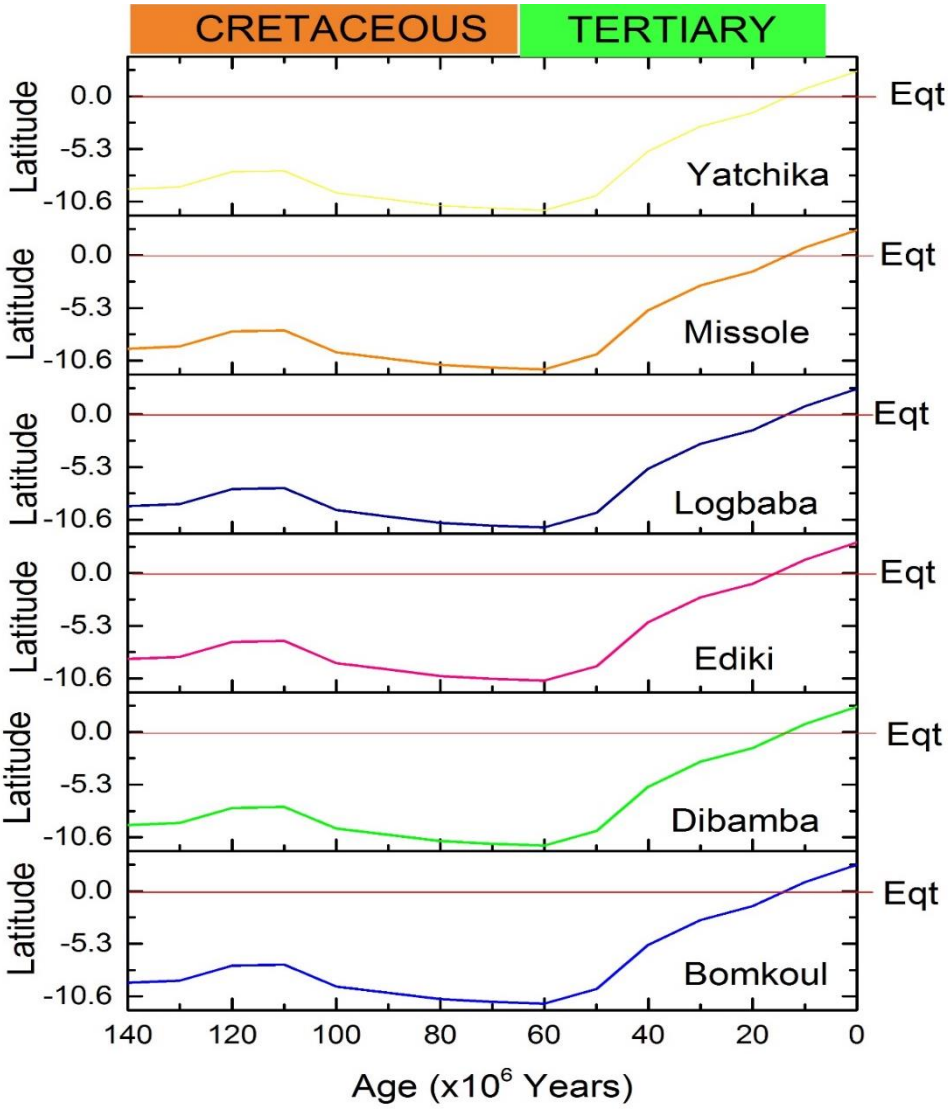

Figure 5.24: Paleolatitudinal evolution of the Douala Sub-Basin from Cretaceous to Present (van Hinsbergen *et al*., 2015). Eqt = Equator.

5.5 Synopsis

Trace elements geochemistry and stable isotopes of Cretaceous-Tertiary kaolins in Douala Sub-Basin were studied to determine their genesis and paleoenvironmental conditions during the time of kaolinisation. The trace elements geochemistry revealed the following:

- Cretaceous-Tertiary kaolins in the Douala Sub-Basin are mainly enriched in REEs compared to the upper continental crust, and they all have a negative Eu anomaly. Large ion lithophiles (mainly Rb and U) were highly enriched in samples, HFSEs (Y and Nb) were enriched in studied samples of all fractions; and TTEs generally had concentrations quite similar to UCC values.

- Studied kaolins are mainly derived from felsic or acidic rocks.
- Bomkoul, Dibamba and Logbaba samples generally showed enrichment in Zr, due to sediment sorting or recycling; unlike Ediki, Missole and Yatchika samples, which had a normal igneous differentiation trend.
- Cretaceous kaolins were deposited in an anoxic reducing environment; whereas Tertiary kaolins were deposited in an oxic or oxidising environment.

Stable isotopes geochemistry revealed the following:

- Cretaceous-Tertiary kaolins in Douala Sub-Basin were formed in a weathering (supergene) environment.
- The temperatures of kaolinitisation (assuming equilibrium with the global meteoric water line) are 21.83^{o}C ± 2.19^{o}C for Cretaceous kaolins and 27.09^{o}C ± 6.17^{o}C for Tertiary kaolins. Assuming equilibrium with the local (Douala) meteoric water line, the temperatures of kaolinitisation were 19.97^{o}C ± 2.14^{o}C for Cretaceous and 25.16^{o}C ± 6.07^{o}C for Tertiary kaolins.
- The mean isotopic composition of the meteoric water in equilibrium with Tertiary kaolins (300.24^{o}K and 298.39^{o}K) and Cretaceous kaolins (294.98^{o}K and 293.12^{o}K), using the GWML, is -5.15 and -31.67‰, for $\delta^{18}O_W$ and δD_W, respectively during the Cretaceous and -4.44 and -26.24‰, for $\delta^{18}O_W$ and δD_W, respectively during the Tertiary. Whereas present day mean isotopic composition of meteoric water in Douala is -3.09 and -10.22‰ for $\delta^{18}O_W$ and δD_W, respectively. This suggests that the meteoric water in Douala is becoming enriched (heavier) in $\delta^{18}O_W$ and δD_W when moving from Cretaceous to present.
- Douala had a cooler and rainy climate during the Cretaceous, and the climate is gradually becoming hotter but more humid.

Validation of hypothesis: The studied Cretaceous-Tertiary kaolin deposits formed in different paleoredox conditions but in similar paleoclimatic conditions.

CHAPTER 6

RADIOGENIC DATING OF CRETACEOUS-TERTIARY KAOLINS

6.1 Preamble

The objective of this chapter was to carry out radiogenic dating of zircons in Cretaceous-Tertiary kaolins in order to constrain their time of kaolinisation (Specific Objective C). It involved dating detrital zircons using U-Pb LA-SFICP-MS, determining the different zircon populations present in each sample, determining the maximum deposition age of the kaolins, and inferring the possible sources of these kaolins. This chapter is based on an identified hypothesis (Hypothesis C).

HYPOTHESIS C: Kaolinisation in Cretaceous-Tertiary Formations of the Douala Sub-Basin occurred during Cretaceous and Tertiary Periods.

6.2 Description of zircon grains (shape and texture)

Backscattered images of zircons in each kaolin are shown in Appendices 6.1-6.6. The description of textures is based on Corfu *et al.* (2003).

6.2.1 Zircons in Bomkoul kaolin

The size of zircon grains in Bomkoul kaolin varies between 90 and 300 µm. The shapes of the grains could be grouped into needle-like, oval to rounded, short to intermediate subhedral to subrounded and euhedral. Of these four shapes, two main shapes dominate: the oval to rounded and the short to intermediate subhedral to subrounded, suggesting that these grains might have travelled a long distance. As texture, growth or oscillatory zonings are dominant, with small rims. Few homogeneous unzoned grains and xenocryst cores were also present. Figure 6.1 shows cathodoluminescence images of representative zircons in Bomkoul kaolins and indicates the different shapes and textures present.

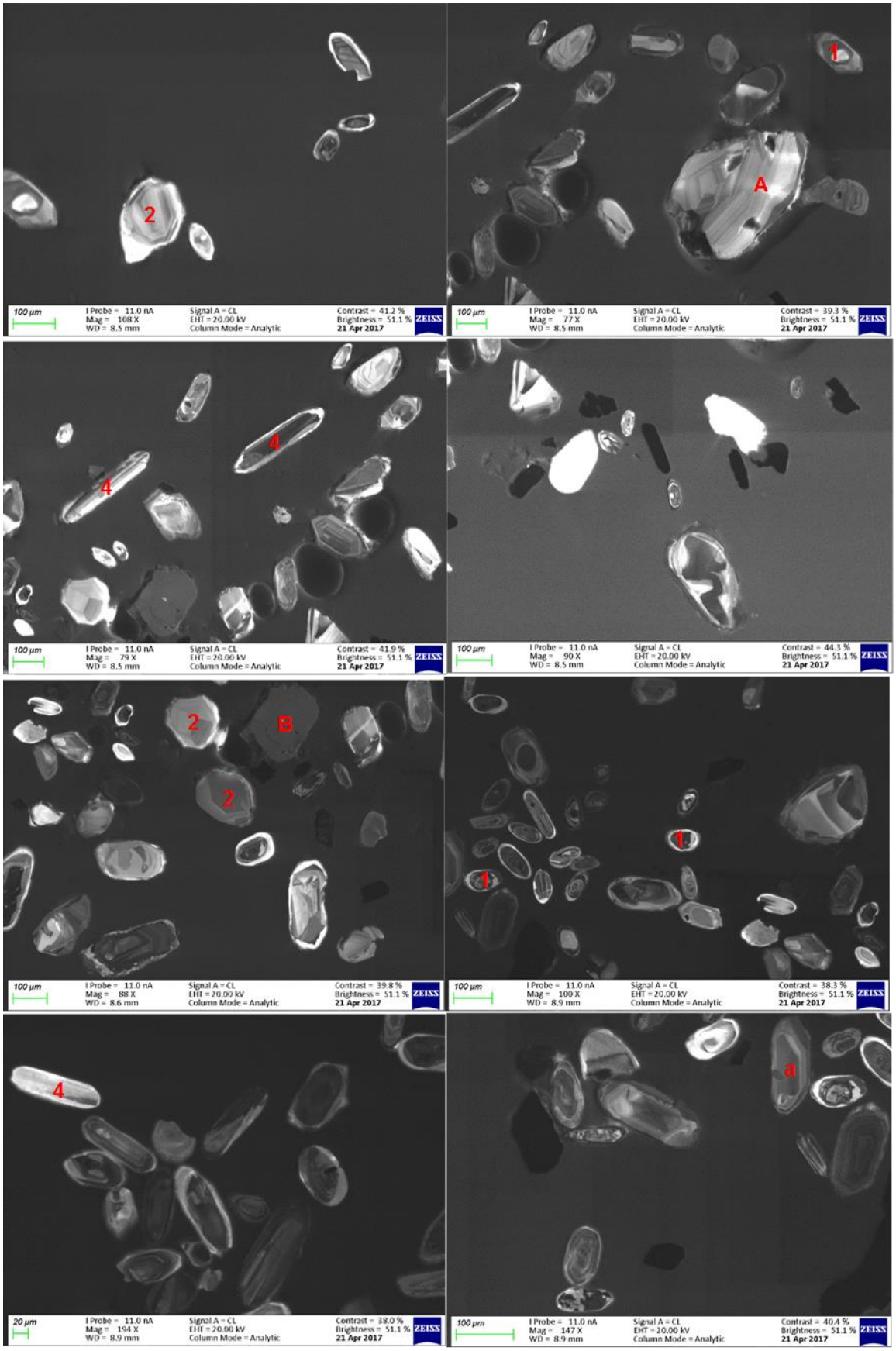

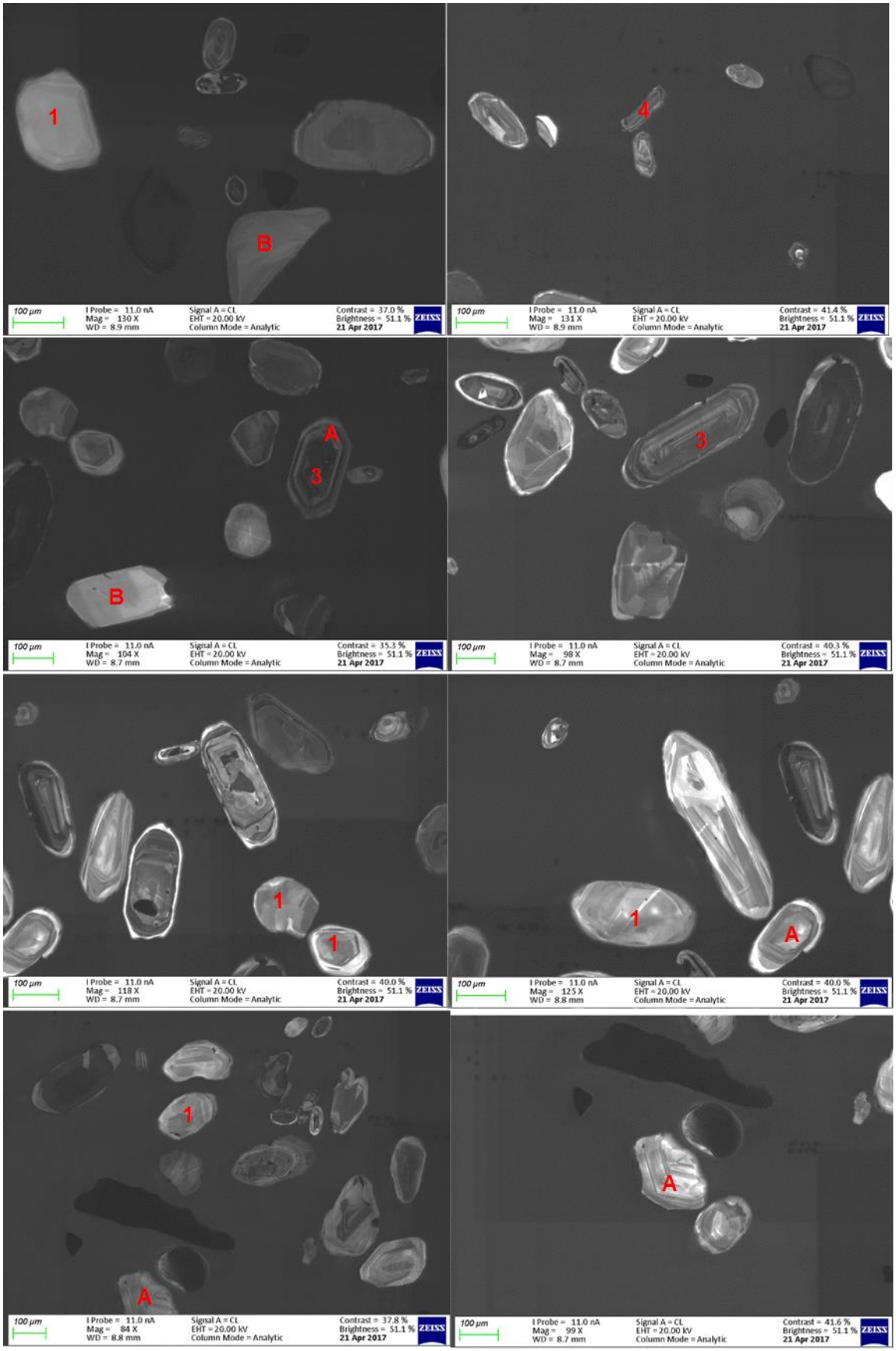

Figure 6.1: Cathodoluminescence images of zircons in Bomkoul kaolin: 1) Short to intermediate subhedral to subrounded grains, 2) Oval to rounded grains, 3) Euhedral grains, 4) Needle-like grains and A) Growth or oscillatory zoning, B) Homogeneous unzoned grains

6.2.2 Zircons in Dibamba kaolin

Dibamba zircons are 80 to ~200 µm in size (Figure 6.2). The grains are mainly short to intermediate subhedral to subrounded in shape, but they also have an oval to rounded shape and few a needle-like. Oscillatory and sector zoning are predominant, few xenocryst cores are observed, having a different colour from the rims (lighter or darker), depending on the uranium content.

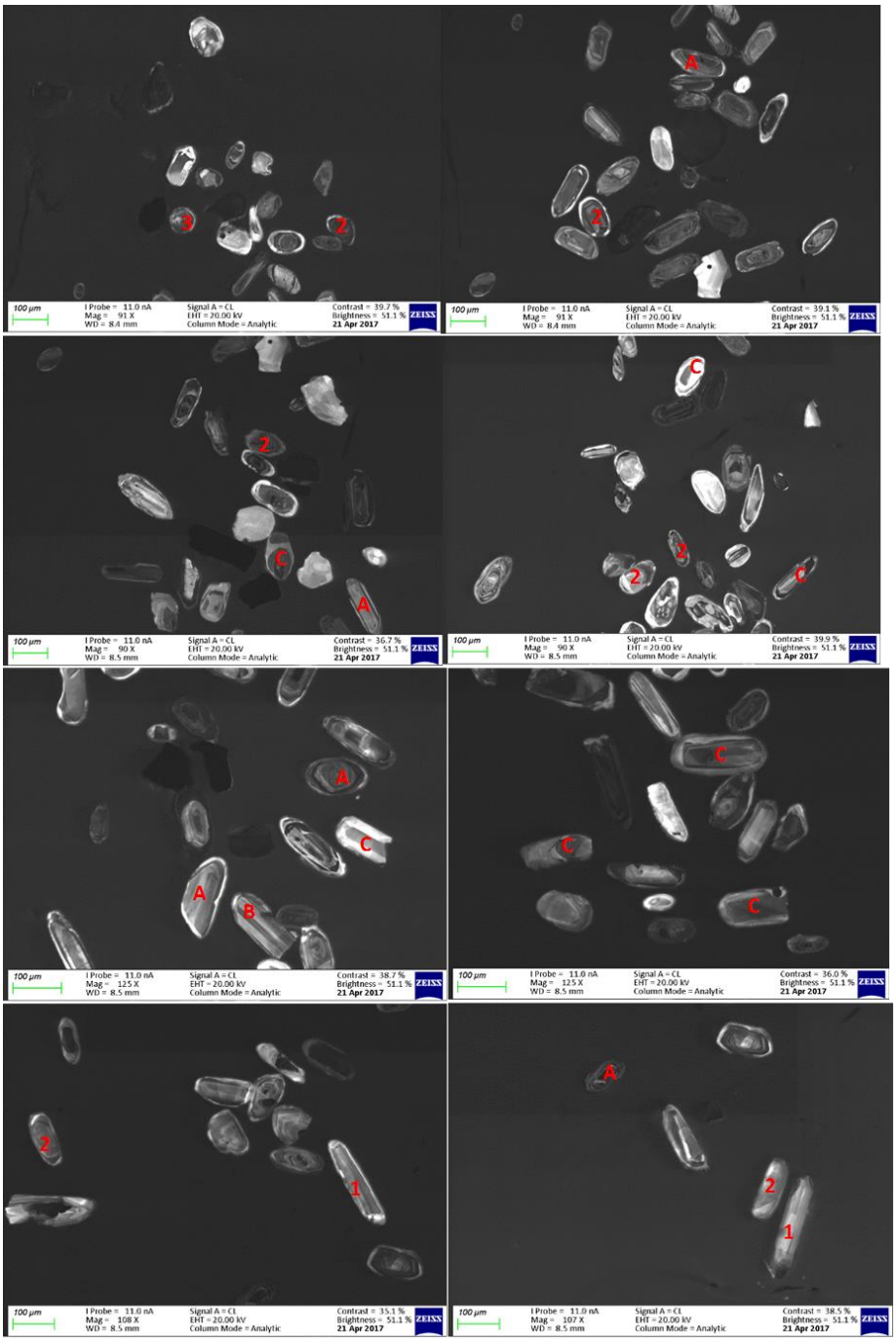

Figure 6.2: Cathodoluminescence images of zircons in Dibamba kaolin: 1) Needle-like grains, 2) Short to intermediate subhedral to subrounded grains, 3) Oval to rounded grains, and A) Oscillatory zoning, B) Sector zoning, C) Xenocryst cores

6.2.3 Zircons in Ediki kaolin

Zircons in Ediki kaolins have sizes varying between 90 and ~200 µm. The zircons are mainly short to intermediate subhedral to subrounded and oval to rounded. This suggests a long travel distance. Euhedral grains are present either with well-defined oscillatory zones or with no zoning (homogenous unzoned grains). Xenocryst cores are also present (Figure 6.3).

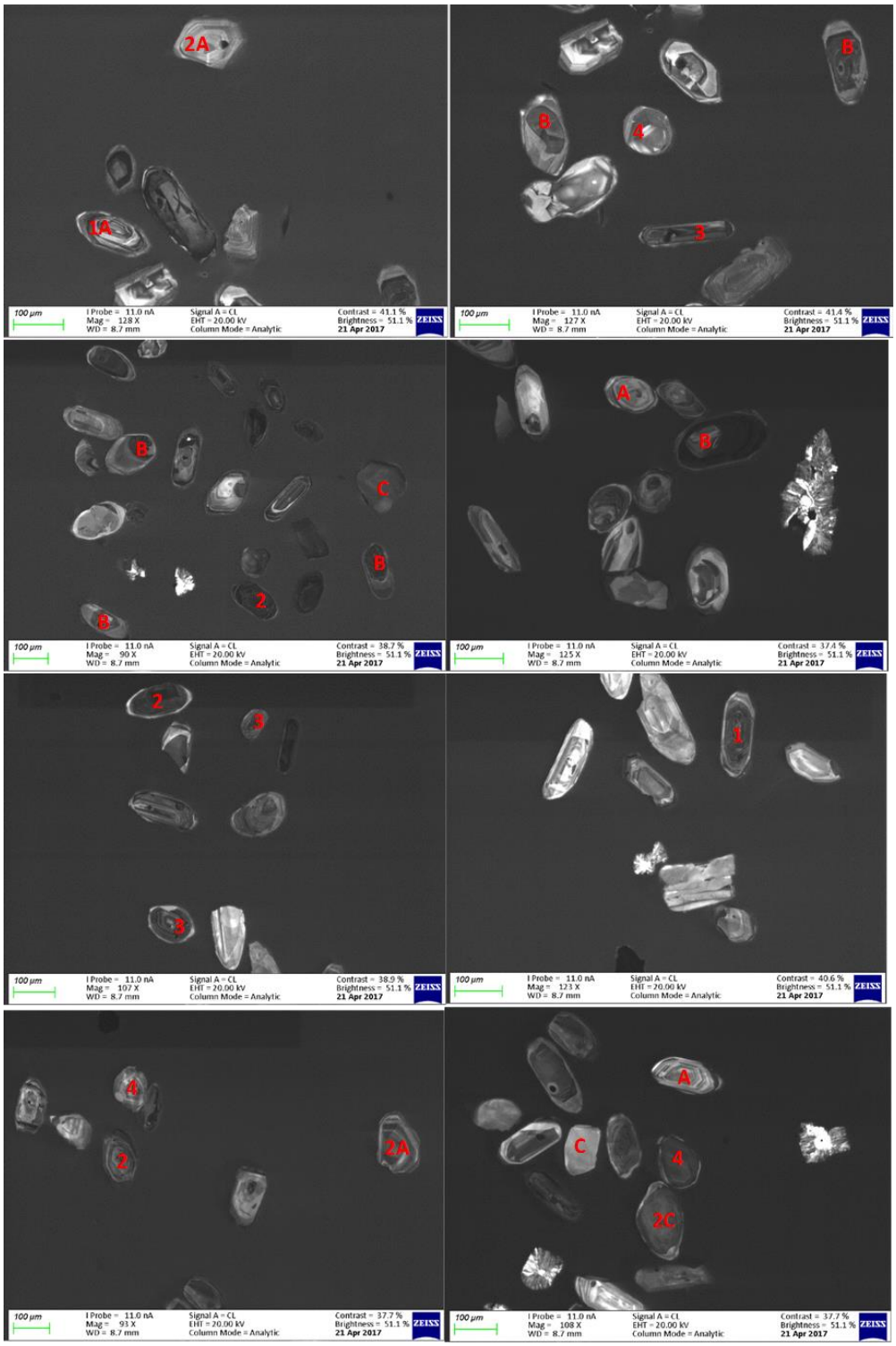

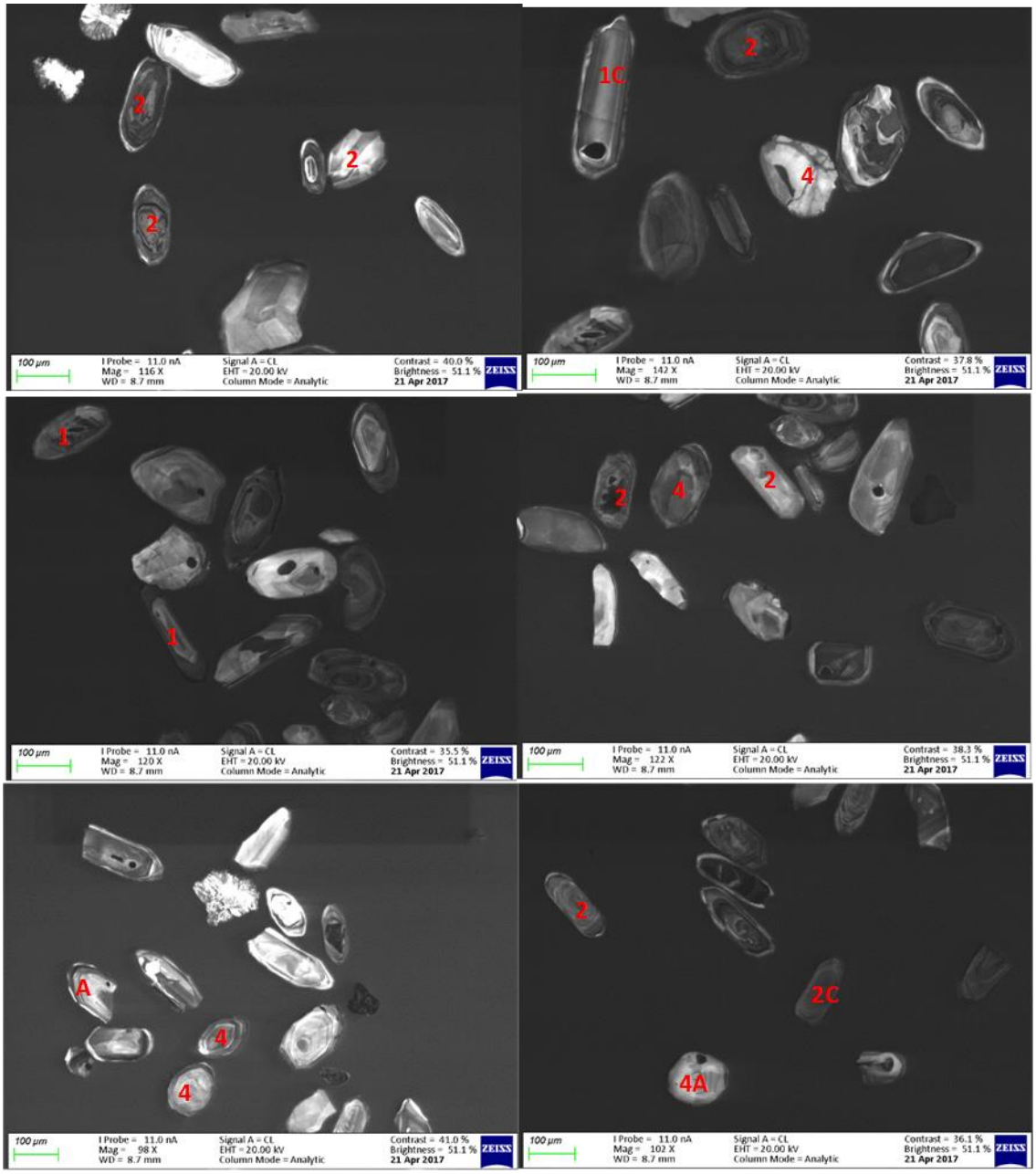

Figure 6.3: Cathodoluminescence images of zircons in Ediki kaolin: 1) Euhedral grains, 2) Short to intermediate subhedral to subrounded grains, 3) Needle-like grains, 4) Oval to rounded grains, and A) Oscillatory zoning, B) Xenocryst cores, C) Homogenous unzoned grains

6.2.4 Zircons in Logbaba kaolin

Zircons in Logbaba kaolins were 100-300 µm. The grains are intermediate euhedral to subrounded (Figure 6.4). More euhedral shapes are observed and few oval to rounded shapes are present. The zircons are characterised by oscillatory and sector zonings.

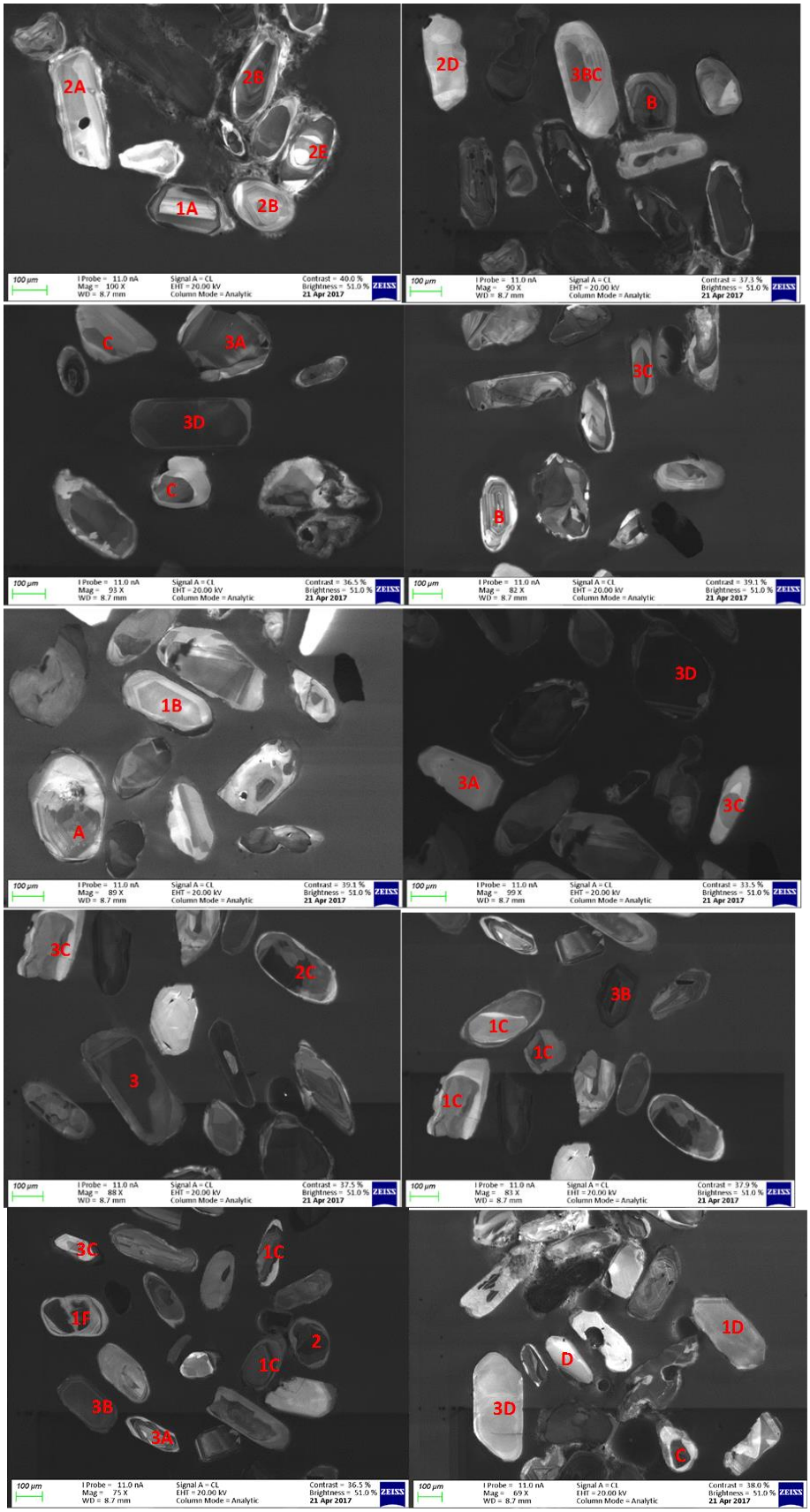

Figure 6.4: Cathodoluminescence images of zircons in Logbaba kaolin: 1) Intermediate subhedral to subrounded grains, 2) Oval to rounded grains, 3) Euhedral grains, and A) Sector zoning, B) Oscillatory zoning, C) Xenocryst cores, D) Homogenous unzoned grains, E) Irregular concentric zoning, F) Chaotic texture

Xenocryst cores are present in some grains, whereas other grains are homogeneous. Two of the grains had unusual texture; one with irregular concentric zoning and the other with a chaotic texture giving an impression of flow.

6.2.5 Zircons in Missole kaolin

Few zircons were obtained from Missole kaolins. The size of the zircons generally varied from 100 to about 200 µm (Figure 6.5). Two groups of shapes were observed: intermediate subhedral to subrounded grains and euhedral grains, with the former being more abundant. Irregular concentric zoning was present in two grains; whereas the remaining grains contained oscillatory zoning and/or xenocryst cores.

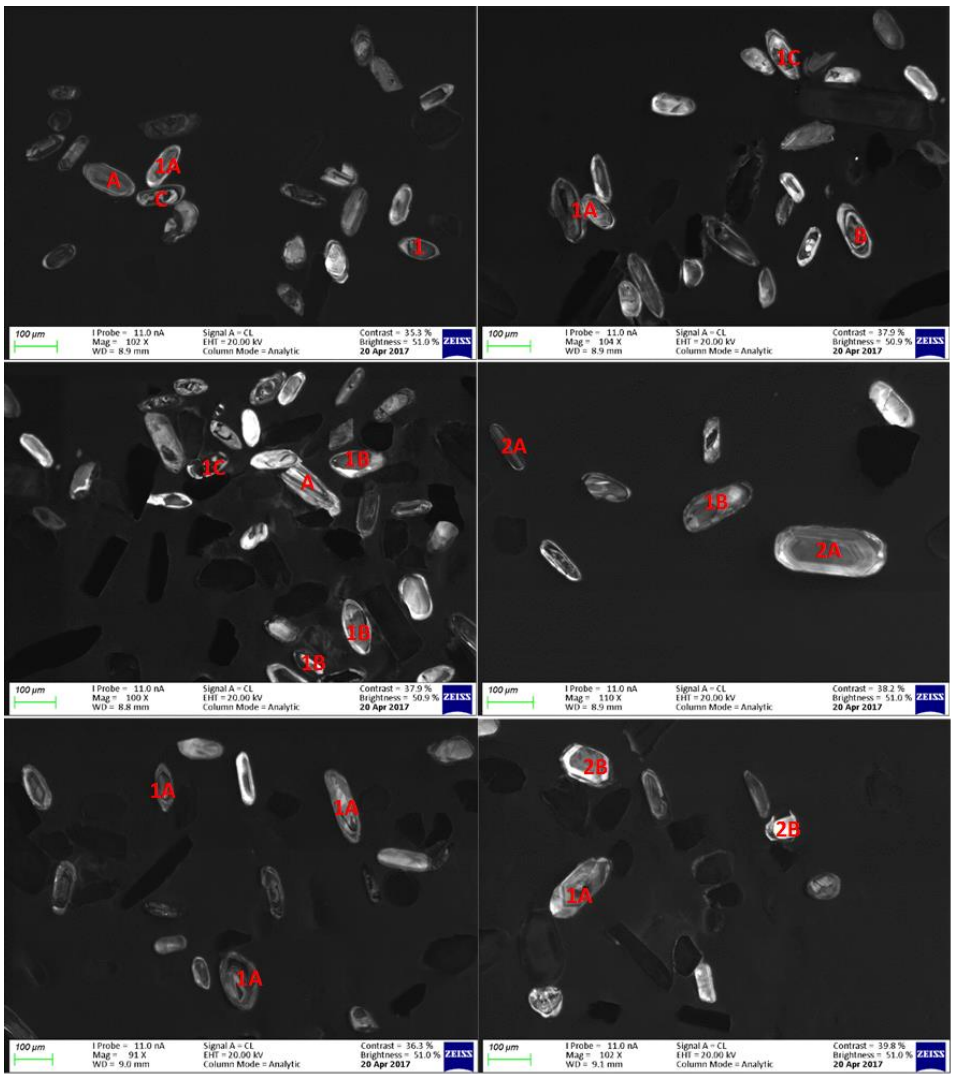

Figure 6.5: Cathodoluminescence images of zircons in Missole kaolin: 1) Intermediate subhedral to subrounded grains, 2) Euhedral grains, and A) Oscillatory zoning, B) Xenocryst cores, C) Irregular concentric zoning

6.2.6 Zircons in Yatchika kaolins

Yatchika kaolins contained both small grains and larger grains. The sizes ranges between 50 to about 500 µm. Most large grains were euhedral (Figure 6.6). Other shapes present were intermediate subhedral to subrounded and oval to rounded grains. Sector zoning was more evident in these zircons. Xenocryst cores with larger rims were present, some of which had oscillatory zoning showing growth of new crystals. Few homogenous grains were also present.

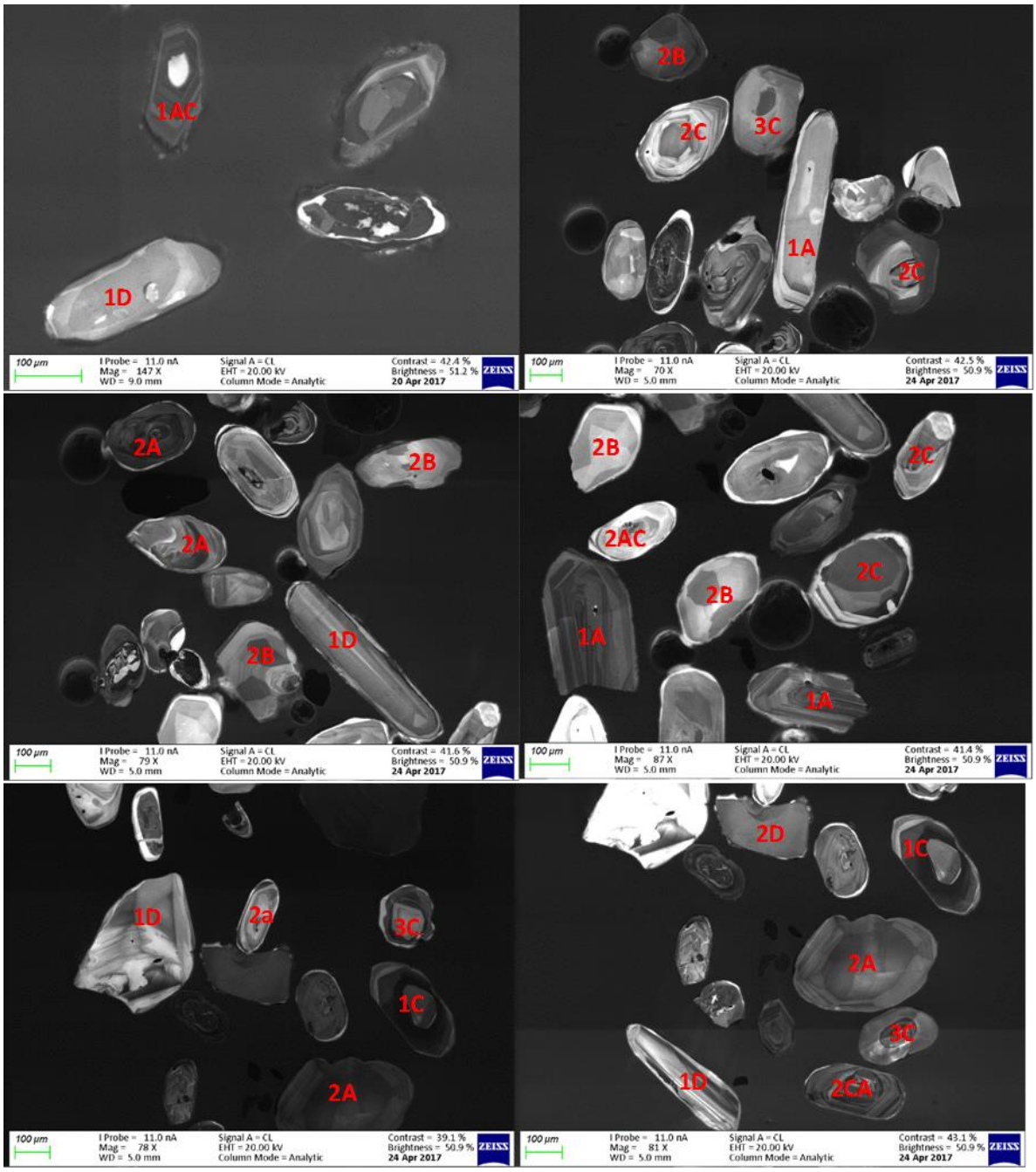

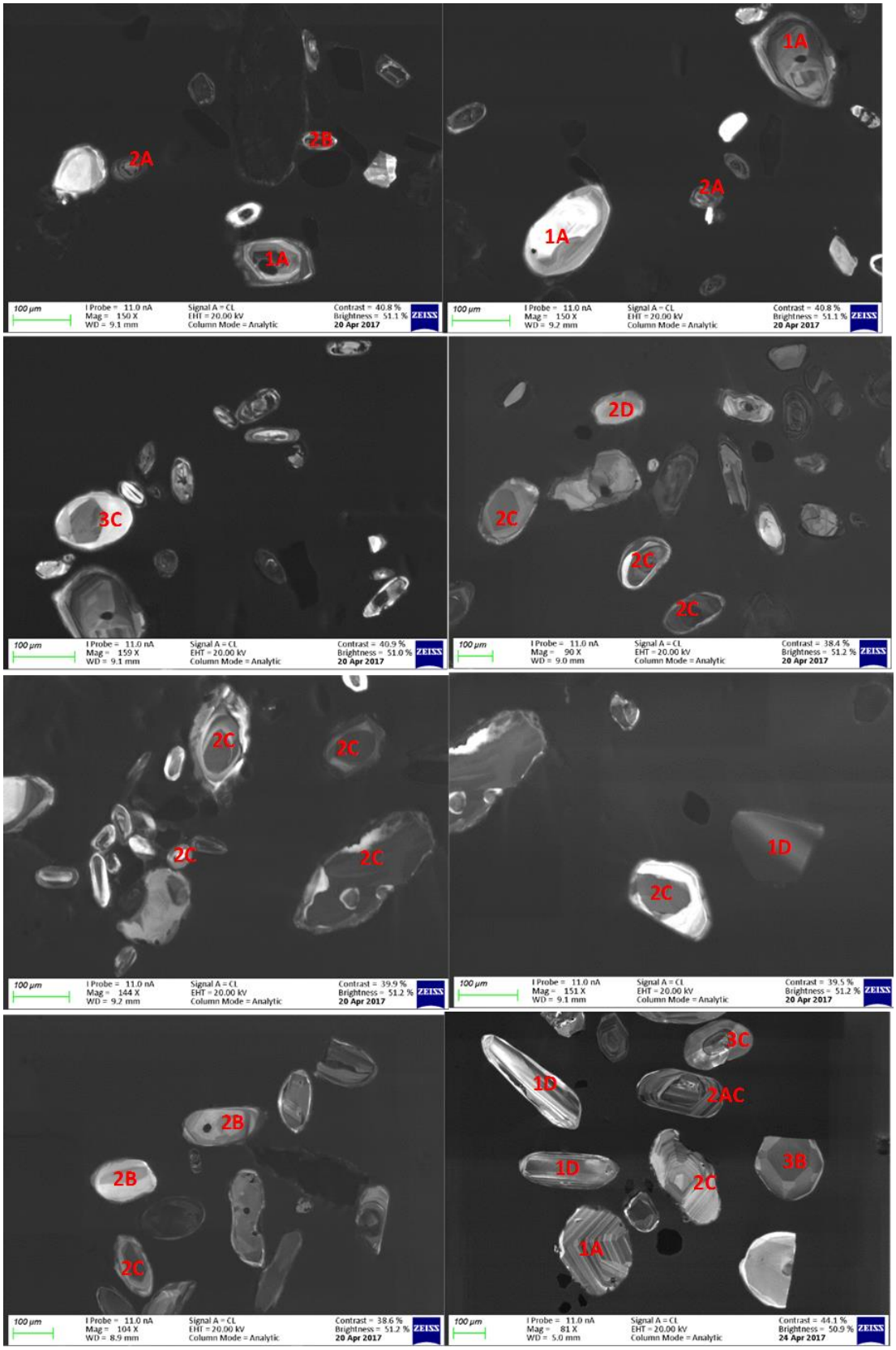

Figure 6.6: Cathodoluminescence images of zircons in Yatchika kaolin: 1) Euhedral grains, 2) Intermediate subhedral to subrounded grains, 3) Oval to rounded grains, and A) Growth/oscillatory zoning, B) Sector zoning, C) Xenocryst cores, D) Homogenous unzoned grains

6.3 Uranium/thorium ratio (Th/U) in zircons

Figures 6.7 and 6.8 show the Th/U ratios of zircons against their $^{238}U/^{207}Pb$ or $^{207}Pb/^{206}Pb$ ages. The ages used are 90-110% concordant. In Bomkoul kaolin, the Th/U ratio of zircons varied between 0.1 and 4.6, though most zircons had a ratio between 0.3 and 2.5 (Figure 6.7A). Younger zircons in Dibamba kaolins (< 700 Ma) had Th/U ratios up to 2.8; whereas older ones (> 700 Ma) had Th/U ratios varying between 0.4 and 1.3 (Figure 6.7B). The Th/U ratios of zircons from Ediki were < 2 (Figure 6.7C).

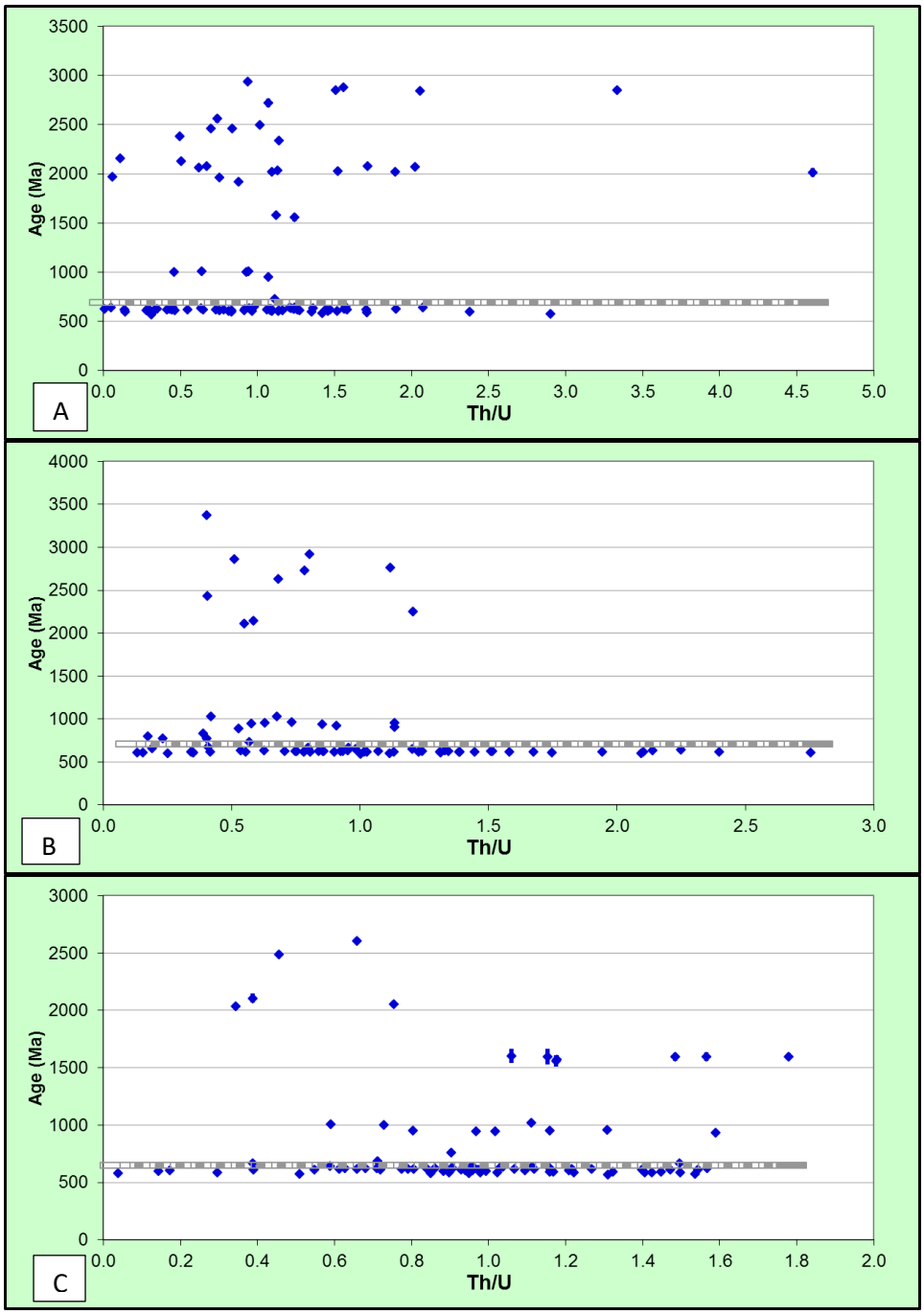

Figure 6.7: Th/U ratios of zircons from A) Bomkoul kaolin, B) Dibamba kaolin and C) Ediki kaolin

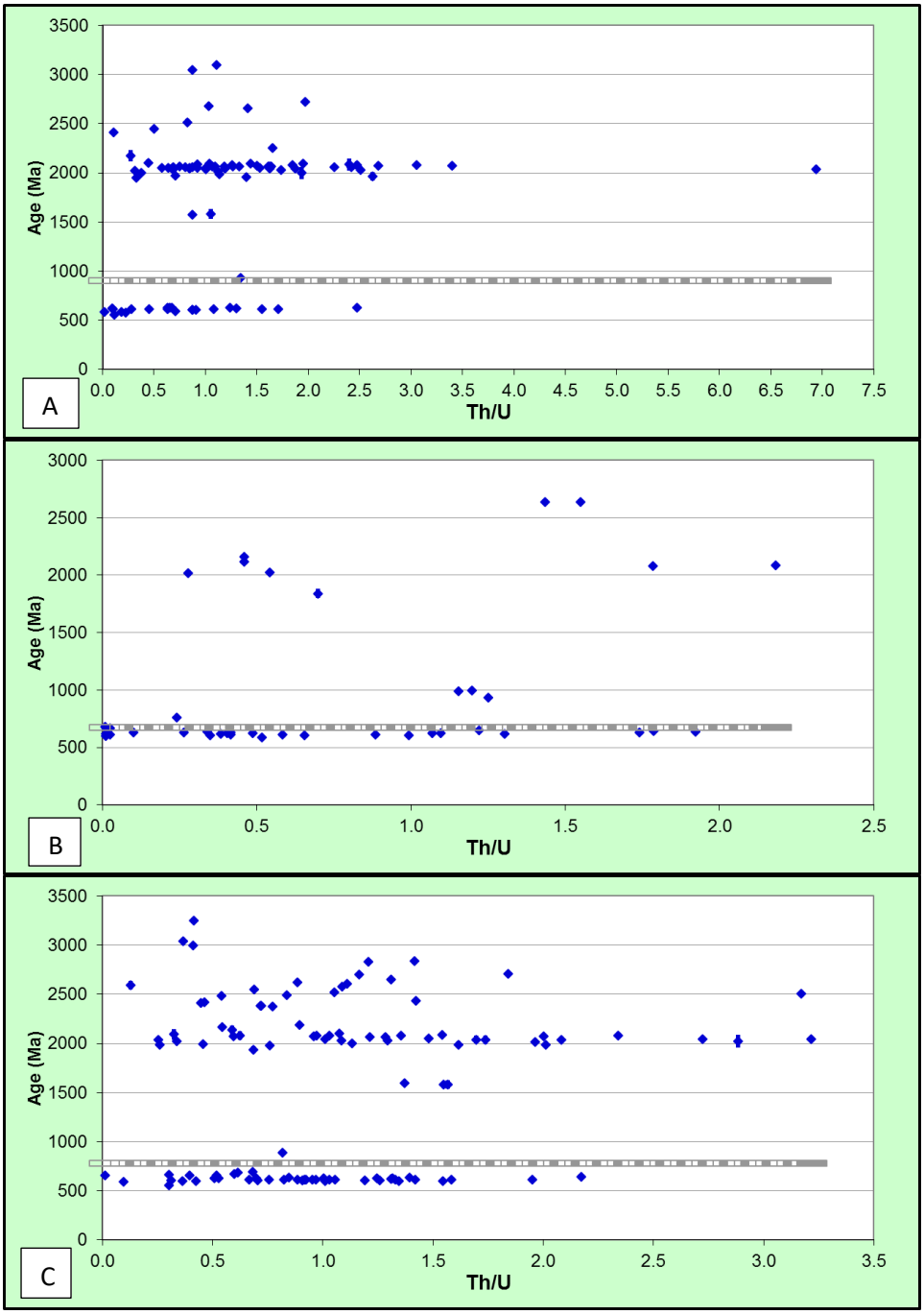

Figure 6.8: Th/U ratios of zircons from A) Logbaba kaolin, B) Missole kaolin and C) Yatchika kaolin

Logbaba, Missole and Yatchika kaolins had zircons with Th/U ratios less than 3.5, though an analysis in zircons in Logbaba kaolin yielded a Th/U ratio of 7. In general, all Th/U ratios of studied zircons were > 0.1, except one or two analyses in each location, which were carried out on rims.

6.4 Detrital zircon population ages

6.4.1 Concordant ages of reference materials

The U/Pb ages of primary reference material (GJ1) and secondary reference materials (Plešovice and M127 zircons) are shown below (Figures 6.9-6.14). Published ages of GJ1 and Plešovice zircon are 602 ± 1 Ma and 337 ± 1 Ma (Horstwood *et al*., 2016); whereas the age of M127 zircon is 524 ± 1 Ma (Nasdala *et al*., 2016). Results of the analyses of reference materials are shown in Appendices 6.7 and 6.8.

6.4.1.1 Sequence 1

Sequence 1 was made up of four samples, namely Bomkoul, Dibamba, Ediki and Logbaba. Thirty-four analyses of GJ1 were carried out, 10 of which were > 3% discordant. The concordia age of GJ1, calculated using the 24 analyses that were ≤ 3% discordant, is 602 ± 1 Ma (as published), with a mean squared weighted average (MSWD) of 0.98 (Figure 6.9).

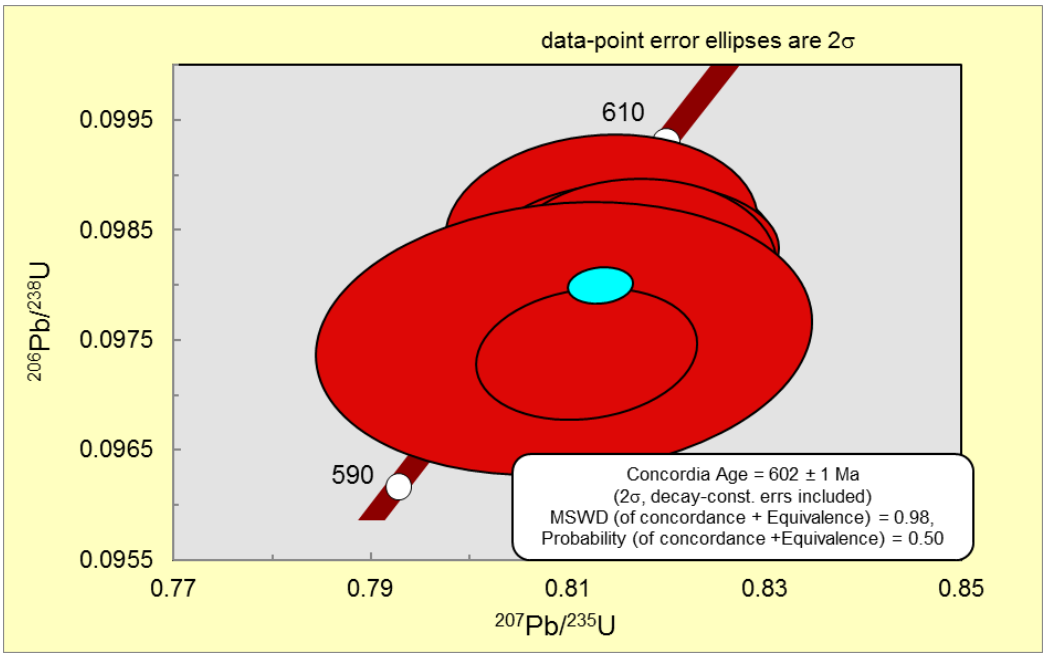

Figure 6.9: Concordia showing the age of analysed GJ1 zircons

Ten analyses of Plešovice zircon were carried out, 5 of which were ≤ 3% discordant. The analysis of the ≤ 3% discordant gave a concordia age of 339 ± 2 Ma, with an MSWD = 0.21 (Figure 6.10). The calculated age of Plešovice zircon during this sequence was very similar to its published age (337 ± 1 Ma).

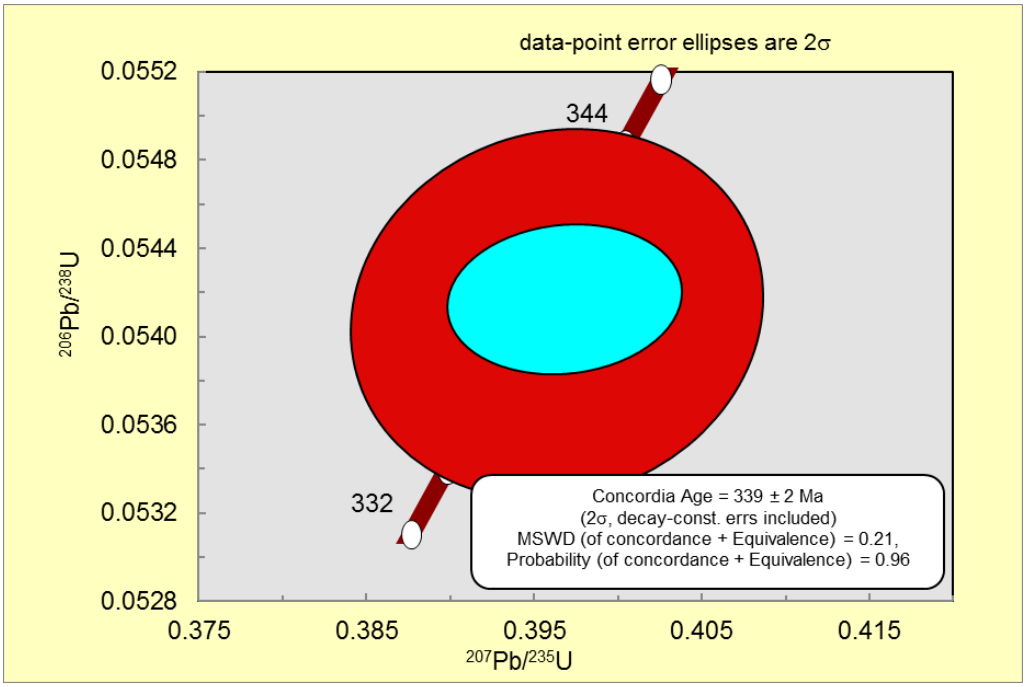

Figure 6.10: Concordia showing the age of analysed Pleşovice zircons

Seven analyses of M127 were carried, with all seven analyses being ≤ 3% discordant. The Concordia age obtained from the seven analyses is 527 ±1 Ma, with an MSWD of 0.79 (Figure 6.11). This age is close to the published age (524 ± 1 Ma).

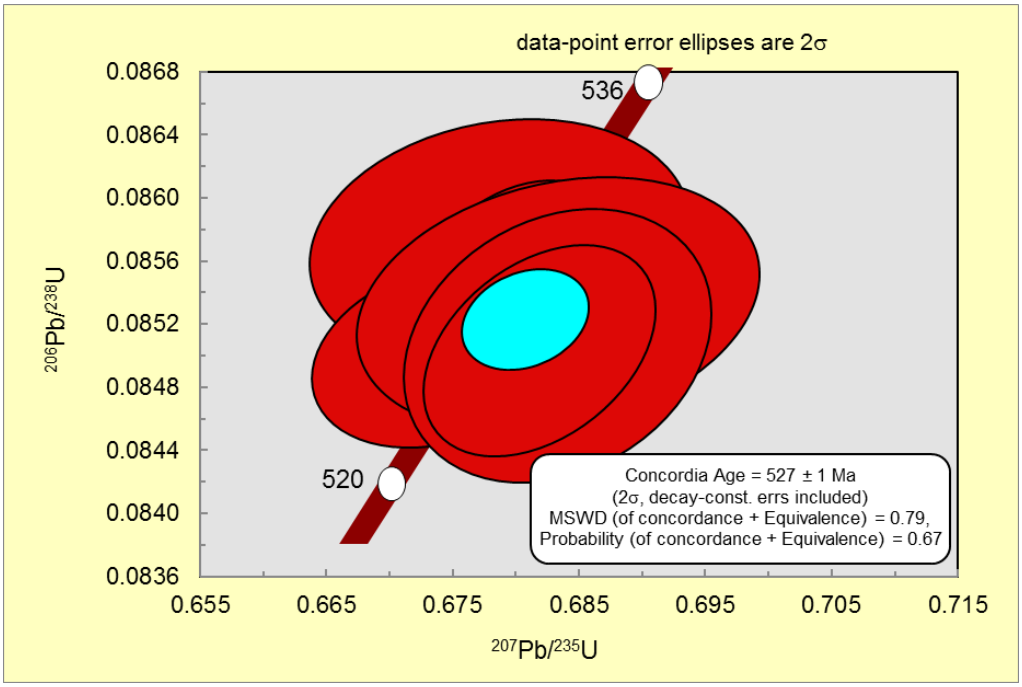

Figure 6.11: Concordia showing the age of analysed M127 zircons

6.4.1.2 Sequence 2

In sequence 2, zircons from two sites were analysed, Missole and Yatchika zircons. Eighteen GJ1 analyses were carried out, 16 of which were ≤ 3% discordant. These 16 concordant GJ1 analyses gave a concordia age of 602 ± 1 Ma, with an MSWD of 0.83 (Figure 6.12). Fifteen analyses of Plešovice were carried out, 6 of which were ≤ 3% discordant. The 6 concordant analyses gave a Concordia age of Plešovice to be 340 ± 1 Ma, with an MSWD of 1 (Figure 6.13). Eight M127 analyses were carried; 6 of these analyses were ≤ 3% discordant and gave a concordia age of 527 ± 1 Ma, with an MSWD of 0.88 (Figure 6.14).

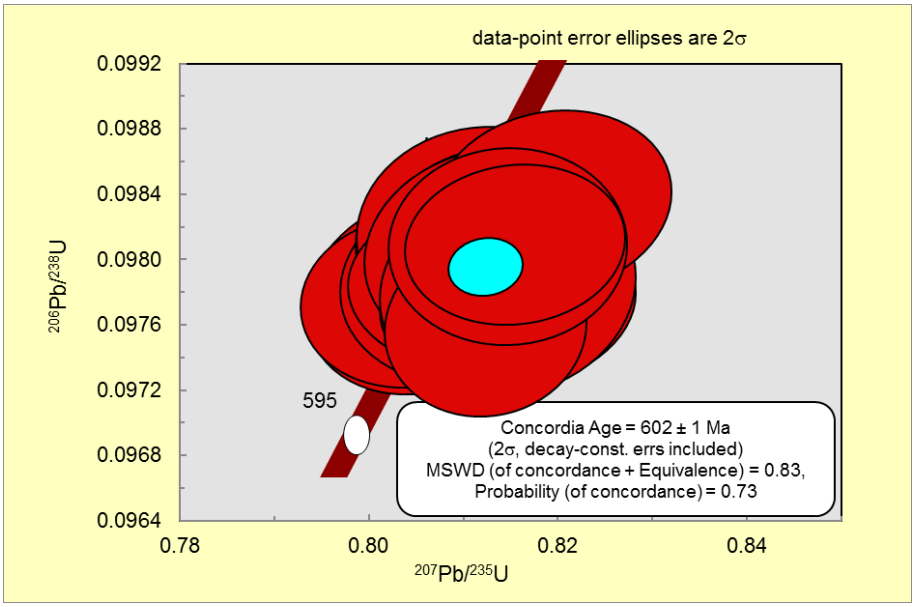

Figure 6.12: Concordia showing the age of analysed GJ1 zircons

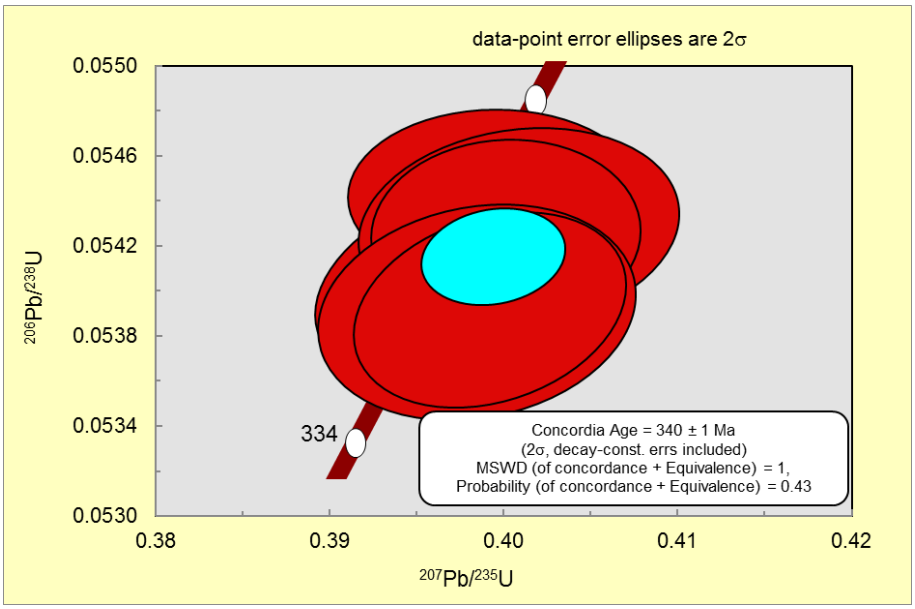

Figure 6.13: Concordia showing the age of analysed Pleşovice zircons

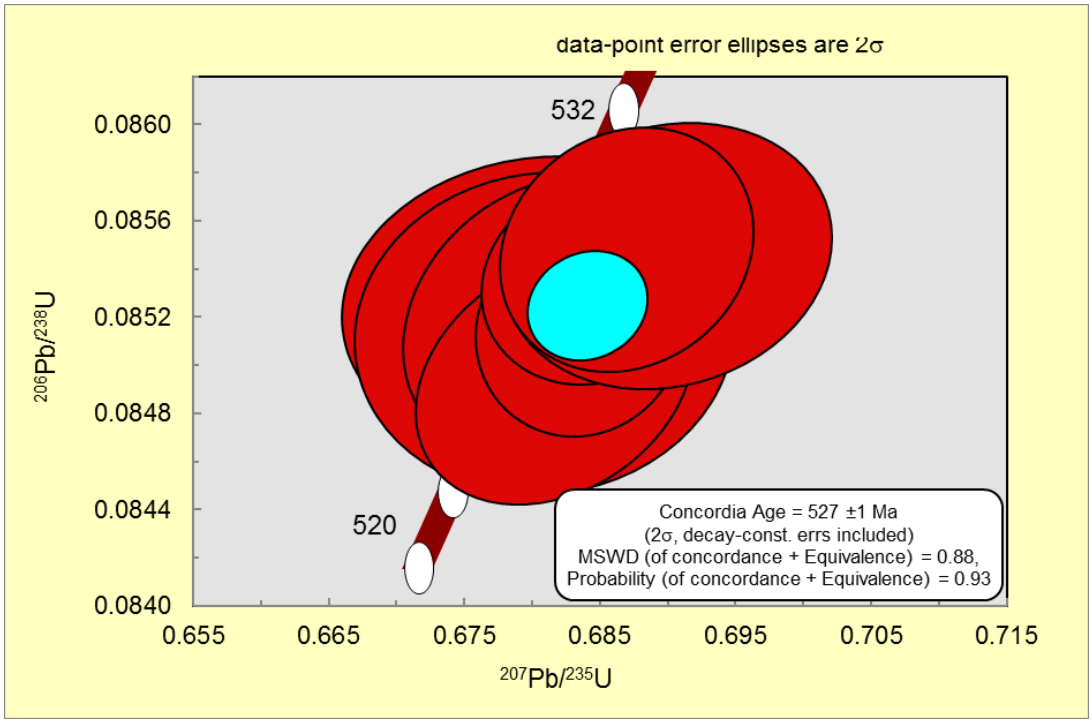

Figure 6.14: Concordia showing the age of analysed M127 zircons

The results of the analyses of all three reference materials used for error propagation and quality control during the analyses of zircons found in Cretaceous-Tertiary kaolins were in agreement with published data. Therefore, all uncertainties caused during analyses were properly corrected during data reduction using these reference materials.

6.4.2 Bomkoul kaolins

Results of the analysis of zircons from Bomkoul kaolin are shown in Appendix 6.9.

6.4.2.1 Concordia of concordant and discordant ages of zircons in Bomkoul kaolin

Figure 6.15 shows the concordia for both concordant and discordant ages of zircons in Bomkoul kaolins, with 114 analyses. Two zircons have $^{206}Pb/^{238}U$ ages < 100 Ma (57 ± 1 Ma and 60 ± 3 Ma); however, these results were the most discordant (16 and 55% concordant, respectively). Figure 6.15A shows that most zircon ages< 1500 Ma are found on the concordia, with two main clusters, one around 600 Ma and another around 1000 Ma. The few analyses that are not on the concordia are believed to have lost common lead (^{204}Pb).

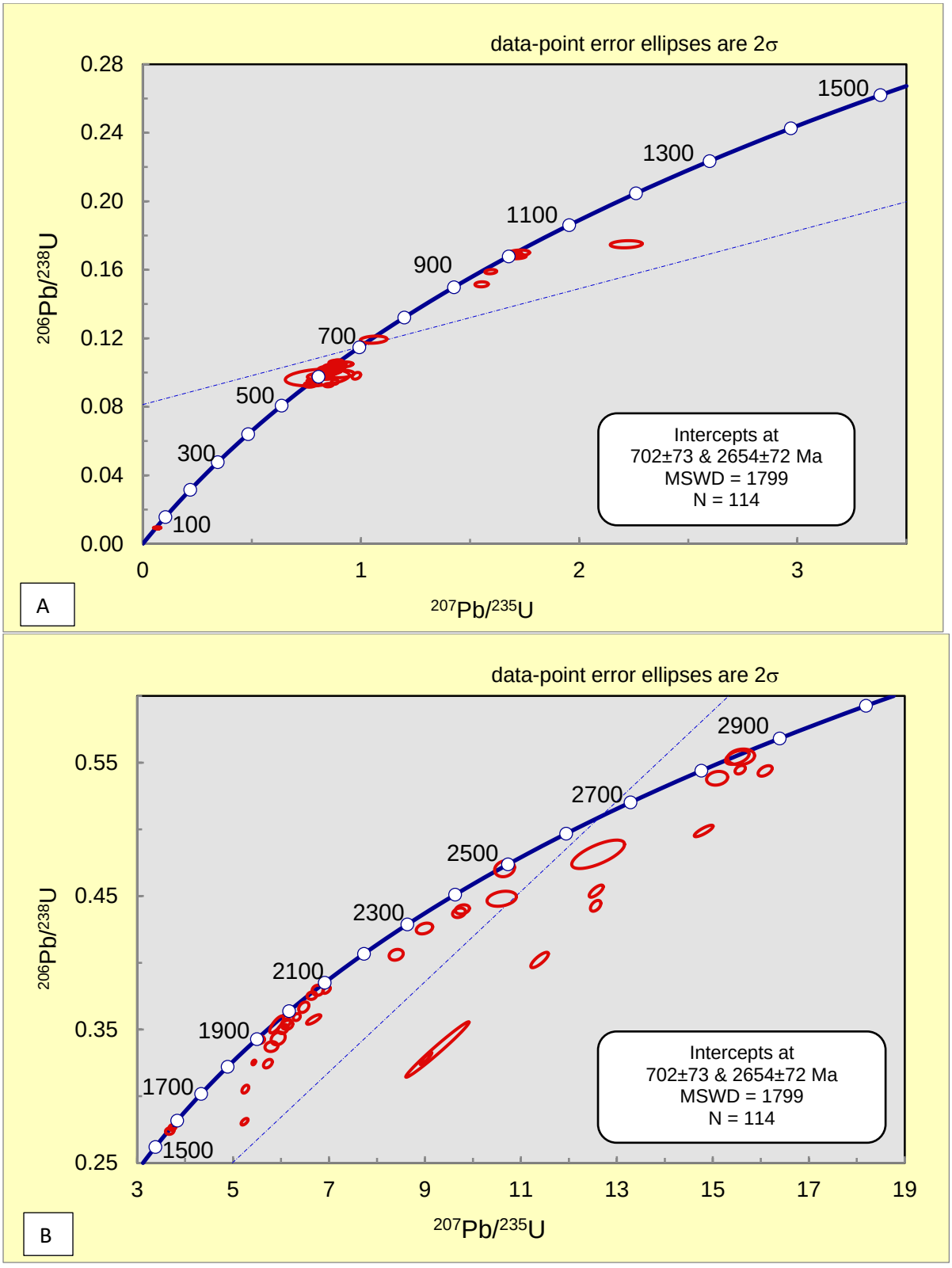

Figure 6.15: Concordia of concordant and discordant ages of zircons in Bomkoul kaolins, A) Ages < 1500 Ma, B) Ages < 1500 Ma

Above 1500 Ma, the analyses were more discordant, due to the loss of ^{204}Pb in older grains, with the oldest grain having a $^{207}Pb/^{206}Pb$ age of 2940 ± 11 Ma (Figure 6.15B). A main cluster of grains is found between 1900 and 2100 Ma.

6.4.2.2 Probability density plot of Bomkoul zircons

The probability density plot of ages of zircons from Bomkoul kaolins, showing the different clusters in zircon ages (≤ 10% discordant), is shown in Figure 6.16. The main cluster is between 600 and 650 Ma, with about 60% of analyses yielding ages in this age range. The second cluster is between 1000 Ma and 1050 Ma, with about 10% of analyses. Little clusters with < 10% analyses were mainly found in older grains.

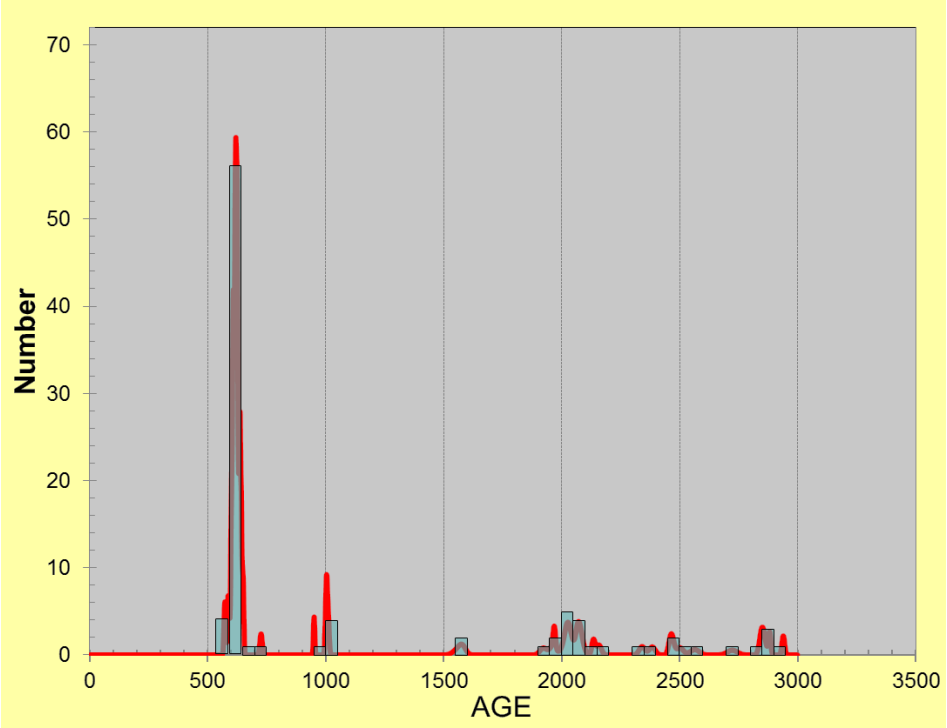

Figure 6.16: Probability density plot of Bomkoul zircons showing different clusters of zircon ages. Bin width = 50 Ma

6.4.2.3 Weighted averages of zircon populations in Bomkoul

Seven zircon populations were obtain from ages ≤ 5% discordance (Figure 6.17). The youngest zircon population (P1) in Bomkoul kaolins has a weighted average of 606.4 ± 2.8 Ma (MSWD = 1.9, N = 9). The 2nd population (P2) has a weighted average of 621.3 ± 1.5 Ma (MSWD = 1.8, N = 23) and it is the population with the largest amount of analyses (N = 23).

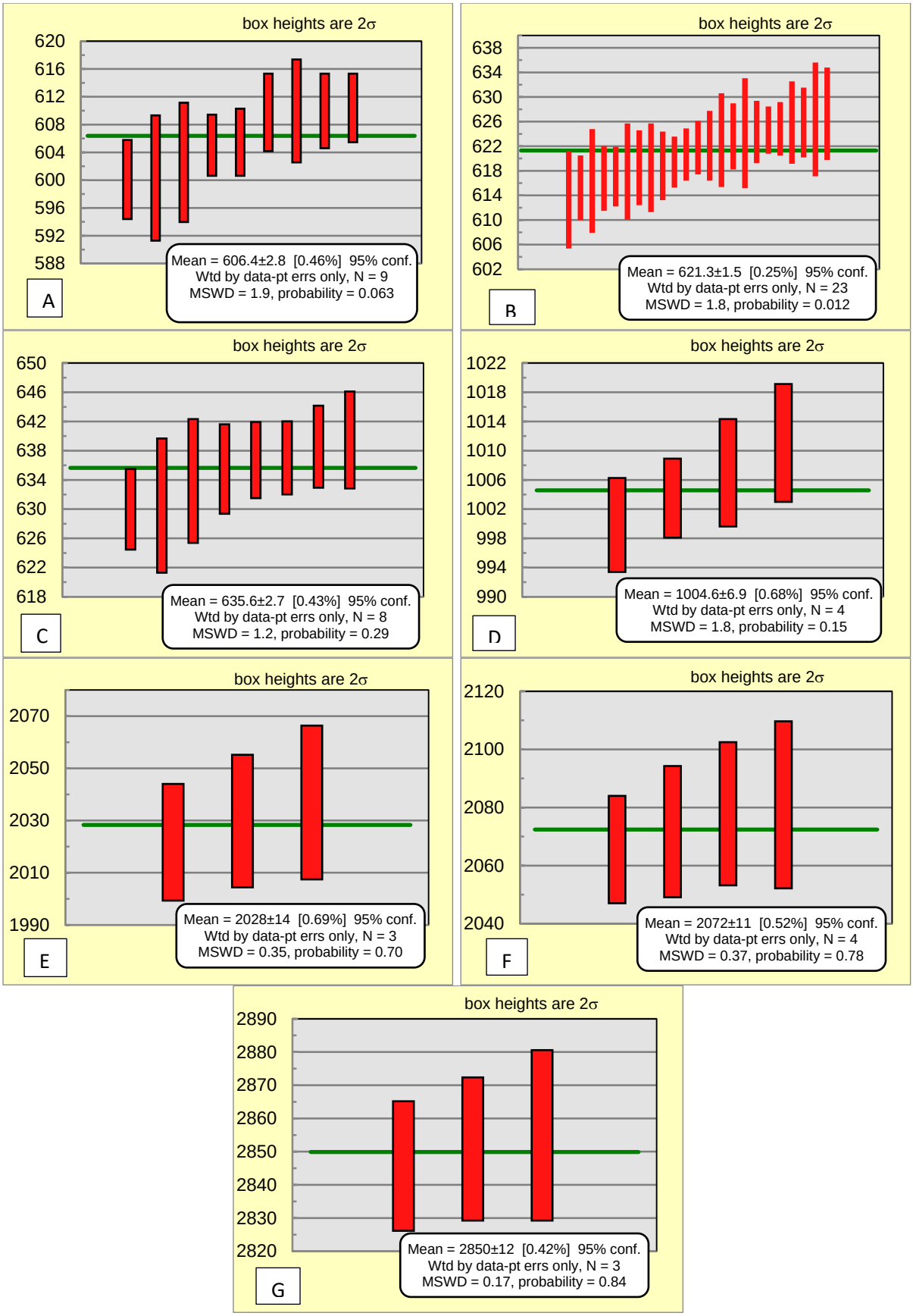

Figure 6.17: Weighted average plots of zircon populations in Bomkoul kaolins, in increasing population age, A) Youngest population (P1), B) P2, C) P3, D) P4, E) P5, F) P6, G) P7. *Ages are in Ma, N = Number of analyses*

The 3rd population (P3) has a weighted average of 635.6 ± 2.7 Ma (MSWD = 1.2, N = 8). These first three populations form a larger cluster between 591 and 639 Ma. The 4th population (P4) has a weighted average of 1004.6 ± 6.9 Ma (MSWD = 1.8, N = 4). The 5th population (P5) has a weighted average of 2028 ± 14 Ma (MSWD = 0.35, N = 3). The 6th population (P6) has a weighted average of 2072 ± 11 Ma (MSWD = 0.37, N = 4); and the last population (P7) has a weighted average of 2850 ± 12 Ma (MSWD = 0.17, N = 3).

6.4.3 Dibamba kaolins

Results of the analysis of zircons from Dibamba kaolins are shown in Appendix 6.10.

6.4.3.1 Concordia of concordant and discordant ages of zircons in Dibamba kaolins

Concordant and discordant ages of zircons found in Dibamba kaolins are shown in Figure 6.18. A total of 110 analyses were carried out. Only one analysis was < 500 Ma (63 ± 1 Ma). For ages < 1500 Ma (Figure 6.18A), most ages were concordant. A first cluster was around 600 Ma, a 2nd cluster was found between 900 and 1000 Ma. Above 1500 Ma (Figure 6.18B), there was no cluster of analyses. Most ages were discordant due to the loss of ^{204}Pb over time.

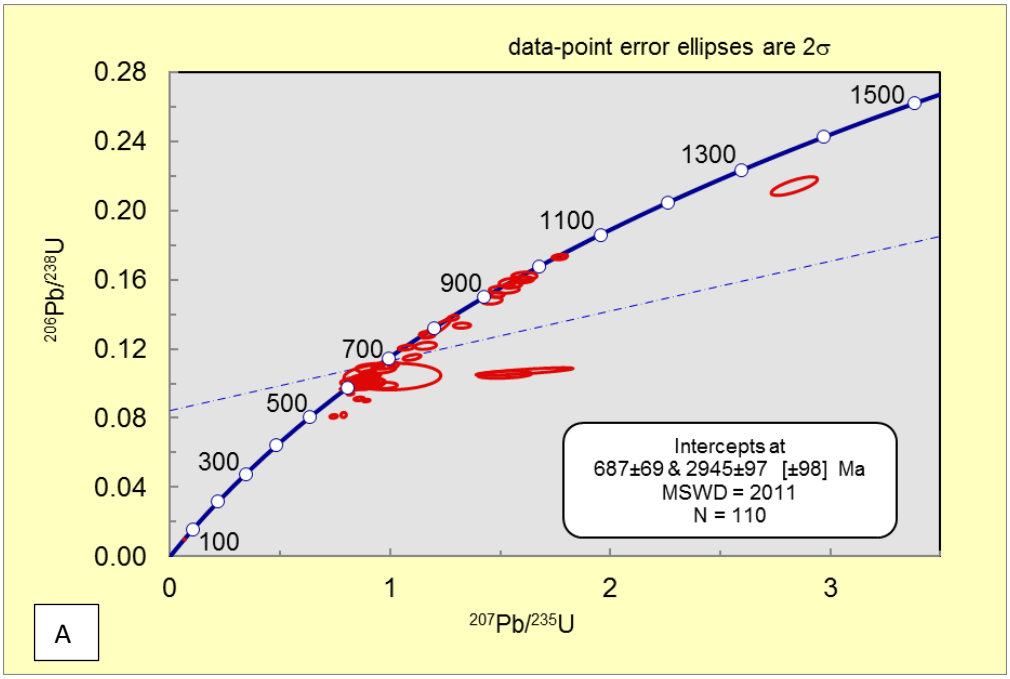

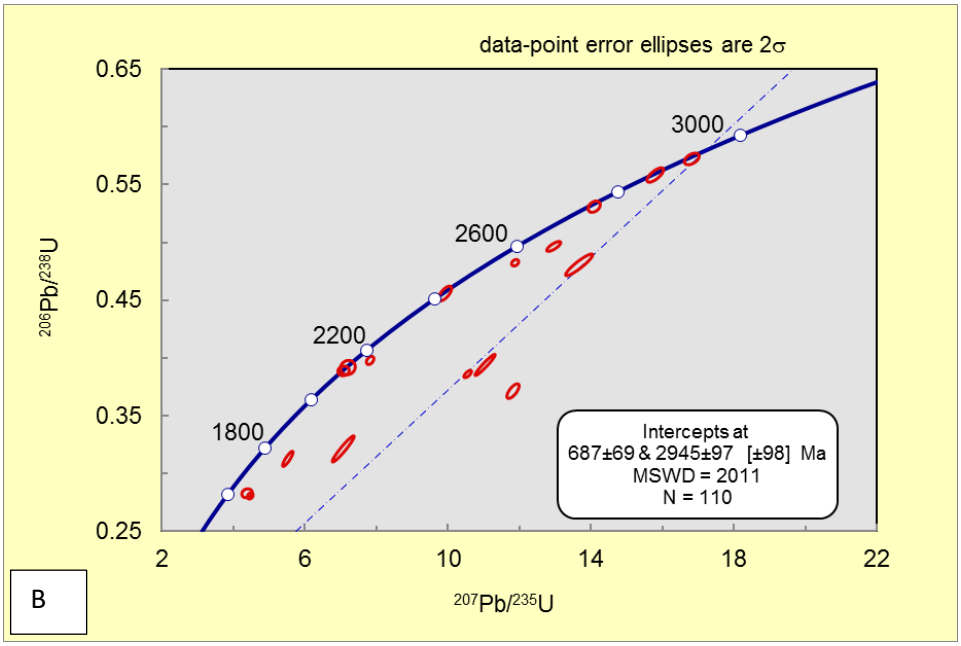

Figure 6.18: Concordia of concordant and discordant ages of zircons in Dibamba kaolins, A) Ages < 1500 Ma, B) Ages < 1500 Ma

6.4.3.2 Probability density plot of Dibamba zircons

Of the 110 analyses, 82 were ≤ 10% discordant. These 82 analyses displayed a main age peak 550 Ma and 650 Ma, represented by about 54% of 82 analyses (Figure 6.19). Insignificant clusters were found above 2000 Ma.

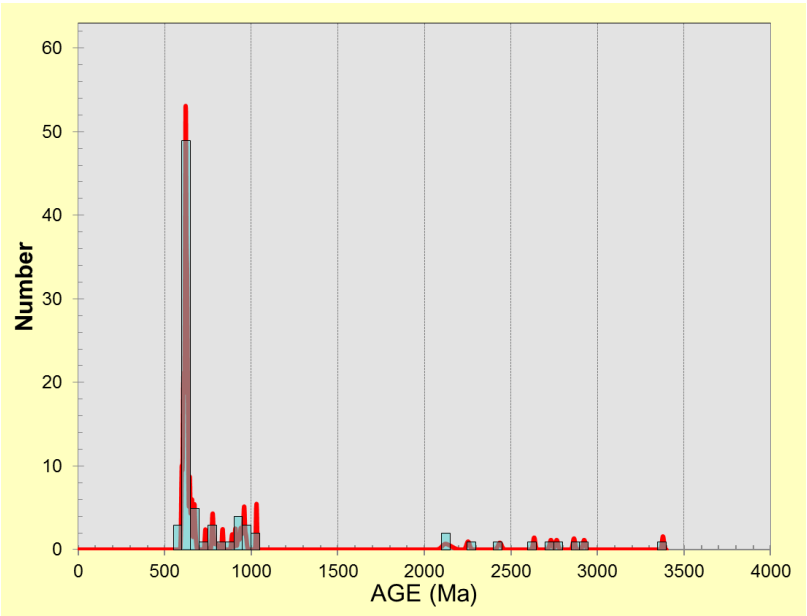

Figure 6.19: Probability density plot of Dibamba zircons showing different clusters of zircon ages. Bin width = 50 Ma

6.4.3.3 Weighted averages of zircon populations in Dibamba

Out of the 110 analyses, 66 were ≤ 5% discordant. These data were used to determine the different zircon populations in the kaolins. Six zircon population were determined in Dibamba kaolins (Figure 6.20). The youngest population (P1) had a weighted average of 607.8 ± 1.9 Ma (MSWD = 0.88, N = 7). The 2nd population (P2), with a weighted average of 620.7±1.3 Ma (MSWD = 0.88, N = 22), was the most abundant of all populations.

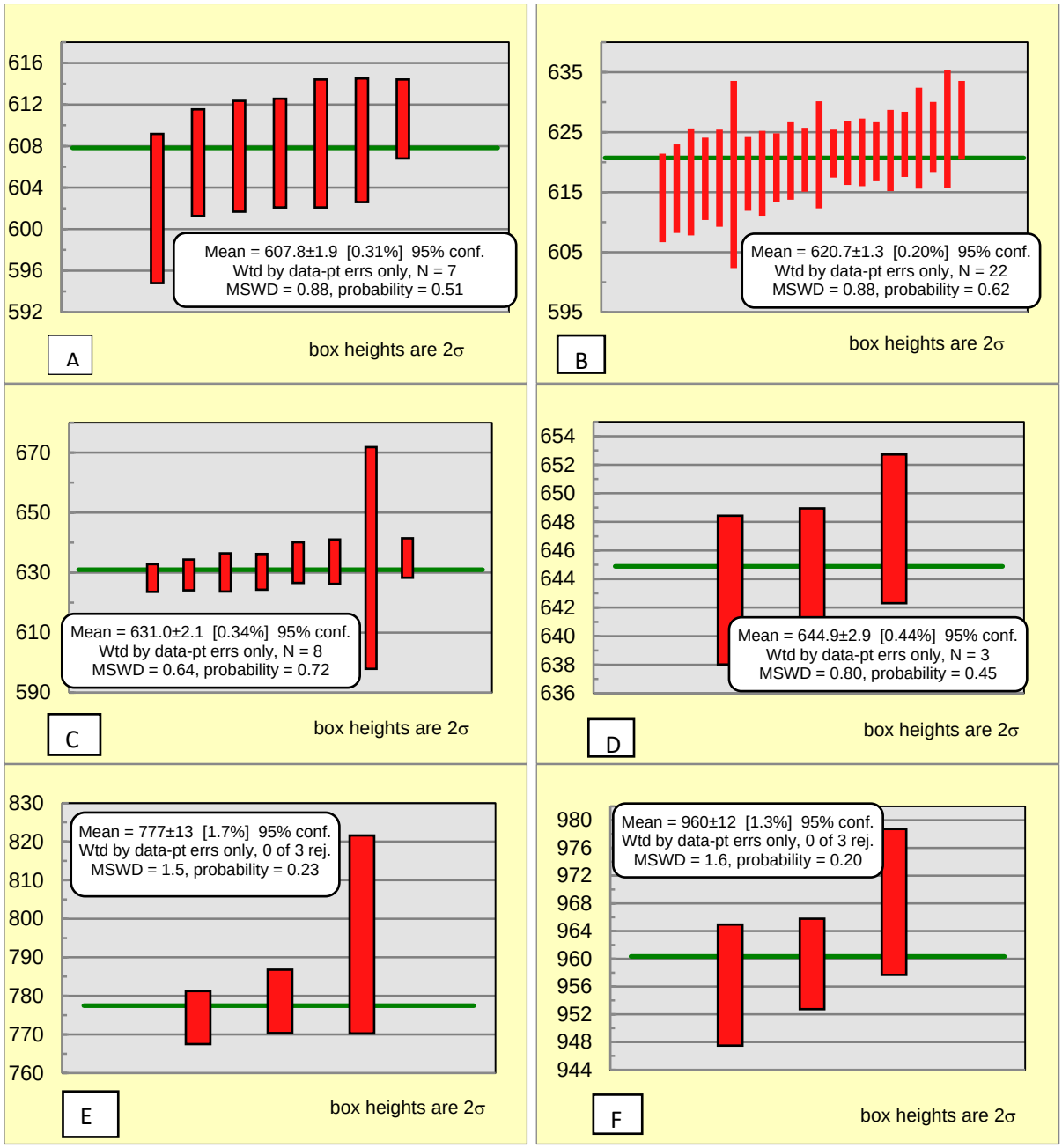

Figure 6.20: Weighted average plots of zircon populations in Dibamba kaolins, in increasing population age, A) Youngest population (P1), B) P2, C) P3, D) P4, E) P5, F) P6. *Ages are in Ma, N = Number of analyses*

The 3rd and 4th populations had weighted averages of 631.0 ± 2.1 Ma (MSWD = 0.64, N = 8) and 644.9 ± 2.9 Ma (MSWD = 0.80, N = 8), respectively. These first four populations re made up of ages varying between 600 and 648 Ma. The 5th population (P5) has a weighted average of 777 ± 13 Ma (MSWD = 1.5, N = 3); and the oldest population (P6) has a weighted average of 960 ± 12 Ma (MSWD = 1.6, N = 3).

6.4.4 Ediki kaolins

Results of the analysis of zircons from Ediki kaolins are shown in Appendix 6.11.

6.4.4.1 Concordia of concordant and discordant ages of zircons in Ediki kaolins

The concordia, showing concordant and discordant ages of 120 zircon analyses, is displayed in Figure 6.21. Though several analyses were discordant, two main clusters are observed for ages < 1500 Ma (around 600 Ma and 1000 Ma) and one cluster in found in ages > 1500 Ma (between 1600 and 1700 Ma). Only five grains were older than 1700 Ma.

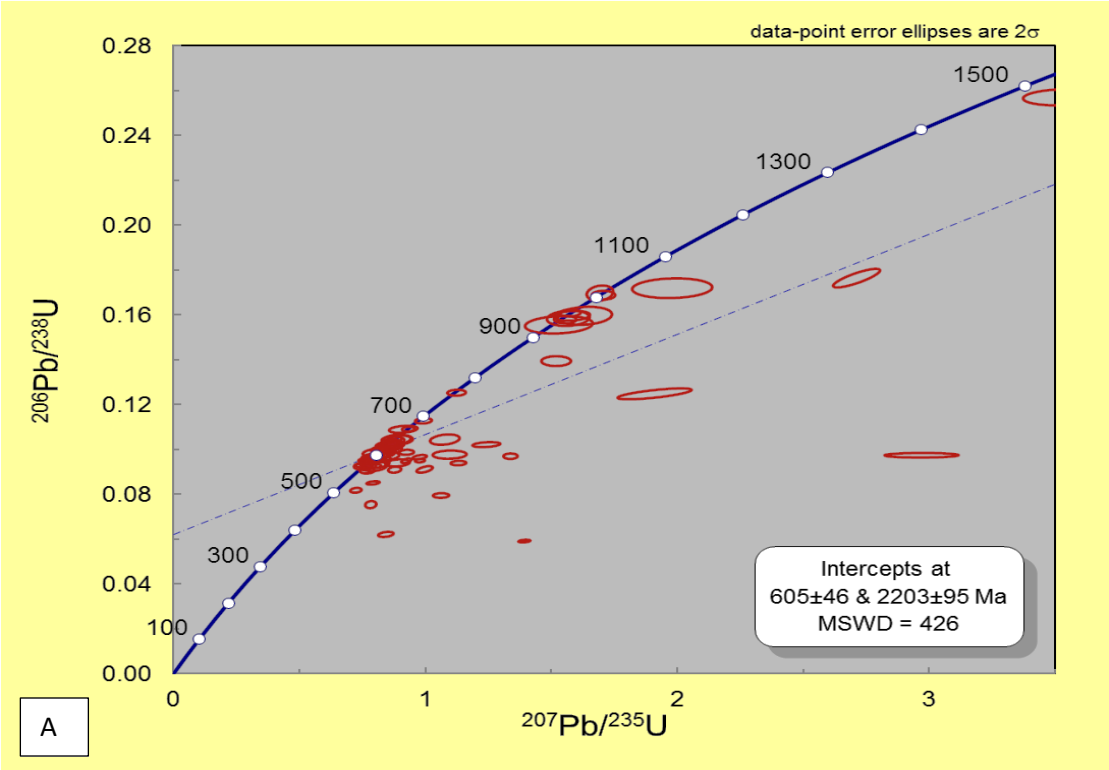

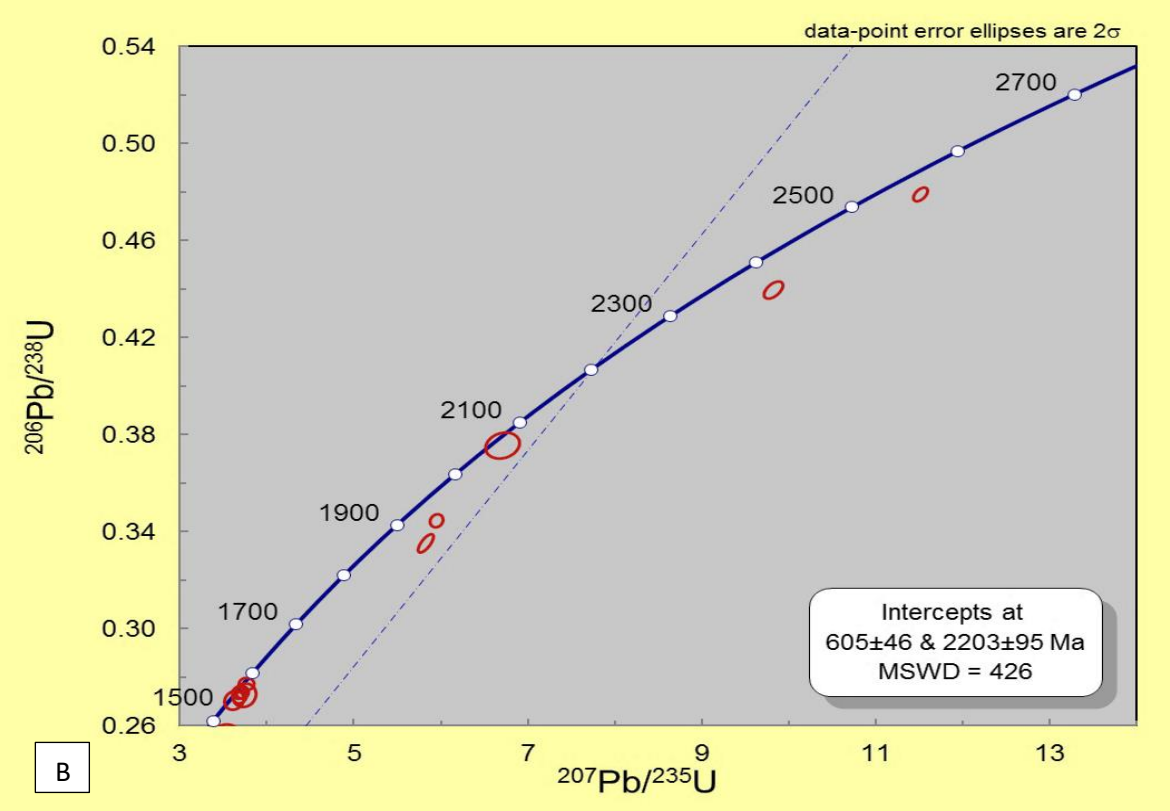

Figure 6.21: Concordia of concordant and discordant ages of zircons in Ediki kaolins, A) Ages < 1500 Ma, B) Ages < 1500 Ma

6.4.4.2 Probability density plot of Ediki zircons

The probability density plot of ages of zircons found in Ediki kaolins is shown in Figure 6.22. The data used were the ≤ 10% discordant (90 analyses). Two main zircon populations are observed between 550 and 650 Ma. Two small clusters are found around 1000 Ma and a 3rd small cluster is found around 1600 Ma.

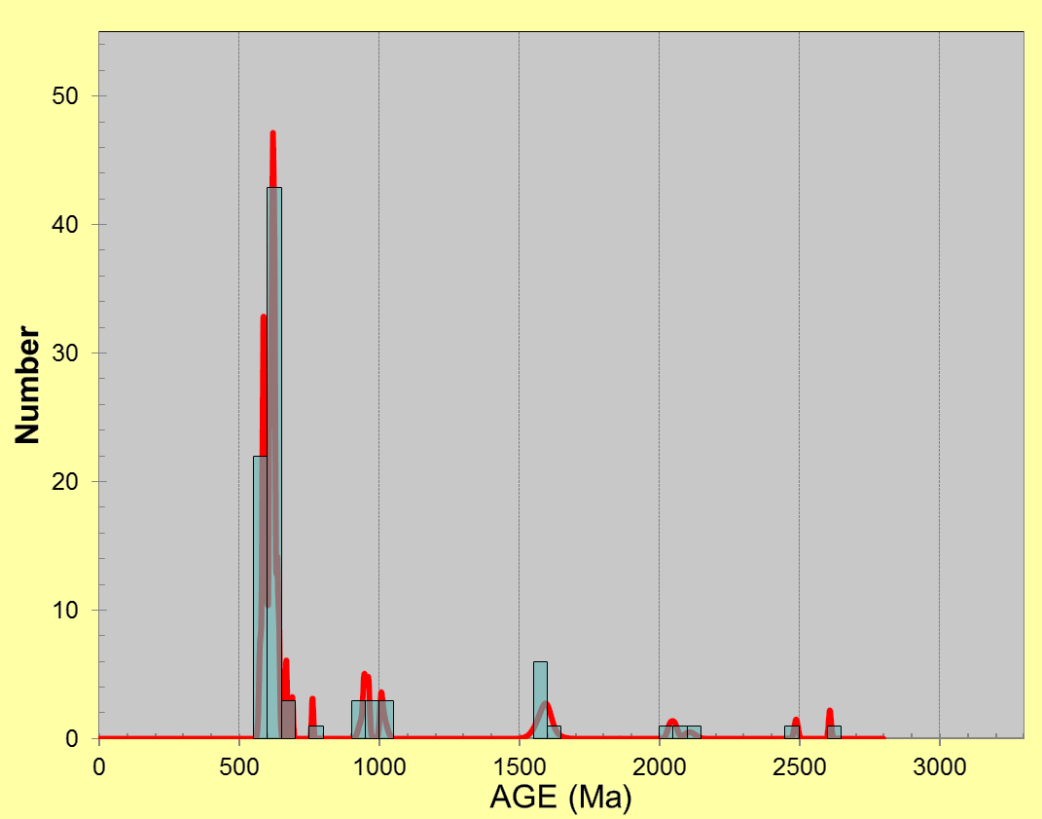

Figure 6.22: Probability density plot of Ediki zircons showing different clusters of zircon ages. Bin width = 50 Ma

6.4.4.3 Weighted averages of zircon populations at Ediki

Using analyses that yielded ages ≤ 5% discordant (72 analyses), six zircon populations were obtained (Figure 6.23). The first and youngest population (P1) had a weighted average of 587.6 ± 2.3 Ma (MSWD = 1.8, N = 13), the 2nd population (P2) had a weighted average of 607.8 ± 2.6 Ma (MSWD =1.8, N = 9). The 3rd and most abundant population (P3) had a weighted average of 622.3 ± 1.6 Ma (MSWD = 1.7, N = 23). The 4th population (P4) had a weighted average of 637.4 ± 6.0 Ma (MSWD = 1.7, N = 4). The 5th population (P5) had a weighted average of 947 ± 12 Ma (MSWD = 1.9, N = 4), and the 6th and last population (P6) had a weighted average of 1589 ± 15 Ma (MSWD = 0.58, N = 6).

Though having a ≤ 5% discordance, some analyses did not belong to a population because they were not up to three (at least three analyses are needed to form a population). Two younger ages than P1 were obtained (571 ± 8 Ma and 578 ± 6 Ma). Two ages were around 1000 Ma. Two ages older than P6 were also obtained (2107 ± 39 Ma and 2607 ± 9 Ma).

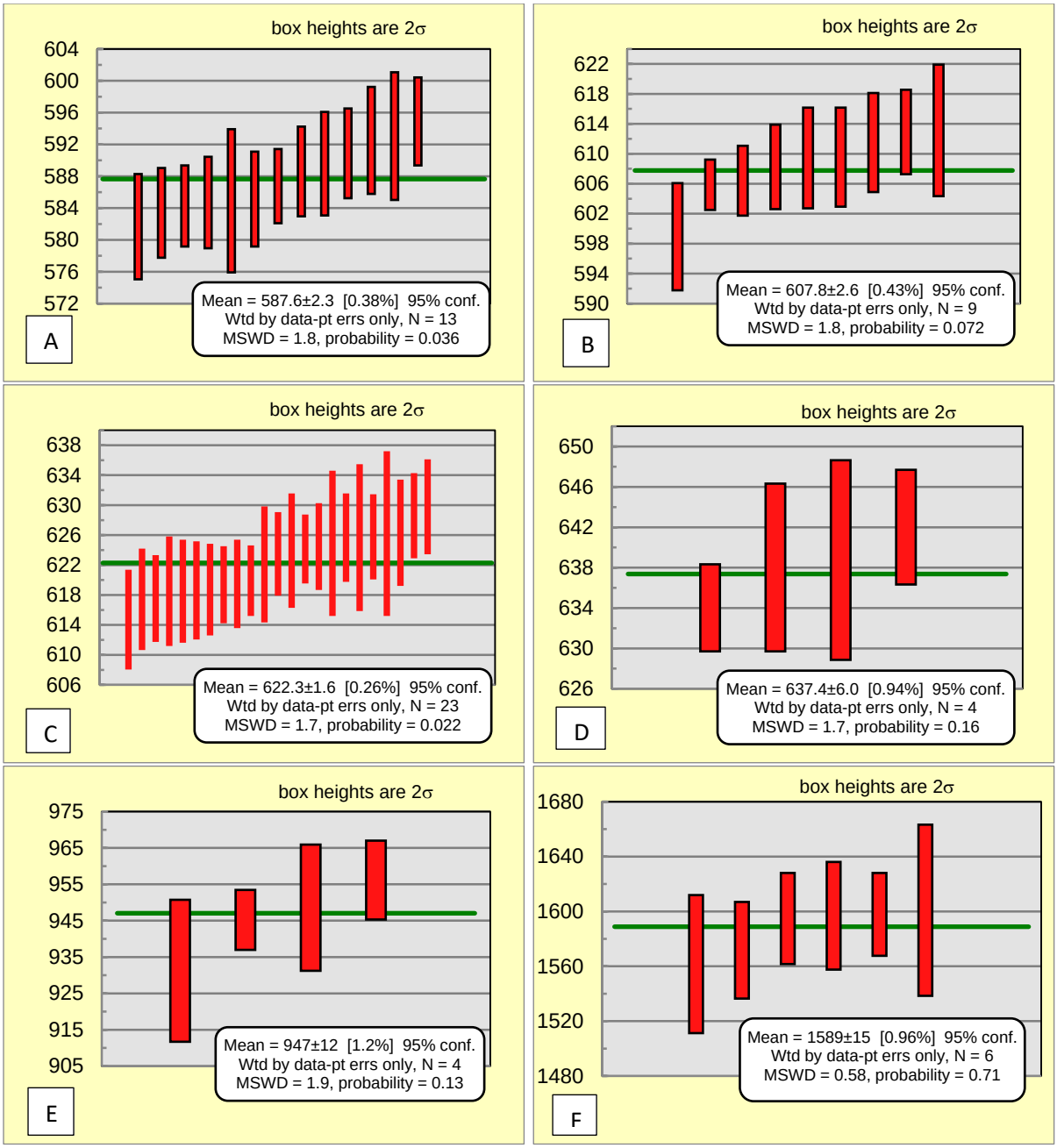

Figure 6.23: Weighted average plots of zircon populations in Ediki kaolins, in increasing population age, A) Youngest population (P1), B) P2, C) P3, D) P4, E) P5, F) P6. *Ages are in Ma, N = Number of analyses*

6.4.5 Logbaba kaolins

6.4.5.1 Concordia of concordant and discordant ages of zircons in Logbaba kaolins

Concordant and discordant ages of 115 analyses are shown in a concordia (Figure 6.24). Below 1500 Ma, one main cluster is observed between 600 and 650 Ma (Figure 6.24A). Two

very discordant analyses yielded ages below 10 Ma. Above 1500 Ma (Figure 6.24B), there were more discordant analyses and a main cluster between 2000 and 2100 Ma.

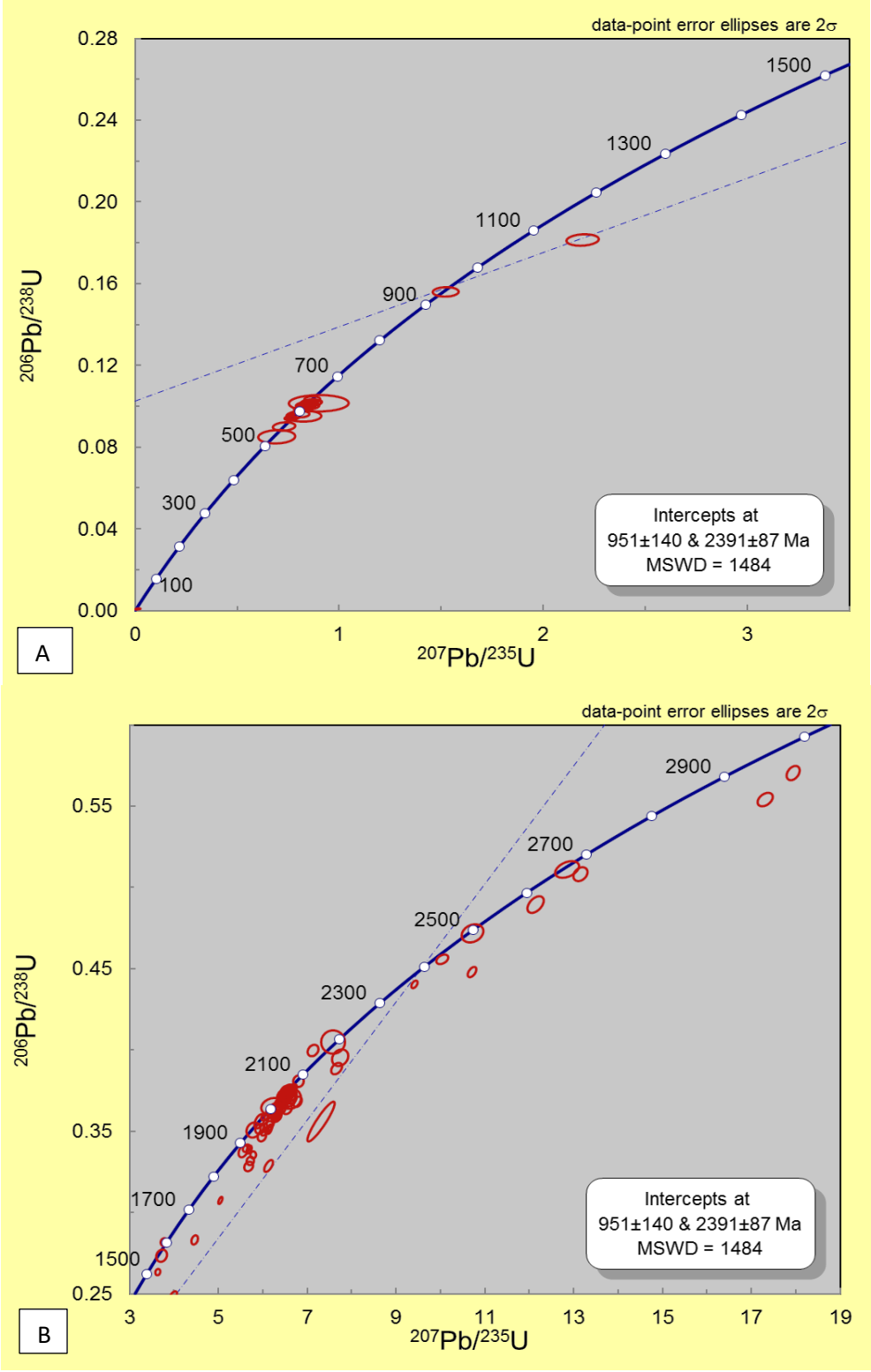

Figure 6.24: Concordia of concordant and discordant ages of zircons in Logbaba kaolins, A) Ages < 1500 Ma, B) Ages < 1500 Ma

6.4.5.2 Probability density plot of Logbaba zircons

A total of 106 analyses were ≤ 10% discordant. Two main peaks were obtained on the probability density plot (Figure 6.25). The most dominant peak was around 600-650 Ma, with about 40 of the analyses. The second peak was between 2000 and 2100 Ma, with about 35 of analyses. Little clusters showed Archean ages (> 2500 Ma).

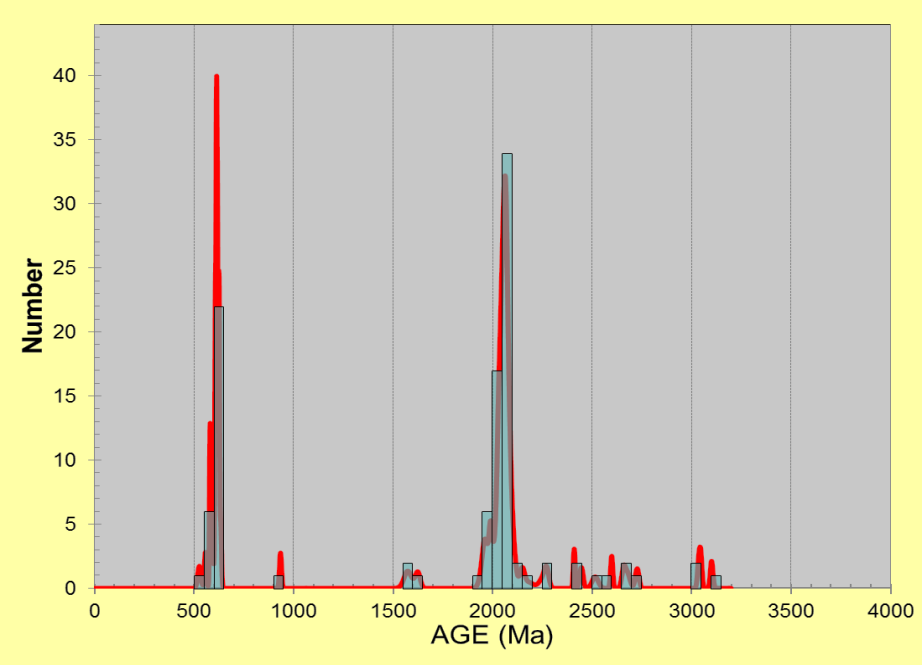

Figure 6.25: Probability density plot of Logbaba zircons showing different clusters of zircon ages. Bin width = 50 Ma

6.4.5.3 Weighted averages of zircon populations at Logbaba

Eighty-eight analyses were ≤ 5% discordant. These gave 6 zircon populations (Figure 6.26). The first and youngest population (P1) had a weighted average of 587.7 ± 4.4 Ma (MSWD = 0.99, N = 3), the 2nd population (P2) had a weighted average of 610.8 ± 2.5 Ma (MSWD = 1.8, N = 10), the 3rd population (P3) had a weighted average of 622.8 ± 2.2 Ma (MSWD = 1.2, N = 7), the 4th population (P4) had a weighted average of 1969 ± 17 Ma (MSWD = 1.6, N = 6). The 5th and 6th populations (P5 and P6, respectively) were the most abundant. They had a weighted average of 2047.0 ± 4.9 Ma (MSWD = 1.18, N = 26) and 2075.9 ± 4.6 (MSWD = 0.92; N = 20), for P5 and P6 respectively. At a discordancy ≤ 5%, older ages were dominant, unlike at a discordance ≤ 10%, younger ages were more dominant.

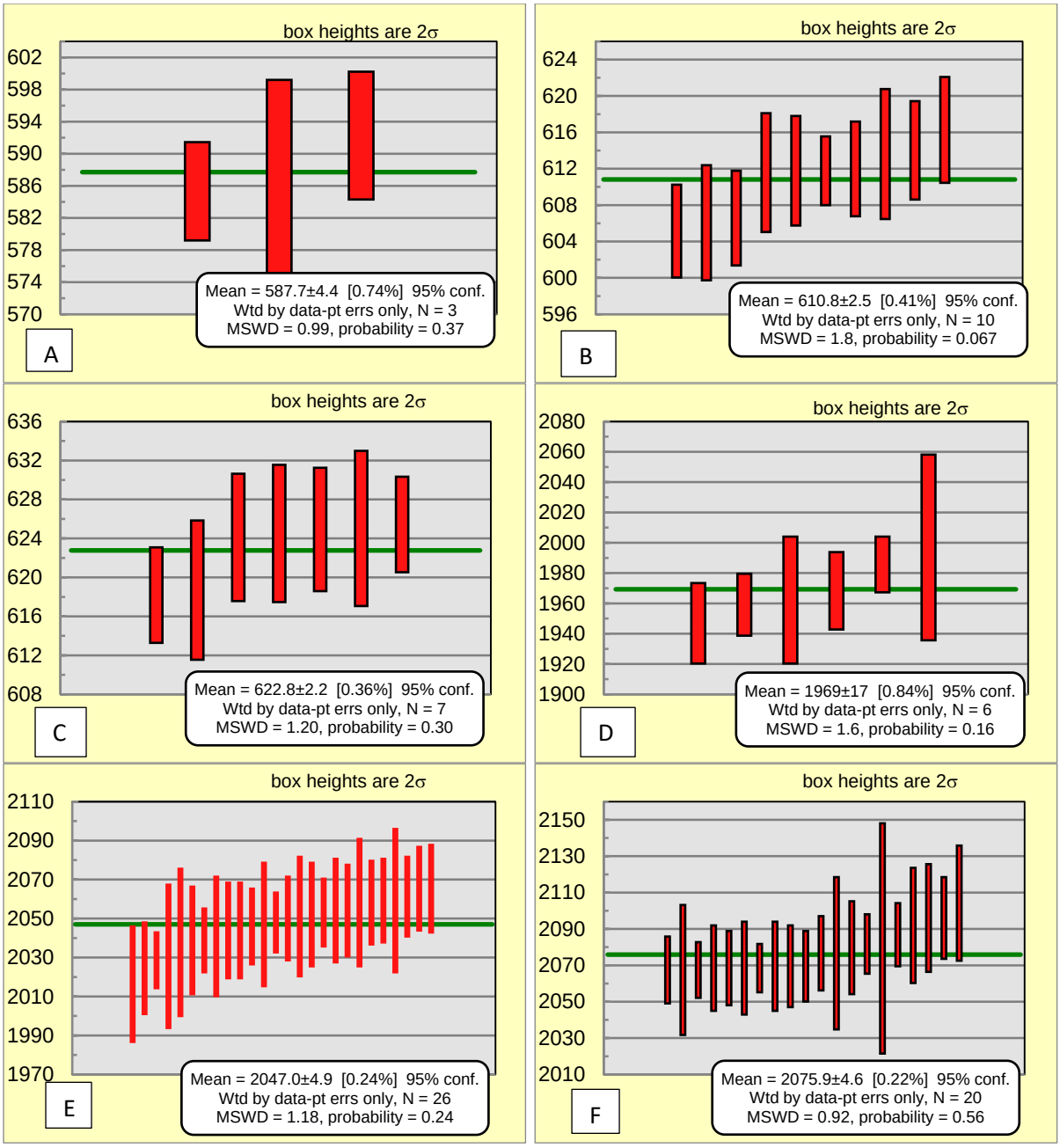

Figure 6.26: Weighted average plots of zircon populations in Logbaba kaolins, in increasing population age, A) Youngest population (P1), B) P2, C) P3, D) P4, E) P5, F) P6. *Ages are in Ma, N = Number of analyses*

6.4.6 Missole kaolins

6.4.6.1 Concordia of concordant and discordant ages of zircons in Missole kaolin

Due to the small particle sizes and the presence of cracks in zircons in Missole kaolin, only 72 analyses were carried out, most of which were discordant. The results are showed in Figure 6.27. Below 1500 Ma, a cluster was obtained between 500 and 700 Ma; whereas above 1500

Ma, no clusters were obtained. The presence of cracks contributed to a gain in ^{204}Pb, which resulted in discordant ages.

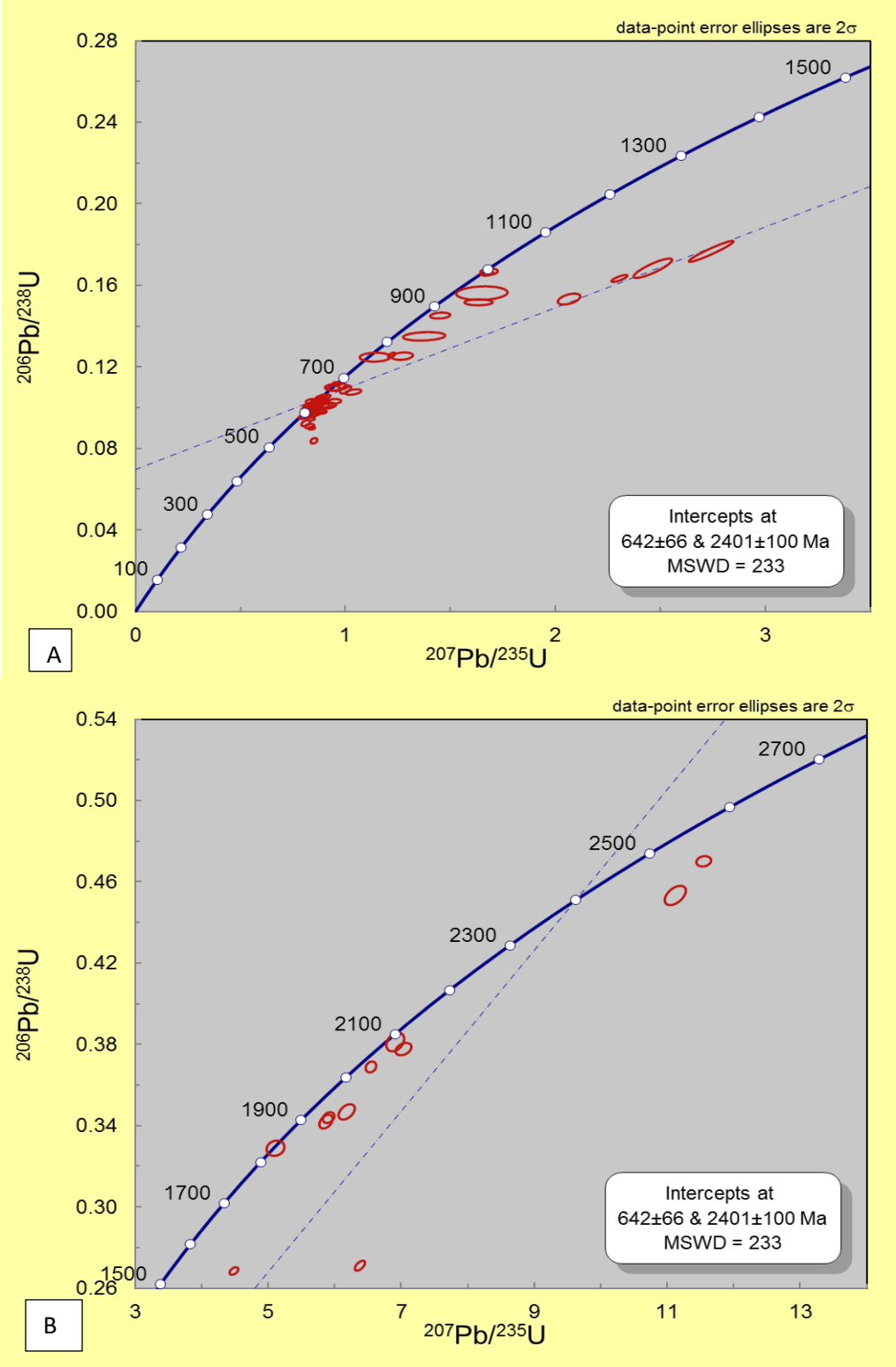

Figure 6.27: Concordia of concordant and discordant ages of zircons in Missole kaolins, A) Ages < 1500 Ma, B) Ages < 1500 Ma

6.4.6.2 Probability density plot of Missole zircons

Of the 72 analyses carried out, 41 yielded ages that were ≤ 10% discordant. One main peak was obtained around 600 Ma, with 18 analyses. A second peak, around 1000 Ma was made up of 4 analyses. About 7 analyses gave ages between 1800 and 2200 Ma, and two analyses gave ages around 2600 Ma (Figure 6.28).

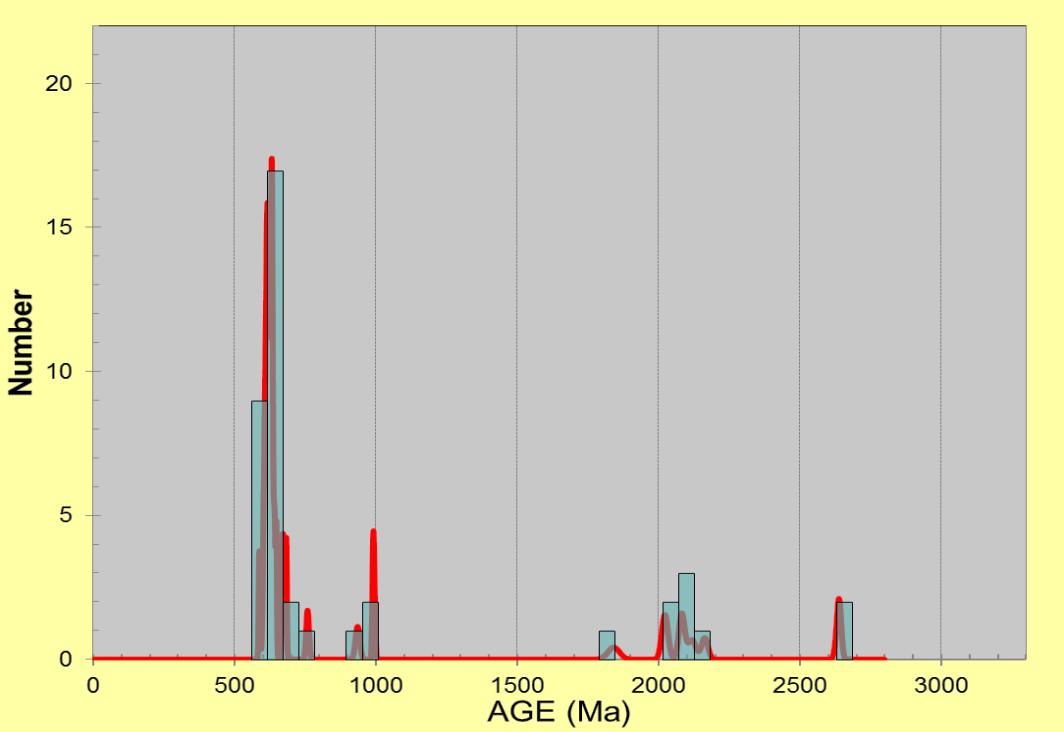

Figure 6.28: Probability density plot of Missole zircons showing different clusters of zircon ages. Bin width = 50 Ma

6.4.6.3 Weighted averages of zircon populations at Missole

Twenty-nine analyses gave ages ≤ 5% discordant, resulting in three populations (Figure 6.29). The first population (P1) had a weighted average of 611.5 ± 2.2 Ma (MSWD = 1.17, N = 6), the 2nd population (P2) had a weighted average of 619.9 ± 2.5 Ma (MSWD = 0.95, N = 4), and the 3rd and last population (P3) had a weighted average of 631.7 ± 1.9 Ma (MSWD = 0.63, N = 6).

Thirteen ≤ 5% discordant ages did not fall in any populations because they didn't form a cluster. The youngest age was 587 ± 4 Ma (96% concordant); whereas the oldest age was 2163 ± 23 Ma (95% concordant).

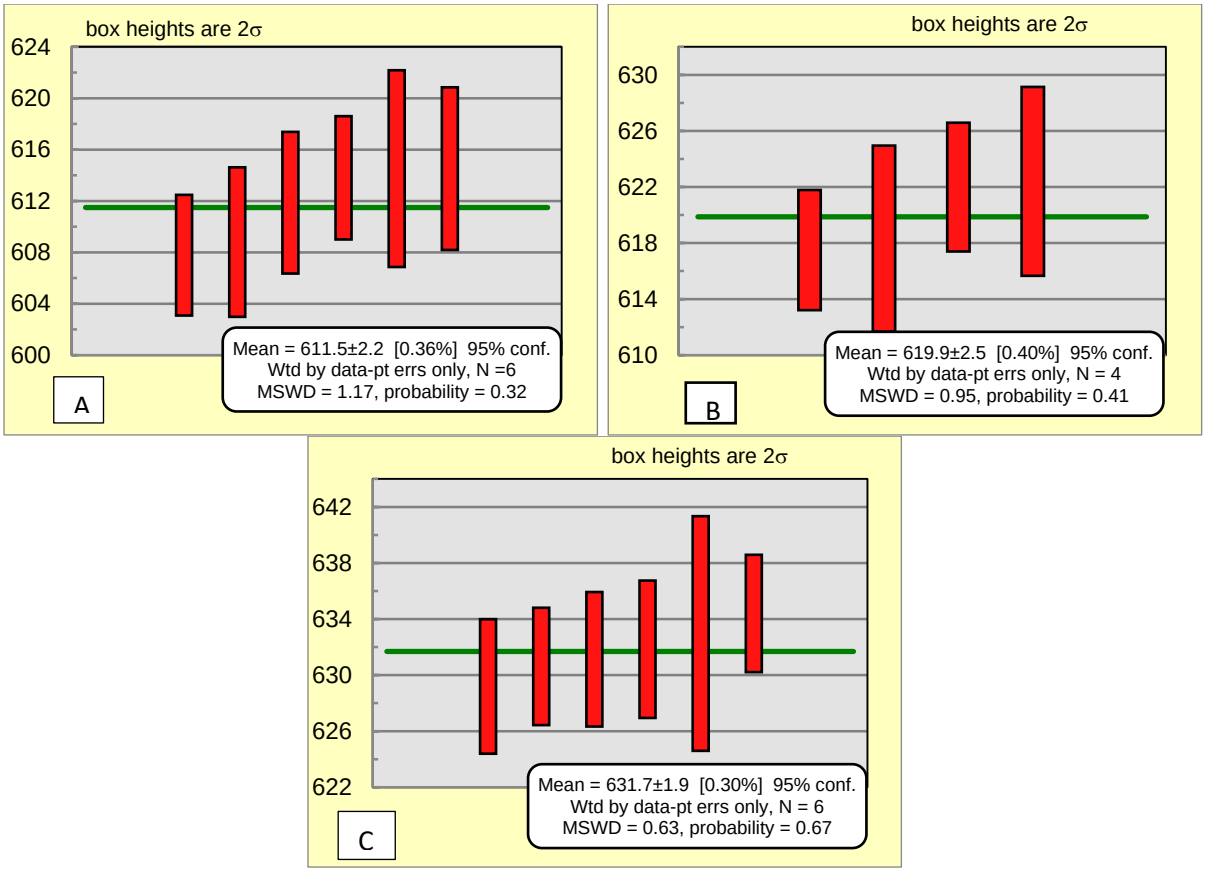

Figure 6.29: Weighted average plots of zircon populations in Missole kaolins, in increasing population age, A) Youngest population (P1), B) P2, C) P3. *Ages are in Ma, N = Number of analyses*

6.4.7 Yatchika kaolin

6.4.7.1 Concordia of concordant and discordant ages of zircons in Yatchika kaolin

Figure 6.30 shows concordant and discordant ages of zircons in Yatchika kaolin. Below 1500 Ma, few discordant ages are observed and a cluster between 500 and 700 Ma (Figure 6.30A). The youngest age was 558 ± 2 Ma (95% concordant). Above 1500 Ma, most of the discordant ages plotted close to the concordia. A main cluster is found between 1900 and 2100 Ma (Figure 6.30B). Another cluster, though made up of discordant ages, is found around 2500 Ma. The oldest grain was 3250 ± 13 Ma (99% concordant).

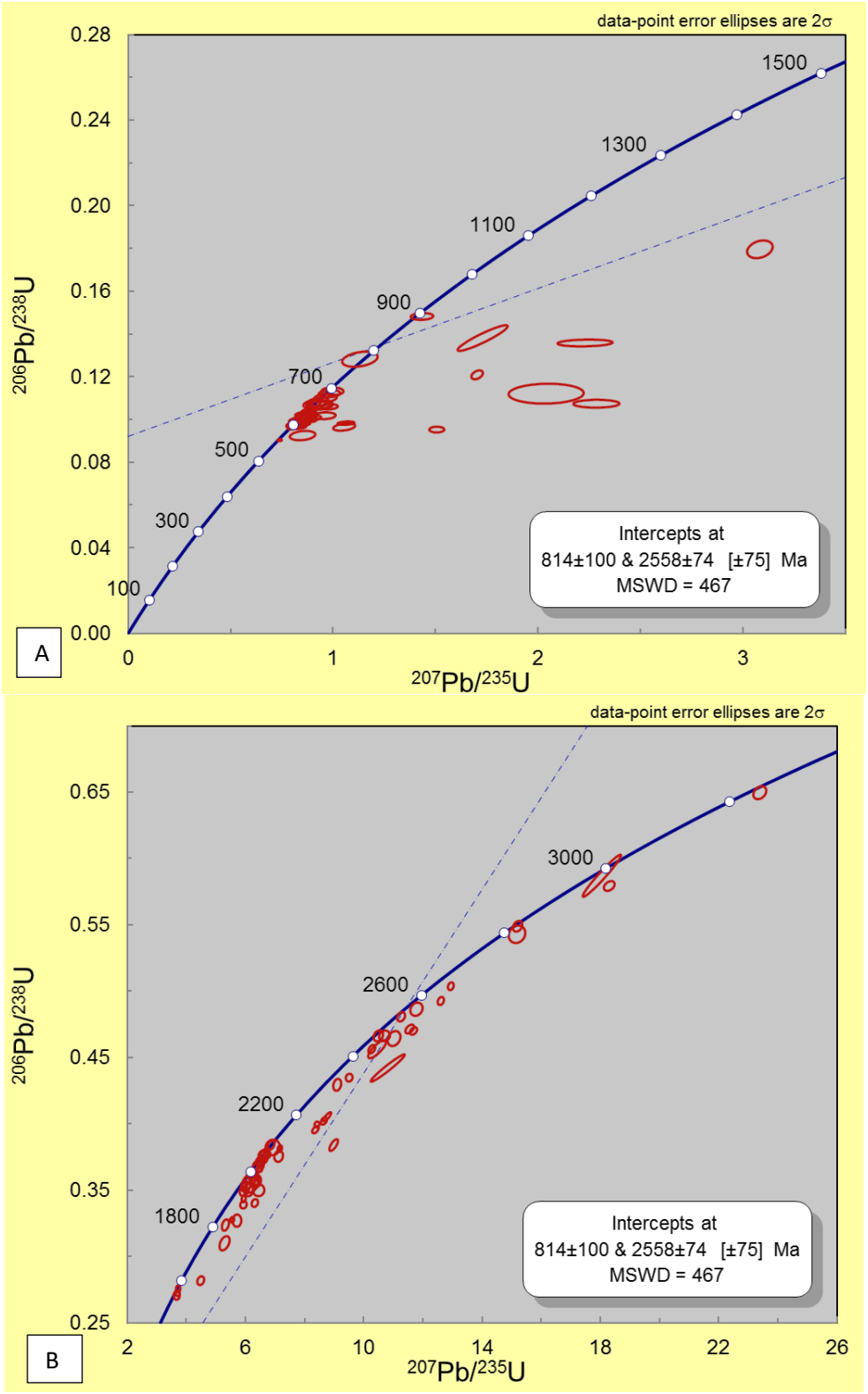

Figure 6.30: Concordia of concordant and discordant ages of zircons in Yatchika kaolins, A) Ages < 1500 Ma, B) Ages < 1500 Ma

6.4.7.2 Probability density plot of Yatchika zircons

The probability density plot of zircon ages that were ≤ 10% discordant is shown in Figure 6.31, with 111 analyses. The most dominant peak was around 600 Ma and contained about 36 analyses, the second peak was around 2100 Ma. Many analyses yielded ages between 2300 and 3300 Ma.

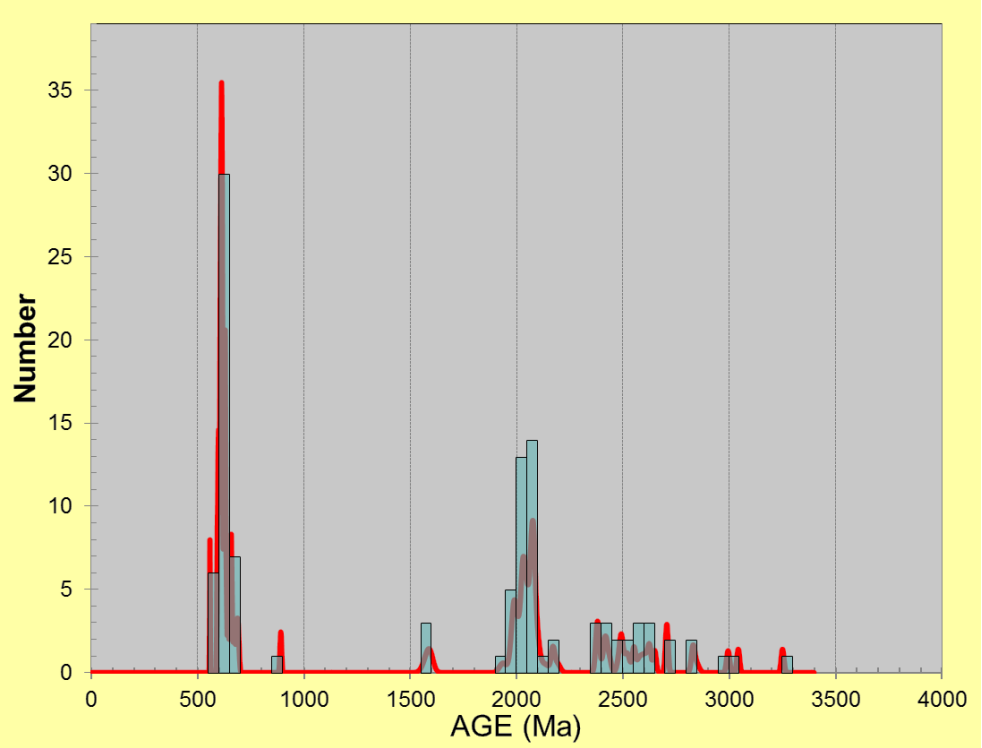

Figure 6.31: Probability density plot of Yatchika zircons showing different clusters of zircon ages. Bin width = 50 Ma

6.4.5.3 Weighted averages of zircon populations at Yatchika

Eight-nine analyses yielded ages that were ≤ 5% discordant (95-105% concordant), and 9 populations were derived. The first and youngest population (P1) had a weighted average of 596.4 ± 4.0 Ma (MSWD = 1.9, N = 6), the 2nd and largest population (P2) had a weighted average of 610.9 ± 1.8 Ma (MSWD = 1.9, N = 18). The 3rd population (P3) had a weighted average of 628.6 ± 3.1 Ma (MSWD = 1.9, N = 8), the 4th population (P4) had a weighted average of 656.2 ± 5.0 Ma (MSWD = 0.65, N = 3), the 5th population (P5) had a weighted average of 1586 ± 19 Ma (MSWD = 0.30, N = 3), the 6th population (P6) had a weighted average of 1988 ± 12 Ma (MSWD = 0.87, N = 4), the 7th population (P7) had a weighted average of 2029.5 ± 7.2 Ma (MSWD = 0.68, N =10), the 8th population (P8) had a weighted

average of 2075.7 ± 5.6 Ma (MSWD = 0.59, N =13). The 9th and oldest population (P9) had a weighted average of 2492 ± 10 Ma (MSWD = 0.90, N =3).

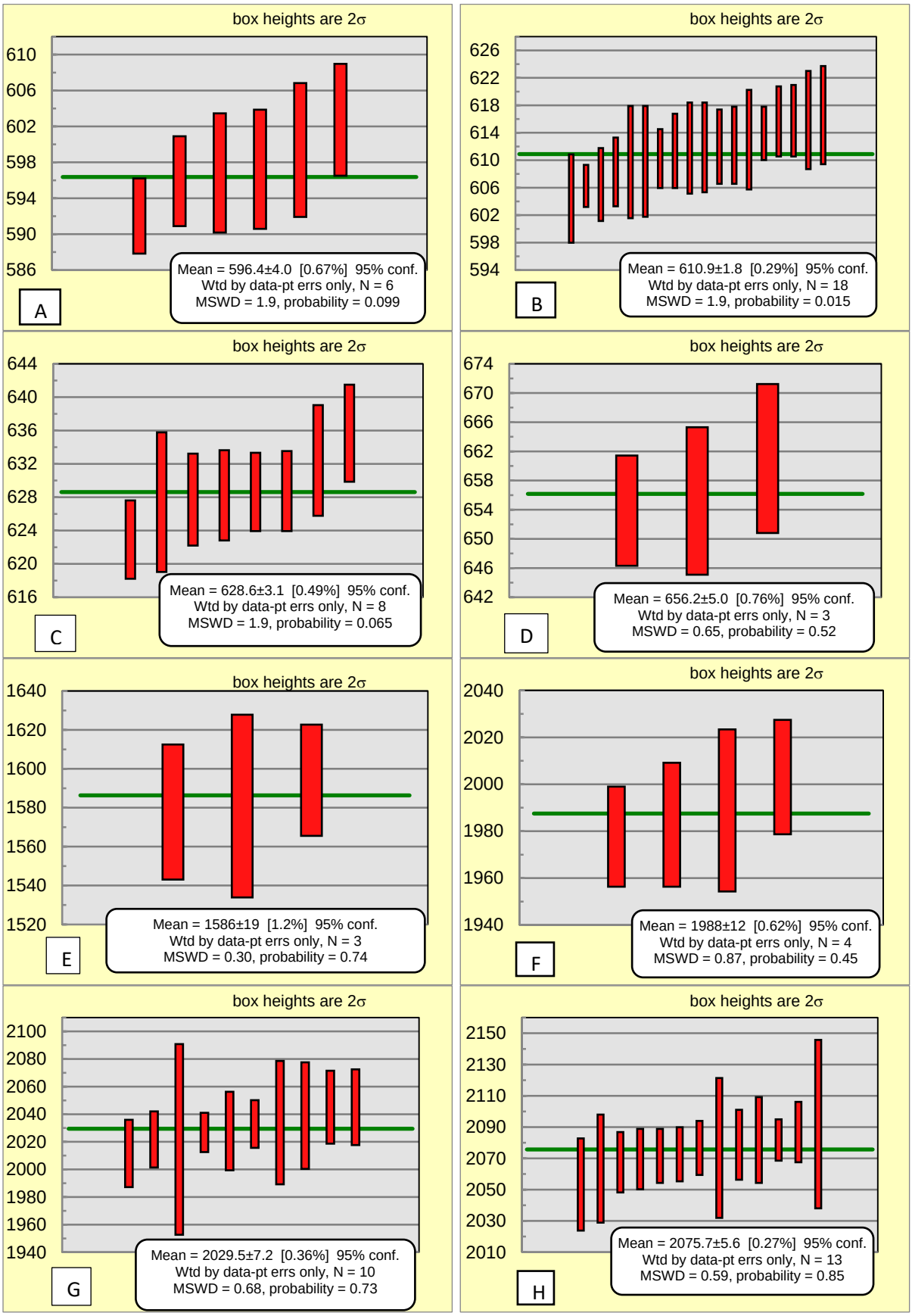

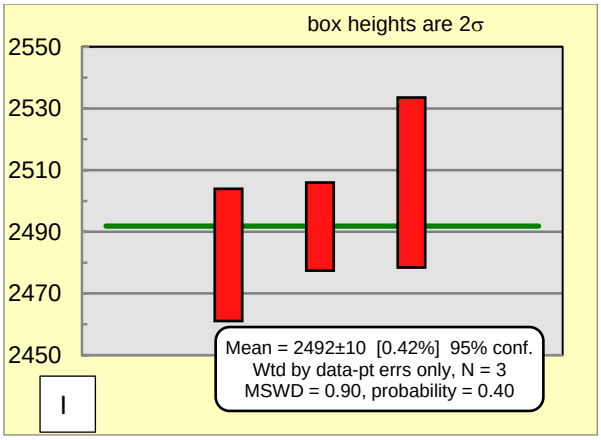

Figure 6.32: Weighted average plots of zircon populations in Yatchika kaolins, in increasing population age, A) Youngest population (P1), B) P2, C) P3, D) P4, E) P5, F) P6, G) P7, H) P8, I) P9. *Ages are in Ma, N = Number of analyses*

Twelve older ages between 2523 ± 10 Ma and 3250 ± 13 Ma were also ≤ 5% discordant but did not form clusters of three to make a population.

6.5 Discussion

6.5.1 Maximum deposition age of kaolins

The maximum possible age of deposition of the kaolins was inferred using the weighted average of the youngest zircon population at 95% confidence (Tucker *et al*., 2013). Table 6.1 shows the youngest zircon population age in each kaolin deposit and its corresponding Period.

Table 6.1: Youngest zircon population age (P1) in kaolins and their corresponding Periods

Kaolin deposit	Age of host Formation	P1	Period	Era
Bomkoul	Tertiary	606 ± 3 Ma		
Dibamba	Tertiary	608 ± 2 Ma		
Ediki	Cretaceous	588 ± 2 Ma	Ediacaran	Neoproterozoic
Logbaba	Cretaceous	588 ± 4 Ma	(630-542 Ma)	(1000-542 Ma)
Missole	Tertiary	612 ± 2 Ma		
Yatchika	Cretaceous	596 ± 4 Ma		

Therefore, the maximum deposition of Cretaceous-Tertiary kaolins in the Douala Sub-Basin was during the Ediacaran Period. It is, however, important to note that the maximum deposition ages of Tertiary kaolins are older than those of Cretaceous kaolins. This could be

due to the fact that the youngest populations in Cretaceous kaolins were obtained from the analysis of zircon rims (therefore having older cores); whereas the youngest populations in Tertiary kaolins were obtained from the analysis of zircon cores.

6.5.2 Provenance of Cretaceous-Tertiary kaolins of the Douala Sub-Basin and implications to tectonics

Figure 6.33 shows probability density plots of zircon ages in kaolin deposits in the Douala Sub-Basin. In this Figure, plots of Cretaceous Formations are separated from Tertiary ones, to better visualise the age clusters of zircons. All six locations have prominent peaks between 650 and 550 Ma, corresponding to the Ediacaran. In all locations, except Yatchika (Cretaceous), peaks are observed between 1050 and 950 Ma, corresponding to Late Stenian and Tonian (1000-850 Ma) Periods. The Cryogenian (850-635 Ma), which is the Period between Tonian and Ediacaran is represented in all zircons, except Logbaba zircons. All three Periods (Ediacaran, Cryogenian and Tonian) belong to the Neoproterozoic Era (1000-541 Ma).

A peak around 1600 Ma, which marks the boundary between the Paleoproterozoic (2500-1600 Ma) and the Mesoproterozoic (1600-1000 Ma), is present in all Cretaceous Formations but absent in Tertiary Formations. The Paleoproterozoic is greatly present in Cretaceous Formations; mainly in Logbaba and Yatchika kaolins (~2200-1900 Ma), which also contain Mesoarchean (3200-2800 Ma) zircons.

Two main orogenies occurred in Central Africa, the Eburnean at ~2400 to 1800 Ma (Owona *et al*., 2013) and the Pan African at ~730-550 Ma (Black and Liegeois, 1993). The main age clusters of zircons in this study show that the zircons probably originated from both orogenies. The Douala Sub-Basin is bounded to the Northeast by the Benue Trough, to the East by the Late Proterozoic Pan-African mobile belt and to the Southeast by the Archean to Early Proterozoic Congo Craton (Meyers *et al*., 1996). The sediments found in the Douala Sub-basin should have their sources from any of these geologic formations. However, the Benue Trough, which is made up of Cretaceous-Tertiary sediments (Petters, 1978), cannot be considered a source of zircons in Cretaceous-Tertiary kaolins in the Douala Sub-Basin because the youngest zircon populations in this study are dated Neoproterozoic. The Benue Trough will therefore not be discussed.

The oldest zircon populations found in Yatchika and Logbaba kaolins (Mesoarchean) might have been derived from the Congo Craton, mainly the Ntem Complex, which is its north-

western part and the oldest (Archean age) geologic unit in Cameroon. Due to high Th/U ratios (> 0.1), reflecting the magmatic origin of the zircons (Verma *et al*., 2016), it is suggested that these older zircons derived from the Late Archaean tonalite–trondhjemite–granodiorites (TTG) and/or high-K granites found in the Ntem Complex (Shang *et al*., 2010).

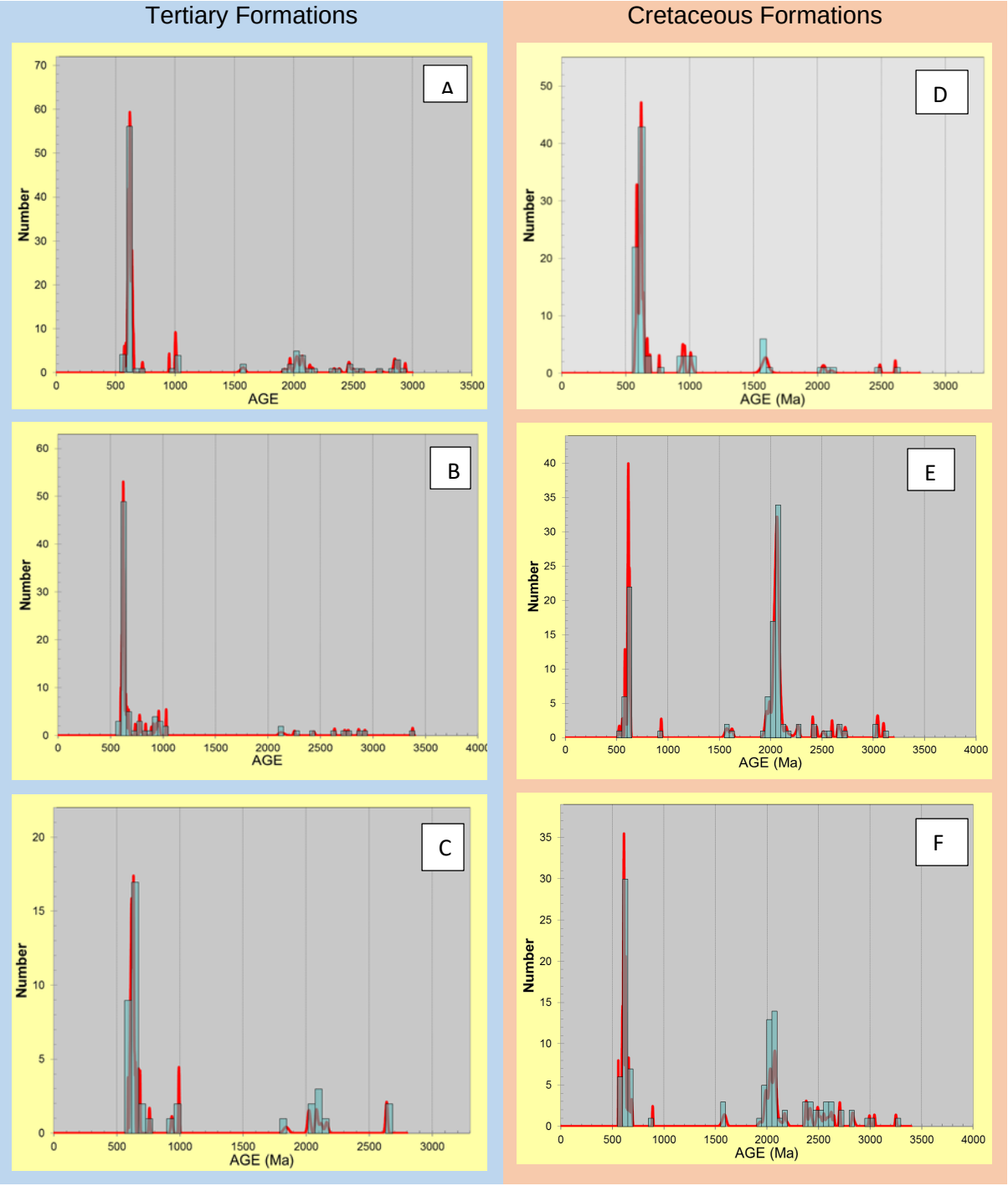

Figure 6.33: Probability density plots of zircon ages in kaolin deposits in the Douala Sub-Basin, A) Bomkoul, B) Dibamba, C) Missole, D) Ediki, E) Logbaba and F) Yatchika

Zircons of Paleoproterozoic ages (1600-2500 Ma) may have been derived from rocks of the Paleoproterozoic Nyong Group. This Group is believed to have been affected by the Eburnean orogeny, which gave rise to metasedimentary and metaplutonic rocks (Lerouge *et al*., 2006); and it is associated to the Borborema and Oaxaquia Provinces in Northeast Brazil and Mexico, respectively (Owona *et al*., 2013).

More than one-third of zircon ages solely fall within the Neoproterozoic Era (541-1000 Ma). Tectonically, this Era is marked by the Pan-African orogeny (730-550 Ma). The Pan-African orogeny was marked by intense reworking of Paleoproterozoic geologic units (Penaye *et al*., 2004). The Yaounde Series is believed to have a Neoproterozoic source marked by the ~650–620 Ma plutonism related to the Pan-African orogeny (Stendal *et al*., 2006). This plutonism (reworking) probably led to the recrystallisation of older zircons or the crystallisation of new zircons and/or zircon rims. The age groups obtained in this research are in agreement with results obtained by Kalsbeek *et al*. (2013), who dated zircons from quartzite, micaceous quartzite and garnet-kyanite paragneiss, all belonging to the Yaounde Group. These zircons yielded ages of Archaean, Palaeoproterozoic, Mesoproterozoic and Neoproterozoic.

Souza *et al*. (2007) dated detrital zircons in sediments of the Cretaceous-Tertiary Capim River kaolins in Brazil; four age plateaus were obtained: 2150, 2020, 1870, and 1510 Ma, belonging to the Paleo- and Mesoproterozoic. Ages between 510 and 800 Ma were also obtained. The most abundant age plateaus were 2150 and 2020 Ma, which were correlated to the Transamazonian orogeny (corresponding to the Eburnean orogeny in Africa). The 2150 and 2020 Ma were also present in Cretaceous kaolins of the Douala Sub-Basin, though they were not the most dominant. The 510 and 800 Ma age plateau were correlated with the Brasiliano orogeny (corresponding to the Pan-African orogeny in Africa). Few Archean ages were also obtained.

Moreover, Kalsbeek *et al*. (2013) also correlated ages of detrital zircons in West Africa to those in the Borborema Province in Northeast Brazil. Analysis of detrital zircons from Brazil yielded two main age ranges, the 1st between 2200-2000 Ma (Paleoproterozoic), the most dominant, and the second between 1000-600 Ma (Neoproterozoic). These ages correspond to the Eburnean (Amazonian in South America) and the Pan-African (Brasiliano in South America) orogenies, respectively.

It is important to note that the detrital zircons from Northern and Northeast Brazil are dominated by older zircons (Eburnean/Transamazonian age); whereas, detrital zircons from Central and West Africa are dominated by younger zircons (Pan-African/Brasiliano age).

6.5.3 Geochronological implications in the paleoclimatic setting of the Douala Sub-Basin and time of kaolinisation

The maximum depositional age of Cretaceous-Tertiary kaolins, obtained from the youngest population ages of zircons contained in these kaolins, indicated Neoproterozoic ages. However, the Neoproterozoic is believed to have been characterised by periods with a global glaciated Earth, referred to as the Snowball Earth (Donnadieu *et al*., 2003; 2004). Hence, kaolins of the Douala Sub-Basin could not have been deposited during the Neoproterozoic. A humid climate characterised by warm temperatures and high rainfall are environmental conditions that favour formation (Harvey and Murray, 1997) and deposition of kaolins.

However, the Late Cretaceous and Early) Tertiary Periods experienced warm temperatures particularly at the Equator, non-varying and without ice (Barron, 1983; 1993; Valdes, 2000; Sijp *et al*., 2014). Moreover, analyses of stable oxygen and hydrogen in studied kaolins showed that kaolinitisation during the Cretaceous occurred at temperatures about 3^{o}C cooler than the Tertiary (26.58^{o}C ± 9.65^{o}C for Cretaceous kaolins and 29.40^{o}C ± 7.22^{o}C for Tertiary kaolins). A 2-3°C temperature change in deep water temperatures was also observed from Mid-Cretaceous throughout the Tertiary by Baron (1983).

In addition, since the Late Cretaceous (Maastrichtian), the Douala Sub-Basin has been in a high rainfall regime (Parrish *et al*., 1982; Tardy *et al*., 1991), due to its proximity to the Equator. The high rainfalls during these Periods would have greatly favoured kaolinisation and resulted to deposition of the studied Cretaceous-Tertiary kaolins in the Douala Sub-Basin.

Therefore, Neoproterozoic maximum depositional ages reflected by the youngest zircon populations probably refer to maximum depositional ages of primary materials that altered in a humid climate during the Cretaceous-Tertiary leading to kaolinisation in the Douala Sub-Basin.

6.6 Synopsis

Radiogenic dating of Cretaceous-Tertiary kaolins in the Douala Sub-Basin using U-Pb LA-SFICP-MS was carried out. Four main zircon populations were identified: the 1st between 650 and 550 Ma, the 2nd between 1050 and 950 Ma, the 3rd around 1600 Ma and the 4th between 3200-2800 Ma. These four zircon populations belong to the Proterozoic (Neo-, Meso- and Paleoproterozoic) and the Archean. The maximum depositional ages of the kaolins, reflected by the youngest weighted averages of zircon populations varied between 588 ± 2 Ma and 612 ± 2 Ma, all belonging to the Ediacaran Period (Neoproterozoic).

It is proposed that the zircons in Cretaceous-Tertiary kaolins originated from primary minerals that formed during two main tectonic events: the Eburnean orogeny, during which older zircons crystallised and the Pan-African orogeny, during which younger zircons crystallised. The main identified sources of these zircons are the Archean Ntem Complex, the Paleoproterozoic Nyong Group and the Neoproterozoic Yaounde Group. Correlation with studies from Brazil showed that though ages of detrital zircons from Brazil and Cameroon correlate with the Eburnean/Transamazonia and Pan-African/Brasiliano orogenies, detrital zircons from Brazil are dominantly older (Eburnean/Transamazonian ages) than those from Cameroon, which are dominantly younger (Pan-African/Brasiliano).

The glacial climate during the Neoproterozoic was not favourable for kaolinisation, which requires a humid climate with warm temperatures and high rainfall. Therefore, Cretaceous-Tertiary kaolins of the Douala Sub-Basin altered from Neoproterozoic primary materials in a humid climate during Cretaceous and Tertiary Periods.

Validation of hypothesis: Kaolinisation in Cretaceous-Tertiary Formations of the Douala Sub-Basin occurred during Cretaceous and Tertiary Periods.

CHAPTER 7

DIAGNOSTIC EVALUATION OF CRETACEOUS-TERTIARY KAOLINS

7.1 Preamble

The diagnostic evaluation of Cretaceous-Tertiary kaolins from the Douala Sub-Basin was carried out and reported in this chapter (Specific Objective D). The evaluation involved the determination of physical characteristics (particle size, texture, colour and moisture content) and physico-chemical characteristics (pH and electrical conductivity). The relationship of physical and physico-chemical components to mineralogical and geochemical characteristics of the studied kaolins were diagnostically evaluated and linked to the paleoenvironments of formation. Potential industrial applications of the Cretaceous-Tertiary kaolins in the Douala sub-basin will were then be inferred. This chapter is based on Hypothesis D.

HYPOTHESIS D: The physical and physico-chemical properties of studied Cretaceous-Tertiary kaolins will aid in assessing their exploitation in Cameroon.

7.2 Physical characteristics

7.2.1. Particle size distribution

Figures 7.1-7.6 show the particle size distribution (PSD) curves of Cretaceous-Tertiary kaolins in the Douala Sub-Basin. These kaolins are mainly rich in sand and have little or no clay size fractions. In Bomkoul kaolins, BKL 01 and BKL 02 had more silt than BKL 03. Dibamba kaolin layer (DBB) was slightly finer than the clay nodules (DBB CN 01 and DBB CN 02). Ediki and Missole II samples were the finest, though they contained little amounts of clay size fraction. Logbaba, Missole I and Yatchika samples were very rich in sands.

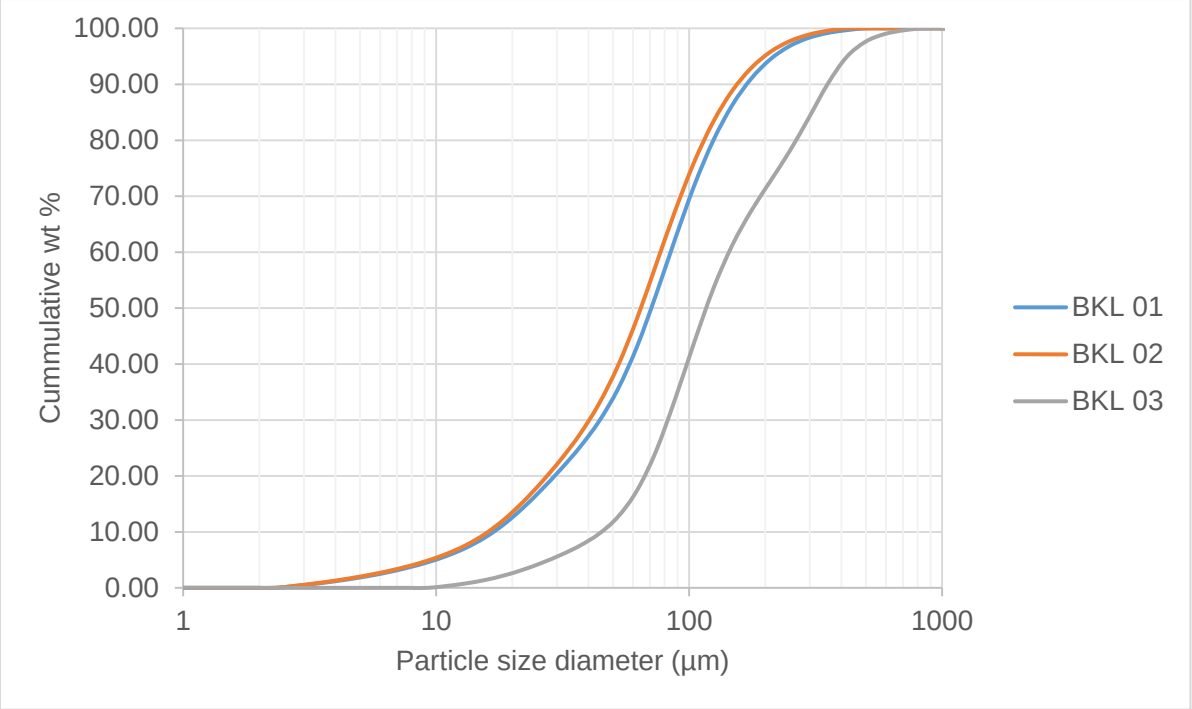

Figure 7.1: Particle size distribution curves of Bomkoul kaolins

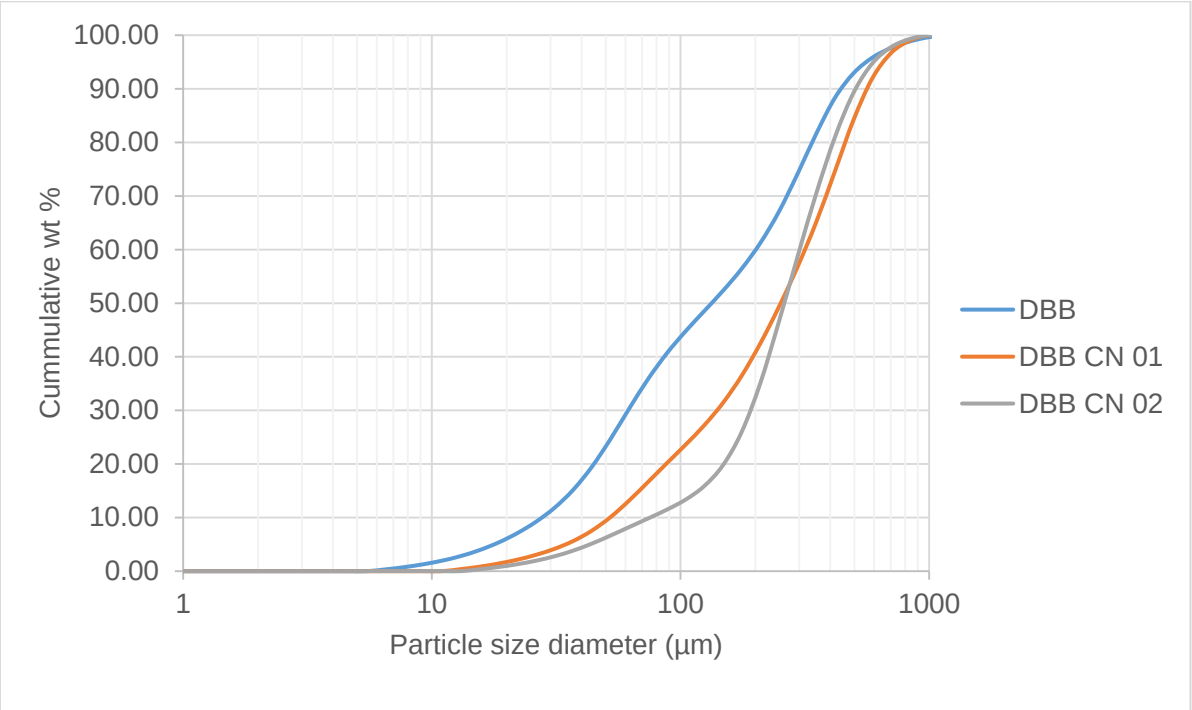

Figure 7.2: Particle size distribution curves of Dibamba kaolins

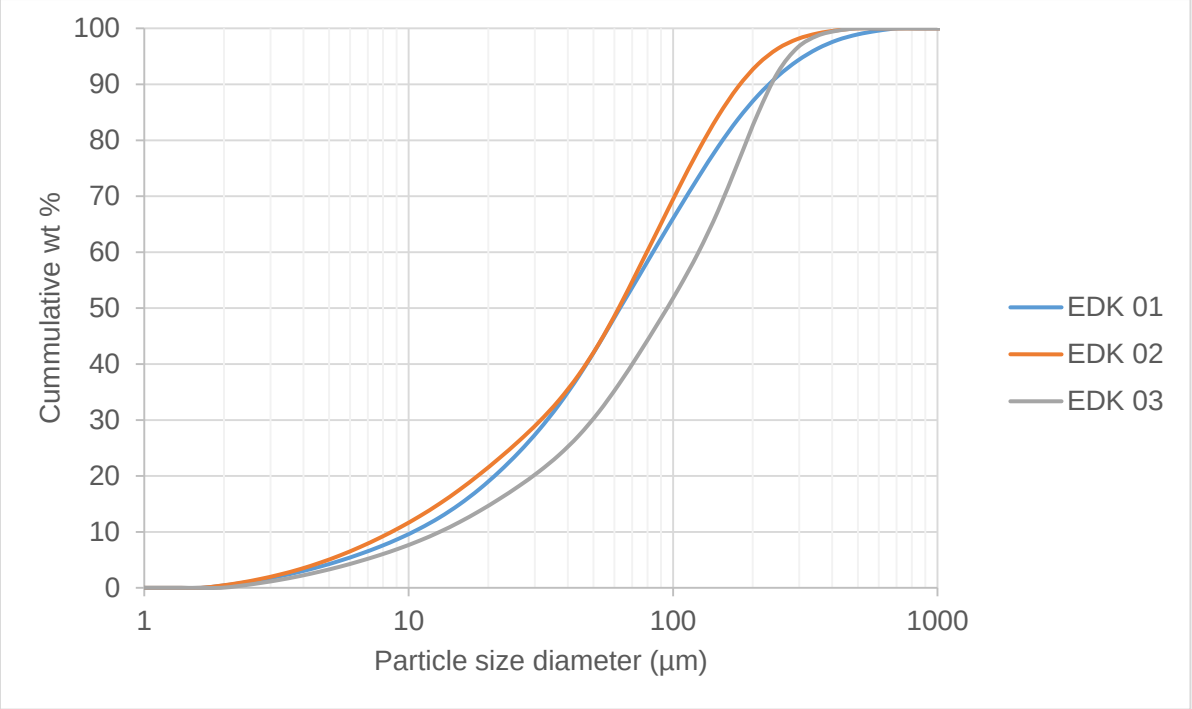

Figure 7.3: Particle size distribution curves of Ediki kaolins

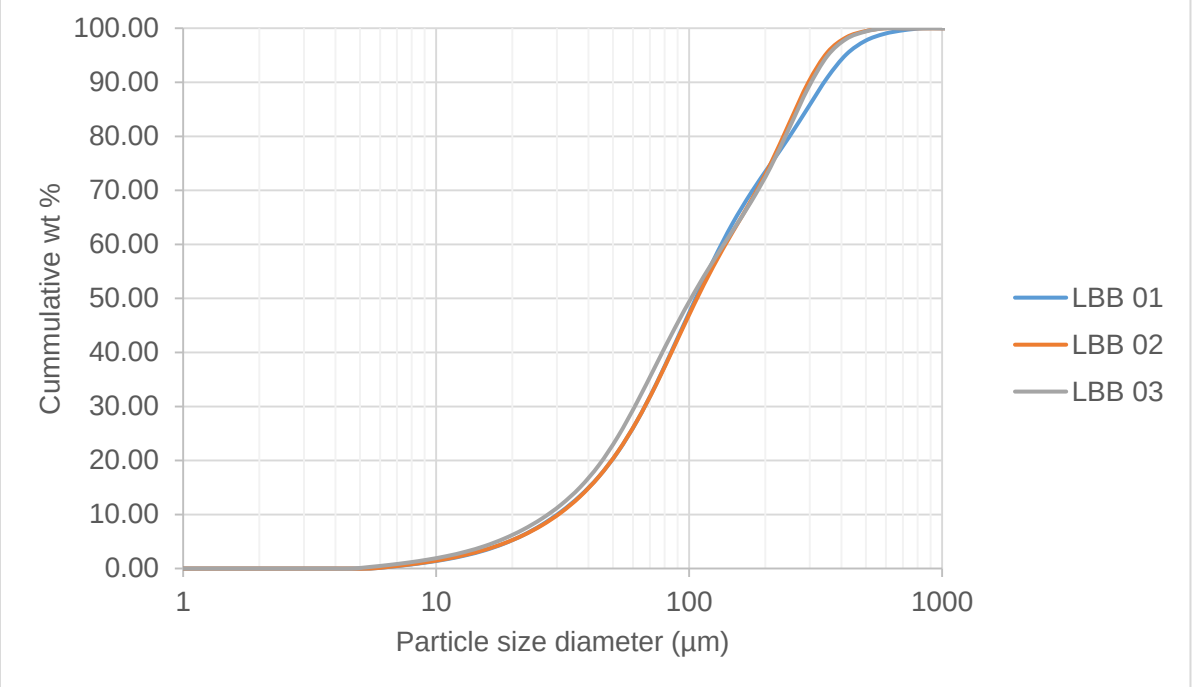

Figure 7.4: Particle size distribution curves of Logbaba kaolins

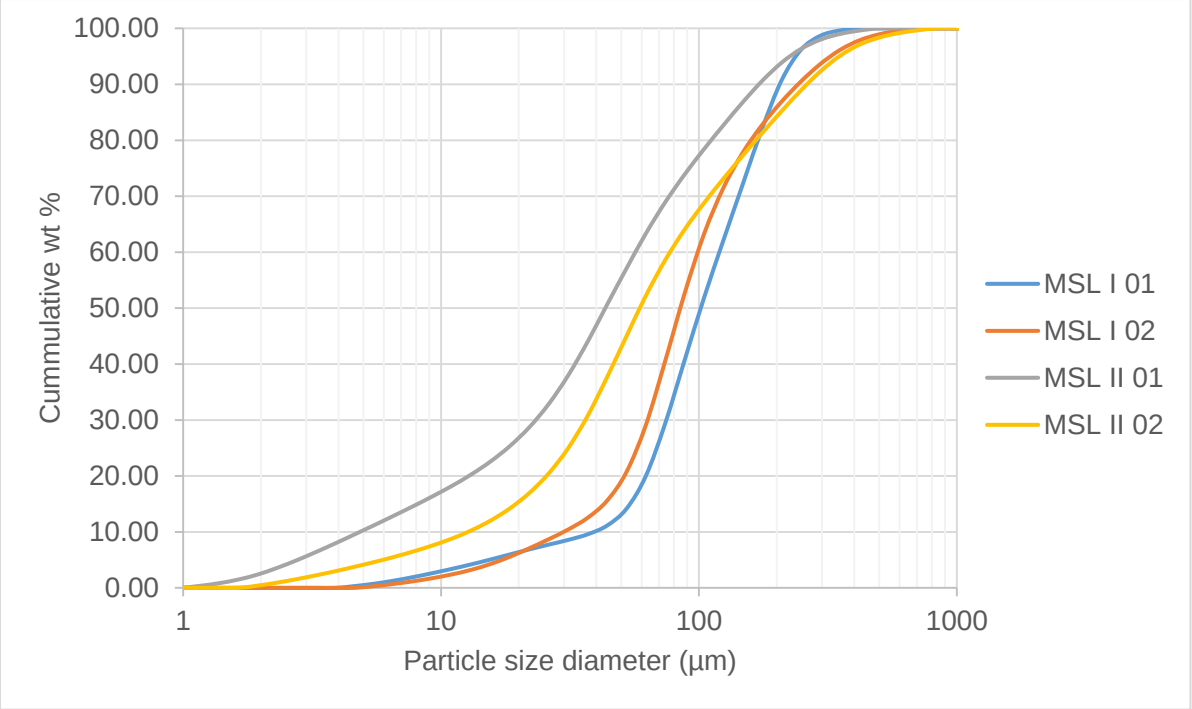

Figure 7.5: Particle size distribution curves of Missole kaolins

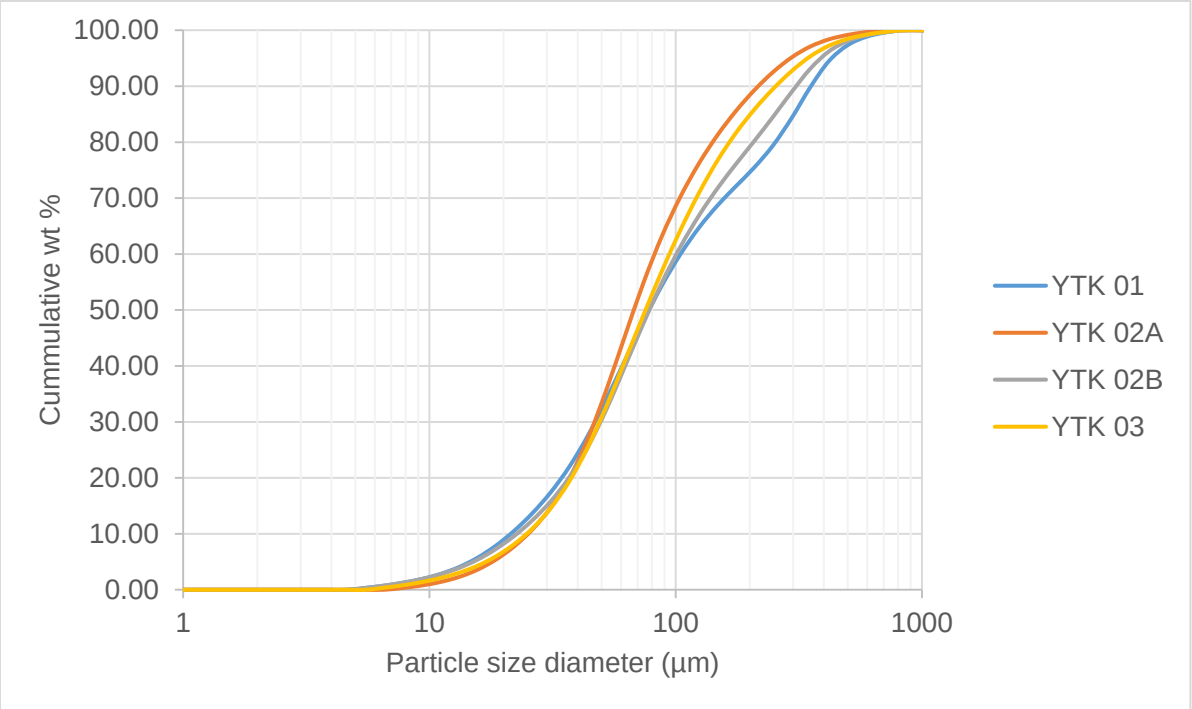

Figure 7.6: Particle size distribution curves of Yatchika kaolins

7.2.2 Texture

Cretaceous-Tertiary kaolin samples of the Douala Sub-Basin have textures that vary from clay to sandy loam, with most samples containing sand (Figures 7.7-7.9). Only 15% of samples had a clay texture (BKL 02, MSL II 02 and YTK 03), 5% had a clay loam texture (EDK 03), 5% had a loamy sand texture (MSL I 02). Sandy clay (BKL 01, Logbaba samples and MSL II 02), sandy loamy clay (BKL 03, DBB, EDK 01, EDK 02 and YTK 01), and sandy loam (DBB CN 01, DBB CN 02, MSL I 02, YTK 02A and YTK 02B) textures were represented by 25% of samples each.

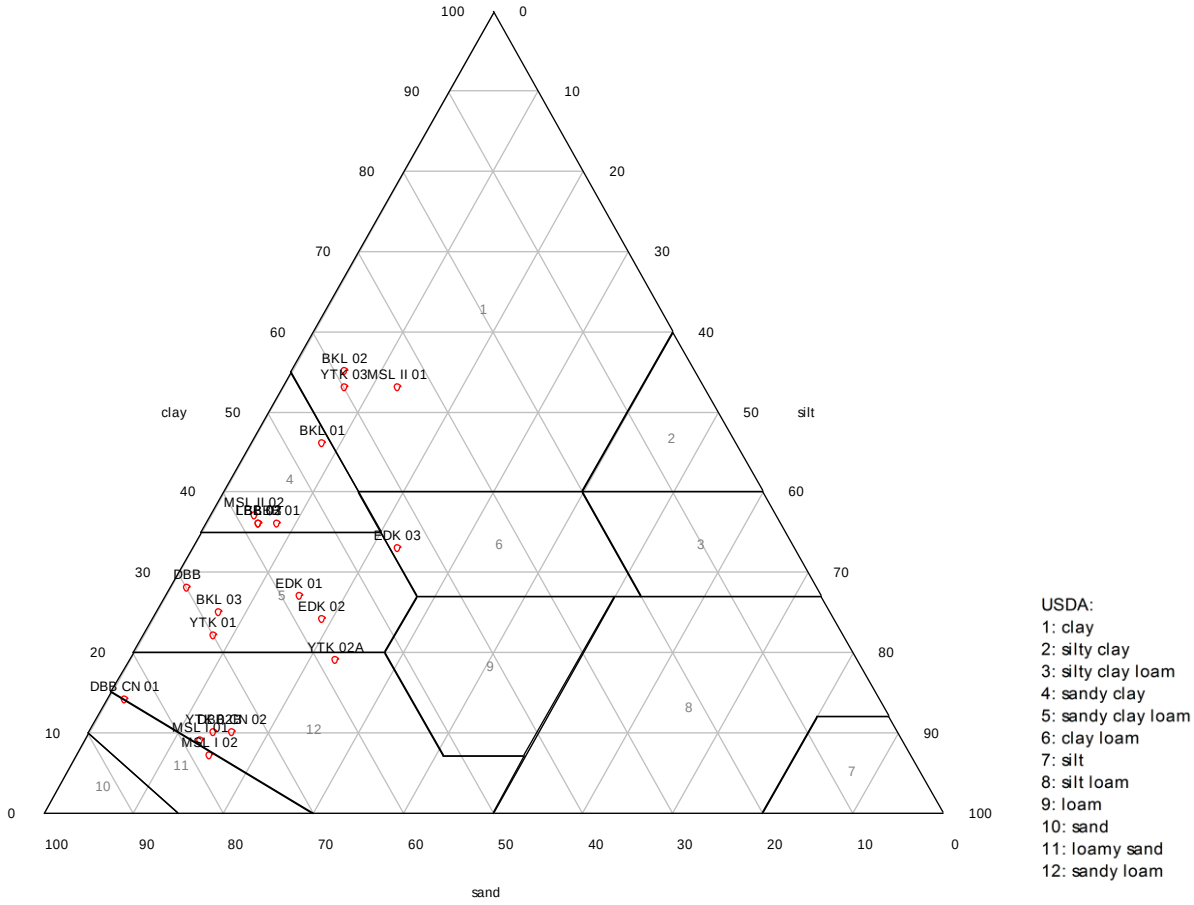

Figure 7.7: Ternary diagram showing kaolins' textures

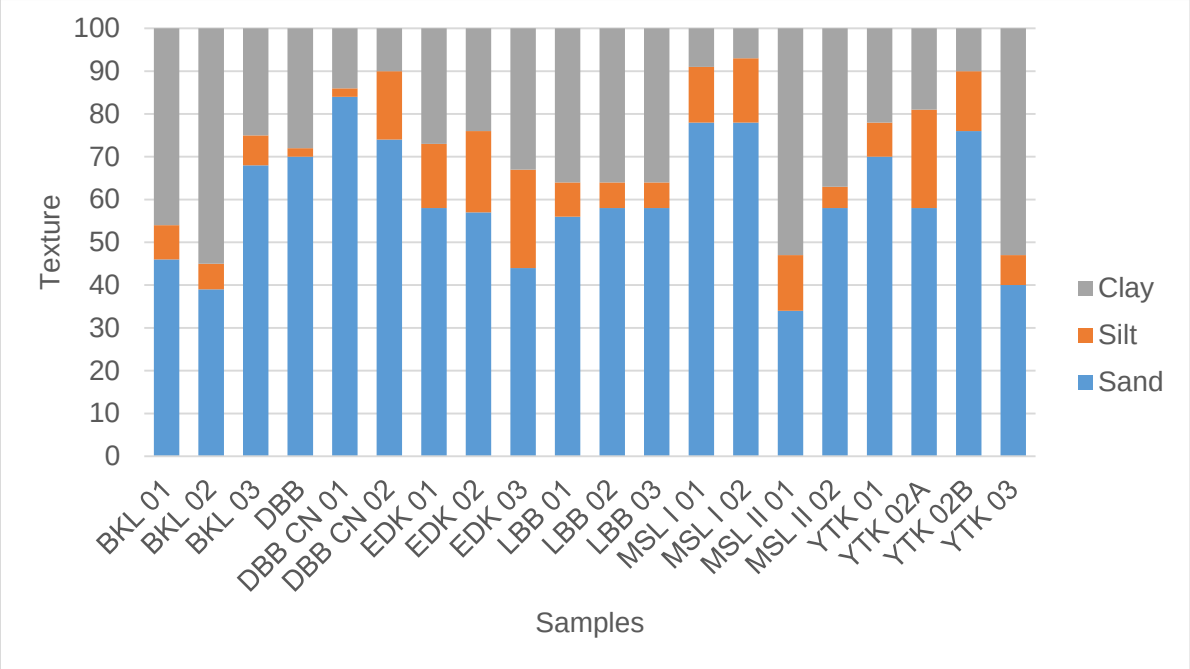

Figure 7.8: Percentage distribution of particle size in studied samples

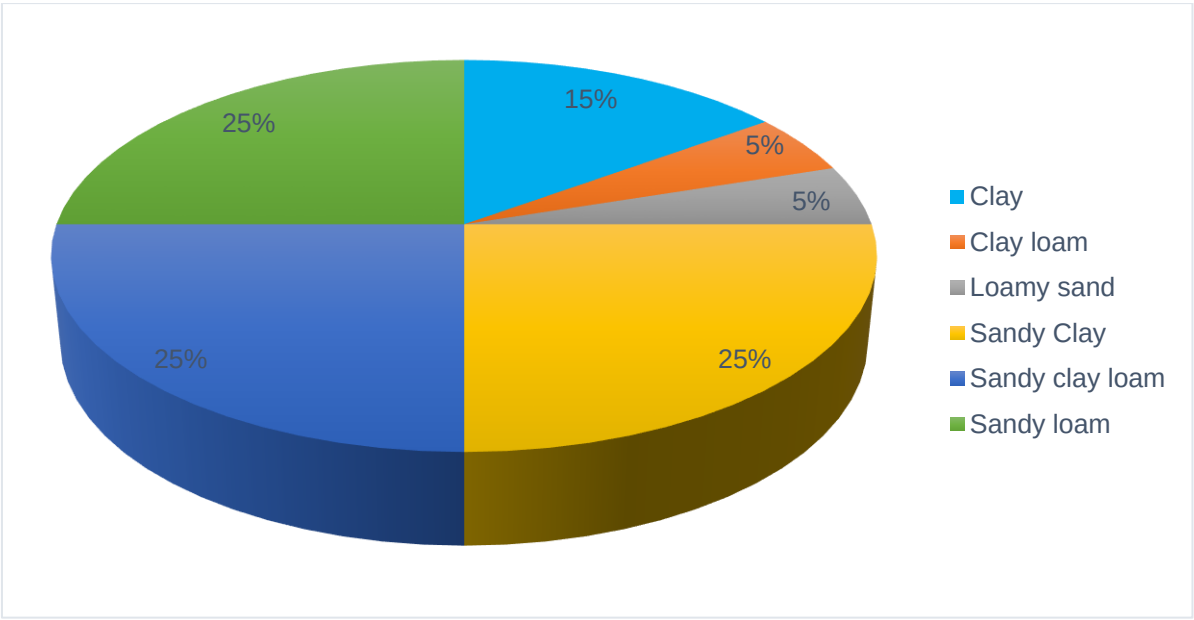

Figure 7.9: Percentage distribution of different textures found in studied kaolins

7.2.3 Colour

Pure kaolin usually has a whitish colour; but most often impurities (iron and titanium) contained in kaolins will cause the colour to have a different tint. Different minerals present in kaolins could also influence their colour. The presence of orthoclase and/or iron-bearing minerals in kaolins will give them a pink, brown, orange or reddish colour. The colour of Cretaceous-Tertiary kaolins of the Douala Sub-Basin, using the hue, value and chroma of samples, is shown in Table 7.1.

Table 7.1: Colour of Cretaceous-Tertiary kaolins of the Douala Sub-Basin

Sample	Hue/Value/Chroma	Colour
BKL 01	5YR/6/4	Light Reddish Brown
BKL 02	5YR/6/4	Light Reddish Brown
BKL 03	10YR/6/6	Brownish yellow
DBB	5YR/8/2	Pinkish white
DBB CN 01	5YR/8/2	Pinkish white
DBB CN 02	10YR/8/6	Yellow
EDK 01	GLEY 1/2/5G	Pale green
EDK 02	GLEY 1/8/5GY	Light greenish grey
EDK 03	GLEY 1/7/5G	Pale green
LBB 01	2.5Y/7/1	Light grey
LBB 02	2.5Y/8/1	White
LBB 03	2.5Y/7/1	Light grey
MSL I 01	5Y/5/1	Grey
MSL I 02	5Y/4/1	Dark grey
MSL II 01	GLEY 1/8/N	White
MSL II 02	GLEY 1/8/10Y	Light greenish grey
YTK 01	10YR/7/8	Yellow
YTK 02A	7.5YR/6/6	Reddish Yellow
YTK 02B	5YR/7/3	Pink
YTK 03	5YR/6/4	Light reddish brown

The colour of Cretaceous-Tertiary kaolins in the Douala Sub-Basin varied greatly in hue, value and chroma; hence, different colours were determined. Bomkoul kaolins were light reddish brown (BKL 01 and BKL 02) and brownish yellow (BKL 03). The Dibamba kaolin layer (DBB) and some clay nodules (DBB CN 01) were pinkish white, whereas the other clay nodule (DBB CN 02) was yellow. Ediki samples were pale green (EDK 01 and EDK 03) and light green (EDK 02). The colour of Logbaba samples varied from white (LBB 02) to light grey (LBB 01 and LBB 03). Missole I samples were grey (MSL I 01) and dark grey (Missole I 02); whereas Missole II samples were white (MSL II 01) and light greenish grey (MSL II 02). Yatchika samples were yellow (YTK 01), reddish yellow (YTK 02A), pink (YTK 02B) and light reddish

brown (YTK 03). Hence, the most dominant colour was light reddish brown, i.e. 15% of kaolins; and the least colours were brownish yellow, dark grey, grey, pink and reddish yellow, each represented by 5% of the kaolins (Figure 7.10).

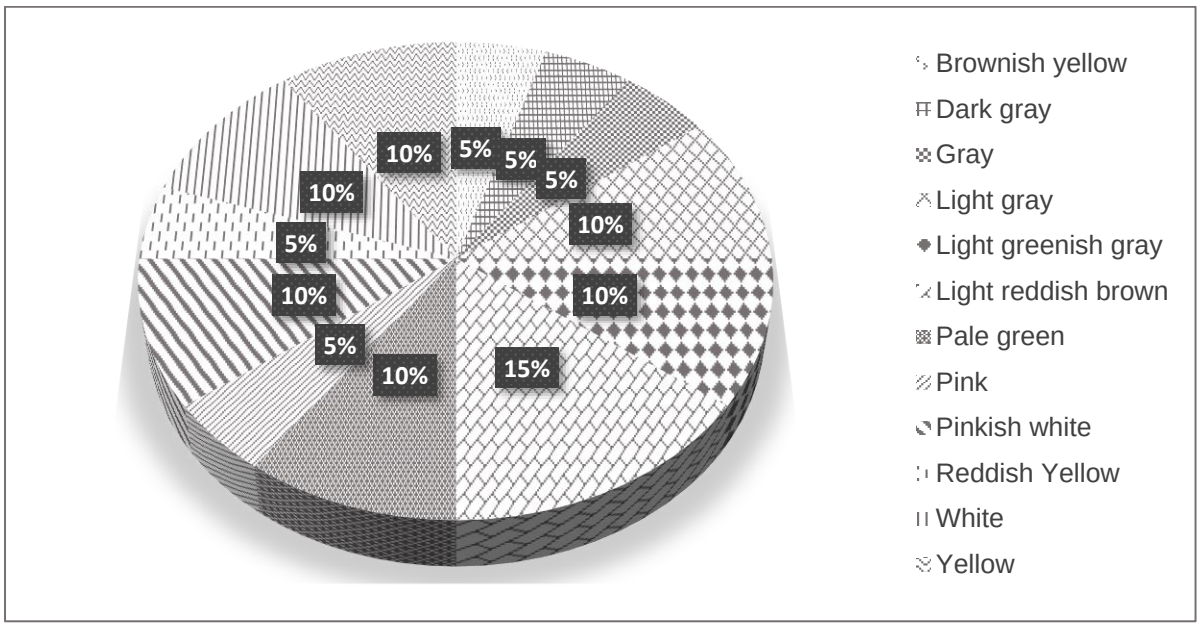

Figure 7.10: Percentage distribution of different colours of studied Cretaceous-Tertiary kaolins

7.2.4 Moisture content

The moisture content of bulk samples varied between 0.00 wt % (DBB CN 02) to 7.00 wt % (YTK 01). YTK samples had a moisture content ≥ 2.00 wt %. Except EDK 01, EDK 03 and LBB 01, which had a moisture content of 1.40 wt %, the remaining samples had a moisture content ≤ 0.80 wt % (Figure 7.11).

Silt samples had a moisture content < 1.00 wt %, except YTK 02A, which had a moisture content of 2.11 wt % (Figure 7.12). All silt fractions had greater moisture content than their corresponding bulk samples. The < 2 µm samples had moisture contents which were greater than their corresponding bulk and silt fractions, except DBB and YTK 01. The moisture content of < 2 µm samples varied between 0.40 wt % (DBB) and 5.20 wt % (YTK 01) (Figure 7.13).

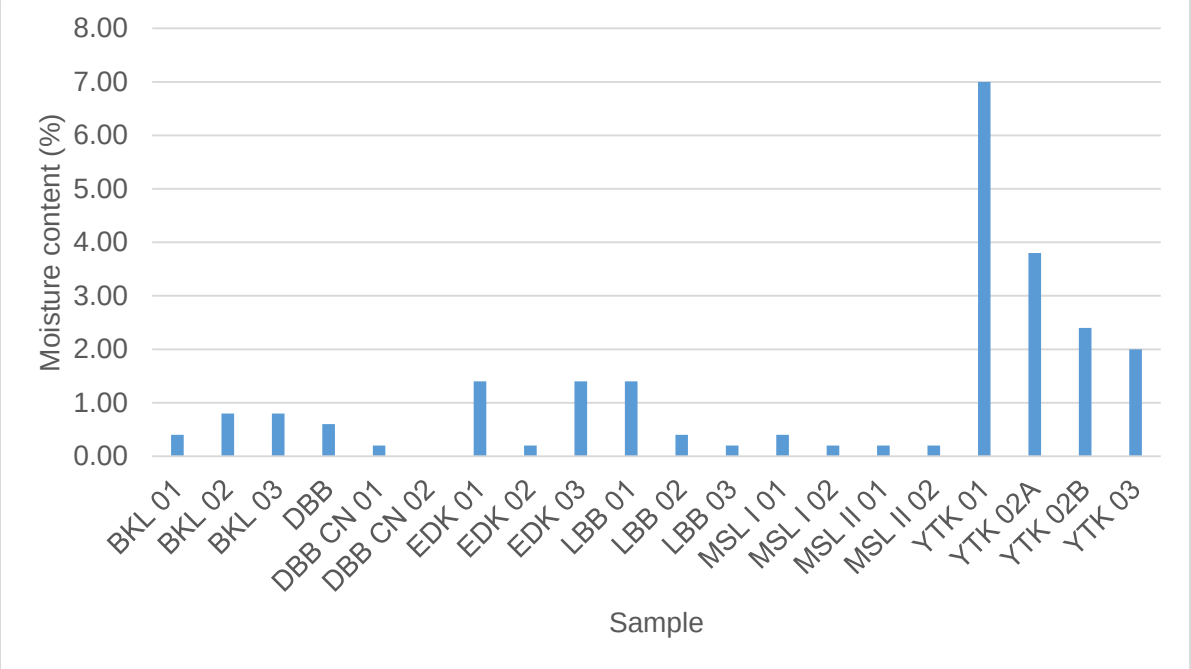

Figure 7.11: Moisture content of bulk kaolins

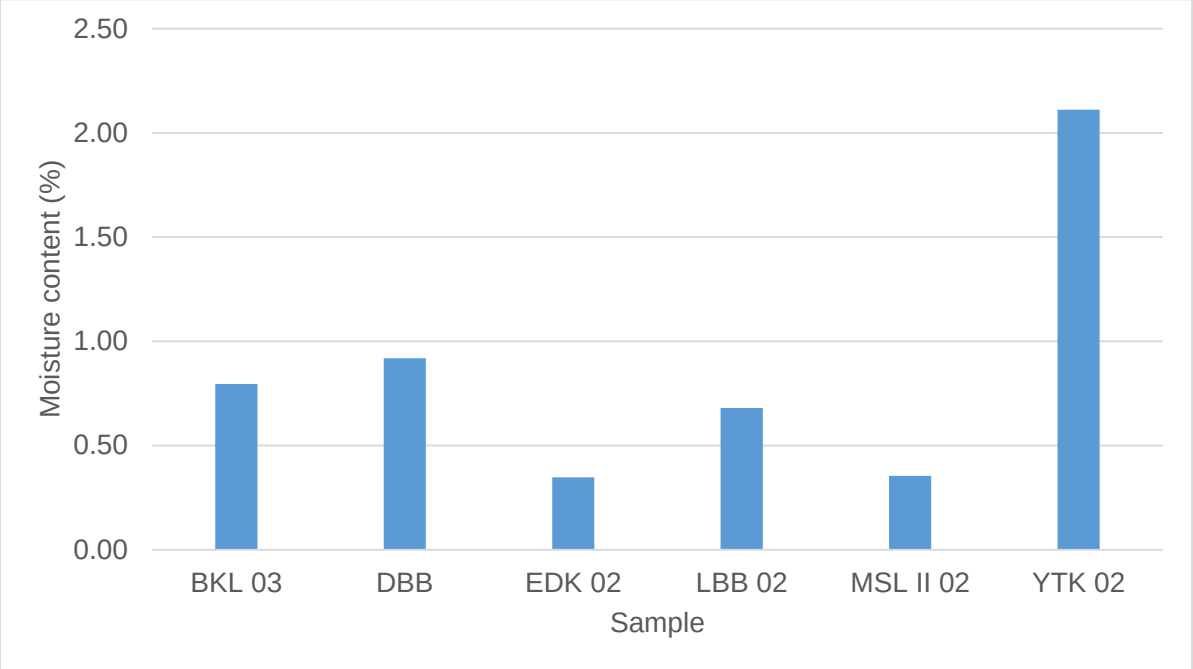

Figure 7.12: Moisture content of silt fraction of kaolins

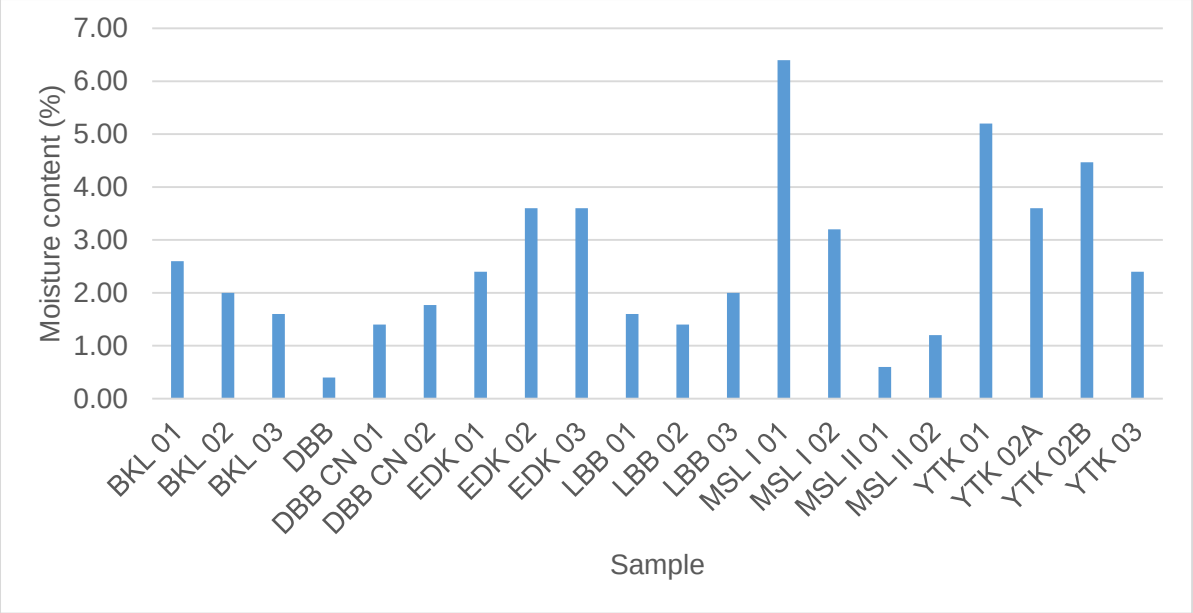

Figure 7.13: Moisture content of < 2 µm fraction of kaolins

7.3 Physico-chemical characteristics

7.3.1 pH

The $pH_{(KCl)}$ of Cretaceous-Tertiary kaolins were all acidic, varying between 1.87 (MSL I 02) and 3.81 (LBB 01), with an average of 3.29. Missole I samples had the lowest pH values; whereas Logbaba samples had the highest pH values (Figure 7.14).

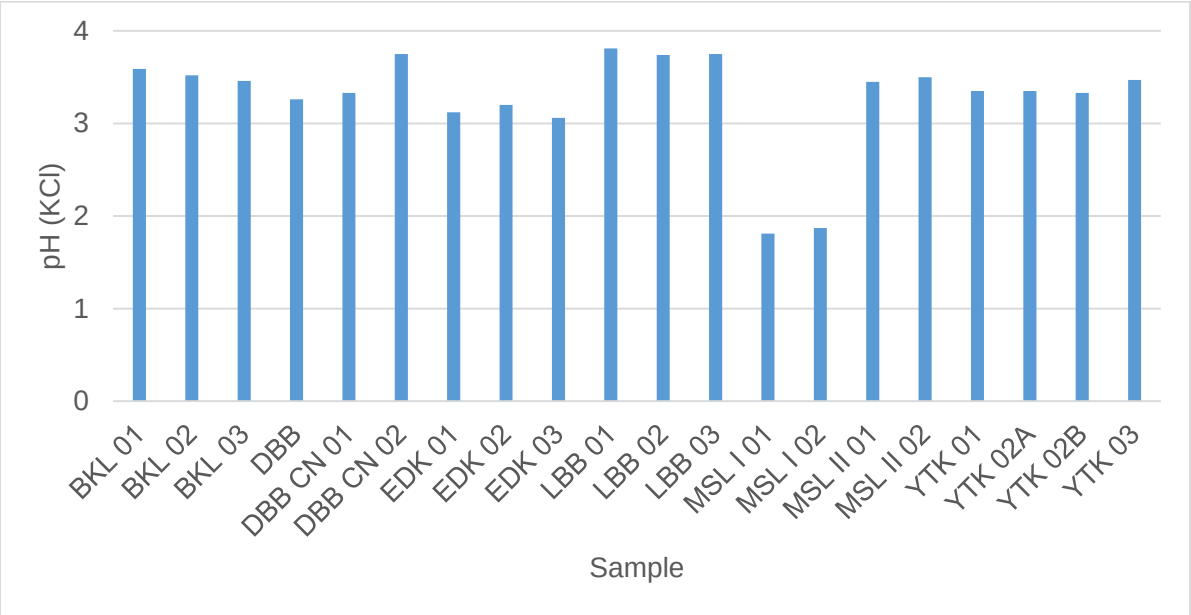

Figure 7.14: pH values of studied Cretaceous-Tertiary kaolins

7.3.2 Electrical conductivity (EC)

The EC of Cretaceous-Tertiary kaolins varied 98 µm/cm (LBB 03) to 8710 µS/cm (MSL I 02). Missole I samples had very high EC compared to other samples, 7860 and 8710 µm/cm for MSl I 01 and MSL I 02, respectively. Excluding these two samples, the mean of EC for all other samples was 35.73 µS/cm. Figure 7.15 shows the EC of studied kaolin samples, excluding MSL I 01 and MSL I 02.

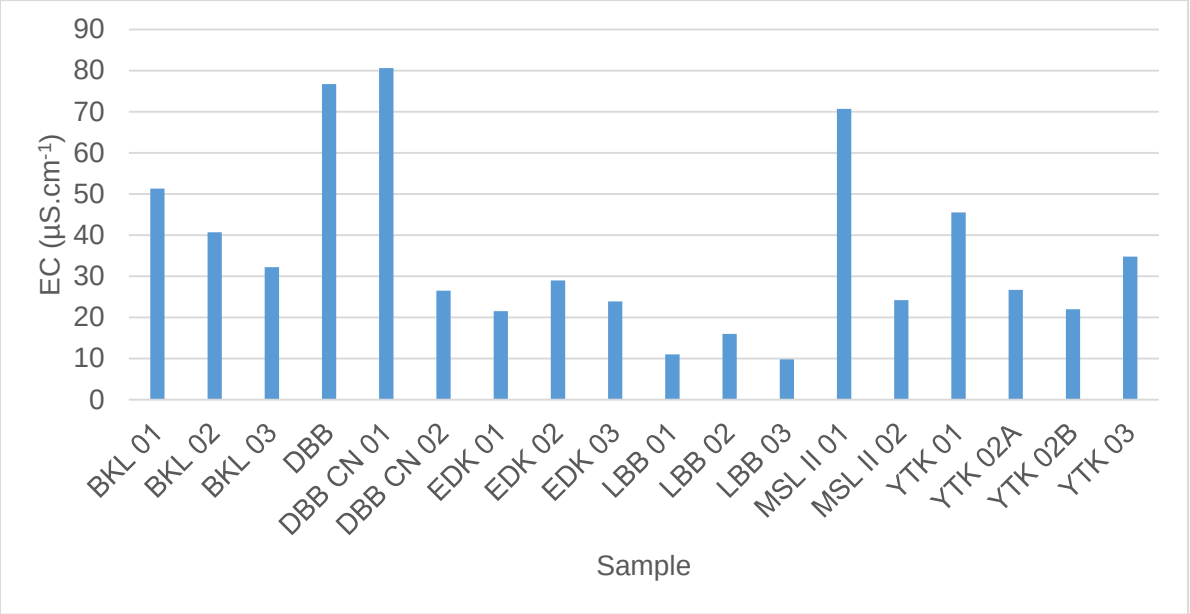

Figure 7.15: Electrical conductivity values of studied Cretaceous-Tertiary kaolins

7.4 Discussion

7.4.1 Physical and physico-chemical properties as indicators of environments of formation of kaolins

Cretaceous-Tertiary kaolins of the Douala Sub-Basin are mainly dominated by sand (60.20%), followed by clay (29.00%) and silt (10.80%), averagely. The dominance of sands in these kaolins is due to the nature of sediments found in the Sub-Basin. These sediments were mainly sandstones, suggesting an acidic source, from which feldspars are believed to have weathered to form kaolins. The lower percentage of silt over clay shows that there is on-going reworking of sediments taking place in the Sub-Basin.

The whitish colour of some of the studied kaolins is indicative of second cycle sediments, formed after recycling of first cycle sediments (Keller, 1978). This has also been observed in

the Georgia kaolins which are second cycle kaolins having a white colour (Schroeder *et al*., 2004). However, some Georgia kaolins are grey. Schroeder *et al*. (2004) indicated that the grey colour in some Georgia kaolins could be more due to the presence of SO_3 than to the presence of organic matter in the kaolins. This was later supported by Pruett (2016), according to whom the grey Georgia kaolins were originally deposited in a reduced anoxic environment in the presence of organic matter and iron sulphides, causing the grey colour.

However, Manju *et al*. (2001) argued that oxidised weathering conditions can enhance the dissolution of the FeS_2 present in the grey kaolins, creating an environment with very low pH, and consequently high EC. Such very acidic environment favours reworking of microcrystalline quartz and authigenic kaolinite (Manju *et al*., 2001). Therefore, similarly to the Georgia grey kaolins, the grey Missole I kaolins were deposited or formed in a reducing environment; then the environment became oxidising, producing the very low pH observed in these kaolins. The V/(V+Ni) ratios of the Missole I kaolins also suggest formation under anoxic to eunixic conditions. The oxidation of the Missole I kaolins led to the formation of the light grey and subsequently white Missole II kaolins by oxidative alteration that removed iron sulfides and formed goethite (Schroeder *et al*., 2004; Pruett, 2016). This confirms that Missole II kaolins are second cycle sediments formed from post-depositional alteration of Missole I kaolins. The light grey and white Logbaba kaolins might have formed in the same conditions, though their colour might be as result of anatase contamination.

The low pH of the kaolins, indicating high acidity (pH < 4), is also an indicator of continuous weathering (Manju *et al*., 2001) and intense hydrolysis processes (Santos *et al*., 2014). The lower the pH of the environment of deposition, the higher the EC, as shown in Figure 7.16.

The yellowish, reddish and brownish colours portrayed in Bomkoul, Dibamba and Yatchika kaolins is indicative of an oxygen-rich environment (oxic), favouring the alteration of feldspar and the presence of goethite. But with reducing oxygen levels in Yatchika samples (according to their Ni/Co, V/Cr and V/(V+Ni) ratios), hematite was formed. The greenish colour of Ediki samples is as a result of the weathering of microcline.

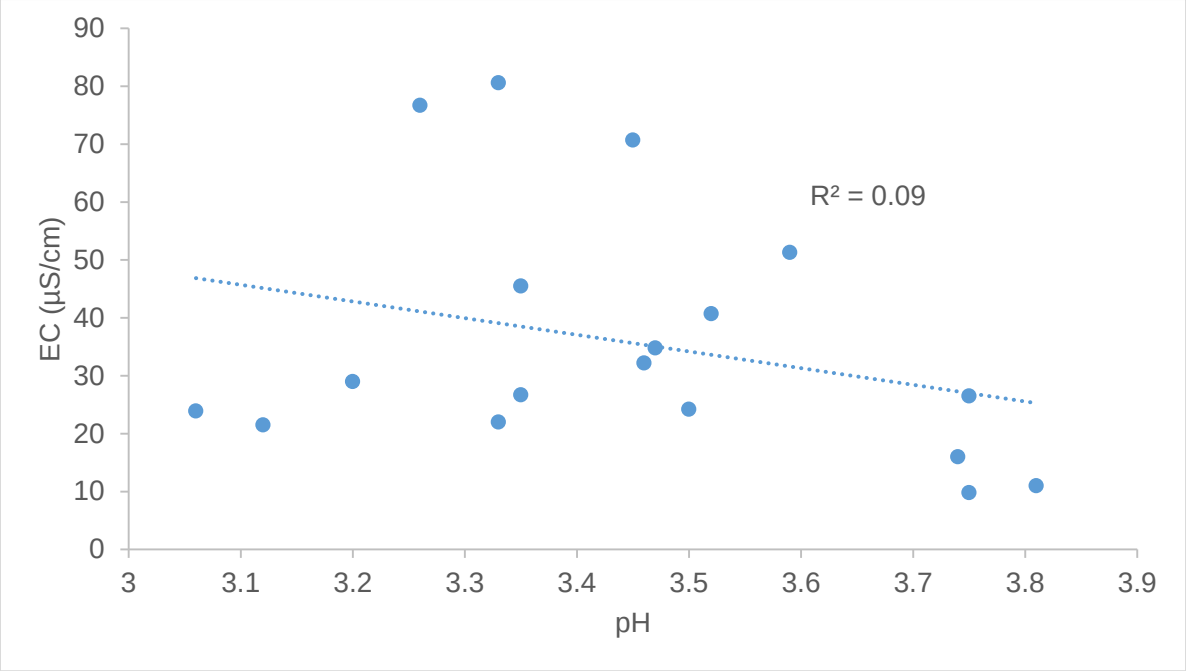

Figure 7.16: Correlation between EC and pH

7.4.2 Influence of particle size on the mineralogy and geochemistry of kaolin

7.4.2.1 Influence of particle size on the mineralogy of kaolin

The six samples for which silt fractions were analysed (BKL 03, DBB, EDK 02, LBB 02, MSL II 02 and YTK 02A) were presented with their corresponding bulk and < 2 µm fractions. The aim was to determine the mineralogical evolution of kaolins with respect to their particle size (Figures 7.17-7.22).

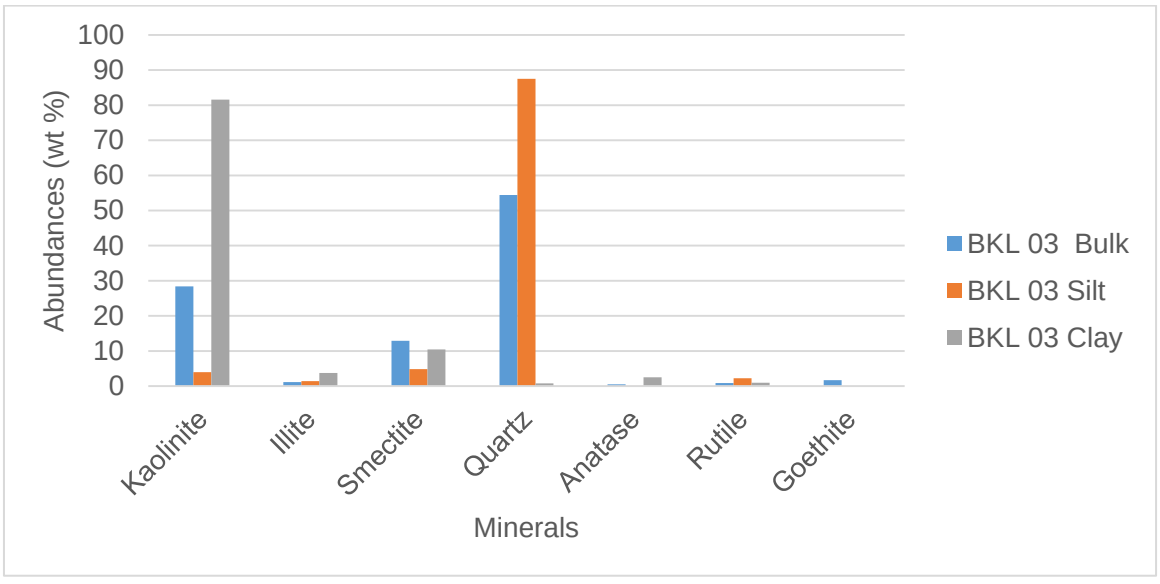

Figure 7.17: Mineralogical composition of BKL 03 with decreasing particle size

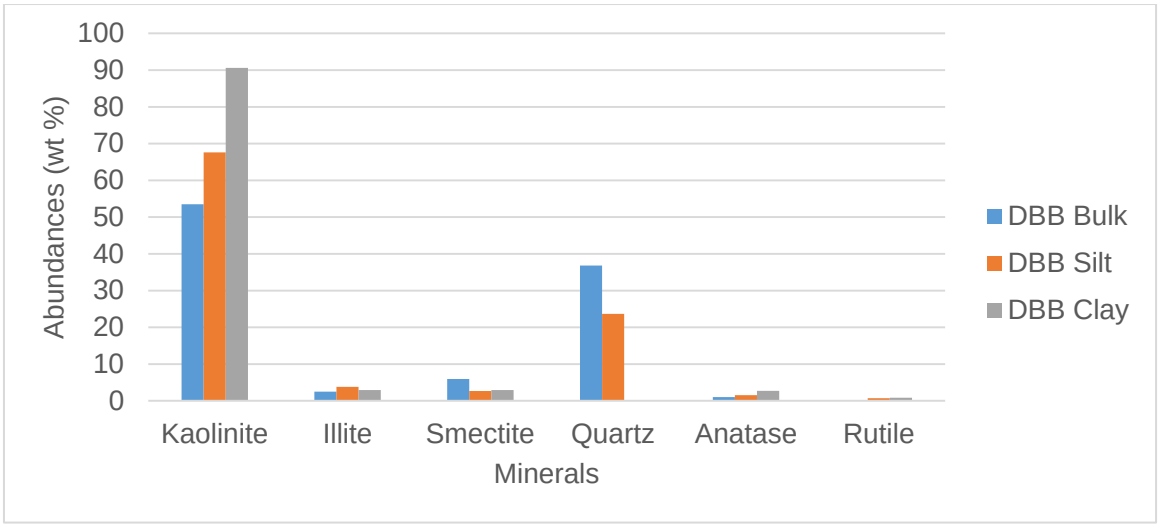

Figure 7.18: Mineralogical composition of DBB with decreasing particle size

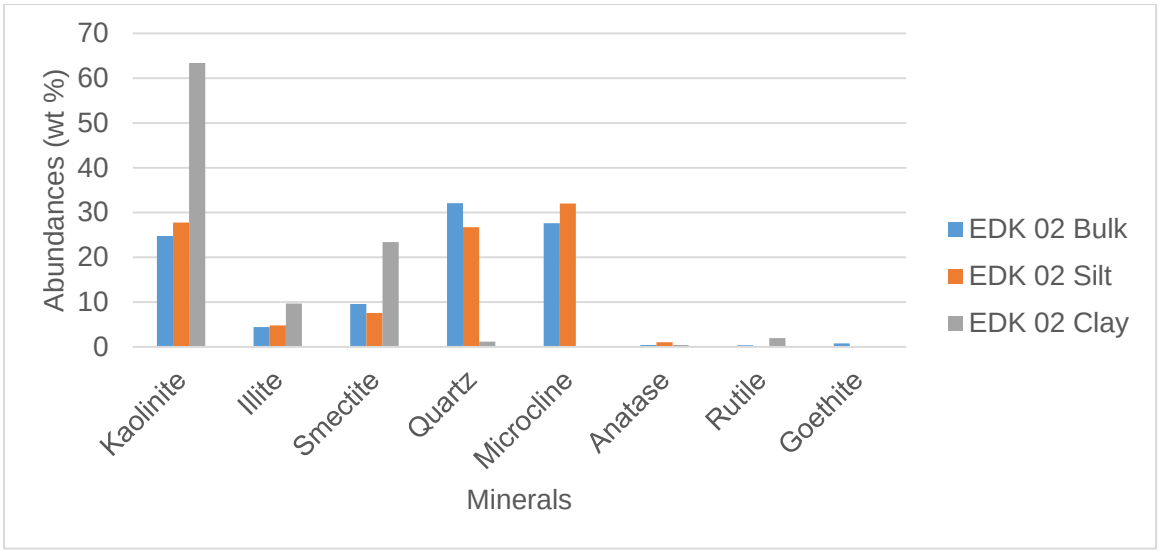

Figure 7.19: Mineralogical composition of EDK 02 with decreasing particle size

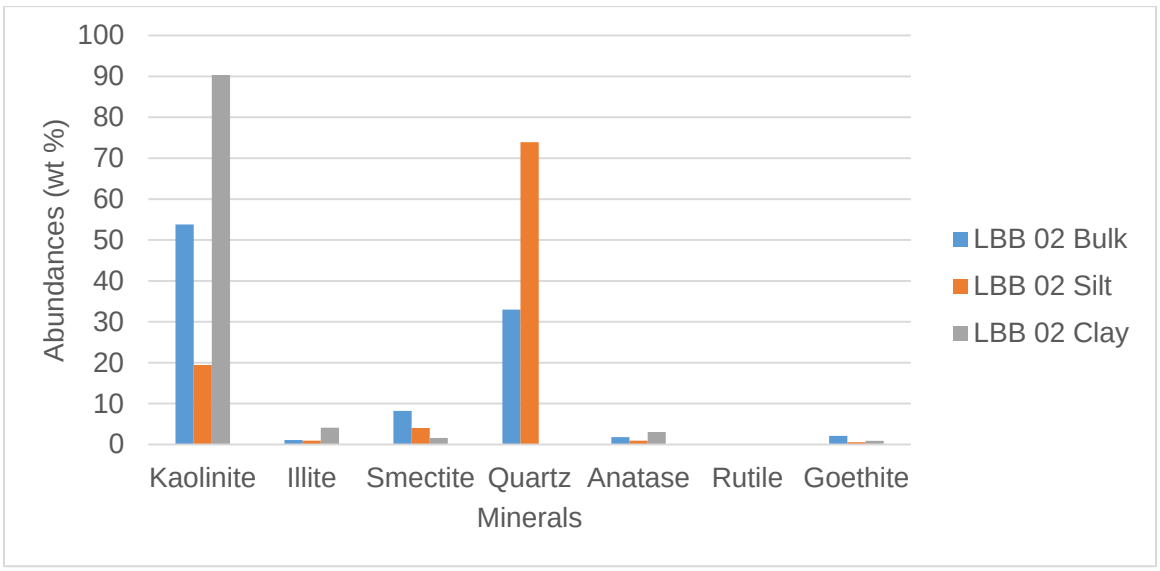

Figure 7.20: Mineralogical composition with of LBB 02 decreasing particle size

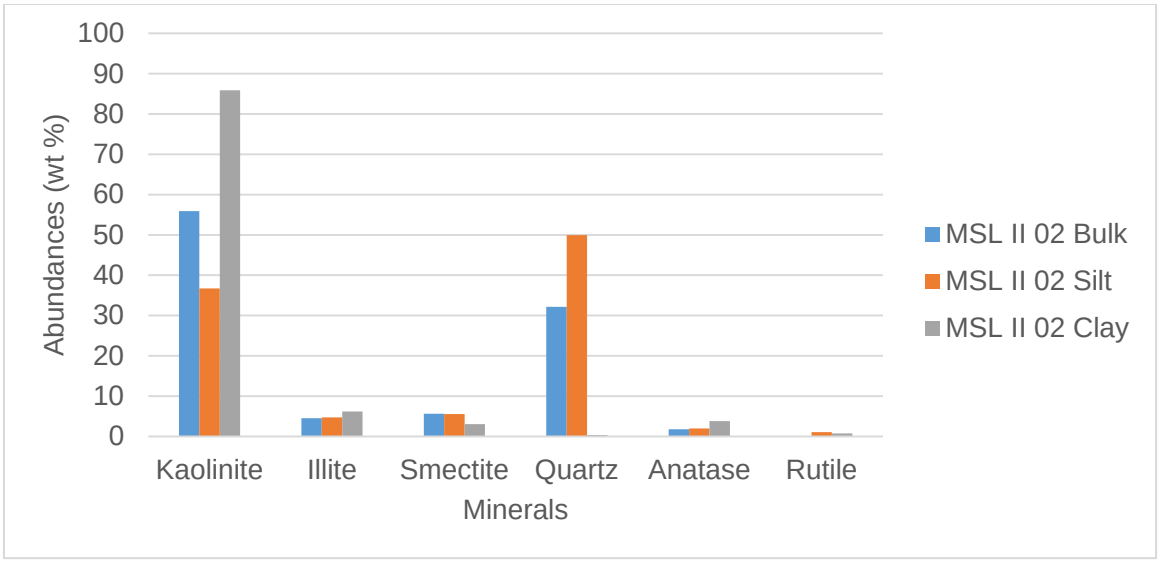

Figure 7.21: Mineralogical composition of MSL II 02 with decreasing particle size

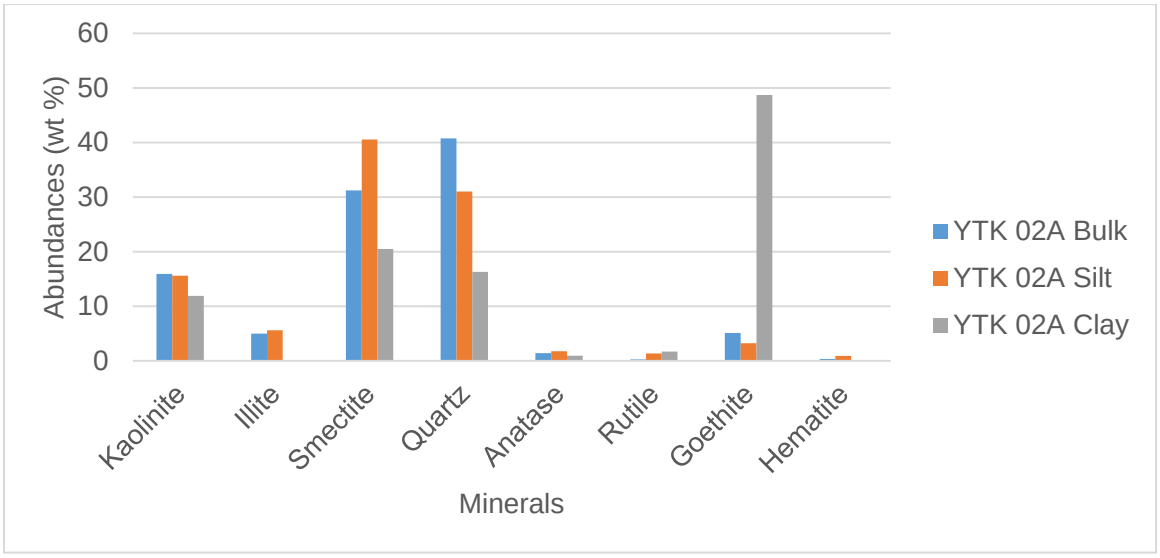

Figure 7.22: Mineralogical composition of YTK 02A with decreasing particle size

Given the fact that clay minerals are more abundant in < 2 µm fraction (clay), their abundances should increase with decreasing particle size, and with decreasing abundances of primary minerals (rock forming minerals). Only one sample (DBB) observed this relationship (Figure 7.18). Kaolinite in DBB increased from 53.5 wt % (bulk) to 90.61 wt % (< 2 µm fraction) through 67.6 wt % (silt); whereas, quartz decreased from 36.83 wt % (bulk) to 0 wt % (< 2 µm fraction) through 23.68 wt% (silt). There also was an increase in anatase and rutile with decreasing particle size, and decrease in smectite. These relationships show that the source rock gradually weathered to form kaolinite.

In EDK 02, there was a similar relationship between kaolinite and quartz relative to decreasing particle size. However, microcline was more abundant in the silt fraction, though not detected in the < 2 µm fraction. Illite, gradually increased with decreasing particle size, probably due to the weathering of microcline; though smectite was more abundant in the < 2 µm sample than illite (Figure 7.19).

A different trend was observed in YTK 02A. The abundance of the primary mineral (quartz) decreased with decreasing particle size (Figure 7.22). Kaolinite also decreased with decreasing particle size. Illite was more abundant in the silt fraction, and it was not detected in the < 2 µm fraction. Smectite was more abundant in the silt fraction, and it was the most abundant clay mineral in the < 2 µm fraction. The abundance of goethite was least in the silt fraction (where smectite and illite were highest) and its abundance was highest (48.7 wt %) in the < 2 µm fraction (where all clay minerals were least). It could, therefore be assumed that Fe^{3+} gradually replaced the Al^{3+} in the clay minerals to form goethite.

The other three samples (BKL 03, LBB 02 and MSL II 02) had a lower kaolinite content in the silt fraction than in the bulk and < 2 µm fraction, with the highest kaolinite content present in the < 2 µm fraction. Higher quartz content and lower kaolinite in the silt fraction could be due to reworking and silicification of the kaolins. Therefore, the kaolinite present in the < 2 µm fraction could be second cycle sediments, as Cretaceous-Tertiary kaolins of Middle Georgia (Ece *et al*., 2003). This is also supported by the white colour of LBB 02 and MSL II 02, which could be due to a subsequent stage of deferritisation (Keller, 1978). These two samples also have similar micromorphologies as Georgia kaolins (Keller, 1978). Moreover, the higher concentrations of smectite in the silt fractions relative to the < 2 µm fraction in LBB 02 and MSL II 02 could be due to a solid-state mechanism in which one smectite layer transformed into one kaolinite layer by stripping of a tetrahedral sheet and the adjacent interlayer region (Amouric and Olives, 1998).

7.4.2.2 Influence of particle size on the geochemistry of kaolin

The major oxides geochemistry of bulk, silt and < 2 µm fractions of six samples (BKL 03, DBB, EDK 02, LBB 02, MSL II 02 and YTK 02A) are presented to evaluate the geochemical evolution with decreasing particle sizes (Figures 7.23-7.28). Geochemical differences among sand, silt and < 2 µm fractions is due to the sorting and recycling of sediments (Hossain *et al*., 2014). Therefore, it is important to assess the differences in kaolins' geochemistry of different particle sizes.

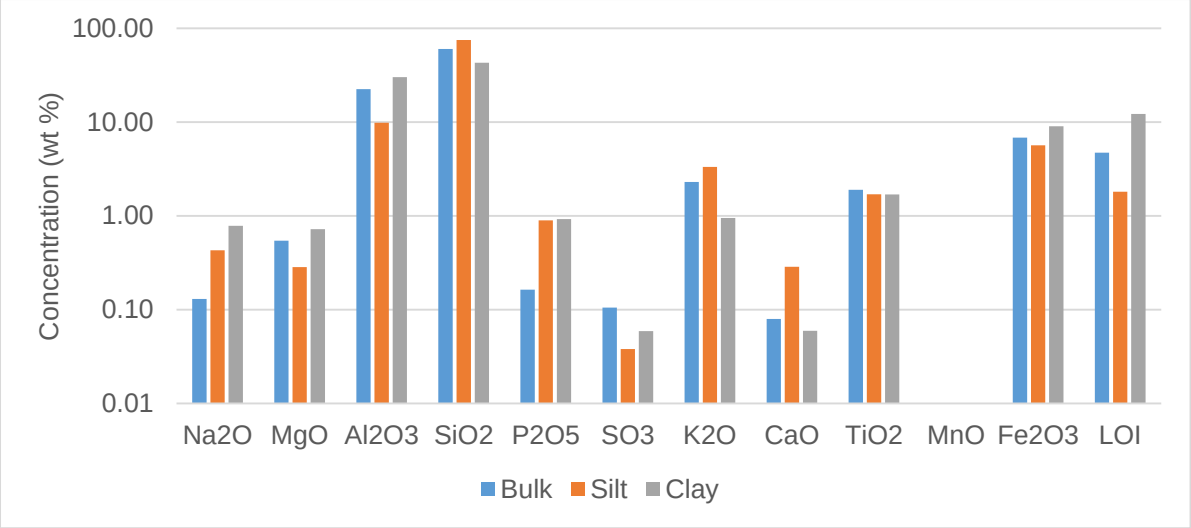

Figure 7.23: Geochemical evolution with decreasing particle size of BKL 03

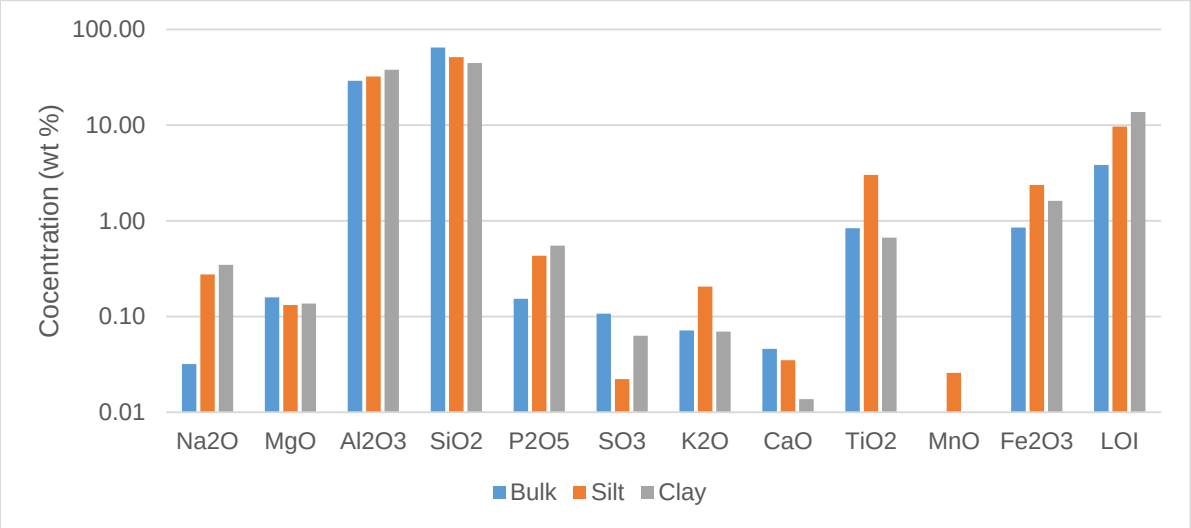

Figure 7.24: Geochemical evolution with decreasing particle size of DBB

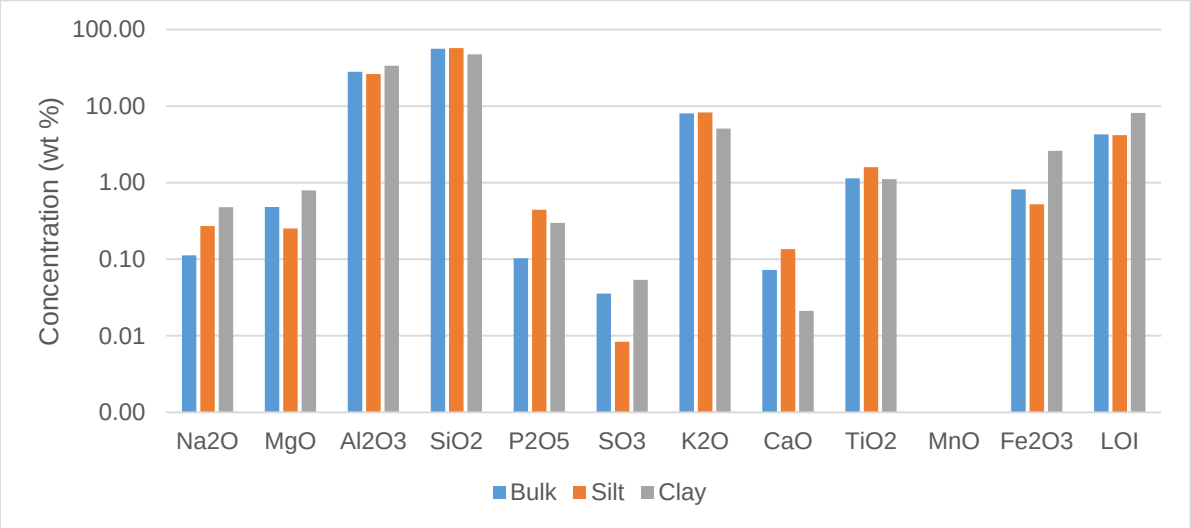

Figure 7.25: Geochemical evolution with decreasing particle size of EDK 02

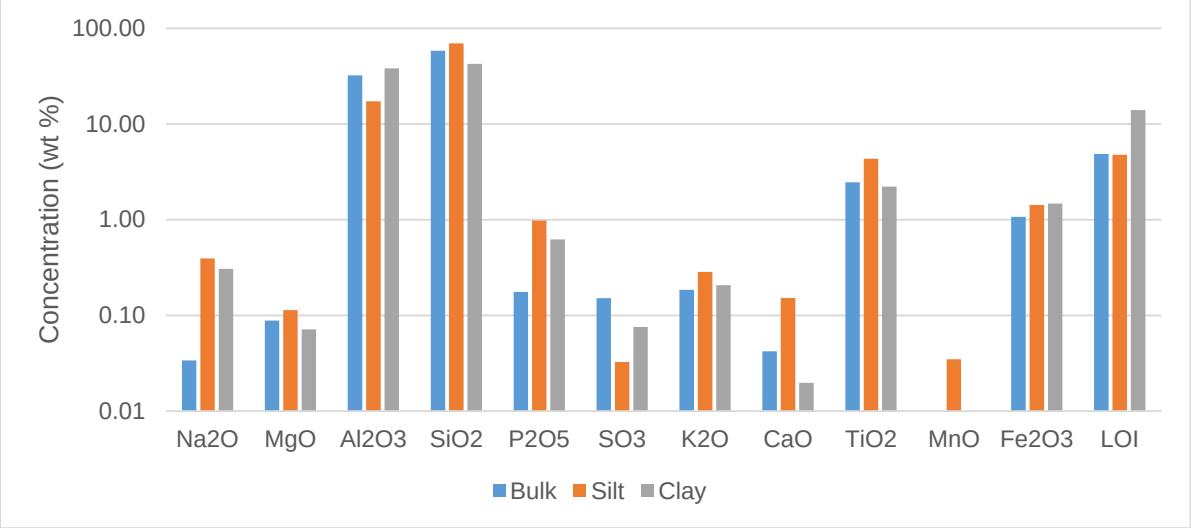

Figure 7.26: Geochemical evolution with decreasing particle size of LBB 02

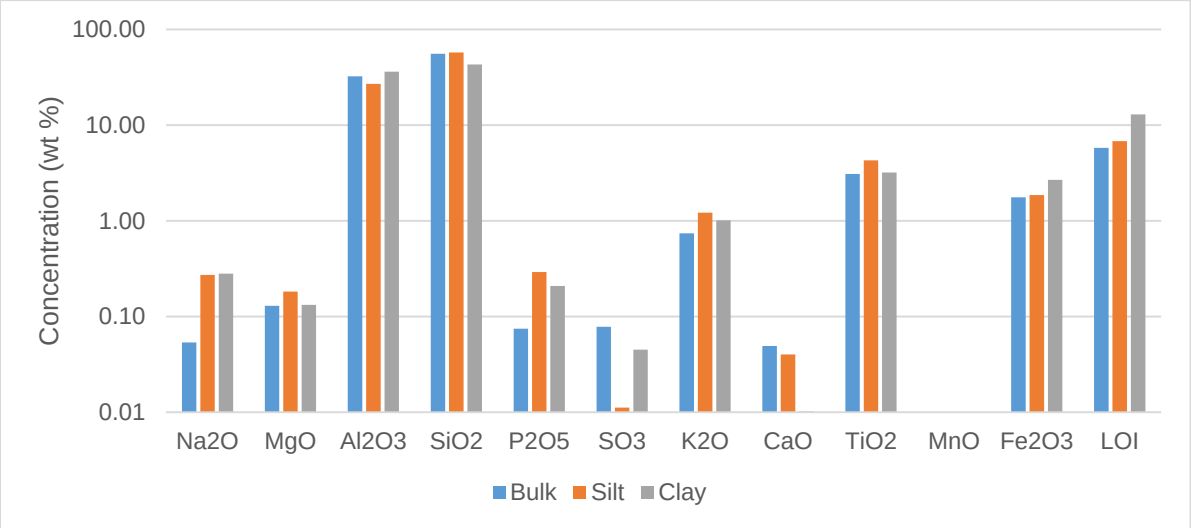

Figure 7.27: Geochemical evolution with decreasing particle size of MSL II 02

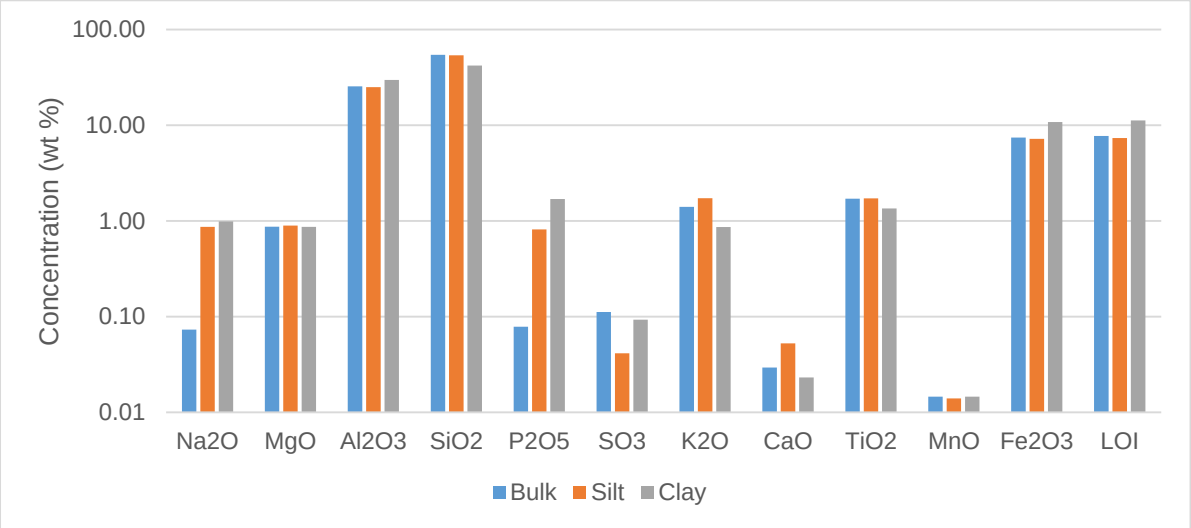

Figure 7.28: Geochemical evolution with decreasing particle size of YTK 02A

The most dominant major oxides, SiO_2 and Al_2O_3 have two major trends with decreasing particle size. The first trend is an increasing Al_2O_3 and a decreasing SiO_2 with decreasing particle size, observed in DBB, EDK 02 and YTK 02A. This is the normal trend because Al_2O_3 is more concentrated in the < 2 µm fraction due to the presence of clay minerals, and there is an inverse relationship between SiO_2 and Al_2O_3. The second trend is lower Al_2O_3 in the silt fraction and a higher SiO_2 in the silt fraction compared to other fractions. This trend was observed in BKL 03, LBB 02 and MSL II 02. The higher concentration of SiO_2 in the silt fractions of these samples indicates reworking of the kaolins (Nagarajan *et al*., 2013).

The concentration of Na_2O increased with decreasing particle size, this is due to the increase in smectite in the < 2 µm fraction. Logbaba were the only ones in which Na_2O was more abundant in the silt fraction. This is consistent with a gradual transformation of smectite into kaolinite (Amouric and Olives, 1998). The concentration of CaO and K_2O were highest in silt fractions and lowest in < 2 µm fractions. The high CaO in silt fractions also suggests the transformation of smectite to kaolinite because both the Ca- and Na-rich smectite were identified in the samples.

However, the high K_2O concentrations in silt fractions suggest the transformation of illite to kaolinite resulting from K^+ dissolution (Lanson *et al*., 2002). It should be noted that K-feldspars and micas were not detected in these samples, except in Ediki samples, where microcline occurred as minor to major mineral. Therefore, the main source of K_2O in the other samples would be due to the presence of illite.

There was no preferred variation in the concentration of TiO_2 according to decreasing particle sizes. However, second cycle sediments (BKL 03, LBB 02 and MSL II 02) had a high TiO_2 concentration in their silt fractions. The concentration of Fe_2O_3 was generally higher in < 2 µm fractions, due to the concentration of goethite in this size fraction. The loss on ignition was highest in the < 2 µm fraction due to more presence of hydrous aluminosilicates in this size fraction.

7.4.3 Potential applications of Cretaceous-Tertiary kaolins of the Douala Sub-Basin

World known and exploited kaolins are the Cornwall (England), Capim River (Brazil), Georgia (USA) and Cape York Peninsula (Australia). One of the common characteristics among these kaolin deposits is their location in Cretaceous-Tertiary sedimentary basins, next to granitic rocks (Harvey and Murray, 1997). These kaolins are exploited for various industrial applications including paper coating, paper filler, ceramics, soap, pharmaceutics and

cosmetics. Therefore, the chemical and physico-chemical characteristics of the Cretaceous-Tertiary kaolins were compared to standards (Prasad *et al*., 1991) set for paper coating, paper filler, ceramics, pharmaceutics and cosmetics (Table 7.2).

The ranges of major oxides and LOI do not correspond to the standards in Table 7.2, except the recommended values for CaO in kaolins to be used in pharmaceutics and cosmetics. However, Dibamba, Logbaba and Missole II kaolins' clay fractions fall in the ranges set for major oxides to be used for paper coating, paper filler, ceramics, pharmaceutics and cosmetics. Therefore, in order for these kaolins to be used for any of these applications, particle size separation must be carried out to obtain the < 2 µm fraction.

Table 7.2: Chemical composition ranges of Cretaceous-Tertiary kaolins of the Douala Sub-Basin compared with standard chemical composition ranges for different applications

Chemical composition	Paper coating*	Paper filler*	Ceramics*	Pharmaceutics and cosmetics*	Bulk	Clay
SiO_2	45–49	46–48	48-50	44.6–46.4	46.87-87.88	36.99-54.70
Al_2O_3	36-38	37-38	36-38	38.1–39.5	9.14-32.90	18.24-38.21
TiO_2	0.5-1.3	0.5–1.5	0.02-0.1	0-1.4	0.18-3.70	0.20-3.21
Fe_2O_3	0.5-1.0	0.5-1.0	0.6-1	0.1-.02	0.58-11.26	1.41-14.34
MnO	-	-	-	-	0.00-0.01	0.00-0.02
MgO	-	-	-	0.1-0.2	0.07-1.57	0.07-1.83
CaO	-	-	-	0.1-0.2	0.01-0.09	0.01-0.11
Na_2O	-	-	-	0-0.1	0.00-0.13	0.27-1.61
K_2O	0.5-1.5	0.5-1.5	1.2-2.7	0-0.2	0.04-8.09	0.06-7.55
P_2O_5	-	-	-	-	0.06-0.93	0.21-7.56
LOI	-	-	11.2-12.5	13.8-13.9	1.21-9.68	6.80-14.57

*Standards from Prasad *et al*. (1991)

In general, the presence of impurities in kaolin usually hinders its potential uses in industries. Such impurities include the presence of Fe_2O_3 and TiO_2. The relatively high Fe_2O_3 averages in Cretaceous-Tertiary kaolins of the Douala Sub-Basin are caused by intense oxidation of iron-bearing silicate minerals (Ariffin *et al*., 2008). High titania in kaolins also reduces their quality. In Cretaceous-Tertiary kaolins of the Douala sub-basin, iron oxides are found in goethite and hematite; whereas titanium oxide is found in anatase. Though these impurities are present in the studied kaolins, it is to be noted that some of their characteristics could be useful for specific industries. For example, the low moisture content indicates that the samples are very dry. This characteristic makes the kaolins suitable for use as paint fillers and for soap production, which should not exceed 2% (Ariffin *et al*., 2008; Aja and Randy, 2013).

Moreover, pH and EC of kaolins are used to detect impurities and salts. High EC values of Missole I kaolin correspond to the presence of SO_3 in these kaolins. Therefore, unlike other deposits which have low EC values, Missole I kaolin cannot be used for ceramics because the presence of salts will lead to the formation of blisters.

7.5 Synopsis

A diagnostic evaluation of Cretaceous-Tertiary kaolins of the Douala Sub-Basin was carried out. The evaluation involved the determination of physical and physico-chemical properties of studied kaolins, which are as follows:

- The particle size distribution and texture of the kaolins showed that the studied kaolins are very rich in sands, with textures varying from clay to sandy loam, with 50% of the samples having a sandy loamy clay or sandy loam texture. The colour of the samples varied considerably. The different colours identified were: dark grey, light grey, light greenish grey, grey, light reddish brown, pale green, pink, pinkish white, reddish yellow, brownish yellow, yellow and white; with the most dominant colour being light reddish brown (15% of samples). The moisture content was generally very low (< 2 wt %) in all size fractions, except in Yatchika samples (moisture content > 2 wt %).
- The kaolins are generally acidic, with a pH (KCl) varying between 3.06 and 3.81, except in Missole I samples, which had a pH (KCl) < 2. The EC generally varied between 20 to ~ 50 µS/cm, except Dibamba and MSL II 01 samples having EC values in the interval 50 µS/cm < EC < 80 µS/cm; and Missole I samples having an EC > 7500 µS/cm.
- The physical and physico-chemical characteristics of studied kaolins showed that the kaolins have an acidic parent rock from which feldspars and/or micas altered to form the kaolins. There is reworking and continuous weathering of the kaolins leading to low pH and whitening of some of the kaolins. The environment of formation/deposition varied from euxenic/dysoxic to oxic.
- The particle size greatly influenced the mineralogy and geochemistry of the kaolins because the finer particles (< 2 µm) have higher amounts of kaolinite and Al_2O_3. But in general, the geochemical composition of samples did not vary much with change of particle size because particle size reduction is a physical process which has little or no change on the chemical composition.
- The moisture content of the kaolins makes them suitable as paint fillers and in soap production. Paper coating, paper filler, ceramics, pharmaceutics and cosmetics are

potential applications for the kaolins, though particle size reduction and beneficiation will give them a higher quality.

Validation of hypothesis: The physical and physico-chemical properties of studied Cretaceous-Tertiary kaolin clearly identified their potential uses.

CHAPTER 8

CONCLUSIONS AND RECOMMENDATIONS

8.1 CONCLUSIONS

Conclusions drawn from this research are as follows:

A) The mineralogical and geochemical characterisations led to the following conclusions:

- Cretaceous-Tertiary kaolins of the Douala Sub-Basin are hosted by sandstone deposits and occur as layers of sandy and clayey kaolins of 1 mm to 5 m thick.
- The mineralogical characterisation showed that quartz and kaolinite were the most dominant mineral phases in bulk and silt fractions; whereas kaolinite was the major mineral phase in clay fractions, with Dibamba, Logbaba and Missole II kaolins, and Ediki kaolin containing the least amount of kaolinite. Other mineral phases identified were: smectite and/or illite (minor phases), anatase and rutile (minor or trace phases), and goethite and hematite (as trace phases). The kaolins exhibited four main morphologies, namely; thin platy or pseudo-hexagonal particles or flakes, books or stacks of kaolinite and swirl texture. Based on the kaolinite's structure, Dibamba, Logbaba and Missole II were well-ordered; Bomkoul and part of Yatchika kaolins have partially to well-ordered; and Ediki and Missole I kaolins have poorly ordered or disordered. Dehydroxylation temperatures in all the kaolins occurred below 570 ^{o}C (as in Georgia Kaolin), and exothermic peak temperatures occurred between 943-988^{o}C.
- The geochemistry generally confirmed that silica and alumina were the most dominant major oxides. Due to the presence of illite and smectite, and probable femic minerals in some kaolins (Ediki, Yatchika and Missole I), potassium and magnesium oxides were relatively higher in these kaolins. Possible inferred source rocks of these kaolins vary between rhyolite/granite and rhyolite/granite + basalt, which have undergone moderate to extreme silicate weathering. An analysis of the geochemistry of Cretaceous-Tertiary kaolins of the Douala Sub-Basin suggest that kaolinisation occurred in a marine environment, except that of Logbaba kaolin, which was a non-marine (probably lacustrine environment).

In general, there was no great distinction between Cretaceous and Tertiary kaolins of the Douala Sub-Basin based on their mineralogy and geochemistry. The best kaolins in terms of these characteristics, and in comparison with the Georgia Kaolins (known for their high kaolinite quality), are the Dibamba (Tertiary), Logbaba (Cretaceous) and Missole II (Tertiary) kaolins. Based on their compositional maturity and mineralogical

characteristics, these three kaolins are believed to be second cycle sediments; unlike Bomkoul, Yatchika and Ediki kaolins, which are believed to be first cycle sediments.

B) Trace elements and stable isotopes composition showed that Cretaceous-Tertiary kaolins in the Douala Sub-Basin were mainly derived from felsic rocks. Sediment sorting and recycling were evident in Bomkoul, Dibamba and Logbaba kaolins. Kaolinisation during the Cretaceous occurred in an anoxic reducing environment, which became oxic during the Tertiary. The temperatures were 26.58^{o}C ± 9.65^{o}C during the Cretaceous and 29.40^{o}C ± 7.22^{o}C during the Tertiary. The mean isotopic composition of the meteoric water during the Cretaceous was -5.15 and -31.67‰, for $\delta 18O_W$ and δD_W, respectively and -4.44 and -26.24‰, for $\delta 18O_W$ and δD_W, respectively during the Tertiary; present day mean isotopic composition of meteoric water in Douala is -3.09 and -10.22‰ for $\delta^{18}O_W$ and δD_W, respectively. Therefore, Douala had a cooler and humid climate during the Cretaceous, and the climate is gradually becoming hotter but more humid.

C) The ages of zircons in Cretaceous-Tertiary kaolins suggested that the zircons formed during two main tectonic events: the Eburnean orogeny, during which older zircons crystallised and the Pan-African orogeny, during which younger zircons crystallised. The main identified sources of these zircons are the Archean Ntem Complex, the Paleoproterozoic Nyong Group and the Neoproterozoic Yaounde Group. The maximum depositional ages of the kaolins varied between 588 ± 2 Ma and 612 ± 2 Ma. However, the glacial climate during the Neoproterozoic was not favourable for kaolinisation. Therefore, Neoproterozoic primary materials altered in a humid climate to form kaolins in the Douala Sub-Basin during Cretaceous and Tertiary Periods.

D) According to the diagnostic evaluation, Cretaceous-Tertiary kaolins of the Douala Sub-Basin are rich in sands, with 50% of the samples having a sandy loamy clay or sandy loam texture. The most dominant colour of the kaolins was reddish brown (15% of kaolins); other occurring colours in the kaolins were dark grey, light grey, light greenish grey, grey, light reddish brown, pale green, pink, pinkish white, reddish yellow, brownish yellow, yellow and white. The $pH_{(KCl)}$ mostly varied between 3.06 and 3.81; rendering the kaolins acidic. The EC generally varied between 20 to ~ 80 µS/cm, with an inverse relationship existing between pH and EC. The physical and physico-chemical characteristics of the kaolins also confirmed that they altered from acidic parent rocks in a euxenic/dysoxic to oxic environment, and there is reworking and continuous weathering of the kaolins leading to low pH and whitening of some of the kaolins. The particle size greatly influenced the mineralogy and geochemistry of the kaolins because the finer

particles (< 2 µm) have higher amounts of kaolinite and Al_2O_3. Paper coating, paper filler, ceramics, pharmaceutics, cosmetics, bricks, pottery and stoneware manufacturing are potential applications for the kaolins, though particle size reduction and beneficiation will give them a higher quality.

8.2 RECOMMENDATIONS

Though this research on the paleoenvironmental reconstruction of Cretaceous-Tertiary kaolins of the Douala Sub-Basin in Cameroon filled identified gaps in the body of knowledge of Clays and Clay Mineral and on Gondwana, it also gave room for future research. The following are recommendations for future research:

- Further characterisation of Cretaceous-Tertiary kaolins in the Douala Sub-Basin should be carried out to confirm the order-disorder in kaolinites, using ^{27}Al and ^{29}Si magic-angle-spinning nuclear magnetic resonance (MASNMR) spectroscopy or other novel technique. Titanium and iron, which were the main impurities in the kaolins, should be better characterised using Raman and Mössbauer spectroscopies, as this will be critical in determining kaolin processing strategies.

- Stable isotopes of African kaolinites of all ages should be investigated to reconstruct African paleoclimates through the geologic time scale.

- The U-Pb LA-SF-ICPMS of other accessory minerals in kaolins, such as rutile and apatite, should be carried out to complement the results obtained from the U-Pb LA-SF-ICPMS of zircons. Moreover, potassium-argon (K-Ar) dating of illites present in Cretaceous-Tertiary Formations of the Douala Sub-Basin should be carried out to better constrain the deposition age of the sediments.

- Beneficiation of the kaolin deposits should be carried out to improve their quality for industrial uses. Dibamba, Logbaba and Missole II kaolins, which might not require beneficiation could be used in a wide range of industries. However, because these kaolin deposits are not big and extensive, they cannot be recommended for large scale industrial applications; but they can be used for bricks, pottery and stoneware manufacturing.

REFERENCES

Ahmad, A.H.M., Noufal, K.N., Masroor Alam, M. and Tavheed K. (2014). Petrography and geochemistry of Jumara Dome sediments, Kachchh Basin: Implications for provenance, tectonic setting and weathering intensity. *Chin.J.Geochem*., **33**, 009-023, DOI: 10.1007/s11631-014-0656-4

Aja, A.A. and Randy, G.J. (2013). Physical properties of kaolin used in soap production in Nigeria. *The International Journal of Engineering and Science*, **2** (10), 10-15.

Ajayi, O.A. and Adefila, S.S. (2012). Comparative study of chemical and biological methods of beneficiation of Kankara kaolin. *International Journal of Scientific and Technology research*, **1** (8), 13-18.

Aka, F.T., Kusakabe, M., Nagao, K. and Tanyileke, G. (2001). Noble gas isotopic compositions and water/gas chemistry of soda springs from the islands of Bioko, São Tomé and Annobon, along with Cameroon Volcanic Line, West Africa. *Applied Geochemistry*, **16**, 323-338.

Akinyemi, S.A., Ogunniyi, S.O., Ojo, A.O., Gitari, W.M., Momoh, A., Akinola, O.O., Talabi, A.O., Afolagboye, L.O., Olaolorun O.A. and Ayodele, O.S. (2014). Mineralogical, physicochemical characteristics and industrial potential of some residual clay deposits within Ekiti State, Southern Nigeria. *Journal of Environment and Earth Science*, **4** (17), 70-88.

Almeida, F.F.M. de, Hasui, Y. and Brito Neves, B.B. (1976). The Upper Precambrian of South America. *Boletim Instituto de Geosciências*, **7**, 45-80.

Amouric, M. and Olives, J. (1998). Transformation mechanisms and interstratification in conversion of smectite to kaolinite: An HRTEM study. *Clays and Clay Minerals*, **46** (5), 521-527.

Ansdell, K.M. and Kyser, T.K. (1993). Textural and chemical changes undergone by zircon during the Pb-evaporation technique. *American Mineralogist*, **78**, 36-41.

Armstrong-Altrin, J.S., Nagarajan, R., Madhavaraju, J., Rosalez-Hoz, L., Lee, Y.I., Balaram, V., Cruz-Martínez, A. and Avila-Ramírez, G. (2013). Comptes rendus Geoscience, 345, 185-202, http://dx.doi.org/10.1016/j.crte.2013.03.004

Aslanian, D., Moulin, M., Olivet, J-L., Unternehr, P., Matias, L., Bache, F., Rabineau, M., Nouze, H. and Klingelheofer, F. (2009). Brazilian and African passive margins of the Central segment of the South Atlantic Ocean: Kinematic constrains. *Tectonophysics*, **468**, 98-112.

Babinski, M., Pedrosa-Soares, A.C., Trindade, R.I.F., Martins, M., Noce, C.M. and Liu, D. (2012). Neoproterozoic glacial deposits from the Araçuaí orogen, Brazil: Age, provenance and correlations with the São Francisco craton and West Congo belt. *Gondwana Research*, **21**, 451-465.

Badmus, B.S. and Olatinsu, O.B. (2009). Geophysical evaluation and chemical analysis of kaolin clay deposit of Lakiri village, southwestern Nigeria. *International Journal of Physical Sciences*, **4** (10), 592-606.

Bain, J.A. (1971). A plasticity chart as an aid to the identification and assessment of industrial clays. *Clay Minerals*, **9**, 1-17.

Baioumy, H.M. (2014). Geochemistry and origin of the Cretaceous sedimentary kaolin deposits, Red Sea, Egypt. *Chemie der Erde*, **74**, 195-203.

Baouimy, H. (2013). Hydrogen and oxygen isotopic compositions of sedimentary kaolin deposits, Egypt: Paleoclimatic implications. *Applied Geochemistry*, **29**, 182-188.

Baouimy, H.M. and Hassan M.S. (2004). Authigenic halloysite from El-Gideda iron ore, Bahria Oasis, Egypt: Characterisation and Origin. *Clay Minerals*, **39**, 207-217, DOI: 10.1180/0009855043920131

Banner, J.L. (2004). Radiogenic isotopes: systematics and applications to earth surface processes and chemical stratigraphy. *Earth-Science Reviews*, **65**, 141-194.

Barron, E.J. (1983). A warm, equable Cretaceous: The nature of the problem. *Earth-Science Reviews*, **19**, 305-338.

Barron, E.J., Fawcett, P.J., Pollard, D. and Thompson, S. (1993). Model simulations of Cretaceous climates: The role of geography and carbon dioxide. *Philosophical Transactions: Biological Sciences Royal Society London*, **341**, 301-316.

Bauer, K., Trumbull, R.B. and Vietor, T. (2003). Geophysical images and a crustal model of intrusive structures beneath the Messum ring complex, Namibia. *Earth and Planetary Science Letters*, **216**, 65-80.

Becker, A., Ammann, B., Anselmetti, F.S., Hirt, A.M., Magny, M., Millet, L., Rachoud, A-M., Sampiero, G., Wüthrich, C. (2006). Paleoenvironmental studies on Lake Bergsee, Black Forest, Germany. *N. Jb. Geol. Paläont. Abh*., **240** (3), 405-445.

Bhattacharyya, K.G. and Gupta, S.S. (2008). Adsorption of a few heavy metals on natural and modified kaolinite and montmorillonite: A review. *Advances in Colloids and Interface Science*, **140**, 114-131.

Bigeleisen, J., Perlman, M.L., Prosser, H.C., (1952). Conversion of hydrogenic materials to hydrogen for isotopic analyses. *Analytical Chemistry*, **24**, 1356–1357.

Bird, M.I. and Chivas, A.R. (1988). Stable-isotope evidence for low-temperature kaolinitic weathering and post-formational hydrogen-isotope exchange in Permian kaolinites. *Chemical Geology*, **72**, 249-265.

Bird, M.I. and Chivas, A.R. (1989). Stable-isotope geochronology of the Australian regolith. *Geochemica et Cosmochemica Acta*, **53**, 3239-3256.

Black, R. and Liegeois, J.-P. (1993). Cratons, mobile belts, alkaline rocks and continental lithospheric mantle: The Pan-African testimony. *Journal of the Geological Society, London*, **150**, 89-98.

Blackwatch (2016). Logbaba Field Reserves Report. Victoria PLC Oil and Gas Report, Blackwatch Petroleum Services Limited, Aberdeenshire, Scotland, 28 Pages.

Bloodworth, A.J., Highley, D.E. and Mitchell, C.J. (1993). Industrial minerals laboratory manual: kaolin. BGS Technical Report WG/93/1.

Bloodworth, A.J., Morgan, D.J. and Briggs, D.A. (1989). Laboratory processing trials on kaolin-bearing sandstones from Pugu, Tanzania, using conventional and new hydrocyclone bodies. *Clay Minerals*, **24**, 539-548.

Boulvais, P., Vallet, J-M., Estéole-Choux, J., Fourcade, S. and Martineau, F. (2000). Origin of kaolinitisation in Brittany (NW France) with emphasis on deposits over granite: stable isotopes (O, H) constraints. *Geochemical Geology*, **168**, 211-223.

Brito Neves, B.B. (2002). Main stages of the development of the sedimentary basins of South America and their relationship with the tectonics of supercontinents. *Gondwana Research*, **5** (1), 175-196.

Brito Neves, B.B. de, Campos Neto, M.C. and Fuck, R.A. (1999). From Rodinia to Western Gondwana: An approach to the Brasiliano-Pan-African Cycle and orogenic collage. *Episodes*, **22**, 155-166.

Brownfield, M.E., and Charpentier, R.R. (2006). Geology and total petroleum systems of the West-Central Coastal Province (7203), West Africa: *U.S. Geological Survey Bulletin,* **2207-B**, 52 pp.

Bullard, E., Everett, J.E. and Smith, A.G. (1965). The fit of the continents around the Atlantic. *Philos. Trans. R. Soc. London*, **258**, 41-51.

Burke, B.C., Heimsath, A.M. and White, A.F. (2006). Coupling chemical weathering with soil production across soil-mantled landscapes. *Earth Surface Processes and Landforms*, DOI: 10.1002/esp.1443.

Burley, S.D. and Flisch, M. (1989). K-Ar geochronology and the timing of detrital I/S clay illitization and authigenic illite precipitation in the Piper and Tartan fields, Outer Moray Firth, UK North Sea. *Clay Minerals*, **24**, 285-315.

Carvalho, H., Tassinari, C., Alves, P.H., Guimaraes, F. and Simoes, M.C. (2000). Geochronological review of the Precambrian in western Angola: links with Brazil. *Journal of African Earth Sciences*, **31** (2), 383-402.

Cavalcante, F., Belviso, C., Piccarreta, G. and Fiore, S. (2014). Grain-size control on the rare earth elements distribution in the late diagenesis of Cretaceous shales from the southern Apennines (Italy). *Journal of Chemistry*, **article ID 841747**, 1-11.

CDC (2010). Meteorological data of Fako; Cameroon Development Corporation.

Chaves, A.O. and Neves, J.M.C. (2005). Radiometric ages, aeromagnetic expression, and general geology of mafic dykes from southeastern Brazil and implications for African-Couth American correlations. *Journal of South American Earth Sciences*, **19**, 387-397.

Chavom, B.M., Ngaha, P.R.N. and Bitom, D.L. (2014). Sedimentary facies and depositional environments of Cenozoic sedimentary Formations cropping out at the central part of the Douala Basin. *American Journal of Geosciences*, **4** (1), 8-23.

Chen, P.-Y., Lin, M.-L., and Zheng, Z. (1997). On the origin of the name kaolin and the kaolin deposits of the Kauling and Dazhou areas, Kiangsi, China. *Applied Clay Science*, **12**, 1-25.

Chen, P.Y., Wang, M.K. and Yang, D.S. (2001). Mineralogy of dickite and nacrite from northern Taiwan. *Clays and Clay Minerals*, **49** (6), 586-595.

Cho, H.M. and Lumetta, G.J. (2001). Preliminary feasibility study of using solid-state nuclear magnetic resonance spectroscopy to characterize hanford tank waste solids. Pacific Northwest National Laboratory Report, PNNL-13701. Batelle Memorial University, United States Department of Energy.

Choudhary, R.P., Sheoran, A.S. and Trivedi, S.K. (2012). A small beneficiation unit: State of the art. *International Journal of Earth Sciences and Engineering*, **5** (4), 775-781.

Clauer, N., Fallick, A.E., Gálan, E., Aparicio, P., Miras, A., Fernández-Caliani, J.C. and Aubert, A. (2015). Stable isotope contraints on the origin of kaolin deposits from Variscan granitoids of Galicia (NW Spain). Chemical Geology, 417, 90-101, http://dx.doi.org/10.1016/j.chemgeo.2015.09.022

Clauer, N., Honty, M., Fallick, A.E., Šucha, V. and Aubert, A. (2014). Regional illitization in bentonite beds from the East Slovak Basin based on isotopic characteristics (K-Ar, δ^{18}O and δD) of illite-type nanoparticles. *Clay Minerals*, **49**, 247-275.

Clauer, N., Rais, N., Schaltegger, U. and Piqué, A. (1995). K-Ar systematics of clay-to-mica minerals in a multi-stage low-grade metamorphic evolution. *Chemical Geology*, **124**, 305-316.

Clauer, N., Zwingmann, H., Liewig, N. and Wendling, R. (2012). Comparative ^{40}Ar/^{39}Ar and K–Ar dating of illite-type clay minerals: A tentative explanation for age identities and differences. *Earth Sciences Reviews*, **115**, 76-96.

Cohen, K.M., Finney, S.C., Gibbard, P.L. and Fan, J.-X. (2013). The ICS International Chronostratigraphic Chart, *Episodes*, **36** (3), 199-204.

Congleton, J., Flynn, L.J., Jacobs, L.L., Brunet, M., Dejax, J., Hell, J. and Pilbeam, D. (1992). Preliminary correlation of continental sediments of the Koum Basin, northern Cameroon. In Mateer, N.J. and Chen, P.J. (Eds.), *Aspects of Nonmarine Cretaceous geology*, China Ocean Press, Beijing, pp. 213-219.

Corfu, F., Hanchar, J.M., Hoskin, P.W.O., Kinny, P. (2003). Atlas of zircon textures. *Reviews in Mineralogy and Geochemistry*, DOI: 10.2113/0530469

Costa, M.L., Souza, D.J.L. and Angélica R.S. (2009). The contribution of the laterisation process to the formation of the kaolin deposits from eastern Amazon. *Journal of South American Earth Sciences*, **27**, 219-234.

Cox, R., Lowe, D.R. and Cullers, R.L. (1995). The influence of sediment recycling and basement composition on evolution of mudrock chemistry in the southwestern United States. *Geochimica et Cosmochimica Acta*, **59** (14), 2919-2940.

Craig, H., 1961. Isotopic variations in meteoric waters. *Science*, **133**, 1702–1708.

Cravero, F., Domínguez, E. and Iglesias, C. (2001). Genesis and applications of the Cerro Rubio kaolin deposit, Patagonia (Argentina). *Applied Science*, **18**, 157-172.

Cravero, F., Gonzalez, I., Galan, E. and Dominguez, E. (1997). Geology, mineralogy, origin and possible applications of some Argentina kaolins in the Neuquen basin. *Applied Clay Science*, **12**, 27-42.

CRC Press (CRC) Handbook of Chemistry and Physics, D.R. Lide (Ed.), Internet Version 2005, CRC Press, Boca Raton, FL.

Cullers, R.L. (1995). The controls on the major- and trace-element evolution of shales, siltstones and sandstones of Ordovician to Tertiary age in the Wet Mountains regions, Colorado, U.S.A. *Chemical Geology*, **123**, 107-131.

Cullers, R.L. (2000). The geochemistry of shales, siltstones and sandstones of Pennsylvanian=Permian age, Colorado, USA: Implications for provenance and metamorphic studies. *Lithos*, **51**, 181-203.

Das, S.S., Rai, A.K., Akaram, V., Verma, D., Pandey, A.C., Dutta, K. and Prasad, G.V.R. (2013). Paleoenvironmental significance of clay mineral assemblages in the southeastern Arabian Sao during last 30 kyr. *Journal of Earth System Sciences*, **122** (1), 173-185.

Deer, W.A., Howie, R.A. and Zussman, J. (1992). An introduction to the rock-forming minerals. 2nd Edition, Pearson Eduction Limited, England, 549 pp.

Delgado, A. and Reyes, A. (1996). Oxygen and hydrogen isotope compositions in clay minerals: A potential single-mineral geothermometers. *Geochemica et Cosmochimica Acta*, **60** (21), 4285-4289.

Dhannoun, H.Y., Othman, S.M. and Al-Dabbagh, S.M. (2010). The relationship between chemical index of alteration and some major and trace elements content in rocks of Injana Formation of northern Iraq. *Iraqi National Journal of Earth Sciences*, **1**, 1-22.

Dickson, W., Schiefelbein, C., Zumberge, J. and Odegard, M. (2005). Basin analysis in Brazilian and West African conjugates: Combining disciplines to deconstruct petroleum systems. *GCSSEPM Foundation 25th Annual Bob F. Perkins Research Conference*, Houston TX December 4-7, 2005.

Diko M., Ekosse G. and Ogola J. (2016). Fourier transform infrared spectroscopy and thermal analyses of kaolinitic clays from South Africa and Cameroon. *Acta Geodyn. Geomater*., **13** (2), xx1–x10, DOI: 10.13168/AGG.2015.0052

Diko, M.L. and Ekosse, G.E. (2012). Physicochemical and mineralogical considerations of Ediki sandstone-hosted kaolin occurrence, South West Cameroon. *International Journal of the Physical Sciences*, **7** (3), 501-507.

Diko, M.L. and Ekosse, G.E. (2013). Characterisation of two kaolin facies from Ediki, Southwest Cameroon. *Scientific Research and Essays*, **8** (18), 698-704.

Diko, M.L., Ekosse, G.E. and Ogola, J. (2013). Industrial suitability of selected Cameroonian and South African kaolins. XV International Clay Conference, Rio de Janeiro, Brazil.

Dill, H.G., Bosse, H.R., Henning, K.H., Fricke, A. and Ahrendt, H. (1997). Mineralogical and chemical variations in hypogene and supergene kaolin deposits in a mobile fold belt the Central Andes of northwestern Peru. *Mineralium Deposita*, **32**, 149-163.

Djouka-Fonkwé, M.L., Schulz, B., Schüssler, U., Tchakounté, J.-P. and Nzolang, C. (2008). Geochemistry of the Bafoussam Pan-African I- and S-type granitoids in western Cameroon. *Journal of African Earth Sciences*, **50**, 148-167.

Domínguez, E., Dondi, M., Etcheverry, R., Recio, C. and Iglesias, C. (2016). Genesis and mining potential of kaolin deposits in Patagonia (Argentina). *Applied Clay Science*, **131**, 44-47, http://dx.doi.org/10.1016/j.clay.2015.12.031

Donnadieu, Y., Fluteau, F., Ramstein, G., Ritz, C, and Besse, J. (2003). Is there a conflict between the Neoproterozoic glacial deposits and the snowball Earth model: an improved understanding with numerical modelings. *Earth and Planetary Science Letters*, **208**, 101–112, doi:10.1016/S0012-821X(02)01152-4

Donnadieu, Y., Ramstein, G., Fluteau, F., Roche, D. and Ganopolski, A. (2004). The impact of atmospheric and oceanic heat transports on the sea-ice-albedo instability during the Neoproterozoic. *Climate Dynamics*, **22**, 293-306, DOI 10.1007/s00382-003-0378-5

dos Santos Jr., A.E.A., Rosetti, D.F. and Murray, H.H. (2007). Origins of the Rio Capim kaolinites (northern Brazil) revealed by $\delta^{18}O$ and δD analyses. *Applied Clay Science*, **37**, 281-294.

Ece, O.I., Nakagawa, Z.-E. and Schroeder, P.A. (2003). Alteration of volcanic rocks and genesis of kaolin deposits in the Şile Region, Northern Istanbul, Turkey. I: Clay mineralogy. *Clays and Clay Minerals*, **51** (6), 675-688.

Effoudou-Priso, E.N., Onana, V.L., Boubakar, L., Beyala, V.K.K. and Ekodeck, G.E. (2014). Relationships between major and trace elements during weathering processes in a sedimentary context: Implications for the nature of source rocks in Douala, Littoral Cameroon. *Chemie der Erde*, http://dx.doi.org/10.1016/j.chemer.2014.05.003.

Ehlers, J. and Gibbard, P.L. (2007). The extent and chronology of Cenozoic global glaciation. *Quaternary International*, **164-165**, 6-20.

Ekosse, G. (1994). Clays: A gateway into the future. *Botswana Notes and Records*, **26**, 139-149.

Ekosse, G. (2000). The Makoro kaolin deposit, southeastern Botswana: its genesis and possible industrial applications. *Applied Clay science*, **16**, 301-320.

Ekosse, G. (2001). Provenance of the Kgwakgwe kaolin deposit in Southeastern Botswana and its possible utilisation. *Applied Clay Science*, **20**, 137-152.

Ekosse, G-I.E. (2005). Fourier transform infrared spectrophotometry and X-ray powder diffractometry as complementary techniques in characterising clay size fraction of kaolin. *Journal of Applied Science and Environmental Management*, **9** (2), 43-48.

Ekosse, G-I.E. (2007). Thermoanalytical characterisation, stable isotope and paleoenvironmental considerations of kaolinite from two genetic sources. *Frenesium Environmental Bulletin*, **16** (12), 1-15.

Ekosse, G-I.E. (2010). Kaolin deposits and occurrences in Africa: Geology, mineralogy and utilisation. *Applied Clay Science*, **50**, 212–236.

Elliot, W.C., Savin, S.M., Dong, H. and Peacor, D.R. (1997). A paleoclimatic interpretation derived from pedogenic clay minerals from the Piedmont Province, Virginia. *Chemical Geology*, **142**, 201-211.

Ernst, R.E., Bleeker, W., Söderlund, U. and Kerr, A.C. (2013). Large Igneous Provinces and supercontinents: Toward completing tectonic revolution. *Lithos*, **174**, 1-14.

Eseme, E., Abanda, P.A., Agyingi, C.M. Foba-Tendo, J. and Hannigan, R.E. (2006). Composition and applied sedimentology of salt from brines of the Mamfe Basin, Cameroon. *Journal of Geochemical Exploration*, **91**, 41-55.

Eseme, E., Agyingi, C.M. and Foba-Tendo, J. (2002). Geochemistry and genesis of brine emanations from Cretaceous strata of the Mamfe Basin, Cameroon. *Journal of African Earth Sciences*, **35**, 467-476.

Fagel, N. and Boës, X. (2007). Clay-mineral record in Lake Baikal sediments: The Holocene and Late Glaciation transition. *Palaeography, Palaeoclimatology, Palaeoecology*, **259**, 230-243.

Farmer, V.C. and Russell, J.D. (1967). Infrared absorption spectrometry in clay studies. *Fifteenth Conference on Clays and Clay Minerals*, **15**, 121-142.

Faure, G. (1998). *Principles and applications of geochemistry: A comprehensive textbook for geology students*. Prentice Hall, 2nd Edition. New Jersey, USA, 615 pages.

Fedo, C.M., Nesbitt, H.W. and Young, G.M. (1995). Unravelling the effects of potassium metasomatism in sedimentary rocks and paleosols, with implications for paleoweathering conditions and provenance. *Geology*, **23** (10), 921-924.

Fehli, M., Tlili, A., Gaied, M.E. and Montacer, M. (2008). Mineralogical study of kaolinitic clays from Sidi El Bader in the far north of Tunisia. *Applied Clay Science*, **39**, 208-217, doi:10.1016/j.clay.2007.06.004

Fernández-Caliani, J.C., Gálan, E., Aparicio, P., Miras, A. and Márquez, M.G. (2010). Origin and geochemical evolution of the Nuevo Montecastelo kaolin deposit (Galicia, NW Spain). *Applied Clay Science*, **49**, 91-97, doi:10.1016/j.clay.2010.06.006

Fiantis, D., Nelson, M., Shamshuddin, J., Goh, T.B. and Van Ranst, E. (2010). Determination of the geochemical weathering indices and trace elements content of new volcanic ash deposits from Mt Talang (West Sumatra) Indonesia. *Eurasian Soil Science*, **43** (13), 1477-1485.

Flögel, S., Wallmann, K. and Kuhnt, W. (2011). Cool episodes in the Cretaceous-Exploring the effects of physical forcings on Antarctic snow accumulation. *Earth and Planetary Science Letters*, **307**, 279-288.

Fluteau, F., Ramstein, G., Besse, J., Guiraud, R. and Masse, J.P. (2007). Impacts of palaeogeography and sea level changes on Mid-Cretaceous climate. *Palaeogeography, Palaeoclimatology, Palaeoecology*, doi:10.1016/j.palaeo.2006.11.016

Folack, J. and Gabche, C.E. (2000). Natural and Anthropogenic characteristics of the Cameroon Coastal Zone.

Földvári, M. (2011). Hanadbook of thermogravimetric system of minerals and its use in geological practice. Occasional Papers of the Geological Institute of Hungary, 213, 180 pages.

Frei, D., Gerdes, A. (2009). Precise and accurate in situ U-Pb dating of zircon with high sample throughput by automated LA-SF-ICPMS. *Chemical Geology*, **261**, 261–270, doi:10.1016/j.chemgeo.2008.07.025

Frost, R.L. (1998). Hydroxyl deformation in kaolins. *Clays and Clay Minerals*, **46** (3), 280-289.

Frost, R.L. and Yang, J. and Cheng, H. and Liu, Q. and Du, X. (2010). Influencing factors on kaolinite-potassium acetate intercalation complexes. *Applied Clay Science*, **50** (4), 476-480.

Fürsich, F.T., Singh, I.B., Joachimski, M., Krumm, S., Schlirf, M. & Schlirf, S. (2005). Palaeoclimate reconstructions of the Middle Jurassic of Kachchh (western India): An integrated approach based on palaeoecological, oxygen isotopic, and clay mineralogical data. *Palaeogeography, Palaeoclimatology, Palaeoecology*, **217**, 289–309.

Gálan, E., Aparicio, P., Fernández-Caliani, J.C., Miras, A., Márquez, M.G., Fallick, A.E. and Clauer, N. (2016). New insights on mineralogy and genesis of kaolin deposits: The Burela kaolin deposit (Northwestern Spain). *Applied Clay Science*, **131**, 14-26, http://dx.doi.org/10.1016/j.clay.2015.11.015

Ganwa, E.E., Frisch, W., Siebel, W., Shang, C.K., Ondoa, J.M., Satir, M. and Numbem, J.T. (2008). Zircon $^{207}Pb/^{206}Pb$ evaporation ages of Panafrican metasedimentary rocks in the Kombé-II area (Bafia Group, Cameroon): Constraints on protolith age and provenance. *Journal of African Earth Sciences*, **51**, 77-88.

Garver, J.I., Royce, P.R. and Smick, T.A. (1996). Chromium and nickel in shale of the Taconic foreland: A case study for the provenance of fine-grained sediments with an ultramafic source. *Journal of Sedimentary Research*, **66** (1), 100-106.

Gaspe, A., Messer, P. and Young, P. (1994). Selection and preparation of clay bodies for stove manufacture. A manual clay/non clay ratio measurement technique. *Clay Testing*, 10 pages.

Gaudette, H.E., Lafon, J.-M., Macambira, M.J.B., Moura, C.A.V. and Scheller, T. (1998). Comparison of single filament Pb evaporation/ionization zircon ages with conventional U-Pb results: examples from the Precambrian of Brazil. *Journal of South American Earth Sciences*, **11** (4), 351-363.

Gerdes, A., Zeh A., (2006). Combined U–Pb and Hf isotope LA-(MC) ICP-MS analyses of detrital zircons: comparison with SHRIMP and new constraints for the provenance and age of an Armorican metasediment in Central Germany. *Earth Planet. Sci. Lett*., **249**, 47–61.

Gilg, H.A. (2000). D-H evidence for the timing of kaolinisation in Northeast Bavaria, Germany. *Geochemical Geology*, **170**, 5-18.

Gilg, H.A. (2003). Isotopic tool of dating paleoweathering in Europe. *Géologie de la France*, **1**, 49-51.

Gilg, H.A. and Frei, R., (1997). Isotope dating of residual kaolin deposits in Europe Tirschenreuth, Germany and St. Yrieix, France. Energy and Mineral Resources for the 21st Century, Geology of Mineral Deposits, Mineral Economics. In: Rongfu, R. (Ed.), *Proceedings of the 30th Internat. Geol. Congress*, Beijing, China 9 VSP Internat. Sci. Pub, Zeist, pp. 123–133.

Gilg, H.A. and Sheppard, S.M.F. (1996). Hydrogen isotope fractionation between kaolinite and water revised. *Geochemica et Cosmochimica Acta*, **60** (3), 529-533.

Gilg, H.A., Hall, A.M., Ebert, K. and Fallick, A.E. (2013). Cool kaolins from Finland. *Paleogeography, Paleoclimatology, Paleoecology*, **392**, 454-462.

Gilg, H.A., Hülmeyer, S., Miller, H. and Sheppard, S.M.F. (1999). Supergene origin of the lastarria kaolin deposit, South-Central Chile, and paleoclimatic implications. *Clays and Clay Minerals*, **47** (2), 201-211.

GTM-13. (2015): Geotechnical Test Method: *Test method and discussion for the particle size analysis of soils by hydrometer method*. Geotechnical Engineering Bureau, Office of Technical Services, Department of Transportation, New York, 33 pages

Guadagnin, F., Chemale, F., Magalhães, A.J.C., Santana, I.D. and Takehara, L. (2013). Age constraints on crystal-tuff from the Espinhaço Supergroup — Insight into the Paleoproterozoic to Mesoproterozoic intracratonic basin cycles of the Congo-São Francisco craton. *Gondwana Research*, http://dx.doi.org/10.1016/j.gr.2013.10.009

Guggenheim, S. and van Groos, A.F.K. (2001). Baseline studies of the Clay Minerals Society Source Clays: Thermal analysis. *Clays and Clay Minerals*, **49** (5), 433-443.

Guo, Y., Li, B., Wen, X., Wang, F., Niu, D., Shi, Y., Guo, Y., Jiang, S. and Hu, G. (2013): Holocene climate variation determined from rubidium and strontium contents and ratios of sediments collected from the Badain Jaran Desert, Inner Mongolia, China. *Chemie Erde*, http://dx.doi.org/10.1016/j.chemer.2013.09.001

Harris, C., Compton, J.S. and Bevington, S.A. (1999). Oxygen and hydrogen isotope composition of kaolinite deposits, Cape Peninsula, South Africa: Low-temperature, meteoric origin. *Economic Geology*, **94**, 1353-1366.

Harvey, C.C. and Murray, H.H. (1997). Industrial clays in the 21st century: A perspective of exploration, technology and utilisation. *Applied Clay Science*, **11**, 285-310.

Hassanipak, A.A. and Elsinger, E. (1985). Mineralogy, crystallinity, O^{18}/O^{16}, and D/H of Georgia kaolins. *Clays and Clay Minerals*, **33** (2), 99-106.

Heckroodt, R.O. (1991): Clay and clay minerals in South Africa. *Journal of South African Institute of Mining and Metallurgy*, **91** (10), 343-363.

Heine, K. and Völkel, J. (2010): Soil clay minerals in Namibia and their significance for the terrestrial and marine past global change research. *African Study Monographs*, **suppl. 40**, 31-50.

Horbe, A.M.C. (2011): Oxygen and hydrogen isotopes in pedogenic minerals-Implications for paleoclimate evolution in Amazonia during Cenozoic. *Geoderma*, **163**, 178-184.

Horstwood, M.S.A., Košler, J., Gehrels, G., Jackson, S.E., McLean, N.M., Paton, C., Pearson, N.J., Sircombe, K., Sylvester, P., Vermeesch, P., Bowring, J.F., Condon, D.J. and Schoene, B. (2016). Community-derived standards for LA-ICP-MS U-(Th-)Pb geochronology – Uncertainty propagation, age interpretation and data reporting. *Geostandards and Geoanalytical Research*, **40** (3), 311-332, doi: 10.1111/j.1751-908X.2016.00379.x

Hossain, I., Roy, K.K., Biswas, P.K., Alam, M., Moniruzzaman, M.D. and Deeba, F. (2014). Geochemical characteristics of Holocene sediments from Chuadanga District,

Bangladesh: Implications for weathering, climate, redox conditions, provenance and tectonic setting. *Chin.J.Geochem*, **33**, 336-350, DOI: 10.1007/s11631-014-0696-9

IAEA/WMO (2017). Global Network of Isotopes in Precipitation. The GNIP Database. Accessible at: http://www.iaea.org/water

Ilić, B.R., Mitrović and Miličić, L.R. (2010). Thermal treatment of kaolin clay to obtain metakaolin. *Hem. Ind*., **64** (4), 351-356, DOI: 10.2298/HEMIND100322014I.

Jackson M.L. (1979). *Soil Chemical Analysis – Advanced Course*, 2nd Edition, published by the author, University of Wisconsin, Madison, WI, 497 pages.

Jackson, S.E., Pearson., N.J., Griffin, W.L. and Belousova, E.A. (2004). The application of laser ablation-inductively coupled plasma-mass spectrometry to in situ U-Pb zircon geochronology. *Chemical Geology*, **211**, 47-69, doi:10.1016/j.chemgeo.2004.06.017

Jenkyns, H.C. (2003): Evidence for rapid climate change in the Mesozoic-Palaeogene greenhouse world. *Philosophical Transactions, Royal Society London*, **361** (1810), 1885-1916.

Jepson, W.B. (1984). Kaolins: their properties and uses. *Philosophical Transactions of the Royal Society London*, **A 311**, 411-432.

Kalsbeek, F., Ekwueme, B.N., Penaye, J., de Souza, Z. and Thrane, K. (2013). Recognition of Early and Late Neoproterozoic supracrustal units in West Afrcia and North-East Brazil from detrital zircon geochronology. *Precambrian Research*, **226**, 105-115, http://dx.doi.org/10.1016/j.precamres.2012.12.006

Kamgang, P., Chazot, G., Njonfang, E., Ngongang, N.B.T. and Tchoua, F.M. (2013). Mantle sources and magma evolution beneath the Cameroon Volcanic Line: Geochemistry of mafic rocks from Bamenda Mountains (NW Cameroon). *Gondwana Research*, **24**, 727-741.

Kearey, P. (2001). Dictionary of Geology. Penguin Books, 2nd Edition, 327 pp.

Keller, G. (2008): Cretaceous climate, volcanism, impacts, and biotic effects. *Cretaceous Research*, **29**, 754-771.

Keller, G., Sahni, A. and Bajpai, S. (2009). Deccan volcanism, the KT mass extinction and dinosaurs. *Journal of Biosciences*, **34** (5), 709-728.

Keller, W.D. (1978). Classification of kaolins exemplified by their textures in scan electron micrographs. *Clays and Clay Minerals*, **26** (1), 1-20.

Kenfack, P.L., Njike Ngaha, P.R., Ekodeck, G.E. and Ngueutchoua, G. (2012a): Fossils Dinoflagellates from the Northern Border of the Douala Sedimentary Sub-Basin (South-West Cameroon): Age Assessment and Paleoecological Interpretations. *Geosciences*, **2** (5), 117-124.

Kenfack, P.L., Njike Ngaha, P.R., Ekodeck, G.E. and Ngueutchoua, G. (2012b). Mineralogic Characterization and Petroleum Potential of Clays (Shales) of the N'Kapa Formation (Paleocene-Eocene) in the Douala Sedimentary Sub-basin (South-West Cameroon). *International Journal of Geosciences*, **3**, 696-709.

King, S.D. (2005). Archean cartons and mantle dynamics. *Earth and Planetary Letters*, **234**, 1-14.

Kirabira, J.B., Jonsson, S. and Byaruhanga, J.K. (2007). Beneficiation and evaluation of Mutaka kaolin. *Proceedings of the Second International Conference on Advances in Engineering and Technology*. AICTE, New Delhi, India, pp 169-175.

Kissinger, H.M. (1956). Variation of peak temperature with heating rate in differential thermal analysis. *Journal of Research of the National Bureau of Standards*, **57** (4), 217-221.

Kober, B. (1986). Whole-grain evaporation for $^{207}Pb/^{206}Pb$-age-investigations on single zircons using a double-filament thermal ion source. *Contributions to Mineralogy and Petrology*, **93**, 482-490.

Kober, B. (1987). Single-zircon evaporation combined with Pb^{+} emitter bedding for $^{207}Pb/^{206}Pb$-age investigations using thermal ion mass spectrometry, and implications to zirconology. *Contributions to Mineralogy and Petrology*, **96**, 63-71.

Komarmeni, S., Fyfe, C.A. and Kennedy, G.J. (1985). Order-disorder in 1:1 type clay minerals by solid-state ^{27}Al and ^{29}Si magic-angle-spinning NMR spectroscopy. *Clay minerals*, **20**, 327-334.

König, M. and Jokat, W. (2010). Advanced insights into magmatism and volcanism of the Mozambique Ridge and Mozambique Basin in the view of the new potential field data. *Geophysical Journal International*, **180**, 158-180.

Kröner, A. and Stern, R.J. (2004). Pan-African orogeny. *Encyclopedia of Geology*, **1**, 1-12.

Kuşcu, R., Özsoy, R., Özçelik, O., Altunsoy, M. (2016). Trace and rare earth element geochemistry of black shales in Triassic Formations, Anamas-Akseki Platform, Western Taurids, Turkey. World Multidisciplinary Earth Sciences Symposium, *IOP Conf. Series: Earth and Environmental Science*, **44**, 042012, doi:10.1088/1755-1315/44/4/042012.

Kusky, T.M. and Polat, A. (1999). Growth of granite-greenstone terranes at convergent margins, and stabilisation of Archean cratons. *Tectonophysics*, **205**, 43-73.

Lang, W.B., Warren, W.C., Thompson, R.M. and Overstreet E.F. (1965). Bauxite and kaolin deposits of the Irwinton District, Georgia. *Geological Survey Bulletin*, **1199-J**, 1-26.

Lanson, B., Beaufort, D., Berger, G., Bauer, A., Cassagnabère, A. and Meunier, A. (2002). Authigenic kaolin and illitic minerals during burial diagenesis of sandstones: A review. *Clay Minerals*, **37**, 1-22, DOI: 10.1180/0009855023710014

Laveuf, C., Cornu, S. and Juillot, F. (2008). Rare earth elements as tracers of pedogenic processes. *C.R. Geoscience*, **340**, 523-532.

Lawrence, J.R. and Meaux, J.R. (1993). The stable isotopic composition of ancient kaolinites of North America. *Climate Change in Continental Isotopic Records, Geophysical Monographs,* **78**, 249-261.

Lawrence, J.R., Taylor, H.P. (1971). Deuterium and oxygen-18 correlation: clay minerals and hydroxides in Quaternary soil compared to meteoric waters. *Geochim. Cosmochim. Acta,* **35**, 993–1003.

Lee, Y.I. (2009). Geochemistry of shales of the Upper Cretaceous Hayang Group, SE Korea: Implications for provenance and source weathering at an active continental margin. *Sedimentary Geology*, **215**, 1-12.

Lerouge, C., Cocherie, A., Toteu, S.F., Penaye, J., Milési, J-P., Tchameni, R., Nsifa, E.N., Fanning, C.M., Deloule, E. (2006). Shrimp U–Pb zircon age evidence for Paleoproterozoic sedimentation and 2.05 Ga syntectonic plutonism in the Nyong Group, South-Western Cameroon: consequences for the Eburnean–Transamazonian belt of NE Brazil and Central Africa. *Journal of African Earth Sciences*, **44**, 413-427.

Li, L., Keller, G., Adatte, T. and Stinnesbeck, W. (2000). Late Cretaceous sea-level changes in Tunisia: a multidisciplinary approach. *Journal of the Geological Society, London*, **157**, 447-458.

Liewig, N., Clauer, N., Sommer, F., (1987). Rb–Sr and K–Ar dating of clay diagenesis in Jurassic sandstone oil reservoirs, North Sea. *American Association of Petroleum*, **71**, 1467–1474.

Ligas, P., Uras, I., Dondi, M., Marsigli, M. (1997). Kaolinitic materials from Romana (north-west Sardinia, Italy) and their ceramic properties. *Applied Clay Science*, **12**, 145-163.

Logmo, E.O., Ngon Ngon, G.F., Samba, W., Mbog, M.B. and Etame, J. (2013). Geotechnical, mineralogical and chemical characterisation of the Missole II clayey materials of Douala Sub-Basin (Cameroon) for construction materials. *Open Journal of Civil Engineering*, **3**, 46-53.

López, J.M.G., Bauluz, B., Fernández-Nieto, C. and Oliete, A.Y. (2005). Factors controlling the trace-element distribution in fine-grained rocks: the Albian kaolinite-rich deposits of the Oliete Basin (NE Spain). *Geochemical Geology*, **214**, 1-19.

Lori, J.A., Lawal, A.O. and Ekanem, E.J. (2007). Characterisation and optimisation of deferration of Kankara clay. *ARPN Journal of Engineering and Applied Sciences*, **2** (5), 60-74.

Loule, J-P. and Pospisil, L. (2013). Geophysical evidence of Cretaceous volcanics in Logone Birni Basin (Northern Cameroon), Central Africa, and consequences for the West and Central African Rift System. *Tectonophysics*, **583**, 88-100.

Ludwig, K.R. (2003). Isoplot/EX version 3.0, A geochronological toolkit for Microsoft Excel, Berkeley Geochronology Center Special Publication.

Madi, K., Tsanwani, M., Zhao, B. and Tongu, E. (2013). Insights on structural, petrographical, mineralogical and geochemical approach on the Grahamstown kaolin deposit genesis in the Eastern Cape, South Africa. *International Journal of Sciences: Basic and Applied Research*, **10** (1), 146-163.

Madukwe, H., Ogungbesan, G., Aturamu, A. and Ajisafe, Y. (2016). Provenance, tectonic setting, source area weathering and paleoenvironment of the Ilaro Formation, Dahomey Basin, Nigeria. *Journal of Environmental and Earth Science*, **6** (10), 95-119.

Maia, A.A.B., Angélica, R.S., Freitas Neves, R., Pöllmann, H., Straub, C. and Saalwächter, K. (2014). Use of ^{29}Si and ^{27}Al MAS NMR to syudy thermal activation of kaolinites from Brazilian Amazon kaolin wastes. *Applied Clay Science*, **87**, 189-196.

Maley, J. (1996). The African rain forest – main characteristics of changes in vegetation and climate from the Upper Cretaceous to the Quaternary. *In*: Alexander, I.J., Swaine, M.D. and Watling, R. (Eds) Essays on the Ecology of the Guinea-Congo Rain Forest. *Proceedings of the Royal Society of Edinburgh*, **104B**, 31-73.

Manju, C.S., Narayanan Nair, V. and Lalithambika, M. (2001). Mineralogy, geochemistry and utilisation study of the Madayi kaolin deposit, North Kerala, India. *Clays and Clay Minerals*, **49** (4), 335-369.

Martin, A.K., Hartnady, C.J.H. and Goodlad, S.W. (1981). A revised fit of South America and South Central Africa. *Earth and Planetary Science Letters*, **54**, 293-305.

Martinez-Ruiz, F., Comas, M. and Vasconcelos, C. (2014). Clay mineral assemblages as proxies for reconstructing Messinian paleoenvironments in the Western Mediterranean. *Geophysical Research Abstracts,* **16**, EGU2012-16767.

Martinez-Ruiz, F., Ortega-Huertas, M. and Rivas, P. (2006). Rare earth element composition as evidence of the precursor material of Cretaceous-Tertiary boundary sediments at distal sections. *Chemical Geology*, **232**, 1-11.

Matike, D.M.E., Ekosse, G.I.E. and Ngole, V.M. (2011). Physico-chemical properties of clayey soils used traditionally for cosmetics in Eastern Cape, South Africa. *International Journal of the Physical Sciences*, **6** (33), 7557-7566.

Matos, M.D. (2000). Tectonic evolution of the Equatorial South Atlantic. *In*: Mohriak, W. and Talwani, M. (eds) *Atlantic rifts and continental margins*. American Geophysical Union, *Geophysical Monographs*, **115**, 331–354.

Mbesse, C-O., Roche, E. and Ngos III, S. (2012). La limite Paléocène-Eocène dans le bassin de Douala (Cameroun). Biostratigraphie et essai de reconstruction des paléoenvironments par l'étude des Dinoflagellés. *Geo-Eco-Trop*., **36**, 83-119.

McLennan, S.M., Hemming, S., McDaniel, D.K. and Hanson, G.N. (1993). Geochemical approaches to sedimentation, provenance, and tectonics. *Geological Society of America*, Special Paper **284**, 21-40.

Meert, J.G. and Van Der Voo (1997). The assembly of Gondwana 800-550 Ma. *Journal of Geodynamics*, **23** (374), 223-235.

Melka, K., Suchy, V., Zeman, A., Bosák, P. and Langrova, A. (2000). Halloysite from karst sediments of the Koněprusy area: Evidence for acid hydrothermal speleogenesis in

the Bohemian karst, Czech Republic. *Acta Universitatis Carolinae-Geologica*, **44**(2-4), 117-124.

Mesquita de, L.M.S., Rodrigues, T. and Gomes, S.S. (1996). Bleaching of Brazilian kaolins using organic acids and fermented medium. *Minerals Engineering*, **9** (9), 965-971.

Meunier, A., Velde, B. and Zalba, P. (2004). Illite K-Ar dating and crystal growth processes in diagenetic environments: A critical review. *Terra Nova*, **16** (5), 296–304.

Meyers, J.B., Rosendhal, B.R., Groschel-Becker, H., Austin J.A. and Rona, P.A. (1996). Deep penetrating MCS imaging of rift-to-drift transition, offshore Douala and North Gabon basins, West Africa. *Marine and Petroleum Geology*, **13** (7), 791-835.

Mineral Diffraction (2001). *Mineral powder diffraction file data book*. International Centre for Diffraction Data, Newton Square, USA, 941 pp.

Miranda-Trevino, J.C. and Coles, C.A. (2003). Kaolinite properties, structure and influence of metal retention on pH. *Applied Clay Science*, **23**, 133-139.

Misi, A., Iyer, S.S.S., Coelho, C.E.S., Tassinari, C.C.G., Franca-Rocha, W.J.S., Cunha, I. de A., Gomes, A.S.R., de Oliveira, T.F., Teixeira, J.B.G. and Filho, V.M.C. (2005). Sediment hosted lead-zinc deposits of the Neoproterozoic Bambuí Group and correlative sequences, São Francisco Craton, Brazil: A review and a possible metallogenic evolution model. *Ore Geology Reviews*, **26**, 263-304.

Mizota, C. and Longstaffe, F.J. (1996). Origin of Cretaceous and Oligocene kaolinites from the Iwaizumi clay deposit, Iwate. Northeastern Japan. *Clays and Clay Minerals*, **44** (3), 408-416.

Mongelli, G., Critelli, S., Perri, F., Sonnino, M. and Perrone, V. (2006): Sedimentary recycling, provenance and paleoweathering from chemistry and mineralogy of Mesozoic continental redbed mudrocks, Peloritani mountains, southern Italy. *Geochemical Journal*, **40**, 197-209.

Moriarty, K. C. (1977). Clay minerals in southeast Indian Ocean sediments, transport mechanisms and depositional environments. *Marine Geology*, **25**, 149—174.

Moulin, M., Aslanian, D. and Unternehr, P. (2010). A new starting point for South and Equatorial Atlantic Ocean. *Earth-Science Reviews*, **98**, 1-37.

Munsell Soil Color Charts (2000). The Munsell Soil Colour Book. Colour charts. Munsell Colour Company Inc., MI 49512, USA

Murphy, J.B. and Nance, R.D. (1991). Supercontinent model for the contrasting character of Late Proterozoic orogenic belts. *Geology*, **19**, 469-472.

Murray, H. (2002). Industrial clays case study. *Mining, Minerals and Sustainable Development*, **64**. International Institute for Environment and Development and World Business Council for Sustainable Development (WBCSD), 9 pages.

Murray, H.H. (1999). Applied clay mineralogy today and tomorrow. *Clay Minerals*, **34**, 39-49.

Murray, H.H. and Kogel, J.E. (2005). Engineered clay products for the paper industry. *Applied Clay Science*, **19**(3-4), 199-206.

Nagarajan, R., Armstrong-Altrin, J.S., Kessler, F.L, Hidalgo-Moral, E.L., Dodge-Wan, D. and Taib, N.I. (2015). Provenance and tectonic setting of Miocene siliciclastic sediments, Sibuti formation, northwestern Borneo. *Arabian Journal of Geoscience*, **8**, 8549-8656, DOI 10.1007/s12517-015-1833-4

Nasdala, L., Hofmeister, W., Norberg, N., Mattinson, J.M., Corfu, F., Dörr, W., Kamo, S.L., Kennedy, A.K., Kronz, A., Reiners, P.W., Frei, D., Košler, J., Wan, Y., Götze, J., Häger, T., Kröner, A. and Valley, J.W. (2008). Zircon M257 – a homogeneous natural reference material for the ion microprobe U-Pb analysis of zircon. *Geostandards and Geoanalytical Research*, **32**, 247-265.

Nesbitt, H.W. and Young, G.M. (1982). Early Proterozoic climates and plate motions inferred from major element chemistry of lutites, *Nature*, **299**, 715-717.

Neves, S.P. (2003). Proterozoic history of the Borborema province (NE Brazil): Correlations with neighbouring cratons and Pan-African belts and implications for the evolution of western Gondwana. *Tectonics*, **22** (4), 1-14.

Ngaha, P.R.N. (2005). Palynostratigraphy and reconstruction of the Cretaceous paleoenvironments of the east of Douala sedimentary basin (Cameroon). Ph.D Thesis: University of Yaounde I, 259 Pages.

Ngako, V. and Njongang, E. (2011). *Plates amalgamation and plate destruction, the Western Gondwana history*. In: Closson, D. (Ed): Tectonics. InTech, 370 pages.

Ngako, V., Njonfang, E., Aka, F.T., Affaton, P. and Nnange, J.M. (2006). The North-South Paleozoic to Quaternary trend if alkaline magmatism from Niger-Nigeria to Cameroon:

Complex interaction between hotspots and Precambrian faults. *Journal of African Earth Sciences*, **45**, 241-256.

Ngon Ngon, G.F., Bayiga, E., Ntamack-Nida, M.J., Etame, J. and Noa Tang S. (2012a). Trace elements geochemistry of clay deposits of Missole II from the Douala Sub-Basin in Cameroon (Central Africa): a provenance study. *Sciences, Technologie & Développement*, **13** (1), 20-35.

Ngon Ngon, G.F., Etame, J., Ntamack-Nida, M.J., Mbog, M.B., Mpondo, A.M.M., Gerard, M., Yongue-Fouateu, R. and Bilong, P. (2012b). Geological study of sedimentary clayey materials of the Bomkoul area in the Douala region (Douala sub-basin, Cameroon) for the ceramic industry. *Comptes Rendus Geoscience*, **344**, 366-376.

Ngon Ngon, G.F., Mbog, M.B., Etame, J., Ntamack-Nida, M.J., Logmo, E.O., Gerard, M., Yongue-Fouateu, R. and Bilong, P. (2014). Geochemistry of the Paleocene-Eocene and Miocene-Pliocene clayey materials of the eastern part of the Wouri River (Douala sub-basin, Cameroon): Influence of parent rocks. Journal of African Earth Sciences, 91, 110-124, http://dx.doi.org/10.1016/j.jafrearsci.2013.12.005

Nguimbous-Kouoh, J.J., Takouang, E.M.T., Nouayou, R., Tabod, C.T. and Manguelle-Dicoum, E. (2012). Structural interpretation of the Mamfe sedimentary basin of Southwestern Cameroon along the Manyu River using audiomagnetotellurics survey. *International Scholarly Research Network*, Article ID **413042**, 1-7, doi:10.5402/2012/413042.

Njoya, A., Nkoumbou, C., Grosbois, C., Njopwouo, D., Njoya, D., Courtin-Nomade, A., Yvon, J. and Martin, F. (2006). Genesis of Mayouom kaolin deposit (western Cameroon). *Applied Clay Science*, **32**, 125-140.

Njoya, D., Hajjaji, H., Baçaoui, A., and Njopwouo, D, (2010). Microstructural characterisation and influence of manufacturing parameters on technological properties of vitreous ceramic materials. *Materials Characterisation*, **61**, 289-295.

Nkoumbou, C., Njoya, A., Njoya, D., Grosbois, C., Njopwouo, D., Yvon, J. and Martin, F. (2009). Kaolin from Mayouom (Western Cameroon): Industrial suitability evaluation. *Applied Clay Science*, **43**, 118-124.

Norris, R.D., Bice, K.L., Magno, E.A. and Wilson, P.A. (2002). Jiggling the tropical thermostat in the Cretaceous hothouse. *Geology*, **30** (4), 299-302.

Ntamack-Nida, M-J., Baudin, F., Schnyder, J., Makong, J-C., Komgeu, P.B. and Abolo, G.M. (2008). Depositional environments and characterisation of the organic matter of the Lower Mundeck Formation (Barremian?-Aptian) of the Kribi-Campo sub-basin (south Cameroon): Implications for petroleum exploration. *Journal of African Earth Sciences*, **51**, 207-219.

Nyakairu, G.W.A. and Koeberl, C. (2001). Mineralogical and chemical composition and distribution of rare earth elements in clay-rich sediments from central Uganda. *Geochemical Journal*, **35**, 13-28.

Nyakairu, G.W.A., Koerberl, C. and Kurzweil, H. (2001). The Buwambo kaolin deposit in central Uganda: Mineralogical and chemical composition. *Geochemical Journal*, **35**, 245-256.

Obaje, S.O., Omada, J.I. and Dambatta, U.A. (2013). Clays and their industrial applications: Synoptic Review. *International Journal of Science and Technology*, **3** (5), 264-270.

Oder, R.R. and Price, C.R. (1973). Brightness beneficiation of kaolin clays by magnetic treatments. *Journal of the Technical Association of the Pulp and Paper Industry*, **65** (10), 75-78.

Oliveira, E.P., Toteu, S.F., Araújo, M.N.C., Carvalho, M.J., Nascimento, R.S., Bueno, J.F., McNaughton, N., Basilici, G. (2006). Geologic correlation between the Neoproterozoic Sergipano belt (NE Brazil) and the Yaoundé belt (Cameroon, Africa). *Journal of African Earth Sciences*, **44**, 470-478.

Ortega, M., Palomo, I., Martinez, F. and Gonzalez, I. (1998). Geological factors controlling clay mineral patterns across the Cretaceous-Tertiary boundary in Mediterranean and Atlantic sections. *Clay Minerals*, **33**, 483-500.

Owen, H.G. (1976). Continental displacement and expansion of the Earth during the Mesozoic and Cenozoic. *Philosophical Transactions of the Royal Society of London. Series A, Mathematical and Physical Sciences*, **281** (1303), 223-291.

Owona, S., Ondoa, J.M. and Ekodeck, G.E. (2013). Evidence of quartz, feldspar and amphibole crystal plastic deformations in the Paleoproterozoic Nyong Complex shear zones under amphibolite to granulite conditions (West Central African Fold Belt, SW Cameroon). *Journal of Geography and Geology*, **5** (3), 186-201.

Pamo, E.T. (2008). Country Pasture/Forage Resource Profiles: Cameroon. Food and Agricultural Organisation. www.fao.org/ag/agp/AGPC/doc/Counprof/cameroon/cameroon.htm

Parnell, J., Baron, M. and Boyce, A. (2000). Controls on kaolinite and dickite distribution, Highland Boundary Fault Zone, Scotland and Northern Ireland. *Journal of the Geological Society, London*, **157**, 635-640.

Parrish, J.T., Ziegler, A.M. and Scotese, C.R. (1982). Rainfall patterns and the distribution of coals and evaporates in the Mesozoic and Cenozoic. *Palaeogeography, Palaeoclimatology, Palaeoecology*, **40**, 67-101.

Paton, C., Hellstrom, J., Paul, B., Woodhead, J., Hergt, J. (2011). Iolite: freeware for the visualisation and processing of mass spectrometric data. *J. Anal. At. Spectrom*., **26**, 2508–2518.

Pedrosa-Soares, A.C., Noce, C.M., Wiedermann, C.M and Pinto, C.P. (2001). The Araçuaí-West-Congo orogeny in Brazil: An overview of a confined orogeny formed during Gondwanaland assembly. *Precambrian Research*, **110**, 307-323.

Penaye, J., Toteu, S.F., Tchameni, R., van Schmus, W.R., Tchakounté, J., Ganwa, A., Minyem, D. and Nsifa, E.N. (2004). The 2.1 Ga West Central African Belt in Cameroon: extension and evolution. *Journal of African Earth Sciences*, **39**, 159-164.

Petrus, J.A., Kamber, B.S. (2012). VizualAge: A Novel Approach to Laser Ablation ICP-MS U-Pb Geochronology Data Reduction: *Geostandards and Geoanalytical Research*, **36**, 247-270.

Petschnick, R., Kuhn, G. and Gingele, F. (1996). Clay mineral distribution in surface sediments of the South Atlantic: sources, transport, and relation to oceanography. *Marine Geology*, **130**, 203-229.

Petters, S.W. (1978). Stratigraphic evolution of the Benue Trough and its implications for the Upper Cretaceous paleogeography of West Africa. *The Journal of Geology*, **86** (3), 311-322.

Pletsch, T., Erbacher, J., Holbourn, A.E.L., Kuhnt, W., Moullade, M., Oboh-Ikuenobede, F.E., Söding, E. and Wagner, T. (2001). Cretaceous separation of Africa and South America: the view from the West African margin (ODP Leg 159). *Journal of South American Earth Sciences*, **14**, 147-174.

Pleuger, J., Manchtelow, N., Zwingmann, H. and Manser, M. (2012). K–Ar dating of synkinematic clay gouges from Neoalpine faults of the Central, Western and Eastern Alps. *Tectonophysics*, **550-553**, 1-16.

Prasad, M.S., Reid, K.J. and Murray, H.H. (1991). Kaolin: processing, properties and applications. *Applied Clay Science*, **6** (2), 87-119.

Price, J.R. and Velbel, M.A. (2003). Chemical weathering indices applied to weathering profiles developed on heterogeneous felsic metamorphic parent rocks. *Chemical Geology*, **202**, 397-416.

Pruett, R.J. (2016). Kaolin deposits and their uses: Northern Brazil and Georgia, USA. *Applied Clay Science*, **131**, 3-13, http://dx.doi.org/10.1016/j.clay.2016.01.048

Ptáček, P., Kubátová, D., Havlica, J., Brandštetr, J., Šoukal, F. and Opravil, T. (2010). *Thermochimica Acta*, **501**, 24-29, doi:10.1016/j.tca.2009.12.018

Rainaud, C., Master, S., Armstrong, R.A. and Robb, L.J. (2005). Geochronology and nature of the Palaeoproterozoic basement in the Central African Copperbelt (Zambia and the Democratic Republic of Congo), with regional implications. *Journal of African Earth Sciences*, **42**, 1-31.

Ramsey, M.H., Potts, P.J., Webb, P.C., Watkins, P., Watson, J.S. and Coles, B.J. (1995). An objective assessment of analytical method precision: comparison of ICP-AES and XRF for the analysis of silicate rocks. *Chemical Geology*, **124**, 1-19.

Renne, P. (2000). K-Ar and 40Ar/39Ar dating. Quaternary Geochronology: Methods and Applications. *The American Geophysical Union*, **AGU Reference Shelf 4**, (77-100).

Rimmer, S.M. (2004). Geochemical paleoredox indicators in Devonian-Mississippian black shales, Central Appalachian Basin (USA). *Chemical Geology*, **206**, 373-391, doi:10.1016/j.chemgeo.2003.12.029

Roaldset, E. (1972). Mineralogy and geochemistry of Quaternary clays in the Numedal area, southern Norway. *Norsk Geologisk Tidsskrift*, **52**, 335-369.

Robertson, R.H.S., Brindley, G.W. and Mackenzie, R.C. (1954): Mineralogy of kaolin clays from Pugu, Tanganyika

Roseneau, N.A. and Tabor, N. (2013). Oxygen and hydrogen isotope composition of paleosol phyllosilicates: Differential burial histories and determination of Middle-Late

Pennsylvanian low-latitude terrestrial palaeotemperatures. *Palaeogeography, Palaeoclimatology and Palaeoecology*, **392**, 382-397.

Roy, A., Singh, S.K., Banerjee, P.C., Dana, K. and Das, S.K. (2010). Bio-beneficiation of kaolin and feldspar and its effect on fired characteristics of triaxial porcelain. *Bull. Mater. Sci.*, **33** (3), 333-338.

Rudnick, R.L., Gao, S. (2003). Composition of the continental crust. *Treatise on Geochemistry*, **3**, 1-64.

Saikia, N.J., Bharali, D.J., Senggupta, P., Bordoloi, D., Goswamee, R.L., Saikia, P.C. and Borthakur, P.C. (2003). Characterisation, beneficiation and utilisation of a kaolinite clay from Assam, India. *Applied Clay Science*, **24**, 93-103.

Sari, A. and Koca, D. (2012). An approach to provenance, tectonic and redox conditions of Jurassic-Cretaceous Akkuyu Formation, Central Taurids, Turkey. *Mineral Res. Expl. Bull.*, **144**, 51-74.

Savin S.M. and Epstein S. (1970). Oxygen and hydrogen isotope geochemistry of clay minerals. *Geochim Cosmochim Acta*, **34**, 25-42.

Savin, S.M. and Hsieh, J.C.C. (1998). The hydrogen and oxygen isotope geochemistry of pedogenic clay minerals: principles and theoretical background. *Geoderma*, **82**, 227-253.

Sayin, S.A. (2007). Origin of kaolin deposits: Evidence from the Hirsacik (Emet-Kütahya) Deposits, Western Turkey. *Turkish Journal of Earth Sciences*, **16**, 77-96.

Schroeder R.J. and Hayes, J.B. (1968). Dickite and kaolinite in Pennsylvanian limestones of southeastern Kansas. *Clays and Clay Minerals*, **16**, 41-49.

Schroeder, P.A., Melear, N.D. and Pruett, R.J. (2003). Quantitative analysis of anatase in Georgia kaolins using Raman spectroscopy. *Applied Clay Science*, **23**, 299-308, doi:10.1016/S0169-1317(03)00129-7

Schroeder, P.A., Pruett, R.J. and Melear, N.D. (2004). Crystal-chemical changes in an oxidative weathering front in a Georgia kaolin deposit. *Clays and Clay Minerals*, **52** (2), 211-220, DOI: 10.1346/CCMN.2004.0520207

Schwaighofer, B. amd Müller, W. (1987). Mineralogy and genesis of the Pugu Hill kaolin deposit, Tanzania. *Clay Minerals*, **22**, 401-409.

Scorzelli, R.B., Bertolino, L.C., Luz, A.B., Duttine, M., Silva, F.A.N.G. and Munayco, P. (2008). Spectroscopic studies of kaolin from different Brazilian regions. *Clay Minerals*, **43**, 1-7.

Scotese, C. R., (2001). *Atlas of Earth History*, Volume 1, Paleogeography, PALEOMAP Project, Arlington, Texas, 52 pages.

Seranne, M. (1999). Early Oligocene stratigraphic turnover on West Africa continental margin: a signature of the Tertiary greenhouse to icehouse transition. *Terra Nova*, **11**, 135-140.

Sewall, J.O. and Sloan, L.C. (2001). Equable Paleogene climates: The results of a stable, positive Arctic oscillation? *Geophysical Research Letters*, **28** (19), 3693-3595.

Shang, C.K., Liégeois, J.P., Satir, M., Frisch, W. and Nsifa, E.N. (2010). Late Archaean high-K granite geochronology of the northern metacratonic margin of the Archaean Congo craton, Southern Cameroon: Evidence for Pb-loss due to non-metamorphic causes. *Gondwana Research*, doi:10.1016/j.gr.2010.02.008.

Shang, C.K., Satir, M., Siebel, W., Nsifa, E.N., Taubald, H., Liégeois, J.P. and Tchoua, F.M. (2004). TTG magmatism in the Congo craton; a view from major and trace element geochemistry, Rb-Sr and Sm-Nd systematics: case of the Sangmelima region, Ntem complex, southern Cameroon. *Journal of African Earth Sciences*, **40**, 61-79.

Shao, J., Yang, S. and Li, C. (2012). Chemical indices (CIA and WIP) as proxies for integrated chemical weathering in China: Inferences from analysis of fluvial sediments. *Sedimentary Geology*, **265-266**, 110-120.

Sheldon, N.D. and Tabor, N.J. (2009). Quantitative paleoenvironmental and paleoclimatic reconstruction using paleosols. *Earth-Science Reviews*, **95**, 1–52.

Sheppard, S.M.F. and Gilg, H.A. (1996). Stable isotope geochemistry of clay minerals. *Clay Minerals*, **31**, 1-24.

Sheppard, S.M.F., Nielsen, R.L., Taylor, H.P. (1969). Oxygen and hydrogen isotope ratios of clay minerals from porphyry copper deposits. *Economic Geology*, **64**, 755–777.

Siddiqui, M.A and Ahmed, Z. (2008). Geochemistry of the kaolin deposits of Swat (Pakistan). *Chemie de Erde*, **68**, 207-219.

Siddiqui, M.A., Ahmed, Z. and Saleemi, A.A. (2005). Evaluation of Swat kaolin deposits of Pakistan for industrial uses. *Applied Clay Science*, **29**, 55-72.

Sijp, W.P., von der Heydt, A.S., Dijkstra, H.A., Flögel, S., Douglas, P.M.J. and Bijl, P.K. (2014). The role of ocean gateways on cooling climate on long time scales. *Global and Planetary Change*, **119**, 1-22.

Sláma, J., Košler, J., Condon, D.J., Crowley, J.L., Gerdes, A., Hanchar, J.M., Horstwood, M.S.A., Morris, G.A., Nasdala, L., Norberg, N., Schaltegger, U., Schoene, B., Tubrett, M.N., Whitehouse, M.J. (2008). Plešovice zircon – a new natural reference material for U-Pb and Hf isotopic microanalysis. *Chemical Geology*, **241**, 1–35, doi:10.1016/j.chemgeo.2007.11.005

SNH/UD (2005). *Stratigraphie Séquentielle et Tectonique des Dépôts Mésozoïques Synrifts du Bassin de Kribi/Cam- po*, Unpublished report.

Souza, D.J.L., Varajão, A.F.D.C., Yvon, J., Scheller, T. and Moura, C.A.V. (2007). Ages and possible provenance of the sediments of the Capim River kaolin, northern Brazil. *Journal of South American Earth Sciences*, **24**, 25-33.

Środoń, J., Clauer, N. and Eberl, D.D.D. (2002). Interpretation of K-Ar dates of illitic clays from sedimentary rocks aided by modelling. *American Mineralogist*, **87**, 1528-1535.

Stendal, H., Toteu, F.S., Frei, R., Penaye, J., Njel, U.O., Bassanak, J., Nni, J., Kankeu, B., Ngako, V. and Hell, J.V. (2006). Derivation of detrital rutile in the Yaoundé region from Neoproterozoic Pan-African belt in southern Cameroon (Central Africa). *Journal of African Earth Sciences*, **44**, 443-458.

Stern, L.A., Chamberlain, C.P., Reynolds, R.C. and Johnson, G.D. (1997). Oxygen isotope evidence of climate change from pedogenic clay minerals in Himalayan molasses. *Geochemica et Cosmochimica*, **61** (4), 731-744.

Štyriaková, I. and Štyriak, I. (2000). Iron removal from kaolins by bacterial leaching. *Ceramics—Silikáty*, **44**, 135-141.

Suárez, M. and García-Romero, E. (2006). FTIR spectroscopic study of palygorskite: Influence of the composition of the octahedral sheet. *Applied Clay Science*, **31**, 154-163.

Sutherland, F.L. (1996). The Cretaceous/Tertiary-boundary impact and its global effects with reference to Australia. *AGSO Journal of Australian Geology & Geophysics*, **16** (4), 567-585.

Tabor, N.J. and Montanez, I.P. (2005). Oxygen and hydrogen isotope compositions of Permian pedogenic phyllosilicates: Development of modern surface domain arrays

and implications for paleotemperature reconstruction. *Palaeogeography, Palaeoclimatology, Palaeoecology*, **223**, 127-146.

Tabor, N.J., Montanez, I.P. and Southard, R.J. (2002). Paleoenvironmental reconstruction from chemical and isotopic composition of Permo-Pennsylvanian pedogenic minerals. *Geochemica et Cosmochimica Acta*, **66** (17), 3093-3107.

Tan, K.H. (1996). *Soil sampling preparation and analysis*. Marcel Dekker Inc. New York, 392 pages.

Tardy, Y., Kobilsek, B. and Paquet, H. (1991). Mineralogical composition and geographical distribution of African and Brazilian periatlantic laterites. The influence of continental drift and tropical paleoclimates during the past 150 million years and implications for India and Australia. *Journal of African Earth Sciences*, **12** (1/2), 283-295.

Tassongwa, B., Nkoumbou, C., Njoya, D., Njoya, A., Tchop, J.L., Yvon, J. and Njopwouo, D. (2014). Geochemical and mineralogical characteristics of the Mayouom kaolin deposit, West Cameroon. *Earth Science Research*, **3** (1), 94-107.

Taylor, S.R. and McLennan, S.M. (1985). *The Continental Crust: Its Composition and Evolution*. Blackwell, Oxford, UK.

Tchameni, R., Mezger, K., Nsifa, N.E. and Poucet, A. (2000). Neoarchaean crustal evolution in the Congo Craton: Evidence from K rich granitoids of the Ntem Complex, southern Cameroon. *Journal of African Earth Sciences*, **30** (1), 133-147.

Tchameni, R., Mezger, K., Nsifa, N.E. and Poucet, A. (2001). Crustal origin of Early Proterozoic syenites in the Congo Craton (Ntem Complex), South Cameroon. *Lithos*, **57**, 23-42.

The Non-Affiliated Soil Analysis Work Committee (1990). *Handbook of standard soil testing methods for advisory purposes*. Soil Science Society of South Africa, P.O. Box 30030, Sunnyside 0132, Pretoria, South Africa.

Thiry, M. (2000). Palaeoclimatic interpretation of clay minerals in marine deposits: and outlook from the continental margin. *Earth-Science Reviews*, **49**, 201-221.

Tobia, H.F. and Shangola, S.S. (2016). Mineralogy, geochemistry, and depositional environment of the Beduh shale (Lower Triassic, Northern Thrust Zone, Iraq. *Turkish Journal of Earth Sciences*, **25**, 367-391, doi:10.3906/yer-1511-10

Tohver, E., D'Agrella-Filho, M.S., and Trindale, R.I.F. (2006). Paleomagnetic record of Africa and South America for the 1200-500 Ma interval, and evaluation of Rodinia and Gondwana assemblies. *Precambrian Research*, **147**, 193-222.

Torrent, J. and Barrón, V. (1993). Laboratory measurement of soil color: Theory and practice. *Soil Science Society of America*, Special Publication **31**, 32-33.

Torsvik, T.H. and Van der Voo, R. (2002). Refining Gondwana and Pangea palaeogeography: estimates of Phanerozoic non-dipole (octupole) fields. *Geophys. J. Int*. **151**, 771-794.

Toteu, S.R., Penaye, J. and Djomani, Y.P. (2004). Geodynamic evolution of the Pan-African belt in central Africa with special reference to Cameroon. *Canadian Journal of Earth Sciences*, **41**, 75-85.

Toteu, S.R., Van Schmus, W.R., Penaye, J. and Michard, A. (2001). New U-Pb and Sm-Nd data from north-central Cameroon and its bearing on the pre-Pan African history of central Africa. *Precambrian Research*, **108**, 45-73.

Tucker, R.T., Roberts, E.M., Hu, Y., Kemp, A.I.S. and Salisbury, S.W. (2013). Detrital zircon age constraints for the Winton Formation, Queensland: Contextualising Australia's Late Cretaceous dinosaur faunas. Gondwana Research, http://dx.doi.org/10.1016/j.gr.2012.12.009

Turc, L., Chevalier, M., Flavier, C., Cheddadi, R., Meadows, M.E., Scott, L., Carr, A.S., Smith, G.F., and Chase, B.M. (2013). Quantification of climate change for the last 20,000 years from Wonderkrater, South Africa: Implications for the long-term dynamics of the Intertropical Convergence Zone. *Palaeogeography, Palaeoclimatology, Palaeoecology*, **386**, 575-587.

Turgeon, S. and Brumsack, H.-J. (2006). Anoxic vsdysoxic events reflected in sediment geochemistry during the Cenomanian-Turonian Boundary Event (Cretaceous) in the Umbria-Marche Basin of central Italy. *Chemical Geology*, **234**, 321-339, doi:10.1016/j.chemgeo.2006.05.008

Vaculíková, L., Plevová, E., Vallová, S. and Koutník, I. (2011). Characterisation and differentiation of kaolinites from selected Czech deposits using infrared spectroscopy and differential thermal analysis. *Acta Geodyn. Geomater*, **8** (161), 59-67.

Valdes, P.J. (2000). Warm climate forcing mechanisms. In: Huber, B.T., MacLeod, K.G. and Wing, S.L. (eds), *Warm climates in earth history*. Cambridge University Press, pp 1-20.

van Hinsbergen, D.J.J., de Groot, L.V., van Schaik, S.J., Spakman, W., Bijl, P.K., Sluijs, A., Langereis, C.G. and Brinkhuis, H. (2015). A Paleolatitude Calculator for Paleoclimate Studies (model version 2.0), *PLOS ONE*, **10**(6): e0126946. doi:10.1371/journal.pone.0126946

Van Reeuwijk, L.P. (2002). *Procedures for soil analysis*. International Soil Reference and Information Centre, Wageningen, The Netherlands, Tech. Paper 9, 100 pp.

Van Wilderode, J., Heijlen, W., De Muynck, D., Schneider, J., Vanhaecke, F. and Muchez, Ph. (2013). The Kipushi Cu-Zn deposit (DR Congo) and its host rocks: A petrographical, stable isotope (O, C) and radiogenic isotope (Sr, Nd) study. *Journal of African Earth Sciences*, **79**, 143-156.

Verma, S.K., Verma, S.P., Oliveira, E.P., Singh, V.K. and Moreno, J.A. (2016). LA-SF-ICP-MS zircon U-Pb geochronology of granitic rocks from the central Bundelkhand greenstone complex, Bundelkhand craton, India. *Journal of Asian Earth Sciences*, **118**, 125-137, http://dx.doi.org/10.1016/j.jseaes.2015.12.021

Violante, A., Cozzolino, V., Perelomov, L., Caporale, A.G. and Pigna, M. (2010). Mobility and bioavailability of heavy metals and metalloids in soil environments. *J. Soil. Sci. Plant Nutr*., **10** (3), 268 – 292.

Walker, J.D., Geissman, J.W., Bowring, S.A. and Babcock, L.E. (2013). The Geological Society of America Geologic Time Scale. *Geological Society of America Bulletin*, **125** (3-4), 259-272, doi: 10.1130/B30712.1

Walter, S., Herrmann, A.D. and Bengtson, P. (2005). Stratigraphy and facies analysis of the Cenomanian-Turonian boundary succession in the Japaratuba area, Sergipe Basin, Brazil. *Journal of South American Earth Sciences*, **19**, 273-283.

Westermann, S., Duchamp-Alphonse, S., Fiet, N., Fleitmann, D., Matere, V., Adatte, T. and Föllmi, K.B. (2013). Palaeoenvironmental changes during the Valanginian: New insights from variations in phosphorous contents and bulk-and clay mineralogies in the western Tethys. *Paleogeography, Paleoclimatology, Paleoecology*, **392**, 196-208.

Wirmvem, M.J., Ohba, T., Kamtchueng, B.T., Tay;or, E.T., Fantong, W.Y. and Ako, A.A. (2016). Variation in stable isotope ratios of monthly rainfall in the Douala and Yaounde cities, Cameroon: local meteoric lines and relationship to regional precipitation cycle. *Applied Water Science*, DOI 10.1007/s13201-016-0413-4

World Bank (2015). Countries, Cameroon Overview. http://www.worldbank.org/en/country/cameroon/overview. Updated on 30 September, 2015.

World Bank (2016a). Countries, Cameroon Overview. http://www.worldbank.org/en/country/cameroon/overview. Updated on 27 March, 2016.

World Bank (2016b). Doing Business 2016: Measuring Regulatory Quality and Efficiency. Washington, DC: World Bank. DOI: 10.1596/978-1-4648-0667-4

www.batatekinc.com Accessed on 04 January 2017.

www.googlr.co.za Accessed on 23 November 2014.

www.paleolatitudes.org Accessed on 21 March 2017.

www.weatherbase.com Accessed on 19 January 2015.

Yaalon, D.H. (1961). Mineral composition of the average shale. *Clay Min. Bull*., **5**, 31-36.

Yuan, Y., Shi, G., Yang, M., Wu, Y., Zhang, Z., Huang, A. and Zhang, J. (2014). Formation of a hydrothermal kaolinite deposit from rhyolitic tuff in Jiangxi, China. *Journal of Earth Science*, **25** (3), 495-505.

Zachos, J.C., Lohmann, K.C., Walker, J.C.G. and Wise, S.W. (1993). Abrupt climate change and transient climates during the Paleogene: A marine perspective. The *Journal of Geology*, **101** (2), 191-213.

Zhu, B., Jiang, S-Y., Yang, J-H., Pi, D., Ling, H-F. and Chen, Y-Q. (2014). Rare earth element and Sr-Nd isotope geochemistry of phosphate nodules from the lower Cambrian Niutitang Formation, NW Hunan Province, South China. *Palaeogeography, Palaeoclimatology, Palaeoecology*, **398**, 132-143.

Zwingmann, H., Offler, R., Wilson, T. and Cox, S.F. (2004). K-Ar dating of fault gouge in the northern Sydney Basin, NSW, Australia-implications for the breakup of Gondwana. *Journal of Structural Geology*, **26**, 2285-2295.

APPENDICES

Appendix 3.1: Replicate samples analyses of Serina Standard

	A	B	C	
Sample	Bulk Serina kao 1	Bulk Serina kao 2	Bulk Serina kao 3	Mean
dD raw (‰)	-61.6	-62.8	-64.0	
d D cor (‰)	-54.5	-55.8	-56.9	
dD corr2 (‰)	-55.5	-56.8	-57.9	
dD corr3 (‰)	-57.4	-58.7	-59.9	**-58.1**
dD corr4 (‰)	-56.3	-57.6	-58.8	**-57.0**
Wt sample	15.34	15.13	15.87	
P	38.3	37.3	39.4	
Mass 2 V	4.264	4.316	4.646	
mg water	1.83	1.85	1.99	
wt.% water	11.93	12.24	12.56	

Appendix 4.1: Results in wt% of quantitative analysis of minerals identified in bulk samples

	Kaolinite	Illite	Smectite	Quartz	Microcline	Anatase	Rutile	Goethite	Hematite	Total
BKL 01	55.82	3.84	2.52	35.76	-	1.3	0.6	0.15	-	99.99
BKL 02	57.64	3.31	6.3	30.96	-	1.68	0.14	-	-	100.03
BKL 03	28.4	1.16	12.9	54.43	-	0.52	0.86	1.67	-	99.94
DBB	53.5	2.5	5.92	36.83	-	1	-	0.23	-	99.98
DBB CN 01	14.15	6.39	4.9	73.4	-	1.11	-	-	-	99.95
DBB CN 02	8.49	2.7	3.78	84.95	-	0.07	-	-	-	99.99
EDK 01	15.6	12.24	35.53	32.4	-	2.14	2.15	-	-	100.06
EDK 02	24.77	4.44	9.56	32.08	27.61	0.41	0.35	0.79	-	100.01
EDK 03	12.91	9.94	38.07	20.76	14.53	1.71	2.12	-	-	100.04
LBB 01	50.23	3.11	1.99	42.53	-	1.76	0.39	-	-	100.01
LBB 02	53.8	1.08	8.2	32.99	-	1.82	-	2.1	-	99.99
LBB 03	40.5	1.5	3.95	51.66	-	1.47	-	0.89	-	99.97
MSL I 01	11.51	0.86	7.4	79.4	-	0.16	-	0.71	-	100.04
MSL I 02	5.28	2.5	3.47	88.19	-	0.57	-	-	-	100.01
MSL II 01	52.43	2.73	3.66	38.32	-	2.08	0.79	-	-	100.01
MSL II 02	55.9	4.51	5.64	32.16	-	1.79	-	-	-	100
YTK 01	41.5	5.15	8.71	40.86	-	0.61	0.07	2.66	0.42	99.98
YTK 02A	15.93	4.97	31.23	40.75	-	1.4	0.24	5.09	0.35	99.96
YTK 02B	46.24	5.55	15.57	31.38	-	0.78	0.04	0.14	0.29	99.99
YTK 03	58.43	4.78	2.77	26.14	-	1.55	0.1	3.21	3.01	99.99
Min	5.28	0.86	1.99	20.76	0	0.07	0	0	0	
Max	58.43	12.24	38.07	88.19	27.61	2.14	2.15	5.09	3.01	
Mean	33.01	4.41	11.20	46.16	2.48	1.20	0.37	0.93	0.27	

Appendix 4.2: Results in wt% of quantitative analysis of minerals identified in silt samples

	Kaolinite	Illite	Smectite	Quartz	Microcline	Anatase	Rutile	Goethite	Hematite
BKL 03	3.95	1.4	4.85	87.49	0	0.06	2.24	0	0
DBB	67.6	3.81	2.66	23.68	0	1.55	0.7	0	0
EDK 02	27.77	4.78	7.57	26.72	32.02	1.03	0.11	0	0
LBB 02	19.44	0.95	4.04	73.92	0	0.96	0.12	0.57	0
MSL II 02	36.74	4.72	5.55	49.93	0	1.99	1.08	0	0
YTK 02A	15.59	5.6	40.55	31.02	0	1.75	1.33	3.21	0.9
Mean	28.52	3.54	10.87	48.79	5.34	1.22	0.93	0.63	0.15

Appendix 4.3: Results in wt% of quantitative analysis of minerals identified in < 2 µm samples

	Kaolinite	Illite	Smectite	Quartz	Microcline	Anatase	Goethite	Hematite	Rutile	Total
BKL 01	88.45	3.77	4.48	-	-	2.52	-	-	0.78	100
BKL 02	88.73	3.6	4.06	-	-	2.83	-	-	0.78	100
BKL 03	81.6	3.74	10.44	0.76	-	2.49	-	-	0.96	100
DBB	90.61	2.91	2.95	-	-	2.72	-	-	0.82	100
DBB CN 01	92.17	1.97	2.29	-	-	2.8	-	-	0.77	100
DBB CN 02	88.94	2.49	4.84	-	-	2.8	-	-	0.93	100
EDK 01	41	14.34	39.67	2.32	-	1.4	-	-	1.24	100
EDK 02	63.4	9.69	23.39	1.17	-	0.42	-	-	1.97	100
EDK 03	8.00	21.9	41.6	6.07	16.03	2.90	-	-	3.5	100
LBB 01	90.43	2.54	3.23	-	-	3.05	-	-	0.76	100
LBB 02	90.33	4.1	1.61	-	-	3.07	-	-	0.89	100
LBB 03	91.14	2	2.9	-	-	3.19	-	-	0.77	100
MSL I 01	58.5	2.6	16.84	20.16	-	1.1	-	-	0.75	100
MSL I 02	31.3	0.9	9.98	57	-	0.1	0.23	-	0.5	100
MSL II 01	87.33	4.94	2.71	0.05	-	4.28	-	-	0.69	100
MSL II 02	85.87	6.18	3.05	0.34	-	3.81	-	-	0.74	100
YTK 01	83.3	-	4.39	0.77	-	1.79	8.42	0.69	0.68	100
YTK 02A	11.91	-	20.48	16.3	-	0.94	48.7	1.69	-	100
YTK 02B	84.07	2.08	10.47	-	-	0.85	-	1.93	0.62	100
YTK 03	87.46	4.06	4.33	0.16	-	2.4	-	0.7	0.89	100
Min	8	0	1.61	0	0	0.1	0	0	0	
Max	92.17	21.9	41.6	57	16.03	4.28	48.7	1.93	3.5	
Mean	72.23	4.69	10.69	5.26	0.80	2.27	2.87	0.25	0.95	

Appendix 4.4: Position and assignment of transmittance bands (cm^{-1}) in the IR spectra < 2 µm fractions of Bomkoul, Dibamba and Ediki samples

KGa-1b	KGa-2	BKL 01	BKL 02	BKL 03	DBB	DBB CN 01	DBB CN 02	EDK 01	EDK 02	EDK 03	Assignment
3689	3691	3690	3690	3690	3688	3690	3688	3586	3684	3688	OH stretching of inner-surface hydroxyl groups
3669	-	3665	3667	-	3667	3667	3667	3665	3667	-	OH stretching of inner-surface hydroxyl groups
3651	3650	3649	3649	3647	3651	3649	3651	3647	3647	3645	OH stretching of inner-surface hydroxyl groups
3619	3619	3621	3619	3618	3619	3621	3619	3619	3619	3619	OH stretching of inner hydroxyl groups
3457	3442	-	-	3439	-	3435	3431	-	-	-	OH stretching of water
3426	-	3435	3431	-	3433	-	-	3425	-	3421	Smectite
1635	1630	1636	1634	1634	1640	1640	1634	1636	1636	1636	OH deformation of water
1115	1114	1114	1114	1114	1114	1114	1114	1114	1114	1111	Si–O stretching (longitudinal mode)
1102	1105	-	-	-	-	-	-	-	-	-	perpendicular Si–O stretching
1027	1028	1024	1026	1026	1024	1026	1026	1024	1022	-	in-plane Si–O stretching
1005	1004	997	999	999	997	997	997	991	993	983	in-plane Si–O stretching
937	935	934	934	936	934	934	934	934	932	-	OH deformation of inner-surface hydroxyl group
912	912	910	910	910	910	908	910	908	908	908	OH deformation of inner hydroxyl groups
788	789	789	790	791	791	790	790	790	790	790	Si–O
751	750	747	748	749	747	749	749	749	747	750	Si–O, perpendicular
681	684	683	679	681	683	681	687	681	681	687	Si–O, perpendicular
645	641	640	640	636	636	636	638	-	636	-	Si–O
541	540	522	526	518	524	538	538	530	522	514	Al–O–Si deformation
472	470	473	477	473	473	465	469	473	469	467	Si–O–Si deformation
432	430	430	420	424	426	430	426	428	434	432	Si–O deformation

(–) not detected

Appendix 4.5: Position and assignment of transmittance bands (cm^{-1}) in the IR spectra of < 2 µm fractions of Logbaba and Missole I samples

KGa-1b	KGa-2	LBB 01	LBB 02	LBB 03	MSL I 01	MSL I 02	Assignment
3689	3691	3690	3690	3690	3692	3694	OH stretching of inner-surface hydroxyl groups
3669	-	3667	3665	3665	-	-	OH stretching of inner-surface hydroxyl groups
3651	3650	3649	3647	3649	3649	3651	OH stretching of inner-surface hydroxyl groups
3619	3619	3621	3621	3621	3621	3619	OH stretching of inner hydroxyl groups
3457	3442	3443	3445	3443	-	-	OH stretching of water
3426	-	-	-	-	-	-	Smectite
1635	1630	1636	1640	1634	1624	1624	OH deformation of water
1115	1114	1114	1114	1114	1114	1114	Si–O stretching (longitudinal mode)
1102	1105	-	-	-	-	1097	perpendicular Si–O stretching
1027	1028	1024	1024	1026	1026	1028	in-plane Si–O stretching
1005	1004	997	997	997	1002	1002	in-plane Si–O stretching
937	935	934	930	934	934	932	OH deformation of inner-surface hydroxyl group
912	912	910	910	910	910	912	OH deformation of inner hydroxyl groups
788	789	789	789	789	791	789	Si–O
751	750	749	747	748	747	749	Si–O, perpendicular
681	684	687	679	683	685	685	Si–O, perpendicular
645	641	636	640	638	638	638	Si–O
541	540	530	528	526	526	529	Al–O–Si deformation
472	470	469	471	475	475	471	Si–O–Si deformation
432	430	432	430	432	432	434	Si–O deformation

(–) not detected

Appendix 4.6: Position and assignment of transmittance bands (cm^{-1}) in the IR spectra of Missole II and Yatchika samples

KGa-1b	KGa-2	MSL II 01	MSL II 02	YTK 01	YTK 02A	YTK 02B	YTK 03	Assignment
3689	3691	3690	3690	3692	3694	3694	3692	OH stretching of inner-surface hydroxyl groups
3669	-	3666	3667	3665	-	-	3665	OH stretching of inner-surface hydroxyl groups
3651	3650	3649	3649	3651	3647		3649	OH stretching of inner-surface hydroxyl groups
3619	3619	3619	3619	3621	3621	3620	3621	OH stretching of inner hydroxyl groups
3457	3442	-	-	-	-	-	-	OH stretching of water
3426	-	-	-	3433	3400	N	3421	Smectite
1635	1630	1636	1630	1636	1630	1634	1636	OH deformation of water
1115	1114	1114	1114	1114	1114	1118	1114	Si–O stretching (longitudinal mode)
1102	1105	-	-	-	-	-	-	perpendicular Si–O stretching
1027	1028	1024	1024	1026	1024	1026	1024	in-plane Si–O stretching
1005	1004	997	997	1002	995	999	997	in-plane Si–O stretching
937	935	928	926	932	934	-	932	OH deformation of inner-surface hydroxyl group
912	912	910	910	910	908	908	910	OH deformation of inner hydroxyl groups
788	789	789	789	793	793	793	791	Si–O
751	750	746	747	749	749	747	749	Si–O, perpendicular
681	684	681	677	681	685	681	677	Si–O, perpendicular
645	641	640	638	-	-	-	636	Si–O
541	540	526	526	524	518	522	520	Al–O–Si deformation
472	470	469	471	471	475	-	471	Si–O–Si deformation
432	430	432	434	430	430	426	426	Si–O deformation

(–) not detected

Appendix 4.7: Major oxides concentrations (wt %) of bulk kaolin samples

	Na_2O	MgO	Al_2O_3	SiO_2	P_2O_5	SO_3	K_2O	CaO	TiO_2	MnO	Fe_2O_3	LOI	Total	CIA	CIW	CNKM	ICV
BKL 01	0.03	0.20	30.18	49.01	0.12	0.11	0.56	0.07	2.08	0.01	8.47	8.72	99.55	97.86	99.69	0.86	0.38
BKL 02	0.01	0.21	32.02	47.41	0.10	0.13	0.45	0.05	2.12	0.00	7.23	9.68	99.42	98.41	99.80	0.73	0.31
BKL 03	0.13	0.54	22.51	60.21	0.16	0.11	2.30	0.08	1.90	0.00	6.84	4.72	99.49	89.97	99.08	3.05	0.52
DBB	0.03	0.16	29.04	64.80	0.15	0.11	0.07	0.05	0.84	0.00	0.85	3.83	99.92	99.49	99.73	0.31	0.07
DBB CN 01	0.00	0.13	21.78	71.73	0.93	0.15	0.08	0.09	0.27	0.00	0.58	3.42	99.15	99.19	99.57	0.30	0.05
DBB CN 02	0.00	0.10	9.14	87.88	0.10	0.08	0.04	0.05	0.18	0.00	1.15	1.21	99.94	98.95	99.41	0.19	0.17
EDK 01	0.07	1.08	25.93	54.83	0.09	0.03	7.71	0.04	1.58	0.00	2.68	5.51	99.56	76.82	99.58	8.91	0.51
EDK 02	0.11	0.48	28.09	56.36	0.10	0.04	8.04	0.07	1.14	0.00	0.82	4.29	99.53	77.36	99.35	8.70	0.38
EDK 03	0.06	1.57	25.87	53.46	0.15	0.05	8.09	0.05	1.58	0.01	4.32	4.29	99.50	75.93	99.58	9.77	0.61
LBB 01	0.03	0.09	30.32	60.31	0.18	0.10	0.19	0.04	2.48	0.00	1.10	4.95	99.78	99.16	99.77	0.35	0.13
LBB 02	0.03	0.09	32.28	58.45	0.18	0.15	0.18	0.04	2.46	0.00	1.07	4.87	99.81	99.20	99.77	0.35	0.12
LBB 03	0.00	0.07	26.36	65.38	0.19	0.10	0.18	0.04	2.12	0.00	0.94	4.46	99.84	99.19	99.86	0.29	0.13
MSL I 01	0.07	0.32	13.15	74.12	0.32	3.07	1.18	0.04	1.83	0.00	2.87	2.63	99.57	91.11	99.22	1.60	0.48
MSL I 02	0.08	0.44	13.78	72.27	0.29	3.33	1.36	0.03	1.99	0.00	2.91	3.04	99.51	90.38	99.21	1.91	0.49
MSL II 01	0.07	0.14	32.90	52.00	0.09	0.08	0.78	0.03	3.70	0.00	2.38	7.47	99.64	97.37	99.69	1.02	0.22
MSL II 02	0.05	0.13	32.35	55.67	0.07	0.08	0.74	0.05	3.09	0.00	1.76	5.79	99.78	97.46	99.68	0.97	0.18
YTK 01	0.08	0.60	29.83	50.53	0.24	0.18	0.52	0.03	1.57	0.00	7.73	8.06	99.37	97.93	99.64	1.23	0.35
YTK 02A	0.07	0.87	25.50	54.55	0.08	0.11	1.40	0.03	1.71	0.01	7.44	7.72	99.51	94.42	99.60	2.38	0.45
YTK 02 B	0.04	0.99	28.53	54.68	0.06	0.08	1.30	0.01	1.57	0.00	4.56	7.82	99.64	95.48	99.82	2.33	0.30
YTK 03	0.04	0.41	28.98	46.87	0.08	0.16	0.72	0.03	1.93	0.00	11.26	9.02	99.51	97.36	99.76	1.20	0.50

Appendix 4.8: Major oxides concentrations (wt %) of silt fraction of kaolin samples

	Na_2O	MgO	Al_2O_3	SiO_2	P_2O_5	SO_3	K_2O	CaO	TiO_2	MnO	Fe_2O_3	LOI	Total	CNKM	CIA	CIW
BKL 03	0.43	0.28	9.86	75.18	0.90	0.04	3.33	0.29	1.70	0.00	5.65	1.81	99.48	4.33	70.89	93.23
DBB	0.27	0.13	32.29	51.34	0.43	0.02	0.21	0.03	3.02	0.03	2.37	9.68	99.83	0.65	98.43	99.05
EDK 02	0.27	0.25	26.30	57.39	0.44	0.01	8.27	0.14	1.59	0.00	0.52	4.18	99.36	8.93	75.19	98.48
LBB 02	0.39	0.11	17.30	69.75	0.98	0.03	0.29	0.15	4.34	0.03	1.43	4.78	99.58	0.94	95.42	96.94
MSL II 02	0.27	0.18	27.07	57.46	0.29	0.01	1.22	0.04	4.28	0.00	1.86	6.80	99.49	1.71	94.65	98.86
YTK 02A	0.87	0.89	25.02	53.86	0.82	0.04	1.73	0.05	1.72	0.01	7.20	7.36	99.58	3.54	90.43	96.45

Appendix 4.9: Major oxides concentrations (wt %) of < 2 µm fraction of kaolin samples

	Na_2O	MgO	Al_2O_3	SiO_2	P_2O_5	SO_3	K_2O	CaO	TiO_2	MnO	Fe_2O_3	LOI	TOTAL	CIA	CIW	ICV	CNKM
BKL 01	0.27	0.14	34.84	40.34	0.54	0.06	0.27	0.04	1.88	0.00	7.27	14.14	99.79	98.35	99.11	0.28	0.72
BKL 02	0.27	0.12	35.83	41.76	0.49	0.05	0.28	0.02	2.03	0.00	5.64	13.03	99.54	98.43	99.18	0.23	0.69
BKL 03	0.78	0.72	30.19	43.05	0.92	0.06	0.95	0.06	1.70	0.00	9.02	12.22	99.68	94.39	97.28	0.44	2.52
DBB	0.35	0.14	38.02	44.67	0.55	0.06	0.07	0.01	0.67	0.00	1.62	13.74	99.88	98.88	99.06	0.07	0.57
DBB CN 01	0.48	0.14	37.27	42.18	2.04	0.14	0.10	0.11	0.20	0.00	1.41	13.82	97.89	98.19	98.45	0.07	0.83
DBB CN 02	0.38	0.12	36.68	42.34	0.68	0.07	0.06	0.03	0.38	0.00	5.71	13.46	99.89	98.76	98.92	0.18	0.58
EDK 01	0.59	1.33	29.06	48.24	0.37	0.04	6.28	0.02	1.74	0.01	4.17	7.76	99.61	80.83	97.95	0.49	8.22
EDK 02	0.48	0.79	33.78	47.46	0.30	0.05	5.09	0.02	1.11	0.00	2.60	8.14	99.83	85.79	98.54	0.30	6.39
EDK 03	0.71	1.83	26.42	48.61	0.52	0.03	7.55	0.04	1.53	0.01	5.63	6.80	99.68	76.11	97.24	0.65	10.12
LBB 01	0.28	0.07	37.91	42.39	0.58	0.10	0.20	0.02	2.12	0.00	1.51	14.57	99.76	98.70	99.22	0.11	0.57
LBB 02	0.31	0.07	38.21	42.60	0.62	0.08	0.21	0.02	2.22	0.00	1.48	14.01	99.82	98.62	99.15	0.11	0.60
LBB 03	0.35	0.07	37.82	42.66	0.62	0.07	0.21	0.01	2.22	0.00	1.50	14.29	99.82	98.52	99.06	0.12	0.64
MSL I 01	0.68	0.52	21.95	38.47	7.56	4.48	1.04	0.03	1.39	0.00	10.10	13.25	99.48	92.62	96.88	0.63	2.27
MSL I 02	0.29	0.52	18.24	54.70	4.69	3.22	1.30	0.03	2.09	0.00	5.95	8.30	99.34	91.82	98.26	0.56	2.15
MSL II 01	0.31	0.14	36.12	42.74	0.27	0.05	0.89	0.01	3.21	0.00	2.91	12.70	99.35	96.78	99.13	0.21	1.35
MSL II 02	0.28	0.13	36.23	43.04	0.21	0.05	1.01	0.01	3.20	0.00	2.68	12.96	99.79	96.53	99.20	0.20	1.43
MSL II 03*	0.30	0.12	36.20	43.14	0.26	0.04	0.91	0.01	3.17	0.00	2.92	12.80	99.88	96.75	99.16	0.52	1.33
YTK 01	0.57	0.41	31.01	36.99	1.31	0.10	0.44	0.03	1.28	0.01	14.34	13.26	99.76	96.77	98.10	0.55	1.45
YTK 02A	0.99	0.87	29.80	42.15	1.70	0.09	0.86	0.02	1.35	0.01	10.80	11.23	99.87	94.08	96.72	0.50	2.74
YTK 02B	1.61	0.98	29.49	43.97	4.47	0.11	0.70	0.02	0.85	0.00	7.89	9.75	99.84	92.65	94.74	0.41	3.31
YTK 03	0.45	0.36	32.89	41.21	0.51	0.09	0.69	0.02	1.97	0.00	9.18	12.50	99.86	96.62	98.62	0.38	1.51
TK*	-	-	39.80	46.30	-	-	-	-	-	-	-	13.90	100.00	-	-		-

*MSL 03: Duplicate sample; TK: Theoretical kaolin (Deer *et al*., 1992)

Appendix 5.1: Rare earth elements concentrations (ppm) in bulk samples

Sample	La	Ce	Pr	Nd	Sm	Eu	Gd	Tb	Dy	Ho	Er	Tm	Yb	Lu
BKL 01	3.12	nd	185.67	nd	nd	nd	25.58	nd	14.25	nd	5544.71	nd	0.59	1.56
BKL 02	44.26	nd	181.87	13.14	nd	nd	32.66	nd	36.34	nd	6155.78	nd	2.51	1.93
BKL 03	24.22	nd	140.21	10.04	nd	2.17	29.15	nd	313.31	nd	8182.36	nd	1.97	1.38
DBB	31.72	69.19	0.00	7.73	nd	0.79	6.54	nd	9.71	nd	565.03	0.20	nd	nd
DBB CN 01	207.58	468.39	25.75	114.97	nd	3.39	18.36	nd	15.37	nd	230.14	1.40	0.40	nd
DBB CN 02	12.53	27.86	nd	nd	nd	0.40	5.37	nd	3.18	nd	246.32	1.19	nd	nd
EDK 01	3.58	nd	61.11	nd	nd	0.20	12.74	nd	11.15	nd	4042.60	0.00	0.20	nd
EDK 02	44.13	84.27	7.79	24.76	nd	1.60	10.18	nd	28.15	nd	1427.72	0.20	0.80	nd
EDK 03	88.87	109.57	90.23	59.18	nd	2.34	25.98	nd	35.35	nd	3401.37	0.39	2.54	2.54
LBB 01	34.33	46.37	11.44	10.46	nd	0.79	9.67	nd	19.34	nd	5801.10	nd	0.59	nd
LBB 02	28.10	50.93	nd	5.02	nd	0.75	10.79	nd	10.04	nd	3913.70	nd	0.25	nd
LBB 03	25.52	31.36	6.82	5.06	nd	0.58	8.57	nd	11.10	nd	4411.76	nd	0.19	nd
MSL I 01	314.82	800.99	372.70	406.14	nd	14.67	93.08	nd	55.14	nd	3959.72	nd	5.67	2.35
MSL I 02	254.56	711.50	251.59	289.68	nd	8.93	70.83	nd	48.81	nd	4553.57	nd	4.76	2.38
MSL II 01	30.13	nd	40.10	nd	nd	1.96	16.04	nd	379.50	nd	6905.32	nd	nd	0.20
MSL II 02	21.45	nd	15.99	nd	nd	1.56	10.73	nd	370.32	nd	4290.17	nd	nd	nd
YTK 01	63.18	nd	367.98	11.31	nd	nd	53.24	nd	24.18	nd	2808.11	nd	1.76	nd
YTK 02A	34.54	2.18	106.23	9.19	nd	nd	19.77	nd	20.37	nd	3224.84	nd	1.40	2.00
YTK 02B	48.98	99.92	73.67	14.50	nd	nd	17.24	nd	25.67	nd	3221.00	nd	1.57	1.96
YTK 03	14.19	nd	283.21	nd	nd	nd	38.43	nd	12.81	nd	5015.77	nd	1.38	nd

nd: not detected

Appendix 5.2: Rare earth elements concentrations (ppm) in silt samples

Sample	La	Ce	Pr	Nd	Sm	Eu	Gd	Tb	Dy	Ho	Er	Tm	Yb	Lu
BKL 03	6.79	nd	59.93	nd	nd	nd	13.18	nd	4.59	nd	3106.27	nd	1.00	0.60
DBB	56.28	73.79	57.65	25.19	nd	0.98	17.71	nd	30.70	nd	7802.05	nd	1.18	0.59
EDK 02	45.40	92.78	2.58	27.95	nd	1.78	10.11	nd	36.88	nd	2388.98	nd	0.79	nd
LBB 02	31.78	34.33	25.50	15.10	nd	0.98	13.93	nd	14.12	nd	8581.80	nd	0.98	nd
MSL II 02	14.42	nd	29.83	0.00	nd	0.40	12.45	nd	16.40	nd	7042.67	nd	0.99	0.40
YTK 02A	33.43	nd	132.71	5.17	nd	nd	24.87	nd	27.46	nd	4058.89	nd	1.59	2.79

nd: not detected

Appendix 5.3: Rare earth elements concentrations (ppm) in < 2 µm fraction of kaolin samples

Sample	La	Ce	Pr	Nd	Sm	Eu	Gd	Tb	Dy	Ho	Er	Tm	Yb	Lu
BKL 01	36.18	0.00	152.88	10.54	nd	nd	24.06	nd	43.94	nd	5188.87	nd	1.59	2.98
BKL 02	63.47	38.32	143.31	30.14	nd	1.40	26.55	nd	48.70	nd	6317.37	nd	2.79	2.40
BKL 03	47.79	0.00	202.11	26.09	nd	nd	34.65	nd	42.81	nd	5029.87	nd	4.38	2.59
DBB	26.49	46.36	22.79	0.00	nd	0.58	9.74	nd	25.71	nd	1121.93	nd	0.78	0.97
DBB CN 01	1257.49	2395.21	188.22	578.84	nd	15.17	81.44	nd	72.85	nd	469.06	1.80	2.79	0.20
DBB CN 02	116.58	160.82	126.54	37.27	nd	0.40	23.52	nd	44.44	nd	1119.97	1.00	0.80	2.19
EDK 01	27.17	nd	93.70	13.58	nd	0.59	21.06	nd	36.22	nd	4753.94	nd	1.18	1.97
EDK 02	3.95	nd	51.58	0.00	nd	nd	13.83	nd	37.55	nd	2994.07	1.58	0.59	0.59
EDK 03	62.62	24.42	137.46	36.83	nd	0.98	29.54	nd	39.78	nd	4302.88	0.98	1.38	2.76
LBB 01	62.48	91.67	29.97	29.39	nd	1.75	14.99	nd	50.21	nd	5975.09	nd	0.78	0.39
LBB 02	54.19	77.39	29.43	28.46	nd	1.56	14.42	nd	15.59	nd	5838.21	nd	0.58	nd
LBB 03	57.31	86.25	29.54	29.15	nd	1.77	14.18	nd	36.83	nd	5848.76	nd	0.59	nd
MSL II 01	31.61	28.65	54.38	3.73	nd	nd	14.92	nd	50.26	nd	8441.30	nd	0.59	0.39
MSL II 02	38.17	12.59	50.18	7.08	nd	nd	11.02	nd	45.26	nd	8638.33	nd	0.59	0.39
YTK 01	64.21	nd	316.50	22.47	nd	nd	45.53	nd	39.96	nd	3121.27	nd	1.59	nd
YTK 02A	65.89	nd	235.62	24.36	nd	nd	35.54	nd	20.97	nd	764.78	2.00	1.60	0.80
YTK 02B	44.49	26.74	114.92	9.18	nd	nd	22.15	nd	36.31	nd	1167.20	1.20	1.20	1.20
YTK 03	40.32	0.00	163.07	6.59	nd	nd	24.55	nd	40.72	nd	5053.89	nd	1.40	2.00

nd: Not detected

Appendix 5.4: Trace elements concentrations (ppm) in bulk samples

Sample	Rb	Sr	Ba	Y	Zr	V	Cr	Co	Ni	Cu	Zn	Th	Pb	Sc
BKL 01	11733.70	31.43	57.01	216.71	286.22	127.29	91.76	13.47	40.02	40.61	40.61	nd	50.96	0.20
BKL 02	14814.46	52.96	56.24	270.78	300.35	144.76	99.73	14.11	37.88	35.18	52.38	18.55	61.27	12.18
BKL 03	16345.02	73.65	172.71	2028.36	290.07	145.92	109.49	10.44	50.81	27.37	61.24	nd	46.28	11.42
DBB	11449.25	9.71	7.53	38.66	42.03	16.26	12.49	nd	13.88	nd	19.83	nd	27.16	1.59
DBB CN 01	12564.87	182.24	131.54	14.77	24.69	16.17	18.17	nd	24.55	nd	15.17	9.98	123.35	4.15
DBB CN 02	8306.80	6.76	5.97	12.14	10.35	9.95	6.17	nd	22.48	nd	14.33	nd	nd	0.80
EDK 01	5965.37	27.87	228.30	208.60	91.36	103.70	94.15	17.91	17.71	34.24	78.82	nd	75.04	0.60
EDK 02	15305.51	214.26	599.04	75.68	54.71	33.15	30.15	nd	36.14	nd	37.74	17.77	62.10	4.59
EDK 03	11774.41	256.84	621.09	170.51	56.64	86.91	78.32	5.86	52.34	23.44	92.19	24.02	120.12	13.67
LBB 01	13891.08	34.73	40.06	249.21	161.40	61.96	76.16	12.43	40.45	nd	34.33	13.02	55.84	5.92
LBB 02	11527.85	24.59	29.35	173.11	97.34	49.17	55.69	6.77	26.59	3.26	48.67	nd	53.69	5.02
LBB 03	13283.99	22.40	24.93	210.36	95.83	49.08	46.75	8.96	15.97	2.14	32.53	10.91	49.28	4.09
MSL I 01	14450.53	48.69	105.79	275.32	213.41	263.59	247.14	12.51	36.57	54.36	57.29	53.58	77.63	17.95
MSL I 02	23551.59	40.48	102.78	249.40	188.69	216.87	198.25	7.34	67.86	33.93	54.37	35.71	51.98	13.26
MSL II 01	10406.89	37.56	62.99	428.40	89.01	213.03	172.73	23.87	39.52	nd	22.69	17.41	56.53	12.72
MSL II 02	7819.81	26.13	45.83	336.00	77.03	144.89	118.17	15.41	34.71	nd	18.72	nd	43.10	9.56
YTK 01	13367.78	21.26	49.34	126.17	130.07	70.01	52.26	4.88	61.43	66.69	51.09	nd	46.61	9.36
YTK 02A	12040.73	26.36	71.88	139.58	142.41	66.29	42.33	5.79	52.12	13.78	48.12	nd	43.73	6.92
YTK 02B	12061.13	26.45	69.95	145.77	122.65	63.48	51.72	5.29	50.35	5.29	46.83	nd	47.61	8.23
YTK 03	10622.78	16.75	37.25	222.11	198.46	144.26	103.47	12.02	37.84	52.82	47.89	nd	47.50	5.12

nd: Not detected

Appendix 5.5: Trace elements concentrations (ppm) in silt samples

Sample	Rb	Sr	Ba	Y	Zr	V	Cr	Co	Ni	Cu	Zn	Th	Pb	Sc
BKL 03	13134.24	52.34	176.79	146.82	120.85	55.93	49.14	3.40	30.76	4.79	26.17	nd	34.36	3.20
DBB	12544.27	38.96	36.99	352.62	236.52	99.37	86.58	22.83	38.96	6.69	53.13	8.66	79.69	6.89
EDK 02	20003.97	327.72	802.93	115.58	84.66	25.18	27.16	nd	41.83	14.67	28.15	16.26	83.07	3.37
LBB 02	12602.98	46.10	46.88	418.99	261.28	105.14	183.41	24.91	68.85	1.57	50.02	19.62	76.89	9.61
MSL II 02	9976.29	17.19	72.30	401.22	96.01	200.91	140.46	21.34	22.72	nd	24.69	24.69	60.65	11.85
YTK 02A	16066.45	47.95	131.12	184.04	156.78	86.35	65.86	7.16	65.26	16.12	44.37	7.96	51.73	8.75

nd: Not detected

Appendix 5.6: Trace elements concentrations (ppm) in < 2 µm fraction of kaolin samples

Sample	Rb	Sr	Ba	Y	Zr	V	Cr	Co	Ni	Cu	Zn	Th	Pb	Sc
BKL 01	11729.62	57.26	42.35	230.22	308.35	125.65	156.00	11.13	41.35	33.40	66.60	14.31	70.58	6.56
BKL 02	13972.06	77.84	53.89	312.38	381.44	119.56	102.79	14.57	31.34	26.55	66.07	23.95	80.44	10.98
BKL 03	11338.11	82.64	59.74	237.95	467.34	207.89	187.18	9.76	56.95	42.81	97.37	15.33	72.88	18.12
DBB	21071.29	11.49	12.27	73.43	167.90	61.55	69.93	nd	42.07	7.60	58.24	nd	75.77	2.14
DBB CN 01	13732.53	858.28	678.64	57.09	121.56	84.03	105.39	nd	37.72	4.19	48.10	70.66	538.92	14.57
DBB CN 02	6514.55	92.07	34.68	49.62	113.19	119.57	101.43	nd	18.33	27.50	47.23	8.77	105.02	1.99
EDK 01	14694.88	172.44	97.24	209.06	62.40	146.06	147.64	15.55	58.46	38.39	134.06	11.22	80.31	13.39
EDK 02	14377.47	156.52	75.10	130.63	56.13	133.40	141.90	10.67	53.56	22.92	130.83	nd	82.21	7.11
EDK 03	16689.64	212.49	374.16	194.56	50.81	143.95	137.65	13.19	64.59	43.13	145.53	22.65	169.16	16.15
LBB 01	10325.03	75.32	94.39	312.18	218.18	115.22	160.57	16.54	34.64	3.89	63.45	27.44	98.09	7.79
LBB 02	9522.42	75.44	185.19	293.18	206.04	115.79	149.32	15.98	30.80	9.16	54.19	24.76	93.57	5.07
LBB 03	16394.25	72.47	89.41	299.33	211.50	108.51	144.35	15.75	38.01	7.29	66.36	28.16	95.51	6.50
MSL II 01	12122.10	46.53	70.08	329.80	42.18	242.25	162.16	27.48	23.36	15.51	22.97	10.40	87.95	11.94
MSL II 02	12249.11	54.11	87.56	364.03	48.41	237.50	196.77	24.60	33.06	11.61	19.48	9.05	79.10	6.10
YTK 01	10516.90	50.30	89.26	161.23	114.71	123.06	92.64	7.95	34.79	58.65	53.88	17.30	89.86	8.35
YTK 02A	66.29	22.56	33.95	46.73	8.39	86.06	73.48	7.39	18.37	54.71	81.27	12.58	59.11	9.38
YTK 02B	828.01	16.76	33.72	55.07	7.58	81.60	97.77	8.18	26.54	36.51	57.66	10.77	48.88	8.18
YTK 03	10227.54	37.52	49.70	222.36	152.50	103.59	95.81	9.98	40.12	26.35	61.68	8.38	70.26	13.17

nd: Not detected

Appendix 6.1: Backscattered images of zircons in Bomkoul kaolin

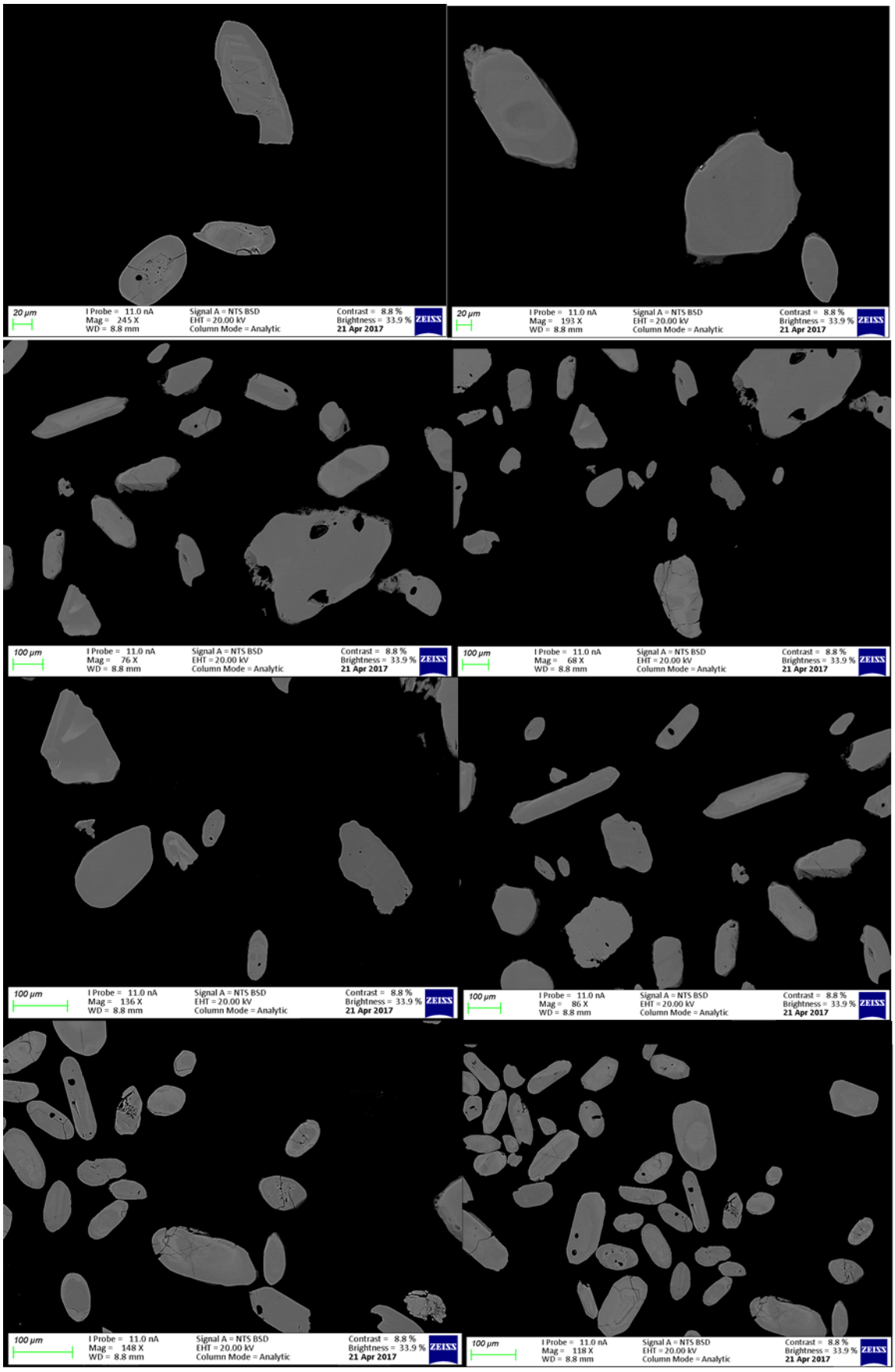

Appendix 6.2: Backscattered images of zircons in Dibamba kaolin

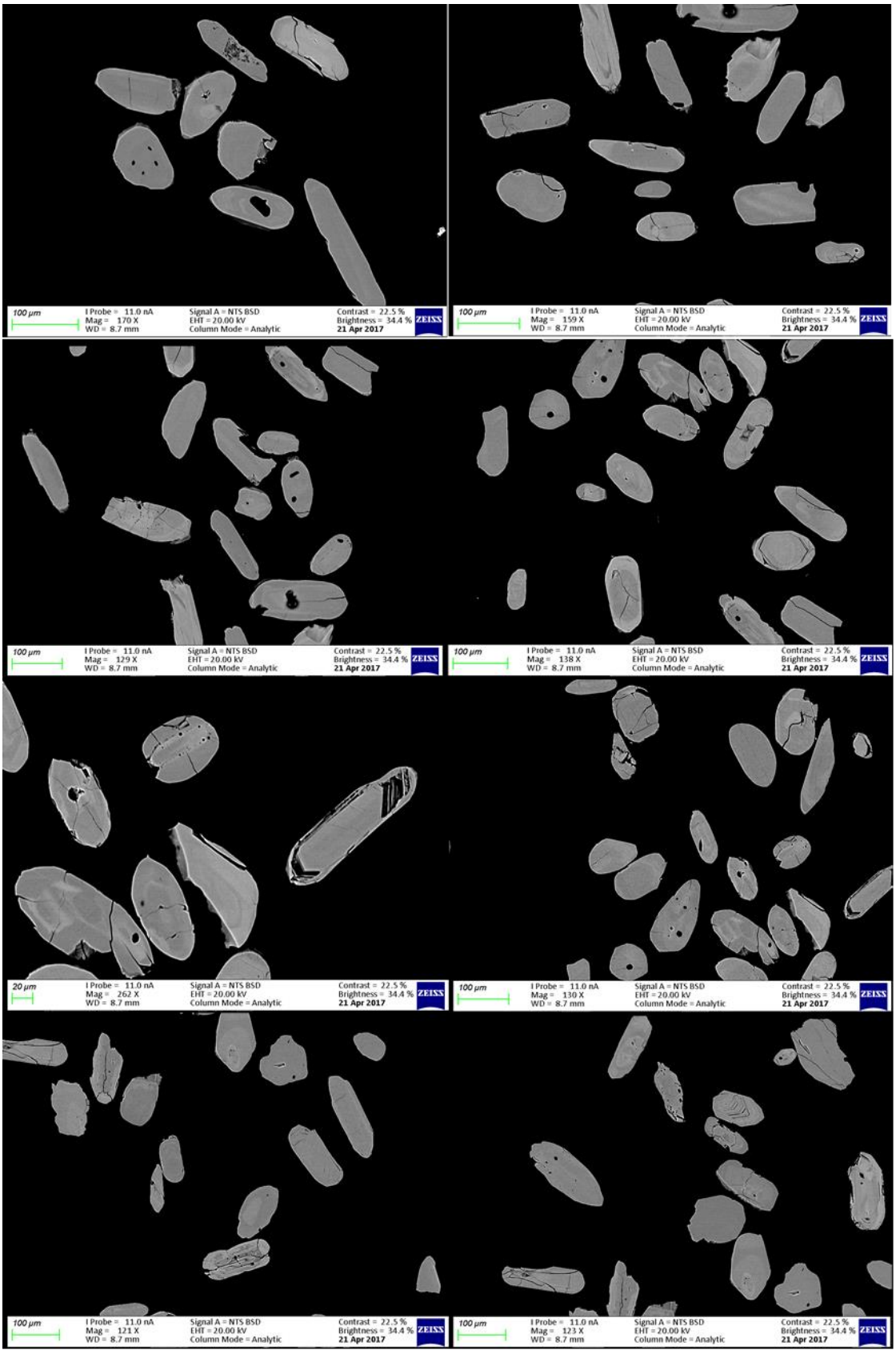

Appendix 6.3: Backscattered images of zircons in Ediki kaolin

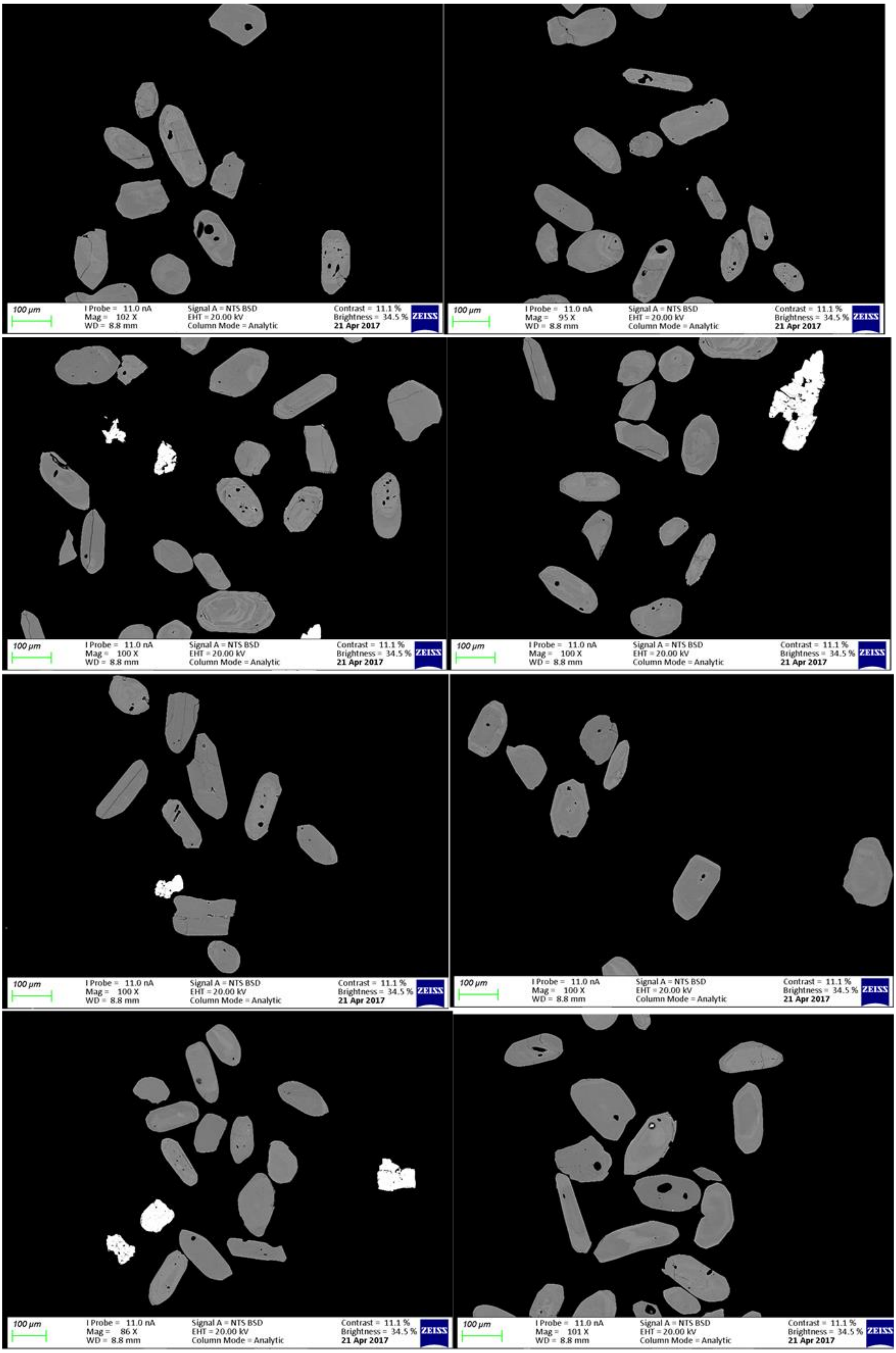

Appendix 6.4: Backscattered images of zircons in Logbaba kaolin

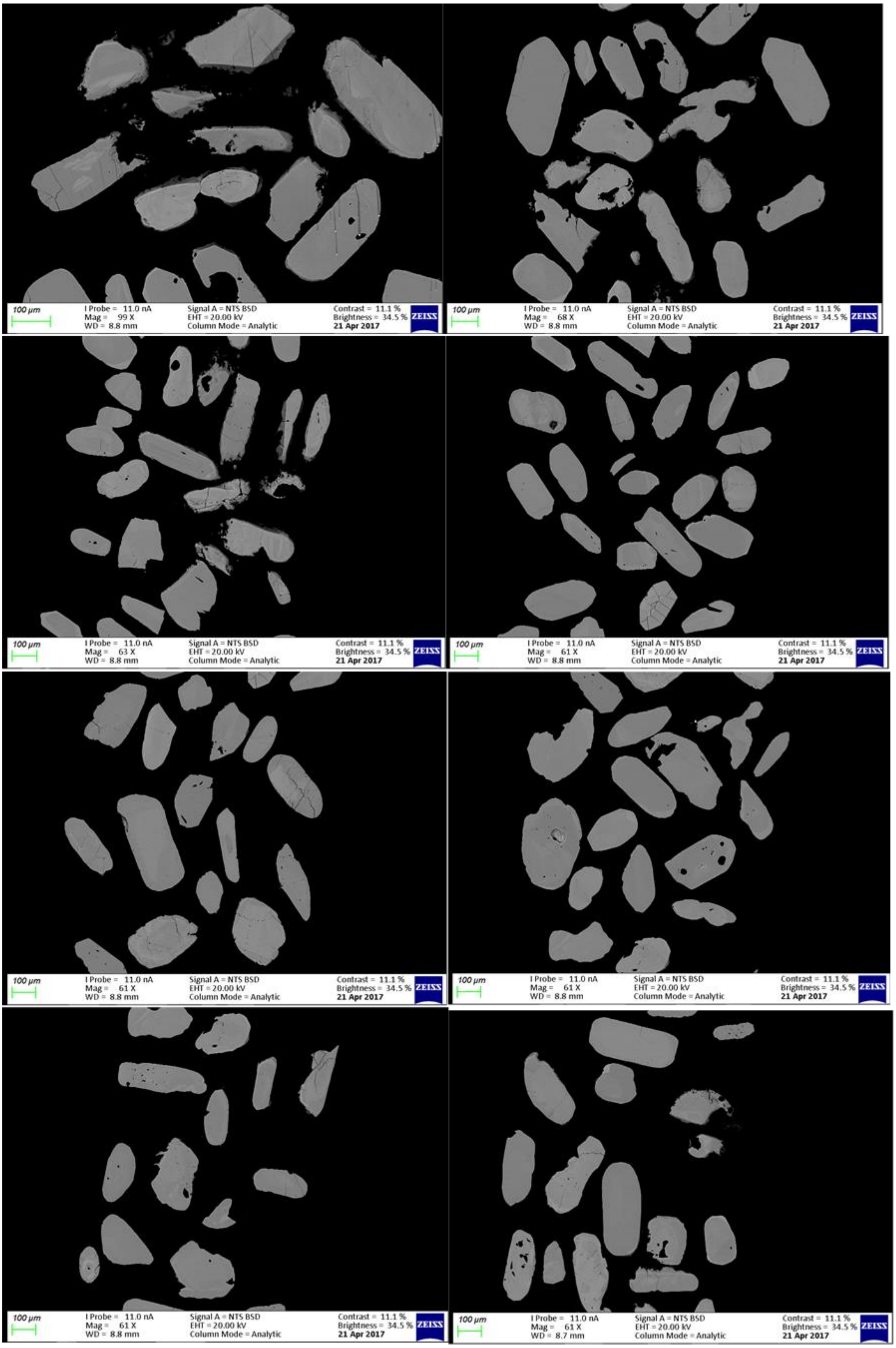

University of Venda
Creating Future Leaders

Appendix 6.5: Backscattered images of zircons in Missole kaolin

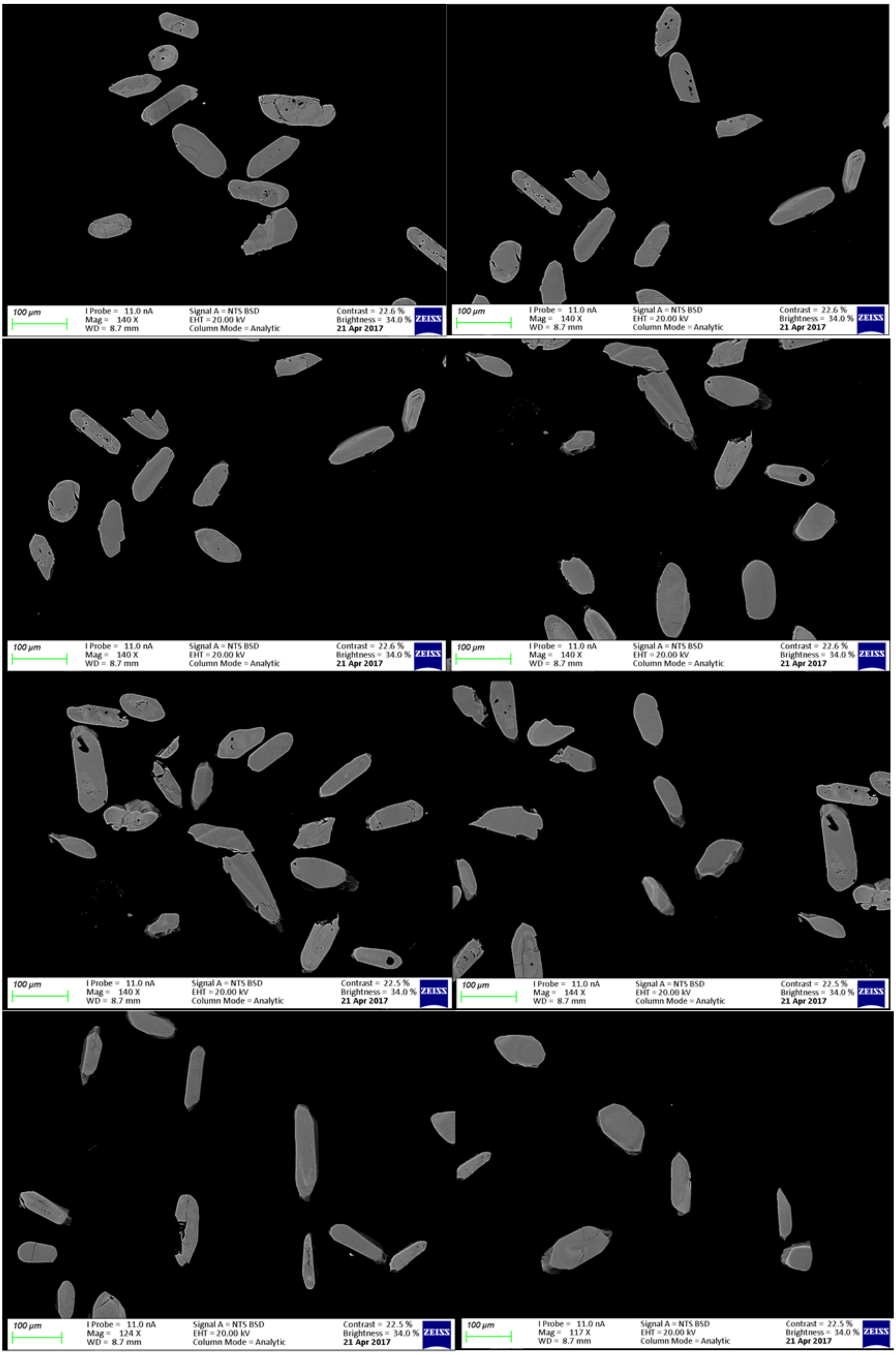

Appendix 6.6: Backscattered images of zircons in Yatchika kaolin

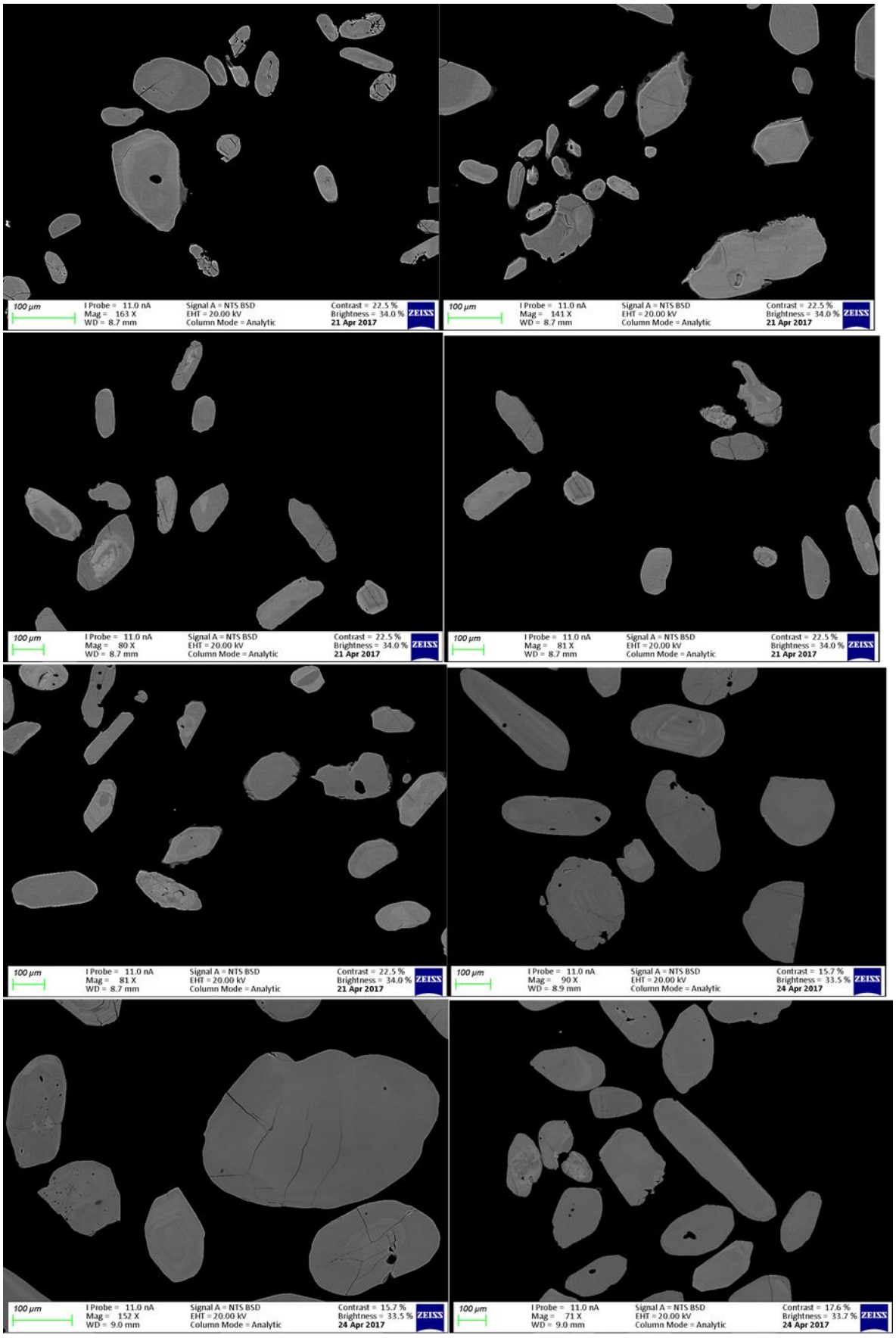

Appendix 6.7: Results of analyses of GJ1, PLES and M127 in Sequence 1

						RATIOS							AGES [Ma]						
Analysis	Sample	U [ppm][a]	Pb [ppm][a]	Th/U[a]	*206/204*	$^{207}Pb/^{235}U$[b]	2 σ[d]	$^{206}Pb/^{238}U$[b]	2 σ[d]	rho[c]	$^{207}Pb/^{206}Pb$[e]	2 σ[d]	$^{207}Pb/^{235}U$	2 σ	$^{206}Pb/^{238}U$	2 σ	$^{207}Pb/^{206}Pb$	2 σ	Conc. %
A_112.FIN2	M127	887	1075	0.54	-6000	0.6800	0.0160	0.0856	0.0007	0.16	0.0580	0.0014	526	10	530	4	519	54	102
A_220.FIN2	M127	899	999	0.52	100	0.6740	0.0110	0.0849	0.0005	0.25	0.0578	0.0010	523	7	525	3	516	37	102
A_273.FIN2	M127	875	958	0.52	-25000	0.6818	0.0092	0.0853	0.0006	0.31	0.0581	0.0008	528	6	528	4	526	29	100
A_056.FIN2	M127	953	1063	0.51	-60000	0.6870	0.0110	0.0851	0.0005	0.07	0.0582	0.0009	531	6	526	3	530	35	99
A_383.FIN2	M127	884	955	0.50	-21000	0.6860	0.0070	0.0852	0.0007	0.24	0.0585	0.0014	530	10	527	4	541	51	97
A_165.FIN2	M127	616	826	0.54	700	0.6860	0.0130	0.0849	0.0008	0.23	0.0585	0.0011	530	8	525	5	541	43	97
A_328.FIN2	M127	879	953	0.50	-1600	0.6841	0.0098	0.0849	0.0006	0.38	0.0584	0.0008	529	6	525	4	541	29	97
GJ1_036.FIN2	GJ1 4	263	23	0.03	-1800	0.8130	0.0170	0.0986	0.0007	0.05	0.0595	0.0013	603	9	606	4	572	48	106
GJ1_444.FIN2	GJ1 29	285	25	0.03	120	0.8060	0.0130	0.0981	0.0006	0.04	0.0594	0.0010	599	7	603	3	571	37	106
GJ1_376.FIN2	GJ1 25	294	27	0.03	-3000	0.8090	0.0130	0.0983	0.0006	0.05	0.0596	0.0010	601	7	604	3	574	36	105
GJ1_070.FIN2	GJ1 6	290	26	0.03	-2100	0.8100	0.0150	0.0977	0.0005	0.29	0.0597	0.0011	601	8	601	3	576	39	104
GJ1_274.FIN2	GJ1 19	279	26	0.03	-200	0.8100	0.0120	0.0983	0.0006	0.16	0.0598	0.0009	602	7	604	3	584	33	103
GJ1_377.FIN2	GJ1 26	283	25	0.03	-4400	0.8130	0.0140	0.0980	0.0005	0.08	0.0601	0.0010	604	8	603	3	587	38	103
GJ1_308.FIN2	GJ1 21	284	26	0.03	3500	0.8150	0.0130	0.0982	0.0005	0.21	0.0601	0.0010	605	7	604	3	590	36	102
GJ1_071.FIN2	GJ1 7	289	24	0.03	-3700	0.8130	0.0130	0.0979	0.0006	0.26	0.0600	0.0010	603	8	602	4	589	36	102
GJ1_240.FIN2	GJ1 17	289	26	0.03	100	0.8120	0.0130	0.0981	0.0006	0.09	0.0600	0.0010	602	7	603	3	593	36	102
GJ1_513.FIN2	GJ1 34	294	26	0.03	-2900	0.8120	0.0160	0.0979	0.0006	0.09	0.0603	0.0012	603	9	602	3	596	43	101
GJ1_003.FIN2	GJ1 3	282	26	0.03	8500	0.8080	0.0160	0.0975	0.0006	0.00	0.0603	0.0013	600	9	600	4	594	46	101
GJ1_173.FIN2	GJ1 14	287	25	0.03	540	0.8090	0.0130	0.0976	0.0006	0.04	0.0603	0.0011	601	8	600	3	597	39	101

GJ1_343.FIN2	GJ1 24	290	27	0.03	-40000	0.8120	0.0130	0.0975	0.0005	0.0116	0.0601	0.0010	602	8	600	3	598	36	100
GJ1_001.FIN2	GJ1 1	288	28	0.03	700	0.8200	0.0150	0.0981	0.0007	0.0592	0.0606	0.0012	607	9	603	4	605	43	100
GJ1_478.FIN2	GJ1 31	288	27	0.03	420	0.8110	0.0130	0.0977	0.0006	0.0583	0.0602	0.0010	603	7	601	3	603	35	100
GJ1_103.FIN2	GJ1 8	292	28	0.03	-2500	0.8150	0.0170	0.0984	0.0008	0.0787	0.0604	0.0014	605	10	605	5	607	48	100
GJ1_172.FIN2	GJ1 13	286	27	0.03	450	0.8190	0.0160	0.0982	0.0006	0.0529	0.0606	0.0012	606	9	604	3	607	44	99
GJ1_037.FIN2	GJ1 5	302	26	0.03	790	0.8180	0.0140	0.0978	0.0006	0.0936	0.0605	0.0010	606	8	601	4	606	38	99
GJ1_104.FIN2	GJ1 9	270	27	0.03	-2400	0.8160	0.0150	0.0978	0.0005	0.0987	0.0606	0.0012	604	8	602	3	610	41	99
GJ1_512.FIN2	GJ1 33	279	25	0.03	-3100	0.8180	0.0150	0.0978	0.0006	0.0768	0.0605	0.0011	606	9	601	4	611	41	98
GJ1_241.FIN2	GJ1 18	288	25	0.03	720	0.8170	0.0130	0.0978	0.0005	0.0886	0.0606	0.0010	605	7	601	3	613	34	98
GJ1_206.FIN2	GJ1 15	276	25	0.03	1730	0.8080	0.0170	0.0972	0.0007	0.0997	0.0603	0.0012	600	10	598	4	615	41	97
GJ1_445.FIN2	GJ1 30	291	26	0.03	4000	0.8200	0.0140	0.0979	0.0005	0.0846	0.0608	0.0010	608	8	602	3	620	37	97
GJ1_342.FIN2	GJ1 23	285	26	0.03	-30000	0.8210	0.0120	0.0977	0.0006	0.0909	0.0609	0.0009	608	7	601	4	619	33	97
GJ1_105.FIN2	GJ1 10	290	29	0.03	-2300	0.8200	0.0150	0.0980	0.0007	0.0133	0.0609	0.0012	607	8	603	4	621	42	97
GJ1_479.FIN2	GJ1 32	286	25	0.03	1760	0.8210	0.0140	0.0978	0.0006	0.0974	0.0607	0.0011	608	8	602	3	620	36	97
GJ1_138.FIN2	GJ1 11	294	26	0.03	1120	0.8100	0.0210	0.0973	0.0011	0.0126	0.0609	0.0021	601	15	599	7	617	73	97
GJ1_309.FIN2	GJ1 22	288	25	0.03	5400	0.8130	0.0120	0.0972	0.0005	0.0768	0.0606	0.0010	603	7	598	3	618	33	97
GJ1_275.FIN2	GJ1 20	296	27	0.03	150	0.8250	0.0150	0.0979	0.0006	0.0422	0.0610	0.0011	610	8	602	4	625	38	96
GJ1_410.FIN2	GJ1 27	287	24	0.03	-8600	0.8200	0.0120	0.0980	0.0006	0.0727	0.0610	0.0009	607	7	602	4	625	34	96
GJ1_207.FIN2	GJ1 16	300	25	0.03	1080	0.8220	0.0130	0.0979	0.0005	0.0101	0.0610	0.0010	608	7	602	3	625	35	96
GJ1_139.FIN2	GJ1 12	256	24	0.03	-470	0.8180	0.0140	0.0977	0.0007	0.0838	0.0609	0.0011	606	8	601	4	625	40	96
GJ1_411.FIN2	GJ1 28	284	26	0.03	-3800	0.8190	0.0140	0.0975	0.0006	0.0779	0.0611	0.0011	606	8	600	3	628	38	95
GJ1_002.FIN2	GJ1 2	293	24	0.03	350	0.8170	0.0170	0.0974	0.0008	0.0714	0.0611	0.0013	605	10	599	5	630	47	95
A_334.FIN2	PLES 6	490	66	0.10	210	0.3889	0.0086	0.0540	0.0003	0.0094	0.0527	0.0013	334	7	339	2	299	54	113

A_509.FIN2	PLES10	547	85	0.10	650	0.3947	0.0092	0.0543	0.0004	0.0940	0.0529	0.0013	337	7	341	3	310	53	110
A_498.FIN2	PLES9	505	77	0.10	280	0.3966	0.0069	0.0541	0.0003	0.0092	0.0531	0.0010	339	5	340	2	316	40	107
A_168.FIN2	PLES3	622	96	0.11	700	0.3970	0.0110	0.0542	0.0004	0.1279	0.0534	0.0016	339	8	340	3	333	68	102
A_280.FIN2	PLES5	459	66	0.10	-1200	0.3999	0.0085	0.0540	0.0003	0.0906	0.0537	0.0012	341	6	339	2	341	47	99
A_114.FIN2	PLES2	590	100	0.11	880	0.3980	0.0130	0.0540	0.0008	0.0930	0.0538	0.0020	340	10	339	5	351	84	97
A_390.FIN2	PLES7	539	75	0.10	560	0.4010	0.0120	0.0540	0.0005	0.1154	0.0537	0.0015	342	8	339	3	353	64	96
A_224.FIN2	PLES4	432	63	0.10	240	0.4007	0.0093	0.0541	0.0005	0.0692	0.0537	0.0013	342	7	339	3	354	57	96
A_443.FIN2	PLES8	499	72	0.10	510	0.4020	0.0140	0.0538	0.0004	0.1619	0.0543	0.0018	342	10	338	3	367	74	92
A_057.FIN2	PLES1	717	102	0.10	680	0.4030	0.0120	0.0537	0.0005	0.2722	0.0543	0.0015	343	8	337	3	367	62	92

Appendix 6.8: Results of analyses of GJ1, PLES and M127 in Sequence 2

Analysis	Sample	U [ppm][a]	Pb [ppm][a]	Th/U[a]	*206/204*	RATIOS $^{207}Pb/^{235}U$[b]	2 σ[d]	$^{206}Pb/^{238}U$[b]	2 σ[d]	rho[c]	$^{207}Pb/^{206}Pb$[e]	2 σ[d]	AGES [Ma] $^{207}Pb/^{235}U$	2 σ	$^{206}Pb/^{238}U$	2 σ	$^{207}Pb/^{206}Pb$	2 σ	Conc. %
A_039.FIN2	M127	809	955	0.52	300	0.6810	0.0160	0.0852	0.0005	0.0736	0.0578	0.0014	527	9	527	3	515	51	102
A_107.FIN2	M127	837	988	0.53	-1000	0.6810	0.0150	0.0850	0.0006	0.0499	0.0581	0.0013	527	9	526	4	525	50	100
A_073.FIN2	M127	844	985	0.52	14000	0.6820	0.0120	0.0851	0.0005	0.1993	0.0583	0.0010	528	7	527	3	532	38	99
A_141.FIN2	M127	858	997	0.52	-2100	0.6820	0.0110	0.0848	0.0005	0.2631	0.0583	0.0010	528	7	525	3	533	39	98
A_209.FIN2	M127	880	1000	0.52	18000	0.6844	0.0082	0.0851	0.0004	0.0569	0.0583	0.0007	529	5	526	2	536	28	98
A_238.FIN2	M127	844	981	0.52	200	0.6858	0.0089	0.0853	0.0004	0.1127	0.0584	0.0008	530	5	528	2	539	29	98
A_239.FIN2	M127	887	981	0.52	-2000	0.6930	0.0130	0.0854	0.0005	0.1383	0.0586	0.0011	534	8	528	3	546	41	97
A_175.FIN2	M127	883	1016	0.52	6100	0.6890	0.0100	0.0854	0.0004	0.1446	0.0588	0.0009	532	6	528	3	552	32	96
GJ1_036.FIN2	GJ1 4	279	24	0.03	-1880	0.8130	0.0140	0.0982	0.0006	0.0107	0.0598	0.0010	603	8	604	3	580	38	104
GJ1_207.FIN2	GJ1 16	282	26	0.03	-690	0.8060	0.0130	0.0976	0.0006	0.1614	0.0598	0.0009	599	7	601	3	587	34	102
GJ1_002.FIN2	GJ1 2	288	26	0.03	400	0.8040	0.0120	0.0976	0.0005	0.0656	0.0598	0.0009	599	7	600	3	591	34	102
GJ1_138.FIN2	GJ1 11	288	26	0.03	3000	0.8120	0.0130	0.0978	0.0005	0.1424	0.0601	0.0010	602	7	602	3	593	35	101
GJ1_001.FIN2	GJ1 1	294	26	0.03	490	0.8140	0.0130	0.0979	0.0005	0.0735	0.0604	0.0010	604	7	602	3	600	38	100
GJ1_240.FIN2	GJ1 17	291	25	0.03	-340	0.8130	0.0150	0.0977	0.0006	0.1082	0.0603	0.0011	603	8	601	3	603	42	100
GJ1_104.FIN2	GJ1 9	291	27	0.03	-39000	0.8150	0.0150	0.0980	0.0006	0.0455	0.0603	0.0012	605	8	603	4	605	40	100
GJ1_172.FIN2	GJ1 13	302	27	0.03	380	0.8140	0.0140	0.0980	0.0006	0.0332	0.0605	0.0011	604	8	603	4	606	41	99
GJ1_105.FIN2	GJ1 10	280	24	0.03	9700	0.8140	0.0120	0.0980	0.0005	0.1174	0.0603	0.0009	604	7	603	3	606	31	99
GJ1_070.FIN2	GJ1 6	296	28	0.03	-2000	0.8140	0.0150	0.0977	0.0005	0.0099	0.0605	0.0011	603	8	601	3	605	41	99
GJ1_139.FIN2	GJ1 12	281	26	0.03	510	0.8170	0.0140	0.0976	0.0005	0.0987	0.0606	0.0011	605	8	600	3	605	39	99

GJ1_103.FIN2	GJ1 8	289	26	0.03	1130	0.8150	0.0140	0.0979	0.0006	0.1000	0.0604	0.0010	604	8	602	3	607	37	99
GJ1_241.FIN2	GJ1 18	278	25	0.03	-940	0.8170	0.0140	0.0977	0.0006	0.1032	0.0606	0.0011	605	8	601	4	609	39	99
GJ1_037.FIN2	GJ1 5	283	26	0.03	230	0.8140	0.0110	0.0974	0.0005	0.0550	0.0604	0.0008	604	6	599	3	609	31	98
GJ1_206.FIN2	GJ1 15	283	26	0.03	280	0.8230	0.0130	0.0983	0.0005	0.1088	0.0608	0.0010	609	7	604	3	618	35	98
GJ1_173.FIN2	GJ1 14	282	26	0.03	-1400	0.8170	0.0130	0.0980	0.0005	0.0202	0.0607	0.0010	606	7	602	3	620	35	97
GJ1_071.FIN2	GJ1 7	283	24	0.03	160	0.8180	0.0120	0.0980	0.0004	0.0848	0.0608	0.0009	606	7	602	3	623	31	97
GJ1_003.FIN2	GJ1 3	280	26	0.03	-360	0.8260	0.0110	0.0981	0.0005	0.0297	0.0612	0.0009	611	6	603	3	631	32	96
A_234.FIN2	PLES 15	548	86	0.10	650	0.3940	0.0120	0.0541	0.0004	0.0104	0.0528	0.0016	337	8	340	3	305	66	111
A_208.FIN2	PLES 8	750	119	0.11	960	0.3943	0.0078	0.0541	0.0004	0.1472	0.0529	0.0011	337	6	340	3	317	45	107
A_230.FIN2	PLES 11	706	111	0.11	860	0.3965	0.0090	0.0540	0.0004	0.1123	0.0531	0.0012	339	7	339	2	320	51	106
A_140.FIN2	PLES 6	672	94	0.10	590	0.3950	0.0078	0.0538	0.0004	0.0907	0.0531	0.0011	338	6	338	2	321	46	105
A_231.FIN2	PLES 12	683	105	0.11	560	0.3963	0.0092	0.0540	0.0004	0.2778	0.0531	0.0012	339	7	339	2	326	50	104
A_212.FIN2	PLES 9	728	125	0.12	780	0.4002	0.0092	0.0544	0.0003	0.0078	0.0534	0.0013	342	7	341	2	336	54	102
A_174.FIN2	PLES 7	751	110	0.11	530	0.3965	0.0082	0.0539	0.0004	0.3172	0.0534	0.0010	339	6	339	2	339	43	100
A_233.FIN2	PLES 14	635	101	0.10	930	0.4020	0.0100	0.0542	0.0004	0.1437	0.0537	0.0014	343	8	340	2	346	57	98
A_217.FIN2	PLES 10	782	124	0.11	800	0.4010	0.0084	0.0542	0.0004	0.0393	0.0535	0.0011	342	6	340	2	346	49	98
A_106.FIN2	PLES 5	604	85	0.10	650	0.3988	0.0099	0.0538	0.0004	0.1662	0.0537	0.0013	340	7	338	3	344	54	98
A_005.FIN2	PLES 2	457	67	0.10	422	0.3998	0.0085	0.0538	0.0004	0.2547	0.0539	0.0011	341	6	338	2	350	46	97
A_038.FIN2	PLES 3	398	60	0.10	390	0.4045	0.0087	0.0540	0.0003	0.1641	0.0544	0.0012	344	6	339	2	367	49	92
A_004.FIN2	PLES 1	460	66	0.10	472	0.4038	0.0078	0.0537	0.0004	0.0439	0.0545	0.0011	344	6	337	2	376	44	90
A_232.FIN2	PLES 13	745	114	0.11	670	0.4061	0.0077	0.0540	0.0004	0.1269	0.0545	0.0010	346	6	339	2	381	43	89
A_072.FIN2	PLES 4	505	78	0.10	460	0.4042	0.0095	0.0537	0.0004	0.3174	0.0547	0.0012	344	7	337	3	386	51	87

Appendix 6.9: Results of the analysis of zircons from Bomkoul kaolin

Analysis	Sample	U [ppm][a]	Pb [ppm][a]	Th/U[a]	*206/204*	RATIOS $^{207}Pb/^{235}U$[b]	2 σ[d]	$^{206}Pb/^{238}U$[b]	2 σ[d]	rho[c]	$^{207}Pb/^{206}Pb$[e]	2 σ[d]	AGES [Ma] $^{207}Pb/^{235}U$	2 σ	$^{206}Pb/^{238}U$	2 σ	$^{207}Pb/^{206}Pb$	2 σ	Conc. %
A_302.FIN2	BKL042	169	48	1.22	0	0.0683	0.0066	0.0089	0.0002	0.0912	0.0566	0.0055	67	6	57	1	360	190	16
A_370.FIN2	BKL104	107	18	0.71	13	0.0660	0.0140	0.0094	0.0004	0.0756	0.0520	0.0110	64	13	60	3	110	340	55
A_325.FIN2	BKL063	523	570	0.44	850	0.8510	0.0160	0.0926	0.0008	0.1340	0.0667	0.0013	624	9	571	5	817	42	70
A_283.FIN2	BKL023	221	158	0.31	430	0.7660	0.0210	0.0927	0.0010	0.0903	0.0601	0.0018	576	12	571	6	588	67	97
A_292.FIN2	BKL032	78	547	2.90	170	0.7790	0.0310	0.0933	0.0010	0.1200	0.0604	0.0024	581	18	576	6	563	85	102
A_317.FIN2	BKL055	363	232	0.28	2800	0.8800	0.0130	0.0945	0.0011	0.1308	0.0677	0.0014	640	7	582	7	843	42	69
A_269.FIN2	BKL013	129	446	1.42	210	0.7770	0.0200	0.0951	0.0007	0.0046	0.0593	0.0016	581	11	586	4	542	57	108
A_278.FIN2	BKL019	243	959	1.71	190	0.7950	0.0160	0.0958	0.0008	0.0455	0.0602	0.0013	594	9	591	5	597	48	99
A_315.FIN2	BKL053	340	656	0.87	60000	0.8510	0.0140	0.0968	0.0006	0.2582	0.0637	0.0011	624	8	595	3	715	37	83
A_339.FIN2	BKL075	8	31	1.33	20	0.8000	0.1200	0.0971	0.0040	0.2677	0.0588	0.0085	599	80	597	23	480	300	124
A_345.FIN2	BKL079	239	490	0.83	-19000	0.8230	0.0230	0.0976	0.0009	0.0281	0.0613	0.0018	608	13	600	5	636	61	94
A_267.FIN2	BKL011	146	51	0.14	226	0.8210	0.0230	0.0976	0.0009	0.1234	0.0608	0.0016	606	13	600	5	625	62	96
A_366.FIN2	BKL100	93	531	2.38	132	0.8180	0.0340	0.0977	0.0014	0.0053	0.0608	0.0028	604	19	601	8	586	97	102
A_365.FIN2	BKL099	108	363	1.35	0	0.8070	0.0430	0.0977	0.0016	0.1428	0.0600	0.0032	597	25	601	9	560	120	107
A_263.FIN2	BKL007	61	170	1.13	76	0.8280	0.0360	0.0980	0.0014	0.0593	0.0616	0.0029	607	20	603	8	600	100	100
A_337.FIN2	BKL073	478	839	0.83	690	0.9790	0.0160	0.0981	0.0016	0.3311	0.0724	0.0015	693	8	603	9	986	41	61
A_304.FIN2	BKL044	403	304	0.31	830	0.8190	0.0180	0.0984	0.0007	0.0859	0.0604	0.0013	607	10	605	4	602	49	100
A_324.FIN2	BKL062	248	599	0.97	7300	0.8260	0.0170	0.0985	0.0008	0.1207	0.0609	0.0012	611	9	605	5	618	44	98
A_295.FIN2	BKL035	104	278	1.09	100	0.8170	0.0260	0.0989	0.0010	0.1285	0.0599	0.0019	604	15	608	6	561	71	108
A_284.FIN2	BKL024	131	267	0.81	-4300	0.8160	0.0240	0.0990	0.0010	0.1164	0.0599	0.0018	604	13	609	6	567	64	107

A_371.FI N2	BKL 105	52	198	1.46	77	0.8210	0.0310	0.0991	0.0010	0.0944	0.0602	0.0022	606	17	609	6	561	81	109
A_262.FI N2	BKL 006	21	53	0.95	29	0.9060	0.0510	0.0992	0.0018	0.0921	0.0662	0.0038	645	28	609	10	700	120	87
A_369.FI N2	BKL 103	86	344	1.52	154	0.8370	0.0240	0.0992	0.0009	0.0697	0.0611	0.0018	614	14	609	5	606	65	101
A_258.FI N2	BKL 002	87	76	0.33	110	0.8350	0.0230	0.0992	0.0009	0.1284	0.0614	0.0018	613	13	610	5	609	60	100
A_257.FI N2	BKL 001	182	190	0.46	133	0.8340	0.0280	0.0992	0.0012	0.0983	0.0613	0.0022	614	15	610	7	625	79	98
A_319.FI N2	BKL 057	196	140	0.28	280	0.8460	0.0250	0.0993	0.0008	0.2336	0.0618	0.0018	621	14	610	5	641	61	95
A_268.FI N2	BKL 012	258	457	0.75	420	0.8470	0.0270	0.0993	0.0011	0.1240	0.0621	0.0020	622	15	611	7	659	67	93
A_285.FI N2	BKL 025	112	236	0.83	-600	0.8260	0.0220	0.0997	0.0008	0.0131	0.0602	0.0017	609	12	612	5	576	60	106
A_259.FI N2	BKL 003	87	265	1.27	87	0.8440	0.0380	0.0999	0.0013	0.1389	0.0616	0.0028	618	22	614	8	640	110	96
A_336.FI N2	BKL 072	301	659	0.91	230	0.8420	0.0210	0.1002	0.0009	0.4282	0.0615	0.0014	619	12	615	5	643	49	96
A_340.FI N2	BKL 076	142	397	1.08	198	0.8340	0.0240	0.1003	0.0009	0.1727	0.0603	0.0017	613	13	616	5	580	61	106
A_291.FI N2	BKL 031	57	167	1.16	1800	0.8530	0.0390	0.1004	0.0014	0.1104	0.0613	0.0028	621	22	617	8	604	99	102
A_279.FI N2	BKL 020	114	327	1.14	226	0.8270	0.0230	0.1004	0.0008	0.0910	0.0602	0.0018	613	14	617	5	570	64	108
A_330.FI N2	BKL 067	186	681	1.47	160	0.8380	0.0210	0.1004	0.0009	0.0961	0.0605	0.0016	616	12	617	5	600	58	103
A_375.FI N2	BKL 109	303	499	0.65	470	0.8430	0.0170	0.1005	0.0008	0.0281	0.0609	0.0013	620	10	617	5	621	47	99
A_276.FI N2	BKL 017	84	358	1.71	128	0.8550	0.0330	0.1006	0.0013	0.1745	0.0617	0.0024	623	18	618	8	627	80	99
A_261.FI N2	BKL 005	79	90	0.44	109	0.8510	0.0350	0.1007	0.0012	0.0827	0.0615	0.0025	621	19	619	7	604	87	102
A_294.FI N2	BKL 034	108	390	1.44	1000	0.8510	0.0250	0.1007	0.0010	0.1114	0.0615	0.0018	623	14	619	6	622	66	99
A_363.FI N2	BKL 097	114	370	1.26	910	0.8470	0.0250	0.1008	0.0009	0.2528	0.0611	0.0018	622	14	619	5	606	63	102
A_265.FI N2	BKL 009	109	215	0.73	225	0.8740	0.0290	0.1008	0.0010	0.0207	0.0629	0.0022	637	16	619	6	673	76	92
A_311.FI N2	BKL 049	444	439	0.41	720	0.8380	0.0140	0.1009	0.0007	0.1990	0.0603	0.0010	618	8	620	4	605	37	102
A_300.FI N2	BKL 040	290	102	0.14	3400	0.8520	0.0160	0.1011	0.0007	0.2828	0.0610	0.0011	625	9	621	4	626	39	99
A_353.FI N2	BKL 087	223	461	0.78	440	0.8520	0.0230	0.1013	0.0007	0.0032	0.0609	0.0017	624	13	622	4	611	61	102
A_351.FI N2	BKL 085	115	168	0.55	3900	0.8560	0.0230	0.1013	0.0009	0.1275	0.0613	0.0017	625	13	622	5	616	61	101

A_374.FIN2	BKL108	76	210	1.06	110	0.8480	0.0370	0.1015	0.0013	0.2962	0.0605	0.0025	620	20	623	7	592	89	105
A_341.FIN2	BKL077	146	597	1.58	248	0.8590	0.0210	0.1016	0.0009	0.0504	0.0614	0.0016	628	12	624	5	639	56	98
A_316.FIN2	BKL054	154	456	1.24	70000	0.8400	0.0300	0.1017	0.0015	0.0788	0.0600	0.0022	622	19	624	9	630	78	99
A_327.FIN2	BKL065	167	148	0.35	800	0.8600	0.0210	0.1017	0.0008	0.0912	0.0614	0.0016	629	11	624	5	639	55	98
A_355.FIN2	BKL089	304	367	0.43	550	0.8600	0.0140	0.1018	0.0006	0.0013	0.0611	0.0011	629	8	625	4	633	40	99
A_289.FIN2	BKL029	313	6	0.01	760	0.8480	0.0180	0.1018	0.0007	0.4090	0.0604	0.0012	622	10	625	4	613	44	102
A_266.FIN2	BKL010	266	187	0.29	490	0.8590	0.0230	0.1019	0.0009	0.0862	0.0615	0.0018	629	13	626	5	638	66	98
A_364.FIN2	BKL098	132	312	0.92	290	0.8790	0.0290	0.1019	0.0011	0.0281	0.0624	0.0021	638	16	626	6	654	76	96
A_323.FIN2	BKL061	57	231	1.56	56	0.8680	0.0420	0.1021	0.0015	0.3952	0.0618	0.0029	629	23	626	9	610	100	103
A_288.FIN2	BKL028	64	303	1.90	4400	0.8710	0.0360	0.1022	0.0012	0.0046	0.0620	0.0027	632	20	627	7	623	92	101
A_312.FIN2	BKL050	185	511	1.09	270	0.8490	0.0260	0.1023	0.0009	0.2475	0.0602	0.0018	624	15	628	5	594	66	106
A_356.FIN2	BKL090	85	290	1.24	400	0.8730	0.0250	0.1027	0.0009	0.0857	0.0617	0.0019	634	14	630	5	620	66	102
A_367.FIN2	BKL101	77	209	1.08	1800	0.8740	0.0400	0.1028	0.0015	0.0846	0.0623	0.0027	638	20	631	9	642	93	98
A_368.FIN2	BKL102	60	238	1.36	700	0.8790	0.0410	0.1033	0.0014	0.0190	0.0617	0.0030	636	23	634	8	610	110	104
A_272.FIN2	BKL016	132	337	0.95	206	0.8680	0.0250	0.1035	0.0009	0.1965	0.0608	0.0017	632	13	635	6	601	60	106
A_271.FIN2	BKL015	317	931	1.22	-1100	0.8800	0.0250	0.1036	0.0010	0.2043	0.0617	0.0017	639	14	636	6	660	57	96
A_354.FIN2	BKL088	207	345	0.63	300	0.8760	0.0200	0.1038	0.0009	0.1491	0.0614	0.0013	638	11	637	5	636	47	100
A_320.FIN2	BKL058	259	1021	1.57	230	0.8690	0.0210	0.1039	0.0008	0.1754	0.0603	0.0014	634	12	637	5	609	55	105
A_307.FIN2	BKL047	112	24	0.05	246	0.8920	0.0250	0.1041	0.0010	0.0655	0.0620	0.0018	645	13	639	6	654	63	98
A_379.FIN2	BKL111	112	359	1.21	0	0.8850	0.0290	0.1043	0.0011	0.0735	0.0616	0.0022	641	15	639	7	618	75	103
A_318.FIN2	BKL056	110	597	2.07	223	0.9180	0.0370	0.1047	0.0012	0.2055	0.0638	0.0028	658	19	642	7	694	94	93
A_306.FIN2	BKL046	377	1047	1.24	2400	0.8970	0.0140	0.1048	0.0006	0.1527	0.0622	0.0010	651	7	642	4	673	32	95
A_326.FIN2	BKL064	145	173	0.45	270	0.9010	0.0260	0.1053	0.0010	0.0185	0.0623	0.0019	650	14	646	6	656	65	98
A_321.FIN2	BKL059	264	659	0.98	3100	0.8860	0.0270	0.1059	0.0011	0.1412	0.0608	0.0019	643	15	649	7	613	67	106

A_270.FIN2	BKL014	269	1083	1.57	451	0.8940	0.0190	0.1063	0.0009	0.1651	0.0611	0.0013	647	10	651	5	633	47	103
A_301.FIN2	BKL041	55	181	1.11	630	1.0580	0.0500	0.1192	0.0017	0.1871	0.0646	0.0030	726	25	726	10	700	100	104
A_314.FIN2	BKL052	240	430	0.45	80000	1.5530	0.0250	0.1515	0.0012	0.0784	0.0744	0.0013	950	10	910	7	1042	36	87
A_282.FIN2	BKL022	373	1462	1.07	1000	1.5950	0.0220	0.1589	0.0010	0.1931	0.0729	0.0010	968	9	951	6	1003	29	95
A_296.FIN2	BKL036	79	287	0.93	197	1.7130	0.0360	0.1678	0.0011	0.0967	0.0739	0.0016	1009	13	1000	6	1011	44	99
A_297.FIN2	BKL037	247	439	0.46	400	1.7100	0.0240	0.1685	0.0010	0.0718	0.0735	0.0011	1011	9	1004	5	1023	29	98
A_357.FIN2	BKL091	162	661	0.94	580	1.6980	0.0320	0.1691	0.0013	0.0973	0.0728	0.0014	1006	12	1007	7	995	41	101
A_281.FIN2	BKL021	92	226	0.64	280	1.7240	0.0400	0.1698	0.0014	0.1559	0.0736	0.0017	1016	14	1011	8	1011	46	100
A_303.FIN2	BKL043	42	178	0.95	280	2.2160	0.0600	0.1749	0.0017	0.1452	0.0917	0.0025	1179	19	1039	10	1425	53	73
A_277.FIN2	BKL018	54	447	1.24	90	3.6800	0.0720	0.2739	0.0020	0.1281	0.0976	0.0020	1564	16	1560	10	1559	40	100
A_298.FIN2	BKL038	84	613	1.12	1100	3.7380	0.0590	0.2767	0.0018	0.2270	0.0980	0.0015	1579	13	1575	9	1579	29	100
A_372.FIN2	BKL106	222	697	0.46	-60000	5.2400	0.0590	0.2809	0.0020	0.5989	0.1349	0.0012	1857	10	1595	10	2159	16	74
A_361.FIN2	BKL095	253	2061	1.06	7600	5.2560	0.0580	0.3053	0.0024	0.4568	0.1246	0.0012	1861	9	1717	12	2024	18	85
A_347.FIN2	BKL081	179	592	0.43	-37000	5.7260	0.0750	0.3244	0.0026	0.4163	0.1283	0.0016	1936	12	1811	13	2072	23	87
A_349.FIN2	BKL083	762	294	0.06	4200	5.4320	0.0310	0.3253	0.0014	0.4249	0.1209	0.0007	1890	5	1815	7	1968	10	92
A_310.FIN2	BKL048	1084	2183	0.61	1047	9.0200	0.1000	0.3283	0.0037	0.9198	0.1988	0.0009	2338	10	1829	18	2816	7	65
A_344.FIN2	BKL078	266	994	0.74	1350	9.2600	0.5400	0.3350	0.0170	0.9853	0.1993	0.0021	2333	52	1851	83	2818	17	66
A_373.FIN2	BKL107	85	1285	1.89	-13000	5.8000	0.1100	0.3372	0.0030	0.1302	0.1248	0.0024	1944	16	1873	14	2019	34	93
A_384.FIN2	BKL115	152	1028	0.88	-200	5.5510	0.0860	0.3425	0.0024	0.0005	0.1181	0.0020	1907	13	1898	12	1922	30	99
A_290.FIN2	BKL030	28	1078	4.60	1100	5.9400	0.1200	0.3433	0.0039	0.2291	0.1251	0.0028	1964	18	1902	19	2016	41	94
A_333.FIN2	BKL070	147	1836	1.52	780	6.0410	0.0850	0.3504	0.0028	0.2736	0.1251	0.0017	1980	12	1936	13	2030	25	95
A_382.FIN2	BKL114	62	401	0.75	170	5.9100	0.1200	0.3538	0.0052	0.7728	0.1208	0.0017	1956	19	1951	25	1961	25	99
A_332.FIN2	BKL069	129	1210	1.13	290	6.1290	0.0950	0.3535	0.0028	0.1746	0.1259	0.0021	1993	14	1951	13	2037	29	96
A_335.FIN2	BKL071	126	1158	1.09	580	6.1070	0.0760	0.3551	0.0025	0.3596	0.1246	0.0015	1991	11	1959	12	2022	22	97

A_293.FIN2	BKL033	155	121	0.11	910	6.6800	0.1200	0.3575	0.0029	0.7766	0.1350	0.0017	2066	15	1970	14	2157	21	91
A_305.FIN2	BKL045	190	964	0.62	5600	6.3270	0.0600	0.3593	0.0021	0.2338	0.1278	0.0013	2022	8	1979	10	2066	18	96
A_381.FIN2	BKL113	159	907	0.67	100	6.4740	0.0870	0.3667	0.0032	0.3558	0.1287	0.0018	2041	12	2014	15	2078	24	97
A_378.FIN2	BKL110	92	1605	2.02	670	6.6430	0.0810	0.3754	0.0023	0.1526	0.1283	0.0016	2065	10	2054	11	2072	22	99
A_352.FIN2	BKL086	103	1609	1.71	470	6.7650	0.0960	0.3794	0.0031	0.0694	0.1291	0.0020	2080	13	2073	15	2081	28	100
A_380.FIN2	BKL112	217	982	0.51	810	6.9480	0.0640	0.3797	0.0021	0.5038	0.1328	0.0011	2104	8	2075	10	2134	14	97
A_286.FIN2	BKL026	306	1012	0.54	1940	11.3900	0.1500	0.4021	0.0047	0.8070	0.2057	0.0016	2554	12	2178	21	2871	13	76
A_359.FIN2	BKL093	57	610	1.14	8700	8.4000	0.1200	0.4060	0.0033	0.2167	0.1501	0.0022	2273	13	2196	15	2340	25	94
A_329.FIN2	BKL066	124	587	0.50	1330	8.9900	0.1400	0.4257	0.0033	0.3128	0.1531	0.0022	2335	14	2286	15	2383	26	96
A_360.FIN2	BKL094	135	942	0.70	690	9.7100	0.1100	0.4375	0.0029	0.2532	0.1610	0.0018	2407	10	2339	13	2463	19	95
A_264.FIN2	BKL008	62	522	0.84	-12000	9.7800	0.1200	0.4400	0.0028	0.2423	0.1615	0.0020	2412	12	2350	12	2465	21	95
A_350.FIN2	BKL084	335	424	0.13	35000	12.5580	0.0890	0.4427	0.0033	0.4730	0.2059	0.0016	2647	7	2363	15	2873	12	82
A_260.FIN2	BKL004	29	219	0.74	137	10.6000	0.2500	0.4480	0.0046	0.2784	0.1720	0.0040	2483	22	2385	21	2563	39	93
A_313.FIN2	BKL051	273	1944	0.70	1850	12.5700	0.1200	0.4537	0.0037	0.7386	0.2004	0.0013	2647	9	2411	17	2828	11	85
A_358.FIN2	BKL092	91	987	1.02	29000	10.6600	0.1700	0.4705	0.0049	0.1721	0.1646	0.0029	2493	15	2485	22	2500	29	99
A_362.FIN2	BKL096	25	243	1.07	220	12.6100	0.4500	0.4813	0.0087	0.7025	0.1894	0.0050	2638	34	2530	38	2722	44	93
A_299.FIN2	BKL039	386	2256	0.52	2800	14.8100	0.1600	0.4988	0.0035	0.8344	0.2147	0.0014	2801	10	2608	15	2940	11	89
A_322.FIN2	BKL060	49	1928	3.34	580	15.0900	0.1800	0.5383	0.0042	0.1714	0.2036	0.0026	2820	11	2776	18	2851	21	97
A_331.FIN2	BKL068	141	1602	0.94	1250	16.0900	0.1200	0.5438	0.0032	0.4983	0.2145	0.0015	2882	7	2799	13	2938	11	95
A_348.FIN2	BKL082	205	4027	1.56	1680	15.5700	0.0870	0.5447	0.0026	0.3632	0.2067	0.0012	2850	5	2803	11	2880	10	97
A_287.FIN2	BKL027	48	1187	2.05	-16000	15.5100	0.2000	0.5540	0.0043	0.4539	0.2030	0.0024	2845	12	2841	18	2846	19	100
A_338.FIN2	BKL074	30	570	1.51	320	15.5900	0.2300	0.5543	0.0048	0.1690	0.2038	0.0032	2849	14	2842	20	2855	25	100

Appendix 6.10: Results of the analysis of zircons from Dibamba kaolin

						RATIOS						AGES [Ma]						Conc.
Analysis	Sample	U [ppm][a]	Pb [ppm][a]	Th/U[a]	*206/204*	$^{207}Pb/^{235}U$[b]	2 σ[d]	$^{206}Pb/^{238}U$[b]	2 σ[d]	rho[c]	$^{207}Pb/^{206}Pb$[e]	2 σ[d]	$^{207}Pb/^{235}U$	2 σ	$^{206}Pb/^{238}U$	2 σ	$^{207}Pb/^{206}Pb$	2 σ	%
A_004.FIN2	DBB 001	1372	254	0.68	198	0.0657	0.0030	0.0098	0.0001	0.0052	0.0488	0.0023	65	3	63	1	139	98	45
A_012.FIN2	DBB 009	611	516	0.78	980	0.7430	0.0140	0.0810	0.0008	0.1756	0.0668	0.0012	564	8	502	5	825	39	61
A_101.FIN2	DBB 092	991	389	0.16	880	0.7880	0.0100	0.0818	0.0012	0.0671	0.0705	0.0016	589	6	507	8	923	44	55
A_016.FIN2	DBB 013	556	1064	0.82	670	0.8920	0.0130	0.0901	0.0006	0.3005	0.0718	0.0010	647	7	556	3	980	29	57
A_054.FIN2	DBB 049	491	387	0.54	710	0.8590	0.0190	0.0911	0.0008	0.2225	0.0683	0.0015	629	10	562	5	867	44	65
A_099.FIN2	DBB 090	495	863	0.82	990	0.8200	0.0120	0.0941	0.0006	0.4080	0.0635	0.0009	607	7	579	4	720	29	80
A_019.FIN2	DBB 016	249	600	1.00	480	0.8030	0.0250	0.0969	0.0009	0.2021	0.0602	0.0018	597	14	596	5	586	67	102
A_066.FIN2	DBB 059	112	616	2.09	180	0.8320	0.0280	0.0974	0.0010	0.0393	0.0617	0.0022	612	15	599	6	627	75	96
A_120.FIN2	DBB 106	235	664	1.12	740	0.8280	0.0220	0.0975	0.0009	0.1904	0.0616	0.0015	611	12	600	5	651	57	92
A_009.FIN2	DBB 006	179	413	0.90	450	0.8780	0.0270	0.0978	0.0011	0.0924	0.0652	0.0021	638	15	601	7	768	72	78
A_078.FIN2	DBB 069	170	101	0.25	248	0.8200	0.0250	0.0979	0.0012	0.0867	0.0608	0.0019	606	14	602	7	623	65	97
A_030.FIN2	DBB 027	369	40	0.15	820	0.8250	0.0190	0.0986	0.0009	0.1261	0.0607	0.0014	610	11	606	5	614	52	99
A_094.FIN2	DBB 085	154	548	1.31	330	0.8170	0.0230	0.0987	0.0009	0.1014	0.0604	0.0018	604	13	607	5	588	66	103
A_091.FIN2	DBB 082	177	1260	2.75	298	0.8220	0.0210	0.0988	0.0009	0.0929	0.0604	0.0016	607	12	607	5	596	57	102
A_052.FIN2	DBB 047	43	35	0.32	75	0.9710	0.0500	0.0989	0.0015	0.0768	0.0713	0.0037	681	26	608	9	890	110	68
A_123.FIN2	DBB 109	95	158	0.61	210	0.9220	0.0330	0.0989	0.0012	0.2288	0.0680	0.0024	660	17	608	7	828	74	73
A_038.FIN2	DBB 033	154	132	0.35	280	0.8380	0.0230	0.0990	0.0010	0.1969	0.0610	0.0018	616	13	608	6	624	60	97
A_045.FIN2	DBB 040	159	147	0.35	320	0.8370	0.0230	0.0990	0.0010	0.0310	0.0611	0.0018	616	13	609	6	616	64	99
A_011.FIN2	DBB 008	368	1207	1.34	890	0.8470	0.0270	0.0991	0.0009	0.0039	0.0625	0.0021	622	15	609	5	687	66	89
A_062.FIN2	DBB 055	329	115	0.13	920	0.8310	0.0180	0.0993	0.0006	0.0201	0.0605	0.0013	613	10	611	4	606	49	101

A_093.FIN2 DBB 084	71	201	1.05	195	0.8860	0.0380	0.0993	0.0013	0.0091	0.0649	0.0030	640	20	612	8	714	97	86
A_074.FIN2 DBB 065	89	386	1.75	190	0.8540	0.0420	0.0997	0.0017	0.0285	0.0630	0.0035	628	25	613	10	650	120	94
A_110.FIN2 DBB 098	111	357	1.23	140	0.8420	0.0280	0.1000	0.0012	0.1711	0.0615	0.0020	618	15	614	7	621	73	99
A_092.FIN2 DBB 083	201	1088	2.10	318	0.8490	0.0290	0.1002	0.0012	0.1402	0.0618	0.0022	622	16	616	7	643	78	96
A_044.FIN2 DBB 039	158	349	0.90	160	0.8610	0.0360	0.1004	0.0014	0.0071	0.0620	0.0028	629	19	617	9	645	96	96
A_060.FIN2 DBB 053	206	702	1.38	300	0.8380	0.0240	0.1005	0.0011	0.1255	0.0603	0.0018	617	13	617	7	595	65	104
A_124.FIN2 DBB 110	53	144	1.03	70	0.8520	0.0400	0.1005	0.0013	0.2081	0.0619	0.0028	619	22	617	8	597	95	103
A_032.FIN2 DBB 029	21	83	1.58	35	0.8760	0.0830	0.1007	0.0026	0.0748	0.0639	0.0065	623	45	618	15	590	200	105
A_050.FIN2 DBB 045	233	538	1.01	530	0.8570	0.0220	0.1006	0.0010	0.2617	0.0615	0.0016	627	12	618	6	640	54	97
A_027.FIN2 DBB 024	93	189	0.81	222	0.8490	0.0310	0.1007	0.0011	0.0153	0.0613	0.0023	622	17	618	7	612	83	101
A_081.FIN2 DBB 072	178	251	0.55	-300	0.8700	0.0430	0.1007	0.0012	0.2896	0.0626	0.0029	633	23	619	7	660	100	94
A_035.FIN2 DBB 032	333	338	0.42	460	0.8500	0.0230	0.1008	0.0009	0.1201	0.0612	0.0017	624	13	619	5	631	62	98
A_084.FIN2 DBB 075	76	231	1.13	217	0.8520	0.0300	0.1010	0.0010	0.0818	0.0608	0.0021	622	16	620	6	607	79	102
A_010.FIN2 DBB 007	172	622	1.39	2500	0.8410	0.0280	0.1010	0.0009	0.1480	0.0607	0.0020	617	15	620	5	596	70	104
A_061.FIN2 DBB 054	46	99	0.78	67	0.8720	0.0350	0.1011	0.0017	0.1108	0.0619	0.0024	637	20	621	10	659	90	94
A_021.FIN2 DBB 018	50	298	2.40	130	0.8600	0.0440	0.1012	0.0015	0.0913	0.0621	0.0033	624	24	621	9	600	110	104
A_048.FIN2 DBB 043	352	1251	1.44	720	0.8530	0.0160	0.1012	0.0006	0.0492	0.0610	0.0012	625	9	621	4	632	41	98
A_077.FIN2 DBB 068	177	895	1.94	320	0.8460	0.0220	0.1012	0.0009	0.0326	0.0607	0.0017	621	12	622	5	605	60	103
A_058.FIN2 DBB 051	266	223	0.34	840	0.8510	0.0200	0.1012	0.0009	0.0176	0.0609	0.0015	624	11	622	5	618	56	101
A_008.FIN2 DBB 005	357	1169	1.31	620	0.8540	0.0180	0.1013	0.0008	0.0367	0.0615	0.0014	626	10	622	5	642	52	97
A_039.FIN2 DBB 034	235	949	1.68	520	0.8530	0.0280	0.1013	0.0011	0.0760	0.0612	0.0021	625	15	622	6	621	76	100
A_083.FIN2 DBB 074	173	342	0.75	310	0.8470	0.0220	0.1015	0.0009	0.1007	0.0606	0.0016	621	12	623	5	599	60	104
A_090.FIN2 DBB 081	62	182	1.07	169	0.8600	0.0310	0.1016	0.0014	0.2467	0.0616	0.0023	626	17	624	8	621	84	100
A_109.FIN2 DBB 097	335	600	0.75	610	0.8460	0.0140	0.1017	0.0009	0.2883	0.0608	0.0010	623	8	624	6	627	37	100

A_080.FIN2 DBB 071	102	232	0.85	228	0.8460	0.0260	0.1017	0.0012	0.0684	0.0600	0.0019	620	14	624	7	585	70	107
A_089.FIN2 DBB 080	75	252	1.24	116	0.8720	0.0380	0.1019	0.0016	0.0513	0.0623	0.0029	633	21	625	9	637	97	98
A_041.FIN2 DBB 036	105	224	0.86	188	0.8880	0.0330	0.1020	0.0011	0.0477	0.0632	0.0025	642	18	626	7	669	85	94
A_085.FIN2 DBB 076	281	523	0.71	710	0.8650	0.0220	0.1021	0.0011	0.2399	0.0613	0.0016	632	12	627	6	636	56	99
A_049.FIN2 DBB 044	212	415	0.78	580	0.8510	0.0250	0.1022	0.0009	0.0793	0.0603	0.0018	623	14	627	6	589	65	107
A_072.FIN2 DBB 063	164	712	1.51	460	0.8610	0.0220	0.1024	0.0008	0.0007	0.0605	0.0016	630	11	629	5	601	57	105
A_100.FIN2 DBB 091	68	281	1.51	177	0.9000	0.0430	0.1026	0.0016	0.1278	0.0640	0.0031	648	23	629	9	690	110	91
A_075.FIN2 DBB 066	45	171	1.34	116	0.8760	0.0390	0.1026	0.0011	0.0474	0.0619	0.0028	631	21	629	7	592	96	106
A_107.FIN2 DBB 095	189	480	0.93	-610	0.8590	0.0220	0.1026	0.0009	0.1579	0.0611	0.0016	628	12	630	5	620	55	102
A_115.FIN2 DBB 101	68	180	0.92	202	0.8690	0.0300	0.1027	0.0011	0.1033	0.0617	0.0021	633	16	630	6	629	71	100
A_015.FIN2 DBB 012	233	486	0.84	640	0.8620	0.0200	0.1028	0.0010	0.1899	0.0612	0.0016	630	11	631	6	626	59	101
A_014.FIN2 DBB 011	229	336	0.63	-26000	0.8950	0.0280	0.1032	0.0010	0.2021	0.0633	0.0020	648	15	633	6	695	67	91
A_069.FIN2 DBB 062	74	260	1.33	217	0.8770	0.0330	0.1033	0.0011	0.0606	0.0618	0.0024	638	18	634	7	616	82	103
A_122.FIN2 DBB 108	61	93	0.53	165	0.8700	0.0360	0.1033	0.0012	0.1105	0.0612	0.0026	631	19	634	7	630	97	101
A_029.FIN2 DBB 026	4	18	2.14	6	1.0100	0.1800	0.1040	0.0063	0.0840	0.0810	0.0160	630	100	635	36	630	370	101
A_046.FIN2 DBB 041	100	251	0.95	186	0.8840	0.0280	0.1035	0.0011	0.0260	0.0620	0.0021	640	15	635	6	634	74	100
A_007.FIN2 DBB 004	200	439	0.76	500	0.9310	0.0210	0.1049	0.0009	0.1313	0.0644	0.0015	668	12	643	5	738	47	87
A_087.FIN2 DBB 078	369	782	0.80	1270	0.8840	0.0200	0.1050	0.0009	0.0709	0.0612	0.0014	642	11	643	5	631	49	102
A_026.FIN2 DBB 023	295	1687	2.25	620	0.8970	0.0200	0.1051	0.0009	0.2232	0.0621	0.0014	651	10	644	5	673	46	96
A_031.FIN2 DBB 028	67	279	1.22	116	1.5200	0.1000	0.1051	0.0017	0.2927	0.1041	0.0066	932	45	644	10	1670	130	39
A_102.FIN2 DBB 093	194	649	1.20	500	0.9030	0.0250	0.1057	0.0009	0.2182	0.0622	0.0017	652	13	648	5	660	60	98
A_055.FIN2 DBB 050	223	587	0.98	860	0.9010	0.0200	0.1066	0.0007	0.0952	0.0609	0.0014	651	11	653	4	614	50	106
A_108.FIN2 DBB 096	45	67	0.10	132	1.6100	0.1800	0.1069	0.0018	0.8138	0.1100	0.0110	939	63	654	11	1540	170	42
A_117.FIN2 DBB 103	547	280	0.19	400	0.9200	0.0110	0.1075	0.0006	0.2381	0.0626	0.0007	662	6	658	4	689	24	96

A_042.FIN2 DBB 037	52	117	0.95	16	0.9340	0.0740	0.1087	0.0023	0.0619	0.0625	0.0050	670	42	665	14	630	170	106
A_067.FIN2 DBB 060	347	751	0.80	900	0.9440	0.0230	0.1097	0.0009	0.0884	0.0627	0.0016	674	12	671	5	678	56	99
A_118.FIN2 DBB 104	88	38	0.41	290	0.9710	0.0380	0.1103	0.0016	0.2334	0.0643	0.0025	685	20	676	9	726	86	93
A_020.FIN2 DBB 017	206	197	1.33	450	1.0150	0.0180	0.1107	0.0014	0.2384	0.0667	0.0012	711	9	676	8	812	39	83
A_053.FIN2 DBB 048	190	320	0.49	350	1.0990	0.0330	0.1151	0.0014	0.4931	0.0689	0.0018	750	16	702	8	884	53	79
A_034.FIN2 DBB 031	196	417	0.57	570	1.0740	0.0310	0.1208	0.0012	0.3968	0.0642	0.0017	739	15	735	7	734	55	100
A_076.FIN2 DBB 067	80	338	1.31	120	1.1610	0.0400	0.1218	0.0017	0.2312	0.0688	0.0023	781	18	741	10	861	74	86
A_047.FIN2 DBB 042	477	337	0.23	680	1.1700	0.0250	0.1278	0.0012	0.1178	0.0664	0.0015	786	12	775	7	811	46	96
A_024.FIN2 DBB 021	245	352	0.40	730	1.1690	0.0300	0.1285	0.0014	0.1454	0.0660	0.0020	785	14	779	8	791	62	98
A_088.FIN2 DBB 079	302	189	0.17	700	1.2090	0.0520	0.1316	0.0044	0.8870	0.0665	0.0013	800	23	796	25	812	41	98
A_028.FIN2 DBB 025	115	160	0.42	276	1.3260	0.0320	0.1335	0.0012	0.0971	0.0720	0.0018	856	14	808	7	965	53	84
A_119.FIN2 DBB 105	273	413	0.39	680	1.2860	0.0200	0.1380	0.0012	0.3685	0.0677	0.0010	838	9	834	7	850	31	98
A_022.FIN2 DBB 019	194	357	0.53	620	1.4620	0.0380	0.1480	0.0017	0.2215	0.0720	0.0019	913	15	890	10	970	53	92
A_113.FIN2 DBB 100	374	1503	1.13	1470	1.4860	0.0260	0.1513	0.0012	0.1346	0.0717	0.0014	924	11	908	7	969	39	94
A_068.FIN2 DBB 061	70	261	0.91	258	1.5180	0.0560	0.1544	0.0018	0.0848	0.0709	0.0027	933	23	926	10	915	83	101
A_006.FIN2 DBB 003	291	1024	0.85	950	1.5540	0.0350	0.1568	0.0013	0.3111	0.0723	0.0016	951	14	939	7	987	43	95
A_023.FIN2 DBB 020	156	375	0.58	960	1.5360	0.0340	0.1586	0.0018	0.3815	0.0700	0.0014	944	14	949	10	920	42	103
A_095.FIN2 DBB 086	69	191	0.63	271	1.6010	0.0410	0.1600	0.0015	0.1722	0.0727	0.0019	969	15	957	8	990	54	97
A_064.FIN2 DBB 057	189	841	1.13	-1700	1.5920	0.0340	0.1605	0.0011	0.0111	0.0719	0.0016	965	13	960	6	967	47	99
A_043.FIN2 DBB 038	77	224	0.73	250	1.6090	0.0470	0.1621	0.0019	0.0766	0.0720	0.0022	970	18	968	10	957	62	101
A_059.FIN2 DBB 052	230	418	0.42	630	1.7680	0.0270	0.1730	0.0011	0.0957	0.0738	0.0011	1033	10	1029	6	1036	30	99
A_063.FIN2 DBB 056	165	503	0.68	420	1.7740	0.0260	0.1735	0.0010	0.2394	0.0738	0.0011	1035	10	1031	6	1033	29	100
A_040.FIN2 DBB 035	74	1280	0.68	35	11.4700	0.9600	0.1824	0.0079	0.7589	0.4410	0.0240	2498	80	1077	42	4001	87	27
A_005.FIN2 DBB 002	183	862	0.66	670	2.8360	0.0860	0.2142	0.0044	0.7437	0.0960	0.0019	1361	23	1250	23	1540	38	81

A_116.FIN2 DBB 102	102	1255	1.55	1050	4.4690	0.0640	0.2807	0.0022	0.2845	0.1161	0.0017	1724	12	1595	11	1888	26	84
A_051.FIN2 DBB 046	43	246	0.80	210	4.3800	0.1200	0.2829	0.0032	0.1403	0.1117	0.0031	1704	22	1606	16	1821	47	88
A_096.FIN2 DBB 087	254	829	0.37	1960	5.5200	0.1200	0.3127	0.0054	0.8743	0.1283	0.0013	1900	18	1753	27	2072	18	85
A_098.FIN2 DBB 089	224	2284	0.91	1440	7.0700	0.2500	0.3213	0.0093	0.9545	0.1597	0.0018	2111	32	1793	45	2450	19	73
A_073.FIN2 DBB 064	183	1566	0.57	294	11.8200	0.1400	0.3713	0.0052	0.7112	0.2297	0.0025	2588	11	2034	24	3047	17	67
A_121.FIN2 DBB 107	365	2444	0.70	1440	10.5540	0.0860	0.3861	0.0026	0.7030	0.1992	0.0012	2484	8	2104	12	2819	10	75
A_086.FIN2 DBB 077	53	273	0.55	610	7.0800	0.1300	0.3888	0.0034	0.1020	0.1316	0.0026	2118	16	2119	17	2116	34	100
A_106.FIN2 DBB 094	60	320	0.58	-300	7.2000	0.1700	0.3917	0.0051	0.1079	0.1343	0.0034	2134	20	2130	24	2147	44	99
A_111.FIN2 DBB 099	224	1747	0.81	940	11.0400	0.2300	0.3940	0.0075	0.9576	0.2046	0.0013	2525	19	2138	34	2863	11	75
A_065.FIN2 DBB 058	157	1798	1.21	1350	7.8230	0.0850	0.3979	0.0029	0.3937	0.1419	0.0016	2210	10	2159	14	2252	18	96
A_018.FIN2 DBB 015	111	449	0.40	840	9.9200	0.1500	0.4558	0.0052	0.6828	0.1584	0.0020	2426	14	2420	23	2436	21	99
A_033.FIN2 DBB 030	124	803	0.47	820	13.6700	0.3100	0.4806	0.0077	0.9184	0.2047	0.0022	2719	23	2527	34	2860	18	88
A_079.FIN2 DBB 070	208	1583	0.68	900	11.8790	0.0810	0.4824	0.0023	0.3418	0.1782	0.0013	2594	7	2538	10	2634	12	96
A_082.FIN2 DBB 073	135	1226	0.78	2830	12.9600	0.1600	0.4965	0.0035	0.7762	0.1889	0.0017	2675	12	2598	15	2731	15	95
A_017.FIN2 DBB 014	198	2750	1.12	1650	14.0900	0.1400	0.5309	0.0040	0.3425	0.1926	0.0018	2755	10	2745	17	2764	15	99
A_097.FIN2 DBB 088	104	742	0.51	1060	15.8000	0.1900	0.5583	0.0051	0.7260	0.2050	0.0017	2863	11	2858	21	2864	13	100
A_013.FIN2 DBB 010	103	1075	0.80	1720	16.8200	0.1700	0.5722	0.0041	0.4679	0.2126	0.0020	2923	10	2916	17	2923	15	100
A_025.FIN2 DBB 022	280	1437	0.40	-72000	23.9200	0.2300	0.6137	0.0055	0.5634	0.2828	0.0021	3265	9	3084	22	3378	11	91

Appendix 6.11: Results of the analysis of zircons from Ediki kaolin

Analysis	Sample	U [ppm][a]	Pb [ppm][a]	Th/U[a]	*206/204*	RATIOS $^{207}Pb/^{235}U$[b]	2 σ[d]	$^{206}Pb/^{238}U$[b]	2 σ[d]	rho[c]	$^{207}Pb/^{206}Pb$[e]	2 σ[d]	AGES [Ma] $^{207}Pb/^{235}U$	2 σ	$^{206}Pb/^{238}U$	2 σ	$^{207}Pb/^{206}Pb$	2 σ	Conc. %
A_199.FIN2	EDK069	827	1291	0.27	121	1.3930	0.0190	0.0592	0.0005	0.3205	0.1719	0.0024	885	8	371	3	2574	23	14
A_157.FIN2	EDK031	327	270	0.62	296	0.8430	0.0250	0.0621	0.0010	0.3382	0.0993	0.0027	620	14	389	6	1600	53	24
A_228.FIN2	EDK094	356	707	1.11	433	0.7830	0.0180	0.0754	0.0013	0.1427	0.0759	0.0021	587	10	469	8	1083	55	43
A_127.FIN2	EDK003	508	593	0.36	240	1.0620	0.0260	0.0795	0.0009	0.0647	0.0979	0.0028	734	13	493	5	1574	52	31
A_186.FIN2	EDK056	171	317	0.91	90	0.7240	0.0180	0.0818	0.0009	0.2195	0.0643	0.0016	551	11	507	5	725	53	70
A_229.FIN2	EDK095	254	235	0.50	240	0.7920	0.0210	0.0851	0.0006	0.4073	0.0674	0.0017	590	12	526	4	839	50	63
A_181.FIN2	EDK051	155	291	0.78	230	0.7690	0.0230	0.0905	0.0010	0.1176	0.0617	0.0018	577	13	558	6	644	66	87
A_225.FIN2	EDK091	195	568	1.26	170	0.8780	0.0210	0.0910	0.0011	0.1737	0.0704	0.0018	638	11	562	6	917	52	61
A_164.FIN2	EDK038	526	1159	0.84	650	0.9970	0.0260	0.0911	0.0012	0.5527	0.0803	0.0028	701	13	562	7	1185	69	47
A_158.FIN2	EDK032	327	249	0.35	1130	0.8050	0.0160	0.0926	0.0007	0.0434	0.0639	0.0014	599	9	571	4	723	48	79
A_244.FIN2	EDK108	93	270	1.31	171	0.7600	0.0360	0.0926	0.0014	0.1344	0.0599	0.0029	570	21	571	8	550	100	104
A_133.FIN2	EDK009	125	151	0.49	239	0.7970	0.0430	0.0927	0.0019	0.2207	0.0631	0.0035	593	24	571	11	720	140	79
A_179.FIN2	EDK049	96	351	1.54	200	0.7580	0.0280	0.0930	0.0009	0.1508	0.0591	0.0021	569	16	573	6	541	78	106
A_180.FIN2	EDK050	152	184	0.51	150	0.7690	0.0220	0.0938	0.0010	0.0331	0.0598	0.0018	577	13	578	6	568	66	102
A_217.FIN2	EDK085	186	433	0.90	249	1.1310	0.0250	0.0939	0.0008	0.1154	0.0880	0.0020	766	12	579	5	1380	45	42
A_211.FIN2	EDK079	81	166	0.85	350	0.7970	0.0490	0.0939	0.0017	0.0801	0.0621	0.0038	591	27	579	10	620	130	93
A_156.FIN2	EDK030	168	421	1.14	230	0.8890	0.0400	0.0940	0.0013	0.2210	0.0693	0.0030	644	22	579	8	913	79	63
A_212.FIN2	EDK080	102	229	0.95	160	0.7780	0.0300	0.0945	0.0010	0.1994	0.0604	0.0022	583	17	582	6	574	78	101
A_141.FIN2	EDK015	123	13	0.04	238	0.7840	0.0220	0.0948	0.0009	0.0886	0.0604	0.0017	586	12	584	5	590	61	99
A_256.FIN2	EDK120	190	659	1.50	260	0.7810	0.0240	0.0949	0.0008	0.0135	0.0599	0.0019	584	14	585	5	567	71	103

A_135.FI N2	EDK 011	389	1250	1.32	675	0.9240	0.0160	0.0950	0.0009	0.5155	0.0709	0.0011	663	9	585	5	943	31	62
A_142.FI N2	EDK 016	108	393	1.40	380	0.7920	0.0220	0.0950	0.0009	0.0041	0.0609	0.0018	590	13	585	5	597	65	98
A_171.FI N2	EDK 043	78	56	0.30	185	0.7950	0.0350	0.0950	0.0014	0.4966	0.0610	0.0026	591	20	585	8	599	93	98
A_188.FI N2	EDK 058	429	1603	1.42	638	0.9780	0.0160	0.0950	0.0006	0.1092	0.0751	0.0013	692	8	585	4	1061	35	55
A_128.FI N2	EDK 004	144	530	1.42	233	0.7880	0.0260	0.0951	0.0009	0.1814	0.0606	0.0020	588	15	585	6	601	76	97
A_234.FI N2	EDK 100	48	137	1.22	65	0.7870	0.0360	0.0951	0.0013	0.0709	0.0604	0.0029	586	21	586	8	550	100	106
A_251.FI N2	EDK 115	64	144	0.96	95	0.7760	0.0340	0.0952	0.0010	0.1501	0.0593	0.0026	581	20	586	6	526	93	111
A_243.FI N2	EDK 107	578	1187	0.90	1310	0.7900	0.0160	0.0953	0.0007	0.1173	0.0603	0.0014	591	9	587	4	604	50	97
A_235.FI N2	EDK 101	228	579	1.02	740	0.8360	0.0240	0.0955	0.0009	0.1188	0.0638	0.0019	618	14	588	5	724	65	81
A_125.FI N2	EDK 001	118	325	1.02	145	0.7980	0.0220	0.0956	0.0009	0.1137	0.0611	0.0017	593	12	589	5	607	60	97
A_197.FI N2	EDK 067	104	239	0.98	290	0.7930	0.0270	0.0958	0.0010	0.1845	0.0605	0.0020	593	15	590	6	588	74	100
A_213.FI N2	EDK 081	246	839	1.32	260	0.8030	0.0210	0.0960	0.0009	0.0524	0.0608	0.0017	597	12	591	5	620	56	95
A_227.FI N2	EDK 093	206	688	1.45	610	0.8020	0.0240	0.0962	0.0011	0.0954	0.0608	0.0019	596	14	592	6	613	69	97
A_216.FI N2	EDK 084	405	2498	2.65	550	0.8280	0.0140	0.0963	0.0007	0.1026	0.0627	0.0011	612	8	593	4	688	38	86
A_204.FI N2	EDK 074	156	431	1.16	120	0.7830	0.0300	0.0963	0.0013	0.1655	0.0595	0.0024	588	18	593	7	563	93	105
A_163.FI N2	EDK 037	230	151	0.15	620	0.9770	0.0230	0.0966	0.0008	0.4437	0.0737	0.0016	690	12	594	5	1031	40	58
A_146.FI N2	EDK 020	292	855	1.17	730	0.8040	0.0190	0.0966	0.0009	0.2177	0.0608	0.0014	598	11	594	5	618	51	96
A_189.FI N2	EDK 059	420	741	0.53	312	1.3380	0.0230	0.0970	0.0010	0.0245	0.1012	0.0020	861	10	597	6	1636	37	36
A_178.FI N2	EDK 048	119	54	0.18	222	0.8350	0.0500	0.0971	0.0016	0.1857	0.0620	0.0036	613	27	597	10	670	130	89
A_215.FI N2	EDK 083	408	142	0.14	210	0.8070	0.0210	0.0971	0.0013	0.0691	0.0599	0.0023	600	12	597	8	618	58	97
A_136.FI N2	EDK 012	328	748	0.88	560	0.8120	0.0350	0.0973	0.0014	0.3037	0.0612	0.0026	603	19	598	9	629	88	95
A_176.FI N2	EDK 046	670	4720	1.75	90	2.9700	0.1200	0.0974	0.0008	0.0395	0.2224	0.0092	1391	32	599	5	2968	72	20
A_161.FI N2	EDK 035	101	257	0.99	180	0.8160	0.0280	0.0975	0.0011	0.0826	0.0616	0.0023	603	16	600	7	623	79	96
A_134.FI N2	EDK 010	50	96	0.74	182	1.0960	0.0550	0.0977	0.0015	0.0932	0.0824	0.0044	745	27	601	9	1180	110	51

A_219.FIN2	EDK087	72	196	1.09	66	0.8150	0.0520	0.0983	0.0017	0.1296	0.0606	0.0038	600	29	604	10	560	130	108
A_193.FIN2	EDK063	150	451	1.21	440	0.8260	0.0340	0.0983	0.0014	0.2968	0.0616	0.0025	609	19	605	8	652	94	93
A_169.FIN2	EDK041	368	920	0.96	850	0.8160	0.0120	0.0986	0.0005	0.1001	0.0603	0.0009	605	7	606	3	608	34	100
A_143.FIN2	EDK017	146	360	0.94	380	0.8210	0.0190	0.0987	0.0007	0.1194	0.0605	0.0013	607	10	607	4	607	51	100
A_170.FIN2	EDK042	268	1045	1.51	380	0.9250	0.0240	0.0988	0.0009	0.0938	0.0685	0.0020	663	13	607	5	864	59	70
A_131.FIN2	EDK007	160	72	0.17	450	0.8160	0.0230	0.0990	0.0009	0.0380	0.0603	0.0018	604	13	608	5	585	65	104
A_177.FIN2	EDK047	130	231	0.72	290	0.8190	0.0250	0.0991	0.0011	0.0913	0.0604	0.0019	605	14	609	6	602	71	101
A_201.FIN2	EDK071	364	492	0.55	460	0.8280	0.0170	0.0991	0.0010	0.1029	0.0610	0.0014	612	10	609	6	640	55	95
A_187.FIN2	EDK057	218	795	1.47	1030	0.8350	0.0260	0.0995	0.0010	0.1427	0.0614	0.0019	615	15	611	6	628	70	97
A_194.FIN2	EDK064	463	1119	0.97	660	0.8380	0.0240	0.0997	0.0009	0.1867	0.0614	0.0017	617	13	613	5	636	61	96
A_175.FIN2	EDK045	156	603	1.54	260	0.8250	0.0330	0.0997	0.0014	0.1201	0.0605	0.0025	609	19	613	8	595	89	103
A_254.FIN2	EDK118	160	364	0.93	221	0.8230	0.0240	0.0998	0.0010	0.0658	0.0601	0.0018	608	14	613	6	580	67	106
A_218.FIN2	EDK086	522	779	0.61	180	0.8610	0.0180	0.0999	0.0009	0.1037	0.0627	0.0013	630	10	614	5	699	47	88
A_223.FIN2	EDK090	270	259	0.39	170	0.8410	0.0130	0.0999	0.0007	0.3732	0.0614	0.0010	619	7	614	4	640	34	96
A_230.FIN2	EDK096	129	432	1.40	272	0.8630	0.0360	0.1001	0.0013	0.0344	0.0630	0.0028	629	20	615	7	669	94	92
A_210.FIN2	EDK078	142	374	1.12	230	0.8430	0.0340	0.1002	0.0010	0.0986	0.0614	0.0025	617	18	615	6	609	84	101
A_247.FIN2	EDK111	104	206	0.77	202	0.8510	0.0280	0.1006	0.0010	0.0189	0.0617	0.0022	622	15	618	6	616	75	100
A_147.FIN2	EDK021	290	462	0.61	770	0.8450	0.0200	0.1006	0.0009	0.1409	0.0614	0.0014	621	11	618	5	651	48	95
A_167.FIN2	EDK040	388	1188	1.22	1480	0.8580	0.0200	0.1007	0.0010	0.2856	0.0622	0.0014	628	11	619	6	669	49	92
A_245.FIN2	EDK109	125	241	0.79	110	0.8450	0.0290	0.1008	0.0011	0.0083	0.0611	0.0022	619	16	619	6	608	78	102
A_198.FIN2	EDK068	267	697	1.07	450	0.8430	0.0220	0.1008	0.0011	0.0366	0.0612	0.0018	620	12	619	7	629	61	98
A_160.FIN2	EDK034	118	317	0.99	460	0.8520	0.0360	0.1008	0.0010	0.0991	0.0618	0.0028	622	19	619	6	618	94	100
A_250.FIN2	EDK114	78	190	0.95	118	0.8530	0.0300	0.1008	0.0009	0.0636	0.0614	0.0022	622	16	619	6	601	75	103
A_246.FIN2	EDK110	212	423	0.80	210	0.8430	0.0210	0.1009	0.0008	0.0034	0.0608	0.0016	619	12	620	5	620	59	100

A_249.FI	EDK						0.030		0.000	0.109		0.002							
N2	113	88	275	1.27	96	0.8680	0	0.1009	9	9	0.0625	2	631	16	620	5	648	74	96
A_162.FI	EDK						0.018		0.000	0.121		0.001							
N2	036	191	351	0.66	1020	0.8460	0	0.1010	7	1	0.0611	3	622	10	620	4	628	46	99
A_252.FI	EDK						0.030		0.001	0.124		0.002							
N2	116	219	613	1.16	430	0.8540	0	0.1013	2	4	0.0615	3	625	16	622	7	632	80	98
A_159.FI	EDK						0.019		0.000	0.265		0.001							
N2	033	201	325	0.63	690	0.8530	0	0.1016	9	1	0.0613	3	625	10	624	5	637	48	98
A_190.FI	EDK						0.034		0.001	0.097		0.002							
N2	060	85	202	0.91	105	0.8510	0	0.1016	2	0	0.0613	6	622	19	624	7	618	94	101
A_191.FI	EDK						0.016		0.000	0.197		0.001							
N2	061	271	510	0.72	430	0.8580	0	0.1017	7	5	0.0616	2	628	9	624	4	650	40	96
A_248.FI	EDK						0.019		0.000	0.091		0.001							
N2	112	278	624	0.90	380	0.8570	0	0.1017	9	6	0.0613	4	627	10	624	5	634	49	98
A_255.FI	EDK						0.037		0.001	0.054		0.002							
N2	119	33	129	1.57	51	0.8610	0	0.1018	5	7	0.0622	8	625	21	625	9	603	95	104
A_200.FI	EDK						0.046		0.001	0.229		0.003						11	
N2	070	84	184	0.86	-30	0.8590	0	0.1019	5	9	0.0616	3	624	26	626	9	600	0	104
A_137.FI	EDK						0.017		0.000	0.202		0.001							
N2	013	308	614	0.68	590	0.8470	0	0.1019	9	3	0.0604	3	622	10	626	5	606	46	103
A_126.FI	EDK						0.019		0.000	0.064		0.001							
N2	002	224	723	1.16	425	0.8430	0	0.1019	9	3	0.0607	5	621	11	626	5	617	50	101
A_130.FI	EDK						0.038		0.001	0.230		0.002							
N2	006	47	102	0.71	176	0.8680	0	0.1021	7	0	0.0618	7	630	21	626	10	619	94	101
A_214.FI	EDK						0.032		0.001	0.186		0.002							
N2	082	166	347	0.84	259	0.8500	0	0.1020	1	8	0.0608	3	622	18	626	6	606	81	103
A_242.FI	EDK						0.045		0.000	0.316		0.003							
N2	106	184	380	0.86	321	1.2420	0	0.1022	9	2	0.0885	1	817	20	627	5	1374	66	46
A_152.FI	EDK						0.024		0.000	0.250		0.001							
N2	026	105	308	1.03	350	0.8560	0	0.1024	9	1	0.0610	7	625	13	628	5	605	58	104
A_153.FI	EDK						0.032		0.001	0.235		0.002							
N2	027	151	379	0.95	320	0.8700	0	0.1026	0	3	0.0620	2	634	17	629	6	650	78	97
A_154.FI	EDK						0.016		0.000	0.114		0.001							
N2	028	275	689	0.87	850	0.8640	0	0.1034	7	6	0.0606	1	631	9	634	4	619	40	102
A_192.FI	EDK						0.022		0.000	0.166		0.001							
N2	062	137	419	1.11	220	0.8650	0	0.1037	8	9	0.0607	5	631	12	636	5	599	56	106
A_155.FI	EDK						0.037		0.001	0.040		0.002							
N2	029	142	343	0.96	350	0.8710	0	0.1041	4	3	0.0613	7	633	20	638	8	615	95	104
A_149.FI	EDK						0.041		0.001	0.333		0.002							
N2	023	88	258	0.96	10	0.8920	0	0.1042	6	0	0.0623	7	644	22	639	9	644	95	99
A_237.FI	EDK						0.048		0.001	0.097		0.003						12	
N2	103	25	68	1.04	21	0.8910	0	0.1044	8	9	0.0622	6	635	26	640	10	570	0	112
A_151.FI	EDK						0.048		0.001	0.273		0.003							
N2	025	48	160	1.26	103	1.0770	0	0.1044	9	6	0.0756	3	735	24	640	11	1016	92	63
A_150.FI	EDK						0.021		0.000	0.071		0.001							
N2	024	155	260	0.59	420	0.8800	0	0.1047	9	1	0.0614	5	639	11	642	5	627	54	102
A_129.FI	EDK						0.046		0.001	0.279		0.003							
N2	005	111	131	0.39	470	0.9120	0	0.1090	3	4	0.0610	0	662	21	667	8	634	91	105

A_132.FI	EDK						0.020		0.000	0.150		0.001							
N2	008	149	665	1.49	600	0.9320	0	0.1091	9	2	0.0624	3	667	10	667	5	672	48	99
A_221.FI	EDK						0.027		0.001	0.151		0.001							
N2	088	208	386	0.71	190	0.9920	0	0.1128	0	0	0.0642	7	698	14	689	6	740	56	93
A_148.FI	EDK						0.120		0.002	0.716		0.006						11	
N2	022	109	326	0.44	207	1.9100	0	0.1248	0	9	0.1111	2	1069	45	758	11	1760	0	43
A_209.FI	EDK						0.030		0.001	0.092		0.001							
N2	077	119	354	0.90	270	1.1240	0	0.1253	1	1	0.0653	8	762	14	761	6	754	59	101
A_184.FI	EDK						0.048		0.001	0.007		0.002							
N2	054	91	234	0.41	254	1.5190	0	0.1394	8	7	0.0798	7	935	19	841	10	1178	66	71
A_208.FI	EDK						0.110		0.003	0.164		0.004						15	
N2	076	38	211	1.59	-90	1.5300	0	0.1556	2	9	0.0721	9	935	43	932	18	930	0	100
A_222.FI	EDK						0.036		0.001	0.012		0.001							
N2	089	75	282	0.97	200	1.5550	0	0.1579	4	9	0.0718	8	950	15	945	8	974	48	97
A_144.FI	EDK						0.069		0.002	0.132		0.003							
N2	018	48	191	1.02	40	1.5670	0	0.1585	8	5	0.0725	2	952	27	948	16	959	95	99
A_174.FI	EDK						0.089		0.003	0.161		0.004						12	
N2	044	55	163	0.80	190	1.6320	0	0.1596	3	9	0.0749	0	977	35	954	19	1020	0	94
A_205.FI	EDK						0.059		0.001	0.189		0.002							
N2	075	80	357	1.16	160	1.5810	0	0.1596	8	8	0.0722	6	957	23	955	10	964	74	99
A_231.FI	EDK						0.034		0.001	0.115		0.001							
N2	097	146	745	1.31	350	1.5750	0	0.1609	3	5	0.0713	6	958	13	962	7	949	45	101
A_183.FI	EDK						0.038		0.001	0.009		0.001							
N2	053	104	313	0.73	160	1.7070	0	0.1688	6	6	0.0739	8	1009	14	1006	9	1023	49	98
A_239.FI	EDK						0.043		0.002	0.185		0.002							
N2	105	107	245	0.59	1370	1.6930	0	0.1697	8	7	0.0729	1	1004	16	1010	15	999	58	101
A_226.FI	EDK						0.130		0.003	0.097		0.005						14	
N2	092	8	38	1.11	0	1.9800	0	0.1719	6	9	0.0846	6	1078	45	1021	20	1130	0	90
A_145.FI	EDK						0.076		0.003	0.828		0.001							
N2	019	336	739	0.38	1900	2.7120	0	0.1764	4	8	0.1122	8	1328	21	1047	19	1831	30	57
A_196.FI	EDK						0.046		0.002	0.307		0.001							
N2	066	289	1044	0.90	630	3.8200	0	0.2127	0	6	0.1312	7	1596	10	1243	10	2111	23	59
A_238.FI	EDK						0.120		0.002	0.138		0.003							
N2	104	37	276	1.15	155	3.5200	0	0.2570	9	3	0.0995	3	1529	27	1474	15	1597	66	92
A_233.FI	EDK						0.091		0.003	0.166		0.002							
N2	099	79	612	1.18	320	3.6230	0	0.2705	2	2	0.0973	5	1552	20	1543	16	1562	50	99
A_236.FI	EDK						0.060		0.002	0.206		0.001							
N2	102	97	1167	1.78	370	3.6910	0	0.2717	0	5	0.0988	6	1569	12	1549	10	1598	30	97
A_253.FI	EDK						0.110		0.004	0.105		0.003							
N2	117	106	786	1.06	450	3.7400	0	0.2726	0	1	0.0993	2	1577	24	1554	20	1601	62	97
A_185.FI	EDK						0.065		0.002	0.076		0.001							
N2	055	57	462	1.18	20	3.6850	0	0.2737	1	7	0.0981	8	1564	14	1559	10	1572	35	99
A_166.FI	EDK						0.059		0.002	0.021		0.001							
N2	039	145	1577	1.48	400	3.7160	0	0.2738	1	8	0.0987	8	1574	13	1560	11	1595	33	98
A_232.FI	EDK						0.071		0.002	0.012		0.002							
N2	098	78	800	1.57	220	3.7650	0	0.2772	1	0	0.0992	1	1585	16	1578	10	1597	39	99
A_182.FI	EDK						0.072		0.003	0.723		0.001							
N2	052	194	1186	0.75	2400	5.8270	0	0.3352	1	6	0.1270	4	1949	11	1863	15	2054	19	91

A_203.FIN2	EDK073	193	532	0.34	310	5.9510	0.0610	0.3445	0.0022	0.1523	0.1258	0.0014	1968	9	1908	11	2037	19	94
A_202.FIN2	EDK072	95	320	0.39	240	6.7100	0.1600	0.3755	0.0044	0.1885	0.1304	0.0031	2071	21	2055	21	2107	39	98
A_195.FIN2	EDK065	335	1507	0.45	3800	9.8250	0.0890	0.4396	0.0029	0.5467	0.1632	0.0013	2418	8	2349	13	2487	13	94
A_140.FIN2	EDK014	360	2868	0.66	4400	11.5160	0.0670	0.4790	0.0023	0.5203	0.1753	0.0009	2566	6	2523	10	2607	9	97

Appendix 6.12: Results of the analysis of zircons from Logbaba kaolin

Analysis	Sample	U [ppm][a]	Pb [ppm][a]	Th/U[a]	*206/204*	RATIOS $^{207}Pb/^{235}U$[b]	2 σ[d]	$^{206}Pb/^{238}U$[b]	2 σ[d]	rho[c]	$^{207}Pb/^{206}Pb$[e]	2 σ[d]	AGES [Ma] $^{207}Pb/^{235}U$	2 σ	$^{206}Pb/^{238}U$	2 σ	$^{207}Pb/^{206}Pb$	2 σ	Conc. %
A_385.FIN2	LOG001	59	198	1.30	76	0.8460	0.0310	0.1008	0.0012	0.0068	0.0611	0.0024	620	17	619	7	591	80	105
A_386.FIN2	LOG002	44	1244	3.06	227	7.1300	0.1000	0.3997	0.0029	0.2493	0.1290	0.0019	2125	13	2167	13	2080	25	104
A_387.FIN2	LOG003	91	264	1.09	110	0.8680	0.0320	0.1034	0.0012	0.0759	0.0609	0.0022	631	17	634	7	599	79	106
A_388.FIN2	LOG004	286	342	0.46	370	0.8360	0.0170	0.0996	0.0006	0.0616	0.0610	0.0012	616	9	612	4	620	46	99
A_389.FIN2	LOG005	81	140	0.67	132	0.8330	0.0270	0.1002	0.0008	0.0211	0.0604	0.0020	611	15	616	5	570	73	108
A_391.FIN2	LOG006	193	752	0.50	1640	5.7820	0.0520	0.3355	0.0018	0.0217	0.1253	0.0013	1944	8	1865	9	2030	19	92
A_392.FIN2	LOG007	91	232	0.31	460	5.9770	0.0780	0.3470	0.0026	0.1969	0.1251	0.0017	1972	11	1920	12	2025	23	95
A_393.FIN2	LOG008	240	1292	0.64	1260	6.2650	0.0570	0.3604	0.0019	0.4556	0.1264	0.0011	2014	8	1984	9	2048	15	97
A_394.FIN2	LOG009	253	1481	0.67	1750	6.3080	0.0680	0.3629	0.0028	0.3925	0.1264	0.0014	2019	9	1996	13	2046	19	98
A_395.FIN2	LOG010	253	413	0.63	610	0.8510	0.0250	0.1019	0.0008	0.0612	0.0606	0.0017	624	14	625	5	608	62	103
A_396.FIN2	LOG011	91	1899	2.42	500	6.5500	0.1100	0.3736	0.0031	0.1215	0.1276	0.0023	2050	15	2046	14	2058	32	99
A_397.FIN2	LOG012	45	402	1.00	210	6.5200	0.0960	0.3747	0.0027	0.2037	0.1262	0.0019	2045	13	2051	13	2039	27	101
A_398.FIN2	LOG013	59	512	1.01	330	6.4700	0.1100	0.3710	0.0028	0.1789	0.1269	0.0022	2039	15	2034	13	2051	30	99
A_399.FIN2	LOG014	115	1559	1.61	660	6.4480	0.0870	0.3667	0.0025	0.1435	0.1282	0.0018	2037	12	2014	12	2069	25	97
A_400.FIN2	LOG015	831	4800	0.58	8000	10.7100	0.0790	0.4480	0.0026	0.5216	0.1741	0.0011	2498	7	2386	12	2598	11	92
A_401.FIN2	LOG016	318	3477	1.33	2010	6.5480	0.0570	0.3733	0.0023	0.3599	0.1279	0.0011	2052	8	2045	11	2068	15	99
A_402.FIN2	LOG017	71	712	1.04	160	6.8010	0.0970	0.3808	0.0029	0.0383	0.1298	0.0022	2084	13	2080	14	2096	29	99
A_403.FIN2	LOG018	111	801	0.81	880	6.5670	0.0750	0.3756	0.0025	0.2689	0.1273	0.0015	2053	10	2055	12	2059	21	100
A_404.FIN2	LOG019	12	0	0.02	17	0.8270	0.0700	0.0952	0.0022	0.0289	0.0637	0.0056	586	39	586	13	560	170	105
A_405.FIN2	LOG020	167	1246	0.64	1510	17.3100	0.1400	0.5541	0.0034	0.3944	0.2279	0.0019	2952	8	2842	14	3036	13	94

A_406.FIN2	LOG 021	122	1335	0.88	1170	17.9400	0.1200	0.5704	0.0036	0.3624	0.2294	0.0017	2986	6	2909	15	3046	12	96
A_407.FIN2	LOG 022	107	74	0.28	152	0.8160	0.0230	0.0995	0.0011	0.1661	0.0605	0.0019	608	14	612	6	589	67	104
A_408.FIN2	LOG 023	14	35	0.88	23	0.9000	0.1200	0.1015	0.0033	0.0218	0.0657	0.0089	625	66	623	19	580	280	107
A_409.FIN2	LOG 024	239	1890	0.92	1970	6.6780	0.0710	0.3763	0.0022	0.4141	0.1294	0.0013	2069	9	2059	10	2087	17	99
A_412.FIN2	LOG 025	131	1374	1.19	990	6.5300	0.0720	0.3714	0.0033	0.3177	0.1275	0.0015	2049	10	2036	15	2065	22	99
A_413.FIN2	LOG 026	95	631	0.85	-9600	6.1180	0.0880	0.3530	0.0027	0.3768	0.1264	0.0017	1991	12	1948	13	2044	24	95
A_414.FIN2	LOG 027	132	518	1.55	-1700	0.8430	0.0260	0.1003	0.0010	0.0216	0.0614	0.0020	618	14	616	6	628	68	98
A_415.FIN2	LOG 028	98	906	1.12	-26000	6.1930	0.0970	0.3623	0.0029	0.1606	0.1246	0.0021	2002	14	1998	14	2017	29	99
A_416.FIN2	LOG 029	121	1183	1.13	-46000	6.0370	0.0610	0.3587	0.0017	0.2928	0.1223	0.0012	1980	9	1976	8	1986	18	99
A_417.FIN2	LOG 030	99	420	1.71	173	0.8440	0.0330	0.0999	0.0012	0.0785	0.0617	0.0025	618	18	614	7	635	92	97
A_418.FIN2	LOG 031	121	714	2.47	166	0.8630	0.0430	0.1018	0.0013	0.2234	0.0621	0.0034	629	24	625	8	640	120	98
A_419.FIN2	LOG 032	61	1242	2.62	500	5.7900	0.1300	0.3508	0.0038	0.1566	0.1206	0.0028	1942	20	1938	18	1963	41	99
A_420.FIN2	LOG 033	65	367	0.87	2500	3.7770	0.0640	0.2818	0.0020	0.0578	0.0978	0.0018	1586	13	1600	10	1571	33	102
A_421.FIN2	LOG 034	142	1624	1.26	790	6.6070	0.0610	0.3761	0.0022	0.2049	0.1281	0.0013	2060	8	2058	10	2068	18	100
A_422.FIN2	LOG 035	130	1229	1.10	820	6.5520	0.0700	0.3722	0.0021	0.1724	0.1282	0.0015	2052	10	2040	10	2069	20	99
A_423.FIN2	LOG 036	182	1321	0.92	780	6.1680	0.0680	0.3553	0.0025	0.1925	0.1267	0.0015	1999	10	1960	12	2050	21	96
A_424.FIN2	LOG 037	74	1141	1.41	570	12.1400	0.1500	0.4895	0.0042	0.4745	0.1809	0.0021	2614	12	2568	18	2658	19	97
A_425.FIN2	LOG 038	81	625	0.86	440	7.3100	0.2500	0.3560	0.0100	0.9141	0.1491	0.0022	2139	33	1959	49	2335	26	84
A_426.FIN2	LOG 039	148	397	1.08	220	0.8250	0.0230	0.0996	0.0009	0.0875	0.0604	0.0017	610	13	612	5	596	63	103
A_427.FIN2	LOG 040	63	729	1.03	250	12.8500	0.2200	0.5111	0.0042	0.3987	0.1832	0.0028	2666	16	2661	18	2678	25	99
A_428.FIN2	LOG 041	86	395	0.91	220	2.1930	0.0650	0.1814	0.0023	0.1469	0.0883	0.0027	1175	21	1074	12	1378	57	78
A_429.FIN2	LOG 042	72	242	1.30	133	0.8160	0.0300	0.0987	0.0011	0.1496	0.0599	0.0021	603	17	607	6	570	79	106
A_430.FIN2	LOG 043	93	157	0.66	166	0.8550	0.0330	0.1017	0.0012	0.0034	0.0613	0.0025	624	18	625	7	602	86	104
A_431.FIN2	LOG 044	118	724	0.92	520	4.4640	0.0610	0.2832	0.0023	0.3076	0.1146	0.0016	1723	11	1607	11	1872	25	86

A_432.FIN2	LOG045	120	898	0.84	250	6.5080	0.0670	0.3734	0.0020	0.2114	0.1269	0.0013	2045	9	2045	10	2053	17	100
A_433.FIN2	LOG046	100	784	0.88	410	6.5200	0.0790	0.3721	0.0022	0.3598	0.1274	0.0015	2047	11	2039	10	2058	21	99
A_434.FIN2	LOG047	56	339	0.69	0	6.5000	0.1200	0.3699	0.0030	0.0800	0.1279	0.0026	2043	16	2028	14	2059	36	98
A_435.FIN2	LOG048	42	829	2.40	170	6.5900	0.2200	0.3704	0.0054	0.0106	0.1301	0.0047	2054	28	2031	26	2085	62	97
A_436.FIN2	LOG049	15	6	0.16	27	0.6940	0.0740	0.0851	0.0027	0.0841	0.0617	0.0070	525	48	526	16	480	220	110
A_437.FIN2	LOG050	159	44	0.11	4900	0.7300	0.0450	0.0901	0.0017	0.1801	0.0588	0.0040	555	27	556	10	530	150	105
A_438.FIN2	LOG051	99	3	0.60	0	0.0140	0.0100	0.0009	0.0002	0.4384	0.2600	0.2000	14	10	6	1	400	160	1
A_439.FIN2	LOG052	139	2045	1.64	330	6.6040	0.0740	0.3754	0.0021	0.1419	0.1278	0.0015	2059	10	2054	10	2065	21	99
A_440.FIN2	LOG053	117	1460	1.44	580	6.6580	0.0840	0.3720	0.0026	0.2699	0.1301	0.0016	2066	11	2038	12	2096	22	97
A_441.FIN2	LOG054	421	1696	0.51	45000	5.6910	0.0470	0.3388	0.0020	0.4426	0.1224	0.0010	1930	7	1881	10	1991	14	94
A_442.FIN2	LOG055	827	1028	0.18	3300	5.0430	0.0380	0.3075	0.0018	0.6095	0.1193	0.0007	1826	6	1728	9	1945	11	89
A_446.FIN2	LOG056	183	4	0.80	28	0.0065	0.0025	0.0008	0.0001	0.0539	0.0790	0.0320	7	3	5	1	-270	620	-2
A_447.FIN2	LOG057	264	1761	0.80	1900	6.1500	0.0510	0.3519	0.0019	0.4953	0.1271	0.0009	1997	7	1943	9	2058	13	94
A_448.FIN2	LOG058	432	2732	0.75	2800	6.3380	0.0530	0.3608	0.0020	0.4934	0.1279	0.0009	2023	7	1986	9	2069	13	96
A_449.FIN2	LOG059	309	1752	0.69	1560	6.0430	0.0660	0.3499	0.0021	0.5320	0.1259	0.0012	1981	10	1936	11	2039	16	95
A_450.FIN2	LOG060	81	687	0.83	670	10.7200	0.2000	0.4718	0.0046	0.2453	0.1655	0.0028	2497	17	2491	20	2515	31	99
A_451.FIN2	LOG061	48	186	0.45	300	6.5300	0.1000	0.3644	0.0031	0.0882	0.1308	0.0023	2050	14	2002	14	2104	31	95
A_452.FIN2	LOG062	52	1175	1.97	450	13.1500	0.1300	0.5082	0.0035	0.2982	0.1886	0.0021	2691	10	2648	15	2726	18	97
A_453.FIN2	LOG063	104	1316	1.50	690	6.3150	0.0700	0.3587	0.0023	0.3260	0.1283	0.0014	2020	10	1976	11	2070	19	95
A_454.FIN2	LOG064	164	3084	2.25	510	6.2830	0.0730	0.3588	0.0025	0.3321	0.1274	0.0014	2015	10	1976	12	2061	20	96
A_455.FIN2	LOG065	98	300	0.38	590	5.9360	0.0890	0.3515	0.0025	0.1696	0.1235	0.0019	1965	13	1942	12	2003	28	97
A_456.FIN2	LOG066	49	162	1.24	57	0.8720	0.0320	0.1017	0.0011	0.0897	0.0624	0.0023	631	18	624	6	626	80	100
A_457.FIN2	LOG067	222	3515	1.84	100	6.4310	0.0610	0.3633	0.0020	0.3333	0.1290	0.0012	2036	8	1998	10	2082	16	96
A_458.FIN2	LOG068	333	708	0.87	530	0.8170	0.0180	0.0987	0.0009	0.2132	0.0606	0.0014	607	10	607	5	618	46	98

A_459.FIN2	LOG069	137	987	1.12	600	3.6340	0.0450	0.2634	0.0016	0.1538	0.1004	0.0013	1555	10	1507	8	1624	24	93
A_460.FIN2	LOG070	98	1438	1.11	930	19.4100	0.1500	0.5955	0.0036	0.3533	0.2373	0.0020	3062	8	3011	14	3100	13	97
A_461.FIN2	LOG071	178	83	0.18	230	0.7800	0.0240	0.0951	0.0010	0.0672	0.0599	0.0020	583	14	585	6	569	72	103
A_462.FIN2	LOG072	35	522	1.65	230	7.7400	0.1500	0.3953	0.0042	0.2159	0.1430	0.0029	2198	18	2147	19	2253	36	95
A_463.FIN2	LOG073	54	485	1.07	370	6.6000	0.1200	0.3748	0.0031	0.1366	0.1286	0.0025	2057	17	2052	14	2068	35	99
A_464.FIN2	LOG074	157	930	0.71	850	5.9240	0.0940	0.3562	0.0036	0.4925	0.1212	0.0017	1963	14	1964	17	1969	25	100
A_465.FIN2	LOG075	30	158	1.34	92	1.5220	0.0520	0.1560	0.0019	0.0464	0.0713	0.0025	935	21	934	10	907	75	103
A_466.FIN2	LOG076	148	1193	0.91	2100	7.6600	0.1000	0.3886	0.0029	0.3844	0.1438	0.0018	2190	12	2116	14	2271	22	93
A_467.FIN2	LOG077	89	775	1.01	1300	6.3430	0.0830	0.3632	0.0025	0.1974	0.1272	0.0017	2023	11	1997	12	2054	23	97
A_468.FIN2	LOG078	31	212	1.05	130	3.7200	0.0990	0.2735	0.0031	0.1697	0.0992	0.0027	1569	21	1560	15	1582	51	99
A_469.FIN2	LOG079	175	2545	1.62	2800	6.5760	0.0840	0.3731	0.0025	0.2878	0.1282	0.0017	2056	12	2044	12	2069	23	99
A_470.FIN2	LOG080	111	1248	1.40	1900	5.6310	0.0680	0.3396	0.0019	0.2674	0.1205	0.0014	1919	10	1884	9	1960	20	96
A_471.FIN2	LOG081	206	4528	2.68	2600	6.3370	0.0680	0.3603	0.0027	0.0611	0.1278	0.0015	2023	9	1983	13	2070	22	96
A_472.FIN2	LOG082	365	9880	3.48	500	6.1330	0.0530	0.3509	0.0021	0.3936	0.1274	0.0011	1994	8	1939	10	2061	15	94
A_473.FIN2	LOG083	124	164	0.53	610	0.7650	0.0200	0.0942	0.0009	0.0999	0.0590	0.0016	575	11	580	5	540	62	107
A_474.FIN2	LOG084	139	768	0.64	1360	6.7800	0.0790	0.3682	0.0026	0.3084	0.1342	0.0016	2082	10	2020	12	2149	22	94
A_475.FIN2	LOG085	66	175	0.33	80	5.5570	0.0860	0.3377	0.0030	0.3561	0.1196	0.0017	1907	13	1875	15	1948	26	96
A_476.FIN2	LOG086	137	757	0.50	330	10.0400	0.1100	0.4558	0.0024	0.3946	0.1593	0.0016	2438	10	2421	11	2446	17	99
A_477.FIN2	LOG087	217	1237	0.72	140	6.1290	0.0810	0.3287	0.0030	0.6292	0.1353	0.0014	1992	12	1832	15	2165	19	85
A_480.FIN2	LOG088	51	538	1.19	340	6.4370	0.0950	0.3706	0.0029	0.0874	0.1263	0.0021	2035	13	2032	14	2041	30	100
A_481.FIN2	LOG089	34	94	1.05	114	0.8450	0.0470	0.1003	0.0015	0.0582	0.0610	0.0034	612	26	616	9	560	120	110
A_482.FIN2	LOG090	171	50	0.10	340	0.8250	0.0200	0.0996	0.0010	0.0227	0.0605	0.0016	609	11	612	6	598	58	102
A_483.FIN2	LOG091	125	2102	1.95	500	6.6100	0.1200	0.3700	0.0025	0.1609	0.1300	0.0023	2058	15	2029	12	2092	31	97
A_484.FIN2	LOG092	32	2016	6.94	70	6.4800	0.1300	0.3708	0.0033	0.1288	0.1268	0.0026	2038	17	2033	15	2038	37	100

A_485.FIN2	LOG 093	239	3687	1.74	470	6.3330	0.0510	0.3673	0.0019	0.3225	0.1251	0.0010	2022	7	2016	9	2029	14	99
A_486.FIN2	LOG 094	44	116	0.28	320	7.5800	0.2200	0.4049	0.0059	0.0021	0.1371	0.0045	2179	26	2191	27	2176	57	101
A_487.FIN2	LOG 095	75	1064	1.63	340	6.3000	0.1000	0.3619	0.0036	0.1924	0.1268	0.0022	2019	14	1990	17	2047	31	97
A_488.FIN2	LOG 096	118	1965	1.87	590	6.4170	0.0870	0.3692	0.0027	0.2864	0.1264	0.0017	2033	12	2025	13	2044	24	99
A_489.FIN2	LOG 097	79	1111	1.53	480	6.5040	0.0880	0.3735	0.0029	0.2333	0.1270	0.0018	2046	12	2045	14	2052	26	100
A_490.FIN2	LOG 098	146	4490	3.40	1000	6.5930	0.0800	0.3726	0.0027	0.1451	0.1282	0.0017	2057	11	2043	13	2070	24	99
A_491.FIN2	LOG 099	358	85	0.09	610	0.8350	0.0170	0.1007	0.0008	0.0640	0.0607	0.0013	616	10	618	5	621	46	100
A_492.FIN2	LOG 100	235	434	0.68	6300	0.8580	0.0240	0.1018	0.0011	0.1873	0.0612	0.0019	628	13	625	6	626	68	100
A_493.FIN2	LOG 101	154	811	0.58	970	6.5120	0.0880	0.3726	0.0031	0.1711	0.1271	0.0018	2046	12	2041	14	2054	26	99
A_494.FIN2	LOG 102	46	86	0.71	61	0.8090	0.0370	0.0962	0.0013	0.0216	0.0609	0.0028	594	21	592	8	563	98	105
A_495.FIN2	LOG 103	191	102	0.23	80	0.7630	0.0250	0.0941	0.0008	0.0235	0.0592	0.0020	574	14	580	5	558	75	104
A_496.FIN2	LOG 104	44	333	1.22	115	3.6940	0.0730	0.2452	0.0023	0.1856	0.1096	0.0021	1568	15	1413	12	1781	36	79
A_497.FIN2	LOG 105	102	1234	1.94	260	3.9840	0.0670	0.2488	0.0023	0.5260	0.1161	0.0017	1627	14	1432	12	1888	27	76
A_499.FIN2	LOG 106	79	984	1.56	170	5.6800	0.0820	0.3284	0.0024	0.2223	0.1255	0.0018	1926	12	1830	12	2035	26	90
A_500.FIN2	LOG 107	37	838	2.48	4000	6.5600	0.1400	0.3694	0.0035	0.0508	0.1290	0.0029	2053	19	2028	17	2077	41	98
A_501.FIN2	LOG 108	31	505	1.94	-2200	6.2200	0.2100	0.3653	0.0043	0.1817	0.1244	0.0041	2000	29	2007	20	1997	60	101
A_502.FIN2	LOG 109	102	1147	1.26	530	6.6230	0.0740	0.3748	0.0023	0.2409	0.1288	0.0015	2061	10	2052	11	2077	20	99
A_503.FIN2	LOG 110	136	316	0.88	220	0.8140	0.0280	0.0986	0.0011	0.1294	0.0603	0.0022	605	16	606	6	593	82	102
A_504.FIN2	LOG 111	158	367	0.91	230	0.8130	0.0210	0.0985	0.0009	0.1450	0.0606	0.0016	602	12	605	5	602	58	101
A_505.FIN2	LOG 112	723	778	0.11	5700	9.4130	0.0570	0.4404	0.0019	0.4913	0.1558	0.0008	2379	6	2352	9	2410	9	98
A_506.FIN2	LOG 113	34	748	2.51	140	6.2900	0.1200	0.3635	0.0032	0.1459	0.1262	0.0026	2012	17	1998	15	2031	36	98
A_507.FIN2	LOG 114	100	169	0.63	156	0.8440	0.0240	0.1000	0.0009	0.0753	0.0618	0.0019	618	14	614	5	621	66	99
A_508.FIN2	LOG 115	123	1725	1.72	750	5.7170	0.0680	0.3318	0.0021	0.0992	0.1258	0.0017	1933	10	1847	10	2035	23	91

Appendix 6.13: Results of the analysis of zircons from Missole kaolin

Analysis	Sample	U [ppm][a]	Pb [ppm][a]	Th/U[a]	*206/204*	RATIOS $^{207}Pb/^{235}U$[b]	2 σ[d]	$^{206}Pb/^{238}U$[b]	2 σ[d]	rho[c]	$^{207}Pb/^{206}Pb$[e]	2 σ[d]	AGES [Ma] $^{207}Pb/^{235}U$	2 σ	$^{206}Pb/^{238}U$	2 σ	$^{207}Pb/^{206}Pb$	2 σ	Conc. %
A_166.FIN2	MSL017	174	274	0.60	350	0.8420	0.0250	0.1029	0.0011	0.1197	0.0595	0.0018	618	14	632	6	558	68	113
A_161.FIN2	MSL012	77	77	0.38	157	0.8370	0.0310	0.1006	0.0012	0.1964	0.0605	0.0022	614	17	618	7	577	80	107
A_219.FIN2	MSL060	44	125	1.10	63	0.8530	0.0350	0.1014	0.0011	0.1249	0.0612	0.0025	624	20	622	7	595	86	105
A_200.FIN2	MSL047	173	114	0.26	-2200	0.8570	0.0180	0.1026	0.0008	0.1548	0.0607	0.0013	627	10	629	5	606	46	104
A_216.FIN2	MSL058	198	6	0.01	510	0.9590	0.0170	0.1117	0.0007	0.0897	0.0622	0.0012	681	9	683	4	666	41	103
A_188.FIN2	MSL035	54	7	0.01	-120	0.9560	0.0440	0.1102	0.0014	0.2155	0.0632	0.0027	676	22	674	8	658	90	102
A_179.FIN2	MSL026	247	609	0.99	400	0.8200	0.0210	0.0989	0.0008	0.2356	0.0602	0.0015	607	12	608	5	595	54	102
A_180.FIN2	MSL027	176	288	0.66	310	0.8240	0.0270	0.0991	0.0010	0.0669	0.0606	0.0020	609	15	609	6	597	73	102
A_178.FIN2	MSL025	116	324	1.07	193	0.8520	0.0220	0.1013	0.0008	0.0184	0.0613	0.0017	624	12	622	5	618	59	101
A_157.FIN2	MSL008	216	1005	1.79	400	0.8860	0.0220	0.1047	0.0009	0.0622	0.0615	0.0016	643	12	642	5	639	58	100
A_214.FIN2	MSL056	270	244	0.42	330	0.8650	0.0160	0.1028	0.0007	0.0358	0.0611	0.0012	632	9	631	4	628	44	100
A_215.FIN2	MSL057	181	7	0.02	270	0.9430	0.0240	0.1095	0.0010	0.1106	0.0625	0.0016	673	13	670	6	671	55	100
A_202.FIN2	MSL049	129	193	0.58	130	0.8440	0.0310	0.1000	0.0013	0.0561	0.0614	0.0023	619	17	615	8	617	81	100
A_193.FIN2	MSL040	76	402	0.70	332	5.1100	0.1100	0.3289	0.0031	0.1495	0.1131	0.0025	1836	19	1833	15	1841	41	100
A_199.FIN2	MSL046	190	622	1.22	-2900	0.9030	0.0210	0.1057	0.0007	0.1230	0.0621	0.0015	651	11	648	4	654	51	99
A_190.FIN2	MSL037	252	69	0.10	480	0.8710	0.0210	0.1030	0.0008	0.0604	0.0614	0.0016	635	12	632	5	639	56	99
A_169.FIN2	MSL020	217	952	0.46	7200	6.9100	0.1100	0.3812	0.0038	0.3276	0.1317	0.0020	2099	14	2082	18	2119	26	98
A_183.FIN2	MSL030	128	677	1.20	323	1.6840	0.0340	0.1667	0.0013	0.1748	0.0735	0.0015	1000	13	994	7	1013	42	98
A_194.FIN2	MSL041	95	227	0.88	185	0.8410	0.0230	0.0996	0.0009	0.0089	0.0615	0.0018	617	13	612	5	627	63	98
A_168.FIN2	MSL019	242	811	1.30	610	0.8450	0.0190	0.1006	0.0007	0.0555	0.0614	0.0015	621	10	618	4	634	51	97
A_162.FIN2	MSL013	186	2930	1.78	1280	6.5450	0.0650	0.3689	0.0022	0.2109	0.1289	0.0013	2051	9	2024	10	2081	18	97

A_197.FIN2	MSL044	324	1406	1.74	480	0.8690	0.0190	0.1029	0.0008	0.1284	0.0614	0.0014	634	10	631	5	649	47	97
A_195.FIN2	MSL042	105	81	0.24	70	1.1410	0.0600	0.1248	0.0018	0.0626	0.0665	0.0037	769	28	758	10	780	110	97
A_176.FIN2	MSL023	185	174	0.34	250	0.8770	0.0180	0.1034	0.0007	0.1672	0.0619	0.0012	638	10	634	4	653	45	97
A_196.FIN2	MSL043	236	1190	1.15	810	1.6730	0.0250	0.1660	0.0010	0.2578	0.0735	0.0011	999	10	990	6	1019	30	97
A_220.FIN2	MSL061	174	23	0.41	210	0.8820	0.0350	0.1032	0.0014	0.1083	0.0620	0.0025	641	19	633	8	653	85	97
A_150.FIN2	MSL001	380	471	0.52	490	0.7970	0.0160	0.0954	0.0007	0.2666	0.0606	0.0012	594	9	587	4	613	41	96
A_177.FIN2	MSL024	295	22	0.03	470	0.8420	0.0170	0.0999	0.0008	0.0724	0.0614	0.0014	620	9	614	5	641	47	96
A_160.FIN2	MSL011	202	13	0.01	200	0.8530	0.0280	0.1007	0.0011	0.2719	0.0615	0.0019	624	15	618	7	647	74	96
A_228.FIN2	MSL069	62	274	0.46	390	7.0340	0.0980	0.3777	0.0025	0.3479	0.1348	0.0018	2115	12	2065	12	2163	23	95
A_189.FIN2	MSL036	329	372	0.42	270	0.8410	0.0220	0.1000	0.0011	0.0949	0.0612	0.0018	619	12	615	6	648	71	95
A_165.FIN2	MSL016	193	859	0.54	2300	5.9080	0.0710	0.3440	0.0022	0.2843	0.1248	0.0015	1962	11	1906	11	2023	21	94
A_185.FIN2	MSL032	122	4	0.01	155	0.8220	0.0280	0.0979	0.0014	0.1838	0.0611	0.0022	608	16	602	8	639	82	94
A_170.FIN2	MSL021	141	2249	1.44	-4800	11.5480	0.0910	0.4701	0.0021	0.1650	0.1787	0.0015	2569	7	2484	9	2639	14	94
A_164.FIN2	MSL015	120	269	0.28	680	5.8700	0.0820	0.3420	0.0028	0.4083	0.1247	0.0017	1956	12	1896	13	2021	23	94
A_184.FIN2	MSL031	308	1292	1.92	510	0.8940	0.0150	0.1041	0.0011	0.1079	0.0626	0.0012	648	8	639	6	684	40	93
A_163.FIN2	MSL014	343	427	0.49	1380	0.8740	0.0190	0.1018	0.0009	0.1084	0.0624	0.0015	637	10	625	5	677	51	92
A_210.FIN2	MSL053	84	1518	2.18	480	6.1800	0.1000	0.3468	0.0031	0.4439	0.1294	0.0019	2000	14	1919	15	2084	26	92
A_187.FIN2	MSL034	670	244	0.40	-50000	0.8730	0.0190	0.1018	0.0009	0.0946	0.0624	0.0014	637	10	625	5	680	48	92
A_154.FIN2	MSL005	226	180	0.35	820	0.8380	0.0220	0.0981	0.0010	0.1585	0.0620	0.0017	617	13	603	6	657	60	92
A_159.FIN2	MSL010	25	122	1.25	29	1.6500	0.1000	0.1562	0.0027	0.1121	0.0771	0.0050	975	39	935	15	1020	140	92
A_167.FIN2	MSL018	103	1816	1.55	1590	11.1200	0.1300	0.4533	0.0039	0.4914	0.1784	0.0019	2532	11	2409	17	2635	18	91
A_158.FIN2	MSL009	136	237	0.44	300	1.4510	0.0390	0.1452	0.0012	0.2060	0.0723	0.0021	908	16	874	7	985	57	89
A_186.FIN2	MSL033	313	551	0.73	440	0.8290	0.0300	0.0970	0.0011	0.0275	0.0627	0.0025	612	16	597	7	673	85	89
A_203.FIN2	MSL050	192	448	1.18	7500	0.8600	0.0350	0.0987	0.0011	0.1086	0.0631	0.0026	628	19	607	6	687	90	88

A_222.FI	MSL						0.017		0.000	0.027		0.001							
N2	063	749	2825	1.66	30000	0.8650	0	0.0994	8	3	0.0631	3	632	9	611	5	704	45	87
A_182.FI	MSL						0.082		0.001	0.195		0.004						12	
N2	029	36	67	0.49	400	1.3750	0	0.1350	7	4	0.0735	1	867	34	816	10	960	0	85
A_192.FI	MSL						0.027		0.000	0.233		0.001							
N2	039	160	121	0.27	-490	0.8900	0	0.1010	9	5	0.0641	9	644	14	620	5	730	66	85
A_198.FI	MSL						0.017		0.000	0.172		0.001							
N2	045	300	1229	2.24	60000	0.8390	0	0.0965	7	7	0.0632	3	619	9	594	4	706	44	84
A_236.FI	MSL						0.030		0.001	0.116		0.002							
N2	072	129	10	0.09	120	0.9040	0	0.1014	2	5	0.0646	1	652	16	623	7	753	74	83
A_155.FI	MSL						0.055		0.001	0.034		0.002							
N2	006	107	301	0.67	310	1.6340	0	0.1517	2	1	0.0777	3	973	18	911	7	1103	61	83
A_227.FI	MSL						0.014		0.001	0.644		0.000							
N2	068	1020	2168	0.80	3600	1.2200	0	0.1258	0	7	0.0701	7	809	6	764	6	929	19	82
A_223.FI	MSL						0.021		0.001	0.365		0.001							
N2	064	815	2635	1.41	400	0.8550	0	0.0971	0	5	0.0637	5	627	12	598	6	728	50	82
A_235.FI	MSL				-		0.021		0.001	0.530		0.001							
N2	071	596	197	0.23	21000	1.0000	0	0.1089	6	7	0.0668	3	703	11	666	10	823	41	81
A_152.FI	MSL						0.027		0.000	0.171		0.002							
N2	003	84	94	0.42	145	0.9460	0	0.1031	9	3	0.0667	0	674	15	633	6	789	63	80
A_153.FI	MSL						0.035		0.001	0.271		0.002							
N2	004	118	437	1.44	190	0.9120	0	0.1010	2	2	0.0661	7	659	20	620	7	782	89	79
A_204.FI	MSL						0.017		0.001	0.449		0.001							
N2	051	279	678	2.18	520	0.8110	0	0.0924	2	7	0.0636	2	602	10	570	7	722	42	79
A_221.FI	MSL				- 10000		0.014		0.000	0.187		0.001							
N2	062	553	524	0.56	0	0.8370	0	0.0945	6	0	0.0642	0	617	8	582	4	739	34	79
A_151.FI	MSL						0.020		0.000	0.082		0.001							
N2	002	181	235	0.57	210	0.8860	0	0.0981	8	1	0.0653	6	643	11	603	5	773	51	78
A_211.FI	MSL						0.053		0.001	0.446		0.001							
N2	054	426	229	0.58	1400	4.4850	0	0.2685	5	1	0.1211	3	1727	10	1534	7	1971	19	78
A_226.FI	MSL						0.041		0.001	0.220		0.002							
N2	067	144	280	0.54	570	1.2710	0	0.1253	5	9	0.0736	4	830	18	761	8	1005	65	76
A_218.FI	MSL						0.031		0.001	0.425		0.001							
N2	059	501	112	0.25	730	1.0370	0	0.1077	1	4	0.0697	9	721	15	659	7	910	56	72
A_213.FI	MSL						0.018		0.000	0.312		0.001							
N2	055	345	442	3.27	420	0.8290	0	0.0910	9	8	0.0661	3	612	10	561	5	798	43	70
A_224.FI	MSL						0.087		0.002	0.521		0.002							
N2	065	119	217	0.28	4700	3.7410	0	0.2307	2	9	0.1174	3	1577	18	1338	12	1908	36	70
A_201.FI	MSL						0.013		0.000	0.270		0.001							
N2	048	348	875	3.60	2000	0.8390	0	0.0900	6	5	0.0676	0	618	7	556	3	852	31	65
A_229.FI	MSL						0.062		0.002	0.581		0.001							
N2	070	404	1005	0.36	5600	6.3790	0	0.2711	0	1	0.1703	4	2029	9	1546	10	2560	14	60
A_225.FI	MSL						0.031		0.001	0.790		0.001							
N2	066	727	988	2.00	1900	2.3050	0	0.1634	4	0	0.1019	0	1213	10	976	8	1660	17	59
A_191.FI	MSL						0.044		0.002	0.483		0.001							
N2	038	252	812	3.28	670	2.0650	0	0.1533	2	2	0.0978	9	1135	14	919	12	1574	36	58
A_156.FI	MSL						0.075		0.003	0.862		0.001							
N2	007	273	694	1.46	500	2.4640	0	0.1684	9	1	0.1060	7	1256	22	1003	22	1725	29	58

A_181.FIN2	MSL028	700	679	0.85	4600	2.7420	0.0870	0.1767	0.0042	0.9534	0.1125	0.0013	1335	24	1049	23	1838	21	57
A_205.FIN2	MSL052	558	1322	2.62	580	0.8500	0.0130	0.0838	0.0011	0.3403	0.0740	0.0013	625	8	519	6	1032	35	50
A_171.FIN2	MSL022	1	8	0.03	3	6.3300	0.9900	0.1930	0.0130	0.2455	0.2480	0.0370	1740	180	1137	70	2490	370	46

Appendix 6.14: Results of the analysis of zircons from Yatchika kaolin

Analysis	Sample	U [ppm][a]	Pb [ppm][a]	Th/U[a]	*206/204*	RATIOS $^{207}Pb/^{235}U$[b]	2 σ[d]	$^{206}Pb/^{238}U$[b]	2 σ[d]	rho[c]	$^{207}Pb/^{206}Pb$[e]	2 σ[d]	AGES [Ma] $^{207}Pb/^{235}U$	2 σ	$^{206}Pb/^{238}U$	2 σ	$^{207}Pb/^{206}Pb$	2 σ	Conc. %
A_069.FIN2	YTK060	37	7	0.03	-4100	1.1310	0.0710	0.1282	0.0029	0.3252	0.0631	0.0037	754	34	777	17	640	120	121
A_020.FIN2	YTK015	16	54	1.24	50	0.9270	0.0590	0.1069	0.0019	0.1097	0.0628	0.0039	653	31	654	11	580	130	113
A_079.FIN2	YTK066	65	88	0.51	99	0.8580	0.0350	0.1021	0.0011	0.0906	0.0611	0.0025	623	19	627	7	580	90	108
A_021.FIN2	YTK016	125	174	0.52	250	0.9100	0.0220	0.1075	0.0008	0.0163	0.0612	0.0016	655	12	658	5	623	56	106
A_050.FIN2	YTK041	74	61	0.30	132	0.9240	0.0440	0.1081	0.0018	0.3967	0.0617	0.0026	657	23	661	10	630	97	105
A_051.FIN2	YTK042	201	673	1.31	640	0.8470	0.0210	0.1015	0.0008	0.0046	0.0602	0.0015	622	12	623	5	600	56	104
A_132.FIN2	YTK114	46	89	0.68	80	0.9970	0.0440	0.1132	0.0015	0.1050	0.0637	0.0029	694	22	691	9	666	95	104
A_116.FIN2	YTK098	128	421	1.26	-30	0.8250	0.0280	0.0987	0.0009	0.0199	0.0606	0.0021	608	16	607	5	585	76	104
A_056.FIN2	YTK047	58	112	0.76	91	0.8370	0.0430	0.0992	0.0014	0.1170	0.0614	0.0033	612	24	610	8	590	110	103
A_115.FIN2	YTK097	144	334	0.89	-5600	0.8360	0.0220	0.1002	0.0009	0.0913	0.0605	0.0016	615	12	616	5	596	58	103
A_017.FIN2	YTK012	72	154	0.61	124	0.9820	0.0430	0.1121	0.0014	0.1642	0.0634	0.0028	689	22	685	8	663	95	103
A_063.FIN2	YTK054	238	414	0.67	420	0.8310	0.0180	0.0999	0.0007	0.2567	0.0603	0.0013	613	10	614	4	595	46	103
A_078.FIN2	YTK065	95	333	1.32	153	0.8630	0.0290	0.1024	0.0009	0.0763	0.0611	0.0021	630	15	628	5	609	76	103
A_121.FIN2	YTK103	35	123	1.35	38	0.8240	0.0380	0.0975	0.0012	0.0173	0.0616	0.0030	603	21	599	7	581	98	103
A_111.FIN2	YTK093	57	141	0.95	-164	0.8470	0.0370	0.0998	0.0012	0.0855	0.0616	0.0027	617	21	613	7	595	94	103
A_089.FIN2	YTK076	53	138	1.03	-12000	0.8510	0.0360	0.1003	0.0012	0.1194	0.0618	0.0027	619	20	616	7	600	90	103
A_075.FIN2	YTK062	78	190	0.92	81	0.8400	0.0300	0.0996	0.0009	0.0132	0.0612	0.0022	614	16	612	5	597	77	103
A_088.FIN2	YTK075	63	256	1.58	780	0.8360	0.0370	0.0992	0.0014	0.0820	0.0614	0.0028	615	20	610	8	595	96	102
A_074.FIN2	YTK061	114	394	1.33	198	0.8360	0.0220	0.1002	0.0009	0.1922	0.0607	0.0016	615	12	616	5	602	57	102
A_064.FIN2	YTK055	134	143	0.40	370	0.9030	0.0270	0.1071	0.0017	0.3605	0.0617	0.0017	650	14	655	10	643	57	102

A_033.FIN2	YTK028	361	495	0.53	7800	0.8610	0.0170	0.1025	0.0008	0.1906	0.0607	0.0012	630	9	629	5	618	42	102
A_144.FIN2	YTK122	94	370	1.39	-900	0.8780	0.0270	0.1031	0.0011	0.1256	0.0618	0.0019	636	15	632	7	624	66	101
A_124.FIN2	YTK106	175	411	0.91	50	0.8250	0.0250	0.0990	0.0008	0.0188	0.0604	0.0019	612	15	608	5	603	72	101
A_008.FIN2	YTK003	140	316	0.85	240	0.8750	0.0230	0.1036	0.0010	0.0912	0.0612	0.0017	638	13	636	6	630	60	101
A_044.FIN2	YTK035	63	776	1.35	490	6.8690	0.0910	0.3841	0.0028	0.3740	0.1288	0.0015	2092	12	2095	13	2079	22	101
A_094.FIN2	YTK081	68	1650	2.72	2200	6.5560	0.0940	0.3763	0.0028	0.1955	0.1266	0.0019	2051	13	2058	13	2045	26	101
A_043.FIN2	YTK034	346	81	0.10	220	0.7980	0.0170	0.0962	0.0007	0.1814	0.0599	0.0012	595	9	592	4	589	45	101
A_114.FIN2	YTK096	130	511	1.55	1800	0.8100	0.0220	0.0969	0.0008	0.0522	0.0606	0.0017	600	12	596	5	593	62	101
A_133.FIN2	YTK115	38	65	0.60	100	0.9630	0.0450	0.1101	0.0016	0.1845	0.0639	0.0031	684	25	673	9	670	100	100
A_120.FIN2	YTK102	45	225	1.95	60	0.8610	0.0370	0.1004	0.0012	0.0175	0.0628	0.0028	626	20	617	7	614	94	100
A_146.FIN2	YTK124	81	174	0.92	-1770	0.8440	0.0320	0.0996	0.0011	0.0661	0.0616	0.0023	617	17	612	7	610	83	100
A_085.FIN2	YTK072	127	408	1.24	227	0.8670	0.0240	0.1025	0.0008	0.0537	0.0615	0.0017	632	13	629	5	627	62	100
A_147.FIN2	YTK125	74	135	0.70	-2800	0.8230	0.0290	0.0980	0.0010	0.0535	0.0613	0.0023	608	17	603	6	602	77	100
A_045.FIN2	YTK036	121	441	1.42	490	0.8410	0.0240	0.0995	0.0009	0.0374	0.0612	0.0018	617	13	611	5	611	64	100
A_096.FIN2	YTK083	65	835	1.48	1700	6.6200	0.1200	0.3754	0.0045	0.3169	0.1272	0.0021	2059	16	2054	21	2054	29	100
A_057.FIN2	YTK048	154	411	1.06	300	0.8370	0.0230	0.0993	0.0007	0.2054	0.0610	0.0016	615	13	610	4	611	59	100
A_093.FIN2	YTK080	75	230	0.34	1440	6.3270	0.0730	0.3676	0.0023	0.3770	0.1247	0.0014	2020	10	2018	11	2022	20	100
A_048.FIN2	YTK039	67	989	1.21	400	15.2000	0.1300	0.5489	0.0033	0.3010	0.2006	0.0019	2827	8	2820	14	2829	15	100
A_082.FIN2	YTK069	13	42	0.33	77	6.9200	0.2000	0.3822	0.0048	0.0650	0.1316	0.0039	2089	25	2085	22	2092	53	100
A_055.FIN2	YTK046	85	218	1.00	154	0.8760	0.0410	0.1022	0.0014	0.1350	0.0621	0.0029	635	22	628	8	630	100	100
A_081.FIN2	YTK068	72	2061	3.22	430	6.4690	0.0960	0.3715	0.0027	0.1836	0.1267	0.0019	2041	13	2036	13	2045	27	100
A_040.FIN2	YTK031	119	251	0.82	170	0.8470	0.0310	0.0996	0.0009	0.1029	0.0614	0.0023	620	17	612	6	615	80	100
A_067.FIN2	YTK058	68	728	1.55	290	3.7230	0.0600	0.2757	0.0021	0.0555	0.0983	0.0018	1573	13	1569	11	1578	34	99
A_059.FIN2	YTK050	75	428	0.54	550	10.4900	0.1300	0.4663	0.0034	0.2583	0.1630	0.0021	2478	11	2467	15	2483	21	99

A_014.FIN2	YTK009	124	222	0.70	270	0.8660	0.0220	0.1023	0.0009	0.0760	0.0614	0.0017	632	12	628	5	632	59	99
A_090.FIN2	YTK077	75	727	1.13	9700	6.1510	0.0830	0.3615	0.0023	0.1562	0.1236	0.0017	1995	12	1989	11	2003	24	99
A_054.FIN2	YTK045	149	892	0.41	1090	23.3900	0.1800	0.6496	0.0040	0.3089	0.2607	0.0021	3243	7	3226	16	3250	13	99
A_097.FIN2	YTK084	141	811	0.41	12700	18.0500	0.5300	0.5870	0.0130	0.9707	0.2221	0.0020	2981	26	2971	52	2994	14	99
A_031.FIN2	YTK026	196	1457	0.69	31000	11.2600	0.1100	0.4807	0.0029	0.2869	0.1694	0.0014	2544	9	2530	13	2551	14	99
A_091.FIN2	YTK078	136	2246	1.96	5000	6.1990	0.0870	0.3627	0.0028	0.2526	0.1240	0.0017	2003	12	1995	13	2012	24	99
A_012.FIN2	YTK007	82	700	0.97	430	6.7250	0.0960	0.3769	0.0024	0.1174	0.1292	0.0020	2074	13	2062	11	2082	27	99
A_134.FIN2	YTK116	32	459	1.70	-130	6.4100	0.1300	0.3677	0.0034	0.0079	0.1260	0.0028	2029	18	2018	16	2039	38	99
A_135.FIN2	YTK117	126	794	0.76	7600	5.9670	0.0680	0.3549	0.0020	0.2224	0.1217	0.0014	1970	10	1958	10	1978	21	99
A_145.FIN2	YTK123	152	2720	2.00	-6900	6.6260	0.0660	0.3737	0.0021	0.3127	0.1283	0.0013	2062	9	2047	10	2073	17	99
A_126.FIN2	YTK108	72	77	0.42	-100	0.8070	0.0290	0.0971	0.0011	0.0589	0.0607	0.0023	600	17	597	7	605	79	99
A_123.FIN2	YTK105	129	400	0.82	-60	1.4340	0.0450	0.1482	0.0013	0.1125	0.0701	0.0022	900	19	891	8	904	66	99
A_065.FIN2	YTK056	348	283	0.31	430	0.8210	0.0130	0.0986	0.0005	0.1178	0.0605	0.0010	609	7	606	3	616	35	98
A_049.FIN2	YTK040	69	1169	1.42	8100	15.1800	0.2300	0.5429	0.0054	0.1491	0.2023	0.0035	2826	15	2795	23	2842	28	98
A_019.FIN2	YTK014	275	1533	2.17	2800	0.8990	0.0230	0.1050	0.0008	0.1433	0.0619	0.0016	650	12	644	4	655	55	98
A_149.FIN2	YTK127	207	1751	0.96	-2200	6.5790	0.0570	0.3713	0.0020	0.1911	0.1282	0.0013	2056	8	2036	10	2072	17	98
A_042.FIN2	YTK033	110	1862	2.01	7500	5.9430	0.0830	0.3523	0.0025	0.1919	0.1222	0.0018	1968	12	1946	12	1983	26	98
A_077.FIN2	YTK064	111	1522	1.54	720	6.6510	0.0740	0.3734	0.0023	0.3042	0.1295	0.0014	2065	10	2045	11	2087	19	98
A_083.FIN2	YTK070	62	758	1.11	440	11.7800	0.1700	0.4864	0.0041	0.1873	0.1758	0.0027	2585	13	2555	18	2609	26	98
A_092.FIN2	YTK079	70	793	1.05	1100	10.7000	0.1500	0.4663	0.0033	0.1262	0.1667	0.0024	2496	13	2467	14	2523	23	98
A_110.FIN2	YTK092	72	797	1.29	1700	6.2170	0.0900	0.3597	0.0022	0.0623	0.1252	0.0021	2007	13	1982	11	2028	28	98
A_053.FIN2	YTK044	65	672	1.57	230	3.6730	0.0840	0.2706	0.0026	0.0257	0.0984	0.0024	1563	18	1544	13	1581	46	98
A_034.FIN2	YTK029	92	8	0.01	90	0.9350	0.0470	0.1068	0.0013	0.1759	0.0632	0.0031	666	25	654	7	670	110	98
A_086.FIN2	YTK073	215	4445	2.34	600	6.5650	0.0480	0.3699	0.0015	0.1833	0.1290	0.0010	2054	7	2029	7	2082	13	97

A_117.FI N2	YTK 099	81	208	0.97	590	0.8480	0.0270	0.0996	0.0011	0.0682	0.0618	0.0020	620	15	612	6	628	70	97
A_052.FI N2	YTK 043	194	1749	1.37	850	3.7100	0.0540	0.2722	0.0017	0.0701	0.0987	0.0015	1573	11	1552	9	1594	28	97
A_143.FI N2	YTK 121	186	1682	1.03	11300	6.5400	0.0600	0.3682	0.0017	0.1697	0.1287	0.0012	2050	8	2021	8	2077	17	97
A_080.FI N2	YTK 067	144	1278	0.84	1290	10.2710	0.0960	0.4563	0.0026	0.4270	0.1634	0.0014	2459	9	2423	12	2492	14	97
A_113.FI N2	YTK 095	48	125	1.01	440	0.8300	0.0330	0.0970	0.0011	0.0316	0.0622	0.0026	608	18	597	7	614	88	97
A_129.FI N2	YTK 111	136	718	0.60	2100	6.4920	0.0630	0.3660	0.0019	0.1587	0.1282	0.0014	2044	9	2011	9	2070	19	97
A_100.FI N2	YTK 087	192	4151	1.84	-19000	12.9410	0.0800	0.5037	0.0024	0.2347	0.1862	0.0012	2675	6	2629	10	2708	11	97
A_029.FI N2	YTK 024	64	877	1.62	390	5.9200	0.0970	0.3488	0.0027	0.0698	0.1228	0.0023	1962	14	1929	13	1989	34	97
A_136.FI N2	YTK 118	132	629	0.37	-4900	18.3000	0.1500	0.5793	0.0030	0.3669	0.2288	0.0019	3005	8	2946	12	3042	13	97
A_058.FI N2	YTK 049	28	666	2.88	99	6.1600	0.2200	0.3551	0.0057	0.1821	0.1260	0.0047	1992	32	1958	27	2022	68	97
A_148.FI N2	YTK 126	76	2492	3.17	-1100	10.4500	0.2500	0.4563	0.0056	0.8124	0.1655	0.0027	2469	23	2422	25	2506	27	97
A_108.FI N2	YTK 090	75	555	0.72	1300	9.1000	0.1100	0.4294	0.0037	0.2203	0.1536	0.0020	2348	10	2303	17	2383	22	97
A_035.FI N2	YTK 030	217	1044	0.54	-500	7.1590	0.0610	0.3813	0.0021	0.2416	0.1356	0.0013	2132	8	2082	10	2170	16	96
A_122.FI N2	YTK 104	156	1656	1.21	1900	6.3710	0.0610	0.3602	0.0018	0.0775	0.1281	0.0013	2027	9	1983	9	2068	19	96
A_087.FI N2	YTK 074	182	3209	2.08	430	6.0890	0.0590	0.3526	0.0018	0.3083	0.1255	0.0012	1988	9	1947	9	2033	17	96
A_060.FI N2	YTK 051	88	1212	1.42	750	9.5050	0.0930	0.4348	0.0024	0.1038	0.1582	0.0018	2387	9	2327	11	2434	19	96
A_098.FI N2	YTK 085	179	2371	1.16	22000	12.6040	0.0860	0.4926	0.0025	0.2683	0.1857	0.0014	2650	6	2582	11	2703	12	96
A_095.FI N2	YTK 082	69	205	1.19	1130	0.8460	0.0350	0.0983	0.0011	0.0870	0.0624	0.0025	618	19	605	6	633	87	96
A_006.FI N2	YTK 001	42	482	1.09	250	11.0200	0.1800	0.4643	0.0046	0.2421	0.1727	0.0031	2526	16	2458	20	2578	30	95
A_119.FI N2	YTK 101	228	2121	1.09	5000	6.0430	0.0510	0.3495	0.0017	0.3049	0.1249	0.0010	1981	7	1932	8	2027	14	95
A_022.FI N2	YTK 017	43	588	1.74	100	6.1200	0.1400	0.3509	0.0045	0.1935	0.1262	0.0031	1989	21	1938	22	2034	44	95
A_137.FI N2	YTK 119	40	440	1.29	20	6.3100	0.1200	0.3564	0.0035	0.2201	0.1279	0.0024	2016	17	1965	16	2064	34	95
A_068.FI N2	YTK 059	663	473	0.30	800	0.7397	0.0085	0.0904	0.0004	0.2066	0.0597	0.0007	562	5	558	2	587	25	95
A_118.FI N2	YTK 100	92	886	0.88	3300	11.5500	0.1200	0.4715	0.0027	0.5148	0.1771	0.0016	2567	10	2490	12	2625	15	95

A_128.FI N2	YTK 110	22	125	0.62	300	6.3500	0.1400	0.3568	0.0040	0.1343	0.1300	0.0033	2027	20	1966	19	2077	44	95
A_109.FI N2	YTK 091	65	502	0.89	1500	7.1200	0.1200	0.3755	0.0034	0.1393	0.1370	0.0024	2124	15	2055	16	2188	31	94
A_130.FI N2	YTK 112	88	1285	1.31	1200	11.6800	0.1000	0.4700	0.0023	0.3983	0.1799	0.0015	2579	8	2483	10	2649	14	94
A_131.FI N2	YTK 113	34	182	0.68	230	5.3190	0.0970	0.3237	0.0035	0.3389	0.1196	0.0022	1871	16	1807	17	1935	33	93
A_112.FI N2	YTK 094	123	1132	1.07	4800	6.3920	0.0770	0.3552	0.0021	0.2615	0.1304	0.0016	2030	11	1959	10	2099	21	93
A_066.FI N2	YTK 057	149	334	0.25	710	5.9390	0.0570	0.3436	0.0022	0.2202	0.1258	0.0013	1966	8	1904	10	2040	18	93
A_030.FI N2	YTK 025	174	158	0.36	390	0.8310	0.0270	0.0976	0.0008	0.1005	0.0615	0.0021	613	15	600	5	646	77	93
A_125.FI N2	YTK 107	63	522	1.01	-1010	5.9290	0.0900	0.3390	0.0023	0.1089	0.1267	0.0020	1963	13	1881	11	2045	29	92
A_032.FI N2	YTK 027	283	589	0.26	4100	5.5390	0.0550	0.3275	0.0015	0.1986	0.1222	0.0012	1906	9	1826	7	1986	18	92
A_142.FI N2	YTK 120	134	508	0.46	3700	5.5510	0.0510	0.3278	0.0016	0.2236	0.1227	0.0012	1907	8	1828	8	1993	17	92
A_102.FI N2	YTK 089	217	1606	0.77	-600	8.4160	0.0670	0.3995	0.0018	0.1118	0.1530	0.0014	2276	7	2167	8	2378	15	91
A_047.FI N2	YTK 038	362	417	0.13	2400	10.8100	0.4700	0.4421	0.0084	0.9688	0.1751	0.0046	2489	41	2358	37	2592	45	91
A_099.FI N2	YTK 086	420	1975	0.46	15000	8.7600	0.1100	0.4053	0.0028	0.8283	0.1567	0.0013	2313	12	2193	13	2420	15	91
A_084.FI N2	YTK 071	39	196	0.59	222	6.4400	0.1600	0.3500	0.0037	0.0178	0.1339	0.0035	2033	21	1934	18	2135	45	91
A_061.FI N2	YTK 052	162	679	0.45	970	8.6500	0.0840	0.4022	0.0023	0.3895	0.1560	0.0014	2301	9	2179	11	2411	16	90
A_062.FI N2	YTK 053	139	1008	0.72	1030	8.3640	0.0890	0.3956	0.0022	0.5098	0.1535	0.0014	2270	10	2148	10	2382	16	90
A_011.FI N2	YTK 006	39	517	1.73	520	5.7100	0.1200	0.3270	0.0038	0.0258	0.1265	0.0030	1929	18	1823	19	2042	41	89
A_127.FI N2	YTK 109	27	67	0.31	-20	5.2900	0.1400	0.3100	0.0044	0.4221	0.1234	0.0030	1859	24	1740	21	1985	45	88
A_101.FI N2	YTK 088	59	351	0.75	-850	6.3140	0.0890	0.3403	0.0024	0.2193	0.1346	0.0018	2020	12	1888	11	2156	23	88
A_076.FI N2	YTK 063	29	489	2.31	91	4.4840	0.0950	0.2818	0.0027	0.2313	0.1154	0.0024	1722	18	1602	14	1878	40	85
A_046.FI N2	YTK 037	98	273	1.04	280	0.9070	0.0290	0.1010	0.0009	0.0087	0.0651	0.0021	652	15	620	5	734	70	84
A_015.FI N2	YTK 010	143	1091	0.88	520	8.9800	0.1200	0.3840	0.0036	0.7108	0.1692	0.0017	2334	13	2094	17	2547	16	82
A_024.FI N2	YTK 019	260	78	0.10	2200	0.8950	0.0210	0.0999	0.0008	0.1614	0.0645	0.0016	648	11	614	5	751	55	82
A_025.FI N2	YTK 020	101	276	0.89	40	0.9830	0.0330	0.1059	0.0010	0.2192	0.0672	0.0022	692	17	649	6	809	73	80

A_041.FI N2	YTK 032	47	109	0.87	-670	0.9600	0.0430	0.1018	0.0013	0.0966	0.0681	0.0030	678	23	625	8	801	98	78
A_016.FI N2	YTK 011	43	78	0.74	160	0.8510	0.0510	0.0925	0.0018	0.2448	0.0666	0.0038	619	28	570	11	760	120	75
A_018.FI N2	YTK 013	146	36	0.06	230	1.7300	0.1000	0.1381	0.0049	0.9244	0.0885	0.0030	999	41	832	28	1363	68	61
A_009.FI N2	YTK 004	203	517	1.29	349	1.0630	0.0340	0.0983	0.0007	0.2651	0.0783	0.0024	738	18	605	4	1139	69	53
A_023.FI N2	YTK 018	101	222	0.88	183	1.0540	0.0440	0.0965	0.0014	0.3439	0.0785	0.0030	726	22	594	8	1119	82	53
A_026.FI N2	YTK 021	374	587	0.26	980	3.0830	0.0510	0.1796	0.0034	0.2803	0.1243	0.0028	1427	13	1064	19	2012	39	53
A_010.FI N2	YTK 005	439	2218	2.29	408	1.7030	0.0230	0.1209	0.0017	0.4000	0.1020	0.0014	1009	9	735	10	1660	27	44
A_028.FI N2	YTK 023	113	288	0.45	177	2.2300	0.1100	0.1358	0.0013	0.1488	0.1184	0.0056	1176	31	821	7	1871	75	44
A_013.FI N2	YTK 008	11	18	0.25	39	2.0400	0.1500	0.1121	0.0038	0.0592	0.1340	0.0100	1097	51	684	22	2000	160	34
A_007.FI N2	YTK 002	436	573	2.50	280	1.5060	0.0300	0.0953	0.0011	0.0108	0.1142	0.0024	932	12	587	7	1867	41	31
A_027.FI N2	YTK 022	60	142	0.26	59	2.2850	0.0920	0.1074	0.0015	0.0283	0.1551	0.0066	1198	29	657	9	2371	74	28